Bacterial abilities to adhere to food components : extent, characterisation, and sensitivity to shear stress

Faustine Gomand

Bacterial abilities to adhere to food components: extent, characterisation, and sensitivity to shear stress

THESIS

presented and publicly defended on October 10, 2019

in order to get the degree of

Doctor of Philosophy of the Université de Lorraine

-

Doctorat de l'Université de Lorraine

(Biotechnology and Food Engineering
Génie Biotechnologique et Alimentaire)

by

Faustine Gomand

Jury composition

President:	Philippe Cayot (Professor)	AgroSup Dijon
Rapporteur:	Mickaël Desvaux (Research Director)	INRA Centre Auvergne Rhône Alpes
Examiners:	Nicolas Desprat (Associate Professor) Fabienne Quilès (Research fellow, HDR)	ENS Paris Université de Lorraine
Guest:	Saverio Spagnolie (Associate Professor)	University of Wisconsin-Madison (USA)
Main thesis advisor:	Claire Gaiani (Professor)	Université de Lorraine
Thesis co-advisor:	Frédéric Borges (Associate Professor)	Université de Lorraine

Université de Lorraine
Laboratoire d'Ingénierie des Biomolécules - LIBio

Mis en page avec la classe thesul.

Acknowledgments

This research project was conducted in the Biomolecule Engineering Laboratory (Laboratoire d'Ingénierie des Biomolécules, LIBio, France) thanks to the LUE initiative (Lorraine Université d'Excellence) and in the Applied Math Lab at the University of Wisconsin-Madison, USA (Jan-Nov 2018) thanks to a Fulbright scholarship.

My first thoughts are for the three people who made this research happen -Claire, Frédéric, and Saverio. Un grand merci à Claire pour avoir construit ce projet, qui m'a fait vivre de belles aventures. Fred, je te suis très reconnaissante pour ta patience et ton écoute qui m'ont accompagnée tout au long de ces trois ans. Merci d'avoir été là pour moi dans les moments difficiles et d'avoir toujours cru en moi, c'est parfois tout ce qu'il faut pour continuer d'aller de l'avant. J'ai une pensée pour les petites leçons de vie et tous les conseils que tu m'as prodigué depuis ce jour où il y a trois ans, tu m'accompagnais pour mes premiers pas de microbiologiste. Merci pour m'avoir donné le goût de la recherche à travers ta curiosité scientifique, qui me motive encore aujourd'hui à approfondir toujours plus d'autres pistes de recherche... Et merci pour tout.

To Saverio, my partner in trouble whenever math or physics get to join the game -it was a great pleasure to get to know you and work with you. Your passion for research and unrestricted enthusiasm for physics and math made me discover and enjoy a world which existence, and labyrinthine paths I would never have imagined, but I now want to make an essential part of my upcoming research path. It has been a lot of fun. A huge thanks for boarding with me on this adventure, never giving in to discouragement, trusting us until the end and bringing our project to a safe harbor. I am also very happy we got to go to New York together for the last part of my stay; I felt happy as a clam in our research team and had love at first sight for the city -these are wonderful times I will always remember with fondness. A special thought for Carina whose presence along the way lightened up the days, and for Elena -sharing common literature delights. Thank you for all -I certainly hope to see you again in the future.

Many thanks to all three labs I got to work with -the LIBio, the Applied Math Lab, and the Biophysical modeling group at the Computational Center for Biology (Flatiron Institute). Merci Jenni pour ton enthousiasme et ton accompagnement tout au long de ces trois ans. Merci à mon groupe de copines doctorantes, Aldjia, Aurélie A. et Asmaa, dont l'enthousiasme (parfois délirant !) et la bonne humeur débordante ont fait vivre le bureau par leurs fous rires et leur optimisme, et donnaient envie d'aller travailler le matin, ainsi qu'à Shirin et aux garçons : Mahmoud, Tristan, Kamil, Loïc. Merci à Aya et Justine pour leurs précieux conseils et leur soutien lors de ma première année. Une pensée pour Nancy, qui a fait en même temps que moi ses débuts en microbio, et pour Marie, toujours là pour m'aider, m'écouter et me conseiller. Merci à Sylvie et Myriam, mes piliers en microbiologie sur lesquelles je pouvais toujours m'appuyer, et à Aurélie C. pour m'avoir sauvée plus d'une fois de situations critiques. Un grand merci aussi à Denis Roegel pour m'avoir aidée à mettre en forme cette thèse en LaTeX ! Enfin, merci à Jiaqi, Lamia et Mina, avec lesquelles discuter était toujours un plaisir.

Thanks to Jean-Luc for having me discover what real maths sound like (from a newborn point of view), to Shingyung for helping me with classes, and to Sara N. and Henry for being there when the Mac crashed down overseas... Many thanks to Chris for always being there to help me out with enthusiasm, and to Will M. for making me want to go work in Madison in the first place, and for his advice and listening in science and on Ph.D. life. It was fun to be in the Applied Math Lab, whether it came to our weekly meetings that always brought something up for curiosity, or to barbecuing and root beers -I am happy I got to know all of you.

I am also really grateful to the Biophysics group for having made me more than welcome during my short stay at the Flatiron Insitute -Claudia, Danxun, Nicholas, Pat... I enjoyed working around you so much! Danny, *Pretty Woman* was a blast -I am very happy I could share it with you!

Enfin, un grand merci à l'équipe Fulbright, Emily et Madeleine, pour toute leur aide, et sans qui ce merveilleux séjour aux Etats-Unis n'aurait pas été possible.

An affectionate thought for my dearest friends in France and everywhere in the world: Aurore, Camille, Mévie, Clémence, Clara H., Thouny, Ida N., Chlo, Michou, Stef, Piffa, Harshad, Alex & Amanda, Ana, Yue, Yujia, Steve & Joan, Larry & Eileen, Nate & his family.

A Aurore et Camille, compagnes de thèse et de thé & petits gâteaux, Mévie pour sa bonne humeur et ses rires, Clara à travers notre correspondance épistolaire aux notes poétiques, Michou pour nos sorties au musée et anecdotes de cuisine, Chlo pour ses après-midi thé... To Stef and Piffa, "i miei piccoli raggi di sole", with who I learn to love italian and Italy -I hope to be soon able to pay you the visit I promised! To Ana & Yue, wonderful friends and roommates for over a year, I would not have made it in Madison if it were not for you and Nate. Nate -all this time we spent together, preparing for the Fulbright scholarship, then on the roads biking, exploring architecture, libraries, parks, the world... I picture you smiling thinking "where will she end up next?" waiting for the next postcard; I owe you a lot -thank you for taking care of me. A special thought to Steve & Joan for being my little family overseas -I send you my love. Warm thoughts also for Larry & Eileen, who have always helped me when in need, and with who I could exchange about everything, and to Yuhua, for making me wonderful breakfasts and meals so I never had to worry about anything!

To my French tutees, Hailey and Emmanuel -it was great to have you as students! I wish you the best in everything!

A mon groupe de danse à Nancy, Marie-Georges, Muriel, Amandine, Jessy, Aramis, Noémie, Aurore D., Julie Z., Pierrick, Matthieu, Taha, Pierrot, Samuel, Essivi, Céline, Sandrine, Luc, Séb, Vincent JG et Vincent L., Célia, Alex, Tabea... Vous avez été comme une seconde famille, c'était un vrai plaisir de se retrouver, aux cours, sous le ciel étoilé de la Pép... N'importe où, du moment que la danse était au rendez-vous ! A thought along to my West Coast partners in Madison, David and Soon-Young.

Un grand merci à toute la classe de CM2 de Thomas F. à l'Ecole primaire La Moisson-

nerie (Pulnoy) pour leur enthousiasme, leur bonne humeur... Et leur affection, qui fait chaud au coeur !

Merci à mes coachs de Brabois, Claude et Denis, pour les séances d'abdos énergisantes, et Denis pour les échappées bucoliques et poétiques, épistolaires et au grand air.

Merci à toute l'équipe du lundi des Restos du Coeur, Maud, Léa, Julie, Pascal, Maxime, Aurélien, Brigitte, Rachel et Laura, Xavier, Dorian, Thomas et Josiane, pour leur bonne humeur et leur ouverture d'esprit.

Un immense merci à P.N., pour ton indéfectible soutien depuis les huit ans qu'on se connaît, pour ton affection qui n'a jamais défailli et qui m'accompagne, partout où je vais. Tu auras toujours une place dans mon coeur.

Une très tendre pensée pour S & S & S, les petites que je vois grandir, et que j'aime comme des soeurs.

Une tendre pensée aussi bien sûr pour Doudou, qui après deux ans mouvementés de déplacements multiples, découvertes, rencontres, retrouvailles... a su me charmer, et (presque !) réussi à m'apprivoiser.

Enfin, mes dernières pensées vont naturellement à ma famille. Mes grand-pères qui, je le sais, auraient été fiers de moi, et mes mamies, Mamie Odette pour sa curiosité et son intérêt pour les sciences, qui est la première à m'avoir poussée dans la direction de la recherche en agroalimentaire. A mon frère Augustin, avec qui j'ai co-construit des cours de maths, et qui a toujours suivi mes projets, même à l'autre bout du monde, et mes parents, que j'aime plus que tout -c'est avec un immense plaisir que je vous dédie à tous les trois ce travail.

"I don't know anything, but I know
that everything is interesting if you go into it deeply enough."
Richard Feynman, 1965.

Contents

Part I Literature review

Part III Material and Methods

Chapter III.1
Material

Chapter III.2
Identification of adhesive interactions

Chapter III.3
Characterisation of adhesive interactions

Part IV Results and Discussion

Chapter IV.1
Identification and characterisation of adhesive interactions

Chapter IV.2
Shaving and breaking bacterial chains under shearing

Part V Conclusions and Perspectives

Part VI Bibliography

Part VII Scientific valorization

Part VIII Appendices

Part IX Résumé de la thèse en français

List of Figures

List of Tables

Preamble

This Ph.D. project was born in the Biomolecule Engineering Laboratory (LIBio), located in Nancy, France. From the beginning, it was conceived as a multidisciplinary project that would lay at the interface of various disciplines, including food engineering, microbiology, biophysics, and mathematical modeling.

The main objectives of LIBio researchers are to understand and control soft matter structuring mechanisms and to get a good grasp at mass transfer phenomena and stability of complex systems by considering biotic and abiotic interactions. Three research axes have been developed around these objectives. They concern (i) the impact of processes and of both biotic and abiotic dimensions of food matrices on their functional properties, (ii) the conception of vulnerable molecules carriers or "vectors", and (iii) the control and study of such vectors and matrices *in situ*.

Previous Ph.D. projects conducted in the LIBio included the development of an encapsulation technique for probiotic lactic acid bacteria [Burgain, 2013], which was patented (patent no. 456357), and a later focus on dairy functional ingredients that allowed optimizing *Lactobacillus rhamnosus* GG encapsulation [Guerin, 2017]. In the latter project, the importance of adhesive phenomena between the strain studied and several dairy components and its impact on the encapsulation process were enhanced. The research presented in the current dissertation was conceived in continuity with those two projects, studying the extent and sensitivity of adhesive interactions occurring between lactic acid bacteria and food components and their potential implications on food structuration and food design.

Part of this research initially included reverse engineering methodology aiming to model and predict food matter structuration depending on interactions between food bacteria and milk components. Because modeling and mathematical skills were not available in the LIBio, building a partnership with another lab was envisioned from the start of the project.

As I had already established strong connections with the University of Wisconsin-Madison during my first year of M.Sc., and because my main Ph.D. supervisor had told me about Fulbright scholarships, I primarily searched for collaborations there. Luckily, I had planned long ago to visit some friends in Madison only two months after starting my thesis, for Thanksgiving. I seized this occasion to knock at some doors in the Food, Biochemistry, Microbiology, and Math departments. And, by chance –I met with a young mathematician who was interested in my research. We spent an hour talking about how our paths may cross in the near future, and could potentially result in a partnership.

Back in France, early 2017 I built up a Fulbright project, which eventually earned a Fulbright scholarship that was going to fund me as a Visiting Researcher at the University of Wisconsin-Madison. The duration of Fulbright projects is left for the researcher to choose depending on the needs of his or her project. I had in mind to develop strong modeling skills that could be a real asset to my home lab when coming back –so I decide to go for a long, nine-month stay.

I spent the first year and a half in Nancy, from October 2016 to December 2017, experimenting and teaching, and left for Madison, WI early 2018. Starting up in this new environment, on a new topic, losing my bearings and having not been doing math for five years –beginnings were difficult. We soon realized, as I started, that because the bacteria I was working with were non motile, most theories my supervisor had worked with before would not be of much use –almost everything was therefore to be recreated.

Trying to find quickly a modeling ground common to both of us that would allow for safe foundations to be rebuilt in relation to food and lactic acid bacteria, we jumped from one field to another, trying to get an overview of diverse theories from totally different branches (statistical physics, biochemical engineering, phase-field modeling, etc.) hoping

to converge faster to a shared point of interest. During several months, every week we switched topics, bringing new questions upon the table, while in parallel I was learning to code and we implemented a simple model inspired from phase-field theory that allowed visualizing bacterial distribution changes in matrices going from a liquid to a solid state.

After four months, coming back from our crusades into the wide world of engineering, math, and physics literature, we eventually sat down to think –too little was known about dairy food structuration and the role played by bacteria during phase transitions to build a decent, predictive model of matter structuration, which was our initial goal. I took the decision to stop looking in that direction, and to valorize our findings into a literature review that would point out the existing gaps that prevented us to come up with a predictive model of matter structuration.

I then chose to adopt a different approach: instead of trying to find how to achieve modeling a topic about which little was known, but which was of interest to us, we tried looking at what we know best how to do, and from it draw topics that could be interesting to us. We came up with a topic relating fluid mechanics and microbiology one month before I came back to France for two weeks for my mid-stay activity report and teaching activities. During that month, I gave all I had to come up with a decent proposal that would be supported by more literature research and even some insight on future modeling that was going to be performed. Although this direction led to a whole new field to explore, this time it was easier as my supervisor at the UW-Madison was an expert of the field we chose and we made progress a lot faster.

Coming back to France, I presented both the literature review I intended to finish writing, and the new project we had just started. It took some explanations and look-backs to manage to integrate it into my Ph.D. project, and general orientations of this project were consequently modified. But once started and framed, this new path was easy to follow. In the next three months I spent in Madison, a numerical model was finalized, alongside with bases for an analytical approach that supported numerical results.

As I was close to finish up numerical experiments and to propose a decent theory supporting our views, another difficulty got in the way: my supervisor was going to spend

the next fall semester in New York, at the Flatiron Institute, as part of a sabbatical year. I was either going to come with him or remain alone in Madison to finish the project. There were two months left before the end of my stay, and we were making a lot of progress on the theory which I know would be a lot harder to develop without daily interactions with my supervisor –our frequent exchanges were essential to the project. I chose to come.

I had to convince both the Fulbright Commission and my supervisors back in France that this mobility was necessary to my project, that I could achieve it without more funding, and that I would be hosted at the Flatiron Institute as well. These last two months were rich in events and discoveries. I integrated a team of ten people on biophysical modeling, who all came from different countries and whose insights on my project broadened my perspectives. It was an extremely stimulating environment which undoubtedly benefited both my project and experience.

Coming back to France mid-November 2018, I had two papers in preparation issued from my stay in addition to the literature review that I projected to write. I spent the next couples of months performing experiments that were going to be coupled with the modeling I had done in the U.S., and refining the underlying mathematical theory. Arriving in June, the two papers issued from the collaboration were almost finalized, and I got accepted as a speaker to two international conferences to present them to both microbiologists and mathematicians.

This dissertation, which was written between May and July, is the result of combined experimental and modeling efforts both overseas and in France that led up to six papers, three of them being already published and three being currently reviewed before submission. The two literature reviews papers were reorganized, completed, and gathered both in one part of this dissertation. The four research articles were integrated and combined if needed in the *Results and Discussion* section. The most recent results led to a number of perspectives that could not be all explored in the remaining time of this Ph.D. project, and were detailed in the *Perspectives* section. I hope to achieve them in future work.

Wishing you a good read...

Part I

Literature review

Chapter I.1

Bacterial adhesion and lactic acid bacteria

I.1.1 Bacterial adhesion: generalities

Bacteria use adhesion apparatus in a wide variety of situations including nutrient sensing and monopolization [Nagara et al., 2017, Yu et al., 1987], twitching motility [Persat et al., 2015, Talà et al., 2019], resistance to mechanical stresses [Björnham and Axner, 2009, Persat et al., 2015], and environment colonization through attachment and growth on biotic and abiotic surfaces [An and Friedman, 1998, Katsikogianni and Missirlis, 2004, Kline et al., 2010, O'Connell, 2003, Lebeer et al., 2008, Lebeer et al., 2012, Pizarro-Cerdá and Cossart, 2006, Segers and Lebeer, 2014, Tripathi et al., 2013, Tassell and Miller, 2011, Whittaker et al., 1996]. Bacterial adhesion can be defined as an action characterised by physicochemical and biological phenomena allowing bacteria to unite with a surface [Quirynen and Bollen, 1995]. It depends on environmental factors (temperature, pH, etc.), surface characteristics (appearance, roughness, etc.), the surface free energy of the couple bacteria/substrate, hydrophylic/hydrophobic characteristics of both bacteria and substrate, the surface charge, the ionic strength of the medium, and the presence of specific structures on bacterial surface or substrate [An and Friedman, 1998, Berne et al., 2018] such as represented on Figure I.1.1.

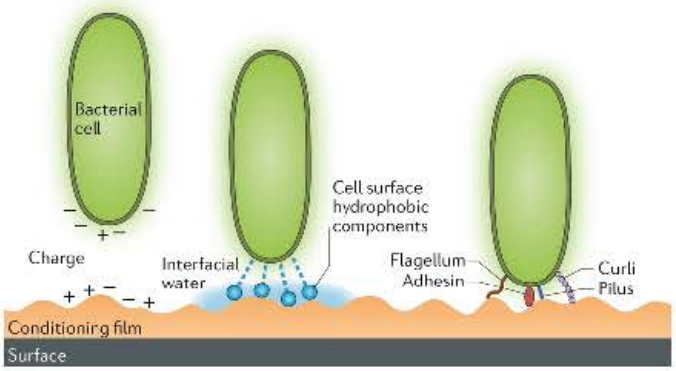

Figure I.1.1: Schematic representation of bacterial-surface first adhesive interactions. These interactions are influenced by both the bacterial and substrate surfaces heterogeneity. The eventual presence of a conditioning film can modify the physicochemical properties of the surface by altering charge, potential and surface tension. At the nanoscale level, the thin layer of interfacial water present on the surface can potentially hinder cell adhesion but may be displaced by cell surface hydrophobic components such as proteins, the polymeric brush layer, and extracellular polysaccharides. Once the bacterium is sufficiently close to the surface, adhesins and bacterial cell appendages such as flagella, pili, and curli can interact with the surface and have direct or indirect roles in adhesion; from Berne et al. [Berne et al., 2018].

Bacterial molecules involved in pathogenic adhesion range from single monomeric proteins, such as adhesins and other surface proteins attached to bacterial cell wall through low-energy binding, to macromolecular complexes such as type III secretion systems and retractile type IV pili [Chagnot et al., 2013, Berne et al., 2018, Desvaux et al., 2018, Desvaux et al., 2006, Jaglic et al., 2014, Pizarro-Cerdá and Cossart, 2006]. In the case of Gram-positive bacteria, bacteria-environment interactions such as bacterial adhesion are generally mediated by sortase-dependent proteins [Comfort and Clubb, 2004, Maresso and Schneewind, 2008], which are anchored through high-energy chemical bonds to the cell wall and possess an LPxTG-like pattern (leucine, proline, X for any amino-acid substitution, threonine, and glycine) at their C-terminal end [Schneewind and Missiakas, 2014b].

Physicochemical adhesive interactions occurring between bacteria and surfaces have been described using different approaches, including thermodynamic approaches [Morra and Cassinelli, 1998] and the Derjaguin–Landau–Verwey–Overbeek (DLVO) theory, which

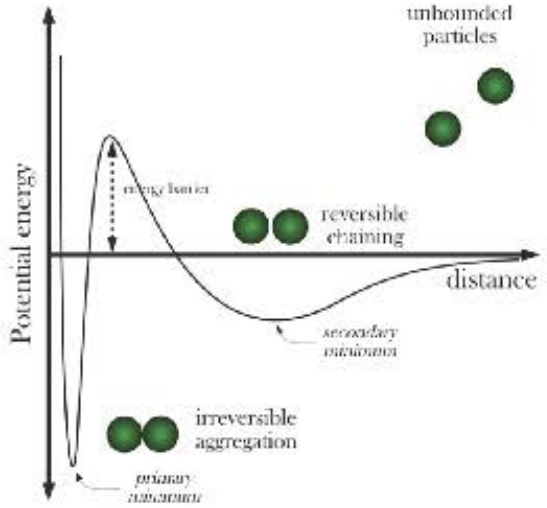

Figure I.1.2: Application of the Derjaguin–Landau–Verwey–Overbeek (DLVO) theory to bacterial adhesion in different states. Potential energy is plotted as a function of distance from the substrate. Both the substrate and the bacterial cell are represented as particles; from Faraudo et al. [Faraudo et al., 2013].

allows predicting the overall state of bacterial adhesion as a function of the free energy involved in the adhesion phenomenon [Alam et al., 2019, Faraudo et al., 2013], as represented in Figure I.1.2. These approaches do not fully comprehend bacterial adhesion [Hermansson, 1999] and therefore the "extended DLVO theory" (XDLVO) was proposed [van Oss, 1989] including acid-base interactions accounting for the hydrophobicity of the surfaces involved [Rosenberg and Doyle, 1990]. However, all these theories are initially meant for soft colloids and fail in taking into account the adaptability and variability of biological systems [Chagnot et al., 2013, Hermansson, 1999, Katsikogianni and Missirlis, 2004] such as morpho- and physiological changes due to different regulatory levels (genes or protein expression).

Both specific and non-specific interactions play an important role in the cell ability to attach to (or to resist detachment from) biomaterial surfaces and have previously been described [An and Friedman, 1998, Berne et al., 2018, Busscher and Weerkamp, 1987, Chagnot et al., 2013, Guerin, 2017, Heilmann et al., 1996, Morra and Cassinelli, 1996, Vaudaux et al., 1990]. First, non-specific and reversible (weak) interactions are

established. Those include van der Waals interactions, which are generally attractive; electrostatic interactions, which are modulated by ionic strength and pH of the liquid environment; hydrophylic/hydrophobic interactions (described by the XDLVO theory); and Lewis acid–base interactions, which are attractive or repulsive depending on the environment, bacterium and surface chemistries [An and Friedman, 1998, Berne et al., 2018, Busscher and Weerkamp, 1987] (Figure I.1.1).

Van der Waals interactions are involved when the bacterium and the substratum are apart but remain fairly close (20-50 nm-distance). They results from electrons interactions. Electrostatic repulsion forces come in to prevent interpenetration of electron clouds [Bos et al., 1999, Marshall et al., 1971, van Loosdrecht et al., 1987] and occur when the surface of the bacterium, commonly negatively-charged in physiologic media due to a higher number of carboxyle and phosphate groups compared to amino groups [Poortinga et al., 2002, van Loosdrecht et al., 1989], comes in contact with the surface of a substrate also negatively charged [Rutter and Vincent, 1984]. They usually involve charged groups such as phosphates, lipopolysaccharides, or carboxyls [Ly et al., 2006] and are considered to be a determining factor controlling bacterial attachment to surfaces [Bellon-Fontaine et al., 1996]. Electrostatic interactions are modulated by environmental factors such as pH, due to its impact on bacterial charge, as presented in Figure I.1.3, and ionic strength. Repulsive energy increases as ionic strength decreases and at very low ionic strength, the energy barrier can become such as impossible to overcome either by swimming or Brownian motion [Marshall et al., 1971, van Loosdrecht et al., 1990], consistently with the DLVO theory [Abu-Lail and Camesano, 2003, Bunt et al., 1995, van Loosdrecht et al., 1989, Zita and Hermansson, 1994]. Below 20 nm, when the bacterium crosses the electrostatic energy barrier, short-distance interactions such as Lewis acid-base or hydrophobic interactions can occur. Lewis acid-base interactions (electron acceptor/donor) enables the formation of hydrogen bonds, which are strong electrostatic interactions.

Then, specific and non-reversible interactions occur [An and Friedman, 1998, Busscher and Weerkamp, 1987]. This second phase of adhesion is achieved through the maturation of some interactions between the bacterial cell and the surface through the repositioning

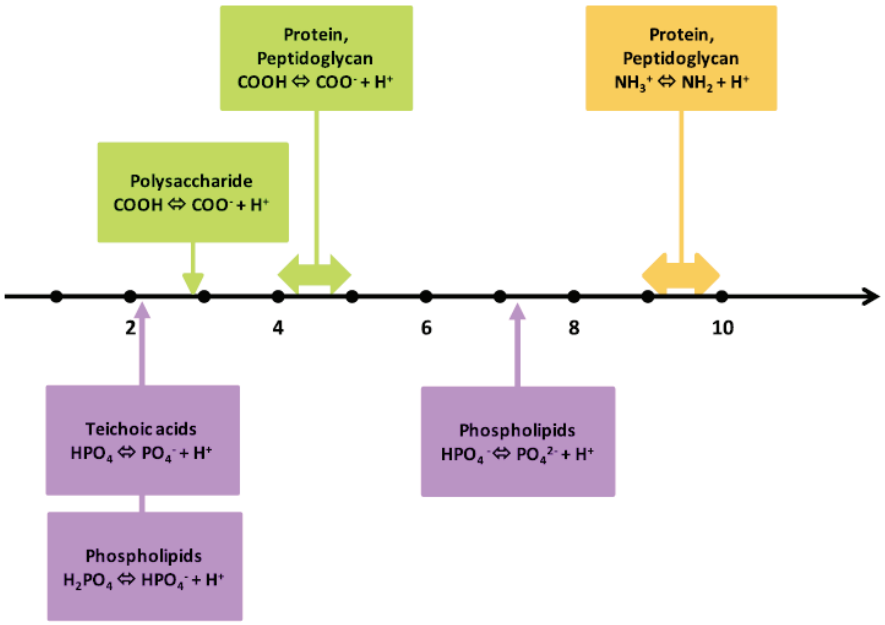

Figure I.1.3: Groups responsible of bacterial surface charges changes depending on pH; from Burgain et al. [Burgain et al., 2014a].

of the cell body and surface structures and by the production of adhesin molecules, which often involves small molecule signalling [Berne et al., 2018]. Other non-protein molecules such as teichoic acids (TA), lipoteichoic acids (LTA), and polysaccharides may also play a role during this phase [Burgain, 2013, Chapot-Chartier and Kulakauskas, 2014, Fischetti, 2019].

Bacterial adhesion can lead to the formation of biofilms, which have been of particular interest in industry [Barnes et al., 2001, Berne et al., 2018, Garrett et al., 2008, Notermans et al., 1991, Pontefract, 1991] and can also mediate host colonization by establishing direct contact with the mucous membrane of various epithelia [Borges et al., 2016b, Conway et al., 1987, Ouwehand et al., 2001, Pizarro-Cerdá and Cossart, 2006, Quinto et al., 2014, Servin and Coconnier, 2003].

Adhesion of pathogens is considered to be a virulence factor as it facilitates host invasion and results in infections [An and Friedman, 1998, Katsikogianni and Missirlis, 2004, Ong et al., 1999, Pizarro-Cerdá and Cossart, 2006, Proft and Baker, 2009, Roszak

and Colwell, 1987, Whittaker et al., 1996]. However, amongst non-pathogenic bacteria such as lactic acid bacteria, adhesion is considered essential in order for the cells to remain functional and therefore provide health benefits to the host, *i.e.* exert a probiotic action [Agrawal, 2005, Borges et al., 2016b, Cousin et al., 2012, Daniel et al., 2006, Ford et al., 2014, Johnson-Henry et al., 2016, Lee and Salminen, 2009, Ouwehand et al., 2001, Pandey et al., 2015, Quinto et al., 2014, Servin and Coconnier, 2003, Tufarelli and Laudadio, 2016].

I.1.2 Lactic acid bacteria

I.1.2.1 Diversity and interest

The interest for lactic acid bacteria (LAB) and foods begins with Pasteur's work on lactic acid fermentation in 1857 and the first isolation of a pure culture, *Bacterium lactis* (now renamed *Lactococcus lactis* subsp. *lactis*) by Leister in 1873. According to Orla-Jensen in 1919, the "true lactic acid bacteria" form a natural group of Gram-positive, non-sporulating rods or cocci that ferment carbohydrates to produce lactic acid as one of their main fermentation products [Axelsson, 2004, Stackebrandt and Teuber, 1988, Stiles and Holzapfel, 1997]. Later, this definition was extended to microorganisms able to ferment various nutrients predominantly into lactic acid [Klaenhammer et al., 2005, Liu, 2003]. General characteristics of LAB are that they are also anaerobic, microaerophilic or facultative aerobic, acid-tolerant [Axelsson, 2004, Klaenhammer et al., 2005], and catalase-negative, although some LAB strains feature a catalase activity mediated by a non-heme "pseudocatalase" [Engesser and Hammes, 1994].

The definition and classification of LAB changed with the introduction of molecular biology and was the focus of intense taxonomic study with approaches involving both phenotypic and phylogenetic characterisation of bacteria [Axelsson, 2004, Pot, 2007]. LAB constitute a heterogeneous group of microorganisms, and the different genera included in the term LAB have been subject to several controversies. Orla-Jensen (1919) initiated a LAB classification based on four main criteria: cellular morphology, mode of glucose fermentation, growth temperature range and carbohydrates utilization patterns. Historically, this classification only included the four genera *Lactobacillus*, *Leuconostoc*,

Pediococcus, and *Streptococcus*, which correspond to the current genera *Carnobacterium*, *Lactobacillus*, *Weissella*, *Leuconostoc*, *Oenococcus*, *Pediococcus*, *Enterococcus*, *Lactococcus*, *Streptococcus*, and *Vagococcus* [Axelsson, 2004, Pot, 2007, Stackebrandt and Teuber, 1988, Stiles and Holzapfel, 1997].

Taxonomic revisions of these genera as well as the description of new genera led to several changes. Among domesticated bacteria widely studied and exploited, LAB are found in two distinct phyla, namely *Firmicutes* and *Actinobacteria*. LAB in the *Actinobacterium* phylum only includes *Atopobium* and *Bifidobacterium* genera (which produce lactic acid but always in combination with acetic acid), with a Guanine-Cytosine (GC) content of 36-46 % and 58-61 %, respectively [de Vos, 2011, Horvath et al., 2009, Makarova et al., 2006]. Within the *Firmicutes* phylum, LAB belong to order *Lactobacillales* and include the genera *Aerococcus*, *Alliococcus*, *Carnobacterium*, *Enterococcus*, *Lactobacillus*, *Lactococcus*, *Leuconostoc*, *Oenococcus*, *Pediococcus*, *Streptococcus*, *Tetragenococcus*, *Vagococcus* and *Weissella* which are all low GC content organisms (31-49 %) [de Vos, 2011, Pot, 2007]. Some minor genera also include *Dolosigranulum* and *Globicatella* [Munoz et al., 2011]. *Lactobacillus* is the main studied genus. Nowadays, phylogenetic relationships among LAB are still a subject of discussion due to their polyphyletic status [Zhang et al., 2011].

LAB are found naturally in a variety of environmental habitats, including plant (fruits, vegetable, cereal), meat and milk environment, and are involved in a large number of industrial and spontaneous food fermentations, notably those based on raw materials derived from these natural habitats. Historically, LAB have been traditionally used and well-known as starter cultures [Carr et al., 2002, Hayek and Ibrahim, 2013, Khalid and others, 2011, Klaenhammer et al., 2005, Pokusaeva et al., 2011, Quinto et al., 2014], which led to their widespread human consumption. Most LAB are Generally Recognized as Safe (GRAS) microorganisms and have numerous applications in foods [Aguirre and Collins, 1993]. Their primary contribution is rapid acid production and acidification of foods, but metabolic processes occurring in parallel to LAB growth also impact flavor, nutrition, and texture quality of a variety of fermented foods [Axelsson, 2004, Klaenham-

mer et al., 2005, Kleerebezem and Hugenholtz, 2003, Pot, 2007]. In addition, LAB have the ability to limit food product deterioration by inhibiting bacterial growth through the production of lactic acid and growth-inhibiting compounds such as acids, H2O2, CO2 and bacteriocins [Cotter et al., 2005]. Some LAB are also closely associated with the mucosal surfaces of animals and human environment, including the gastrointestinal tract, the oral, the respiratory and the vaginal cavities. Moreover, many species of lactic acid bacteria are considered to be important components of the normal intestinal microbiota, which contribute to a variety of functions including intestinal integrity, immunomodulation, and pathogen resistance.

More recently, their probiotic potential has also made them very attractive in the design of functional foods [Klaenhammer et al., 2005, Pot, 2007, Quinto et al., 2014, Stiles and Holzapfel, 1997]. Few LAB feature the European probiotic claim, but some have already obtained it in other countries [Ebner et al., 2014]. In order to benefit human health, LAB most often need to remain both viable and functional *i.e.* able to adhere when reaching the targeted tract, although in some cases even nonviable organisms can induce positive health effects [Ditu et al., 2014]. Strategies to ensure bacterial protection and efficient delivery have therefore been developed, and in this context probiotic food products have drawn increasing interest since the early 2000's, representing already 65 % of the international market of functional foods in 2005 [Agrawal, 2005], valued at approximately USD 40.09 billion in 2017 and estimated to generate revenue of around USD 65.87 billion by end of 2024, with an annual growth rate of more than 7 % (Zion Market Research).

Functional genomics approaches have been used to understand better the response of LAB to their environment and in particular, their adaptaion in artisanal and industrial food fermentations as well as their interactions with the human host in case of probiotic action [Douillard and de Vos, 2014]. These approaches revealed characteristics shared by the group involved in colonization, persistence, interaction and signaling towards to the human host and its health. Within the *Lactobacillus casei* group, the respective LPxTG protein-encoding genes repertoires of *L. rhamnosus*, *L. casei*, and *L. paracasei*

share several similarities such as pili gene clusters [Toh et al., 2013]. A recent review discussed the central role of sortases and LPxTG proteins for LAB, especially for the ones found in the gastrointestinal tract (GIT) [Call and Klaenhammer, 2013].

Mucin adhesion factor	**Species**	**Anchoring type**	**Reference**
Mucus-binding protein (MUBs)	*L. acidophilus*, *L. reuteri*	LPxTG	[Boekhorst et al., 2006, Buck et al., 2005, Etzold et al., 2014, Mackenzie et al., 2010] [Roos and Jonsson, 2002]
Mannose-specific adhesin (Msa)	*L. plantarum*	LPxTG	[Pretzer et al., 2005]
Mucus-binding factor (MBF)	*L. rhamnosus*	LPxTG	[Von Ossowski et al., 2011]
CmbA protein	*L. reuteri*	LPxTG	[Etzold et al., 2014, Jensen et al., 2014]
SpaCBA and SpaFED pili	LGG	LPxTG (fimbriae type)	[Kankainen et al., 2009, Reunanen et al., 2012, Rintahaka et al., 2014, von Ossowski et al., 2010]
Lam29 protein	*L. mucosae*	Membrane	[Watanabe et al., 2010]
MapA protein	*L. reuteri*	Membrane	[Miyoshi et al., 2006]
32-Mmupb protein	*L. fermentum*	Membrane	[Macías-Rodríguez et al., 2009]
Elongation factor Tu (EF-Tu)	*L. johnsonii*, *L. reuteri*, *L. plantarum*	Anchorless	[Dhanani and Bagchi, 2013, Granato et al., 2004, Mukai et al., 2002, Nishiyama et al., 2013]
Glyceraldehyde 3-phosphate dehydrogenase (GAPDH)	*L. acidophilus*, *L. plantarum*	Anchorless	[Kinoshita et al., 2008, Patel et al., 2016]
Chaperon protein GroEL	*L. johnsonii*	Anchorless	[Bergonzelli et al., 2006]

Table I.1.1: Mucin adhesion factors characterised in lactobacilli species; adapted from Nishiyama et al. [Nishiyama et al., 2016].

Numerous papers have been published dealing with probiotic lactic acid bacteria adhesion to the host [Apostolou et al., 2001, Borges et al., 2016b, Conway et al., 1987, Daniel et al., 2006, Klemm and Schembri, 2000, Kline et al., 2009, Lebeer et al., 2012, Lee et al., 2000, Lee and Salminen, 2009, Morelli, 2007, Muñoz-Provencio et al., 2009, Ouwehand et al., 2001, Pizarro-Cerdá and Cossart, 2006, Quinto et al., 2014, Scott and Zäh-

ner, 2006, Servin and Coconnier, 2003, Tassell and Miller, 2011, Van Loosdrecht et al., 1987, Whittaker et al., 1996]. The composition of the bacterial cell wall and, in particular, the presence of some surface appendages such as pili, adhesins, and non-protein molecules including teichoic and lipoteichoic acids, and polysaccharides are essential to the adhesion process of lactic acid bacteria [Berne et al., 2018, Boekhorst et al., 2006, Burgain, 2013, Chagnot et al., 2013, Chapot-Chartier and Kulakauskas, 2014, Danne and Dramsi, 2012, Delcour et al., 1999, Desvaux et al., 2006, Desvaux et al., 2018, Dimitrov et al., 2014, Fischetti, 2019, Granato et al., 1999, Hynönen and Palva, 2013, Katsikogianni and Missirlis, 2004, Klemm and Schembri, 2000, Kline et al., 2009, Le et al., 2013, Lebeer et al., 2010, Mandlik et al., 2008, Meyrand et al., 2013, von Ossowski et al., 2010, Weidenmaier and Peschel, 2008, Welman and Maddox, 2003]. In particular, mucin adhesion factors characterised in lactobacilli species have recently been reviewed (Table I.1.1).

Main cell wall components involved in adhesion amongst lactic acid bacteria and, in particular, present on the model strain *Lactobacillus rhamnosus* GG (LGG) will be detailed in the next section.

I.1.2.2 Description and adhesive role of the bacterial cell wall

The cell wall of lactic acid bacteria is typically composed of a thick peptidoglycan layer in which are inserted proteins, teichoic acids, and polysaccharides, some of which being anchored in the underlying cytoplasmic membrane such as represented in Figure I.1.4. Peptidoglycans and teichoic acids are respectively the first and second major components of the cell wall in terms of dimensions and molecular weight. Teichoic acids are usually made of repeated units of polyglycerol phosphate or polyribitol phosphate, which can be either anchored through high-energy chemical bonds ("covalent") to peptidoglycans (wall teichoic acids, WTAs), or to the cytoplasmic membrane (lipoteichoic acids, LTAs) [Lebeer et al., 2010]. Both are often substituted with glycosyl residues or D-alanyl esters. Cell wall-associated polysaccharides such as capsular polysaccharides (CPS) are often long heteropolysaccharides which feature repeating subunits with different sugar moieties but can also be occasionally homopolysaccharides; they do not have a common core structure.

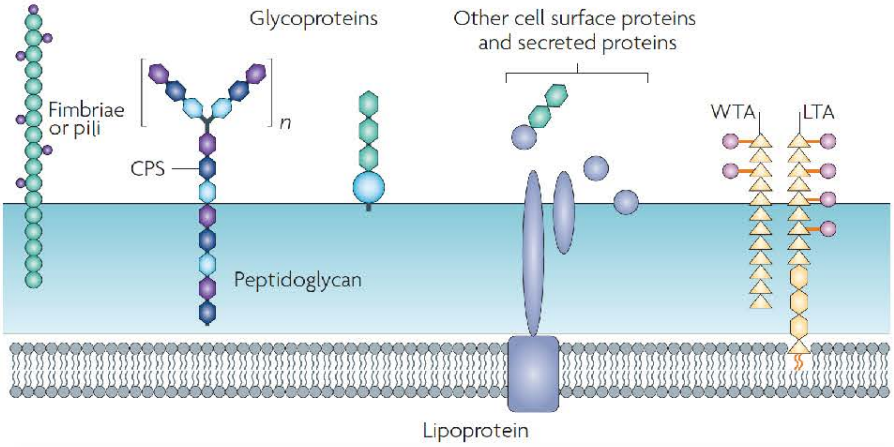

Figure I.1.4: Bacterial cell wall architecture for Gram-positive bacteria, featuring peptidoglycans, teichoic acids (wall teichoic acids: WTAs, and lipoteichoic acids: LTAs), various cell wall-associated polysaccharides such as capsular polysaccharides (CPS) sometimes with repeated subunits, glycoproteins, lipoproteins, secreted proteins, other surface proteins, and proteinaceous appendages that are called fimbriae or pili. From Lebeer et al. [Lebeer et al., 2010].

Additionally, lactic acid bacteria can secrete adhesive proteins, such as the lectin-like moonlighting proteins that bind to sugar residues on host surfaces [Kinoshita et al., 2008]. Some strains also present long surface appendages with adhesive properties, named fimbriae or pili [Kankainen et al., 2009] and a S-layer of rigidly arrayed protein molecules covering the outside of the cell, attached to the cell wall through low-energy bonding [Sleytr and Beveridge, 1999]. WTAs, LTAs, CPS, secreted proteins and proteins of the S-layer, and external appendages may all be involved in adhesive phenomena [Busscher and Weerkamp, 1987].

I.1.2.2.1 Proteins

Proteins are organic compounds that consist of amino acids residues joined by peptide bonds in one or several assembled chains. The subset of proteins interacting with the extracellular environment may be called surfaceome [Desvaux et al., 2018]. In LAB, surface-associated proteins represent roughly 80 % of predicted secreted proteins [Zhou et al., 2010] and most of them are secreted by the universally conserved Sec pathway [Chapot-Chartier and Kulakauskas, 2014] although many other protein secretion systems are

present on LAB such as the TAT system (twin-arginine translocation), the ABC protein exporter, and the FPE (fimbrilin-protein exporter) [Chagnot et al., 2013]. The Sec-machinery mediated secretion is an essential pathway that provides for the transport of most proteins into and accross the plasma membrane and has been best studied in *Escherichia coli* [Schneewind and Missiakas, 2014b]. Details on this secretion system and its modes of action can be found in previous reviews [Chapot-Chartier and Kulakauskas, 2014, Schneewind and Missiakas, 2014b], and other secretion systems presents on LAB have also been thoroughly reviewed [Chagnot et al., 2013]. More generally, information on surface proteins present on Gram-positive bacteria can be found in the recent review by Fischetti [Fischetti, 2019]. It can also be noted that in the field of protein secretion, the description of monoderm bacteria (species exhibiting only one biological membrane) and diderm bacteria (species exhibiting two biological membranes, a cytoplasmic and an outer membrane), such as presented by Chagnot et al., may be more appropriate than the traditional distinction between Gram-negative and Gram-positive terminology which may sometimes presents some ambiguities [Chagnot et al., 2013]. Secreted proteins can be highly bound to the cell surface by sortase-mediated reactions, in which case the protein contains both a Sec-dependent N-terminal signal peptide and a C-terminal cell wall sorting signal, consisting of a LPxTG-like motif, a hydrophobic domain and a positive charged tail [Navarre and Schneewind, 1999]. They can also be poorly bound to the cell surface via (i) transmembrane anchors, (ii) lipids anchors, or (iii) different cell wall binding domains [Chapot-Chartier and Kulakauskas, 2014]. Main proteins present on the surface of LAB that can be involved in adhesion include pili, which are long proteinaceous structures composed of associated proteins subunits called pilins or fimbrins, and monopolypeptides such as MUBS, MucBP, and MBF, some of them being included in supramolecular protein structures such as the S-layer. Other proteins with uncharacterised cell-envelope interacting domains, called "moonlighting proteins", may also act as adhesins towards host components such as plasminogen, fibronectin, laminin, or mucin [Desvaux et al., 2018].

Pili Bacterial pili are defined as filamentous, non-flagellar, proteinaceous, multi-subunit surface appendages involved in adhesion to other bacteria, host cells, or environmental surface [Fronzes et al., 2008, Kline et al., 2009, Kline et al., 2010, Reunanen et al., 2012, Scott and Zähner, 2006]. In Gram-negative bacteria four types of pili have been characterised in detail over the last decades: (i) the type I and type P of *Escherichia coli* (chaperone/usher pathway), (ii) the type III or *Yersinia*, *Shigella*, and *Salmonella* (secretion needle), (iii) the type IV of *Neisseria*, and (iv) curli of *E. coli* and *Salmonella*. The structure, secretion, and roles of these pili have been previously described and will not be detailed here [Danne and Dramsi, 2012, Kline et al., 2010]. In the case of Gram-positive bacteria, pili are usually composed of a single major pilin subunit and one or two accessory subunits, the genes for which are all clustered in genetic loci which contains a sortase gene(s) which encodes the enzyme that catalyses the polymerization of these sortase-assembled pili [Kline et al., 2010]. Pili have been predicted in numerous lactic acid bacteria strains including *L. rhamnosus*, *Lactobacillus casei* and *paracasei*, *Lactococcus lactis*, *Lactobacillus salivarius* [Douillard et al., 2013, Sun et al., 2015], a subset being presented in Appendix A.1. Out of 213 *Lactobacillus* strains a total of 67 pili gene clusters were predicted in 51 bacterial strains, most strains harboring a single pili gene cluster. Only about one-third of the piliated strains possessed pili gene clusters similar to those of the model strain LGG [Sun et al., 2015]. In terms of phylogenetic dispersion, the ecologically diverse *L. casei*/*L. rhamnosus* clade harbored the greatest number of piliated species, whereas other strains such as *Lactobacillus equicursoris*, *Weissella confusa*, and *Lactobacillus parabuchneri* DSM 15352 are the only piliated species within their respective clades [Sun et al., 2015].

LGG pili have first been observed by Lebeer et al. [Lebeer et al., 2009] when characterising the mutant strain EPS-depleted LGG *welE*. A complete genome sequencing performed by Kankainen et al. the same year allowed precising the genes coding for LGG pili [Kankainen et al., 2009]. Two main gene clusters have been evidenced, the first one coding for the SpaFED pilus and the second coding for the SpaCBA pilus, the latter being the only one that was seen expressed in laboratory conditions [Douillard et al.,

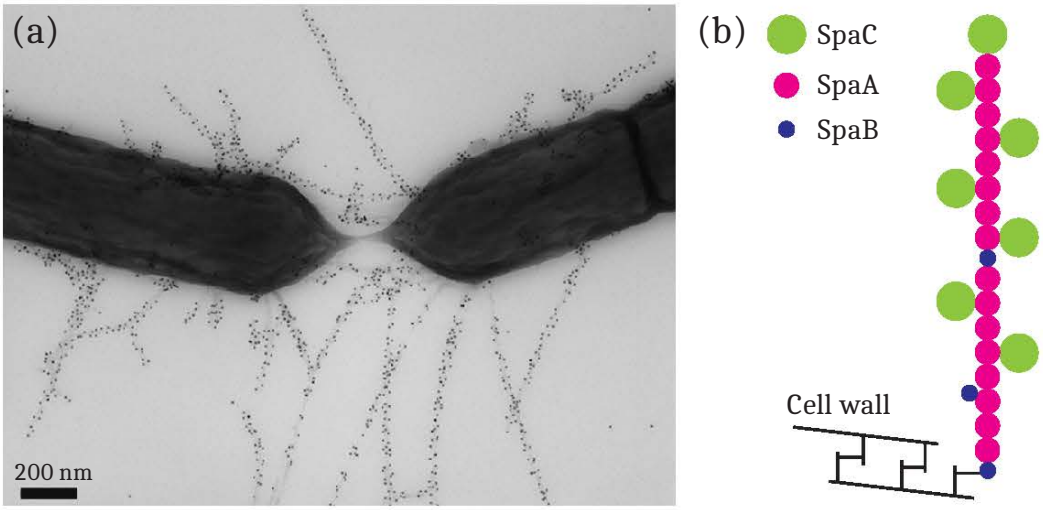

Figure I.1.5: Microscopic observation (a) and structure description (b) of the SpaCBA pilus of *Lactobacillus rhamnosus GG*; (a) has been obtained by transmission electron microscopy (TEM) using antibodies against the subunit SpaA with gold particles of 10 nm [Reunanen et al., 2012]; (b) was adapted from Reunanen et al. [Reunanen et al., 2012].

2013, Reunanen et al., 2012]. LGG was found to remain piliated with SpaCBA pili under different stress conditions such as bile salts and low pH [Douillard et al., 2013]. Comparative genome and functional analysis of *L. rhamnosus* species showed that functional SpaCBA pili are significantly more prevalent in human than in dairy isolates (13 %), and most prevalent in intestinal isolates compared to oral and vaginal isolates [Douillard et al., 2013]. Immunostaining techniques confirmed the presence of about 10 to 50 SpaCBA pili by LGG cell, each measuring approximately 1 μm (Figure I.1.5a). The SpaCBA pilus is constituted of three protein subunits named SpaA, SpaB, and SpaC. The subunit SpaA constitutes the core of the pilus on which SpaB (located preferentially near the pilus basis) and SpaC (all along the subunit SpaA and also at its tip) are anchored (Figure I.1.5b).

The glycosylation of the SpaCBA pilus was also recently evidenced [Tytgat et al., 2016]. Mannose and fucose residues were identified and are likely associated with the SpaC subunits [Tripathi et al., 2013, Tytgat et al., 2016]. Mechanically speaking, LGG

pili are helical-shaped (spring-like) and measure about 1.0 ± 0.3 μm for a diameter of 5 ± 1 nm, with a persistence length of 0.4 nm [Tripathi et al., 2013]. They are mostly concentrated at the tips of a given bacterium and each bacterium features between 10 and 50 pili [Tripathi et al., 2013].

Mucus-binding monopolypeptides Mucus-binding proteins (MUBs) are cell-surface proteins containing a typical signal peptide and a LPxTG anchoring motif in the C-terminal end for high energy attachment to the bacterial cell wall. They are characterised by the presence of multiple Mub repeats [Juge, 2012] and play an important role in bacterial adhesion to mucins under shear flow conditions [Le et al., 2013]. One of the best studied examples of MUBs is from *Lactobacillus reuteri*, which contains two types of amino-acids repeats called Mub1 and Mub2 [MacKenzie et al., 2009, Roos and Jonsson, 2002]. MUBs binding to mucus components is pH-dependent, with maximum binding at pH 4-5 [Juge, 2012]. Rencently, the first 3D-structure of a type 2 Mub repeat (Mub-R5) from *L. reuteri* ATCC 53608 was analyzed and revealed a previously undetected immunoglobulin-binding activity common to the repeat structural unit of MUBs [MacKenzie et al., 2009]. In a biocomputing study screening several bacterial genome database gathering information on more than 260 strains, only nine LAB species were identified to contain at least one MUB domain, and complete MUB domains were found exclusively in LAB [Boekhorst et al., 2006]. The phylogenetic distribution of the Pfam-MucBP domain is much broader than the one of MUB proteins as [Juge, 2012]. For example amongst 25 *L. reuteri* strains, only one featured a predicted MUB protein, whereas all strains exhibited MucBP domains [Mackenzie et al., 2010]. Pfam-MucBP domains are also found in the internalin family of leucin-rich repeat-containing surface proteins from *Listeria monocytogenes* [Bierne et al., 2007]. However, despite the multiple copies of MucBP homologs predicted by genome analysis, only a few have been functionally characterised [Juge, 2012]. Strains on which at least partial MucBP characterisation was performed include *Lactobacillus plantarum* (WCFS1, Lp9, 299 v, Lp6), *Lactococcus lactis* subsp. *cremoris* IBB477 [Radziwill-Bienkowska et al., 2016], and LGG [Juge, 2012, Von Ossowski et al., 2011]. Further research is needed to precise the role and mech-

anisms of action of these predicted proteins *in vivo*. The mucus-binding factor (MBF) is a mucus-specific adhesin predicted from LGG which primary structure and domain organization has been identified and presents several MucBP repeats, but was suggested to be different from the MUB-containing proteins found in other lactobacilli [Von Ossowski et al., 2011]. They are not easily visible on the surface of LGG as they are hidden within the EPS layer of the wild type strain and do participate to adhesive phenomena, although to a less extent than SpaCBA pili [Juge, 2012, Von Ossowski et al., 2011].

The S-layer Mucus-binding proteins may or may not be included in supramolecular structures such as the S-layer, which may also contain other proteins potentially involved in adhesion phenomena. S-layers are planar, monomolecular-thick crystalline lattices produced by the self-assembly of proteinaceous subunits on the surface of both Gram-positive and Gram-negative bacteria [Sleytr and Beveridge, 1999]. Some gram-positive and Gram-negative bacteria can produce two super-imposed S-layers. Because they are ubiquitous, S-layers may have very diverse functions depending on both the organism and environmental conditions. They have, for example, been suggested to act as molecular sieves and as molecule or ion traps in cell adhesion or surface recognition, and are known to mediate cell adhesion for some pathogens such as *Clostridium difficile* and *Bacillus cereus* [Sleytr and Beveridge, 1999].

I.1.2.2.2 Cell wall-associated polysaccharides

Cell wall-associated polysaccharides may be either anchored to the cell membrane as O-antigen lipopolysaccharides (LPS), linked to the cell wall through high-energy bonding as capsular polysaccharides (CPS), or released in the environment as exopolysaccharides (EPS) which can however readsorb onto the bacterial surface. EPS biosynthesis is common amongst lactic acid bacteria and present similarities between some species of streptococci, lactobacilli, and lactococci [Jolly and Stingele, 2001] although *eps* loci may vary a lot between LAB species. EPS may protect the cell from desiccation and other environmental stresses, and facilitate adherence of bacteria to solid surfaces [Badel et al., 2011, Jolly and Stingele, 2001, Dimitrov et al., 2014]. They have also been increasingly

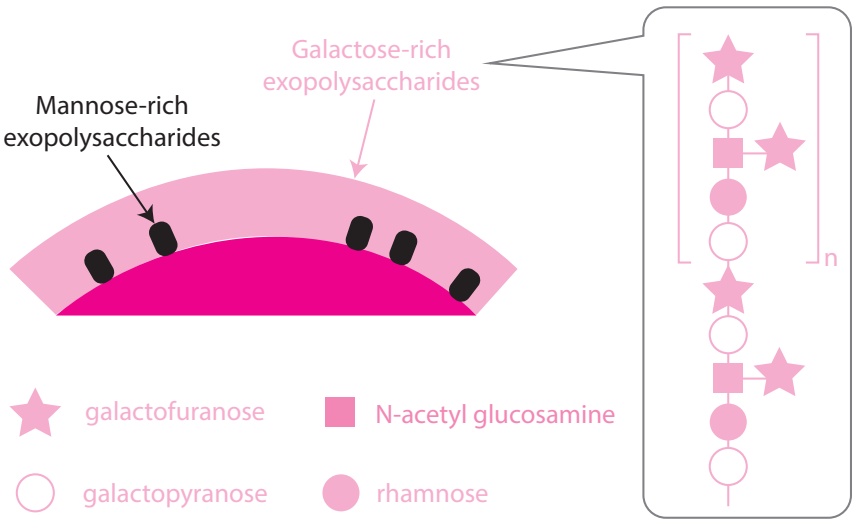

Figure I.1.6: Exopolysaccharides (EPS) present at the surface of *Lactobacillus rhamnosus* GG (LGG) and structure of galactose-rich EPS; adapted from Guerin et al., 2017 [Guerin, 2017].

used in the past fifteen years in food industry for their thickening and health-related properties [Badel et al., 2011, Bajpai et al., 2015, Lebeer et al., 2009, Ruas-Madiedo et al., 2002, Welman and Maddox, 2003]. On the model strain LGG, two main types of EPS have been identified: galactose-rich and mannose-rich EPS [Francius et al., 2009], such as represented on Figure I.1.6. Galactose-rich EPS are the ones that are both the longest and the most present on LGG and constitute a dense, homogeneous layer [Guerin, 2017]. Mannose-rich EPS are shorter and have been less studied. Both have been identified to play a role in reducing adhesion of the LGG "wild type" (WT) strain compared to mutant strains EPS-depleted [Guerin et al., 2016, Guerin et al., 2018a, Lebeer et al., 2009]. Indeed, the mutant impaired in EPS synthesis showed increased mucin adherence and biofilm capacity [Lebeer et al., 2009]. Enhanced adherence of this mutant onto milk components was also later demonstrated [Guerin et al., 2016, Guerin et al., 2018a]. The thickness of the galactose-rich EPS layer has also been identified to increase with decreasing pH, which can impact the adhesive abilities of other adhesive components embedded within this layer such as pili [Burgain et al., 2015].

I.1.2.2.3 Teichoic acids

Teichoic acids and in particular LTA are known to mediate microorganism-associated molecular pattern (MAMP)-pattern recognition receptor (PRR) interactions, such as adhesive interactions [Granato et al., 2010, Grangette et al., 2005, Lebeer et al., 2010]. Lipoteichoic acids were shown to be involved notably in adhesion of *Lactobacillus johnsonii* La1 to Caco-2 cells [Granato et al., 1999]. They are anionic, cell surface glycopolymers containing phosphodiester-linked polyol repeat units [Brown et al., 2013]. The structure, biosynthesis, and biological roles of WTA and LTA in Gram-positive bacteria have been previously described in comprehensive reviews [Brown et al., 2013,Schneewind and Missiakas, 2014a, Reichmann and Gründling, 2011, Weidenmaier and Peschel, 2008]. LTA are widely present in LAB and are found in enterococci, lactobacilli, lactococci, leuconostoc, and streptococci [Fischer, 1994].

I.1.3 Adhesive interactions with food components

I.1.3.1 Generalities

In addition to be able to adhere to the host, LAB have been shown to be able to adhere to food components, especially to meat [Firstenberg-Eden, 1981,Piette and Idziak, 1989], some cereals [Chumphon et al., 2016], and more recently to dairy components [Burgain et al., 2014a, Gomand et al., 2019b, Gomand et al., 2018, Guerin et al., 2016]. Some of these interactions have been shown to be mediated by pili, in particular when in relation to β-lactoglobulin [Guerin et al., 2016]. Several reviews have highlighted the need of further research on the important role played by these interactions on preserving probiotic action and achieving efficient probiotic delivery [Hickey et al., 2015b, Mortazavian et al., 2012, Ranadheera et al., 2010, Sanders and Marco, 2010].

Encapsulating probiotic bacteria using components to which they feature adhesive affinities may indeed result in a higher resistance to gastric digestion [Burgain et al., 2013a, Burgain et al., 2014b, Guerin et al., 2017a], thus improving probiotic protection. However, bacterial adhesion to food components was also suggested to be able to compete

with bacterial adhesion to the host in a study involving TC7 Caco-2 cell lines, *Lactobacillus rhamnosus* GG, and milk fat globule membrane [Guerin et al., 2018b] as well as in a review mentioning the anti-adhesive power of various food components regarding bacterial adhesion to different kinds of epithelial cell lines [Sun and Wu, 2017]. Therefore food components such as milk fat globule membrane [Douëllou et al., 2017, Guerin et al., 2018a], milk proteins [Halpin et al., 2008], and milk oligosaccharides [Lane et al., 2012] may play an anti-adhesive role by decreasing bacterial adhesion to the intestine [Guerin et al., 2018b]. Some food additives including stabilizers (such as sucrose fatty acid esters) and colors (gardenia yellow, monascus pigment, etc.), as well as some phenolic compounds and plant-derived polysaccharides and peptides have also been found to feature similar effects [Islam et al., 2014, Signoretto et al., 2012, Sun and Wu, 2017].

In food matrices, adhesive interactions are also likely to play an important part in bacterial spatial distribution and viability during the structuration of the food matrix [Gomand et al., 2019a, Guerin et al., 2017b, Laloy et al., 1996], as well as on food texture and flavor [Laloy et al., 1996, Lopez et al., 2006, Tarazanova et al., 2018a]. Indeed, adhesive interactions between genetically engineered *Lactococcus lactis* producing pili and dairy components result in texture alteration in fermented milk [Tarazanova et al., 2018a] and can modulate this strain distribution in cheese curd [Tarazanova et al., 2018b]. Similarly, during curdling and cheese ripening, bacterial cells mostly co-localize with fat globules or at the casein-fat interface, which suggest adhesive interactions between fat and LAB strains [Laloy et al., 1996, Lopez et al., 2006] which may favor fat degradation [Hickey et al., 2015a]. This is likely to play a role in lipolysis thus affecting the development of characteristic flavors and textures during ripening [Laloy et al., 1996, Lopez et al., 2006] but also to help with bacteria survival [Gomes et al., 1998, Jeanson et al., 2011]. For example, dairy matrices have been found to be able to better preserve bacterial viability during food structuration compared to non-dairy matrices [Mortazavian et al., 2012, Sanders and Marco, 2010].

The structure of the main dairy components to which LGG has been shown to adhere, as well as the nature of bacterial-food interactions, will be detailed in the next subsections.

I.1.3.2 Dairy components: structure and properties

I.1.3.2.1 Proteins

The protein composition of skimmed cow milk is represented in Table I.1.2. Main protein elements will be detailed in following sections.

		Concentration in milk (g/L)	**Molecular mass (kDa)**
Caseins	Casein α_{s1}	12-15	22.1-23.7
	Casein α_{s2}	3-4	25.2-25.4
	Casein β	9-11	23.9-24.1
	Casein κ	2-4	19.0
	TOTAL	26-34	N/A
Whey Proteins	β-lactoglobulin	2-4	18.3
	α-lactalbumin	1-1.5	14.2
	bovine serum albumin (BSA)	0.1-0.4	66.3
	Immunoglobulins (Ig)	0.6-1.0	146.0-1,030.0
	Lactoferrine (Lf)	0.1	80.0
	TOTAL	3.8-7	N/A

Table I.1.2: Protein composition of skimmed cow milk; N/A means "non applicable"; adapted from Fox and MacSweeney [McSweeney and O'Mahony, 2016], from Livney [Livney, 2010].

Caseins Caseins constitute the main protein fraction of milk and include α-caseins (α_{s1} and α_{s2}), β-caseins, and κ-caseins (Table I.1.2). Native caseins are organized in spherical superstructures called micelles and are able to precipitate at pH = 4.6 [McSweeney and O'Mahony, 2016]. The mean casein micelles diameter is 150 nm. The exact structure of casein micelles has been subjected to countless controversies and is still not established. Numerous models have been proposed and refined over the years [Bouchoux et al., 2010, Dalgleish, 2011, De Kruif et al., 2012, Holt, 1992, Horne, 1998, McMahon and Oommen, 2008, Schmidt, 1982, Walstra, 1990] as presented in Figure I.1.7. At first, organization in submicelles was hypothesized [Schmidt, 1982, Walstra, 1990], where submicelles would be connected to one another thanks to colloidal calcium phosphate bonds. Core submicelles would be composed of α- and β-submicelles and submicelles at the boundaries would be composed of α- and κ-caseins. (Fig. I.1.7a,b). Later models include micelles were caseins

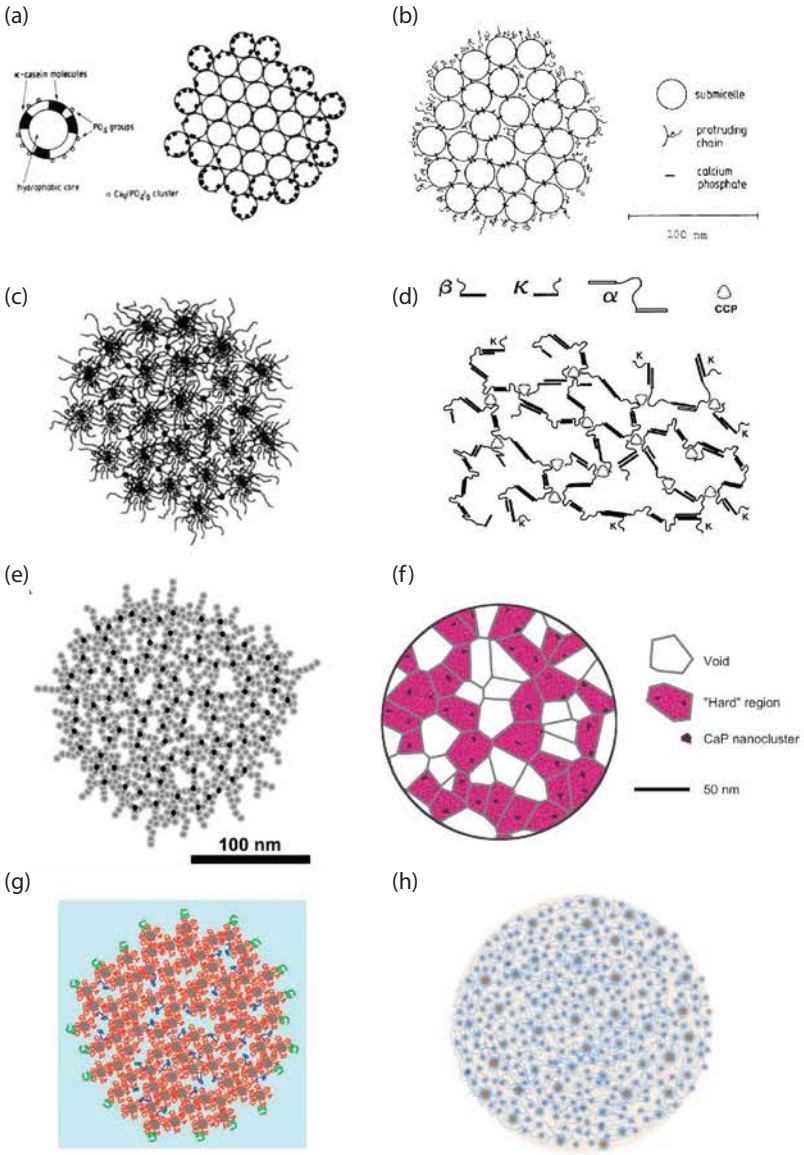

Figure I.1.7: Evolution of casein micelles models from 1982 to 2012; models are successively proposed by : (a) [Schmidt, 1982]; (b) [Walstra, 1990]; (c) [Holt, 1992]; (d) [Horne, 1998]; (e) [McMahon and Oommen, 2008]; (f) [Bouchoux et al., 2010]; (g) [Dalgleish, 2011]; (h) [De Kruif et al., 2012]. Adapted from Guerin et al. [Guerin, 2017].

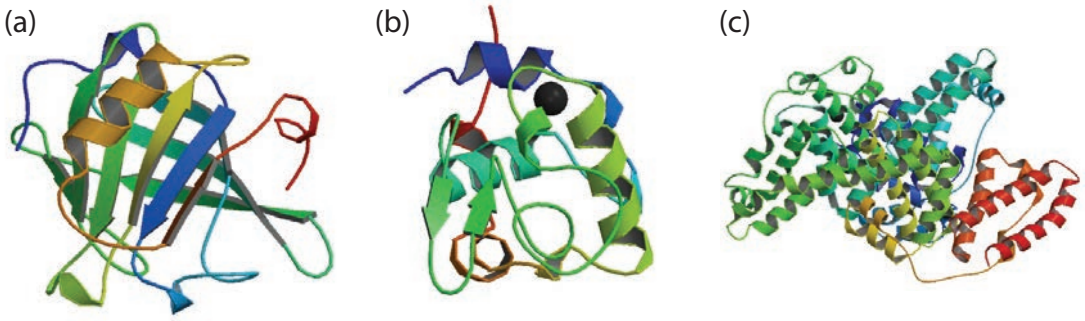

Figure I.1.8: Structure of the main whey proteins: (a) bovine β-lactoglobulin (RCSB PDB code 1BEB) [Brownlow et al., 1997]; (b) bovine α-lactalbumin (RCSB PDB code 1ALC) [Pike et al., 1996]; (c) bovine serum albumin (BSA; RCSB PDB code 3V03) [Majorek et al., 2012].

chains are fully unfolded and hydrated [Holt, 1992], with calcium phosphate nanoclusters (Fig. I.1.7c), porous structures where calcium phosphate nanoclusters interact with one another through hydrophobic interactions [Horne, 1998] (Fig. I.1.7d), and sponge structures with high protein regions and voids [Bouchoux et al., 2010, McMahon and Oommen, 2008] (Fig. I.1.7e,f). The latest models [Dalgleish, 2011, De Kruif et al., 2012] consist in core micelles constituted of water-filled canals, stabilized by interactions between β-caseins and hydrophobic nanoclusters (Fig. I.1.7g,h). Despite controversies, it has been established that micelles surface is mainly constituted of κ-caseins which feature a hydrophilic C-terminal end, negatively charged, and which allows for steric and electrostatic stability of casein micelles in fresh milk.

Whey proteins Whey proteins (WP), also called soluble proteins, represent 20 % of total milk proteins *i.e.* 5 to 6 g/L of milk. WP include β-lactoglobulin, α-lactalbumin, bovine serum albumin (BSA), immunoglobulins (Ig), and lactoferrine (Lf) as presented in Table I.1.2. All these proteins are soluble at the casein isoelectric point (pH = 4.6).

β-lactoglobulin is the main whey protein (Table I.1.2). It is constituted of 162 amino-acids residues and weighs 18.3 kDa with an isoelectric point of 5.2 [Tavares et al., 2014]. Its secondary structure includes eight antiparallel β sheets which form a hydrophobic pocket called calyx (allowing β-lactoglobulin to act as a molecule carrier) and three α

helices [Brownlow et al., 1997, Monaco et al., 1987], such as represented in Figure I.1.8a, as well as two disulfide bonds and three free thiols groups [Livney, 2010]. This protein is able to bind various hydrophilic and hydrophobic molecules such as retinol, cholesterol, fatty acids, D3 vitamin, mucin, and lactose [Domínguez-Ramírez et al., 2013, Kontopidis et al., 2002, Kontopidis et al., 2004]. Milk at native pH (6.7) usually features dimers of β-lactoglobulin.

α-lactalbumin is the second main whey protein (Table I.1.2). This small metalloprotein is constituted of 123 amino-acids residues and weighs 14.2 kDa with a isoelectric point between 4.3 and 4.7 [Tavares et al., 2014]. Its structure includes four disulfide bonds [Edwards et al., 2008] and is very close to the lysozyme's (Figure I.1.8b).

Bovine serum albumin (BSA) represents less than 5 % of whey proteins. It is a larger protein constituted of 582 amino-acids residues which weighs 66.3 kDa with an isoelectric point of 5.0 [Tavares et al., 2014]. BSA features numerous disulfide bonds (17 total) and one free thiol group [Edwards et al., 2008]. Its structure is represented in Figure I.1.8c.

Whey Protein Isolate (WPI) is a commercial powder with a high protein content obtained from the lactoserum phase of cheese manufacturing during the curd gelation process. It contains all proteins mentioned above. It is usually manufactured by either ion exchange chromatography or microfiltration, followed by spray-drying [Smithers et al., 1996]. Main process parameters impacting WPI structure are extrusion/spray-drying temperature, moisture content, and pH [De Souza Lima et al., 2018, Gao et al., 2019, Qi and Onwulata, 2011b, Qi and Onwulata, 2011a].

I.1.3.2.2 Milk fat globule membrane

Native milk fat globules are constituted of a triglycerides-rich core stabilized by three phospholipid layers constituting the milk fat globule membrane (MFGM), represented in Figure I.1.9. The MFGM is constituted of phospholipids, sphingolipids, and membrane-specific proteins (mostly glycoproteins). MFGM composition depends on the cow's age, milk quality, milking stage, season, but also on the chosen method for extraction and purification [Evers, 2004]. The lipid fraction is essentially constituted of polar lipids (26-40%) such as phospholipids [Fong et al., 2007]. Polar lipids are minor am-

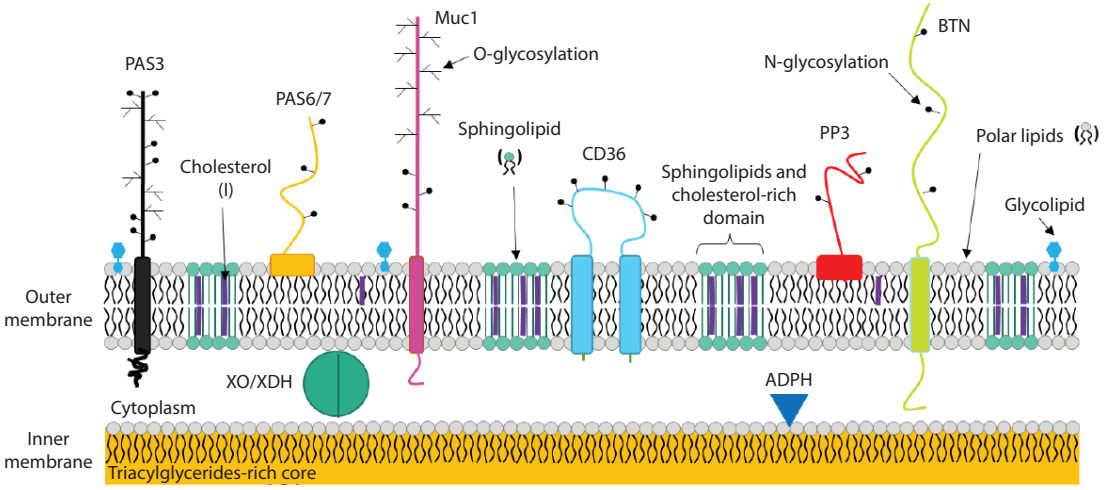

Figure I.1.9: Native milk fat globule membrane composition; adapted from Guerin et al. [Guerin, 2017].

phiphilic components constituted of a hydrophobic tail combined with a hydrophilic head group. Major polar lipids found in mammal species are phosphatidylethanolamine (PE), phosphatidylcholine (PC), phosphatidylserine (PS), phosphatidylinositol (PI), lysophosphatidylcholine (LPC), and sphingomyelin (SM) [Dewettinck et al., 2008, Fong et al., 2007,Guerin et al., 2017b]. The protein fraction stand for 25 to 70% of the MFGM [Elias-Argote et al., 2013, Riccio, 2004]. Main MFGM proteins include the mucin MUC1, the redox enzyme xhantine deshydrogenase/oxidase (XDH/XO), butyrophilin (BTN), cluster of differentiation (CD36), periodic acid schiff 6/7 (PAS 6/7), periodic acid schiff III (PAS III), adipophilin (ADPH), and fatty-acid binding proteins (FABP), all of which are glycosylated except the latter two [Dewettinck et al., 2008, Guerin et al., 2017b, Mather, 2000,Le et al., 2009]. The MFGM can be isolated from raw milk, buttermilk, butterserum, or lactoserum [Holzmüller and Kulozik, 2016, Le et al., 2009, Sachdeva and Buchheim, 1997]. In laboratory MFGM extraction involves (i) fat globules separation, (ii) cream washing, (iii) MFGM release from fat globules, and (iv) MFGM collection [Dewettinck et al., 2008,Guerin et al., 2017b]. Up to 70% of the peripheral MFGM membrane proteins can be collected [Holzmüller and Kulozik, 2016,Holzmüller et al., 2016]. Coagulation and microfiltration may also impact phospholipids collection [Sachdeva and Buchheim, 1997].

I.2

Food matrix impact on bacterial viability and functionality

I.2.1 Context and evaluation methods

I.2.1.1 Generalities

Food matrix structure and composition, as well as food manufacturing, storage, and digestion conditions, play an important role in enhancing or lowering the adhesive abilities, viability, and health effects of LAB strains [Ranadheera et al., 2010, Sanders et al., 2014]. Several reviews have recently pointed out the need for further research on the comparative impact of different food matrices on LAB viability and functionality [Ranadheera et al., 2010, Sanders et al., 2014, Sanders and Marco, 2010]. This review aims to meet this need by performing a meta-comparison of all studies that compare the efficiency of different food matrices in sustaining LAB viability in order to draw conclusions regarding food structure and composition (Tables I.2.1, I.2.2, and I.2.3). The food matrix impact on LAB delivery can be studied at three main times: during food manufacturing, food storage, and digestion (Figure I.2.1). For clarity, each of these aspects is detailed separately in this review.

In addition to LAB, bacteria studied within this article also include bifidobacteria,

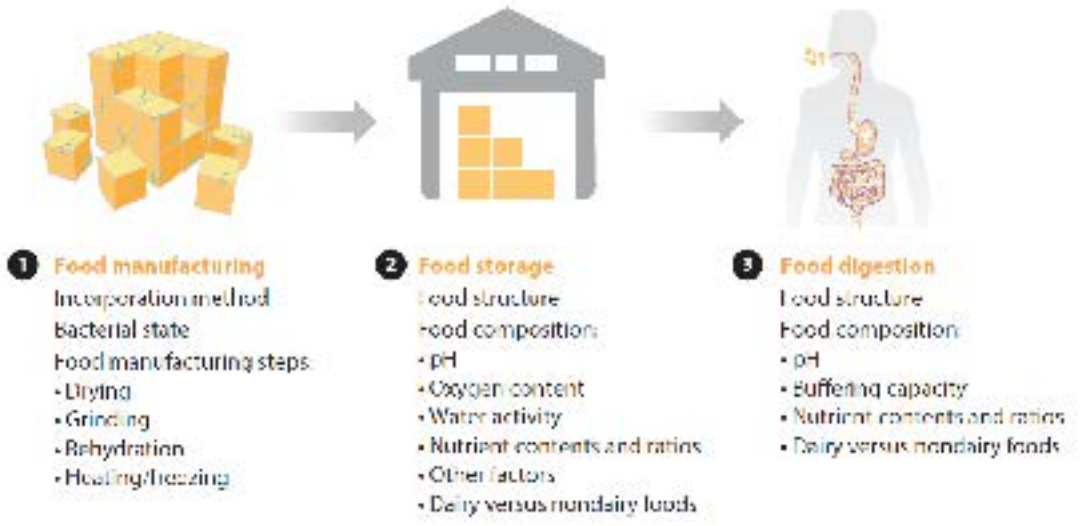

Figure I.2.1: Food matrix impact on lactic acid bacteria protection, carrying and delivery through food manufacturing (incorporation method, bacterial state, drying, grinding, rehydration, heating/freezing), food storage (food structure, pH, oxygen content, water activity, nutrient contents and ratios) and digestion (food structure, pH, buffering capacity, nutrient contents and ratios). A distinction is made between dairy and nondairy foods.

which have common metabolism and structural characteristics with LAB [Cronin et al., 2011,Khalid and others, 2011]. Although the distinction between LAB and bifidobacteria has been acknowledged [Sonomoto and Yokota, 2011], some authors still use a broader definition of LAB that includes bifidobacteria. This confusion is common and accepted when dealing with probiotic strains [Hickey et al., 2015b]. Other food bacteria, such as *Propionibacterium*, that present an interest for human health may also be included in the present study.

I.2.1.2 Methods to evaluate lactic acid bacteria viability

The ability of LAB to survive in a given matrix (*i.e.*, their viability) varies with many conditions, including the strain(s) considered, the delivery matrix, manufacturing steps, and storage conditions. The three most critical steps impacting the delivery of viable and functional LAB to the host are food matrix manufacturing, storage, and digestion [Champagne et al., 2005,Mortazavian et al., 2012]. Although not part of the scope of this review

because of its occurrence prior to the introduction of bacteria in food products, bacteria stabilization also plays an important role in preserving the viability and functionality of LAB and must be considered carefully before engaging in the food design process [Champagne et al., 2005, Mortazavian et al., 2012]. In most cases, LAB viability is assessed through bacterial enumeration. Samples are collected from the media at different times and are inoculated on specific growth media; colony counts are then performed. This approach can be completed by other techniques, such as confocal laser scanning microscopy associated with rapid epifluorescence staining, which allows metabolically active bacteria to be set apart from bacteria featuring a damaged membrane [Boulos et al., 1999]. This method uses two nucleic acid-binding stains: SYTO 9, which penetrates all bacterial membranes and stains cells in green, and propidium iodide, which only penetrates cells with damaged membranes; the combination of the two stains produces redfluorescing cells [Boulos et al., 1999]. This method is mostly used for qualitative purposes.

Bacterial enumeration can also be performed on feces when monitoring the impact of the delivery format on probiotic viability through fecal recovery after digestion [Sanders et al., 2014]; the higher the recovered fecal quantity of LAB, the more bacteria have survived and possibly multiplied in the GIT.The impact of digestion is mostly analyzed in vitro; animal and clinical tests are only performed when looking for a specific health effect [Isolauri et al., 1991]. In vitro digestion assays include the use of saliva, gastric, and/or intestinal juices; the gastric step is the most commonly simulated, using a range of pH from 2 to 4. Some studies feature dynamic GIT models [Bove et al., 2013, Klindt-Toldam et al., 2016], but these models remain rarely used for LAB foods. Recently, a standard static digestion procedure has been internationally accepted [Minekus et al., 2014], although later reviews request more standardization [Singh et al., 2015].

I.2.1.3 Methods to evaluate lactic acid bacteria functionality

Bacterial functionality, although crucial to probiotic action, is less often assessed than bacterial viability because a lot more complex. Clinical studies can provide a general, comprehensive assessment of both LAB viability and functionality as but only as indirect

causes of resulting health effects, as presented in this review, and are extremely long and costly procedures.

Biophysical methods are traditionally used to evaluate the adhesive properties of bacteria, such as atomic force microscopy (AFM) and single-cell force spectroscopy [Beaussart et al., 2013, Burgain et al., 2013b, Burgain et al., 2014b, Deutsch et al., 2012, Guerin et al., 2016, Sullan et al., 2013, Tripathi et al., 2012, Tripathi et al., 2013], and cell cultures [Deutsch et al., 2012, Dimitrov et al., 2014, Lee et al., 2000, Servin and Coconnier, 2003]. These methods have been designed to evaluate the behavior of a few strains of interest in a restricted range of conditions corresponding to their future use.

Other approaches to study bacterial adhesion to biopolymers include bacterial radiolabeling [Douillard et al., 2013, Kankainen et al., 2009], fluorescent or Fluorescein Isothiocyanate (FITC) labeling [Avadhanula et al., 2006, Shimaoka et al., 2001], and spectrophotometric assays on 96-well microtiter plates [Patton et al., 2006, Rosendale et al., 2008].

A recent high-throughput method was recently developed for testing interactions between a wide range of food proteins and a few pathogen strains involving microarray platform development [Utratna et al., 2017]. However this method is not applicable to screen a large number of strains as it involves fluorescent staining, which would be tedious work as it has to be done individually on each tested strain [Utratna et al., 2017].

Most of these methods are time-consuming and therefore cannot be applied to screen a large number of strains as they have not been intended for this purpose. They can be difficult to implement and require many steps. High-throughput methods are therefore needed to estimate quickly bacterial adhesion preferences for components of interest for a wide range of strains. To our best knowledge, no study was published that would describe a high-throughput screening method specifically designed to study bacteria-molecule adhesion amongst all possible interactions. Perspectives will be provided to guide future research in this direction (Section I.2.6), that led to the development of the high-throughput screening method described in Chapter IV.1.1.

I.2.2 Impact of food manufacturing processes

LAB can be grown in either the food matrix or an intermediary industrial medium from which they are harvested [Makinen et al., 2012]. They are then added to food products as frozen, dried, encapsulated dried, or liquid cultures. Many studies have been published on drying and encapsulation techniques [Burgain et al., 2011, D'Orazio et al., 2015, Guergoletto et al., 2012, Haffner et al., 2016, Iaconelli et al., 2015, Makinen et al., 2012, Meng et al., 2008, Muller et al., 2010]. The comparative efficiency of these methods is not discussed here. Instead, we focus on the methods used to incorporate LAB into foods as well as the influence of the bacterial state (*i.e.*, dried, frozen, etc.). The impact of food manufacturing steps, such as drying and grinding, on viability is also detailed. Comparative studies mentioned in this paragraph appear in Table I.2.1.

I.2.2.1 Impact of the method used to incorporate probiotics in foods

Food Category	Food Structure	Compared Food Products	Strains	Critical step	Effects on strain viability[1]	Reference
Dairy	Solid, Liquid	Acidified milk, Yogurt: liquid, low fat versus set, full fat	*Bifidobacterium bifidum*, *Lactobacillus acidophilus*, *Lactobacillus delbrueckii* subsp. *bulgaricus*	Incorporation method	Direct Inoculation > Indirect	Vinderola et al., 2000a
	Solid	Ice cream: full versus low fat, full versus low sugar, full versus low oxygen	*Lactobacillus johnsonii, Lactobacillus rhamnosus*	Incorporation method, freezing step	Low fat/sugar contents increase the detrimental effect of freezing	Alamprese et al., 2002, 2005
			B. bifidum, Bifidobacterium longum, L. acidophilus, Lactobacillus casei	Freezing step	Freezing and oxygen incorporated during manufacturing decrease viability	Homayouni, 2008
Nondairy	Powder	Fruits (strawberry, pomegranate, blackcurrant, cranberry): dried versus rehydrated	*Lactobacillus plantarum*	Rehydration step	Strawberry > blackcurrant > pomegranate > cranberry; high water activity and low pH decrease viability upon reconstitution	Nualkaekul et al. 2012
	Solid, Liquid	Pineapple–grape versus mandarin juice, Apple impregnated with mandarin juice (dried, rehydrated)	*L. acidophilus, Lactobacillus salivarius* subsp. *salivarius*	Incorporation method, drying/ rehydration steps	Viability loss was minimal during impregnation with mandarin juice and rehydration	Betoret et al., 2012

[1] A > B means that A is more efficient than B.

	Liquid	Oils (flaxseed, canola, extra-virgin, olive pomace)	*L. rhamnosus*	Bacterial state, heating step	Freeze-dried > cultured cells	Endo et al., 2014
Dairy versus Nondairy	Solid	Apple impregnated with milk versus with apple juice (sole, dried, rehydrated)	*L. rhamnosus*	Incorporation method, drying/ rehydration steps	Milk > apple juice as impregnation media and during rehydration	Betoret et al., 2003
	Powder	Fruits (apple, strawberry, banana) with/without skim milk powder	*L. plantarum*	Incorporation method, drying/grinding steps	Milk > buffer against mechanical stress; strawberry and banana > apple during drying and grinding; separate drying of fruit and LAB > drying of fruits infused with LAB	Borges et al., 2016a
	Solid, liquid, emulsion, mix	Sandwich (including tomato and ham), sushi, burger, oil, tamarin vinaigrette, mayonnaise, fruit versus ice cream–based smoothie, butter	*Bifidobacterium animalis* subsp. *lactis, L. acidophilus*	Bacterial state, heating step	Freeze-dried > frozen cells (higher inocula); high matrix temperatures during manufacturing kill LAB	Rodgers, 2007

Table I.2.1: Food matrix impact on lactic acid bacteria (LAB) viability during food manufacturing.

LAB can be incorporated into foods using various techniques such as dry-mixing [Makinen et al., 2012], direct inoculation in beverages and mixes [Alamprese et al., 2002, Alamprese et al., 2005, Céspedes et al., 2013, Champagne and Gardner, 2008, Lupien-Meilleur et al., 2016], and immersion and vacuum impregnation [Alegre et al., 2011, Betoret et al., 2003, Betoret et al., 2012, Rößle et al., 2010, Russo et al., 2014, Russo et al., 2015]. The compared efficiency of these different methods is described in Table I.2.1. Direct inoculation is found to be more effective than indirect inoculation [Vinderola

et al., 2000a]. Borges et al. (2016a) show that a higher LAB survival is achieved by separately drying fruits and LAB before mixing them together. Two studies described the impregnation medium impact [Betoret et al., 2003, Borges et al., 2016a] but led to contradictory results and therefore cannot be conclusive. Betoret et al. (2003) found that whole milk is a more effective medium than fruit juices, whereas Borges et al. (2016a) assessed no viability difference when comparing skim milk to a buffer. Important properties of the impregnation medium include its pH and viscosity, which latter should allow diffusion of the medium inside the pores or in intercellular spaces during rehydration [Martinez-Monzo et al., 1998].

I.2.2.2 Impact of the bacterial state

Rodgers (2007) showed that freeze-dried cells resulted in higher initial viable populations upon inoculation in a variety of different foods compared to frozen cells [Rodgers, 2007]. Freeze-dried cells of *Lactobacillus rhamnosus* GG also showed better survival than cultured cells in oils during storage [Endo et al., 2014]. According to Iaconelli et al. (2015), freeze-drying also gives the best results for cultivability, residual enzymatic activity, and cell integrity compared to spray-drying (second-best technique) and air-drying [Iaconelli et al., 2015]. Freeze-drying seems therefore the best option for incorporating LAB into foods.

I.2.2.3 Impact of food manufacturing steps

Food manufacturing processes and steps are very diverse. In this section, we discuss the impact of general manufacturing steps such as drying, grinding, rehydration, heating, and freezing on the efficiency of final food products as LAB carriers. These findings may easily translate into specific manufacturing steps, food products, and LAB strains.

I.2.2.3.1 Drying

Techniques such as spray-drying can be used in the process of producing milk powders and fruit juices,which can incorporate probiotics. The main parameter impacting probiotic viability during spray-drying is the outlet air temperature [Barbosa and Teix-

eira, 2017, Kim and Bhowmik, 1990]. Atomization pressures were also found to have an impact [Barbosa and Teixeira, 2017]. The shear rate to which probiotics are exposed during atomization is arguably a parameter decreasing viability [Riveros et al., 2009,Santivarangkna et al., 2008], but a recent study [Ghandi et al., 2012] showed that the survival of *Lactococcus lactis* subsp. *cremoris* was greatly diminished by an increased shear rate. This study also demonstrates that damage caused by oxygen exposure resulted in higher cell inactivation compared to thermal and dehydration stresses. The drying medium has also been shown to have an impact on probiotic preservation. Skim milk is probably the most common carrier, and its protective effect has been demonstrated for various species [Ananta et al., 2005, Barbosa et al., 2015, Paéz et al., 2012, Teixeira et al., 1995]. A medium with a high solid content requires more time under high temperatures to dry out, which results in a decrease of probiotic survival [Santivarangkna et al., 2007]. A negative impact of the drying step on probiotic viability was reported by two studies featuring an apple matrix [Betoret et al., 2003, Borges et al., 2016a], which is likely due to low pH values and the presence of organic acids. No impact was reported for strawberries and bananas [Borges et al., 2016a].

I.2.2.3.2 Grinding

Borges et al. (2016a) report the impact of grinding on the viability of *Lactobacillus plantarum* during the manufacturing of fruit powders [Borges et al., 2016a]. Fresh fruits were impregnated with *L. plantarum* using either skim milk or a buffer, then subsequently dried and ground. Survival was best for milk-impregnated fruits and much higher for strawberry and banana than for apples. This confirms that apple is a poor carrier compared to other fruits and shows that skim milk protects bacteria against mechanical stress. This might be explained by the capacity of skim milk to stabilize cell membranes, thereby preventing cellular injury [Meng et al., 2008].

I.2.2.3.3 Rehydration

Rehydration has been shown to affect LAB viability for dried apple matrices. This is especially true for apples impregnated with apple juice compared to whole milk–impregnated

apples [Betoret et al., 2003]. However, apples impregnated with mandarin juice containing *Lactobacillus salivarius* subsp. *salivarius* are little affected by the rehydration step [Betoret et al., 2012]. These two studies suggest that the rehydration impact is strain-dependent and related to the impregnation medium used. Nualkaekul et al. (2012) studied the rehydration impact on various fruit powders containing *L. plantarum*. The highest viability decrease was observed with the cranberry matrix and the best survival was observed with the strawberry matrix. Pomegranate and blackcurrant feature a slightly worse survival rate than does strawberry, but viability loss remained low for both. The main physicochemical factors of the food matrix that negatively impact cell survival upon reconstitution of fruit juice powders were low pH and high water activity (a_w), the latter fostering the migration of acids and other bactericidal compounds toward probiotics upon rehydration [Nualkaekul et al., 2012].

I.2.2.3.4 Heating/freezing

Extreme temperatures during food manufacturing can cause lethal stress to probiotics [Cruz et al., 2009, Endo et al., 2014, Homayouni, 2008, Santivarangkna et al., 2008]. Food processes that include a heating step above 65 °C are highly detrimental to probiotics. Even short exposure times up to 1 min can be destructive depending on the species; Rodgers (2007) pointed out that no viable population was detected after inoculation in melted cheese (70–80 °C) for *Lactobacillus acidophilus* and *Bifidobacterium animalis* subsp. *lactis* [Rodgers, 2007], and cold temperatures are also known to reduce the membrane fluidity and enzymatic activity and to increase sensitivity toward sodium chloride, which may cause membrane damage [Corcoran et al., 2008]. Alamprese et al. (2002, 2005) reported that lower amounts of sugar or fat in ice cream led to higher viability losses right after freezing. This can mean that sugar and fat help protect LAB cells against external stresses such as temperature changes and ice crystal formation. Furthermore, when the fat:sugar ratio does not get below one-third but both fat and sugar contents are reduced, no significant decrease in viability is observed [Alamprese et al., 2002, Alamprese et al., 2005]. This leads to the assumption that there is an optimum fat:sugar ratio in ice cream formulation that allows maximum protection for LAB cells.

I.2.3 Impact of food storage

Viability can be assessed easily during storage,which is also more flexible than most manufacturing steps. These two reasons explain that storage time and conditions have been extensively studied and that storage viability has been assessed on a wide range of dairy and nondairy foods [Cruz et al., 2009, Karimi et al., 2011, Martins et al., 2013, Pasqualin Cavalheiro et al., 2015, Ranadheera et al., 2010, Shori, 2015, Vijaya Kumar et al., 2015, Yeo et al., 2011]. Food matrices are compared during storage on the basis of their structure, composition, and physicochemical parameters (Table I.2.2). A distinction is made between dairy and nondairy foods.

Food Category	Food Structure	Compared Food Products	Strains	Critical factor	Effects on strain viability[2]	Reference
Dairy	Solid	Peanut butter: full versus low fat	Mix 1: *Bifidobacterium bifidum*, *Bifidobacterium lactis*, *Lactobacillus acidophilus* Mix 2: *B. bifidum*, *Bifidobacterium breve*, *B. lactis*, *Bifidobacterium longum*, *L. acidophilus*, *Lactobacillus brevis*, *Lactobacillus bulgaricus*, *Lactobacillus casei*, *Lactobacillus gasseri*, *Lactobacillus lactis*, *Lactobacillus paracasei*, *Lactobacillus plantarum*, *Lactobacillus rhamnosus*, *Lactobacillus salivarius*, *Streptococcus thermophilus* Mix 3: *B. bifidum*, *B. longum*, *L. acidophilus*, *L. bulgaricus*, *L. plantarum*, *L. rhamnosus*, *L. salivarius*, *S. thermophilus* Alone: *L. rhamnosus*	Oxygen content, nutrient contents and ratios	Mix 1 > mix 2 > mix 3 across 1 year; fat content impacts negatively LAB survival only at high storage temperatures; refrigerated matrices with high initial inocula presented better viability	Klu et al., 2012, 2014
	Solid	Ice cream: full versus low fat, full versus low sugar, full versus low oxygen	*Lactobacillus johnsonii, Lactobacillus rhamnosus*	Nutrient contents and ratios	No significant viability losses during storage	Alamprese et al., 2002, 2005

[2] A > B means that A is more efficient than B.

			B. bifidum, B. longum, L. acidophilus, L. casei	Oxygen content, nutrient contents and ratios	Oxygen scavengers (L-cysteine) increase *L. casei* and *B. bifidum* survival; *L. casei* survives best; sugar content does not influence viability	Homayouni, 2008
		Cheese: full fat, low fat, and fat-free	Mix: *Lactococcus lactis* subsp. *cremoris*, *L. lactis* subsp. *lactis* Alone: *L. lactis* subsp. *cremoris*	Nutrient contents and ratios	Full fat > 50 %-reduced fat > fat-free before pressing; fat content directly influences LAB retention and growth in the fresh curd	Laloy et al., 1996
		Ice cream versus yogurt (various fat/sugar ratios)	*L. rhamnosus*	Nutrient contents and ratios	Fat and sugar contents and ratios do not influence cell survival during storage; no difference between matrices	Deepika et al., 2011
		Cheese versus yoghurt	*L. casei*	Food structure	No significant difference between matrices	Sharp et al., 2008
		Yogurt versus yogurt with fruits	*Bifidobacterium animalis* subsp. *lactis*, *L. acidophilus*	Food pH, oxygen content, nutrient contents and ratios	Fruit addition in yogurt lowers pH and decreases LAB survival; increased oxygen content due to stirring decreases viability	Kailasapathy et al., 2008
	Solid, liquid	Acidified milk Yogurt: liquid, low fat versus set, full fat	*B. bifidum*, *L. acidophilus*, *Lactobacillus delbrueckii* subsp. *bulgaricus*	Nutrient contents and ratios	Inconclusive on yogurt versus milk Liquid, low-fat > set, full-fat yogurt, especially for *B. bifidum*	Vinderola et al., 2000a
Nondairy	Liquid	Fruit juices (orange, pineapple, cranberry)	*B. animalis* subsp. *lactis*, *L. casei*, *L. paracasei*, *L. rhamnosus*	Food structure, food pH	Orange juice > Pineapple > Cranberry	Sheehan et al., 2007

		Cereal-based, yogurt-like beverages (rice, rice and soy, rice and barley, rice and emmer, rice and oat)	*L. plantarum* (mix of two strains)	Food structure	Rice and barley = rice and emmer > rice and oat > rice; they also have the highest viscosity and water-holding capacity	Coda et al., 2012
		Cereal extracts (barley, wheat, malt)	*L. plantarum*	Nutrient contents and ratios	Malt > wheat > barley; highest cereal content = highest survival	Charalampopoulos and Pandiella, 2010
			L. acidophilus, Lactobacillus fermentum, L. plantarum, L. reuteri	Nutrient contents and ratios	Malt > barley = wheat; *L. plantarum* and *L. fermentum* grow the best; *L. acidophilus* grow poorly on cereals	Charalampopoulos et al., 2002
		Cereals extracts (barley, malt, barley and malt)	*L. plantarum* and *L. acidophilus* alone and in a mix	Nutrient contents and ratios	Malt = malt–barley mix > barley; no difference between strains	Rathore et al., 2012
	Solid, liquid	Pineapple–grape versus mandarin juice, apple impregnated with mandarin juice (dried, rehydrated)	*L. acidophilus, L. salivarius* subsp. *salivarius*	Water activity	Mandarin > pineapple–grape for incubation	Betoret et al., 2012
		Apple juice versus chocolate-coated cereals	*L. rhamnosus*	Food structure, food pH, water activity	Chocolate-coated cereals > apple juice; most important loss at the beginning of storage	Saarela et al., 2006b
	Powder	Fruits (apple, strawberry, banana) with/without skim milk powder	*L. plantarum*	Food structure, food pH	Banana and strawberry > apple; the fiber content of bananas could have a positive impact; minimal loss during storage compared to manufacturing	Borges et al., 2016a

		Fruits (strawberry, pomegranate, blackcurrant, cranberry) dried versus rehydrated	*L. plantarum*	Food structure, food pH, water activity	Blackcurrant was the best carrier and cranberry the worst; water activity < 0.25 results in very low losses	Nualkaekul et al., 2012
Dairy versus nondairy	Solid	Dark versus milk chocolate	*B. animalis* subsp. *lactis*, *L. acidophilus*	Nutrient contents and ratios, dairy versus nondairy foods	No viability difference between matrices or strains	Klindt-Toldam et al., 2016
			B. lactis, L. acidophilus	Dairy versus nondairy foods	No viability difference between matrices; *B. lactis* better than *L. acidophilus*	Lalicic-Petronijevic et al., 2015
		Milk-based versus water-based pudding	Mix: *B. animalis* subsp. *lactis*, *L. acidophilus* Alone: *B. animalis* subsp. *lactis*, *L. acidophilus*, *L. rhamnosus*	Food pH, dairy versus nondairy foods	Milk-based $>$ water-based for all strains; *L. rhamnosus* is the only strain to remain viable in water-based pudding; *B. animalis* and *L. acidophilus* better when mixed	Helland et al., 2004
		Rice (*Oryza sativa*; nine different cultivars)	*Lactobacillus amylovorus*	Food structure	Adhesion to food matrix during storage is higher in sticky rice (Luem Pua); riceberry and black jasmine also give good results; amylopectin embeds LAB (mucous coating); rough surface can retain better LAB	Chumphon et al., 2016
	Solid, Emulsion	Cheese (fresh, semihard, hard), ice cream, chocolate (milk, dark), organic jam, chocolate mousse, salami (Ciauscolo/ Italian, Swiss)	Mix: *L. paracasei*, *L. rhamnosus*	Food structure, Food pH, dairy versus nondairy foods	All carriers remain viable except jam; ice cream is the best carrier on the long-term; on short term, Ciauscolo and chocolate mousse are good carriers; cheese is a good carrier for half its life	Coman et al., 2012
	Solid, Liquid	Artichoke, olives, skim milk	*L. paracasei, L. plantarum*	Food structure	Both strains survived over 3 months; no significant reduction after 30 days	Valerio et al., 2006

	Solid, Liquid, Emulsion, Mix	Sandwich, sushi, burger, oil, tamarin vinaigrette, mayonnaise, fruit-based versus ice cream–based smoothie, butter	*B. animalis* subsp. *lactis*, *L. acidophilus*	Food structure, food pH, oxygen content, dairy versus nondairy foods	Sandwich and sushi are good carriers; lipid oxidation if high temperatures (oil, butter); low-pH products have a poor viability (vinaigrette, mayonnaise); viability properties are strain-specific	Rodgers, 2007
	Purée, Liquid	Milk-based, vanilla-flavored drink versus fruit purées/juices	*B. animalis* subsp. *lactis*	Food structure, food pH, dairy versus nondairy foods	Apple-based products were less reliable carriers due to their lower pH	Vinderola et al., 2012
	Liquid	Skim milk versus fruit juices	*B. animalis* subsp. *lactis*	Food structure, food pH, water activity, dairy versus nondairy foods	Skim milk > fruit juices	Saarela et al., 2006a
		Milk and drinking yogurt versus soy milk, orange juice	*B. animalis, B. animalis* subsp. *lactis*	Food pH, dairy versus nondairy foods	Milk = soy milk > yogurt for one strain > orange juice (all strains)	Charnchai et al., 2016

Table I.2.2: Food matrix impact on lactic acid bacteria (LAB) viability during food storage.

I.2.3.1 Food structure

The physical structure, *i.e.*, solid, gel, emulsion, or liquid, of food plays a role during storage in protecting LAB cells from an unfavorable environment. This has especially been highlighted for cheese matrices [Castro et al., 2015, Karimi et al., 2011]; additional observations of cheese microstructure during ripening showed that some bacteria adhere to the matrix, which helps with their protection [Gobbetti et al., 1998, Hickey et al., 2015b]. Solid and gel matrices have been found to physically and chemically bind with detrimental factors such as hydrogen ions and organic acids, therefore reducing the exposure of bacteria to these factors [Karimi et al., 2011, Mohammadi and Mortazavian,

2011,Mortazavian et al., 2012,Ranadheera et al., 2010]. Furthermore, the complexation of hydrogen ions by the matrix decreases the amount of undissociated organic acids to which the bacterial membrane is permeable [Russell and Diez-Gonzalez, 1997], thus resulting in the reduction of subsequent bactericidal effect [Mortazavian et al., 2012]. However, to our knowledge, no study has been published that compares LAB viability during storage of two food matrices that differ by their physical structure but are identical in composition. Compared food matrices are often different commercialized food products and more rarely food models. More attention is also often given to food composition versus food structure because changes to the latter are more difficult to implement within a given manufacturing process and more likely to impact the consumer's acceptance. Therefore, it is difficult to ascertain how much of the protection during storage provided by a dense matrix is due, for example, to its density regardless of other physicochemical factors.

However, several studies comparing foods with different structures point out that differences in LAB viability during storage are mostly due to differences in physicochemical composition or storage conditions [Coman et al., 2012, Rodgers, 2007, Saarela et al., 2006b, Vinderola et al., 2012], meaning that food structure has not been found to be a dominant factor compared to other characteristics of the food matrix, such as pH. Solid and liquid food matrices are compared throughout storage for their efficacy to preserve LAB viability (Table I.2.2). Storage induces minimal viability losses in fruit powders compared to other fruit media such as fruit juices [Borges et al., 2016a, Nualkaekul et al., 2012, Saarela et al., 2006a, Sheehan et al., 2007]. Coman et al. (2012) showed that some solid or gel products such as ice cream and Ciauscolo salami are better or equally good LAB carriers compared to emulsions such as chocolate mousse [Coman et al., 2012]. This could be attributed to structural differences, as LAB are more likely to be retained in gels than in more aerated matrices. Sharp et al. (2008) did not find out any significant difference between semi-hard cheese and yogurt during storage [Sharp et al., 2008]. Rice and barley and rice and emmer mixes feature the highest LAB survival during storage [Coda et al., 2012] and also exhibit the highest viscosity and water holding capacity; one could then argue that the beverage density plays a role in protecting LAB during

storage. Valerio et al. (2006) showed that two strains survived over several months on artichokes preserved in brine without presenting any significant viability loss [Valerio et al., 2006]. The roughness of the vegetable structure was hypothesized to have contributed to protecting bacteria from the acidic environment. Borges et al. (2016a) suggested that the banana structure and its fiber content might contribute to its efficiency as a carrier [Borges et al., 2016a]. The high amylopectin content of some Thai rice cultivars was found to foster LAB preservation during storage [Chumphon et al., 2016]. LAB adhesion to these cultivars was observed using scanning electron microscopy (SEM) and was revealed to foster *Lactobacillus amylovorus* embedded within the mucous membrane of glutinous Luem Pua, therefore better protecting it from the action of external detrimental factors [Chumphon et al., 2016].

I.2.3.2 Food composition

Differences in food matrix efficacy in sustaining good LAB viability during storage can often be at least partly explained by the food matrix composition. Food composition is the combined result of three main underlying factors: nutrient contents, nutrient ratios, and physicochemical parameters such as food pH, a_w, and O_2 content. Cooperative and competitive interactions between probiotic LAB and starter cultures may also enhance or reduce probiotic LAB survival and growth [Boylston et al., 2004, Champagne et al., 2005, Yeo et al., 2011] but are not discussed in this review; the authors refer the public to other reviews for more details on these topics [Ford et al., 2014, Pandey et al., 2015, Sieuwerts et al., 2008, Tufarelli and Laudadio, 2016].

I.2.3.2.1 pH

Low pH has been pointed out as one of the main factors affecting probiotic growth and survival during storage [Borges et al., 2016a, Charnchai et al., 2016, Coman et al., 2012, Helland et al., 2004, Kailasapathy et al., 2008, Mortazavian et al., 2012, Nualkaekul et al., 2012, Rodgers, 2007, Saarela et al., 2006a, Saarela et al., 2006b, Sheehan et al., 2007, Vinderola et al., 2012]. A very low pH value increases the concentration of undissociated

organic acids in fermented products, therefore enhancing the bactericidal effect of these acids [Mortazavian et al., 2012, Tripathi and Giri, 2014]. Vegetable- and fruit-based beverages with low pH are very challenging probiotic carriers. Low pH tolerance is strain-specific; globally, optimum pH ranges from 5.5 to 6 for L. acidophilus and from 6 to 7 for bifidobacteria [De Vuyst, 2000]. Lactobacilli are capable of growing and surviving in fermented products with pH ranges between 3.7 and 4.3 [Tripathi and Giri, 2014], whereas survival of bifidobacteria decreases below pH 4.6 to 5 or above 8.0 [Boylston et al., 2004, Lourens-Hattingh and Viljoen, 2001, Tripathi and Giri, 2014] and growth is inhibited below 4.0 [Karimi et al., 2011].

I.2.3.2.2 Oxygen content

Most LAB can grow under aerobic conditions but the impact of oxygen can range from insignificant to harmful depending on the species [Pedersen et al., 2012]. Lactobacilli are usually more oxygen tolerant than bifidobacteria. Oxygen can affect LAB in three ways [Mortazavian et al., 2012]: (a) It is directly toxic to anaerobic cells such as bifidobacteria; (b) in the presence of oxygen, certain cultures produce peroxides that are toxic to other species (this is especially true in dairy products); and (c) free radicals produced from the oxidation of components (*e.g.*, fats) called reactive oxygen species (ROS) are toxic to LAB. Food matrices with high fat contents can increase oxidation rates therefore decreasing LAB survival [Klu et al., 2012, Rodgers, 2007]. The negative impact of oxygen has been reported by two comparative studies [Homayouni, 2008, Kailasapathy et al., 2008]. The oxygen incorporated into yogurt during stirring was assumed to contribute to the viability loss of *B. animalis* subsp. *lactis* [Kailasapathy et al., 2008]. Furthermore, the addition of oxygen scavengers such as L-cysteine and of reducing agents has been shown to successfully increase LAB survival in ice cream [Homayouni, 2008]. Some vitamins, such as vitamins C and E, that are naturally present within certain food products have been reported to help with oxygen scavenging [Bagchi et al., 1997]. Other matrices, *e.g.*, cheese, proved to offer good protection against oxygen thanks to their density and structure [Karimi et al., 2011]. It has also been shown that some bacteria, such as *Lactococcus lactis*, are able to respire oxygen when heme is added, thus helping detoxify

the medium and increase LAB growth [Lechardeur et al., 2012, Sonomoto and Yokota, 2011]. The presence of heme in foods (*e.g.*, naturally present in some meat products) would then allow reducing oxygen concentration.

I.2.3.2.3 Water activity

Food matrices such as dry fermented meat that have a very low a_w are not favorable to LAB growth or survival during incubation and therefore reduce the initial quantity of LAB present before storage [Yeo et al., 2011]. However, foods with high a_w are unstable, as they favor overall microorganism growth, including unwanted microorganisms [Betoret et al., 2012]. A high moisture content after inoculation can therefore be detrimental to LAB viability during subsequent storage [Tripathi and Giri, 2014]. A_w is not too commonly referenced as a critical parameter [Nualkaekul et al., 2012, Saarela et al., 2006a, Saarela et al., 2006b].This can be due to the fact that the impact of some other parameters on LAB (*e.g.*, pH) overcomes the a_w impact.

I.2.3.2.4 Nutrient contents and ratios

Charalampopoulos and Pandiella (2010) demonstrated that in cereal-based beverages, higher cereal content led to higher survival rates during storage [Charalampopoulos and Pandiella, 2010], whereas fruit addition to stirred yogurts decreased *L. acidophilus* survival because it lowers the pH [Kailasapathy et al., 2008]. This shows that when the added substrate changes the food physicochemical composition unfavorably, LAB viability can decrease as a result. The influence of the fat:sugar ratio as well as the fat and sugar content has been studied within several dairy products for their assumed protective capabilities [Alamprese et al., 2002, Alamprese et al., 2005, Deepika et al., 2011, Homayouni, 2008, Klu et al., 2012, Klu et al., 2014, Laloy et al., 1996, Vinderola et al., 2000a]. Indirectly, the protective effect of fat content was also studied within chocolate [Klindt-Toldam et al., 2016]. From a global point of view, these studies suggest that fat and sugar do not significantly impact LAB viability in ice cream, peanut butter, or yogurt during storage. A study performed by Vinderola et al. (2000a) is the only one showing that LAB strains can better survive in liquid, reduced-fat yogurt than in set, full-fat

yogurt [Vinderola et al., 2000a]. In cheese, however, fat content was found to be a determining factor for the retention and therefore survival of LAB starters during ripening under normal conditions [Laloy et al., 1996]. Bacteria were found to be located at the interface of the milk-fat globule membrane and milk proteins, thus confirming the adhesion phenomenon occurring between LAB and fat [Guerin et al., 2017b, Laloy et al., 1996, Lopez et al., 2006]. The high fat content, associated with the anaerobic environment and buffering capacity of the cheese matrix, helps protect LAB during storage [Lee and Salminen, 2009]. In beverages containing malt, barley, and wheat, malt has been found to be the most effective medium, which promotes LAB growth and protection. This is likely due to the high content of fermentable and reducing sugars as well as of free nitrogenous compounds [Charalampopoulos et al., 2002, Charalampopoulos and Pandiella, 2010,Rathore et al., 2012]. The most important factor influencing cell survival in cereal-based beverages seems to be the amount of residual sugars [Charalampopoulos and Pandiella, 2010].

I.2.3.2.5 Additives

Sweeteners, salts, aroma compounds, flavoring, coloring agents, and preservatives can affect both LAB growth and viability [Vinderola et al., 2002]. High salt levels have been found to cause high losses during ripening [Gomes et al., 1995, Gomes et al., 1998]. Disaccharides can be used for LAB protection [Önneby et al., 2013]. Sorbitol prevents cell damage during storage by interacting with membrane components and prevents lipid oxidation thanks to its antioxidant properties [Carvalho et al., 2004]. It was also found to stabilize protein functionality and structure in *Lactobacillus delbrueckii* subsp. *bulgaricus* [Yoo and Lee, 1993].

I.2.3.2.6 Dairy versus nondairy foods

Dairy products are traditionally considered very good delivery vehicles for probiotic LAB. The importance of adhesive interactions occurring between LAB and dairy food components and their impact on resulting health effects have been previously highlighted [Burgain et al., 2014a]. However, a growing interest in the development of nondairy probiotic

products must be acknowledged. Main underlying reasons are the rising vegan trend, lactose intolerance, and other factors such as the unfavorable cholesterol content of some dairy products [Ranadheera et al., 2010, Shori, 2015, Yeo et al., 2011].

No LAB viability difference was reported between dark and milk chocolate [Klindt-Toldam et al., 2016, Laličić-Petronijević et al., 2015] nor between a milk-based drink and several fruit purées [Vinderola et al., 2012]. Rodgers (2007) and Coman et al. (2012) compared the efficiency during storage of a variety of products as LAB carriers including fruit-based and ice cream–based smoothies, butter, cheese, ice cream, milk chocolate, and nondairy products [Rodgers, 2007, Coman et al., 2012]. The efficiency of dairy versus nondairy foods as LAB carriers might not be revealed for very short incubation times [Rodgers, 2007]. When food products are inoculated directly upon delivery, smoothies and butter were indeed found to be poor carriers, whereas other products such as sandwiches and sushi showed a better viability:shelf-life ratio [Rodgers, 2007]. Ice cream, fermented meat, and chocolate mousse were the best carriers for a given probiotic mix, although all food matrices remained viable except the organic jam. Buscion (fresh Swiss cheese), Caciotta, and Pecorino cheeses (seasoned Italian cheeses) count among carriers with the highest viability loss [Coman et al., 2012]. Skim milk [Saarela et al., 2006a] and dairy beverages [Charnchai et al., 2016] more efficiently carried *B. animalis* subsp. *lactis* through storage than fruit juices. *L. acidophilus*, *L. rhamnosus*, and *B. animalis* subsp. *lactis* showed better growth and survival in milk-based versus water-based pudding [Helland et al., 2004]. Proposed reasons for the efficiency of dairy products include the presence of proteins or protein derivatives, such as whey protein concentrate, acid casein hydrolysate, and tryptone, which have been found to promote probiotic growth and survival by reducing the food redox potential and increasing its buffering capacity, thus maintaining a near-neutral pH [Dave and Shah, 1998, Mortazavian et al., 2010]. Probiotics proliferate well in dairy-based media because of the lactose-hydrolyzing enzyme and proteolytic system involved in casein utilization, which provides cells with carbon and essential amino acids [Yeo et al., 2011]. Casein and whey protein hydrolysates enhance growth and thus increase the acidification rate of *Streptococcus*

thermophilus. The increased acidity reduces the growth rate of some LAB, *e.g.*, *L. acidophilus* and *L. rhamnosus*, during manufacturing; however, dairy protein hydrolysates improve survival of LAB during storage [Lucas et al., 2004]. Within dairy foods, the kind and amount of carbohydrates available, degree of protein hydrolysis and thus of available amino acids, and composition and degree of lipid hydrolysis are important factors controlling the efficiency of matrices as LAB carriers [Heller, 2001].

For all these reasons, dairy foods have excellent potential as probiotic carriers. However, this potential may or may not be expressed depending on other conditions, such as a low pH or the presence of antimicrobial compounds resulting from the addition of fruits [Vinderola et al., 2002, Yeo et al., 2011]. Furthermore, other media such as chocolate [Gadhiya et al., 2016, Klindt-Toldam et al., 2016, Laličić-Petronijević et al., 2015, Possemiers et al., 2010] and fermented meat [De Vuyst, 2000, Khan et al., 2011, Pasqualin Cavalheiro et al., 2015] have also been found to be very promising probiotic carriers. Because very little research has focused on comparing these media with dairy foods, no assumption can be made regarding which medium is a more efficient probiotic carrier.

I.2.4 Impact of food digestion

The main factors that have been acknowledged to influence the viability of probiotic LAB in food during their passage through the GIT are (a) the food matrix, (b) the low pH in the stomach, which is the most impactful digestion step, (c) bile salts and gastroenzymes in the small intestine, (d) lysozyme in saliva, and (e) colonic environment [Bove et al., 2013, Mortazavian et al., 2012]. Here, we focus only on the food matrix impact on LAB effective gastrointestinal delivery (Table I.2.3). Food structure and composition influences are detailed separately for more clarity.

Food Category	Food Structure	Compared Food Products	Strains	Critical factor	Effects on strain viability[3]	Reference
Dairy	Solid	Ice cream versus yogurt (various fat/sugar ratios)	*Lactobacillus rhamnosus*	Food pH, nutrient contents and ratios, dairy versus nondairy foods	Yogurt > ice cream for adhesion to Caco-2 cells; this is attributed to changes in the bacteria surface conformation that may have occurred during storage; fat/sugar contents/ratios do not impact	Deepika et al., 2011
		Ice cream versus yogurt (plain versus stirred fruits)	*Bifidobacterium animalis* subsp. *lactis*, *Lactobacillus acidophilus*, *Propionibacterium jensenii*	Food structure, buffering capacity, nutrient contents and ratios, dairy versus nondairy foods	Yogurt > ice cream for *L. acidophilus* versus ice cream > yogurt for *P. jensenii* and *B. animalis*; ice cream > yogurt for acid and bile tolerance of all strains but fruit yogurt > ice cream and plain yogurt for adhesion	Ranadheera et al., 2012
		Cheese versus yogurt	Mix: *B. animalis* subsp. *lactis*, *L. rhamnosus*, *Propionibacterium freudenreichii*	Food structure, buffering capacity, dairy versus nondairy foods	Yogurt > cheese for *P. freudenreichii*/*B. animalis* (fecal quantities, recovery time); no matrix effect for lactobacilli	Saxelin et al., 2010
			Lactobacillus casei	Food structure, food pH, buffering capacity, dairy versus nondairy foods	Cheese > yogurt	Sharp et al., 2008
	Liquid	Fermented milk versus whey beverage	*L. rhamnosus*	Nutrient contents and ratios	Whey-based beverage > fermented milk (counts and longer period)	Goldin et al., 1992
	Solid, Liquid	Cheese versus milk (fermented/ unfermented)	*L. rhamnosus*	Food structure	Cheese > unfermented milk > fermented milk (feces recovery)	Saxelin et al., 2003

[3] A > B means that A is more efficient than B.

Dairy versus nondairy	Solid	Dark versus milk chocolate	*B. animalis* subsp. *lactis*, *L. acidophilus*	Dairy versus nondairy foods	No significant difference between matrices	Klindt-Toldam et al., 2016
	Solid, Liquid	Pasta (ordinary, β-glucan enriched) versus skim milk	*Lactobacillus plantarum*	Food structure, dairy versus nondairy foods	Skim milk = β-glucan pasta > pasta; carbohydrate polymers may physically protect LAB in enriched pasta	Bove et al., 2013
			Artichoke, olives, skim milk	*Lactobacillus paracasei, L. plantarum*	Food structure, buffering capacity, nutrient contents and ratios, dairy versus nondairy foods	Valerio et al., 2006
	Purée, Liquid	Milk-based, vanilla-flavored drink versus fruit purées/juices	*B. animalis* subsp. *lactis*	Food structure, dairy versus nondairy foods	Milk-based drink and banana–carrot juice > fruit purées > orange juice	Vinderola et al., 2012
	Liquid	Skim milk versus fruit juices	*B. animalis* subsp. *lactis*	Dairy versus nondairy foods	Milk > fruit juice for bile and pepsin tolerance	Saarela et al., 2006a

Table I.2.3: Food matrix impact on lactic acid bacteria (LAB) viability during food digestion.

I.2.4.1 Food structure

The physical food structure is one of the most important factors influencing the viability of LAB within the GIT as well as its adhesion to the intestinal epithelium, but it has been insufficiently studied [Mortazavian et al., 2012, Ranadheera et al., 2012, Saxelin et al., 2010]. However, more studies have been done on nutraceutical and nutrient delivery. Singh et al. (2015) reported that food structure has a significant impact on food breakdown and release of nutrients, and McClements (2015) presents guidelines to design structural foods to optimize nutraceutical delivery [Singh et al., 2015, McClements,

2015]. The impact of the physical structure of dairy products on the digestion rate has also been studied [Barbé et al., 2013, Guo et al., 2016, Ye et al., 2016]. The food disintegration rate in the stomach depends on food rheology and is lower for hard or tough foods. Changes in the food structure caused by processing such as boiling, roasting, and frying impact the digestion rate; the network strength of gel matrices is also involved in the release or separation of food components and nutrients [Barbé et al., 2013, Singh et al., 2015]. In cheese, caseins were found to build stronger and denser networks than did whey [Guerin et al., 2017a] and high cohesiveness and elasticity were associated with slower degradation [Lamothe et al., 2012]. Porous structure and weak milk-based gels disintegrate quickly during the gastric step and are inefficient LAB carriers, whereas strong gels and dense matrices (with elastic component G' ranging from 200 to 300 Pa and viscous component G" ranging from 50 to 100 Pa) prevent the total disintegration of the matrix, thus preventing bacteria delivery; an optimum texture can therefore be determined [Guerin et al., 2017a]. Gastric emptying is influenced mainly by the disintegration rate and the particle size of the bolus entering the stomach [Singh et al., 2015]. Articles comparing the efficiency of different food matrices with different structures on LAB delivery are presented in Table I.2.3. The cheese matrix was shown to protect LAB during their passage through the GIT [Corbo et al., 2001, Gardiner et al., 1998, Vinderola et al., 2000b]. Sharp et al. (2008) showed that low-fat cheese improved *Lactobacillus casei* survival when exposed to lethal acid challenge compared to yogurt [Sharp et al., 2008]. The same study also showed that the fecal recovery of *L. casei* was higher when originating from the cheese versus yogurt matrix. This suggests that the cheese matrix impact goes beyond its shielding and entrapment of LAB, which would have limited bacteria release within the intestine, therefore reducing the counts in feces compared to yogurt. Beta-glucan may physically shield bacteria due to its high intrinsic viscosity, as *L. plantarum* showed enhanced resistance to orogastric stress in β-glucan-enriched versus normal pasta [Bove et al., 2013, Ruas-Madiedo et al., 2002, Stack et al., 2010]. Several studies suggest that the rough structures of some matrices can help with LAB survival through digestion [Lavermicocca et al., 2005, Lavermicocca, 2006, Valerio et al., 2006].

Vinderola et al. (2012) showed that various fruit purées improved GIT survival of *B. animalis* subsp. *lactis* compared to orange juice when all media had similar pH and featured similar nutrients [Vinderola et al., 2012]. However, its survival was five times higher in banana-carrot juice versus several fruit purées for which pH and buffering capacity were presumably lower [Vinderola et al., 2012]. This shows that physicochemical differences between food matrices are likely to govern LAB survival during digestion over differences in the physical food structure.

These studies confirm that food structure does play a role in LAB delivery and that denser, more viscous or complex matrices better protect LAB during digestion but also tend to limit their release. However, the relative importance of food structure compared to other food matrix parameters such as composition still remains to be determined, and data comparing food matrix based on structural differences remain scarce. Further research needs to focus on the impact of food structure on effective LAB delivery during digestion.

I.2.4.2 Food composition

Similar to what happens during food storage, the nutrient and physicochemical composition of food matrices also play a role during digestion in LAB survival and effective delivery (Table I.2.3).

I.2.4.2.1 pH

Food pH has been reported to act on the bacterial surface conformation during storage and therefore affect LAB adhesion capacity, *i.e.*, effective delivery within the GIT. This was argued in a study in which neutral pH in ice cream was assumed to preserve better LAB adhesive capabilities than low pH in yogurt [Deepika et al., 2011]. Sharp et al. (2008) also argued that the higher pH of cheese compared to yogurt can contribute to its higher protective effect on *L. casei* during digestion [Sharp et al., 2008].

I.2.4.2.2 Buffering capacity

The buffering capacity of a food matrix can be defined by its ability to be acidified or alkalinized [Ranadheera et al., 2012, Salaün et al., 2005]. Matrices with low pH have

a low buffering effect [Valerio et al., 2006]. Dairy products have very good buffering capacities due essentially to their protein and salt, such as phosphate, citrate, and lactate, contents. The buffering capacities of whey proteins and caseins are maximal at pH 3–4 and pH 5–5.5, respectively. During acidification, milk features the highest buffering capacity at pH 5 [Salaün et al., 2005]. Cheese has been argued to feature high buffering capacities [Boylston et al., 2004, Lee and Salminen, 2009, Sharp et al., 2008], although some studies show no difference in lactobacilli survival during digestion with othermedia such as yogurt [Saxelin et al., 2010]. Some components such as fat are likely to improve the food matrix buffering capacity [Mortazavian et al., 2012, Ranadheera et al., 2012]. Buffering food matrices offer good storage protection to LAB by limiting acidification. They are, however, less favorable to LAB delivery within the GIT, as they also increase stomach pH, thus limiting the action of gastric acids, which contribute to food breakdown and LAB release [Ranadheera et al., 2010,Ranadheera et al., 2012]. Finally, buffering food matrices can also lower LAB recovery and persistence in feces [Guerin et al., 2017a,Saxelin et al., 2010].

I.2.4.2.3 Nutrient contents and ratios

Fat features good buffering capacities, which help with LAB survival throughout the GIT [Ranadheera et al., 2012] but also tend to lower LAB strains' adhesive capabilities as previously reported in milk [Ouwehand et al., 2001]. However, these properties are likely to be strain dependent and also vary with the other nutrients present within the matrix [Deepika et al., 2011]. Some components such as whey are likely to improve LAB fecal recovery and persistence [Goldin et al., 1992] and can protect LAB during digestion [Madureira et al., 2005, Madureira et al., 2011]. Fermentable sugars also improve LAB survival during digestion [Corcoran et al., 2005,Lacroix and Yildirim, 2007] and stimulate ATP production in bacteria cells, which is required for pumping acid out the cytoplasm and therefore protecting bacteria from the low gastric pH. Prebiotic carbohydrates, such as inulin contained in artichokes, have also been assumed to contribute to the high LAB recovery rate in feces [Valerio et al., 2006].

I.2.4.2.4 Dairy versus nondairy foods

Because dairy products are conventional LAB carriers, they are often used as baselines in comparative studies (Table I.2.3). Matrices with close compositions and similar structures, such as dark versus milk chocolate, do not feature significant viability differences [Klindt-Toldam et al., 2016]. However, when comparing milk to a range of media, including pasta, artichoke, olives, fruit purées, and fruit juices [Bove et al., 2013, Saarela et al., 2006a, Valerio et al., 2006, Vinderola et al., 2012], milk always proved to be the most efficient medium for LAB preservation during digestion. This has been assessed for a variety of strains including *L. plantarum*, *Lactobacillus paracasei*, and *B. animalis* subsp. *lactis*. The presence of fermentable substrates and the occurrence of milk fat and proteins can sustain bacterial metabolism and shield bacteria cells from drastic environmental conditions [Charteris et al., 1998, Valerio et al., 2006]. The high buffering effect of milk contributes to increasing the acid and bile tolerance of LAB strains [Bove et al., 2013, Saarela et al., 2006a, Vinderola et al., 2012] and calcium ions increase the LAB binding capacity to epithelial cells [Larsen et al., 2007]. Comparing the efficiency of individual dairy carriers in delivering LAB appears to be more difficult than comparing the efficiency of dairy versus nondairy foods. When compared based on LAB recovery from feces, cheese was found to increase LAB recovery compared to milk [Saxelin et al., 2003]. Cheese was also found to increase the survival of *L. casei* [Sharp et al., 2008] and decrease the survival of *Propionibacterium freudenreichii* and *B. animalis* subsp. *lactis* compared to yogurt [Saxelin et al., 2010]. *L. acidophilus* better survives in yogurt versus ice cream, whereas the opposite is the case for *Propionibacterium jensenii* and *B. animalis* subsp. *lactis* (Ranadheera et al. 2012). In another study, *L. rhamnosus* originating from a yogurt model was shown to be more adhesive to Caco-2 cells than strains issued from an ice cream model [Deepika et al., 2011]. Overall, these studies show that dairy matrices optimize LAB delivery compared to nondairy but that within dairy products survival rates are highly strain dependent.

I.2.5 Food matrix design proposal

The delivery potential of five main food matrix types, i.e., cereals, vegetables and fruits, chocolate, meat, and dairy products, on LAB protection, carrying, and delivery has been discussed throughout this review (Figure I.2.2). Cereal-based products feature many positive aspects, including high viscosity, water-holding capacity, and fiber content, but their consumer acceptability is often low. Vegetables and fruit-based products are becoming more and more attractive to consumers but often feature a low pH and high organic acid content as well as oxygen and other bactericidal compounds. Chocolate and meat products are promising carriers because of their high nutrient and fat contents, buffering capacity, and solid or gel structure that keeps LAB entrapped and protected during storage, although they can sometimes feature low pH and preservative agents. Long shelf-life LAB also need to be used when designing long shelf-life food products such as chocolate bars. Chocolate and meat matrices are becoming increasingly studied, as they feature a good potential as LAB carriers. Lastly, dairy products remain very good LAB carriers because of their excellent buffering capacity and high milk protein and fat contents, even though some factors, such as a high oxygen content in ice cream, antagonistic interactions with starters in yogurt, and pH decrease in fermented dairy products, are susceptible to decreased LAB viability. This review has highlighted seven essential food matrix parameters that act on LAB protection, carrying and delivery: pH, a_w, matrix buffering capacity, physical food structure, and fat, oxygen, and nutrient contents. These parameters have been integrated within a hypothetical food matrix optimal for effective LAB delivery (Figure). A neutral or slightly acidic pH (5–6) is optimal for LAB growth during food manufacturing and survival during storage. It also helps with efficient LAB delivery during digestion by preserving the ability of LAB to adhere to intestinal cells. A_w should remain high during manufacturing but preferably lower during storage to first foster LAB growth and then promote their protection and stability. A high matrix buffering capacity helps with LAB protection during food manufacturing and storage by lowering the impact of mechanical, physicochemical, and temperature-related

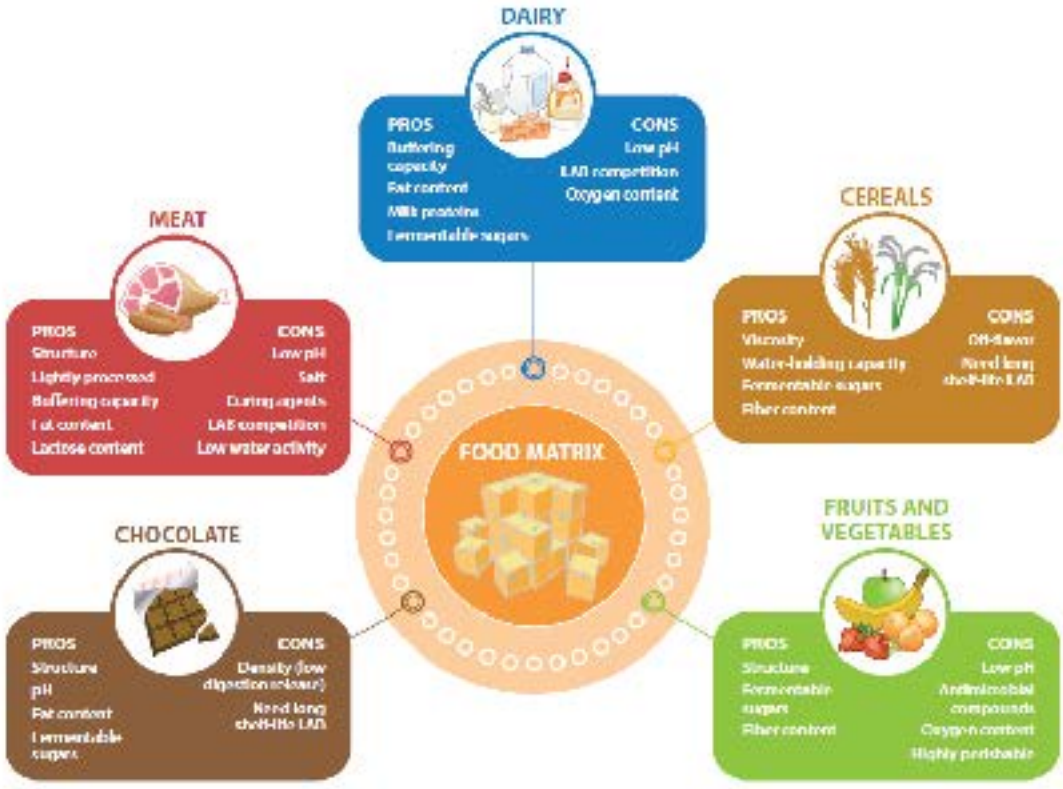

Figure I.2.2: Advantages and disadvantages of five main food matrix types (dairy, cereals, fruits and vegetables, chocolate, and meat) on lactic acid bacteria (LAB) protection, carrying, and delivery.

stresses, including acidification. It may also increase the pH of the stomach, thus improving LAB protection during digestion. Solid and gel food structures are recommended to improve LAB growth and stabilization during food manufacturing by taking advantage of LAB adhesive capabilities. The entrapment of LAB into such matrices limits their accessibility to detrimental factors during storage, which also promotes their survival. Solids and gels also prevent LAB from being killed in harsh environments such as the stomach when they are being embedded within the food structure. However, when the physical structure of food is too hard (*i.e.*, with a high elastic modulus G' or a high loss modulus G") or when the matrix binds very strongly with LAB, food breakdown during digestion is restricted and LAB release within the GIT might not be optimal. A high fat content has been shown to feature the same positive effects as a good matrix

buffering capacity during food manufacturing and storage, especially for cheeses. The incorporation of oxygen within the matrix should be avoided as much as possible, as it can be toxic to LAB, preventing growth and decreasing survival during storage. A solid physical structure can limit oxygen access during storage. Manufacturing steps such as stirring and mixing should be monitored with great care, especially for products with long shelf-lives such as ice cream. Highly fermentable sugars and nutrients promote LAB growth during manufacturing and foster LAB survival during food storage and digestion. A high fiber content can also foster LAB adhesion to the matrix, thus increasing LAB survival during storage.

I.2.6 Lactic acid bacteria functionality and perspectives

Although this review mainly focuses on LAB viability, LAB functionality, *i.e.*, the ability of bacteria to interact with their host and multiply, is also essential for them to be able to provide health benefits. Many factors can impact LAB physiology and functionality including their level of entrapment within the food matrix and the loss or inactivation of bacterial surface markers modulating bacterial-host interactions and adhesion, etc. [Sanders and Marco, 2010]. Main factors related to the food matrix affecting LAB functionality are a_w of the carrier, access to nutrients, matrix pH, growth promoters [De Vuyst, 2000], oxygen content, and storage temperature [Shori, 2016]. LAB need to be functional during digestion to colonize the GIT and exert their health benefits on the host. A common approach to evaluate their colonization capabilities consists of monitoring the adhesive behavior of LAB strains to models of intestinal cells; however, this approach needs to be completed by a viability study because dead bacteria have also been shown to adhere to Caco-2 cells [Deepika et al., 2011, Ouwehand et al., 2001]. Clinical studies are the most reliable way to assess LAB functionality; probiotics are *de facto* considered functional if resulting health effects are observed. However, assessment methods are numerous, and clinical studies comparing different LAB food matrices are rare, long, and hardly comparable with one another. Further research should concentrate on how food can impact LAB functionality to determine whether LAB remains both

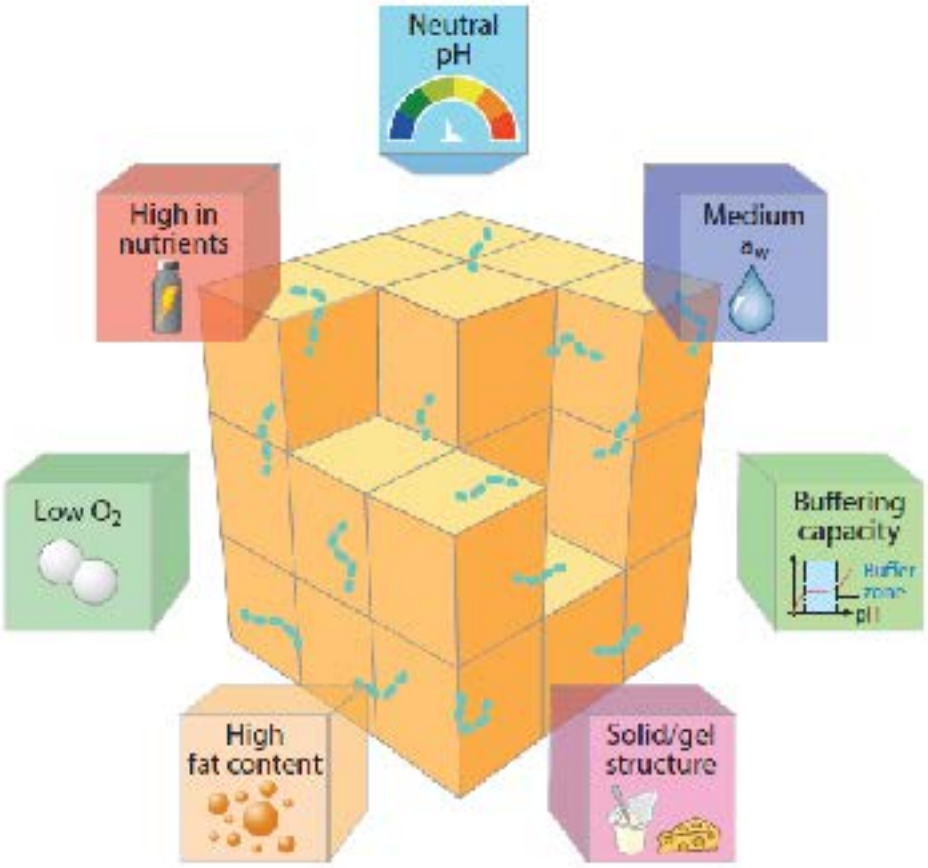

Figure I.2.3: The ideal food matrix for effective lactic acid bacteria protection, carrying and delivery: optimization of seven essential parameters (pH, a_w, buffering capacity, food structure, fat content, oxygen content, nutrient contents).

viable and functional when reaching the GIT. It is of great interest to study LAB probiotic activity indicators such as effective adhesion to the GIT, metabolite production (*e.g.*, bacteriocins), stress tolerance, and gene expression. Recent work has been performed on the functionality of dairy propionibacteria through the use of new imaging techniques that assess their colonizing capabilities [Daniel et al., 2006] or of new ingredients that enhance multistress tolerance [Huang et al., 2016]. Such work could be adapted to LAB, although these studies have not always been on food products. Studying LAB functionality will help to develop methods to assess LAB activity a priori; such outcomes could be combined with existing knowledge on LAB viability and prove very useful when performing food matrix design for effective LAB delivery.

I.3

Modeling shearing impact on bacteria

I.3.1 Modeling shearing impact on bacterial viability, functionality, and shape

I.3.1.1 Factors impacting bacterial adhesion

Bacteria-food adhesive interactions are likely to be affected by many unfavorable environmental conditions that may generate stress [Arnaud et al., 1993, Berzins et al., 2001, Boylston et al., 2004, Champagne et al., 2005, Corcoran et al., 2008, Golowczyc et al., 2011, Iaconelli et al., 2015, Pontefract, 1991, Sanders et al., 2014, Tripathi and Giri, 2014].

Factors likely to influence LAB adhesion are indeed numerous and include the level of bacterial entrapment within the food matrix as well as the loss or inactivation of bacterial surface components modulating bacterial-host interactions and adhesion [Sanders and Marco, 2010]. Environmental stresses may damage bacterial surface molecules or in some cases induce partial or even total removal, "shaving the bacterial surface" [Tripathi et al., 2012, Kiekens et al., 2019], thus altering bacterial cells adhesive abilities. Bacterial stress can occur in a wide variety of situations including common food and ferment

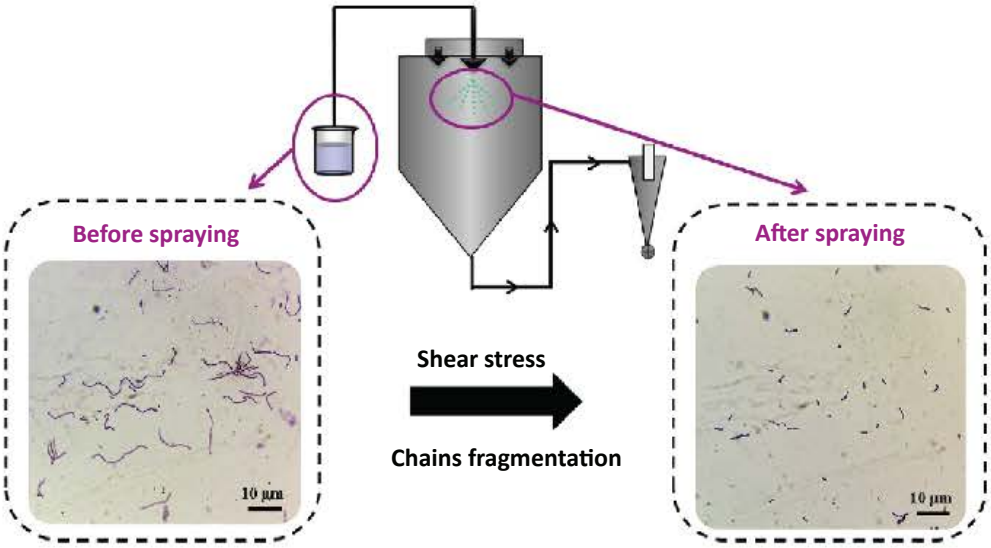

Figure I.3.1: Effect of spraying-induced shear stress on bacterial chain organization; from Guerin et al. [Guerin et al., 2017c].

manufacturing steps. These situations include acid stress during fermentation [Ouwehand et al., 2001], heat stress upon drying which may induce permanent structural changes related to significant cell collapse and membrane integrity loss [Doherty et al., 2010], preventing bacteria from colonizing the host, and shear stress occurring in spray-drying, encapsulating, and extrusion processes [Arnaud et al., 1993, Berzins et al., 2001, Doherty et al., 2010, Edwards et al., 1989, Ghandi et al., 2012, Guerin et al., 2017b, Joshi et al., 1996, Kiekens et al., 2019, Lange et al., 2001, Taskila, 2017], but also during the biological process of digestion [Aziz et al., 2019, Yang et al., 2017]. Shear stress may cause bacterial chain fragmentation as shown in Figure I.3.1 [Guerin et al., 2017c]. Observed changes in terms of cellular organization were not found to impact bacterial viability (evaluated at the end of the encapsulated process), however bacterial functionality was not assessed in this study although bacterial surface was found to be impacted in similar conditions in a very recent study [Kiekens et al., 2019]. The following sections will focus on shear stress and the impact of shearing steps in manufacturing processes on bacterial viability and functionality, for bacteria alone in suspensions as well as for bacteria incorporated in food matrices.

I.3.1.2 Shearing impact on bacterial viability and functionality

In the case of Gram positive bacteria, cell metabolism was found to be stimulated by intermediate shear stress levels in the case of *Lactobacillus delbrueckii* subsp. *bulagricus* as evidenced by increased biomass concentration [Arnaud et al., 1993], but higher shear forces could weaken bacterial cells [Toma et al., 1991, Arnaud et al., 1993] and even cause inhibition of microbial growth and productivity, which phenomenon is called turbohypobiosis [Toma et al., 1991]. It can therefore be concluded that shearing is likely to markedly affect bacterial viability.

In terms of functionality, bacterial surface proteins mediating adhesion, such as pili, are also likely to be affected by shear stress. Indeed, the role of pili is to maintain adhesion to surfaces, and their action to optimize surface colonization in stressful conditions has previously been investigated [Persat et al., 2015, Björnham and Axner, 2009] although mostly for Gram-negative bacteria responsible of infections. Cell adhesion forces range from a few to hundreds of picoNewtons, which is sufficient to maintain adhesion in many flow environments. In some rare cases, bacterial strains are able to withstand as high as 1 MPa both in terms of functionality and survival shear stresses [Persat et al., 2015]. Pathogenic strains featuring type I and type IV-pili (thin, helix-shaped protein filaments allowing bacteria to interact with and colonize a broad array of chemically diverse surfaces) were even found to feature shear stress-enhanced adhesive properties [Weaver et al., 2011, Pappelbaum Karin I. et al., 2013, Lecuyer et al., 2011], thus contributing to biofilm formation in low shear stress conditions [Persat et al., 2015]. Shear sensitivity of bacterial cells was also found to depend on the composition of their growing medium, which may sometimes favor enzyme production under increased agitation [Joshi et al., 1996]. In some cases, time variations in applied stresses were found to have a higher impact on bacterial cell integrity than the stress magnitude [Foster et al., 1962, Brookman, 1975, Engler and Robinson, 1981b, Engler and Robinson, 1981a].

Only two studies describe the impact of shearing on the adhesive abilities of lactic acid bacteria [Kiekens et al., 2019, Golowczyc et al., 2011]. *Lactobacillus kefir 8321* and *Lactobacillus plantarum* 83114 were found to be still able to adhere to intestinal cells

after spray-drying for atomizing air pressures of 3 bars whereas the strain *Lactobacillus kefir* 8348 showed a significant loss of adhesion capacity [Golowczyc et al., 2011]. In the case of *Lactobacillus rhamnosus* GG, high shear rates were shown to completely shear off pili and significantly affect adhesion ability to Caco-2 cells [Kiekens et al., 2019]. These two studies are first steps in the direction of a better understanding on how food and ferment manufacturing steps may affect bacterial functionality. However, they do not allow distinguishing between mechanical stress (generated by shearing), heat stress (generated by drying), and osmotic stress (experienced during rehydration), all of which that could have different impact on pili expressed by probiotic bacteria or on their adhesive functionality, both being crucial to bacterial probiotic action.

I.3.1.3 Shearing impact on bacterial shape

Environmental stresses such as heat and shear stresses, occurring during powder formulation and LAB encapsulation by spray-drying and extrusion were also shown to induce changes in bacterial shape and organization, such as bacterial chain breakage or fragmentation [Doherty et al., 2010, Guerin et al., 2017b, Kiekens et al., 2019] which in some cases was associated with increased colony forming [Guerin et al., 2017b, Kiekens et al., 2019].

Very little is known about why some bacteria may organize preferentially in chains versus filaments or isolated cells, and whether bacterial chain breakage may be beneficial or detrimental to their survival and functionality in stressful environments. The excellent review by Young et al. proposes possible rationales to explain why bacteria may be of a certain shape or organize in a certain way in given environments [Young, 2006]. This review deals with bacterial shape, and more generally, bacterial organization, in relation to the evolutionary process and their survival value. Different shapes and organizations in different settings were found to enhance nutrient access, motion from one place to another, and escaping predators [Young, 2006, Young, 2007].

Some strains were found to be more likely to grow in chains in high shear force-environments where they would form biofilms, which would increase the number of con-

tacts intertwining with surface elements to resist detachment [Edwards et al., 1989]. Chaining may also provide selective advantage against predation in grazing environments (*i.e.* predation by "peeling" or "shaving" a surface, like what do cleaner fish) [Güde, 1979, Hahn and Höfle, 1999, Jürgens and Matz, 2002, Posch et al., 1999, Shikano et al., 1990], and in environments where chaining is helpful, some bacteria such as *Lactococcus lactis* were found to produce lysins dismantling bacterial chains of their competitors [Mercier et al., 2000, Young, 2006]. Other forms of bacterial organization, such as bacterial filamentation, caused by blocking of bacterial division and elongation of the initial bacterial cell, can also be triggered by environmental conditions or antibiotic treatment and may provide competitive advantages for colonization of biopassive surfaces [Möller et al., 2013]. Under shear stress, some bacteria have indeed been observed to increase in size and featured increased stretching of cell walls, partly due to osmoregulation phenomena which are impacted by a shear-induced increased calcium ion transfer [Berzins et al., 2001, Joshi et al., 1996].

However, most of these perspectives are provided in relation to bacterial survival in tough environments (where survival is difficult), and not in relation to bacterial functionality. Only one study suggests that bacterial organization and bacterial functionality may be correlated in the case of *Lactobacillus acidophilus*, as the gene identified to be responsible of cell-division and cell elongation, *cdpA*, was found to control bacterial adhesion abilities as well [Altermann et al., 2004]. This study does not link with environmental stresses such as shear stress though.

Further research should therefore concentrate on the impact of distinct stresses on bacterial functionality and its relationship to bacterial shape, and aim to draw general trends at the level of bacterial groups such as the LAB group. In this sense, modeling may be a promising approach allowing generalizing trends observed on isolated strains. Shearing impact on bacteria could also be compared for bacterial suspensions and bacteria integrated in a food matrix, in order to evaluate the potential protective effect of the matrix on bacterial integrity.

I.3.1.4 Modeling lactic acid bacteria chains in a shear flow

Lactic Acid Bacteria often grow in chains, which can be modeled by bodies connected to one another by springs with various bending and stretching stiffnesses, that be adapted to stand for different chain rigidity values. In this sense, modeled chains of bacteria can be considered as long entities constituted of smaller building blocks which we will call "dumbbells".

The dumbbell is a toy model arising in all branches of mechanics which features in the development of more complex theories like continuum models of viscoelastic fluids, such as polymer suspensions [Barrett and Süli, 2009, Barrett and Süli, 2018, Bird et al., 1987, Bonito et al., 2006, Degond et al., 2010, E et al., 2004, Isihara, 1951, Luo and Yin, 2017, Masmoudi, 2008, Sato et al., 2017, Schieber, 1991, Stadler et al., 2011, van den Brule, 1990], liquid crystals [Adams and Corbett, 2018, Maffettone and Marrucci, 1992, Uneyama et al., 2014], and active gels and suspensions including bacterial suspensions [Córdoba et al., 2014, Ishikawa, 2019, Furukawa et al., 2014].

As such it has seen extensive consideration, particularly in linear flows and Brownian fluctuations [Sharma and Cherayil, 2011, Zhang and Zhou, 1998, Hernández Cifre et al., 2003, Chiba et al., 1999b, Chiba et al., 1999a, Kobayashi and Yamamoto, 2010, Takamura et al., 1981], alongside with the case of internal viscosity dumbbells [Kailasham et al., 2018, Schieber, 1993]. The elasticity considered in past works has mostly focused on dumbbell stretching as mostly aiming for far-field approximations, especially with the development of the finite extensible nonlinear elastic dumbbell model (FENE) [Bird et al., 1987, Luo and Yin, 2017, Masmoudi, 2008, Samaey et al., 2011, Wang et al., 2009, Watanabe and Matsumiya, 2017], neglecting other modes of deformation and relaxation such as bending, as well as traction forces exerted on the body surfaces in a linear flow.

These modes may translate into interesting behaviors which, combined with the study of traction forces, could help improving our understanding of the potential surface damages suffered by a bead-like chains like such as polymer and bacterial chains, which in some cases may lead to rupture and cause functionality losses. For chains of polymers, these phenomena are commonly called "polymer degradation" and "depolymerization",

"polymer fragmentation", or "chain scission" [Banasiak and Noutchie, 2010, El'darov et al., 1995, Göpferich, 1996, Kostoglou, 2000, Mantzaris, 2005, Mao et al., 2017, Montroll and Simha, 1940, Paturej et al., 2011]. For bacterial chains however, very little is known about dynamics, traction forces, and underlying rationale governing chain integrity and breakage in linear flows [Arnaud et al., 1993, Edwards et al., 1989, Guerin et al., 2017c, Lange et al., 2001], although a better understanding would considerably help optimizing industrial processes involving bacteria, such as in the ferment and food industries.

Another, still under-exploited use of dumbbell models lies in adhesion settings, when considering each body of a dumbbell as a component engaged in adhesive interactions, which may be of relevance in many biological occurrences, ranging from muscle contraction [Smith, 1998] to bacterial adhesion. As shearing has been previously described to impact altogether bacterial viability, functionality, and shape (Sections I.3.1.2 and I.3.1.3), the dumbbell model could push investigations further by evaluating how bacterial adhesion to various molecules, such as fat globules and whey proteins, could impact the way shearing may damage bacterial cell surfaces. A protective or damaging role of bacterial adhesive interactions, such as those occurring in food matrices, on bacterial adhesive abilities could then be investigated.

I.3.2 Modeling shearing impact on dairy matrices containing lactic acid bacteria

I.3.2.1 Importance of lactic acid bacteria and fat on the rheology of dairy matrices

The importance of fat globules in the coagulation process has been especially highlighted in the past ten years [Michalski et al., 2002, Ion Titapiccolo et al., 2010, Corredig et al., 2011, Luo et al., 2017]. Fat globules have been found to modulate casein network formation depending on their size as well as on the composition of the milk fat globule membrane [Michalski et al., 2002, Ion Titapiccolo et al., 2010, Luo et al., 2017]. Small

globules get coated by caseins and actively fasten the gelation process [Ion Titapiccolo et al., 2010, Luo et al., 2017], leading to the formation of fine strands and high storage modulus-cheeses [Luo et al., 2017] whereas native fat globules cannot interact with caseins and their size can cause steric hindrance, therefore leading to the formation of coarser gel strands [Luo et al., 2017]. Fat-protein interactions may also impact cheese texture and rheology [Lamichhane et al., 2018] and Liu et al. (2019) demonstrated that thixotropic properties of composite milk gels such as cheeses were likely to increase with protein content [Liu et al., 2019].

The impact of fat globules on rennet-induced gelation in cheeses is also susceptible to be affected by the presence of bacteria. Lactic Acid Bacteria have indeed been found to gather around fat globules [Oberg et al., 1993, Laloy et al., 1996, Fitzsimons et al., 2001, Lopez et al., 2006] which may hinder the participation of fat globules to cheese network build-up. Bacterial adhesion and production of EPS have also been previously pointed out as key factors impacting dairy products texture [Gentès et al., 2011, Mende et al., 2013, Patrício et al., 2014, Ruas-Madiedo et al., 2002, Surber et al., 2019, Tarazanova et al., 2017, Tarazanova et al., 2018a, Tarazanova et al., 2018b]. As for cheeses which coagulation origins mostly from lactic acidification, as well as for other fermented dairy products, Lactic Acid Bacteria play an even more important role on texture and rheological changes of the product, and their influence on dairy structuration is more complex.

If fat and bacteria play a key role in dairy matrix structuration, they can also in return be affected by various stresses generated by structuration steps. The impact of these stresses on dairy matrices containing fat and bacteria, and in particular of shear stress induced by structuration steps such as stirring, stretching, rolling, and spray-drying, will be investigated in Section I.3.2.

I.3.2.2 Dairy matrices as thixotropic elasto-viscoplastic (TEVP) fluids

During manufacturing, dairy matrices such as cheeses and yoghurts may experience different stresses, including mechanical stresses, such as shearing [Robert and Sherman, 1988, Goh et al., 2005, McCulloch, 2008, Vandenberghe et al., 2017] and heating

stresses [Bonanno et al., 2017]. These stresses are known to play a role in dairy matrices structuration and to influence the final structure of the product [Kindstedt et al., 2004, Goh et al., 2005, McCulloch, 2008, McMahon and Oberg, 2011, Vandenberghe et al., 2017, Gonçalves and Cardarelli, 2019]. Some types of cheeses, such as pasta filata or string cheeses, also experience thermomechanical stresses later in structuration (past flocculation, during cross-linking) during the characteristic step of stretching, the curd being subjected to mechanical work in hot water leading the amorphous structure to transform into an organized, elastic and compact network [Kindstedt et al., 2004, McMahon and Oberg, 2011, Gonçalves and Cardarelli, 2019]. The way dairy products behave in reaction to stress, and therefore the way stress may influence their structuration, depend on the rheological properties of the products considered. Despite the wide diversity of products, a few common rheological characteristics can be drawn out from the existing literature. Previous reviews have indeed identified many dairy matrices to present thixotropic properties, especially acid milk gels, fresh (soft), and semi-hard cheeses [Massaguer-Roig et al., 1984, Korolczuk, 1993, Javanmard et al., 2018, Lakemond and Van Vliet, 2007, Omar et al., 1995, Foegeding et al., 2011, Lamichhane et al., 2018].

Thixotropic fluids can be defined as fluids featuring a flow-induced decrease in viscosity over time [Mewis and Wagner, 2009]. Models integrating both kinetic and thixotropic approaches are called structural-kinetic models. Such models are usually defined by coupling a model describing the fluid behavior under shear stress (using viscosity-related functions), called "constitutive model", and a kinetic model including a shear rate-dependence [Wei et al., 2018, Javanmard et al., 2018]. The kinetic part of such models usually features a structural parameter, often called λ, which monitors the instantaneous degree of structure of the considered fluid, varying between 0 (random dispersion of particles) and 1 (fully structured), often used to describe shear-induced breaking of structure (varying from 1 to 0). Reviews to be addressed when comparing the efficiency and range of applications of structural-kinetic models of thixotropic fluids are those by Mewis and Wagner [Mewis and Wagner, 2009] and Larson [Larson, 2015], although none of these reviews specifically addresses food applications. In single-lambda thixotropic

models, the structural parameter λ is often interpreted as the instantaneous number of links (or other structural units) normalized by the maximum number of units in a fully structured state [Goodeve and Whitfield, 1938, Azikri de Deus and Dupim, 2013]. For example, for acid milk gels, λ could be the normalized number of casein aggregates; for mature cheeses submitted to shearing, λ could be the ratio between the existing number of cross-links and the maximum number of cross-links in a mature, undisturbed state. In the latter case, this ratio can be estimated experimentally using the shear modulus ratio $\frac{G}{G_\infty}$ [Carlson et al., 1987b]. As a first approximation, it is usually assumed that all links have the same strength, and break or form at the same rate.

In addition to present thixotropic properties, dairy products are also known to feature viscoelastic [Faber et al., 2017, Foegeding and Drake, 2007, Houzé et al., 2005, Lucey et al., 2003, Muliawan and Hatzikiriakos, 2007, Muthukumarappan and Swamy, 2017, Niki et al., 2000] and viscoplastic properties [Blair and W, 1953, Javanmard et al., 2018, Kothari et al., 2016, Muliawan and Hatzikiriakos, 2007]. It therefore makes sense to consider dairy matrices as thixotropic elasto-viscoplastic (TEVP) fluids such as described by Ewoldt and McKinley [Ewoldt and McKinley, 2017] and reviewed by De Souza Mendes et al. [de Souza Mendes and Thompson, 2012]. If models for thixotropic [Barnes, 1997, Mewis and Wagner, 2009], viscoelastic [Fraggedakis et al., 2016], and viscoplastic fluids [Balmforth et al., 2014, Bonn et al., 2017] have been proposed, frameworks encompassing all these characteristic to describe the behavior and structuration of TEVP fluids are still rare as important challenges need to be faced when attempting to describe each isolated aspect of the constitutive response of those fluids [Bonn et al., 2017].

In the next section, we will essentially focus on a recently-published TEVP model using a structural-kinetic framework [Wei et al., 2018]. This model is especially interesting as it focuses on transient rheology, describing changes occurring during shearing of TEVP fluids. It uses a comprehensive set of constitutive equations allowing monitoring the fluid behavior and structuration rate when submitted to rheological constraints (stress, strain) [Wei et al., 2018] in a very general case. It is, to our knowledge, the most advanced and "up-to-date" model describing the behavior of matrices in response

to shearing.

I.3.2.3 The ML-IKH model: a comprehensive framework describing TEVP fluids behavior under shear

I.3.2.3.1 General features of this model

Wei et al. generalize a previous scalar thixotropic-only "multilambda" (ML) model [Wei et al., 2016] combined with an isotropic kinematic hardening (IKH) model [Dimitriou and McKinley, 2014]. The "multilambda" part of this model allows taking into account multiple overlapping time scales. In our case, this could be useful to describe the shearing of dairy matrix at a microscopic level, the time scale being different for each matrix component *e.g.* caseins, whey proteins, fat, bacteria, etc. The IKH part of this model allows accounting for hardening behavior, which is a phenomenon in which the amount of stress required to deform a material increases more than proportionally to the strain value, both at constant strain rate and increasing strain [Bast et al., 2015]. This phenomenon has been observed since the early 1950s and an official distinction was made between isotropic and kinematic hardening in 1980 [Weng, 1980]. Isotropic hardening consists in a global increase of the elastic limit (also called "yield stress") which could be due either to tension or compression, when punctually-applied; materials featuring isotropic hardening properties harden until they respond elastically. Kinematic hardening account for tension and compression when applied in cycles, introducing the Bauschinger effect, *i.e.* the fact that the characteristic response to stress and/or strain of materials change as a result of microscopic stress distribution (*e.g.*, materials can globally soften during cyclic compression in addition to harden punctually. Materials featuring hardening properties can therefore exhibit isotropic or kinematic behaviors depending on stress conditions [Weng, 1980]. Although more studied in relation to bread-making [van Vliet, 2008], several dairy products were also found to exhibit hardening behavior and this especially during shearing steps, including whey protein gels [Lowe et al., 2003], β-lactoglobulin gels [Pouzot et al., 2006], casein gels [Rohm et al., 2014], and pasta filata cheeses such as Mozzarella [Huc et al., 2014,Bast et al., 2015,Sharma et al., 2017,Sharma

et al., 2018]. The hardening behavior of these latter cheeses play an essential role during cheese structuration as hot water stretching, rolling, and kneading are indispensable steps in the traditional manufacture of Mozzarella cheeses [Sharma et al., 2018]. Strain hardening behavior was observed during shearing in the longitudinal (fiber) direction and softening in the perpendicular direction [Bast et al., 2015, Sharma et al., 2018] thus resulting in anisotropic plastic deformations (Bauschinger effect). A structural model was recently proposed to explain this behavior at the molecular level, based on microscopic alignments of elongated casein clusters and cross-linked polymers [Sharma et al., 2018]. This model was found to be in agreement with experimental observations [Bast et al., 2015, Sharma et al., 2018]. Main features of this model are represented in Figure for the case of cheeses I.3.2.

Based on Sharma et al. (2018), during the cross-linking phase cheese can be thought of as a continuous, building-up protein gel containing a dispersed phase of fat particles and whey pockets, elongated in the direction of rolling. Although bacteria were not explicitly taken into account, one can reasonably think of them as dispersed particles present in the vicinity of fat or trapped inside whey pockets [Guerin, 2017, Guerin et al., 2017b]. As rolling is performed, generating shear stress, fat inclusions as well as whey pockets get stretched out (due to viscoelastic properties) and cheese experience strain hardening, which leads to three major changes: casein clusters align, initial cross-links become more tightly bound and additional cross-linking occur. The potential role of calcium in the casein network strengthening process is also mentioned [Sharma et al., 2018].

In our case, it is therefore important for hardening behavior to be taken into account when modeling cheese and more generally dairy matrices structuration, in addition to thixotropic and viscoelastic properties; the comprehensive model developed by Wei et al. to describe the transient rheology of TEVP fluids allows encompassing all these charateristics. Four main features of this model enable capturing different aspects of TEVP rheology: (1) Multiple thixotropic structure parameters ("multilambda"), all exhibiting a stretch-exponential thixotropic relaxation behavior when recovering their viscosity af-

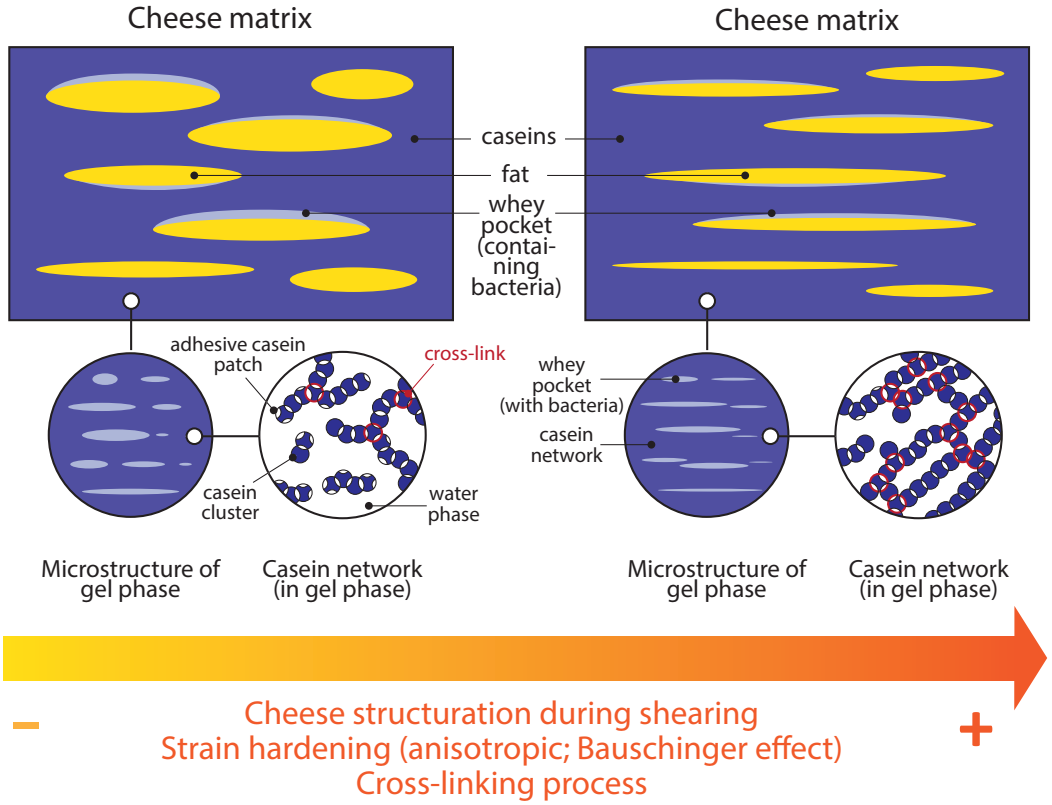

Figure I.3.2: Cheese anisotropic hardening and viscoelastic behavior during shearing for pasta filata cheeses such as mozzarella; "adhesive casein patches" represent the areas of micelles depleted of κ-casein, which are able to stick to other depleted areas in order to form casein clusters during the curd-firming process. This figure was inspired from Sharma et al. [Sharma et al., 2018].

ter earlier shearing; (2) nonlinear thixotropic kinetic equations in both the shear rate or stress and the structure parameters; (3) incorporation of the Armstrong-Frederick kinematic hardening rule [Frederick and Armstrong, 2007] for the evolution of the elastic limit, introducing a term which influences plastic flow differently whether tension or compression forces are applied, depending on the accumulated plastic strain; and (4) viscoelasticity.

This model features 12 equations governed by 12 parameters, four of them controlling the transient response and the others governing steady state. Wei et al. provide both a scalar and tensorial form of their model. The model equations in their scalar form in

relation to dairy matrix structuration, and in particular in relation to pasta filata cheese shearing, will be detailed in the next sections.

I.3.2.3.2 The multilambda parameter as a thixotropic multimodal response to stress

Wei et al. chose to define the structural parameter λ as a linear combination of substructural parameters λ_i such as presented in Eq. (I.3.1). In this section, we will focus on the cross-linking phase of cheeses submitted to shearing such as presented in Fig. I.3.2. In this case, introducing multiple lambdas λ_i allows distinguishing different structuration rates within our system, which could each be associated with a different cheese component such as those represented in Fig. I.3.2 namely fat pockets (potentially including bacteria in their vicinity), whey pockets containing bacteria, casein strands (elongated), and casein polymers. In Eq. (I.3.1), C_i are constant coefficients and N the number of thixotropic relaxation modes of the system. In practice in our case, as a first approximation, a different relaxation mode could be associated with each cheese component earlier mentioned.

$$\lambda = \sum_{i=1}^{N} C_i \lambda_i, \tag{I.3.1}$$

$$\frac{d\lambda_i}{dt} = D_i[-k_{bd}\psi^a \lambda_i^n + k_{bu}\psi^b(1-\lambda_i)^m + k_B(1-\lambda_i)^m]; \qquad b = 0.5,\ m = 1. \tag{I.3.2}$$

Equation (I.3.2), which monitors the evolution of the structure λ_i under shearing, is a modified form of the general λ equation for ideal thixotropic fluids [Wei et al., 2016, Wei et al., 2018]. This equation includes a break-down term $-(k_{bd}\psi^a\lambda_i^n)$ with a break-down constant k_{bd}, and two build-up terms, one shear-induced $k_{bu}\psi^b(1-\lambda_i)^m$ and one Brownian $k_B(1-\lambda_i)^m$ with two build-up constants, k_{bu} and k_B.

Parameters b and m have been fixed numerically by Wei et al. from previous experimental studies [Onogi, 1970, Dullaert and Mewis, 2006, Wei et al., 2016, Armstrong et al., 2016, Wei et al., 2018], in which flow-induced aggregation rate was found to have a square-root dependence on the shear rate or stress ($b = 0.5$), and which showed that

$m = 1$ assuming a linear relationship between λ and viscosity, or between λ and the elastic limit (yield stress). However, these studies did not concern foodstuffs but diverse polymer suspensions, and therefore further experiments may be required to adjust these parameters to our case. In particular, the relationship between viscosity and λ may not be linear; indeed, experimental data collected by Javanmard et al. on acid milk gel suspensions show that λ is more likely to evolve exponentially with decreasing viscosity in a way closer to Michaelis-Menten kinetics [Javanmard et al., 2018], thus the value of m in Eq. (I.3.2 would have to be reconsidered.

Parameters a and n in the break-down term of Eq. (I.3.2) are two adjusting model parameters and can be determined experimentally. The non-linearity of λ_i in ψ in the break-down term was shown by Wei et al. to improve model predictions for the rheology of fumed silica suspensions. This still remains to be proven for cheeses. The best-fit value of n depends on the choice of the flow parameter ψ, which may stand for shear rate, shear stress, or a combination of both [Wei et al., 2018]. The preferred definition for ψ in our case may depend on the manufacturing parameters that can be controlled during the cheese-making process. Wei et al. propose the following expressions for ψ depending whether the stress-controlled (SC) or rate-controlled (RC) form is chosen:

$$\begin{cases} \text{SC form:} \psi & = \max(0, |\sigma_{eff}| - \lambda k_y) \\ \text{RC form:} \psi & = |\dot{\gamma}_p|. \end{cases} \tag{I.3.3}$$

These expressions can be used assuming that thixotropy only occurs upon plastic deformation, *i.e.*, that structural changes occurring during elastic deformations do not lead to the breakage of internal structures (the global degree of structure λ is only affected once the elastic limit k_y is overcome). This appears plausible in our case since experimentally, the microstructural cheese elements were found to fracture irreversibly only for very high shear work [Bast et al., 2015, Sharma et al., 2017, Sharma et al., 2018].

All λ_i share the same steady-state value but their transient behavior differs, *i.e.*, all cheese components would reach in the end a similar structuration level, but on different

time scales. These different transient behaviors constitute the multimodal response of the system to shear stress and are accounted for in Eq. (I.3.2) by the dimensionless pre-factors D_i leading to different time derivatives for each λ_i.

Following stress, the ML-IKH model predicts a global stretched exponential response of the system during relaxation *i.e.* an immediate viscoelastic response which intensity decreases over time. The relevance of such a behavior is attested by previous experimental studies on various polymer suspensions and gels [Berry and Plazek, 1997, Quemada, 1998, de Gennes, 2002, Wei et al., 2018]; however not having been demonstrated for foodstuffs, this behavior appears sensible in regard to the viscoelastic/plastic properties exhibited by pasta filata cheeses once they reach the stretching step. In order to satisfy the global stretched exponential response experienced by the system, C_i and D_i are consequently determined by Eq. (I.3.4)

$$\exp(-t^{\beta}) \approx \sum_{i=1}^{N} C_i(\beta) \exp^{-D_i t} \tag{I.3.4}$$

Where β is the stretching exponent, $0 < \beta < 1$. Eq. (I.3.4) shows the decomposition of the global stretched exponential response into a linear combination of simple exponentials, *i.e.* each cheese component experiences a stretched exponential response during relaxation on a different time scale.

So far, equations have been provided that govern the transient behavior of the system under shear stress as well as during post-stress relaxation, such as what would occur for pasta filata cheeses submitted to shear during stretching and post-stretch relaxation (cross-linking phase). They describe a multimodal response accounting for different time scales depending on the cheese component considered, assuming a global stretched exponential response.

I.3.2.3.3 Incorporation of viscoelastic, viscoplastic, and hardening characteristics

The viscoelastic, viscoplastic, and hardening features of the ML-IKH model are captured by the following set of equations:

$$\sigma = \eta_m \dot{\gamma} + \sigma_s, \tag{I.3.5}$$

$$\lambda\theta\dot{\sigma_s} + max\left(0, \frac{|\sigma_{eff}| - \lambda k_y}{|\sigma_{eff}|}\right)\sigma_{eff} = \lambda\eta_{thi}\dot{\gamma}, \tag{I.3.6}$$

$$\sigma_{eff} = \sigma_s + \sigma_{back}, \tag{I.3.7}$$

$$\sigma_{back} = k_h A, \tag{I.3.8}$$

$$\dot{\gamma}_p = \begin{cases} 0 & \text{if } |\sigma_{eff}| < \lambda k_y, \\ \dfrac{|\sigma_{eff}| - \lambda k_y}{\lambda\eta_{thi}} \cdot \text{sign}(\sigma_{eff}) & \text{if } |\sigma_{eff}| \geq \lambda k_y, \end{cases} \tag{I.3.9}$$

$$\dot{A} = \dot{\gamma}_p - qA|\dot{\gamma}_p| \tag{I.3.10}$$

In equation (I.3.5), σ stands for the total stress experienced by the system, composed of contributions by the medium $\sigma_m = \eta_m\dot{\gamma}$ as well as by internal elastic forces $\sigma_s = G\gamma_e$. In cheese, σ_m could be assimilated to the continuous protein phase (at the macroscopic scale), and σ_s to internal structures such as fat, whey pockets, and bacteria. The expression of σ_m originates from the assumption that the system reaches a constant viscosity η_m once all internal structures (pockets and casein network) are broken down (*e.g.*, cheese melts), and that in the transient regime σ_m is controlled by the total rate of deformation under shear $\dot{\gamma}$. If the latter assumption appears plausible in our case, the first may need some adjustements. Indeed, Sharma et al. have found Mozzarella cheeses to exhibit work-thickening behavior when melting for high applied shear work [Sharma et al., 2016b, Sharma et al., 2016a] and proposed thickening exponential equations to describe this behavior [Sharma et al., 2016b]. The nature of η_m in Eq. (I.3.1) would therefore need to be consequently adjusted, η_m becoming a stretched exponential function. The expression of σ_s comes from the assumption of a linear relationship between elastic de-

formations γ_e induced by internal structures (*e.g.*, when fat or whey pockets move with respect to the medium) and internal forces σ_s, which appear plausible in our case as a first approximation, as the flowability of Mozzarella cheeses was found to be linearly proportional to shear work [Sharma et al., 2016a].

Equation (I.3.6) describes the evolution and potential irreversible deformation of the global structure λ of the system (with η_{thi} plastic viscosity and $\dot{\gamma}$ total strain rate, $\dot{\gamma} = (\dot{\gamma}_e + \dot{\gamma}_p)$, $\dot{\gamma}_e$ and $\dot{\gamma}_p$ respectively elastic and plastic rates) as a function of viscoelastic changes induced by internal forces during the relaxation time θ, and viscoplastic changes induced by the effective stress σ_{eff}. In practice in our case, it means that the cheese structure (how far we are in the cross-linking process and in the rearrangements of cheese matrix components) depends on a balance between viscoelastic internal forces and plastic deformations. Viscoelastic forces are driven by fat and whey pockets trying to "bounce back" to their original form when stretching has been applied, and plastic deformation results from overcoming the elastic limit or yield stress k_y (*e.g.*, the cheese matrix structures irreversibly anisotropically in the direction of elongation, such as what can be found experimentally for high shear work [Bast et al., 2015, Sharma et al., 2016a, Sharma et al., 2016b, Sharma et al., 2017, Sharma et al., 2018]).

Viscoplastic changes are accounted for by the viscoplastic strain rate $\dot{\gamma}_p$, which starts evolving past the elastic limit k_y; the higher the effective stress exerted on the system, the faster the plastic deformation occurs, and the more structured and/or viscous the system is, the more plastic deformations are slowed down.

The effective stress is defined by the sum of internal forces σ_s and of a back stress term σ_{back}, which relates to the hardening properties of the fluid through a hardening constant k_h and a back strain A. Equation (I.3.10), namely the Armstrong-Frederick equation for kinematic hardening, implies that A depends exclusively on the strain histories. In the case where the system considered was only elastic, the material constant q would be null and σ_{back}, A would resume respectively as elastic stress and elastic strain. Depending on the fluid, Jiang et al. mention that slight modifications to Eq. (I.3.10) may need to be accounted for in order to accommodate specific material properties [Jiang and Kurath,

1996]. They propose the following adjustment:

$$\dot{A} = \dot{\gamma}_p - (q|A|)^c \, \text{sign}(A)|\dot{\gamma}_p| \tag{I.3.11}$$

This equation resumes to the original Armstrong-Frederick equation for $c = 1$. Experimentally, Wei et al. work on weakly aggregated fumed silica suspension which validate the original Armstrong-Frederick equation, whereas Dimitriou et al. (2014) needed $c = 0.25$ to accurately predict the rheology dynamics of waxy crude oils [Dimitriou and McKinley, 2014, Wei et al., 2018]. Therefore in the case of cheese, c may need to be adjusted as well.

I.3.2.3.4 Application of the ML-IKH model to cheese structuration

Main variables and parameters used in the ML-IKH model have been summarized in Table I.3.1 and gathered according to the model feature they describe (multimodal relaxation, viscoelasticity, viscoplasticity, thixotropy, hardening).

Quantity	Type	Definition	Cheese analog
Associated model features: Thixotropy, Multimodal relaxation			
λ	variable	structural variable	degree of structural organization of the whole cheese matrix
λ_i	variable	structural variable	degree of structural organization for the i^{th} cheese matrix component
ψ	variable	flow variable	applied stress or strain rate
N	parameter	number of thixotropic relaxation modes	number of components in the cheese matrix
β	parameter	stretching exponent	duration of the relaxation phase after cheese matrix stretching

k_{bd}, k_{bu}, k_B	parameters	break-down and build-up constants	structuration constants for fat globules, casein polymers, bacteria aggregates, and whey proteins after stretching
a,b,n,m	parameters	non-linear dependence of break-down and build-up terms in λ_i	the structuration process of each cheese component depends non-linearly on the intensity of stress/strain ψ applied and of its current structural state λ_i
Associated model features: Viscoelasticity, Viscoplasticity			
σ	variable	total stress	total stress applied on the whole cheese matrix
σ_m	variable	stress arising from the medium	stress arising from the continuous protein phase
σ_s	variable	stress arising from internal forces	stress arising from singular cheese components *e.g.* fat globules, whey pockets, bacteria, caseins if envisioned as discontinuous clusters
θ	variable	viscoelastic relaxation time in the fully structured state	time during which elastic deformations occur due to singular components in the cheese matrix (fat, whey pockets, bacteria, casein clusters)
$\dot{\gamma}$	variable	shear rate	evolution of the total deformation of the cheese matrix overtime (elastic and plastic)
$\dot{\gamma}_e$	variable	elastic rate	evolution of the elastic component of deformation of the cheese matrix overtime
η_m, η_{thi}	parameters	asymptotic and plastic viscosity	viscosity of the whole matrix once all internal elements have broken down* (*variable for thickening pasta filata cheeses) and viscosity of the matrix once stress overcome the elastic limit
G	parameter	elastic modulus	elasticity of the whole cheese matrix

Associated model features: Thixotropy, Viscoplasticity, Hardening			
σ_{eff}	variable	effective stress	total stress felt by the cheese matrix if in the plastic domain
σ_{back}	variable	back stress	stress associated with increased and oriented cross-linking (hardening behavior)
$\dot{\gamma}_p$	variable	plastic rate	evolution of the plastic component of deformation of the cheese matrix overtime
A	variable	back strain	deformation induced by the elongation of casein clusters and increased and oriented cross-linking (hardening behavior)
c	parameter	hardening exponent	the hardening behavior depend on the composition of the whole cheese matrix
k_y, k_h	parameters	elastic limit (yield stress) and hardening constant	threshold between elastic and plastic domain for the whole cheese matrix, intensity of the hardening phenomenon during cross-linking
q	parameter	material constant	characteristic constant related to the overall plasticity of the cheese matrix

Table I.3.1: Variables and parameters used in the ML-IKH (multilambda isotropic kinematic hardening) model for thixo-elasto-visco-plastic (TEVP) fluids proposed by Wei et al. adapted in relation to cheese structuration for pasta filata cheeses during stretching; quantities have been gathered according to the model features they relate to (multimodal relaxation, viscoelasticity, viscoplasticity, thixotropy, hardening).

The model parameters governing the steady state of the system are (assuming $b = 0.5$, $m = 1$, $c = 1$): a,n, k_y, $\frac{k_h}{q}$,$\frac{k_{bd}}{k_B}$, $\frac{k_{bu}}{k_B}$, η_m, η_{thi}.

The model parameters controlling transient response during shearing and shear-induced structuration are: k_B, β, q, G. The parametrization of the ML-IKH model requires three types of experimental data as presented in Table I.3.2: the steady state flow curve, shear stress variations induced by flow reversal tests, and shear stress variations induced by step tests [Wei et al., 2018]. In addition to these three data sets,

Data type	**Definition**	**Parameters determined**
Steady state flow curve	Recorded stress variations when varying the applied strain (or *vice versa*) on the fully mature cheese matrix	η_m $(k_h/q+k_y)$ a n k_{bd}/k_B k_{bu}/k_B η_{thi}
Shear stress variations induced by flow reversal tests (hardening behavior)	Recorded stress variations when, after reaching steady state under shearing, an instantaneous reversal of the shear direction is imposed, while holding fixed the shear rate magnitude	k_h/q q
Shear stress variations induced by step tests (global transient behavior)	Recorded stress variations when the shear rate (or stress) undergo a stepwise change after a period of steady shear	k_B β G

Table I.3.2: Experimental data required to fix the parameters of the ML-IKH (multil-ambda isotropic kinematic hardening) model to fit cheese structuration for pasta filata cheeses during stretching.

additional tests may be needed to adjust parameters b, m as previously mentioned in Section I.3.2.3.2, and parameter c as mentioned in Section I.3.2.3.3.

Although the ML-IKH model has not yet been applied experimentally to foodstuffs, it provides a comprehensive framework which, if applied to cheese structuration during shearing, will allow good understanding and monitoring of structural changes occurring during cheese manufacturing. This model can especially be useful for pasta filata and string cheeses undergoing stretching steps, but may also be of use to understand more generally the impact of shearing on dairy matrices containing lactic acid bacteria. In the next section, a different (simpler) TEVP model will be reviewed, which has been applied

to acid milk gel suspensions. Both TEVP models will be compared, and we will then conclude on the interest of TEVP models in relation to shear-induced dairy matrices structuration.

I.3.2.4 Experimental modeling of sheared acid milk gel suspensions as TEVP fluids

I.3.2.4.1 Dairy matrix microstructure: characteristic particle dimensions

Another recent approach developed by Javanmard et al. (2018) allows correlating λ, *i.e.* the instantaneous global degree of structure of the dairy matrix, with some characteristic dimensions of the aggregates constituting the matrix that could contain bacteria, *i.e.* with the matrix microstructure, when the matrix is subjected to shear stress. These dimensions are the surface-weighted mean diameter $D_{3,2}$, also called Sauter mean diameter (SMD) or surface area moment mean diameter, and the volume-weighted mean diameter $D_{4,3}$, also called De Brouckere mean diameter (BMD) or mass momen mean diameter. Both these dimensions are based on the concept of "equivalent sphere", which consists in measuring some property of an aggregate (surface area, volume, weight, etc.) and assuming that it refers to a sphere instead of an aggregate [Rawle, 2003, Pabst and Gregorová, 2007]. This theoretical sphere would thus be equivalent to our aggregate relatively to the measured property (surface-equivalent, volume-equivalent, etc.), and therefore the diameter of this sphere characterises our aggregate relatively to this same property.

This concept has been illustrated for cross-linked polymers such as those present in cheeses (although this is also valid for simpler clusters such as those present in yogurts) in Figure I.3.3.

The most common ways to approximate an aggregate by a sphere are by using its surface or its volume, using the concept of surface-equivalent and volume-equivalent spheres [Pabst and Gregorová, 2007], such as represented in Fig. I.3.3. For a matrix constituted of n aggregates, each k^{th}-aggregate being approximated by the k^{th}-sphere (equivalent in surface or in volume, depending on the adopted equivalence concept), the Sauter and De Brouckere diameters give information on a theoretical mean particle which

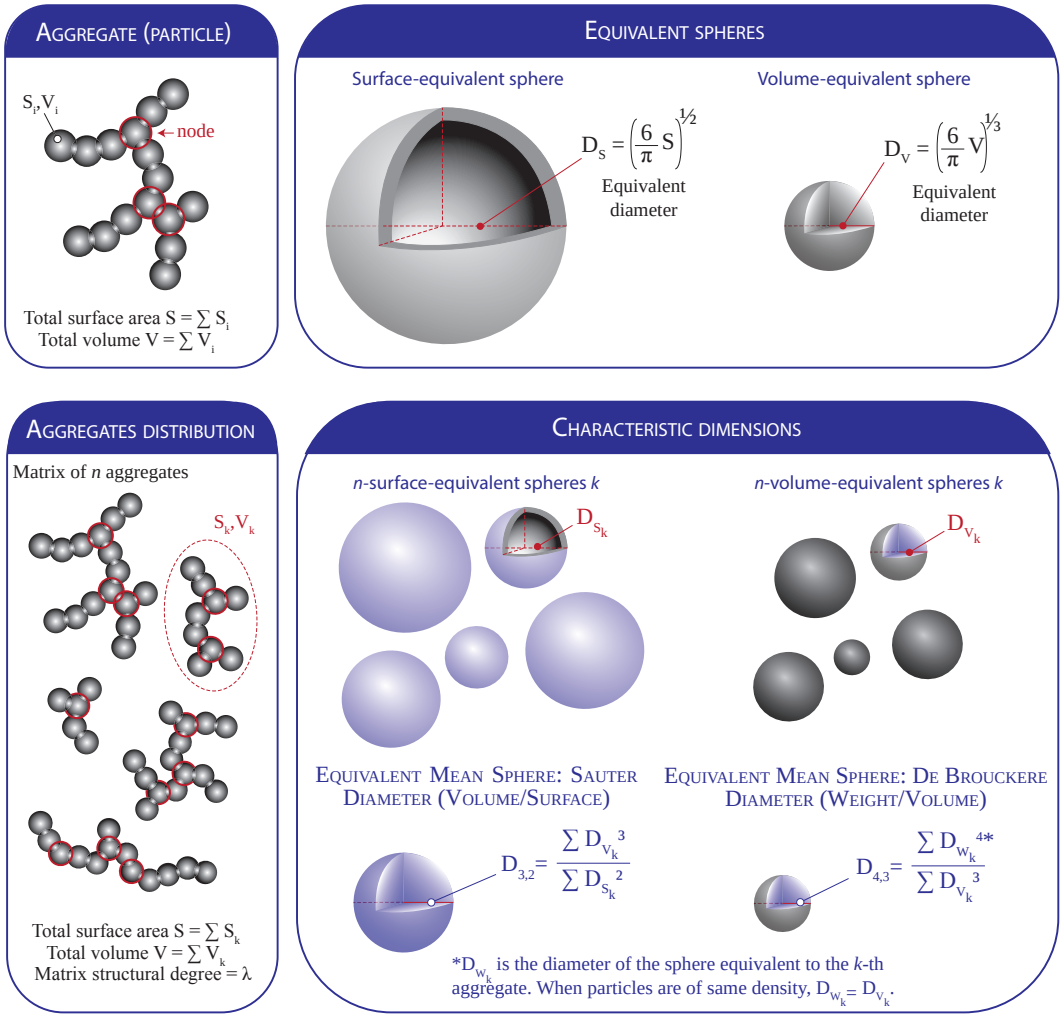

Figure I.3.3: Correlation between the global degree of structure of the dairy matrix λ and the characteristic dimensions $D_{3,2}$ and $D_{4,3}$, respectively the surface-weighted mean diameter and the volume-weighted mean diameter (also called the Sauter and De Brouckere mean diameters) of the bacteria-containing aggregates constituting the matrix.

characterises the matrix microstructure. The diameter of this mean particle depends on the volume:surface ratio using volume-equivalent and surface-equivalent spheres (SMD), or on the weight:volume ratio using weight-equivalent and volume-equivalent spheres (BMD) [Piacentini, 2014], the weight-equivalent sphere being the same as the volume-equivalent sphere in the case of particles of same density [Pabst and Gregorová, 2007].

However in practice, most experimental methods are only able to compute for one type of equivalent sphere at a time [Pabst and Gregorová, 2007], which undifferentiated diameter is called D_i for the i^{th}-particle. The exponential dependence of D_i, *i.e.* $(D_i)^4$, $(D_i)^3$, and $(D_i)^2$ then respectively represents the approximate weight-, volume-, and surface-dependence of the i^{th}-aggregate. This unique equivalent diameter D_i is generally the one used in studies which do not mention the concept of equivalent spheres, such studies providing approximate values of $D_{3,2}$ and $D_{4,3}$, which can lead to confusion. When a unique diameter D_i is used, the expressions for both the Sauter and the De Brouckere diameters are indeed approximated as follows:

$$D_{3,2} = SMD = \frac{\sum(D_{i_V})^3}{\sum(D_{i_S})^2} \approx \frac{\sum(D_i)^3}{\sum(D_i)^2} \tag{I.3.12}$$

(I.3.13)

$$D_{4,3} = BMD = \frac{\sum(D_{i_W})^4}{\sum(D_{i_V})^3} \approx \frac{\sum(D_i)^4}{\sum(D_i)^3} \tag{I.3.14}$$

Where D_{i_W}, D_{i_V}, and D_{i_S} are respectively the diameters of the i^{th}-weight-, volume-, and surface-equivalent spheres, and are approximated by the uniquely measured equivalent diameter D_i, which may be any one of them. When this is the case, the experimental method used may be a clue to determine to which equivalent sphere D_i refers to [Pabst and Gregorová, 2007]. In the case of the Javanmard approach, characteristic particle dimensions were measured using dynamic light scattering with a Mastersizer 2000 (Malvern Instruments, Malvern, UK), which results are volume-based according to the manufacturer. Therefore, the values of $D_{3,2}$ provided by Javanmard et al. are approximates of the real SMD values, using $D_i = D_{i_V}$. However, assuming our aggregates of same density, we have $D_{i_W} = D_{i_V}$ for all spheres, and therefore the values of $D_{4,3}$ provided by Javanmard et al. are the real BMD values. Providing both diameters $D_{3,2}$ and $D_{4,3}$ allows a better characterisation of the microstructure of the matrix in relation to its global degree of structure λ.

I.3.2.4.2 Relationship between macro- and micro-structure of the matrix during shearing

The study by Javanmard et al. was performed on acid milk gel suspensions (dispersions of aggregating particles, which may or may not contain bacteria), which may serve as fresh cheese, spread cheese, or yoghurt models in order to establish a relationship between shear processing, rheology, and food matrix structure [Javanmard et al., 2018] thus providing an interesting insight on the possible physical meaning of λ. Although the work of Javanmard et al. seems to have been more motivated by stirred yoghurt manufacturing than cheese-making, their gelation process, involving glucono-delta-lactone, is similar to those of fresh cheeses such as cottage cheese [Sharma et al., 1980, Makhal et al., 2013], and of low-fat pasta filata cheeses [Joshi et al., 2003,Mizuno and Lucey, 2005,Ismail et al., 2007, Wadhwani et al., 2011]. Indeed, the use of glucono-delta-lactone in cheese-making is known for allowing a better control of pH during gelation as its behavior is more predictable and more easily controlled than bacterial behavior [Lablée, 1988]. A similar gelation process has also been used in cheese models studies [Kelly and O'Kennedy, 2001, Møller et al., 2013]. In this section, we will point out the main features of the approach proposed by Javanmard et al. which can be of value regarding dairy matrix structuration.

Javanmard et al. consider acid milk gels as TEVP fluids and focus on those exhibiting shear-thinning properties [Javanmard et al., 2018]. Such properties have been found mostly in relation to yoghurts, spread, fresh and semi-hard cheeses [Lakemond and Van Vliet, 2007, Korolczuk, 1993, Omar et al., 1995, Foegeding et al., 2011, Huc et al., 2014, Ningtyas et al., 2018], which experience shearing during their manufacturing process and will consequently be our main focus here. Low-fat pasta filata cheeses such as Mozzarella cheeses, although involving a similar gelation process, have been found to exhibit shear-thickening behavior [Sharma et al., 2016b, Sharma et al., 2016a, Sharma et al., 2018].

To apprehend acid milk gels as TEVP fluids, Javanmard et al. combined the thixotropic elasto-viscoplastic model developed by Baravian et al. (1996) for shear-thinning disper-

sions of aggregated particles, with the model developed by Cross for materials exhibiting pseudoplastic behavior in response to structure breakage [Cross, 1965, Baravian et al., 1996]. These models were chosen for their simplicity and their good experimental fit with the case of interest [Javanmard et al., 2018]. The global degree of structure λ was found to evolve exponentially with both characteristic dimensions $D_{4,3}$ and $D_{3,2}$ of the aggregates [Javanmard et al., 2018]. The three constitutive equations of the approach proposed by Javanmard et al. are detailed below:

$$\begin{cases} \text{Baravian model: } \begin{cases} \lambda(t) &= \frac{1}{K}\left(1-\sqrt{\frac{\eta_\infty}{\eta}}\right) \\ K &= 1-\sqrt{\frac{\eta_\infty}{\eta_0}} \end{cases} & \text{(I.3.15)} \\ \text{Cross model: } \eta = \eta_\infty + \dfrac{\eta_0-\eta_\infty}{1+(\tau\dot{\gamma})^m} & \text{(I.3.16)} \\ \text{Characteristic aggregate size: } \lambda(t) = 1-e^{(D_0-D/b)} & \text{(I.3.17)} \end{cases}$$

The Baravian model involves the limiting Newtonian viscosities *i.e.* the zero-shear and the infinite-shear viscosities respectively η_0 and η_∞. As matrices considered are thixotropic, λ and η both depend on shear and time. This model essentially describes the fact that a decrease in viscosity *i.e.* a decrease in η is correlated with the break-down of the global matrix structure, *i.e.* a decrease in λ (shear-thinning behavior). Before the matrix is subjected to any shear *i.e.* at $t = 0$, λ is equal to 1, *i.e.* assuming a fully gelled dairy matrix. Limiting viscosities η_0 and η_∞ can be determined experimentally through steady state measurements [Javanmard et al., 2018] using the narrow-gaps method [Davies and Stokes, 2008, Kravchuk and Stokes, 2013].

The Cross model is a time-independent model which features an inverse exponential dependence of the viscosity on the shear rate $\dot{\gamma}$, modulated by the exponent m and the time constant τ. At low shear rates, viscosity changes are very little, *i.e.* the global degree of structure of the matrix λ is conserved (experimentally, λ remains superior to 0.9 until shear rates becomes higher than 1 s^{-1}). However, at shear rates higher than 1 s^{-1}, viscosity decreases exponentially with the shear rate as fast as $\dot{\gamma}^m$, and λ consequently decreases at the exponential rate of $\frac{m}{2}$ (featuring an inverse square-dependence in η).

This means that the global structure of the matrix, once the effects of shear start to show, gets broken down very fast. It can be noticed that the dependence of η on $\dot{\gamma}$, as well as the dependence of η on λ, present good resemblance with Michaelis-Menten kinetics described by $f(x) = \frac{A}{1+B/x}$, where A and B constants.

The third equation, derived from empirical observations, show that even small changes in the global structure actually translate in big changes at the microstructure level, as the dependence of λ on the characteristic aggregate dimension D (undifferentiated dimension which can refer either to $D_{4,3}$ and $D_{3,2}$, both featuring the same dependence on λ) follows an inverse exponential function, D_0 being the minimal aggregate size reached when $\lambda = 0$. As a result, although λ only lose 5 % of its original value for $\dot{\gamma} = 1$ s^{-1}, $D_{4,3}$ has decreased by 60 % for the same shear rate. Even at very small shear rates such as $\dot{\gamma} = 0.01$ s^{-1}, the aggregates can lose up to 30 % of their original size. This suggests that there is a threshold, which could be argued to be the elastic limit, below which shear-induced microstructural changes are invisible at the global structural level. This is coherent, considering cheese structuration, with the fact that this same phenomenon also occurs earlier: although casein flocculation starts occurring once 60-80 % of the caseins micelles have been hydrolyzed [Carlson et al., 1987a], more extensive hydrolysis (80-90 %) needs to occur for the flocculation to become visible [Dalgleish, 1979, Fox, 1993, McSweeney and O'Mahony, 2016].

Another phenomenon that can be observed using the approach proposed by Javanmard et al. is that, after an intense exposure to high shear rates, applying low shear rate levels (0.001-0.1 s^{-1}) actually promote aggregation phenomena, thus inducing a partial recovery of the original gel structure, in the limit of small aggregates (overgrown aggregates may subsequently get broken down again). This shows the existence of a balance between breakdown (hydrodynamic forces during shear) and recovery (adhesion forces between caseins) depending on the applied level of shear rate. Matrices issued from "breakdown and recovery" experiments where shown to feature a more heterogenous microstructure (wider size distribution) than matrices solely undergoing breakdown, which may favor the formation of electrostatic and hydrogen bonds between aggregates [Hin-

richs and Keim, 2007], thus leading to an observed increase in viscosity and size.

Javanmard et al. support the fact that the global structural variable λ may be used as a proxy for either the instantaneous normalized number of links between aggregates, such as suggested in previous studies [Goodeve and Whitfield, 1938, Azikri de Deus and Dupim, 2013], or for the characteristic size of mean aggregates, thus providing a instantaneous picture of the microstructure in relation to the global structure at a given time. Their study also supports the fact that some aggregation phenomena during dairy structuration may be partially reversible, therefore providing a trigger in the shear-induced structuration process which can be used to obtain a specific final cheese texture [Javanmard et al., 2018]. Javanmard et al. also mention that λ may provide indication on the effective volume fraction occupied by the aggregates in the system, which they aim to look at in future work.

Both the ML-IKH model and the approach proposed by Javanmard et al. provided a better understanding of dairy matrices shear-induced behavior. The ML-IKH model is a comprehensive, detailed model which can be applied to shear-induced structuration of dairy matrices modeled by TEVP fluids. It can take into account hardening behavior as well as the presence of several matrices components through the use of the multilambda parameter. The approach proposed by Javanmard et al. relies on very simple structural expressions but still achieve relating the global structure of shear-thinning dispersions of aggregated particles, such as yogurts, fresh cheeses and semi-hard cheeses, to their microstructural state using characteristic aggregate dimensions. Both these models provide complementary information and may relate to distinct application fields. However, they remain mostly matrix-centered, making it more difficult to estimate the impact of shearing at the scale of the dairy matrix biotic fraction, and in our case especially on bacteria. Although bacteria can be taken into account as a matrix fraction in the ML-IKH model, they are only considered through their rheological properties, as if they were a sole, inert material. The response of living organisms to shear stress applied to their embedding matrix cannot be analyzed from these models. Similarly, no insight can be provided on specific damages that may be caused by shearing, and could lead to bacterial

functionality losses and spatial rearrangements. Further research should concentrate on evaluating and modeling the impact of shearing on the living fraction of food matrices, in order to determine in which cases the matrix can provide a good protection to bacteria with a probiotic potential.

Part II

Questions & Objectives

Most studies discussing bacterial adhesion to food components focused on very few strains at a time [De Bellis et al., 2010, Chumphon et al., 2016, Tarazanova et al., 2017, Tarazanova et al., 2018b, Tarazanova et al., 2018a, Utratna et al., 2017], and up to now no rationale was evidenced which would allow extrapolating results obtained for some strains to a larger group of strains, such as the LAB group. Whereas viability can often be reliably assessed, bacterial functionality, including bacterial adhesive abilities, remains more difficult to ascertain because of its complexity and the lack of information on the associated assessment criteria. Several reviews have highlighted the need for further research targeting bacterial–food interactions and how these interactions are affected by changes in food, thus implying changes in resulting health benefits [Hickey et al., 2015b, Mortazavian et al., 2012, Sanders and Marco, 2010]. The impact of LAB strains on their human hosts has been extensively studied [Carr et al., 2002, Quinto et al., 2014, Sanders and Marco, 2010], but research focusing on the interactions between probiotic LAB and their delivery food format remains relatively scarce. Developing tools allowing characterising adhesive interactions for a wide range of strains and components or molecules of interest would therefore answers the increasing need of industry to better understand the conditions that may favor or hinder probiotic bacteria viability and functionality at the LAB group level, generalizing trends observed on single strains. In particular, a better knowledge of the impact of manufacturing steps that may generate stress on bacteria and potentially induce bacterial functionality losses, such as shearing steps, would especially help with the optimization of food and ferment process design.

Therefore, the three core questions constitutive of my research project have been defined as follows:

1. What are the characteristics and strength of bacterial adhesion to dairy components amongst the lactic acid bacteria group and, in particular, to β-lactoglobulin?

2. How does shear stress impact bacterial integrity (shape and functionality) for the model strain *Lactobacillus rhamnosus* GG?

3. What is the influence of bacterium-particle adhesive interactions on the dynamics

and forces exerted on the bacterial cell?

The scope of the first question concerning dairy components was reduced after preliminary assays to the β-lactoglobulin for two main reasons, which are (i) the fact that adhesive interactions between the model strain LGG and three mutant strains with β-lactoglobulin have been well-studied through atomic force microscopy techniques, thus providing good reference points for future comparison with adhesive abilities featured by other lactic acid bacteria strains, and (ii) the possibility, contrary to micellar caseins and whey protein isolate, to prepare pure β-lactoglobulin solutions, which may simplify results analysis and interpretation.

These questions translated into three objectives, which have been represented in Figure II.0.1.

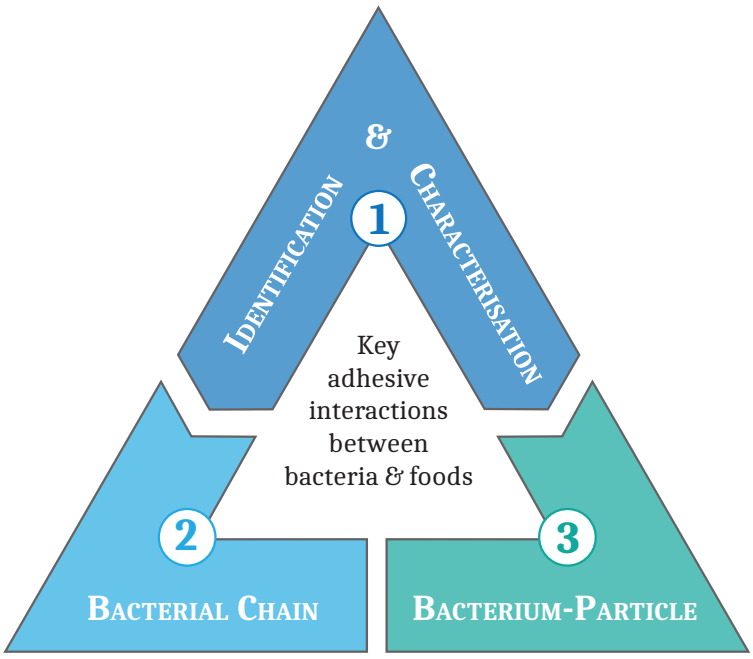

Figure II.0.1: The three objectives of the multidisciplinary research project "Key adhesive interactions between bacteria and food components".

The first objective consisted in identifying and characterising strains presenting adhesive affinities for β-lactoglobulin amongst a collection of 73 lactic acid bacteria strains,

in order to draw general adhesion characteristics within the lactic acid bacteria group.

From this first objective arose the second and third objectives: what and how could these strains be deprived from their adhesive abilities in response to exterior stress? We chose to focus on the impact of shear stress, common in food industry, on the model strain LGG. This impact was studied both for bacteria alone in suspension (second objective) and bacteria engaged in a bacteria-particle interaction (third objective), as if they were part of a more complex matrix.

The adopted strategy to fulfill these objectives involved the following techniques and approaches:

1. Developing a high-throughput method allowing screening quickly bacterial-component adhesive interactions for a wide range of strains and components of interest, later applied to a collection of 73 lactic acid bacteria strains; biophysical techniques were used for characterising the adhesive strains: atomic force microscopy, confocal microscopy, surface protein analysis (genomic approach),

2. A double approach, experimental and theoretical, was used; the experimental approach involved process engineering using a two-fluid nozzle and bacterial suspensions, and the theoretical approach involved both analytical modeling (applied mathematics) and numerical simulations (fluid mechanics),

3. This objective was only studied through modeling for now (analytical and numerical), although experiments have been planned that may be achieved in future work.

This multidisciplinary research project allowed considering bacterial adhesion and adhesive abilities from both a biological perspective and from a physical and mathematical perspective. Experimentally, adhesive interactions and their influence on bacterial location were investigated at the scale of the lactic acid bacteria group, as well as the impact of shearing on bacterial behavior and functionality. Mathematically, the intensity of shear-induced damages occurring on bacterial cell surfaces were correlated with the intensity of surface traction forces exerted on these cells, and tracked numerically on individual bacterial cells, represented as ellipsoidal bodies, as well as on bacterial chains.

The major novelty of this work dwells in the fact that, when experiments drove main research orientations tackled in this project, modeling allowed pushing further some hypotheses and unexplained facts to establish interesting relationships between isolated, experimental conclusions. Most studies up to now have focused either on the biological aspect of bacterial adhesion through *in vitro* and *in vivo* studies [Altieri, 2016, An and Friedman, 1998, Barnes et al., 1999, Burgain et al., 2013b, Conway et al., 1987, Dimitrov et al., 2014, Douëllou et al., 2018, Fernandez et al., 2011, Morelli, 2007, Pizarro-Cerdá and Cossart, 2006, Valerio et al., 2006] and genomics/protemics studies [Desvaux et al., 2006, Desvaux et al., 2018, Chagnot et al., 2013, Giaouris et al., 2014, Jaglic et al., 2014], or on the physical aspect of adhesive interactions using modeling and biophysical techniques [Andersson et al., 2006b, Andersson et al., 2006a, Beaussart et al., 2013, Björnham and Axner, 2009, Jeanson et al., 2011, Kowalik et al., 2018, Lu et al., 2015, Ong et al., 1999, Ponnuraj et al., 2003, Rangel et al., 2013]. However studies allowing relating both biological and physical aspects to explain a given phenomenon remain rare.

Another innovative feature of this project resides in the multiscale approach. Indeed, bacterial adhesion is studied both at the bacterial suspension level through laboratory-scale experiments and at the single-cell level through the use of biophysical techniques and modeling. This double approach thus allows refining our understanding of collective bacterial behavior and relating it to micro-phenomena likely to induce macro-scale responses.

This dissertation has been organized around five main parts which are a literature review (Part I), research questions & objectives (Part II), material and methods (Part III), results and discussion (Part IV), and conclusions and perspectives (Part V).

This research project led to six first-author publications, four of them included as chapters in *Results and Discussion* and the latter two incorporated in the *Literature review* section. Scientific valorization (effective publications, oral communications, posters, collaborations, etc.) is detailed in Part VII.

Part III

Material and Methods

III.1

Material

III.1.1 Preparation of milk components solutions

Micellar caseins (Promilk 872 B) and Whey Protein Isolate (WPI, Promilk 752 FB) powders were provided by Ingredia IDI (Arras, France). β-lactoglobulin (β-lac), α-lactalbumin (α-lac), and Bovine Serum Albumin (BSA) were provided by Sigma-Aldrich Co. LLC, St Louis, MO, USA. Milk Fat Globule Membrane (MFGM) was extracted from bovine raw milk at the laboratory following a two-steps isolation method previously described [Holzmüller and Kulozik, 2016].

Milk proteins and MFGM solutions were prepared by dissolving each component in sterile water (1 % w/w) and solutions were homogenized for a minimum of 2 h at ambient temperature. All proteins and MFGM solutions were used to validate the screening method. Only β-lactoglobulin and BSA were used for shearing experiments.

III.1.2 Bacterial strains and cultures

III.1.2.1 Bacterial strains

Four control strains were used to validate the high-throughput screening method as well as for the shearing experiments, which are the model strain *Lactobacillus rhamnosus* GG ATCC53103 (LGG wild type, "WT") and three derivative mutant strains: LGG *spaCBA* CMPG 5357, impaired in pili synthesis [Tripathi et al., 2013], LGG *welE* CMPG5351, im-

paired in long, galactose-rich exopolysaccharides (EPS) production [Lebeer et al., 2009], and LGG *welE-spaCBA* CMPG5355, double mutant [Lebeer et al., 2012] impaired both in pili synthesis and exopolysaccharides production. The adhesion properties of these strains have been previously described [Guerin et al., 2016, Lebeer et al., 2012, Tripathi et al., 2013, Tripathi et al., 2012]. These four control strains were kindly provided by Dr Sarah Lebeer (Centre of Microbial and Plant Genetics, K.U. Leuven, Leuven, Belgium, and Department of Bioscience Engineering, University of Antwerp, Antwerp, Belgium).

The screening method was then applied to a collection of 73 LAB strains. The 73 LAB strains used in this work are listed in detail in Appendix A.1 This collection of strains has previously been studied for their genomics and surface properties [Sun et al., 2015]. The model strains LGG WT and the mutant strain LGG *spaCBA*, which adhesive properties of both are well-known [Guerin et al., 2016, Lebeer et al., 2012, Tripathi et al., 2012, Tripathi et al., 2013] were respectively used as positive (adherent) and negative (non-adherent) control strains.

Two strains out of the collection of 73 LAB strains were analyzed using AFM, *Lactobacillus aquaticus* DSM 21051 and *Lactobacillus sharpeae* DSM 20505. The model strains LGG WT and the mutant strain LGG *spaCBA*, were respectively used as positive (adherent) and negative (non-adherent) control strains.

III.1.2.2 Bacterial cultures in tubes

III.1.2.2.1 Screening method validation

All strains were cultivated at 37 °C overnight in 10 mL of liquid MRS medium [De Man et al., 1960] inoculated each with 100 μL of frozen cultures stored at -80 °C. The next day, the suspensions were centrifuged at 3618 *g* (*i.e.* 3,000 rcf) for 10 min. The resulting cell pellets were resuspended in phosphate buffered saline (PBS, P4417, Sigma-Aldrich Co. LLC, St Louis, MO, USA) adjusted at pH 6.8, centrifuged (3,618 *g*, 10 min) and resuspended again in PBS (pH 6.8). Bacterial suspensions were then diluted until reaching an optical density of 0.5 at 595 nm (OD_{595nm}=0.5) and were subsequently used for adhesion assay. Triplicates on independent cultures were performed as well as duplicates

by strain.

III.1.2.2.2 Experimental shearing

All strains were pre-cultivated at 37 °C overnight in 10 mL of MRS medium (de Man, Rogosa and Sharpe) inoculated with 100 μL of frozen cultures previously stored at -80 °C. The next day, 100 μL of the pre-cultures were used to inoculate 10 mL of MRS medium and the suspensions were left for incubation at 37 °C until they reached an optical density of 0.8 at 595 nm. Bacterial suspensions were then centrifuged at 3,618 g for 10 min at ambient temperature. The resulting cell pellets were resuspended in phosphate buffered saline (PBS, P4417, Sigma-Aldrich Co. LLC, St Louis, MO, USA) adjusted at pH 6.8 and the resulting bacterial suspensions were subsequently used for shearing experiments. Triplicates on independent cultures were performed as well as six replicates of shearing experiments by strain for a given culture.

III.1.2.3 Bacterial cultures in 96-well microplates

III.1.2.3.1 Screening method validation

Bacterial cultures describe in this paragraph relate to the validation of the high-throughput screening method. Four tubes containing 10 mL of MRS were inoculated each with 100 μL of frozen cultures stored at -80 °C and homogenized. Their content was immediately distributed on a medium binding 96-well microplate (200 μL by well) and incubated overnight at 37 °C. The mother microplate was replicated the next day using 5 μL to inoculate 200 μL of MRS by well using an automated liquid handling system for 96-well plates (Freedom Evo, TECAN Gmbh., Austria); daughter microplates were cultivated at 37 °C overnight and frozen at -80 °C. For each series of experiments a daughter microplate was thawed and replicated on working microplates using 5 μL to inoculate 200 μL of MRS by well. The working microplates were prepared the day before the adhesion assay and incubated overnight at 37 °C. The day of the adhesion assay, the working microplates were centrifuged at 1,642 *g* (*i.e.* 2,000 rcf) for 20 min. The resulting cell pellets were resuspended in PBS (pH 6.8), washed by centrifugation (1,642 *g*, 20 min) and resuspended again in PBS (pH 6.8). Bacterial suspensions were then diluted until

reaching an OD_{595nm} of 0.5 and were subsequently used for adhesion assay. Triplicates on independent cultures were performed as well as twelve repetitions by strain.

III.1.2.3.2 Collection of 73 lactic acid bacteria strains

For each series of experiments, a 96-well microplate previously stored at -80 °C was thawed and replicated on working microplates using 50 μL of bacterial suspension to inoculate 150 μL of MRS by well. The working microplates were incubated at 30 °C two days before the adhesion assay. During the adhesion assay, microplates were only centrifuged once at 1,642 *g* for 20 min, emptied and the resulting cell pellets were resuspended in 200 μL of PBS adjusted at pH 6.8. Triplicates on independent cultures were performed as well as duplicates by strain on each plate (6 repetitions for control strains).

III.1.2.4 Bacterial cultures for atomic force microscopy

Cultures were prepared according to Guerin et al. (2018a). Precultures of *Lactobacillus aquaticus* DSM 21051 and *Lactobacillus sharpeae* DSM 20505 were prepared by inoculating 9 mL of MRS broth with 100 μL of bacterial stock and grown overnight at 37 °C. These precultures were used to inoculate 9 mL of fresh MRS broth the next day and the growth was performed at 37 °C until an optical density of 1.2 was reached at 660 nm (for about 8 h). Cultures were then centrifuged at 3,000 *g* for 10 min at 156 room temperature. Pellets were suspended in 1 mL of PBS (pH 6.8).

III.2

Identification of adhesive interactions

III.2.1 Microplate coating

Six-well high-binding microplates were used for microscopy measurements (Costar 3506, 6-well cell culture plate, non-pyrogenic polystyrene, Corning Inc.). Other experiments involved 96-well microplates (Corning 3361, 96-well assay plate, clear flat bottom, high-binding, polystyrene sterile, and Corning 3370, 96-well assay plate, clear flat bottom, medium binding, polystyrene sterile, Corning Inc.). Two hundred microliters vs. 1.5 mL of the milk component solution were then respectively introduced by well on high-binding 96-well vs. 6-well microplates (for shearing experiments, one half of each microplate contained β-lactoglobulin-filled wells, and the other half contained BSA-filled wells). Microplates were stored at 9 °C overnight. Immobilization occurred through physicochemical interactions between the microplates' material and the components of interest. Wells were washed twice the next day with 300 μL vs. 3 mL of PBS supplemented with the blocking reagent Tween 20 (PBST, 5 % Tween 20 v/v, pH adjusted at 6.8) and adjusted at pH 6.8, respectively for 96- well vs. 6-well microplates.

III.2.2 Strain adhesion and growth monitoring

One hundred and twenty μL and 1.5 mL of each diluted bacterial suspension were introduced into each well of high-binding 96-well and 6-well microplates, respectively, where the milk components had been immobilized. This was done either manually (cultures in tubes and 6-well plates) or automatically (cultures in 96-well plates). The high-binding microplates were incubated for 1 h respectively either at 37 °C for the LGG strains when validating the method, or 30 °C for the collection of 73 LAB strains in order to match the diversity of the growing conditions for all strains [Gomand et al., 2018]. Each well was then washed 5 times using 300 μL and 3 mL of PBST (pH 6.8) for 96-well and 6-well microplates, respectively, to eliminate non-adherent strains. Two hundred microliters and 1.5 mL of MRS for 96-well and 6-well microplates, respectively, were finally introduced into each well and bacterial growth was monitored through OD_{595nm} measurements over 24 h (respectively 48 h for the collection of 73 LAB strains). For 96-well microplates, 5 μL of fresh, non-diluted cultures of LGG WT, *spaCBA*, *welE*, and *welE-spaCBA* were also added into additional wells already filled in with MRS; these wells stand for controls allowing to assess the viability of the strains tested through growth monitoring. All actions featuring 96-well microplates were automatized using automated liquid handling system for 96-well microplates.

III.2.3 Correlation between bacterial growth and bacterial adhesion

The wild type strain and derivative mutant strain *spaCBA* CMPG 5357 were tested with β-lactoglobulin using two 6-well microplates. Culture in tubes were performed and bacterial adhesion was assayed in two microplates in parallel. Adhesion ability was measured either directly by visual observation of adhered cells using a microscope, or indirectly by monitoring growth. Microplates used for microscopic measurements were dried, stained with crystal violet and washed with PBS (pH 6.8). The wells were then emptied, washed once with 1.5 mL of PBS (pH 6.8) and dried out again. Microscopic observations were

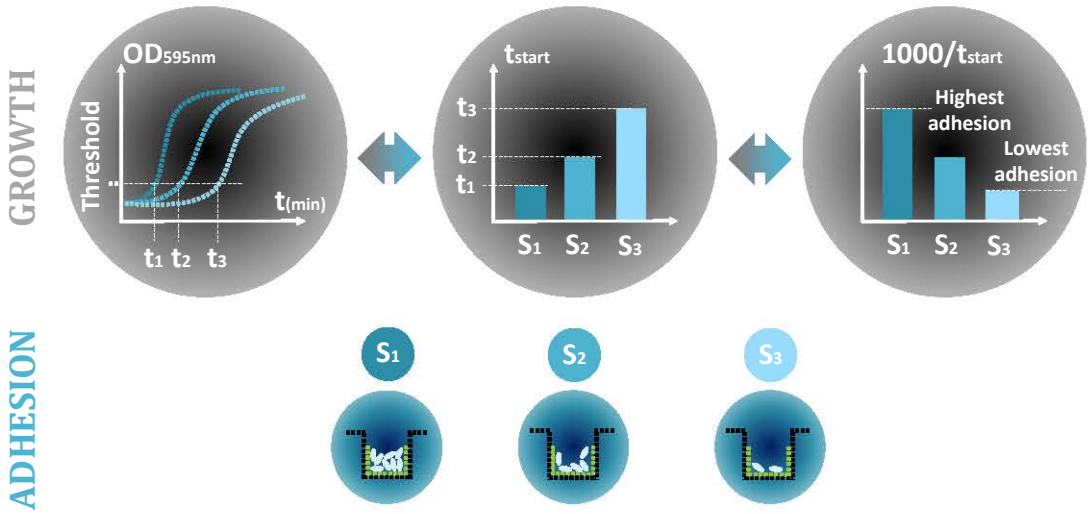

Figure III.2.1: Visual representation of the times values t_{start} at which apparent growths start and the corresponding levels of adhesion for three hypothetical strains presenting adhesive differences.

performed using an Olympus microscope alongside with Toupcam software. Experiments were performed in triplicates for independent cultures with duplicates by strain.

III.2.4 Strain growth comparison

Strain growth comparison was performed using (i) times at which the apparent bacterial growth starts, called t_{start} , and (ii) Minimum Adhesion Values (MAV). Figure III.2.1 gives a visual representation of the equivalence between the t_{start} and the level of adhesion for three hypothetical strains presenting different adhesive affinities: S_1 is a highly adhesive strain, S_2 a medium adhesive strain, and S_3 a poorly adhesive strain.

The time values t_{start} match an OD_{595nm} threshold which was defined according to the baseline corresponding to the absence of growth detection. This baseline was defined by experiment and baseline values used range from 0.3 to 0.4. The higher the t_{start} values are, the later the growth starts *i.e.* the fewer bacteria have adhered *i.e.* the lower the affinity. In order to be proportionally and visually representative of adhesion ability the value of $1000/t_{start}$ was calculated.

For a given strain, the Minimum Adhesion Value corresponds to the difference be-

tween the smallest averaged t_{start} (highest adhesion) obtained on a control without β-lactoglobulin, and the highest t_{start} (lowest adhesion) obtained on β-lactoglobulin:

$$\text{Minimum Adhesion Value (MAV)} = (t_{start} - \sigma)_{control} - (t_{start} + \sigma)_{\beta-lac} \qquad \text{(III.2.1)}$$

Where σ stands for standard deviation. A strain is considered to adhere to β-lactoglobulin if its MAV is significantly superior to zero for all three series of experiments.

III.3

Characterisation of adhesive interactions

III.3.1 Adhesive interactions characterised through atomic force microscopy

Atomic force microscopy (AFM) allows observing and characterising the physico-mechanical properties of a surface, but also interactions occurring between two components of interest, one of them being fixed on the probe which is then called "functionalized", and the other immobilized on a piezoelectric surface (Figure III.3.1). Monitoring structural dynamics in response to environmental stimuli is also possible [Burgain, 2013]. Two main acquisition modes can be distinguished: the topographic mode and the spectroscopic mode. In our case, we used the spectroscopic mode to characterise the interactive behavior between bacterial cells (immobilized on mica) and dairy components. The topographic mode was only used to ensure that interactions monitored were those between the cells and the dairy components (and not the mica itself).

Protocols used in this part have been adapted from previous work [Guerin et al., 2018b]. Briefly, in our case, this method consists in immobilizing the bacterial strains of interest on functionalized gold-coated mica by deposing the bacterial suspension during

15 h at 4 °C (pH 6.8). The mica is rinsed with PBS (pH 6.8) before use. Milk proteins are prepared in distilled water (1 % w/w) and adsorbed on modified AFM probes (gold-coated and with NH2-terminated PEG linker) by immersion for 15 h at 4 °C and then rinsed with milli-Q-grade water before use. Force measurements are performed at room temperature in PBS buffer (pH 6.8). AFM force distance curves are obtained by following the cantilever deflection as a function of the vertical displacement of the piezoelectric scanner with a scan speed of 400 mm/s. Adjustments to this protocol are listed below.

III.3.1.1 Preparation of bacteria-coated mica and protein-coated tips

According to Guering et al. (2018a), a mica coated with a gold layer functionalized with a NH2-terminated PEG-linker (Novascan, Ames, Iowa, USA) was used, as well as AFM probes with borosilicate glass particle (2 μm), coated with gold and modified with NH2 terminated PEG linker (Novascan, Ames, Iowa, USA). The bacterial suspension is deposed on mica at 4 °C and left overnight (pH 6.8). Preparation of the β-lactoglobulin and Bovine Serum Albumine (BSA) 1 % (w/w) solutions (Sigma-Aldrich Co. LLC, St Louis, MO, USA) was done according to Guerin et al. (2018a). Probes tips were left to incubate overnight at 4 °C in wells containing 1 mL of the β-lactoglobulin or BSA solutions to maximize protein adsorption. β-lactoglobulin was the candidate protein tested and BSA was the negative control.

III.3.1.2 Atomic force microscopy measurements

Protocol followed is described by Guerin et al. (2018a) and experimental settings are represented in Figure III.3.1. AFM allows obtaining force-distance curves from cantilever deflections as a function of vertical displacements of the piezoelectric scanner such as represented on Figure III.3.2. Deflection events are measured using a laser beam focused on the terminal part of the cantilever (Fig. III.3.1). Deflection events are then converted to forces using Hooke's law $F = -kd$ where k is the cantilever spring constant in N.m^{-1} and d the cantilever deflection in m. Force-distance curves are obtained in two steps (Fig. III.3.2). The probe tip and the surface are first far apart from one another (1). As the tip gets closer to the surface, the cantilever may bend up- or downwards due to attractive or

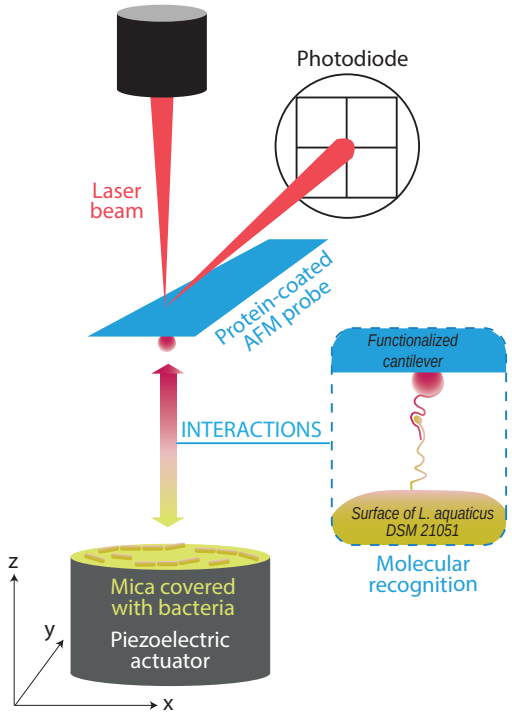

Figure III.3.1: Experimental settings of atomic force microscopy (AFM) when measuring adhesive interactions between lactobacilli (*Lactobacillus aquaticus* DSM 21051 *e.g.*), and milk proteins.

repulsive forces (2). The probe finally comes into contact with the surface when attractive forces exceed the sum of the spring constant and the gradient of repulsive forces (3). The second step consists in the probe retraction from the surface (Fig. III.3.2). Retraction curves resulting from this step are the ones that have been analyzed in our study. As the probe pulls away from the surface, interactions may cause the stretching of components involved in the interaction thus giving an evaluation of their viscoelastic properties (4). Eventually, the probe detaches from the sample (5). The number of rupture peaks, the maximal adhesion force, the maximal rupture force, and the rupture length are all characteristics of the interaction and components studied. For a given experiment many force-distance curves are analyzed. The percentage of specific signatures observed on all curves analyzed which is called "percentage of adhesive events" constitutes therefore another indicator of the interaction specificity. In our case, we focused essentially on

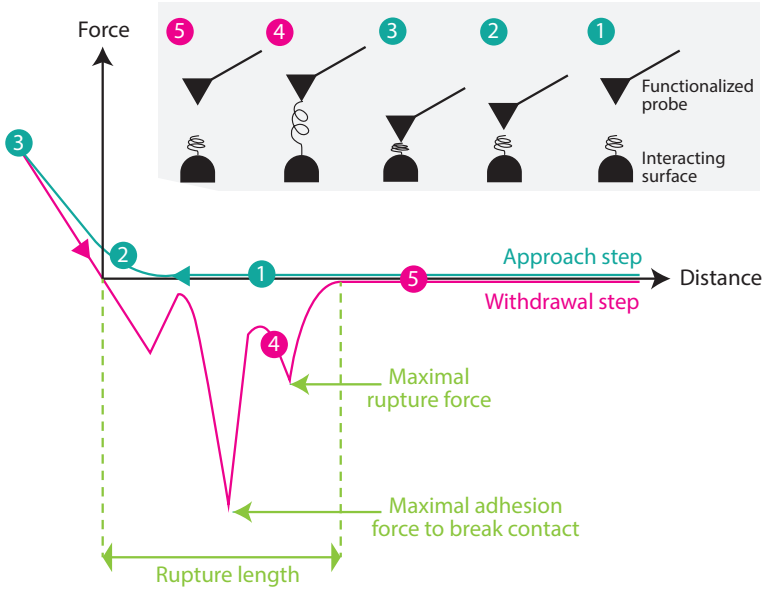

Figure III.3.2: Typical force-distance curve obtained using atomic force microscopy in spectroscopic mode for specific interactions occurring between a functionalized probe and an interacting surface.

three indicators: the percentage of adhesive events, the adhesion force, and the rupture length.

Force-volume measurements are performed at room temperature in PBS buffer (pH 6.8) using a Bruker Bioscope Resolve atomic force microscope (Bruker corporation, Santa Barbara, CA) mounted on an inverted microscope (DMi8, Leica 171 microsystems). The spring constants of the cantilevers was measured using the thermal noise method and found to be 0.01 N m^{-1}. Force distance curves were recorded between the bacteria deposited on functionalized mica and the probe coated with β-lactoglobulin or BSA.

Some shortcomings of this method can be pointed out. Like all microscopic methods, the representativity of the data sets analyzed remains a sensitive subject. Several repeats must be done to ensure the reliability of the results. Also, as the two components/organims involved in the interaction are immobilized (one on the probe, the other on the surface), part of complex components such as unfolded globular proteins or micelles may be overexposed. The interaction is "forced to occur" between the two

components/organisms: therefore, it may not be representative of interactions occurring in suspensions, where the part exposed in AFM may remain hidden within the structure in its native state. Therefore, it is interesting to compare this technique with other less "invasive" techniques mimicking conditions closer to real suspensions.

III.3.2 Adhesive interactions imaged by confocal microscopy

The cultures were prepared as described in Section III.1.2, then centrifuged at 3,000 *g* for 10 min at room temperature. Pellets were suspended in 10 mL of WPI solution (15 %, w/w). The WPI solution was prepared using PRODIET 90 S (Ingredia, Arras, France) which is a soluble milk protein isolate containing native whey proteins including β-lactoglobulin. One milliliter of resuspended cells was stained with the LIVE/DEAD BacLight viability kit (1:200 v/v; LIVE/DEAD BacLight viability kit was prepared according to the procedure described for the kit L13152 by ThermoFisher Scientific). Two hundred microliters of suspension containing LAB were introduced on chambered glass slides (Nunc Lab-Tek, ThermoFisher Scientific). Confocal Laser Scanning Microscopy (CLSM) images were taken using a Leica TCS SP5-X-AOBS confocal laser scanning microscope (Leica Microsystems CMS GmbH, Mannheim, Germany) equipped with WLL lasers. Experimental settings are represented in Figure III.3.3. The objective lens used was a HCX PL APO CS 100 x 1.40 (oil immersion). The excitation wavelength was 488 nm and emission bandwidth was of 495-510 nm for SYTO 9 and 600-620 nm for propidium iodide.

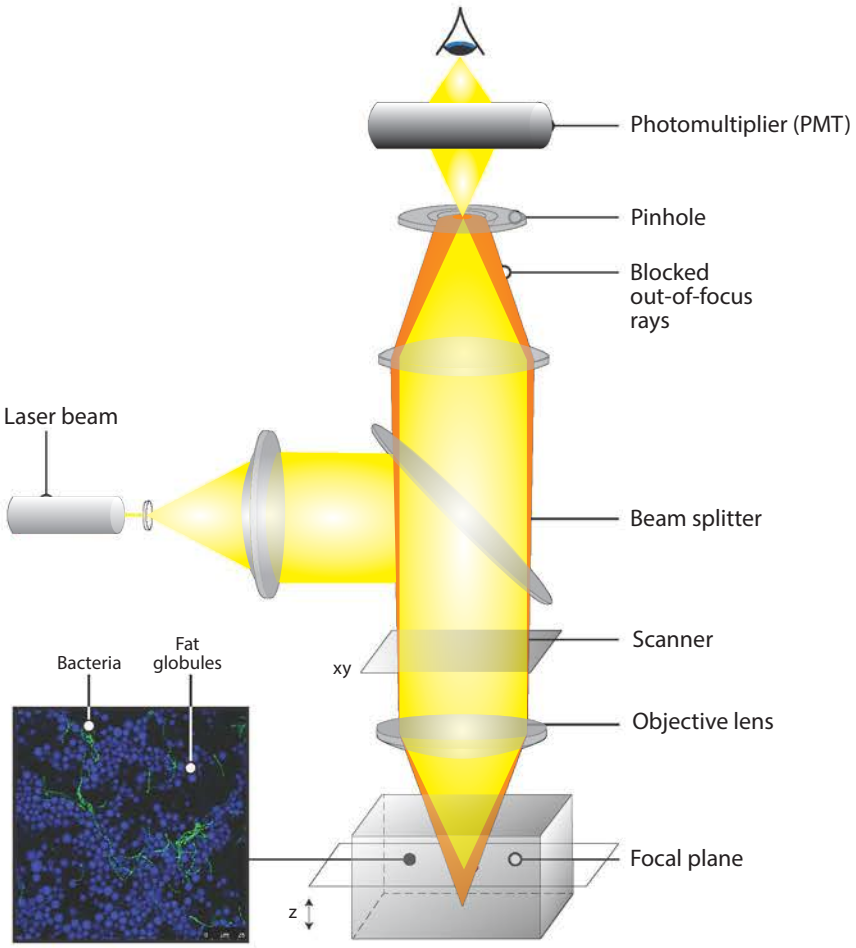

Figure III.3.3: Experimental settings of confocal laser scanning microscopy (CLSM) when observing bacterial spatial distribution relatively to fat globules in various milk media.

III.4

Shearing experiments

Bacterial adhesion to β-lactoglobulin and bacterial chain size distribution were experimentally evaluated on model strains before and after shearing in order to estimate the impact of shear stress on bacterial functionality and physical state. In this study, bacterial adhesion was considered to constitute an indicator of bacterial surface integrity. Bacterial adhesion to bovine serum albumin (BSA) was also recorded as a negative control, owing to the low adhesive affinity of LGG for BSA [Guerin et al., 2018a,Guerin et al., 2016, Gomand et al., 2018]. A general overview of the experimental setup is displayed in Figure III.4.1.

III.4.1 Calculation of spray-drying characteristic shear rates

Bacterial suspensions were sheared using a bi-fluid nozzle composed of a Fluid Cap 60100 and an Air Cap 120 (Spraying Systems Co., Wheaton, IL, USA; inner and outer diameters of the liquid channel: $D_{i_L} = 1.524$ mm and $D_{o_L} = 2.540$ mm; air channel inner diameter: $D_A = 3.048$ mm). The bacterial suspension was pumped into the nozzle through a 48-mm tube using a peristaltic pump (VWR International Europe bvba, Leuven, Belgium) such as presented in Fig. III.4.1. Liquid flow rate was fixed at $\dot{q}_B = 20.3 \pm 0.32$ mL.s^{-1}. Shear rate was monitored by modifying the air pressure (0.2, 0.4, 0.6, 1, and 4 bars).

A review on two-fluid atomization written by Hede et al. (2008) [Hede et al., 2008] and a study performed by Ghandi et al. (2012) [Ghandi et al., 2012] were used to calculate

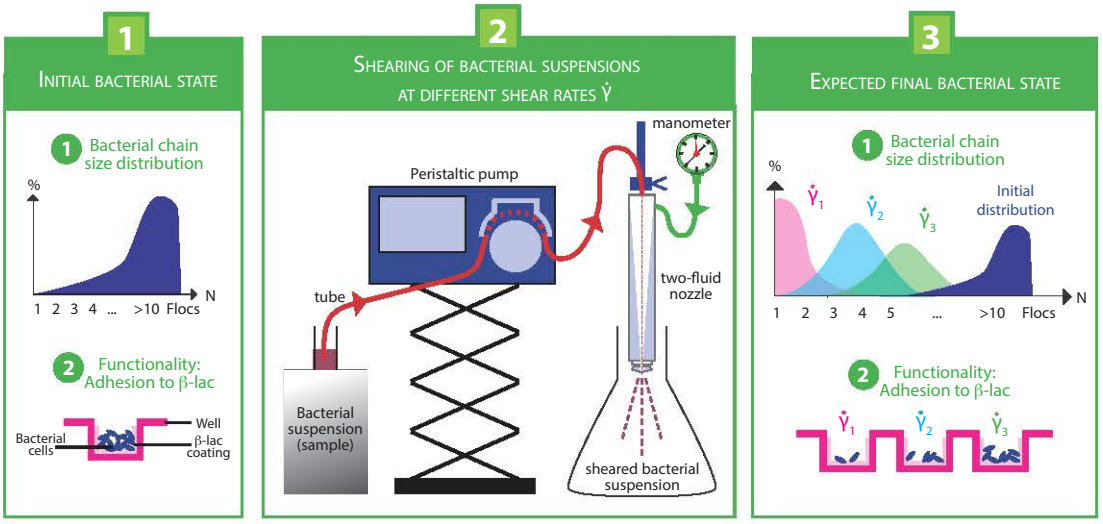

Figure III.4.1: Overview of the experimental system allowing the determination of the impact of shear stress on bacterial functionality (through bacterial adhesion) and bacterial physical state (through bacterial chain size distribution); "β-lac" stands for "β-lactoglobulin".

the shear rates corresponding to the investigated range of air pressures. Hede et al. give a comprehensive overview of the role of formulation, nozzle geometry, and feed and gas flow rates for two-fluid nozzles introducing basic nozzle theory and thermodynamics, and can be referred to for more detailed information on these matters [Hede et al., 2008]. Ghandi et al. (2012) give directions to determine characteristic shear rates for an external mixing two-fluid nozzle such as represented in Figure III.4.2 from the velocities of air and bacterial suspension v_A, v_B, the mass flow rates of air and bacterial suspension $\dot{m}_A$, $\dot{m}_B$, and nozzle characteristics (diameters D_{i_L}, D_{o_L}, D_A). Characteristic shear rates were calculated based on the two following equations [Ghandi et al., 2012]:

$$\dot{\gamma} = \frac{2(v_{av} - v_B)}{D_{i_L}} \tag{III.4.1}$$

$$v_{av} = \frac{v_A \dot{m}_A + v_B \dot{m}_B}{\dot{m}_A + \dot{m}_B} \tag{III.4.2}$$

Where v_{av} is the average velocity in the mixing zone, assuming transfer of momentum between the bacterial suspension and air which both leave the atomization zone at con-

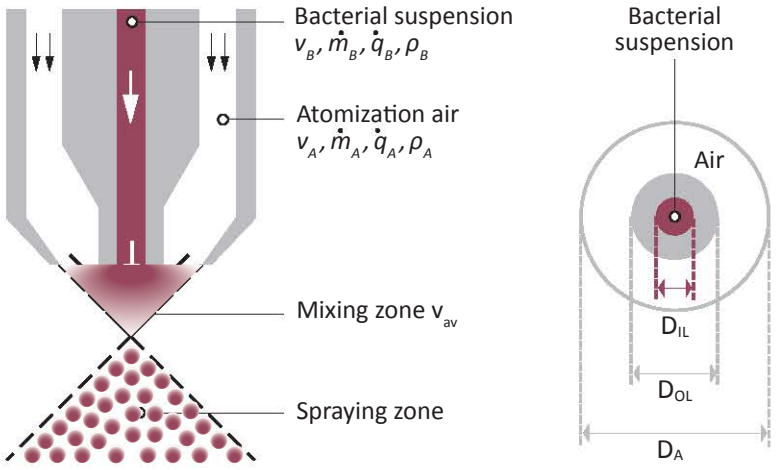

Figure III.4.2: Vertical (*left*) and horizontal (*right*) cross-sections of the external two-fluid nozzle used for shearing experiments, adapted from Ghandi et al. (2012) [Ghandi et al., 2012]. Bacterial suspension and atomization air respectively have velocities v_B, v_A, mass flow rates $\dot{m}_B$, $\dot{m}_A$, volumetric flow rates $\dot{q}_B$, $\dot{q}_A$, densities ρ_B, ρ_A, and v_{av} average velocity in the mixing zone; inner and outer diameters of the liquid channel: D_{i_L}, D_{o_L}; air channel inner diameter: D_A.

stant velocities, respectively v_B, v_A. Air and liquid velocities were calculated using the following relationships:

$$v_A = \frac{\dot{q}_A}{\frac{\pi D_A^2}{4} - \frac{\pi D_{O_L}^2}{4}} \tag{III.4.3}$$

$$v_B = \frac{4\dot{q}_B}{\pi D_{i_L}^2} \tag{III.4.4}$$

The liquid and air volumetric flow ratesn $\dot{q}_B$, $\dot{q}_A$ were determined experimentally; $\dot{q}_B$ was found to be independent of applied air pressure, and $\dot{q}_A$ was measured at ambient temperature (20 °C) using a gas meter (Gallus G4, Itron) for air pressures of 0.2, 0.4, 0.6, and 1 bar. This experimental set of flow rates was combined with the nominal flow rate at 4 bars given by the supplier in the technical sheet and a polynomial model was fitted allowing linking the air flow rate to the air pressure (with $\dot{q}_A$ in L.min^{-1} and P in

bars):

$$\dot{q}_A = -1.67\ P^2 + 26.78\ P + 30.58, \qquad R^2 = 0.999 \tag{III.4.5}$$

The mass flow rates have been calculated using the relation $\dot{m} = \rho\dot{q}$ where ρ is the fluid density (in kg.m^{-3}) and $\dot{q}$ the volumetric flow rate (m^3.s^{-1}). The bacterial suspension density ρ_B has been averaged experimentally on 10 samples of 10 mL of bacterial suspension in PBS with an optical density of 0.8. The relevant parameters used to calculate characteristic shear rates have been gathered in Table III.4.1.

Parameter	**Unit**	**Bacterial suspension**	**Air**
D_i	mm	1.524	3.048
D_O	mm	2.540	NA
ρ	kg.m^{-3}	1025.8	1.204
$\dot{q}$	L.min^{-1}	20.3×10^{-3} ± 0.32	34.8 ± 0.4
		41.8 ± 0.4	
		47.2 ± 0.7	
		54.8 ± 1.2	
		111 (fitted nominal value)	

Table III.4.1: Parameters used to determine the characteristic shear rates used in shearing experiments. D_i, D_O inner and outer channel diameters; ρ densities; $\dot{q}$ volumetric flow rates; The different values of $\dot{q_A}$ correspond to different air pressures (0.2, 0.4, 0.6, 1, and 4 bars). "NA" means "Non Applicable".

For each air pressure, 5 mL of sheared bacterial suspension were sampled at about 50 cm of the nozzle exit. Five milliliters of sheared bacterial suspension were also collected at 0 bar air pressure, to determine whether going through the nozzle itself could impact bacterial functionality. In this case, the shear rate was determined using the following formula:

$$\dot{\gamma} = \frac{2v_B}{D_{i_L}} \tag{III.4.6}$$

Based on these calculations, the characteristic shear rates investigated in shearing experiments have been gathered in Table III.4.2. A linear relationship can be established between the air pressure and shear rate:

$$\dot{\gamma} \approx (1.93 \times 10^5)P + (2.89 \times 10^5), \qquad R^2 = 0.996 \tag{III.4.7}$$

Air pressure (bar)	**Characteristic shear rate ($10^5 s^{-1}$)**
0	0.00244
0.2	3.0
0.4	3.7
0.6	4.2
1.0	4.9
4.0	11

Table III.4.2: Characteristic shear rates and air pressures applied in shearing experiments.

with $\dot{\gamma}$ in s^{-1} and P in bars.

The influence of repeated shear stress was also studied by shearing three times the same bacterial suspension.

III.4.2 Functionality assessment

Bacterial functionality was evaluated through bacterial adhesion to β-lactoglobulin using the method described by Gomand et al. (2018) [Gomand et al., 2018]. Briefly, sheared and control (without shearing) bacterial suspensions were diluted until reaching an optical density of 0.5 at 595 nm. One hundred and twenty microliters of diluted sampled were then introduced into each well of the high-binding 96-well microplates containing immobilized β-lactoglobulin and BSA and left 1 h for incubation at 37 °C. Each well was then washed 5 times using 300 μL of PBST (pH 6.8) to eliminate non-adherent strains. Two hundred microliters of MRS were finally introduced into each well and bacterial growth was monitored through measurements of optical density at 595 nm over 20 h. The quicker the apparent growth started, the higher the bacterial affinity towards β-lactoglobulin, *i.e.* the less shear-impacted the bacterial suspension. Strain growth comparison was performed using times at which the apparent bacterial growth starts (right after the lag phase), called t_{start}, and results have been expressed in terms of $1000/t_{start}$ to match high adhesion abilities with high values [Gomand et al., 2018].

III.4.3 Bacterial chain distribution assessment

Bacterial chain distribution was evaluated through microscopic observations. For each assay, 5 μL of half-diluted sheared and control bacterial suspension were sampled, dried, stained with crystal violet, and washed with distilled water. Microscopic observations were performed using an Olympus microscope (Olympus Corp., Shinjuku, Tokyo, Japan) alongside with Toupcam software (ToupTek Photonics, Zhejiang, P.R. China). Thirty pictures by sample were taken and analyzed.

III.5

Model and numerics

III.5.1 Model presentation

The model developed and used in this section allows representing elastic chains of bodies of various shapes and sizes in a shear flow as presented in Figure III.5.1 and has been adapted from Mitchell & Spagnolie [Mitchell and Spagnolie, 2017]. Modeling for chains of bacteria experiencing shearing, bacterial chains were represented as chains of ellipsoids in a pure shear flow, *i.e.*, no extensional flow component was considered (Figure III.5.2). Flow is studied locally around bacteria, therefore viscous forces are dominant and the Reynolds number $Re \approx 0$. All bacterial cells are identical ellipsoids ("bodies") of same half-length a and half-width b, connected to one another by clusters of springs, each connection featuring sixteen springs in 3D. Surface traction forces can be tracked visually by color scale changes on the surface of each body (Fig. III.5.1 and III.5.2).

III.5.2 Hydrodynamics with a traction integral equation

The flow in this problem is driven by the spring forces described in the next subsection together with the influence of an imposed linear background flow. We will consider a boundary integral equation method for solving the mobility problem, that is, we impose net forces and torques and we seek rigid body motions. To derive the integral equation, we begin from a formulation known as the *completed traction boundary integral equation*,

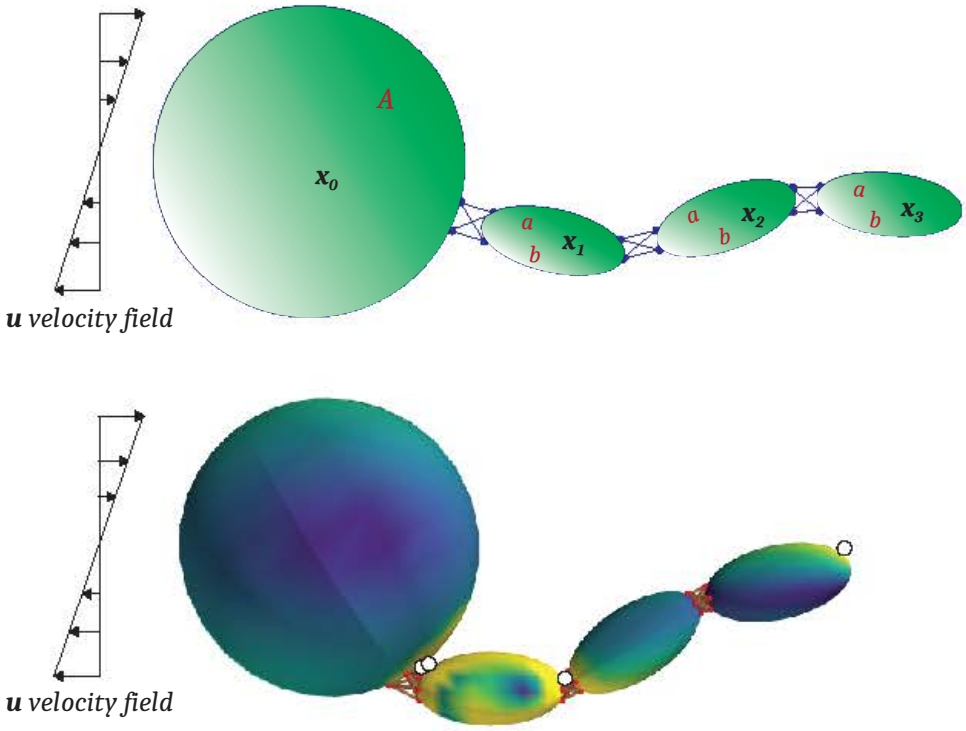

Figure III.5.1: General representation of an elastic chain of bodies of various shapes and sizes *(top)* and the equivalent output generated by the model *(bottom)* in a shear flow. The position of each body i of radius A or half-length b and half-width a is defined by a centroid $\mathbf{x_i}$. Color scale changes on the model output represent variations in surface traction forces on each body. Maximal traction force location by body is represented by an open circle. The color scale is reset at each timestep, therefore a given color corresponds to different values at different times.

henceforth referred to as the CTBIE [Mitchell and Spagnolie, 2017, Keaveny and Shelley, 2011]. The advantages of the CTBIE include the desirable conditioning of second-kind integral equations and the ability to directly solve for surface tractions, which in our case will be useful to evaluate the extend of shear-induced damage to the bacterial cell surface. This method presents two general limitations, that are (i) the restriction to rigid-body motions, which will be triggered in the present study in the limit of tiny bending and stretching displacements, and (ii) the discretization of the continuous equation for the purpose of solving for traction forces over the surface of the bodies, requiring an adaptive timestepping method when two particles approach each other more closely than

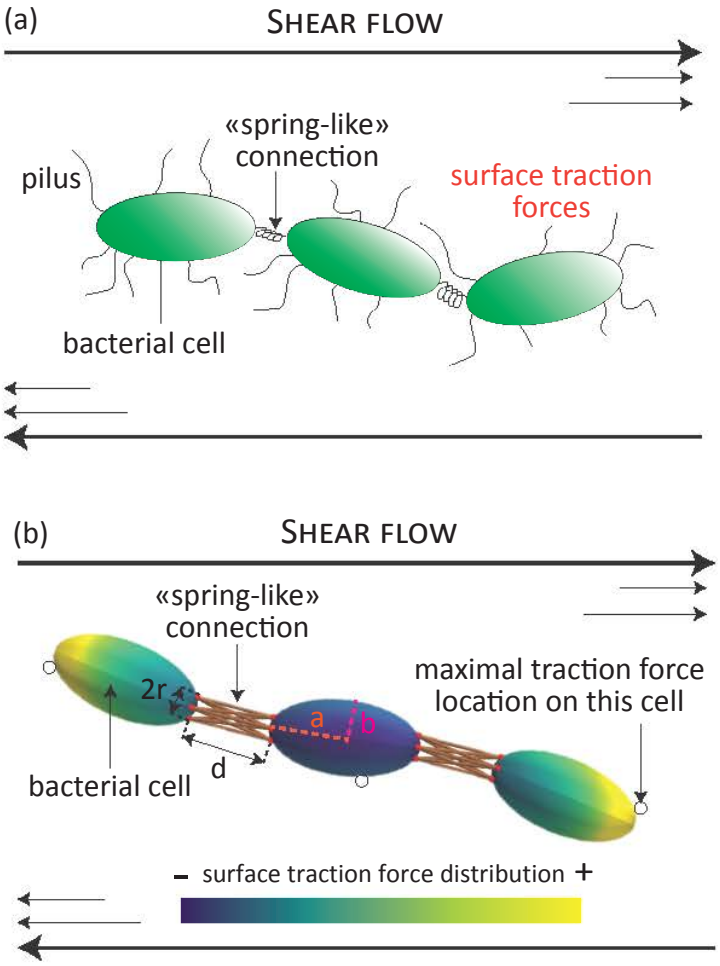

Figure III.5.2: Visual representation of a model 3-cell bacterial chain in a shear flow (a) and output of the numerical model with full hydrodynamic color scale for surface traction forces (b); a, b, r, and d are respectively the dimensionless half-length and half-width of one ellipsoid, the dimensionless radius of the cluster of springs connecting one ellipsoid to the other, and the resting distance separating one ellipsoid from the other. Maximal traction force location by body is represented by an open circle.

the typical mesh scale, which cost increases with the flexibility of the system. Both limitations appear neglectable in our case as we mostly solved in the limit of rigid body motion, assuming that bacterial chains are stiff to some extent.

For the case of a single body, the equation has the form

$$\begin{aligned}\frac{1}{2}f_j(\boldsymbol{y}) + \frac{1}{8\pi}n_k(\boldsymbol{y})\int_D^{P.V.} T_{ijk}(\boldsymbol{y}',\boldsymbol{y})f_i(\boldsymbol{y}')dS_{\boldsymbol{y}'} + \frac{1}{8\pi}\int_D C_{ij}(\boldsymbol{y}',\boldsymbol{y})f_i(\boldsymbol{y}')dS_{\boldsymbol{y}'} \\ -\mu\left(U_j + \varepsilon_{jk\ell}\Omega_k(y_\ell - Y_\ell)\right) \\ = -\mu(A_{jk}+A_{kj})n_k(\boldsymbol{y}) + \frac{\mu}{2}(A_{jk}-A_{kj})y_k + \frac{\mu}{2}(A_{jk}+A_{kj})Y_k.\end{aligned} \tag{III.5.1}$$

The quantities appearing in this equation are:

- D, the particle surface
- $\boldsymbol{f}$, the hydrodynamic surface traction, *i.e.* $f_i = \sigma_{ij}n_j$
- $\boldsymbol{n}$, the normal vector pointing from the body into the fluid
- $\boldsymbol{y}$, any source point on the particle surface (the equation must hold for any $\boldsymbol{y} \in D$)
- $T_{ijk}(\boldsymbol{y}',\boldsymbol{y}) = -6(y_i'-y_i)(y_j'-y_j)(y_k'-y_k)|\boldsymbol{y}'-\boldsymbol{y}|^{-5}$, the free-space stresslet
- $C_{ij}(\boldsymbol{y}',\boldsymbol{y}) = \delta_{ij}/r + r_i r_j/r^3 + \varepsilon_{m\ell j}\varepsilon_{mpi}r_p(y_\ell - Y_\ell^q)$ with $r_i = x - Y^q$ and $r = |\boldsymbol{r}|$, the adjoint of the Power and Miranda completion flow
- $\boldsymbol{U}$ and $\boldsymbol{\Omega}$, the rigid-body translational and rotational motions of the particle
- A, the matrix defining the linear background flow through $u_i^{BG} = A_{ij}x_j$
- μ, the viscosity
- $\boldsymbol{Y}$, the particle centroid

This equation holds for each $\boldsymbol{y}$ on the particle surface D; the stresslet integral has to be interpreted in the principal value sense because the integrand diverges as $\boldsymbol{y}' \to \boldsymbol{y}$. We note that $\boldsymbol{U}$ and $\boldsymbol{\Omega}$ appear on the left-hand side of (III.5.1) because they are unknowns in the mobility formulation; to impose a given force and torque we also enforce the six scalar equations

$$\boldsymbol{F} = \int_D \boldsymbol{f}(\boldsymbol{y}')\,dS_{\boldsymbol{y}'}, \qquad \boldsymbol{L} = \int_D (\boldsymbol{y}'-\boldsymbol{Y})\times\boldsymbol{f}(\boldsymbol{y}')\,dS_{\boldsymbol{y}'}. \tag{III.5.2}$$

We now adapt the system (III.5.1)-(III.5.2) for a flow with several independently moving particles. To do this we replace D with a union of particle surfaces $\cup_{p=1}^{N} D_p$ with centroids $\{\boldsymbol{Y}^p\}$, subject respectively to forces $\boldsymbol{F}^p$ and torques $\boldsymbol{L}^p$. This yields a new equation which holds for each source point $\boldsymbol{y}$ on the surface of each particle D_q. Separating the integral over D_q from the others, we obtain

$$\begin{aligned}
&\frac{1}{2}f_j(\boldsymbol{y}) + \frac{1}{8\pi}n_k(\boldsymbol{y})\int_{D_q}^{P.V.} T_{ijk}(\boldsymbol{y}',\boldsymbol{y})f_i(\boldsymbol{y}')dS_{\boldsymbol{y}'} + \sum_{p\neq q}\frac{1}{8\pi}n_k(\boldsymbol{y})\int_{D_p} T_{ijk}(\boldsymbol{y}',\boldsymbol{y})f_i(\boldsymbol{y}')dS_{\boldsymbol{y}'} \\
&+\sum_{p=1}^{N}\frac{1}{8\pi}\int_{D_p} C_{ij}(\boldsymbol{y}',\boldsymbol{y})f_i(\boldsymbol{y}')dS_{\boldsymbol{y}'} - \mu\left(U_j^q + \varepsilon_{jk\ell}\Omega_k^q(y_\ell - Y_\ell)\right) \\
&= -\mu(A_{jk}+A_{kj})n_k(\boldsymbol{y}) + \frac{\mu}{2}(A_{jk}-A_{kj})y_k + \frac{\mu}{2}(A_{jk}+A_{kj})Y_k^q
\end{aligned} \tag{III.5.3}$$

where $\boldsymbol{U}^q + \boldsymbol{\Omega}^q \times (\boldsymbol{y} - \boldsymbol{Y}^q)$ is the rigid motion of the q-th particle. Because $\boldsymbol{y}$ is exterior to the other surfaces, the remaining integrands are smooth. To regularize the integrand over D_q we use a singularity subtraction as in Mitchell and Spagnolie (2017) [Mitchell and Spagnolie, 2017]. The resulting equation together with the force and torque balance is

$$\begin{aligned}
&\frac{1}{8\pi}\int_{D_q} T_{ijk}(\boldsymbol{y}',\boldsymbol{y})\Big(f_i(\boldsymbol{y}')n_k(\boldsymbol{y}) + f_i(\boldsymbol{y})n_k(\boldsymbol{y}')\Big)dS_{\boldsymbol{y}'} + \sum_{p\neq q}\frac{1}{8\pi}n_k(\boldsymbol{y})\int_{D_p} T_{ijk}(\boldsymbol{y}',\boldsymbol{y})f_i(\boldsymbol{y}')dS_{\boldsymbol{y}'} \\
&+\sum_{p=1}^{N}\frac{1}{8\pi}\int_{D_p} C_{ij}(\boldsymbol{y}',\boldsymbol{y})f_i(\boldsymbol{y}')dS_{\boldsymbol{y}'} - \mu\left(U_j^q + \varepsilon_{jk\ell}\Omega_k^q(y_\ell - Y_\ell^q)\right)
\end{aligned} \tag{III.5.4}$$

$$\begin{aligned}
&= -\mu(A_{jk}+A_{kj})n_k(\boldsymbol{y}) + \frac{\mu}{2}(A_{jk}-A_{kj})y_k + \frac{\mu}{2}(A_{jk}+A_{kj})Y_k^q \\
&\int_{D_q} f_j(\boldsymbol{y})\,dS_{\boldsymbol{y}} = F_j^q, \qquad \int_{D_q}\varepsilon_{jk\ell}(\boldsymbol{y}_k - \boldsymbol{Y}_k^q)f_\ell(\boldsymbol{y}) = L_j^q
\end{aligned} \tag{III.5.5}$$

For the computations presented in this work, we discretize the system (III.5.4)-(III.5.5) using a collocation scheme where the continuous equation (III.5.4) is enforced only on a finite collection of points $\boldsymbol{y} \in \{\boldsymbol{x}_n\}_{n=1}^{N_x}$ which coincide with the nodes of quadrature rules surface integration rules for each body. We employ discrete quadrature rules

based on spherical coordinates with Gauss-Legendre integration in the zenith and the trapezoidal rule in the azimuth. The subtracted singularity in (III.5.4) still has a bounded jump discontinuity on D_q at $\boldsymbol{y}' = \boldsymbol{y}$, which we address using the simple heuristic of taking the integrand to be zero there. The resulting linear equation for $\boldsymbol{f}$ and $\{(\boldsymbol{U}^p, \boldsymbol{L}^p)\}_p$ is dense and non-normal and we solve it using GMRES (Generalized Minimal Residual) after explicitly building the matrix. This scheme was previously found to be second-order accurate for the case of a single body [Mitchell and Spagnolie, 2017], and since the integrals over other bodies are smooth we expect the same convergence rate in the multibody setting, with the caveat previously mentioned that increased discretization or small timesteps may be required when two particles approach each other more closely than the typical mesh scale.

III.5.3 Model parametrization for bacterial chains

Parameter	Physical meaning	Numerical value
N_{bodies}	Number of bodies in the chain	1 to 5
a	Half-length of one ellipsoid	1
b	Half-width of one ellipsoid	0.5
d	Resting distance separating one ellipsoid from another	1
k_L	Stretching constant	350
r	Radius of the spring cluster (defining bending ability)	0.3
$\max_f$	Maximum force leading to chain breakage	10^6
$\max_l$	Maximum torque leading to chain breakage	10^6
ρg	Inertia factor	0
$\dot{\gamma}$	Shear rate	1
α	Extensional rate	0
T_{final}	Duration of the simulation	25
timestepping_method	Time-stepping method (Euler or adaptive)	adaptive
NT	Number of time steps	100
N_{pics}	Number of pictures taken	25

Table III.5.1: Numerical parameters used to simulate the behavior and surface traction forces exerted on bacterial chains in a shear flow for quasi-rigid body motion. All presented variables are dimensionless and scale with the radius of the smallest body (longest half-length) defined as the characteristic length scale a.

Parameters and variables used in the model are dimensionless and scale with the radius (longest half-length) of the smallest cell in the chain, defined as the characteristic

length scale a. The set of parameters used in simulations of bacterial chains in Chapter IV.2 is presented in Table III.5.1. The characteristic velocity scale is $\dot{\gamma}a$, $\dot{\gamma}$ being the dimensionless shear rate, and the characteristic time $1/\dot{\gamma}$. The dimensionless stretching constant k_L scales with a as follows: $k_L = \frac{k_L^*}{\mu^* a^* |\dot{\gamma}^*|}$, with k_L^*, μ^*, a^*, and $\dot{\gamma}^*$ respectively the real values of the stretching constant ($\mathrm{kg.s^{-2}}$), the viscosity ($\mathrm{kg.m^{-1}.s^{-1}}$), the half-length of one bacterial cell (m), and the shear rate ($\mathrm{s^{-1}}$). Simulations were run at fixed k_L, defined in order to maintain quasi-rigid body motion for chains up to 5 cell-length in a shear flow of shear rate $\dot{\gamma} = 1$. Because chains evolve in quasi-rigid body motion, the rotation behavior of a chain is periodic on half its rotation period. Therefore, the duration of the simulation T_{final} was defined in order to allow approximately for a half-rotation period for the longest chain tested (number of cells $N_{\text{bodies}} = 5$). Traction forces were studied over time on all cells of a chain, for chains with N_{bodies} varying from 1 (reference case) to 5, using the full version of the code solving for all hydrodynamic interactions. Chain breakage phenomena were observed on chains of spherical bodies using the simplest version of the code not taking into account hydrodynamic interactions in order to limit computing costs. Indeed, the proximity reached by bodies before breaking is very costly computationally. Therefore, when studying traction forces over the cells of a chain, maximum rupture force and torque $\max_f$, $\max_l$ were set high enough so that cells would not get too close (quasi-rigid body motion), *i.e.* chains would only rotate and slightly deform in shear flow, and not break. Gravity forces were neglected.

III.6

Data treatment

III.6.1 Statistical analysis

III.6.1.1 High-throughput screening

For the validation of the high-throughput screening method, results were standardized for tube cultures using the measured adhesion of LGG WT to β-lactoglobulin averaged for all experiments; standard errors were calculated. Principal Component Analysis (PCA) was used to determine which main underlying factors could explain the observed differences in strain affinities for LGG strains using Unscrambler (CAMO software AS).

In all cases, statistical analysis was performed via t-tests and Tukey tests (cross-analysis for multiple comparisons of parametric data) for normal data and Wilcoxon-Mann Whitney and Steel-Dwass tests (cross-analysis for multiple comparisons of non-parametric data) for data that did not fit normal distribution using Kyplot software (Kyens Lab Inc.).

III.6.1.2 Atomic force microscopy measurements

Three adhesion force maps (20 μm x 20 μm, 256 force curves) were recorded for each protein-bacteria interaction analysis. Data analysis was performed using the Nanoscope Analysis software from Bruker (Santa Barbara, CA, USA) and the last peak was calculated for each curve before plotting adhesion forces and last rupture length histograms.

The last peak is used for analysis instead of the maximum peak in order to characterise the last interacting point between the β-lactoglobulin and the cell receptor and not the unfolding of a biomolecular domain.

III.6.1.3 Confocal microscopy measurements

Two independent repetitions were performed and approximately twenty representative images were acquired and analyzed for each sample.

III.6.1.4 Shearing experiments

Bacterial functionality results were normalized for each shearing experiment using the measured adhesion of control LGG WT (before shearing) to β-lactoglobulin. Cross-analysis were performed via Tukey HSD (honestly significant difference) tests (parametric for multiple comparisons) for normal data and Steel-Dwass tests (non-parametric for multiple comparisons) for data that did not fit normal distribution using Kyplot software to highlight the main observed differences according to shearing conditions for each strain.

III.6.2 Functional domain prediction for the bacterial surface proteome

Bacterial surface proteins featuring LPxTG motif were predicted using the InterPro resource, that provides functional analysis of protein sequences provided in FASTA format by classifying them into families and predicting the presence of domains and important sites [Finn et al., 2017]. Protein sequences with LPxTG motif were obtained from Sun et al. (2015) and were scanned against InterPro's signatures using the software package InterProScan [Sun et al., 2015, Jones et al., 2014]. Gene sequence resemblance with known domains was performed using the Basic Local Alignment Search Tool resource (BLAST) previously developed [Altschul et al., 1990]. InterProScan analysis allowed predicting for each predicted protein the family to which it belongs, a homologous superfamily if a match was found, and assigned predicted molecular functions or roles in biological processes to identified domains and repeats. Signature matches with known proteins or surface components were provided when available. An example of analysis

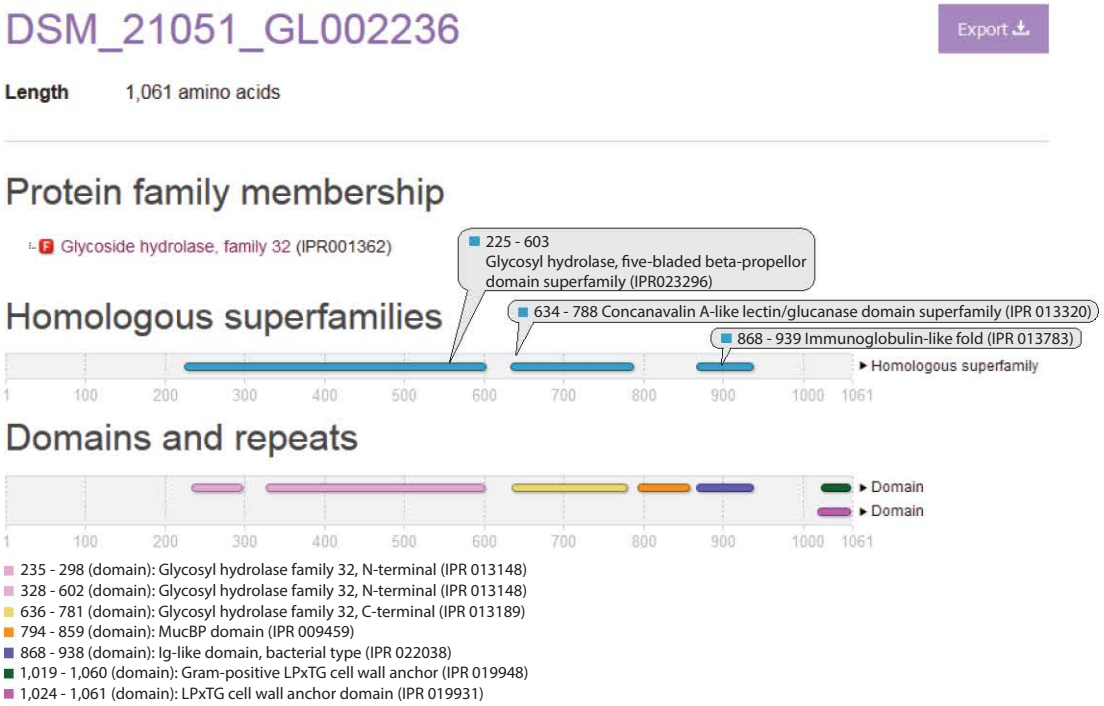

Figure III.6.1: InterProScan functional analysis of the protein GL002236 predicted from the strain *Lactobacillus aquaticus* DSM 21051.

for the predicted protein GL002236 of the strain *Lactobacillus aquaticus* DSM 21051 is given in Figures III.6.1, III.6.2, and III.6.3.

III.6.3 Model and numerics

III.6.3.1 Bacterial chains

For each simulation, one traction force profile was analyzed by cell, and the location (identified visually by an open circle on each of the cells such as represented in Figure III.5.2) and intensity of the maximum surface traction force $\mathrm{Max}_{\mathrm{STF}}$ exerted on each cell were monitored over time. Variations in distance d_{i-i+1} between cells i and $i+1$, as well as cells rotation rates Ω_i, and traction forces exerted at both ends of each cell, were also recorded and compared between chains of different lengths, as well as for all cells within a given chain.

Figure III.6.2: InterProScan functional analysis of glycoside hydrolase, family 32, predicted from the protein GL002236 of the strain *Lactobacillus aquaticus* DSM 21051.

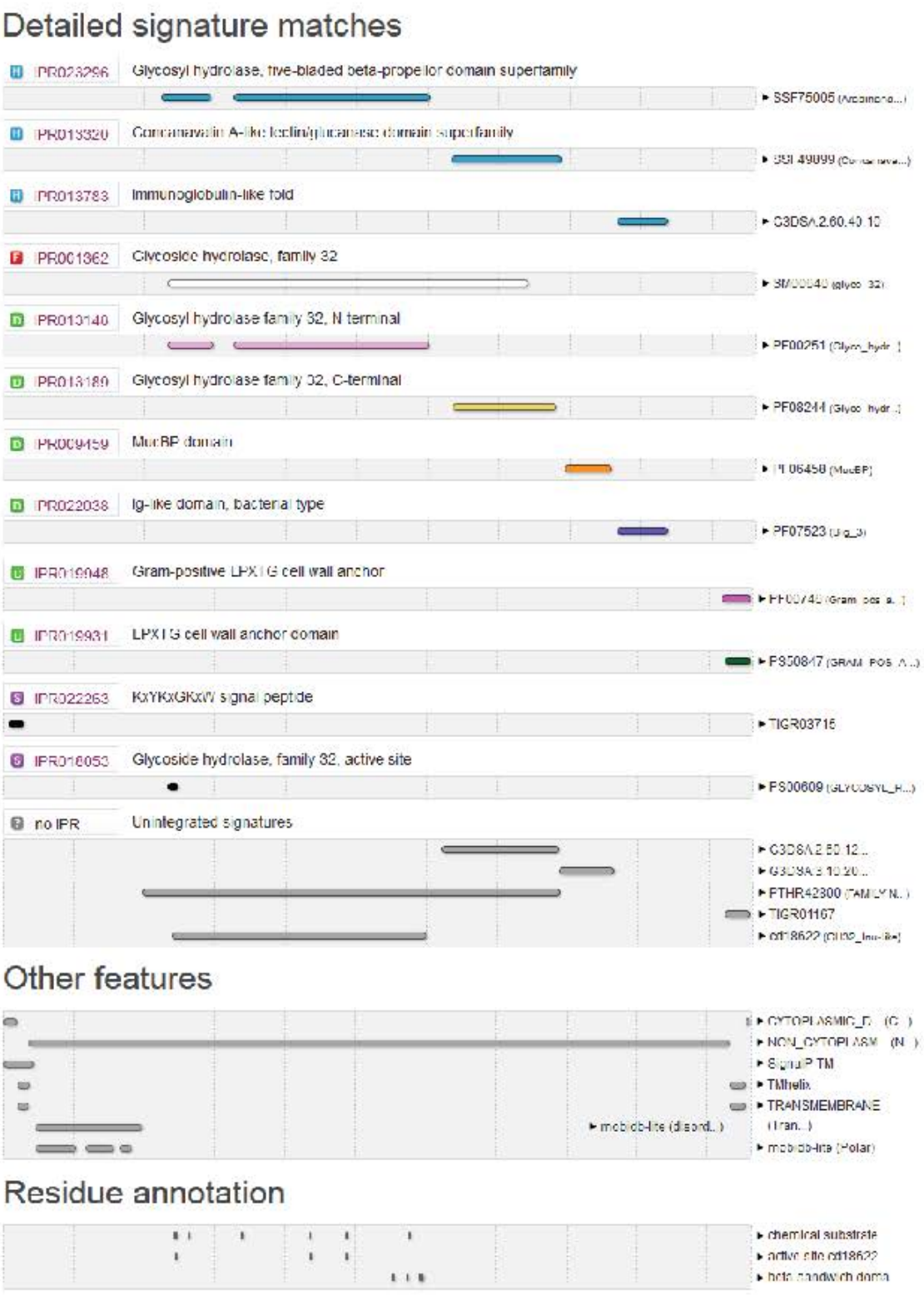

Figure III.6.3: InterProScan functional analysis of the protein GL002236 predicted from the strain *Lactobacillus aquaticus* DSM 21051: detailed signature matches.

III.6.3.2 Dumbbells

Parameters monitored depend on the case studied *i.e.* rigid body motion (RBM) or flexible regimes ("locking-tumbling"), and are precised by case in the text. Three indicators were built and analyzed on each dumbbell body to help compare the dynamics of the different cases:

- The periodicity of period T (dimensionless number) of the body behavior (rotation, locking, swinging),
- The first time $t_{\pi/2}$ at which the system rotation angle ζ reaches $\pi/2$ (expressed in % of period completion), and
- The highest (absolute) rotation rate value $\mathbf{\Omega}_{\text{high}}$ reached over the course of one period.

Part IV

Results and Discussion

IV.1

Identification and characterisation of adhesive interactions

IV.1.1 Method development to identify adhesive interactions

IV.1.1.1 Method concept

Milk components are immobilized on the surface of 96-well adherent microplates exhibiting high affinity for charged polymers such as represented in Figure IV.1.1.

Microplates are then washed with a blocking agent to remove all unbound molecules and to block the sites that had remained empty. Strain suspensions are then added into the wells and incubated for 1 h in order to allow bacterial adhesion to the immobilized components. Non-adherent bacteria are removed by successive washes using the same blocking agent. The amount of immobilized bacteria is measured through bacterial growth monitoring (turbidity measurements at 595 nm) after the addition of culture growing medium in the wells. The higher the initial quantity of bound bacteria, the earlier the growth starts.

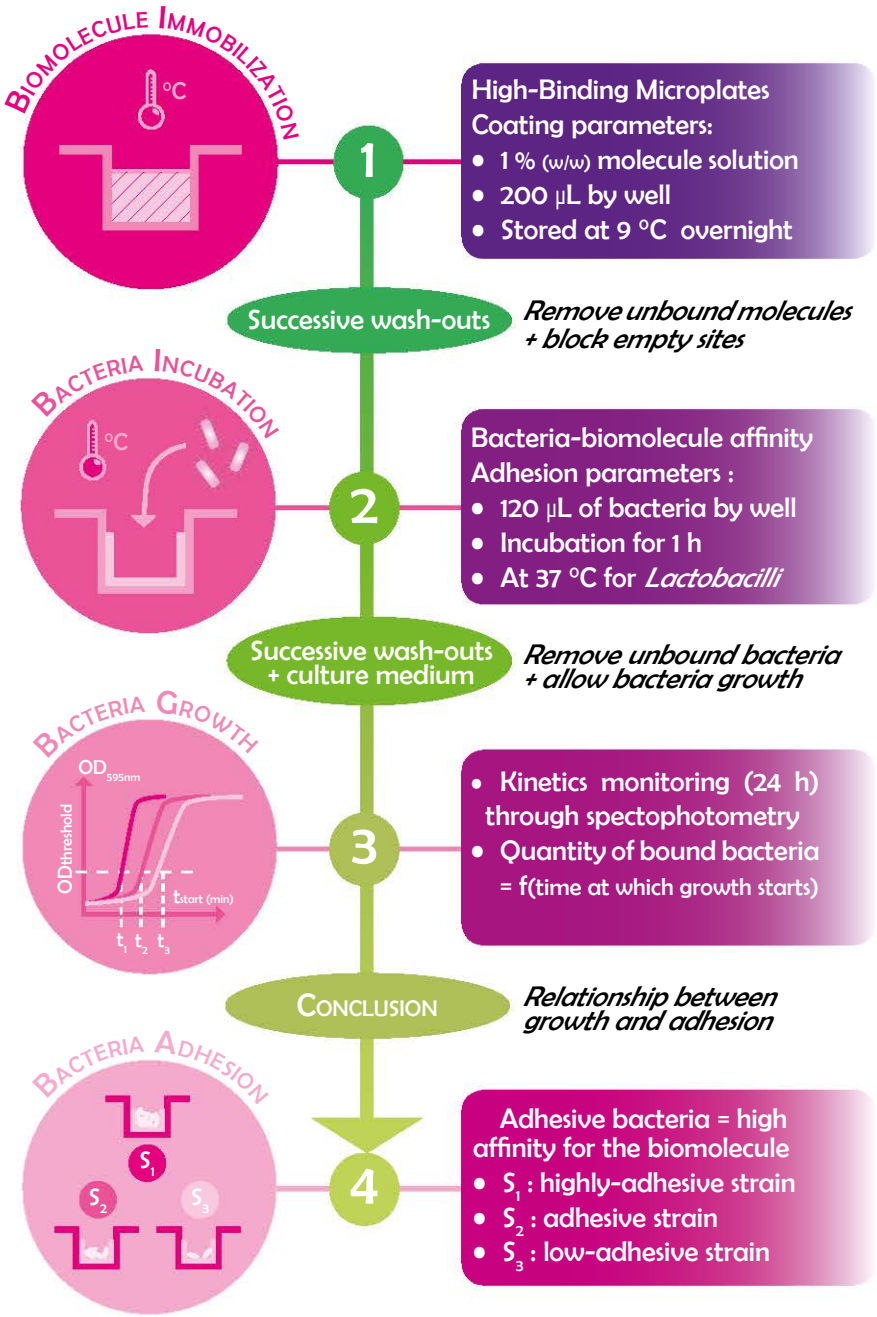

Figure IV.1.1: Main steps of the high-throughput screening method allowing estimating quickly the affinity of a wide range of strains for various components.

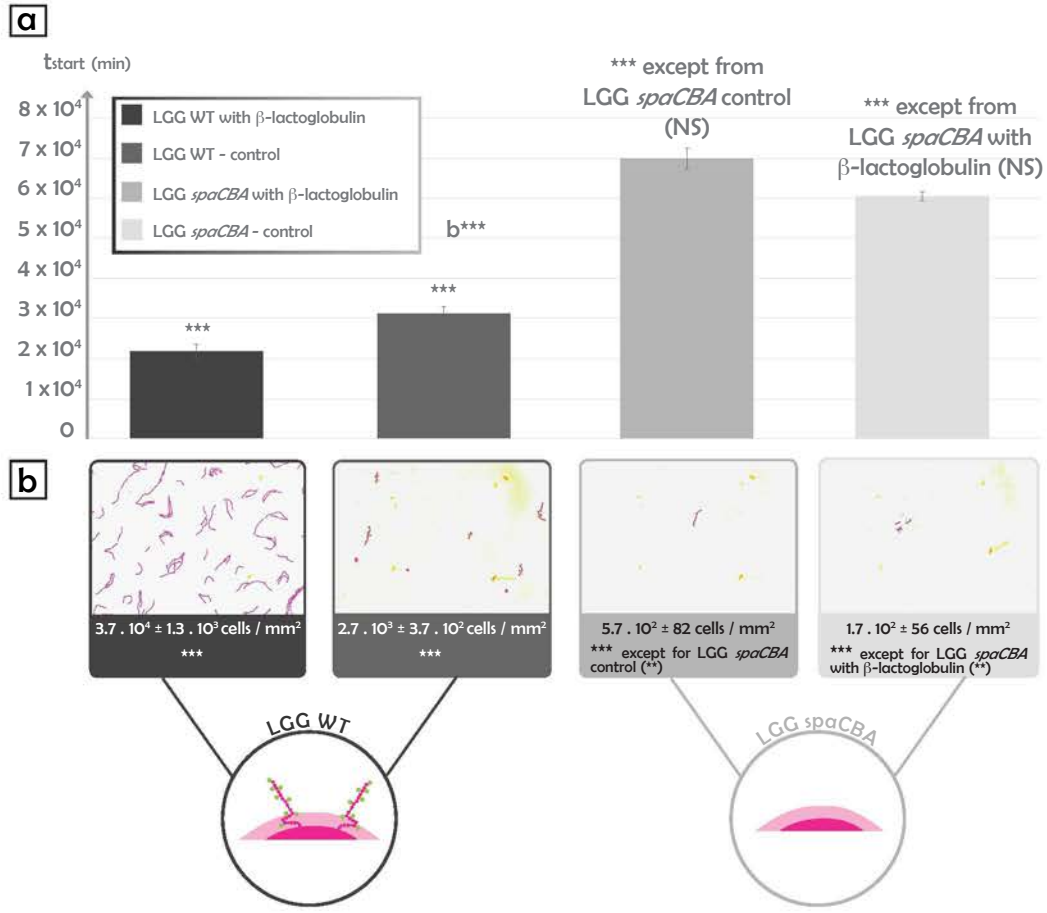

Figure IV.1.2: Relationship between indirect adhesion measurements through bacterial growth start times monitored through optical density measurements at 595 nm (a) and direct measurement of bacterial adhesion through microscopy observation (b). All series are significantly different from one another except when mentioned otherwise. Levels of significance are indicated on the figure (** stands for P $\leq$ 0.01 and *** for P $\leq$ 0.001). Standard errors are represented.

IV.1.1.2 Correlation between bacterial growth and bacterial adhesion

The growth monitoring of adherent bacterial cells show that the time required for the apparent growth to start (t_{start}) is shorter for the LGG WT in wells coated with β-lac compared to control wells (Figure IV.1.2a).

Microscopic observations reveal that LGG WT adheres approximately fifteen times

more to β-lac than to control wells (Figure IV.1.2b). Compared to LGG WT, the non-adherent mutant strain *spaCBA* showed high tstart values when the adhesion assays were performed both in wells coated with β-lac and in uncoated wells. Accordingly low adhesion ability was recorded under the same conditions for the mutant strain *spaCBA* by microscopy observation. These results show the adhesion ability is inversely related to the time required for the growth to start (t_{start}) after adhesion assays. For more convenience, in the manuscript the adhesion ability will be expressed as $1000/t_{start}$, to which it is directly related.

IV.1.1.3 Affinity results for the model strain LGG WT and three mutant strains

IV.1.1.3.1 Tube culture assays

Strain differences by component. Globally, the values of $1000/t_{start}$ are very low for all components for the mutant strain *spaCBA* when compared those obtained for LGG WT; this means that the mutant strain *spaCBA* adheres less to all components compared to LGG WT. These results were confirmed significantly on β-lac, α-lac, and MFGM and trend differences were observed for the other tested components (Figure IV.1.3).

A contrario, all $1000/t_{start}$ values were significantly high for the mutant *welE* whichever strain it was compared to, except for β-lac and α-lac when compared with LGG WT. This means that the mutant strain *welE* is more adhesive to almost all components compared to the three other strains. The strains *spaCBA* and *welE* can therefore be considered respectively the least and most adhesive strains. The double mutant *welE-spaCBA* features a low-affinity behavior very close to the *spaCBA* behavior as the $1000/t_{start}$ values obtained for this strain are significantly lower for β-lac, α-lac, and MFGM when compared to those obtained for LGG WT. Although mean comparison of $1000/t_{start}$ values would suggest that the strain *welE-spaCBA* would be a little more adhesive than the mutant strain *spaCBA* on most components, this was not supported statistically.

Component differences by strain. All controls *i.e.* wells without protein coating are not significantly different from one strain to another and therefore each control was used

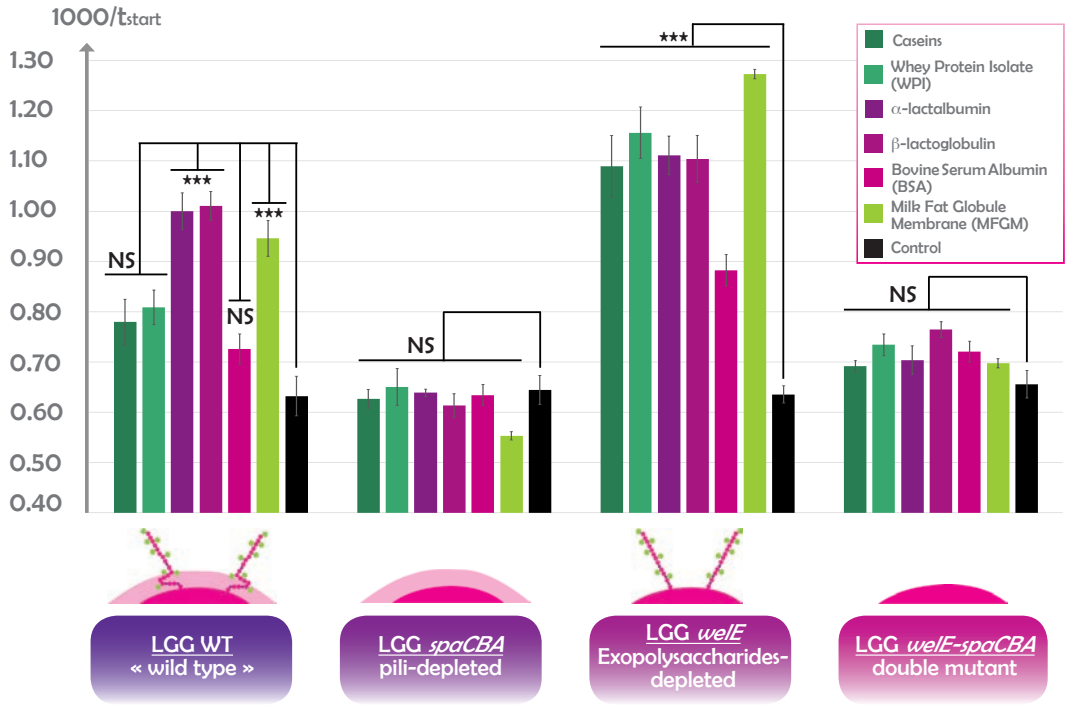

Figure IV.1.3: The adhesive behavior of *Lactobacillus rhamnosus* GG and the three mutant strains for various milk components (*** stands for $P \leq 0.001$). Standard errors are represented.

as a reference for the strain to which it stands (Fig. IV.1.3). The values of $1000/t_{start}$ for LGG WT were found significantly higher for β-lac, α-lac, and MFGM compared to the values obtained for the control, which means that this strain features a high affinity for these molecules. *A contrario*, low values of $1000/t_{start}$ for LGG WT were found for BSA as well as for non-purified milk proteins including caseins and WPI, which means that LGG WT adheres very little to these molecules compared to the control. All the values of $1000/t_{start}$ for the mutant strain *spaCBA* were very low and so were the values of the double mutant *welE-spaCBA* when compared to the values of their controls; this implies that the strains *spaCBA* and *welE-spaCBA* showed very low affinity for all the components. The mutant *welE* however featured high $1000/t_{start}$ values for all components but significantly less for BSA compared to the others. This means that the strain *welE* highly adheres to all components although a little less to BSA than to

the others.

Principal Component Analysis (PCA). Two main factors were found to explain most of the observed adhesion differences (Figure IV.1.4).

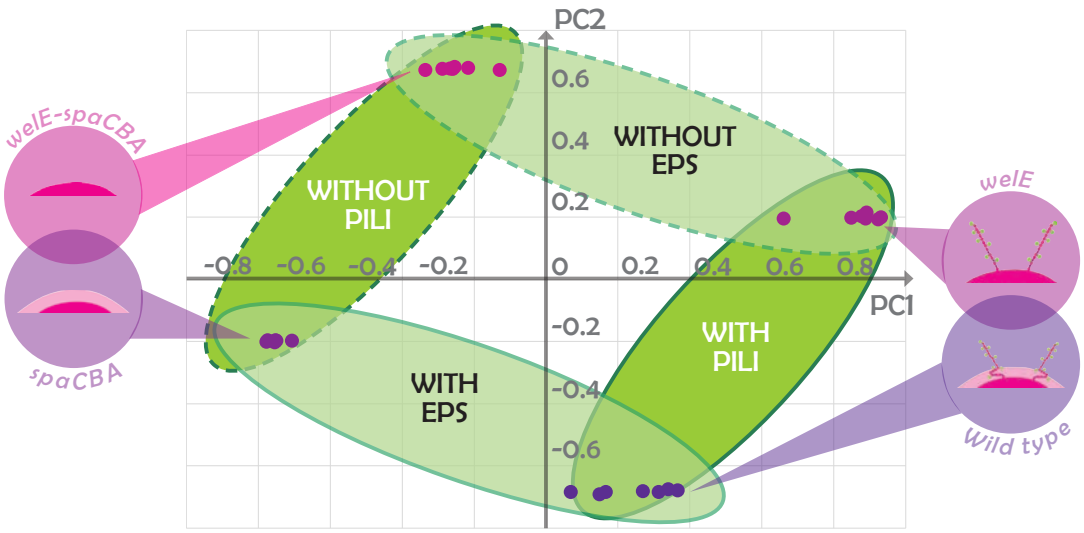

Figure IV.1.4: The two main factors explaining the observed adhesion differences between the *Lactobacillus rhamnosus* GG strains (principal component analysis) for various milk components.

Both factors relate to changes on the surface of the bacteria considered: 54 % of the adhesive differences are explained by the presence or absence of pili (first PCA component, PC1) and 40 % are due to the presence or absence of exopolysaccharides (second PCA component, PC2). These two strain characteristics seem to explain most of the adhesive differences observed for the four strains studied.

IV.1.1.3.2 Microplate culture assays

Results from cultures on 96-well microplates confirmed those obtained via tube culture assays (Figure IV.1.5) thus validating the method. Microplate cultures can therefore be substituted to tube cultures; this allows automatizing most steps using an automated liquid handling system in order to implement high-throughput screening to test a wider number of strains and components.

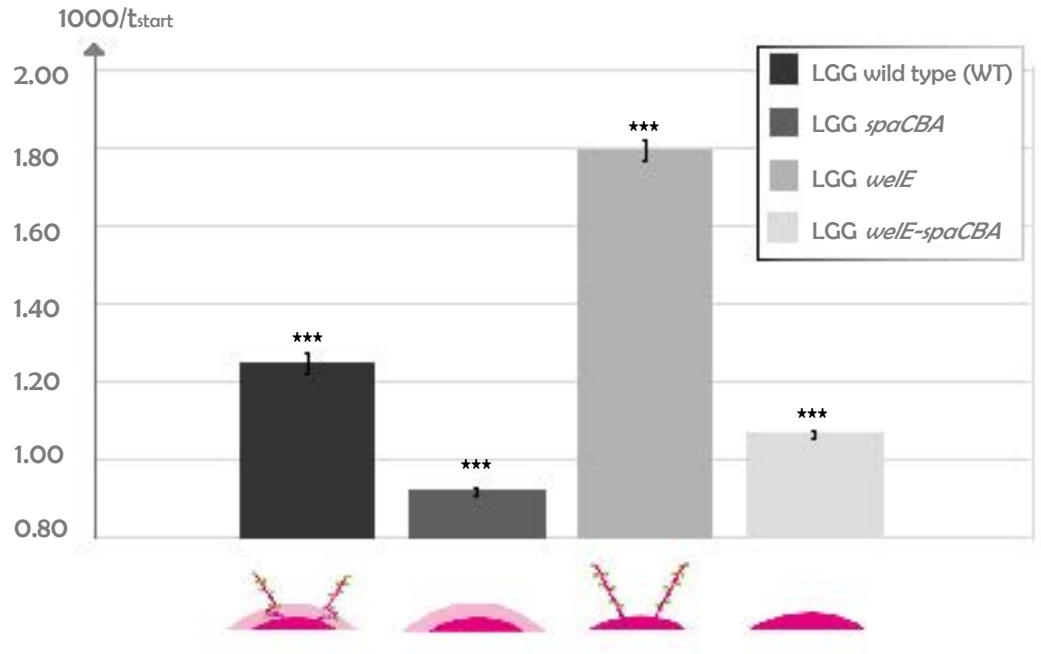

Figure IV.1.5: Confirmation of the adhesive behavior of *Lactobacillus rhamnosus* GG and the three mutant strains on milk fat globule membrane (MFGM) with microplate culture assays. All series are significantly different from one another (*** stands for $P \leq 0.001$). Standard errors are represented.

IV.1.1.4 Interest of the high-throughput screening approach

Classical biophysical approaches used to evaluate the adhesive behavior of bacteria *i.e.* AFM with Single-Cell Force Spectroscopy have been designed to decipher precisely the interactions between a restricted number of bacteria and [Burgain et al., 2013b, Guerin et al., 2016,Sullan et al., 2013,Tripathi et al., 2013]. These techniques are time-consuming and therefore cannot be applied to screen a large number of strains. Some microbiological approaches, such as bacterial radiolabeling or FITC labeling, have been developed which allow to study more strains simultaneously. However labeling is a cumbersome process which requires many steps [Auletta et al., 2016, Avadhanula et al., 2006, Douillard et al., 2013, Dutta et al., 2017, Kankainen et al., 2009, Shimaoka et al., 2001, Utratna et al., 2017] whereas the number of steps should be restricted to the minimum when dealing with microorganisms. In addition, preliminary assays to this study revealed

that FITC abolished the adhesion properties of LGG, probably because FITC directly bound pili structures therefore preventing cell adhesion to the tested polymers (data not shown). A recent approach based on bacterial labelling with crystal violet was used to determine adhesion differences between strains to intestinal mucin [Kimoto-Nira et al., 2015]. The amount of crystal violet was correlated to the cell affinity for the tested component. This method derives from a classical approach used to estimate the biofilm capacity of bacteria [Diaz et al., 2016, Kubota et al., 2008]. However, in our case this method was not considered applicable because interferences between crystal violet and dairy proteins were susceptible to occur; dairy proteins such as caseins have indeed been found to be able to bind crystal violet [Santhanalakshmi and Balaji, 2001]. Two studies used spectrophotometric methods to screen potential functional ingredients for beneficial bacteria [Rosendale et al., 2008] and microbial sensitivity of pathogens to honey [Patton et al., 2006]. Bacteria were incubated in media supplemented with the tested component and bacterial growth was directly correlated to a positive or negative (inhibitory) impact of this component. However, both these studies only take into account the initial and final optical densities regardless of bacterial growth kinetics; one can wonder whether only two measurements can be representative of bacterial growth preferences whereas kinetics could have been monitored through optical density measurements [Lee and Lim, 1980]. Indeed, this might not provide enough information to determine what underlying factor induced growth differences as the composition of the supplemented medium is complex and other changes, such as pH variations, may have occurred during growth [Patton et al., 2006, Rosendale et al., 2008]. In order to estimate with more accuracy the effect of the tested components on bacteria, it would be more relevant to immobilize them on a given support and monitor bacterial adhesion to this support, which is possible using our method.

The approach described in our article allows to screen the adhesion of a wide number of strains for a range of components while reducing the number of steps. Our method is not specific to a given strain and do not require to know much information on the components of interest nor on the tested strains, apart from their growing conditions. It

has proven to be highly repeatable as standard errors are very low and successive washes allow to standardize the protocol. By cultivating strains directly in microplates, automatization of all operations allows to fasten and standardize the experiments. However, preliminary experiments to this study (Fig. IV.1.2) showed that monitoring bacterial growth is less precise than counting bacteria when determining bacterial affinity for a given component. Differences between bacterial counts appeared magnified compared to OD_{595nm} differences when monitoring bacterial growth, and some differences could be brought to light using microscopy but not through kinetics monitoring such as a higher adhesion of the mutant strain spaCBA to wells containing β-lac compared to control wells.

When applied to other strains than LGG, this method may require some adjustments related to the growth properties of the tested strains, in order to accurately discriminate adhesion levels between strains and tested components. Such adjustments include the choice of an adequate OD_{595nm} threshold to discriminate t_{start} for the different strains, which must fit a baseline corresponding to the absence of growth detection, defined according to the average OD (for all strains) during the lag phase of bacterial growth, plus its standard deviation (rounded to the nearest value). The monitoring duration of the growth phase might also be extended if needed, for strains featuring a slower growth rate. Finally, the growing medium, the incubation temperature, and the time allowed for initial growth of the microplate cultures may also need to be modified to fit best other strains than LGG.

IV.1.1.5 Choice of blocking reagent

Our experiments and previous work highlighted that bacterial adhesion to dairy components can highly vary from one component to another as well as by strain [Burgain et al., 2014b, Guerin et al., 2016] whereas dairy components such as caseins and BSA are commonly used in the literature as blocking agents for adhesive assays [Muzzio et al., 2017, Steinitz, 2000, Vogt et al., 1987]. Diluted Tween 20 in PBS adjusted at pH 6.8 (5 % v/v) was used as blocking reagent to block remaining empty sites on coated microplates.

Tween 20 belongs to polysorbate surfactants and contains lauric acid. It is commonly used as washing agent in immunoblotting and ELISA in order to minimize nonspecific binding of antibodies and to remove unbound moieties [Diao et al., 2013,Dilly and Rajala, 2008, Gulati et al., 2008, Habashi et al., 2011, Li et al., 2008, Scholler et al., 2008]. Tween 20 is often used to prevent non-specific interactions and especially non-specific binding to occur [Steinitz, 2000]. Tween 20 can indeed block vacant binding sites after bacterial removal during the washing phase thus preventing low affinity interactions from occurring, as well as limiting strain interaction with microplates' material. Since our experiments demonstrated that bacterial affinity can vary a lot for milk components, including for caseins and BSA which are traditionally used as blocking reagents, we highly recommend to use exclusively Tween 20 as a blocking reagent when performing adhesion experiments in order to avoid biases.

IV.1.1.6 Comparison with atomic force microscopy results

The adhesive behaviors of the strains LGG WT, *spaCBA* and *welE* towards caseins, WPI, and β-lac have previously been studied using AFM [Burgain et al., 2013b, Burgain et al., 2014b, Guerin et al., 2016]. In addition, the affinity of LGG WT for α-lac and BSA has also been tested. The affinity of the strains towards the different components was estimated through the amount of adhesive events occurring during the retraction of the AFM probe [Burgain et al., 2013b] and are presented in Table IV.1.1.

Both AFM and high-throughput screening show that the strain *spaCBA* features very little affinity for caseins, WPI, and β-lac. AFM also reveals that LGG WT and *welE* are highly adhesive to both WPI and β-lac and that LGG WT feature a low affinity for caseins and BSA, all these outcomes being in adequacy with our results. However, LGG WT and *welE* are also found to feature a low affinity for α-lac and a high affinity for WPI whereas when using the screening method LGG WT is shown to adhere as little to WPI as to caseins and the adhesion to α-lac is similar to the one on β-lac. An hypothesis which can be proposed to explain this observation is that the screening method could be sensitive to the degree of purity of the tested components. Pure proteins such as

Adhesive events (%)	**LGG WT**	**LGG *spaCBA***	**LGG *welE***	**References**
Caseins	3.2 ± 1.50	0.05± 0.05	1.6 ±0.78	[Burgain et al., 2014b]
Whey Protein Isolate (WPI)	53.7± 6.70	0.24 ± 0.15	88.7 ± 0.39	[Burgain et al., 2014b]
β-lactoglobulin	51.4 ± 9.90	0.00 ± 0.00	84.1 ± 3.00	[Guerin et al., 2016]
α-lactalbumin	9.3 ± 3.40			[Guerin et al., 2016]
Bovine Serum Albumin (BSA)	13.1 ± 0.80			[Guerin et al., 2016]

Table IV.1.1: The different adhesive behaviors of the three *Lactobacillus rhamnosus* GG strains (wild type WT, *spaCBA* pili-depleted, *welE* exopolysaccharides-depleted) identified through atomic force microscopy (AFM).

β-lac and α-lac may have been immobilized more efficiently than complex proteins such as micellar caseins and WPI. Also, β-lac may be entrapped in WPI and therefore less accessible for bacterial adhesion.

AFM studies have shown that the key component involved in the adhesion with β-lac had previously been found to be the glycosylated SpaC subunit of bacterial pili [Guerin et al., 2016]. This explains the very limited adhesion observed for the mutant strain *spaCBA* through both AFM and high-throughput screening. Pili are stretched out in the exopolysaccharides-depleted strain *welE* which explains its higher adhesive capabilities for most components compared to the wild strain. These two behaviors were identified very clearly using high-throughput screening. The higher affinity of LGG WT for β-lac compared to other components which had previously been demonstrated using AFM was also revealed through this new binding assay.

IV.1.2 Characterisation of the adhesive potential of 73 strains and impact on bacterial spatial distribution

IV.1.2.1 Identification of strains adhesive to β-lactoglobulin

Most strains of the collection were found not to be adhesive to β-lactoglobulin as the average MAV calculated on the 73 strains was negative (-180 ± 22) although higher

than the MAV of the negative control LGG *spaCBA* (-386), known to be non-adhesive to β-lactoglobulin [Guerin et al., 2016]. The microplate adhesive assays revealed four adhesive candidates to β-lactoglobulin amongst the 73 strains tested: *Lactobacillus aquaticus* DSM 21051 (MAV = 61.5), *Lactobacillus murinus* DSM 20452 (MAV = 12.8), *Lactobacillus plantarum* DSM 13273 (MAV = 12.6), *Lactobacillus brantae* DSM 23927 (MAV = 6.97), although these strains were still less adhesive than the positive control LGG WT (MAV = 104). Nine strains were also found to have a MAV inferior to the one of the negative control LGG spaCBA: *Lactobacillus sharpeae* DSM 20505 (MAV = -857), *Lactobacillus kefiri* DSM 20587 (MAV = -787), *Lactobacillus similis* DSM 23365 (MAV = -780), *Lactobacillus pobuzihii* DSM 28122 (MAV = -617), *Lactobacillus namurensis* DSM 19117 (MAV = 516), *Lactobacillus satsumensis* DSM 16230 (MAV = -490), *Pediococcus parvulus* DSM 20332 (MAV = -477), *Lactobacillus senmazukei* DSM 21775 (MAV = -404), *Lactobacillus lindneri* DSM 20690 (MAV = -387). The MAV for all strains are listed in Appendix A.1.

IV.1.2.2 Biophysical deciphering of adhesive interactions

The adhesive interactions between β-lactoglobulin and the strains at the extremes of the adhesion spectrum, *L. aquaticus* DSM 21051 (the most adhesive strain) and *L. sharpeae* DSM 20505 (the least adhesive strain) were studied through AFM, in order to characterise them in further depth. Results are represented in Figures IV.1.6 and IV.1.7.

Only two strains were chosen to precise our understanding of the interaction mechanism of the LAB surface with β-lactoglobulin since AFM is not a suitable method for screening of large populations. This is why we decided to select only the two strains at the extreme of the adhesion spectrum for this analysis. BSA was used as a negative control as LAB strains have previously been found to feature low adhesion to it [Gomand et al., 2018, Guerin et al., 2016]. The percentages of adhesive events (frequencies) observed between *L. aquaticus* DSM 21051 and the two proteins, β-lactoglobulin and BSA, were respectively of 82.6 $\pm$ 7.1 % and 27.6 $\pm$ 10.4 % (Figure IV.1.6a). The frequencies of adhesive events observed between *L. sharpeae* DSM 20505 and the same two proteins

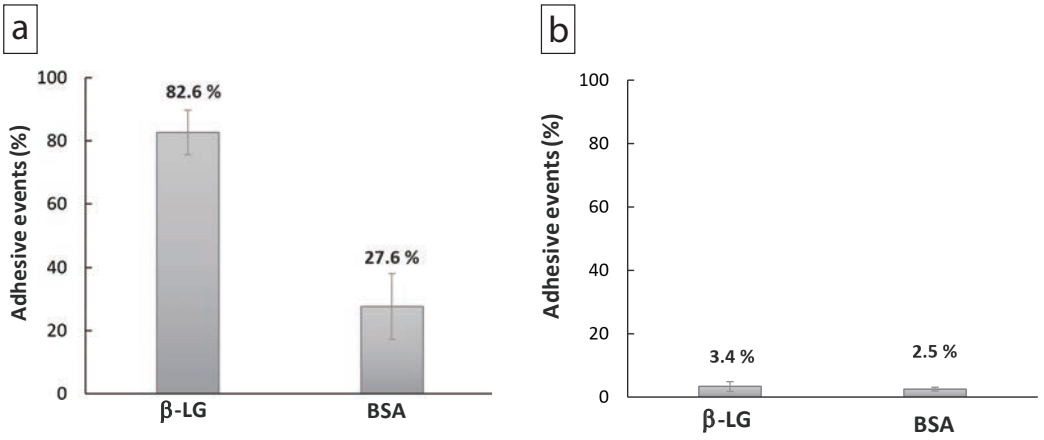

Figure IV.1.6: Comparison of the adhesive properties of two strains (*Lactobacillus aquaticus* DSM 21051, *Lactobacillus sharpeae* DSM 20505) for whey proteins isolates probed by atomic force microscopy (AFM): frequency of adhesive events occurring between whey proteins and *L. aquaticus* DSM 21051 (a) and *L. sharpeae* DSM 20505 (b).

were respectively of 3.4 ± 1.5 % for β-lactoglobulin and 2.5 ± 0.6 % for BSA (Figure IV.1.6b). Typical force-distance curves obtained for the interactions occurring between the two strains and the AFM probes functionalized with the two proteins are presented, *i.e. L. aquaticus* DSM 21051 and β-lactoglobulin (Figure IV.1.7a$_1$), *L. aquaticus* DSM 21051 and BSA (Figure IV.1.7a$_2$), *L. sharpeae* DSM 20505 and β-lactoglobulin (Figure IV.1.7b$_1$), and *L. sharpeae* DSM 20505 and BSA (Figure IV.1.7b$_2$). During the withdrawal of functionalized β-lactoglobulin-coated probe from the surface of *L. aquaticus* DSM 21051 several specific adhesive events occur (Fig. IV.1.7a$_1$), whereas more than 70 % of the curves observed for BSA-coated probes did not feature any adhesive event (Figure IV.1.7a$_2$). Moreover, the few adhesive events observed between BSA and *L. aquaticus* DSM 21051 appeared to be random and therefore could not be associated to any specific interaction (Fig. IV.1.7a$_2$). Almost no adhesive event was observed for both BSA- and β-lactoglobulin-coated probes on *L. sharpeae* DSM 20505 cells (Figures IV.1.6b, IV.1.7b$_1$, IV.1.7b$_2$). These results are consistent with those obtained using the screening method: *L. aquaticus* DSM 21051 significantly adheres to β-lac whereas poor adhesion was observed for *L. sharpeae* DSM 20505. Retraction curves recorded between

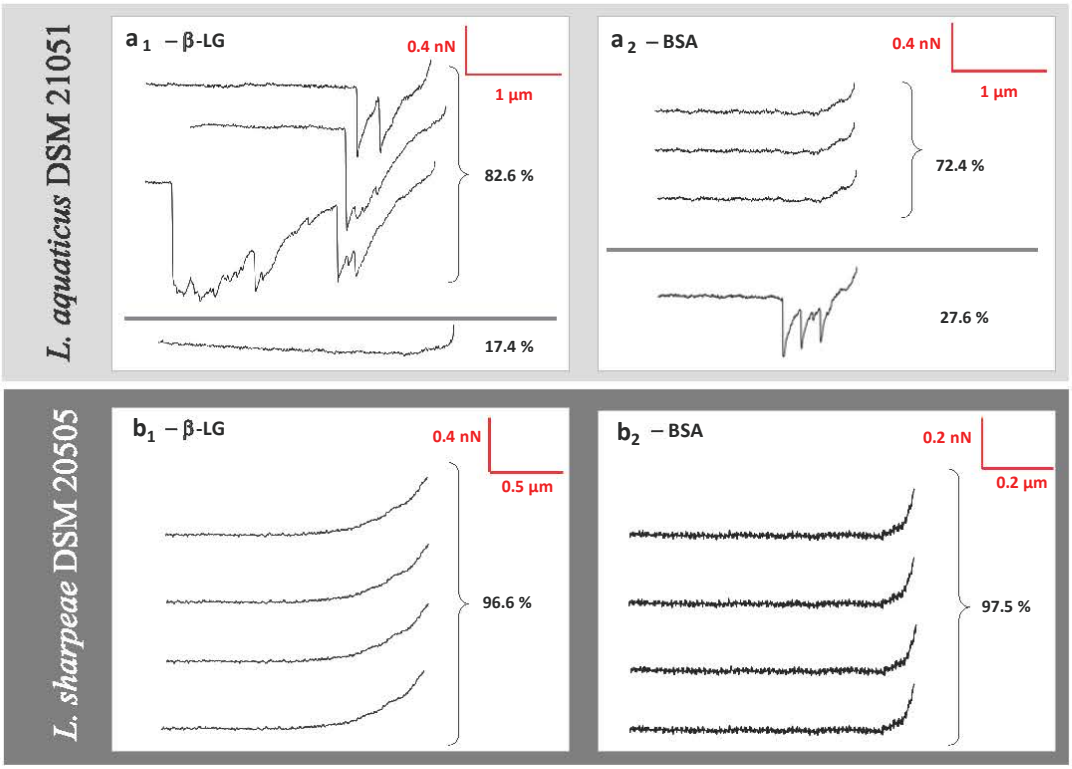

Figure IV.1.7: Comparison of the adhesive properties of two strains (*Lactobacillus aquaticus* DSM 21051, *Lactobacillus sharpeae* DSM 20505) for whey proteins isolates probed by atomic force microscopy (AFM): representative examples of retraction curves obtained for force measurements between *L. aquaticus* DSM 21051 and β-lactoglobulin (a_1), *L. aquaticus* DSM 21051 and BSA (a_2), *L. sharpeae* DSM 20505 and β-lactoglobulin (b_1), and *L. sharpeae* DSM 20505 and BSA (b_2).

L. aquaticus DSM 21051 and β-lactoglobulin attest the specificity of occurring adhesive interactions, which would happen according to a lock and key mechanism (Fig. III.3.1). 3D-AFM images recorded on mica attest of the good coverage of *L. aquaticus* DSM 21051 and therefore that adhesive events recorded did occur between *L. aquaticus* DSM 21051 cells and β-lactoglobulin-coated probes such as presented on Figure IV.1.8.

The biophysical properties of the adhesion between *L. aquaticus* DSM 21051 and β-lac were analyzed using additional force parameters including adhesion forces and final rupture length, respectively presented on Figure IV.1.9a and IV.1.9b.

Retraction curves exhibited adhesion forces averaging around 1.43 $\pm$ 0.03 nN. Final

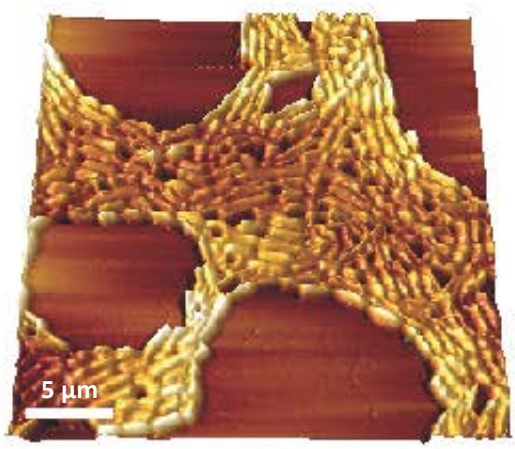

Figure IV.1.8: 3D-AFM (atomic force microscopy) image of Lactobacillus aquaticus DSM 21051 recorded in liquid in phosphate buffered saline.

rupture length averaged around 0.90 ± 0.03 μm. These results will be compared with those of LGG WT and the mutant strains LGG *spaCBA* and *welE* in the discussion section.

IV.1.2.3 Impact of adhesive interactions on bacterial location

L. aquaticus DSM 21051, *L. sharpeae* DSM 20505, LGG WT and LGG *spaCBA* were first imaged in MRS to make sure that they were originally homogeneously distributed (Figures IV.1.10a$_1$, IV.1.10b$_1$ and IV.1.11a$_1$, IV.1.11b$_2$).

Live cells of *L. aquaticus* DSM 21051 were found to aggregate in the WPI solution whereas *L. sharpeae* DSM 20505 live cells remained homogeneously distributed (Fig. IV.1.10a$_2$ and IV.1.10b$_2$). This is consistent with the adhesive properties of the control strains: LGG WT (positive control) aggregate in the WPI solution whereas LGG *spaCBA* remained homogeneously distributed (Figure IV.1.11a$_2$ and IV.1.11b$_2$). Dead bacterial cells or cells with a damaged membrane gathered in flocs for all 4 strain types (data not shown).

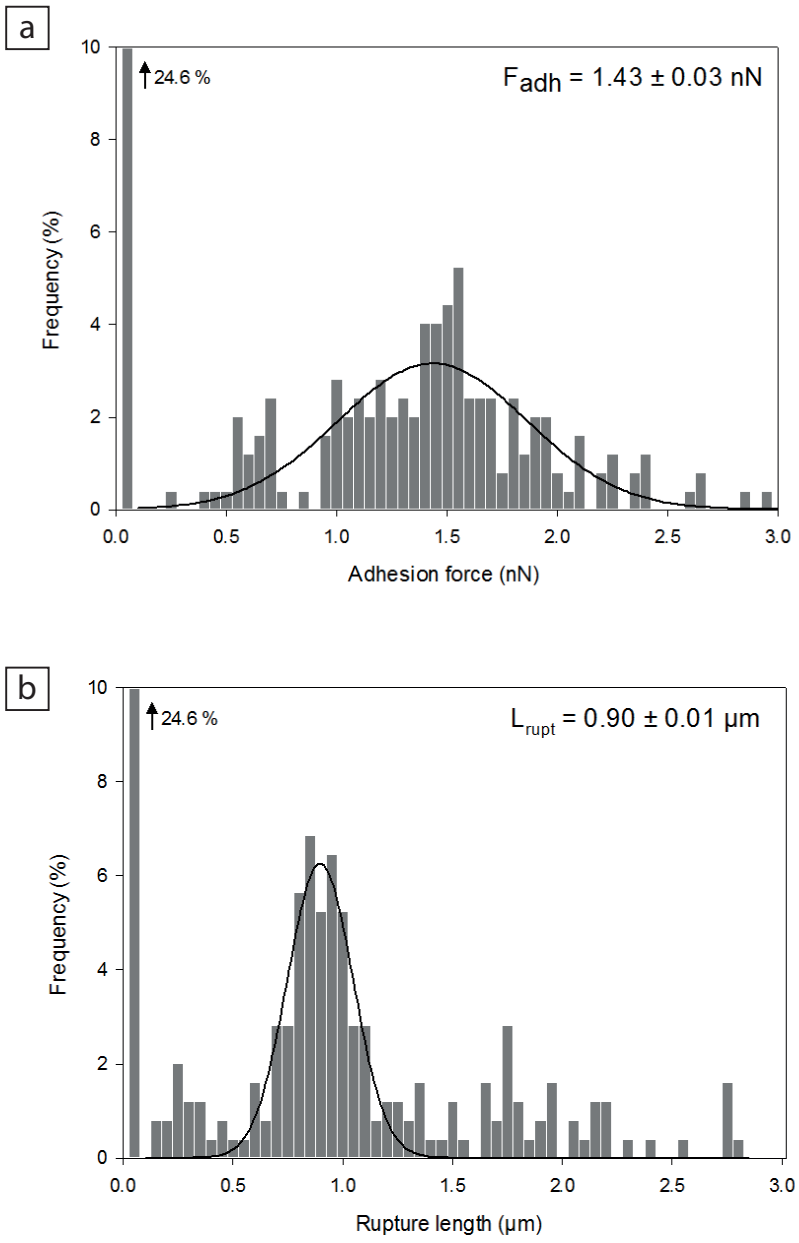

Figure IV.1.9: Interactions between β-lactoglobulin and *L. aquaticus* DSM 21051 explored by force measurement using atomic force microscopy: adhesion forces (a) and final rupture lengths (b); averages of adhesion forces and rupture lengths are precised in (a) and (b) with standard errors.

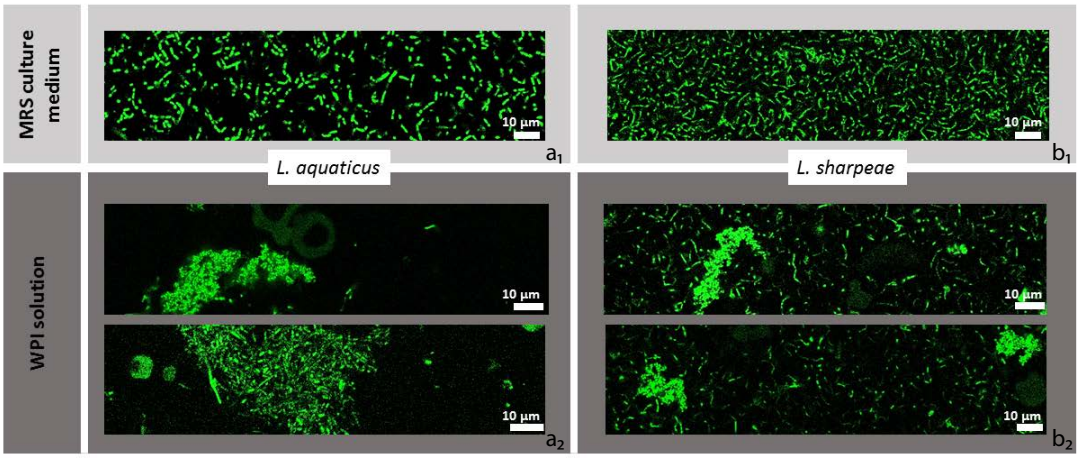

Figure IV.1.10: Spatial distribution of *L. aquaticus* DSM 21051 and *L. sharpeae* DSM 20505 in MRS culture medium [A1 and B1] and in whey protein isolate (WPI) solution [A2 and B2], imaged by confocal laser scanning microscopy (CLSM). Bacterial concentration is 107 u.f.c./ mL. Bacteria cells are represented in green on this figure whether they are viable or damaged (no difference is made here that would depend on bacterial status).

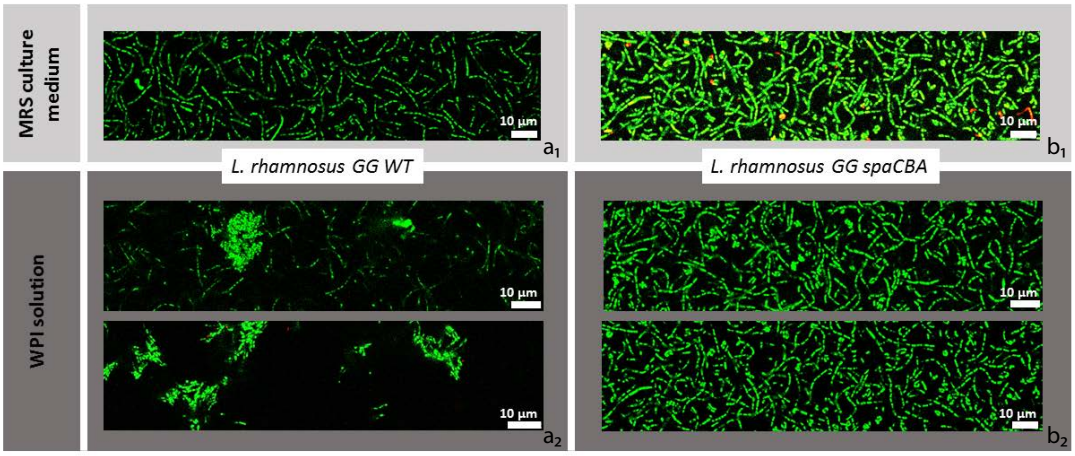

Figure IV.1.11: Spatial distribution of LGG WT and LGG *spaCBA* in MRS culture medium (a_1 and b_1) and in whey protein isolate (WPI) solution (a_2 and b_2), imaged by confocal laser scanning microscopy (CLSM). Bacterial concentration is 107 u.f.c./ mL. Bacteria cells are represented in green on this figure whether they are viable or damaged (no difference is made here that would depend on bacterial status).

IV.1.2.4 Relation between bacterial adhesion to β-lactoglobulin and predicted bacterial surface characteristics

IV.1.2.4.1 Presence of pili genes clusters (PGCs)

Predicted bacterial surface characteristics were analyzed in relation to the results of the adhesive assays in order to delineate gene candidates predicted to encode surface proteins that could be involved in bacterial adhesion to β-lactoglobulin. Amongst the 73 strains tested, 32 of them possessed at least one sortase-dependent pilus gene cluster (PGC) and therefore were predicted to express pili on their surface [Sun et al., 2015]. The average MAV of these 32 strains was -163 $\pm$ 33.2 whereas the average MAV of the 41 non-piliated strains was -194 $\pm$ 30.1. Amongst the 32 strains presenting PGCs, 16 possessed PGCs similar to LGG pilus clusters in terms of gene order, that is, a cluster of three pilin genes and one pilin-specific sortase gene [Sun et al., 2015]. The MAV of these 16 strains was -165 $\pm$ 53.8 whereas the MAV of the 16 strains with PGCs different from LGG was -160 $\pm$ 38.8. Although a mean comparison of the MAV for strains featuring PGCs compared to non-piliated strains would suggest that the presence of PGCs fosters adhesion to β-lactoglobulin, this was not supported statistically. No difference could be observed between strains featuring PGCs similar to LGG WT's and PGCs different from LGG WT's. The number of PGCs, sortase enzymes or proteins with LPxTG motif (listed for all strains in Appendix A.1) were not found either to impact strain adhesion to β-lactoglobulin (data not shown).

IV.1.2.4.2 Predicted protein domains candidates for mediating bacterial adhesion to β-lactoglobulin

More predicted surface characteristics were analyzed for the four strains found to be adhesive to β-lactoglobulin. Predicted protein domains featuring LPxTG motif found for each strain are listed in Table IV.1.2.

Strains were analyzed for gene sequence resemblance with the spaCBA domain, known

[4]proteins containing-domains written in **bold characters** for the four adhesive strains are likely to mediate adhesive interactions with β-lactoglobulin

Strain	MAV	Predicted adhesion-related protein domains[4]
Lactobacillus aquaticus DSM 21051	61.5	Immunoglobulin-like fold, **MucBP**
Lactobacillus murinus DSM 20452	12.8	**Immunoglobulin-like fold**
Lactobacillus plantarum DSM 13273	12.6	**Immunoglobulin-like fold**, **MucBP**, CMBE-CBM3 (carbohydrate-binding), **fibrinogen-binding**, collagen-binding
Lactobacillus brantae DSM 23927	6.97	**Immunoglobulin-like fold**, Collagen-binding surface protein Cna-like (type B), **Leucin-rich repeat**, **SD-repeat (type B)**
Lactobacillus rhamnosus GG WT	104	**Immunoglobulin-like fold**, **MucBP**, **Leucin-rich repeat**, Fn3-like (frequently found in the adhesin/invasin streptococcal C5a), Gram positive pilin subunit D1 N-terminal (**containing *spaCBA* domain**, responsible of adhesion to β-lactoglobulin)

Table IV.1.2: Predicted protein domains with LPxTG motif which may play a role in bacterial adhesion to β-lactoglobulin. Domains present on *L. rhamnosus* GG (known to be adhesive to β-lactoglobulin) are included as a reference. Proteins sequences used were those provided by Sun et al. (2015).

to be responsible for adhesion to β-lactoglobulin for LGG WT [Guerin et al., 2016] but no homologue sequence could be identified for any of the four adhesive strains. All strains are predicted to feature immunoglobulin-like (Ig-like) fold domains, which are usually involved in binding or molecular recognition processes [Bodelon et al., 2013]. Other and more specific adhesion-related domains present on the five strains studied include MucBP (mucin-binding), CBME/CBM3 (carbohydrate-binding), figbrinogen- and collagen-binding domains, cysteine- and leucine-rich domains, and SD-repeat B-domain. Most of these domains are present once in the genome of the adhesive strains (*L. plantarum* DSM 13273 is the only adhesive strain presenting 3 MucBP domains) and are not repeated within a given protein.

The MucBP domain is the only domain with a known adhesive-related function (apart from the Ig-like fold domain) which could be identified on *L. aquaticus* DSM 21051, the most adhesive strain to β-lactoglobulin. MucBP domains have been found predominantly in lactobacilli found naturally in intestinal niches, which suggests that they play an important role in establishing host-microbial interactions in the gut by binding mucus [Roos and Jonsson, 2002, Tassell and Miller, 2011]. *L. plantarum* DSM 13273 is the strain featuring the highest number of adhesion-related domains in its genome (Table IV.1.2). This is also the only strain out of the four presenting fibrinogen- and collagen-binding domains. The fibrinogen-binding domain has been found to accommodate linear peptides with a certain degree of ligand sequence variability [Ponnuraj et al., 2003] and therefore might be able to interact with β-lactoglobulin. *L. brantae* DSM 23927 features leucine-rich repeats (LRRs) and SD-repeat (Sdr) domains (Table IV.1.2), both of them susceptible to play a role in adhesive interactions to β-lactoglobulin. LRRs have been found to provide a structural framework for the formation of protein-protein binding and interactions [Gay et al., 1991, Kobe and Kajava, 2001] and are likely to allow a broad range of ligands [Kobe and Kajava, 2001]. Sdr-repeat domains are surface proteins that play an important role in Staphylococcus aureus adhesion and pathogenesis [McCrea et al., 2000, Wang et al., 2013]. The protein containing Sdr-repeat domains may therefore be a good candidate for mediating adhesion to β-lactoglobulin for the strain *L. brantae* DSM 23927. No other adhesion-related domain than the Ig-like fold domain was identified on *L. murinus* DSM 20452 (Table IV.1.2), which would suggest that the protein containing this domain would likely be the one involved in adhesive interactions with β-lactoglobulin.

IV.1.2.5 Adhesion specificity and common adhesion characteristics

The aim of this study was to evaluate and characterise adhesive interactions occurring between lactic acid bacteria and β-lactoglobulin. A collection of 73 LAB strains was screened for their adhesive behavior towards β-lactoglobulin and strains at the extreme of the adhesion spectrum *i.e.* a highly adhesive and a poorly adhesive strains were studied

in further depth.

Only four strains out of 73 were found to present adhesive affinities toward β-lactoglobulin. Therefore, adhesion to β-lactoglobulin appears not to be a common characteristic of the LAB group. The consequences of these adhesive interactions, when they occur, are not fully understood. However, it could be hypothesized that strains featuring adhesive affinities toward whey proteins would be lost during the drainage step of cheese manufacturing processes, alongside with whey expulsion from the cheese network. It would be interesting to test the affinity of this same strain collection to other food components in future work, in order to dispose of more comparison points to our study and to get a better understanding of the importance of adhesion to β-lactoglobulin compared to adhesion to other food components. Currently, the rare existing studies discussing bacterial adhesion to food components other than β-lactoglobulin generally concern up to four strains at most at a time [De Bellis et al., 2010, Chumphon et al., 2016, Tarazanova et al., 2017, Tarazanova et al., 2018b, Tarazanova et al., 2018a, Utratna et al., 2017], therefore failing to provide an overview of adhesion to food components amongst wide bacterial groups such as the LAB group.

The study performed by Tarazanova et al. (2017) is the only one to our knowledge that compares the adhesion level of a wide number of strains (55) to food (casein-derived) components, however these strains are all of the same species, *L. lactis* [Tarazanova et al., 2017]. Out of 55, 30–40 strains presented adhesive affinities toward casein-derived components, depending on their growth phase, and strains isolated from a dairy environment presented much stronger binding of milk proteins versus strains isolated from plants, suggesting a selective advantage [Tarazanova et al., 2017]. However, this was not confirmed in our case, as the four strains out of 73 that were originally isolated from dairy products, *i.e.*, *Lactobacillus casei* DSM 20011, *L. paracasei* subsp. *tolerans* DSM 20258, *Lactobacillus bifermentans* DSM 20003, and *L. kefiri* DSM 20587, did not present more adhesive affinities toward β-lactoglobulin in average than the strains isolated from nondairy sources (data not shown).

The strain found to be the most adhesive to β-lactoglobulin, *L. aquaticus* DSM

21051, exhibited a specific adhesive behavior when studied by AFM. The signature of the observed retraction curves was identified as specific of components stretching, suggesting that the surface of L. aquaticus DSM 21051 features a strong affinity towards β-lac. This has also been shown previously for the model strain LGG WT by our team as well as for the mutant strain LGG *welE*, expolysaccharide-depleted and known to adhere more to β-lactoglobulin than LGG WT due to its increased pili exposure [Guerin et al., 2016, Guerin et al., 2018b]. *A contrario*, *L. sharpeae* DSM 20505 which screening results show not to adhere to β-lactoglobulin presented retraction curves characteristic of a lack of adhesion to β-lac when studied by AFM (frequency of adhesive events was inferior to 5 %). Similarly, our team demonstrated previously this same fact for the model strain non-adhesive to β-lactoglobulin, LGG *spaCBA* [Guerin et al., 2016]. Comparative results are presented in Table IV.1.3.

	Adhesive events (%)		**Adhesion forces to β-lac (nN)**	**Length of the stretched component (μm)**	**Reference**
	To β-lac	**To BSA**			
L. aquaticus	82.6 ± 7.1	27.6 ± 10.4	1.43 ±0.03	0.90 ± 0.01	/
LGG WT	51.4 ± 9.9	13.1 ± 0.8	[0.13-0.81] ± 0.01	0.39 ± 0.02	Guerin et al., 2016
LGG *welE*	84.1 ± 3.0	88.5 ± 2.5	[0.58-1.31] ± 0.01	0.93 ± 0.03	Guerin et al., 2016; Guerin et al., 2017
L. sharpeae	3.4 ± 1.5	2.5 ± 0.6	NS[5]	/	/
LGG *spaCBA*	NS	/	NS	/	Guerin et al., 2016

Table IV.1.3: Comparison of the adhesive capabilities of five strains to β-lactoglobulin when studied by atomic force microscopy: *L. aquaticus* DSM 21051, *L. sharpeae* DSM 20505, and the model strains LGG WT, LGG *spaCBA* (pili-depleted) and LGG *welE* (expolysaccharides-depleted).

The adhesive behavior of *L. aquaticus* DSM 21051 towards β-lactoglobulin appears relatively close to the one of LGG *welE* in terms of frequency of adhesive events. The high specificity of the adhesion phenomenon occurring between *L. aquaticus* DSM 21051 and β-lactoglobulin is highlighted by the fact that the frequency of adhesion is almost

[5]NS *i.e.* "Non Significant" means that the frequency of adhesive events was inferior to 5 %.

twice as high as the one characterising adhesive interactions between LGG WT and β-lactoglobulin, whereas the frequency of adhesion of *L. aquaticus* DSM 21051 on BSA is almost four times lower than the one occurring between LGG *welE* and BSA. The mean adhesion force recorded on the last peak is also three times higher than the mean adhesion force recorded for LGG WT and β-lactoglobulin, and higher than the highest adhesion force recorded on the last peak for LGG welE and β-lactoglobulin, reaffirming the idea of a very strong specificity and adhesion strength. When comparing the length of components stretched by adhesive interactions with β-lactoglobulin, *L. aquaticus* DSM 21051 and LGG welE both exhibit molecules stretched up to 1 μm *i.e.* three times longer than the molecule stretched in the case of LGG WT (Table IV.1.3). The molecule mediating adhesive interactions with β-lactoglobulin in the case of *L. aquaticus* DSM 21051 is therefore comparable in length to LGG pili when stretched, which may explain the higher specificity and adhesion strength found for *L. aquaticus* DSM 21051 compared to LGG WT, which pili are partially hidden within the expolysaccharides layer [Guerin et al., 2016].

On the other hand, the frequency of adhesive events observed between *L. sharpeae* DSM 20505 and β-lactoglobulin is inferior to 5 % and similar to the frequency of adhesive events observed on BSA for both this strain and *L. aquaticus* DSM 21051. The frequency of adhesive events recorded when using BSA-coated probes is also 4 times lower for *L. sharpeae* DSM 20505 than for LGG *spaCBA* (negative control). Overall, *L. sharpeae* DSM 20505 has demonstrated very poor adhesive capacities towards β-lactoglobulin. However, when analyzed for predicted adhesion-related protein domains, this strain revealed a total of 23 adhesion-related domains, 8 of which being different, including MucBP and Gram positive pilin subunit D1 N-terminal, although no sequence homologue to the *spaCBA* domain was found (data not shown). The *spaCBA* domain is known to mediate adhesion to β-lactoglobulin for the piliated strain LGG WT (Guerin et al., 2016). This confirms that adhesive interactions with β-lactoglobulin are specific, and cannot be predicted accurately using only genomic predictions (the functions of these domains may not be accurately predicted or they may not be expressed).

The gathering behavior observed by CLSM for the adhesive strains in the WPI solution also pledges in favor of a specific bacterial adhesion to β-lactoglobulin for *L. aquaticus* DSM 21051. CLSM results indicate that the location of bacteria in a dairy matrix strongly depends on bacterial surface properties. These observations are important as it was evidenced recently that physical properties of dairy products, such as viscosity and gel hardness, are affected by bacterial surface properties in the case of surface-engineered strains [Tarazanova et al., 2018a]. In light of our results, it would be interesting to see if that is also the case for wild strains presenting different surface properties inducing different adhesive behaviors. Some peptides shown to be linked to bacterial aggregation were also recently evidenced to be able to promote bacterial adhesion to functionalized surfaces and Caco-2-cells [Okochi et al., 2017]. This typical behavior was responsible for observed enhanced interactions between LAB and the host intestinal mucosa [Okochi et al., 2017]. Adhesive interactions with β-lactoglobulin leading to the aggregation of *L. aquaticus* DSM 21051 and LGG WT cells might therefore be considered for further study in order to determine whether they would promote such kind of behavior as well.

IV.1.3 Adhesive interactions amongst lactic acid bacteria: extent and characteristics

Bacterial adhesion is likely to play a key role on the protection and distribution of probiotic bacteria in a given matrix. However, evaluating and characterising bacterial adhesion at the LAB group level is difficult because of the lack of reliable, fast methods allowing assessing bacterial affinity on a wide number of strains.

The new microbiological method developed in Section IV.1.1 answers this need by allowing determining and comparing quickly affinities by strain and by component for a wide range of strains and components of interest. It can thus provide a good overview of all bacteria-components interactions, although slight differences in affinities between strains or components might require complementary methods to be identified. This method was validated on four well-known strains for six milk components based on times at which bacterial growth starts, and results obtained were mostly in adequacy with

those obtained through AFM. This method only requires to know the growing conditions of the tested bacteria and involves high-throughput screening and automatized handling using an automated liquid handling system for 96-well plates. It has a wide range of applications as it encompasses all fields where determining the affinity of bacteria to a given range of components can be useful. Direct applications include determining the efficacy of a range of biopolymers as probiotic encapsulating materials, and the affinity of pathogenic bacteria to food matrix components compared to intestinal components in order to help designing food matrices for preventing bacterial infection and host colonization.

In Section IV.1.2, this method was applied to a collection of 73 LAB strain, seeking to go beyond bacterial species differences in revealing common adhesive characteristics of LAB in relation to dairy food components such as β-lactoglobulin. We first looked for LAB species featuring adhesive affinities for β-lactoglobulin, then focused on the molecular characteristics of this adhesion. We observed adhesion to β-lactoglobulin for few LAB (less than 6 % of our collection). However, for those which did feature adhesive affinities, some common characteristics were pointed out that matched the characteristics previously identified on the model strain LGG. These characteristics include the specificity of the affinity, as well as the impact on bacterial spatial distribution in the matrix.

Major findings are that (i) Adhesion to whey proteins is apparently not a common characteristic to the LAB group (few strains presented adhesive affinities towards β-lactoglobulin), (ii) Strains featuring adhesive affinities towards β-lactoglobulin present common adhesive characteristics (specific β-lactoglobulin-adhesion domains related to the specificity of the AFM signature), and (iii) Adhesion to β-lactoglobulin was shown to strongly influence bacterial distribution in dairy matrices featuring this component (adhesive bacteria gathered in flocs in whey matrices whereas non-adhesive bacteria distribute more homogeneously), and could therefore modulate their accessibility and later delivery when designing functional foods containing probiotic LAB.

According to these findings, food matrices could play a protective role on bacteria by influencing their spatial distribution, which may prove especially useful for probiotic

bacteria. Indeed, as bacteria adhering to a component have been found to flocculate in the food matrix containing this component, this could result in later heterogeneous delivery in the gastro-intestinal tract (GIT) which would impact host colonization, but may also better protect bacterial survival until they reach the GIT. These findings also pave the road to future experiments aiming generalizing bacterial adhesion characteristics to broad bacterial groups, thus helping with practical food matrix design. It would therefore be interesting to study the potential protective effect of components to which bacteria are adherent, such as fat globules, during critical steps of the food manufacturing process. Indeed, steps such as spray-drying during probiotic milk powder production may generate stress and thus potentially induce damages to bacterial cell surfaces, which may hinder both their viability and functionality.

IV.2

Shaving and breaking bacterial chains under shearing

IV.2.1 Shearing impact on bacterial functionality and spatial organization

IV.2.1.1 Bacterial flocs categories

Distinct categories created to describe bacterial chain size distribution include from single cells to 10-cell chains, chains featuring more than 10 cells (which will be called "long chains" throughout the manucript), and flocs. Flocs have been defined to stand either for (i) bacterial cells that stick together by their sides (and not their ends), meaning that they were not part of the same chain, when 3 or more cells are stuck in parallel, (ii) two or more bacterial chains close to one another bend excessively ("destructured chains" with apparent overlaps), or (iii) bacterial chains combine both bending (case (ii)) and sticking (case (i)) characteristics. The floc type (ii) has been shown to be caused by mechanical strain sensing amongst other factors, which was identified as an important component of bacterial cell shape regulation for *Escherischia coli* [Wong et al., 2017]. Bacterial floc types (i) and (ii) are represented in Figure IV.2.1. Flocs can be of various sizes, as long as all cells within the flocs remain connected to one another.

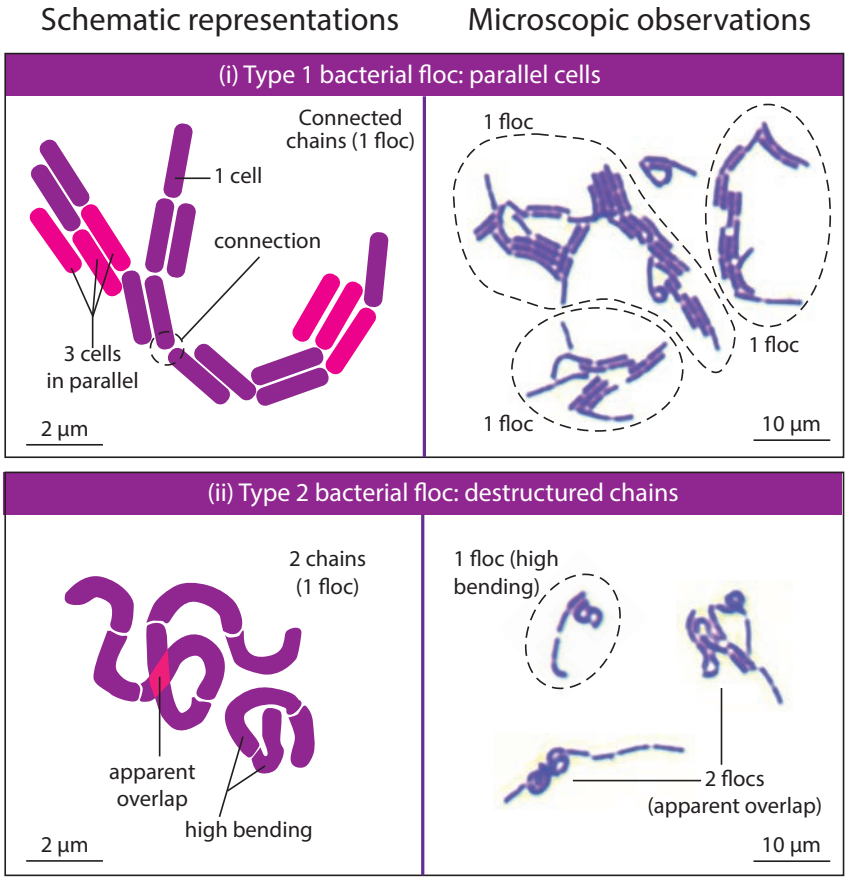

Figure IV.2.1: Representation of bacterial flocs types: parallel bacterial cells (i) and destructured chains (ii); representative microscopic pictures of each floc type for *Lactobacillus rhamnosus* GG WT are presented to illustrate the proposed schematic representations.

IV.2.1.2 Bacterial chain size distribution

IV.2.1.2.1 One-time shearing experiments

Bacterial chain size distribution has been monitored before and after shearing for the characteristic shear rates of 244 (no air pressure applied), 3.0×10^5, 3.7×10^5, 4.2×10^5, 4.9×10^5, and 11×10^5 s^{-1} for LGG WT, LGG *spaCBA*, and LGG *welE* and Figure IV.2.2 presents results obtained at 244, 3.0×10^5, 4.9×10^5, and 11×10^5 s^{-1}. Comprehensive data sets for all shear rates tested are available for LGG WT, *spaCBA*, and *welE* in respective

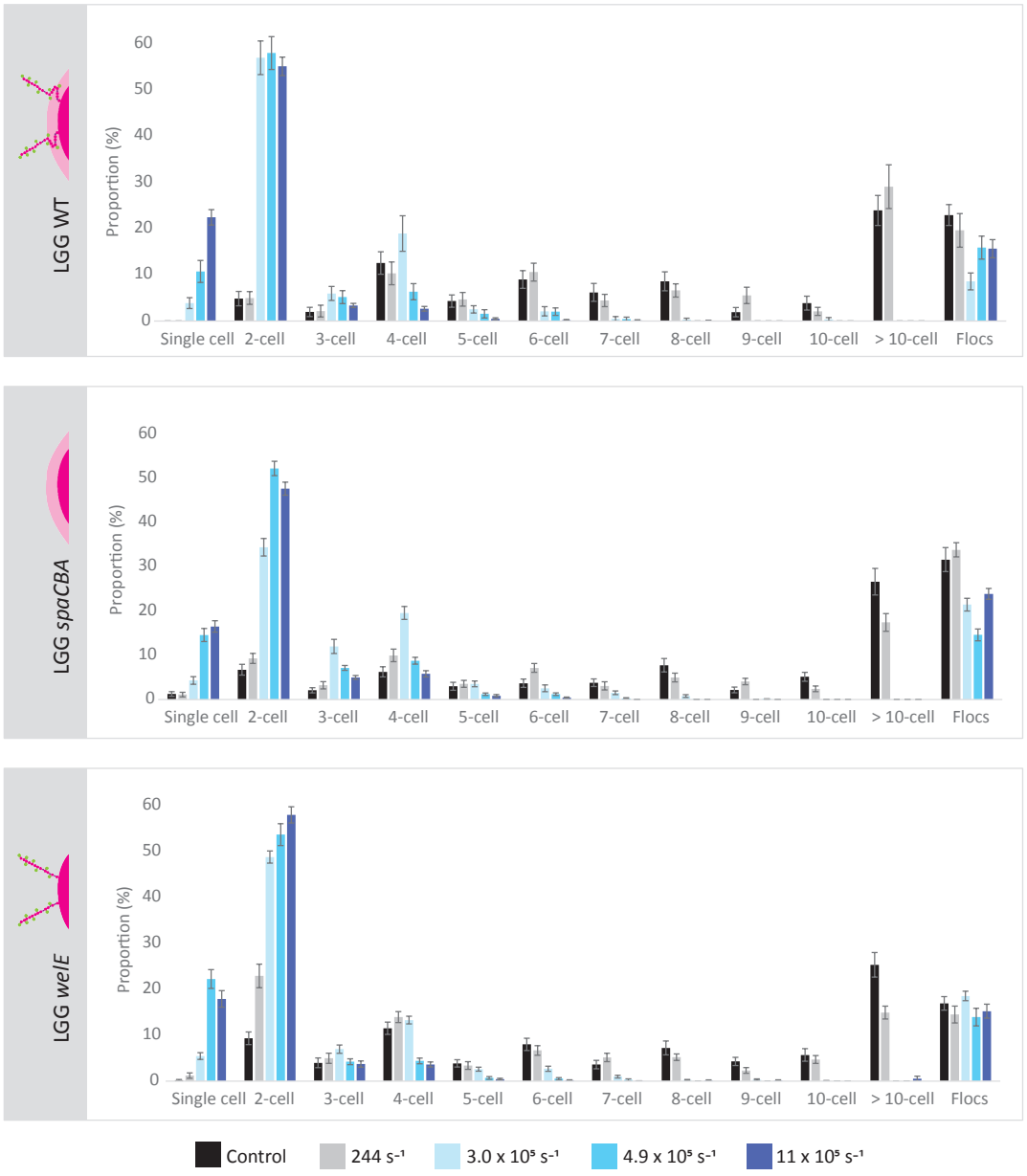

Figure IV.2.2: Bacterial chain size distribution for the strains *Lactobacillus rhamnosus* GG "wild type" (WT), *spaCBA*, and *welE* before and after shearing at 244, 3.0×10^5, 4.9×10^5, and 11×10^5 s^{-1}. Error bars correspond to standard errors.

appendices B.1, B.2, and B.3.

In their initial state before shearing, for all strains 25% of the total number of chains

and flocs featured more than 10 cells. Flocs also represent an important proportion of the initial bacterial suspension when observed after adhesion assays, varying between between strains from 16% for LGG *welE* to more than 30% for LGG *spaCBA*. Little or no single cells were initially found, and other chain lengths appeared to be randomly distributed, with proportions ranging from 1 to 10%.

When sheared at very low shear rate (244 s^{-1}), the chain distribution of LGG WT remained mostly similar to the control. For the two other strains, however, a significant decrease (by about 10 %) in long chains occurred. This loss was compensated by a proportional increase in 2-cell chains for LGG *welE*, whereas it was more homogeneously distributed amongst the different chain length categories for LGG *spaCBA*.

When performing atomization even at low air pressures (0.2 bar, *i.e.* 3.0×10^5 s^{-1}), the proportion of 2 cell-chains drastically increased by a factor of 6, representing at least 35 % of the total number of chains and flocs in solution, and almost all chains featuring more than four cells get broken whichever the strain. The proportions of chains featuring from seven to more than ten cells remains inferior to 1 %; 6-cell and 5-cell chains represented each around 2 % of the total number of chains and flocs (up to 4 % for LGG *welE*). The proportion of 4-cell chains also increased of 10 % for shear rates as low as 3.0×10^5 s^{-1} (0.2 bar) for the strains LGG WT and *spaCBA*.

The strain LGG *spaCBA* was the one the less impacted by chain breakage at low air pressures, as 2-cell chains represented only 35 % of its total chain distribution, versus 50 % or more for the two other strains. LGG *spaCBA* was also identified as the strain the most likely to flocculate, flocs representing the major category of bacterial organization even in the initial solution. For this strain, the increased proportion of 2-cell chains due to shearing may result from floc breakage instead of chain breakage (the loss in flocs being relatively equivalent in proportion to the gain in 2-cell chains). Given the fact that a 2-cell chains proportion of 50% was reached for a shear rate of 4.9×10^5 s^{-1} for LGG *spaCBA* versus for a shear rate of 3.0×10^5 s^{-1} for LGG WT and *welE*, it can be proposed that interactions between bacterial cells in flocs involve higher interaction forces than those involved between bacterial cells in chains, thus, that flocculation would

tend to preserve bacterial chains from breaking. However, although the ability to form flocs in different proportions after adhesion assays seems to depend both on the strain and on the applied shear rate, flocculation may result from the fixation of bacterial cells onto a surface and therefore our results might not be representative of what occurs in suspension.

Most of the shearing impact on bacterial chain distribution can be observed from an air pressure of 0.2 bars ($\dot{\gamma} = 3.0 \times 10^5$ s^{-1}). Higher shear rates generated very little additional changes in bacterial chain structuration. Globally, all proportions of chains featuring more than two cells decreased (up to 10 % decrease). However, some additional changes appeared to be more strain-dependent. Proportion of 2-cell chains did not evolve much for LGG WT and LGG *welE*, but kept on increasing for LGG *spaCBA* until reaching a threshold similar to the two other strains (between 50 and 60 %), while the proportion of flocs of LGG *spaCBA* proportionally decreased. Very high pressures *i.e.* elevated shear rates, were required to obtain single cells, which proportion gradually increased for LGG WT as shear rate increases, whereas it suddenly increased of respectively 10 and 20 % for the two mutant strains *spaCBA* and *welE*.

Overall, this suggests that chain breakage is more likely to occur for strains organized in long chains than for strains which tend to flocculate. Moreover, chain breakage is triggered at low spraying air pressures ($P = 0.2$bars, $\dot{\gamma} = 3.0 \times 10^5$ s^{-1}.). In fact, most breakage events occurred at very low air pressures and led to a drastic increase in 2-cell chains, which seem to be the major and most stable form of bacterial chains in flow. Indeed, this form is able to resist even shear rates as high as $11{\times}10^5$ s^{-1} without breaking. Higher shear rates than $3.0{\times}10^5$ s^{-1}, although not inducing as drastic a change to bacterial chain distributions compared to low shear rates, generated additional strain-dependent bacterial chain breakage and led to an increased proportion of single cells. A hypothesis for why 2-cell chains appear to be a more favorable configuration in shear flow than longer bacterial chains could be that forces exerted on the cells of 2-cell chains are minimized compared to other forms. This hypothesis will be furthered explored in the modeling part.

Four-cell chains are the second major and most stable form; their breakage occurs in parallel of an increase in proportions of single cells and 2-cell chains, suggesting that it would break in three pieces, two single chains and one 2-cell chain. The breaking mechanisms of bacterial chains will also be furthered discussed in the modeling part.

IV.2.1.2.2 Repeated versus one-time shearing

	LGG WT		
	Control (%)	One-time (%)	Repeat (%)
Single cells	0.0 ± 0.0^a	$22 \pm {}^b$	38 ± 2^c
2-cell chains	4.8 ± 1.5^a	55 ± 2^b	47 ± 2^b
3-cell chains	2.0 ± 1.0^a	3.4 ± 0.5^b	1.4 ± 0.4^a
4-cell chains	12 ± 2^a	2.6 ± 0.5^b	1.6 ± 0.4^b
Flocs	23 ± 2^a	16 ± 2^b	11 ± 2^b

Table IV.2.1: Impact of repeated shear stress ('Repeat') compared to one-time shear stress ('One-time') at high shear rate (11×10^5 s^{-1}) on bacterial chain distribution (expressed in proportion of total number of chains and flocs) for *Lactobacillus rhamnosus* GG wild type. Standard errors are presented for thirty measurements; for each strain, different letters within the same row attest of statistically significant differences.

	LGG *spaCBA*		
Control	One-time	Repeated	
Single cells	1.2 ± 0.5^a	16 ± 1^b	36 ± 1^c
2-cell chains	6.7 ± 1.2^a	48 ± 2^b	43 ± 1^b
3-cell chains	2.1 ± 0.6^a	5.0 ± 0.4^b	3.4 ± 0.3^c
4-cell chains	6.2 ± 1.1^a	5.8 ± 0.7^a	1.7 ± 0.3^b
Flocs	32 ± 3^a	24 ± 1^b	16 ± 1^c

Table IV.2.2: Impact of repeated shear stress ('Repeat') compared to one-time shear stress ('One-time') at high shear rate (11×10^5 s^{-1}) on bacterial chain distribution (expressed in proportion of total number of chains and flocs) for *Lactobacillus rhamnosus* GG *spaCBA*. Standard errors are presented for thirty measurements; for each strain, different letters within the same row attest of statistically significant differences.

The effect of repeated versus one-time shearing on bacterial chain size distribution is presented in Tables IV.2.1, IV.2.2, and IV.2.3 respectively for LGG WT, *spaCBA*, and *welE* using a characteristic shear rate of 11×10^5 s^{-1}. Initial chain distributions are used as controls. Only impacted bacterial chain categories are presented in Tables IV.2.1,

		LGG *welE*	
Control	One-time	Repeated	
Single cells	0.2 ± 0.2^a	18 ± 2^b	52 ± 2^c
2-cell chains	9.3 ± 1.3^a	58 ± 2^b	33 ± 2^c
3-cell chains	4.0 ± 1.1^a	3.7 ± 0.7^a	2.9 ± 0.9^a
4-cell chains	11 ± 1^a	3.6 ± 0.6^b	0.3 ± 0.2^c
Flocs	17 ± 2^a	15 ± 2^{ab}	11 ± 1^b

Table IV.2.3: Impact of repeated shear stress ('Repeat') compared to one-time shear stress ('One-time') at high shear rate (11×10^5 s^{-1}) on bacterial chain distribution (expressed in proportion of total number of chains and flocs) for *Lactobacillus rhamnosus* GG *welE*. Standard errors are presented for thirty measurements; for each strain, different letters within the same row attest of statistically significant differences.

IV.2.2, and IV.2.3. Comprehensive data sets including results for other categories are available in Appendices B.1, B.2, and B.3 respectively for LGG WT, *spaCBA*, and *welE*.

Whichever the strain, repeated shearing reduced the proportions of all kind of chains and flocs and increased the proportion of single cells. However, the impact of repeated shearing also appeared both strain- and chain length-dependent. When comparing between strains, the chain distribution of the mutant strain LGG *welE* was indeed more impacted than those of the two other strains. The proportion of single cells of LGG *welE* after repeated shearing increased by a factor of 2.5 compared to one-time shearing, while the proportion of 2-cell chains was divided by a factor of 2. For LGG WT and *spaCBA*, the proportion of single cells after repeated shearing increased by a factor of 2 compared to one-time shearing, while the proportion of 2-cell chains only slightly decreases (not significantly). Similarly, the 4-cell chains proportion was divided by a factor of 10 for LGG *welE*, whereas it was only divided by 2 for LGG WT and by 3 for LGG *spaCBA*. LGG *welE* appeared therefore to be more sensitive to repeated shearing than the two other strains.

When comparing LGG WT chain lengths, 3-cell and 4-cell chains appeared to be more sensitive to repeated shearing than 2-cell chains and flocs. A similar behavior was observed for LGG *spaCBA*: the proportion of 2-cell chains did not change from one-time shearing to repeated shearing. However, proportions of 3-cell and 4-cell chains after

repeated shearing were significantly lower than after one-time shearing, reduction factors being respectively of 2.4 and 1.6 for LGG WT, and of 1.5 and 3.4 for LGG *spaCBA*. Two hypotheses can explain this fact for both LGG WT and *spaCBA*: (i) the increase in single cells at higher shear rates actually resulted rather from the breakage of 4-cell and 3-cell chains than from the breakage of 2-cell chains, or (ii) 3-cell and 4-cell chains broke into 2-cell chains and single cells, and part of the 2-cell chains broke into single cells. The second hypothesis may however appear less likely, since there does not seem to be any reason for why only part of the 2-cell chains could break into single cells. Assuming the existence of a shear rate threshold leading to chain breakage, which is coherent with observations for the range of one-time shear rates previously tested in Section IV.2.1.2.1, most 2-cell chains should be affected the same way by repeated shearing, which would lead to a much higher increase in proportion of single cells than the one observed. The sensitivity to shearing of bacterial chains of LGG *welE* decreased in the following order: 4-cell chains > 2-cell chains > flocs. In this case, 3-cell chain proportion remained stable.

For all strains, the proportion of flocs after repeated shearing decreased compared to one-time shearing, although this decrease was only statistically significant for the mutant strain LGG spaCBA. Floc breakage may also have contributed to the increased proportion of single cells. Pönisch et al. (2016) previously showed that certain types of pili mediate the merging dynamics of single cells and self-assembly of colonies [Pönisch et al., 2017].

This suggests that the impact of repeated shearing on bacterial cell chain size distribution depends both on the considered strain and the preferred bacterial organization (in terms of chain length and floc proportion). One-time shearing did not seem to be able to break 2-cell chains even when applying high shear rates (Figure IV.2.2), contrarily to repeated shearing, for which the degree of breakage was found to be strain-sensitive. Flocs seemed to be more resistant to shearing. LGG *welE* was found to be the most sensitive strain to repeated shearing. Two hypotheses can be formulated to explain this. On one hand, as this strain is impaired in EPS production, connections between cells within a chain are less protected from shearing. EPS could also play a protective role

on the way shearing constraints apply to the cells, by increasing the fluid viscosity for example [Badel et al., 2011]. However, this hypothesis does not explain the differential impact of shearing according to chain length, especially for repeated stress. On the other hand, LGG *welE* is expected to be the most adhesive of the three investigated strains due to its increased pili exposure [Guerin et al., 2016, Guerin et al., 2018a]. This could have resulted in a higher degree of adhesion to the walls of the nozzle. As bacteria attached to walls would be likely to undergo a higher shearing stress under flow, LGG *welE* would be more affected by shearing and its chains therefore more easily broken. Proximity to the walls could be fostered for some chain types depending on their length and weight, therefore resulting in a differential shearing impact according to chain length. A similar phenomenon was observed for blood cells with different densities and shape properties when undergoing shear stress in channels, leading to differential cell distribution [Goldsmith and Marlow, 1979, Aarts et al., 1988]. For blood cells, this differential distribution has been identified as one essential factor leading to differential adhesion to the channel walls [Aarts et al., 1988, Gidaspow and Chandra, 2014].

IV.2.1.3 Bacterial functionality

The impact of shearing on bacterial adhesive abilities was evaluated for shear rates ranging from 244 to 11×10^5 s^{-1} for LGG WT and the three mutant strains LGG *spaCBA*, LGG *welE*, and LGG D2 (double mutant). Adhesion results are presented in Tables IV.2.4, IV.2.4, IV.2.4, and IV.2.4 respectively. They were expressed both in $1000/t_{start}$ normalized on the adhesion of the control LGG WT to β-lactoglobulin (without shearing) to allow inter-strain comparison, and in functionality losses expressed in percentages (normalized on the bacterial functionality of the control without shearing for each strain, which is set equal to 100 %) to determine the influence of shearing for each strain independently. Overall, bacterial adhesive abilities appeared to be affected by shearing. However, the shearing impact seemed to be strain-dependent. Indeed, the highest functionality losses recorded for one-time-applied shearing amongst adhesive strains ranged from 1% (LGG WT) to more than 30% for LGG *welE*. Surprisingly, in the case of the

$\dot{\gamma}$ (10^5 s^{-1})	LGG WT	
	$1000/t_{start}$	Loss (%)
Control	1.01 ± 0.09^a	0
0.00244	1.05 ± 0.14^a	-1
3.0	1.03 ± 0.16^a	-5
3.7	1.06 ± 0.13^a	-3
4.2	1.02 ± 0.15^a	-6
4.9	1.00 ± 0.14^a	-2
11 (one-time)	0.99 ± 0.16^a	1
11 (repeated)	0.86 ± 0.020^a	14

Table IV.2.4: Impact of shearing on bacterial adhesive abilities of LGG WT. Results are expressed in means ± standard deviations; values of $1000/t_{start}$ are normalized on the control and therefore expressed without units. Different letters attest of statistically significant differences.

$\dot{\gamma}$ (10^5 s^{-1})	LGG *spaCBA*	
	$1000/t_{start}$	Loss (%)
Control	0.41 ± 0.050^a	0
0.00244	0.41 ± 0.038^a	0.5
3.0	0.50 ± 0.067^b	-22
3.7	0.49 ± 0.057^b	-19
4.2	0.49 ± 0.057^b	-20
4.9	0.49 ± 0.056^b	-19
11 (one-time)	0.48 ± 0.048^b	-18
11 (repeated)	0.43 ± 0.0090^{ab}	-5

Table IV.2.5: Impact of shearing on bacterial adhesive abilities of LGG *spaCBA*. Results are expressed in means ± standard deviations; values of $1000/t_{start}$ are normalized on the control and therefore expressed without units. Different letters attest of statistically significant differences.

strain featuring the lowest adhesive abilities, LGG *spaCBA*, an increase of adhesive abilities was also acknowledged after shearing compared to the initial adhesion level (marked as "negative adhesion losses" in Table IV.2.5).

The wild type strain was the one whose adhesive abilities were the less affected by shearing: in particular, one-time shearing appeared not to impact on bacterial adhesive abilities. Even when applying the highest shear rate repeatedly, losses remained inferior to 20 %. However, for higher shear rates such as those applied by Kiekens et al. on

$\dot{\gamma}$ (10^5 s^{-1})	LGG *welE*	
	$1000/t_{start}$	Loss (%)
Control	1.8 ± 0.09^a	0
0.00244	1.5 ± 0.06^b	17
3.0	1.6 ± 0.04^b	11
3.7	1.4 ± 0.03^{bc}	19
4.2	1.4 ± 0.02^{bc}	18
4.9	1.4 ± 0.02^{bc}	22
11 (one-time)	1.2 ± 0.05^c	31
11 (repeated)	0.78 ± 0.016^d	56

Table IV.2.6: Impact of shearing on bacterial adhesive abilities of LGG *welE*. Results are expressed in means ± standard deviations; values of $1000/t_{start}$ are normalized on the control and therefore expressed without units. Different letters attest of statistically significant differences.

$\dot{\gamma}$ (10^5 s^{-1})	LGG D2	
	$1000/t_{start}$	Loss (%)
Control	0.77 ± 0.11^a	0
0.00244	0.70 ± 0.049^b	9
3.0	0.71 ± 0.063^a	8
3.7	0.73 ± 0.083^a	5
4.2	0.72 ± 0.062^a	6
4.9	0.69 ± 0.054^b	10
11 (one-time)	0.67 ± 0.069^b	13
11 (repeated)	0.57 ± 0.010^b	26

Table IV.2.7: Impact of shearing on bacterial adhesive abilities of LGG D2 (*welE-spaCBA*). Results are expressed in means ± standard deviations; values of $1000/t_{start}$ are normalized on the control and therefore expressed without units. Different letters attest of statistically significant differences.

the same strain (using an air flow rate $\dot{q}_A$ five times higher than the highest value of $\dot{q}_A$ used in the current study), LGG WT was imaged without pili after shearing and functionality losses went over 70 % when evaluated as the ability to adhere to Caco-2 cells [Kiekens et al., 2019]. This drastic decrease found in previous literature can look surprising in regard to our results. Three hypothesis can be made to explain this difference: (i) different surface molecules are involved in adhesion to β-lactoglobulin compared to Caco-2 cells and some of them may be more or less shear-sensitive, (ii),

there is a shear rate threshold below which bacterial surface is little affected, but can be almost completely "shaved" once past it, or (iii) other kinds of stresses, such as heat stress and osmotic stress (spray-drying and rehydration) may have come into play and, combined with shearing, may have had a lot more impact on bacterial surface.

The adhesion of the pili-depleted strain LGG *spaCBA* increased by 20 % for shear rates over % 3×10^5 for one-time shearing experiments. However, when the highest shear rate was repeatedly applied, bacteria in both sheared and control suspensions presented similar adhesive abilities. This could be explained by the partial removal of the surface EPS layer of LGG *spaCBA* upon shearing, which would expose other adhesive surface proteins [Guerin et al., 2018a]. This is supported by the fact that the double mutant strain LGG D2 (pili- and EPS-depleted) was found to have an adhesive capacity superior to LGG *spaCBA* in control conditions (initial unsheared suspensions), which could be due to the presence of other adhesive proteins on the cell surface (usually buried in the EPS layer). The existence of such surface adhesive proteins hidden within the EPS layer has previously been brought to light [Guerin et al., 2018a]. Potential candidates that would mediate adhesion in the absence of pili include the Mucus Binding Factor MBF, the MbA protein, lipoteichoïc acids or peptidoglycans, all being present at the surface of LGG cells within the EPS layer [Guerin et al., 2018a, Lebeer et al., 2012]. The EPS themselves have previously been found to play a positive role in adhesion, although of less importance than the role played by pili [Guerin et al., 2018a].

However, LGG D2 also featured adhesive abilities losses for the highest shear rates (reaching 10% after shearing at 4.9×10^5 s^{-1}), suggesting that these other surface proteins contributing to bacterial adhesion may also get damaged by shearing. On the contrary, LGG *spaCBA* adhesive abilities were always increased by shearing, the lowest increase resulting from repeated shearing. A hypothesis could be that, in the range of investigated shear stresses, the EPS layer of LGG *spaCBA* could not be completely removed after one-time shearing, and that the remaining parts of this layer may surround and therefore "protect" the other underlying surface adhesive proteins. Less forces were therefore exerted on these more buried sites, which are thus more preserved and could later act as

adhesive patches. However, under repeated shearing, the EPS of LGG *spaCBA* would be more completely removed and therefore the underlying surface adhesive molecules more damaged, leading to a smaller gain in adhesive abilities.

The LGG *welE* strain, initially the most adhesive strain (before shearing), was also found to be the most sthear-sensitive strain. Adhesive abilities losses seemed to incrementally increase with shear stress even from shear rates as low as 244 s^{-1}. For shear rates from 3.0×10^5 to 4.9×10^5 s^{-1}, adhesive abilities losses approached 20 %, whereas for the highest shear rate, adhesive abilities losses respectively reached 31 % and 56 % for one-time vs. repeated shearing. The fact that LGG *welE* is a lot more sensitive to shearing than LGG WT may be due to the fact that pili would be partially protected by the EPS layer featured by LGG WT, which could prevent their removal and limit the forces exerted at the pili basis. EPS have indeed recently been found to feature a protective effect against shearing in terms of bacterial functionality for *Lactococcus lactis* subsp. *cremoris* in fermented milk compared to non-EPS-producing strains [Girard and Schaffer-Lequart, 2007]. The full pili-exposure of LGG *welE*, presented in previous studies as a competitive advantage allowing higher adhesive abilities [Guerin et al., 2016, Burgain et al., 2014b, Lebeer et al., 2009], was found here to be a competitive disadvantage in matter of strain resistance to shearing.

It can also be noticed that even after repeated shearing at the highest shear rate, strains still presented significant adhesive abilities differences. This suggests that each strain possesses a minimal adhesion level below which it does not seem possible to get. However, the classification of strains according to their adhesive abilities is changed by repeated shearing. Before shearing, adhesive abilities increased in the following order: LGG *spaCBA* < LGG D2 < LGG WT < LGG *welE*, whereas after repeated shearing at the highest tested shear rate, it increased in the following order: LGG *spaCBA* < LGG D2 < LGG *welE* < LGG WT. This confirms that LGG *welE* was the most sheared-sensitive strain in this study.

Finally, adhesive abilities losses can be correlated with chain breakage for most strains (except the wild type), as the major impact of shearing on adhesive abilities occurred at

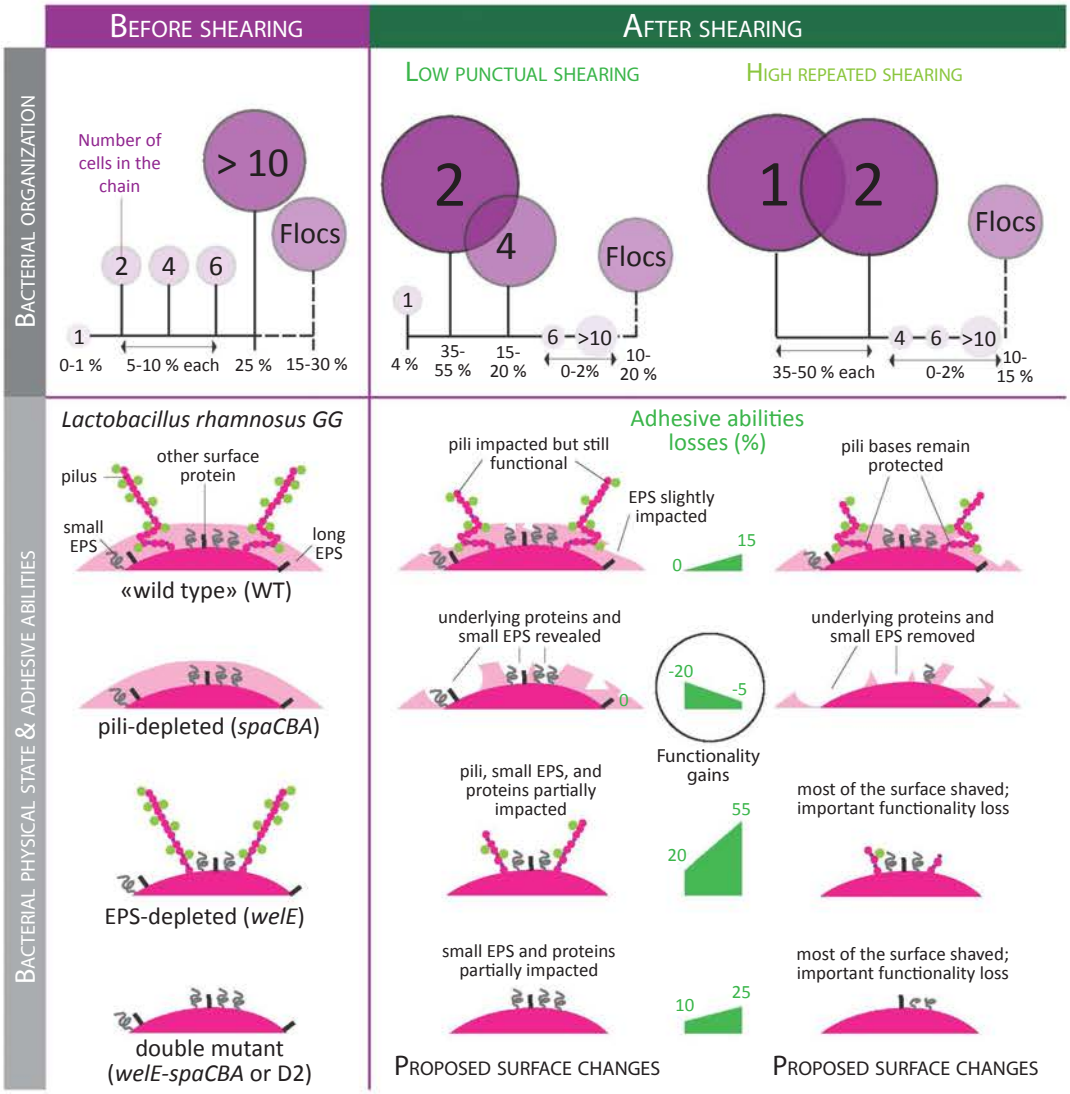

Figure IV.2.3: Summary of the effects of shearing on bacterial organization (chain size distribution), physical state, and adhesive abilities for the strain *Lactobacillus rhamnosus* GG and three mutant strains. Negative adhesive abilities losses indicate an increase in adhesive abilities.

the lowest air pressure ($P = 0.2$ bars, $\dot{\gamma} \approx 3.0 \times 10^5\ s^{-1}$), concomitantly with the drastic increase in the proportion of 2-cell chains. Although adhesive abilities losses further increased at higher shear rates, it evolves slightly compared to the first adhesive abilities loss experienced at the lowest air pressure. Reasons for why most of the adhesive abilities

losses seem to occur at low shear rates will be explored in the modeling part.

Figure IV.2.3 sums up the main effects of shearing on bacterial chain size distribution (chains and flocs) and bacterial adhesive abilities evidenced in this study on bacterial suspensions. Corresponding shear-induced nanoscale changes at the surface of bacterial cells are also proposed.

IV.2.2 Modeling the impact of shear flow on bacterial chain integrity

This section focuses on the impact of shearing on bacterial chains integrity at the cell scale by answering one central question: do bacterial chains matter in a shear flow in terms of bacterial adhesive abilities? This question will be investigated by looking at the influence of the position of a body within a chain, the chain angle with the horizontal during a chain rotation period, and the chain length on bacterial surface adhesive proteins (SAP) removal, such as pili and small filamentous adhesive proteins, through the proxy of traction forces exerted on the surface of ellipsoidal bodies in a chain.

IV.2.2.1 Bacterial surface adhesive proteins removal and their relationship to surface traction forces

This section aims at proving that it can be sensible to use the maximum surface traction force exerted on the surface of a bacterial cell as a proxy for pili removal or, more generally, SAP removal, when considering the problem at cell scale (when viscous forces are dominant, and the sedimentation phenomenon is neglected). Addressing this question, we will first explore briefly the simple case of pili removal through high-speed centrifugation, which has been acknowledged experimentally [Tripathi et al., 2012]. Then, we determine the expression of the traction force on the surface of a spherical body, identified to a single bacterial cell, in background shear flow in three different scenarii *i.e.* (i) when the sphere is freely translating/rotating with the flow, (ii) when the sphere is fixed in space (*i.e.* the bacterial cell adheres to a surface), and (iii) when the sphere is part of a bacterial chain which is moving in the flow. Then, we will determine the viscous force

applied to a pilus fixed on a given cell of a bacterial chain in a shear flow and compare it to the traction force expressions previously established.

IV.2.2.1.1 Bacterial pili removal through high-speed centrifugation

Pili removal has been shown to occur for LGG WT cells collected during the exponential growth phase when centrifugated once at $8,000g$ for 30 min [Tripathi et al., 2012]. In this section, we propose a general approach to evaluate pili removal through tangential traction forces for a simplified, individual spherical bacterium experiencing centrifugal forces. We point out the limitations of this approach, some will be addressed in the following sections.

Considering a individual bacterium in a linear flow of global velocity field $\boldsymbol{u}$ such as represented in Figure IV.2.4, we solve the Stokes equation for the local velocity field $\boldsymbol{u}_S$, calculated for a Stokeslet, *i.e.* a solution of the Stokes equation for a singular point to which is given a Dirac impulse, where $\boldsymbol{x_0}$ is the center of mass (centroid), a the radius of

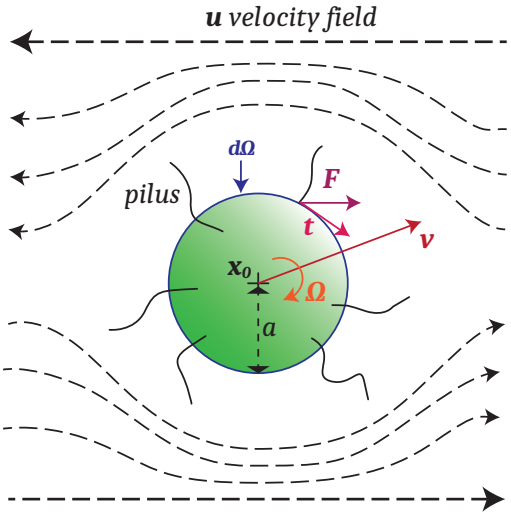

Figure IV.2.4: Individual spherical bacterium with pili in a linear flow of velocity field $\boldsymbol{u}$.

the sphere, $\boldsymbol{d\Omega}$ the surface of the body, $\boldsymbol{t}$ the traction force exerted by surface area, $\boldsymbol{v}$ the local velocity field, $\boldsymbol{F}$ the net force by surface area, and $\boldsymbol{\Omega}$ the local torque of the body. The background velocity field $\boldsymbol{u}$ can be expressed in function of a tensor matrix $\boldsymbol{T}$ which

can be itself separated in a stresslet $\boldsymbol{S}$ (extensional component of the field) and a rotlet $\boldsymbol{R}$ (rotational component of the field). $\boldsymbol{S}$ is the *symmetric rate* of the strain tensor. It corresponds to a *stretching stress* (elongating/compressing). $\boldsymbol{R}$ is the *antisymmetric rate* of the strain tensor. It corresponds to a *rotative stress* (rotational motion). A graphic representation of these tensors is given in Figure IV.2.5.

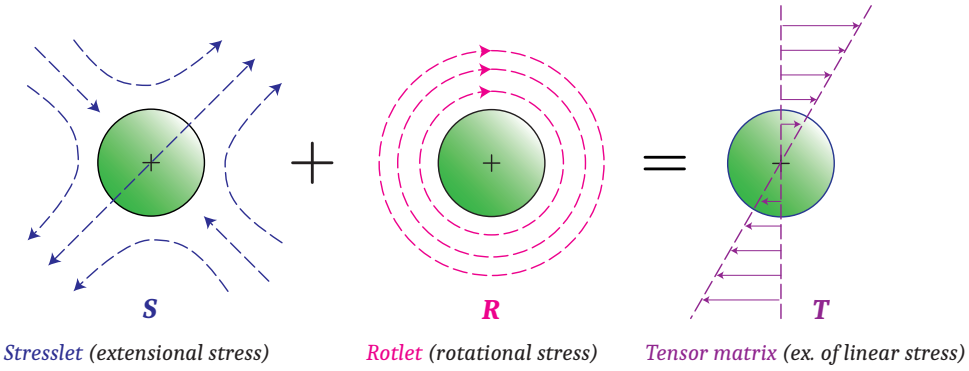

Figure IV.2.5: Graphic representation of the two types of stress applied on spherical bodies in a linear flow such as a shear flow; these stresses are related such as $\boldsymbol{S} + \boldsymbol{R} = \boldsymbol{T}$ with $\boldsymbol{u} =\propto \boldsymbol{T}$.

At the equilibrium, the system presented in Fig. IV.2.4 is such as:

- the net force on the sphere is equal to $\mathbf{0}$: $\boldsymbol{F_{net}} = \int_{\boldsymbol{d\Omega}} \boldsymbol{F}.d\boldsymbol{S} = \mathbf{0}$
- the net moment on the sphere is equal to $\mathbf{0}$: $\boldsymbol{M_{net}} = \int_{\boldsymbol{d\Omega}} (\boldsymbol{x} - \boldsymbol{x_0})\boldsymbol{F}.d\boldsymbol{S} = \mathbf{0}$

The following conditions are fixed at the boundaries:

$$\begin{cases} \lim_{|\boldsymbol{x}|\to\infty} \boldsymbol{u} & = \boldsymbol{x} \cdot \boldsymbol{T} \\ \lim_{|\boldsymbol{x}|\in \boldsymbol{d\Omega}} \boldsymbol{u} & = \boldsymbol{v} + \boldsymbol{\Omega}(\boldsymbol{x} - \boldsymbol{x_0}) \end{cases}$$

With $\boldsymbol{x}$ being the directional vector of the sphere.

When solving the Stokes equation using the singularity method *i.e.* giving to the body an initial Dirac impulse $\delta\boldsymbol{F}$ at the origin, $\boldsymbol{F}$ being the force of this impulse, we get the following expressions for the $\boldsymbol{u}$, the Stokeslet $\boldsymbol{u}_S$, the global pressure p and the

Stokeslet pressure p_S:

$$\begin{cases} \boldsymbol{u} &= \boldsymbol{u}_S + \dfrac{a^2}{6}\nabla^2 \boldsymbol{u}_S \\ \boldsymbol{u}_S &= \dfrac{1}{8\pi\mu}\boldsymbol{G}\boldsymbol{F} \\ \boldsymbol{G} &= \left(\dfrac{\boldsymbol{I}}{|\boldsymbol{x}|} + \dfrac{\boldsymbol{x}\boldsymbol{x}^T}{|\boldsymbol{x}|^3}\right) \end{cases} \quad and \quad \begin{cases} p &= p_S + \dfrac{a^2}{6}\nabla^2 p_S \\ p_S &= \dfrac{2(\boldsymbol{x}\cdot\boldsymbol{F})}{|\boldsymbol{x}|^3} \end{cases}$$

Where $\boldsymbol{I}$ is the identity tensor and $\boldsymbol{x}^T$ the transposed of $\boldsymbol{x}$.

Knowing $\boldsymbol{u}$ and p we can calculate the stress tensor $\boldsymbol{\sigma}$ and the traction force exerted on the bacterium by surface area (projection of the stress tensor on the bacterium surface) defined such as:

$$\begin{cases} \boldsymbol{\sigma} &= -p\boldsymbol{I} + \mu\left(\nabla\boldsymbol{u} + \nabla\boldsymbol{u}^T\right) \\ \boldsymbol{t} &= \hat{\boldsymbol{n}}\cdot\boldsymbol{\sigma} \end{cases}$$

Where $\hat{\boldsymbol{n}}$ unitary vector such as at $|\boldsymbol{x}| = a$, $\hat{\boldsymbol{n}} = \dfrac{\boldsymbol{x}}{a}$. By solving for the traction force with Mathematica we get:

$$\boldsymbol{t} = \frac{-1}{4\pi a^2}\boldsymbol{F} \tag{IV.2.1}$$

And at equilibrium we know that the sum of the forces exerted on the bacterium is equal to $\mathbf{0}$. Therefore:

$$\begin{aligned} \boldsymbol{F_{net}} + \int_{\boldsymbol{d\Omega}} \boldsymbol{t}.d\boldsymbol{S} &= \mathbf{0} \\ \implies \boldsymbol{F_{net}} &= \boldsymbol{F} \end{aligned}$$

Therefore the expressions for the local traction force $\boldsymbol{t}$ and the local velocity $\boldsymbol{v}$ near the

sphere are:

$$\boldsymbol{t} = \frac{-1}{4\pi a^2}\boldsymbol{F_{net}} \tag{IV.2.2}$$

$$\boldsymbol{v} = \frac{\boldsymbol{F_{net}}}{6\pi\mu a} \tag{IV.2.3}$$

The net force $\boldsymbol{F_{net}}$ exerted on the sphere (neglecting hydrodynamic interactions with the fluid for now) is gravitational:

$$\boldsymbol{F_{net}} = \frac{4}{3}\pi a^3 \left(\rho_{water} - \rho_{bacteria}\right) Mg\hat{\boldsymbol{z}} \tag{IV.2.4}$$

Where a is the radius of the sphere (Fig. IV.2.4), ρ_{water} and $\rho_{bacteria}$ the mass densities, g the gravitational constant (g = 9.8 m.s^{-2}), $\hat{\boldsymbol{z}}$ a unitary vertical vector and M a multiplicative factor if needed (*i.e.* when a centrifugal force of M x g is applied *e.g.*). Therefore the final expressions for $\boldsymbol{t}$ and $\boldsymbol{v}$ are:

$$\boldsymbol{t} = \frac{\Delta\rho Mga\hat{\boldsymbol{z}}}{3} \tag{IV.2.5}$$

$$|\boldsymbol{v}| = \left(\frac{2a^2}{9\mu}\right)\Delta\rho Mg \tag{IV.2.6}$$

Where a radius of the bacterium, μ dynamic viscosity of the suspension, $\Delta\rho$ difference between the mass densities of water and bacteria, M a multiplicative factor and g the gravitational constant. Assuming that pili would be removed proportionally to the tangential section, we name τ the **tangential component of $\boldsymbol{t}$** (in $N.m^{-2}$), which we can

calculate using polar coordinates:

$$\begin{aligned}
\tau &= (\boldsymbol{I} - \hat{\boldsymbol{n}}\hat{\boldsymbol{n}}) \cdot \boldsymbol{t} \\
&= \boldsymbol{t} - (\hat{\boldsymbol{n}} \cdot \boldsymbol{t})\, \hat{\boldsymbol{n}} \\
\text{and} \begin{cases} \hat{\boldsymbol{n}} = \cos\theta \hat{\boldsymbol{z}} + \sin\theta \hat{\boldsymbol{e}}_\phi(\phi) \\ \hat{\boldsymbol{n}} \cdot \hat{\boldsymbol{z}} = \cos\theta \end{cases} \\
\implies \tau = |\boldsymbol{t}| &= \frac{\Delta\rho M g a}{3}
\end{aligned} \tag{IV.2.7}$$

We know that pili can be removed from LGG when applying a centrifugal force of $8,000\ g$ for 30 min [Tripathi et al., 2012]. When calculating the corresponding theoretical local velocity $\boldsymbol{v}$ and tangential traction τ by surface area and when applied on a point (infinitestimal surface) using the equations (IV.2.3) and (IV.2.7) with $M = 8,000$, $a \in [5; 10]\ \mu m$, $\mu = 10^{-3}\ Pa.s$, $\Delta\rho \in [0.1.10^{-3}, 0.2.10^{-3}]\ kg.m^{-3}$ (ρ_{bacteria} was assumed identical to the one found for *E. coli* by Lewis et al. [Lewis et al., 2014]), we find that:

$$\begin{cases} \boldsymbol{v} & \approx 1\ mm.s^{-1} \\ \tau & \approx 1\ N.m^{-2} \\ \tau_{point} & \approx 1\ pN \end{cases}$$

This would mean that a pellet starts to be formed 1 min after starting the centrifugation (for a 10 cm-tube), which sounds reasonable.
However, in the literature local traction forces (applied on an infinitesimal surface) necessary to remove pili range between 250-300 pN for LGG [Tripathi et al., 2013] and up to 500 pN for type I pili for *Escherischia coli* [Miller et al., 2006]. The theoretical value of τ_{point} would therefore not be sufficient to remove pili from bacteria, whereas it occurred in reality. Several reasons can explain that difference:

- Pili have been considered until now as short filaments feeling the velocity $\boldsymbol{v}$ only locally near the bacterial surface, whereas in reality they sometimes can be on the

same length scale as the bacterium itself and would therefore experience the entire velocity field $\boldsymbol{u}$; in reality, the average length of a pili is intermediary (1.0 ± 0.3 μm whereas the length of a bacterium is of 2-3 μm),

- Pili were also considered uniform filaments, but in the case of LGG are in fact elongating, extensible (spring-like) coils [Tripathi et al., 2012, Tripathi et al., 2013], meaning they are likely to feel more the flux of the velocity field,

- Bacteria are not individual spheres but chains of rods, which can modify their global dynamics,

- Bacteria can interact with the walls of the tube when being centrifuged, which would make them experience more shear flow,

- Bacteria are numerous in the suspension and therefore can run into one another during the centrifugation, which would foster friction.

The real force experienced by the bacterium on its surface for a centrifugal force of 8,000 g expressed during 30 min would therefore be greater than 1 pN.
It is also to be noted that pellets could in some cases found to start forming even for very low centrifugal forces such as 500 g applied for 1 min (data not shown), whereas the equation (IV.2.3) does not reflect it as sedimentation is found to start theoretically after 10 min of centrifugation at 500 g.
The reasons detailed above for explaining the difference between the experimental and the theoretical values of the traction force could also contribute to explain the velocity difference. Another reason explaining this latter difference could be that sedimentation is not the only process happening during centrifugation as other flux (backflow *e.g.*) could occur thus impating the overall dynamics.

From this brief study, we conclude that tangential traction forces obtained from single spheres calculations cannot be used as quantitative proxies for pili removal occurring in centrifugation settings. In the next sections, we will consider the case of surface traction forces for bacteria in a simple shear flow and see if it can be sensible to use them as

qualitative proxies for pili removal on bacterial cells in a chain.

IV.2.2.1.2 Traction on a lone, freely-moving spherical cell

Consider a background shear flow $\boldsymbol{u}^\infty = \dot{\gamma} y \hat{\boldsymbol{x}}$ and a sphere with center at $\boldsymbol{x}_0 = x_0\hat{\boldsymbol{x}} + y_0\hat{\boldsymbol{y}}$. The velocity field due to the presence of the sphere at a point $\boldsymbol{x} = (x, y, z)$ in the flow is given by

$$\begin{aligned}\boldsymbol{u}(\boldsymbol{x}) = \boldsymbol{u}^\infty(\boldsymbol{x}) + \frac{1}{8\pi\mu}\left(1 + \frac{a^2}{6}\nabla^2\right)\boldsymbol{G}(\boldsymbol{x} - \boldsymbol{x}_0)\cdot\boldsymbol{F} \\ + \frac{1}{8\pi\mu}\boldsymbol{G}^c(\boldsymbol{r}(s) - \boldsymbol{x}_0)\cdot\boldsymbol{L} + \left(1 + \frac{a^2}{10}\nabla^2\right)\nabla\boldsymbol{G}(\boldsymbol{r}(s) - \boldsymbol{x}_0) : \boldsymbol{S},\end{aligned} \tag{IV.2.8}$$

where the force $\boldsymbol{F}$ and torque $\boldsymbol{L}$ depend on whether or not the sphere is free to rotate in the flow, and $\boldsymbol{S}$ is the stresslet. Generically, with $\boldsymbol{U}$ and $\boldsymbol{\Omega}$ the translation and rotation rate of the sphere, we have $\boldsymbol{F} = 6\pi\mu a(\boldsymbol{U} - \boldsymbol{u}^\infty(\boldsymbol{x}_0))$, $\boldsymbol{L} = 4\pi\mu a^3(2\boldsymbol{\Omega} - \nabla\times\boldsymbol{u}^\infty(\boldsymbol{x}_0))$, and $\boldsymbol{S} = (20\pi\mu a^3/3)\boldsymbol{E}^\infty$, where $\boldsymbol{E}^\infty = (\dot{\gamma}/2)(\hat{\boldsymbol{x}}\hat{\boldsymbol{y}} + \hat{\boldsymbol{y}}\hat{\boldsymbol{x}})$ is the symmetric rate-of-strain tensor describing the background flow. The associated traction is given by (with $\boldsymbol{x} \in D$, the surface of the sphere),

$$\boldsymbol{f}(\boldsymbol{x}) = -\frac{1}{4\pi a^2}\boldsymbol{F} - \frac{3}{8\pi a^4}\boldsymbol{T}\times\boldsymbol{x} + \frac{5\mu}{a}\boldsymbol{E}^\infty\cdot\boldsymbol{x}. \tag{IV.2.9}$$

If the sphere is free to rotate in the flow, then $\boldsymbol{U} = \boldsymbol{u}^\infty(\boldsymbol{x}_0)$ and $\boldsymbol{\Omega} = \nabla\times\boldsymbol{u}^\infty(\boldsymbol{x}_0)/2$ (and the body is force and torque free), so the traction is

$$\boldsymbol{f}(\boldsymbol{x}) = \frac{5\dot{\gamma}\mu}{2a}((y - y_0)\hat{\boldsymbol{x}} + (x - x_0)\hat{\boldsymbol{y}}), \tag{IV.2.10}$$

which is notably independent of the sphere size.

IV.2.2.1.3 Traction on a fixed spherical cell

Looking back at Equation (IV.2.9), if the spherical cell is held fixed in the flow, then $\boldsymbol{U} = \boldsymbol{\Omega} = \mathbf{0}$, thus finding

$$\begin{aligned}\boldsymbol{f}(\boldsymbol{x}) = \frac{3\dot{\gamma}\mu y_0}{2a}\hat{\boldsymbol{x}} + \frac{3\dot{\gamma}\mu}{2a}\left((y-y_0)\hat{\boldsymbol{x}} - (x-x_0)\hat{\boldsymbol{y}}\right) \\ + \frac{5\dot{\gamma}\mu}{2a}((y-y_0)\hat{\boldsymbol{x}} + (x-x_0)\hat{\boldsymbol{y}}) \\ = \frac{\dot{\gamma}\mu}{2a}\left[(3y_0 + 8(y-y_0))\hat{\boldsymbol{x}} + 2(x-x_0)\hat{\boldsymbol{y}}\right].\end{aligned} \tag{IV.2.11}$$

If the sphere is centrally located at $y_0 = 0$, then the traction remains independent of the size. But if the sphere is held in the oncoming flow the traction now depends on the size of the sphere. If the sphere is held at $y_0 = 0$ then the maximum traction is larger than that for a freely moving sphere but only by a factor of 8/5. This is because the boundary conditions are naturally not satisfied by a fixed sphere without disturbing the background flow, but this is also true of a rotating sphere with nearly identical consequences.

IV.2.2.1.4 Traction on a spherical cell in a chain

One way for a cell to be "held in the flow" in some sense is if it is part of a chain of bodies, which rotates with zero net force and torque, but each component along the chain may still experience a force and torque. Using the simplest resistive force theory to describe the motion of a chain of bodies, we find that the rotation rate is $\boldsymbol{\Omega} = -\dot{\gamma}/2(1-\cos(2\theta))\hat{\boldsymbol{z}}$, where θ is the orientation angle relative to $\hat{\boldsymbol{x}}$, such as presented in Figure IV.2.6. Associated with this rotation, with the chain centered at the origin, the n^{th} sphere away from the origin moves with speed $\boldsymbol{U} = \boldsymbol{\Omega} \times [na(\cos\theta\hat{\boldsymbol{x}} + \sin\theta\hat{\boldsymbol{y}})] = a\dot{\gamma}n\sin^2\theta\,(\sin\theta\hat{\boldsymbol{x}} - \cos\theta\hat{\boldsymbol{y}})$, and rotates with rate $\boldsymbol{\Omega}$, resulting in a traction (which neglects hydrodynamic interac-

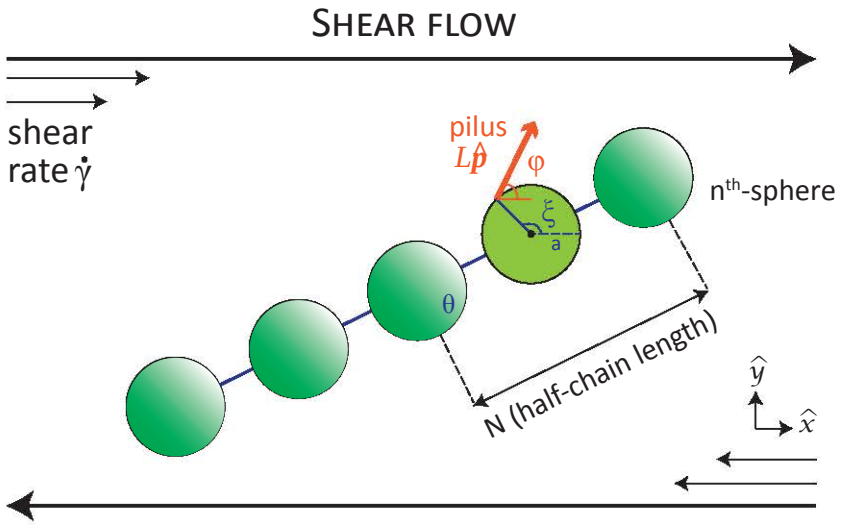

Figure IV.2.6: Schematic of the pilus on body $(n-1)$ of the chain. Only one pilus has been represented for better readability of the figure. n is measured from the center, and the chain is of length $2N$. The pilus has length L, points in the $\hat{\boldsymbol{p}}$ direction, and is connected to the sphere by a connection point located on the sphere at an angle ξ relative to $\hat{\boldsymbol{x}}$, and fixed at an orientation angle ϕ relative to $\hat{\boldsymbol{x}}$. The chain makes an angle θ with the horizontal. Chain motion is assumed here to be semi-rigid.

tions among the bodies),

$$\begin{aligned}\boldsymbol{f}(\boldsymbol{x}) &= \frac{3\mu\dot{\gamma}n}{2}\sin\theta\cos\theta\,(\cos\theta\hat{\boldsymbol{x}}+\sin\theta\hat{\boldsymbol{y}}) + \frac{3\dot{\gamma}\mu\cos(2\theta)}{2a}\,((y-y_0)\hat{\boldsymbol{x}}-(x-x_0)\hat{\boldsymbol{y}}) \\ &+ \frac{5\dot{\gamma}\mu}{2a}((y-y_0)\hat{\boldsymbol{x}}+(x-x_0)\hat{\boldsymbol{y}}) \\ &= \frac{\dot{\gamma}\mu}{2a}\left(3an\sin\theta\cos^2\theta+(5+3\cos(2\theta))(y-y_0)\right)\hat{\boldsymbol{x}} \\ &+ \frac{\dot{\gamma}\mu}{2a}\left(3an\sin^2\theta\cos\theta+(5-3\cos(2\theta))(x-x_0)\right)\hat{\boldsymbol{y}}\end{aligned} \tag{IV.2.12}$$

where $\boldsymbol{x}_0 = an(\cos\theta\hat{\boldsymbol{x}}+\sin\theta\hat{\boldsymbol{y}})$. Since $\boldsymbol{x} = \boldsymbol{x}_0 + O(a)$, the traction is independent of a. However, it increases linearly with n, the position along the chain. The traction on the n^{th} sphere away from the center is now a factor of $3n/5$ larger than that of a freely moving sphere. In this sense, the traction on the bodies far from the center is

considerably reduced by their abandoning the chain.

IV.2.2.1.5 Relationship between surface adhesive protein removal and surface tractions

It is simpler to analyze and compute the traction on the surface of a bacterium in a flow than to study the forces on individual small pilus or other SAP attached to the cell body. Here the question of to which extent the surface tractions described in Equations (IV.2.10), (IV.2.11), and (IV.2.12) may be used as proxies to understand the force on the SAP. The surface traction is proportional to the velocity gradient, which we expect to be relevant to the force on the SAP. If the SAP is small relative to the body size, then the no-slip boundary condition on the cell body is particularly relevant, as it renders the fluid motionless there relative to the body motion. So the velocity of the base of the SAP is given by $\boldsymbol{U}+\boldsymbol{\Omega}\times(\boldsymbol{X}-\boldsymbol{x}_0)$, where $\boldsymbol{X}-\boldsymbol{x}_0$ is the location of the SAP connection point. To determine the viscous force on the SAP, $\boldsymbol{f}_p(s)$, a function of the arc-length $s \in [0, L]$,the resistive force approximation can be used again although in a different context, writing

$$\boldsymbol{f}_p(s) = \frac{2\pi\mu}{\log(2/\varepsilon_p)}[2\boldsymbol{I} - \hat{\boldsymbol{p}}\hat{\boldsymbol{p}}] \cdot (\boldsymbol{u}(\boldsymbol{r}(s)) - \boldsymbol{r}_t(s)), \tag{IV.2.13}$$

where ε_p is the aspect ratio of the SAP (radius/length), $\hat{\boldsymbol{p}}$ is the orientation of the SAP, $\boldsymbol{r}(s) = \boldsymbol{X} + s\hat{\boldsymbol{p}}$ is the position along the SAP at arc-length s, and $\boldsymbol{r}_t(s)$ is the velocity of the SAP itself there. At this point, semi-rigidity of the SAP is assumed, in order to consider first that only slight (neglectable) deformation of the SAP under flow can occur. The SAP is considered in the xy-plane, with the connection point located on the sphere at an angle ξ relative to $\hat{\boldsymbol{x}}$, and fixed at an orientation angle ϕ relative to $\hat{\boldsymbol{x}}$ (Fig. IV.2.6). With its rigid body motion, it thus moves with velocity

$$\boldsymbol{r}_t = \boldsymbol{U} + \boldsymbol{\Omega} \times (\boldsymbol{r}(s) - \boldsymbol{x}_0) = \boldsymbol{U} + \boldsymbol{\Omega} \times (\boldsymbol{X} - \boldsymbol{x}_0 + s\hat{\boldsymbol{p}}). \tag{IV.2.14}$$

The expression for the velocity field in the fluid determined above considered that $\boldsymbol{x} = \boldsymbol{r}(s)$ along the SAP. When evaluating the force per length on the SAP above with this

velocity inserted, and integrate on $s \in [0, L]$, because this is generally a rather long expression, SAP will be assumed short only terms up to $O(L/a)$ with L/a assumed small will be conserved.

Looking at a spherical cell free to move in the fluid, the fluid velocity along the SAP is

$$\boldsymbol{u}(s) = \frac{a\dot{\gamma}s}{2}\left(\sin(\xi-\phi)\hat{\boldsymbol{x}} - \cos(\xi-\phi)\hat{\boldsymbol{y}}\right) + O(s^2). \tag{IV.2.15}$$

The force on the SAP is then:

$$\begin{aligned}\boldsymbol{F}_{SAP} &= \int_0^L \boldsymbol{f}_p(s)\,ds \\ &= \frac{5\pi\mu\dot{\gamma}\cos(\xi-\phi)L}{2\log(2/\varepsilon_p)}\left[2\sin\xi\cos(2\xi)\hat{\boldsymbol{x}} - (\cos\xi + \cos(3\xi))\hat{\boldsymbol{y}}\right] \\ &+ O((L/a)^2),\end{aligned} \tag{IV.2.16}$$

or at worst,

$$\|\boldsymbol{F}_{SAP}\|_\infty \leq \frac{5\pi\mu\dot{\gamma}L}{\log(2/\varepsilon_p)} + O((L/a)^2), \tag{IV.2.17}$$

Now considering a SAP on the n^{th} sphere away from the origin on a chain, the fluid velocity is

$$\boldsymbol{u}(s) = a\dot{\gamma}s\sin^2\theta\left[(n\sin(\theta-\phi)+\sin(\xi-\phi))\hat{\boldsymbol{x}} - (n\cos(\theta-\phi)+\cos(\xi-\phi))\hat{\boldsymbol{y}}\right], \tag{IV.2.18}$$

resulting in

$$\begin{aligned}\boldsymbol{F}_{SAP} &= \frac{\pi\mu\dot{\gamma}\cos(\xi-\phi)L}{2\log(2/\varepsilon_p)} \\ &\times \left[\sin\xi\cos(\xi-\phi)(-6\cos(2\theta)+3n\sin(2\theta)\sin(\theta-\xi)+10\cos(2\xi))\hat{\boldsymbol{x}}\right. \\ &\left.-\cos\xi(6\cos(2\theta)-3n\sin(2\theta)\sin(\theta-\xi)-10\cos(2\xi))\hat{\boldsymbol{y}}\right] + O((L/a)^2),\end{aligned} \tag{IV.2.19}$$

or at worst,

$$\|\boldsymbol{F}_{SAP}\|_\infty \leq \frac{\pi\mu\dot{\gamma}(2+3n/2)L}{\log(2/\varepsilon_p)} + O((L/a)^2), \tag{IV.2.20}$$

so just as with the traction on the cell body, the force acting on the SAP is larger if it is on a sphere towards the end of the chain. Therefore, using the maximal surface traction force as a proxy for SAP removal does appear sensible.

IV.2.2.2 Impact of the position of bacterial cells within a chain

The impact of the position of bacterial cells within chains of 2 up to 5 cells in a shear flow on the maximal surface traction force ($\mathrm{Max}_{\mathrm{STF}}$) exerted on each bacterial cell (ellipsoid body) has been investigated. Results are presented in Figure IV.2.7 for chains of 3, 4, and 5 cells.

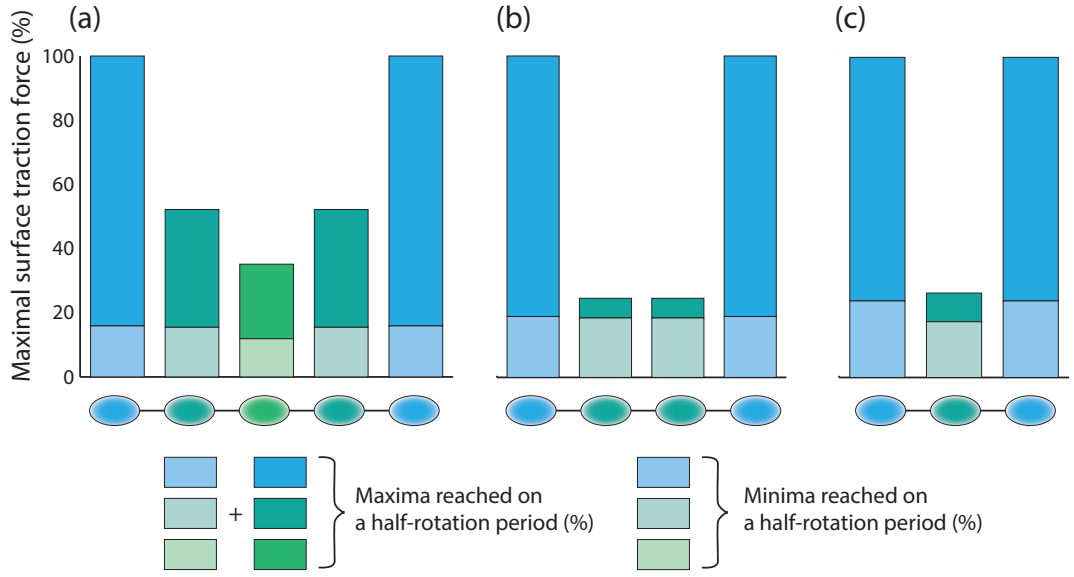

Figure IV.2.7: Maximal surface traction force (dimensionless) exerted on each bacterial cell (ellipsoid body) for 5-cell chains (a), 4-cell chains (b), and 3-cell chains (c). Each bar matches the cell position represented below. Results are normalized by chain length on the highest value reached over one rotation period. Minima (light colors) and maxima (sum of light colors and dark colors) reached over one rotation period are represented. Dark colors represent the range of values between which the maximal surface traction force varies over one period for a given cell position in a chain.

Because shear flow acts equally on both sides of a single given chain centered at the origin, $\mathrm{Max_{STF}}$ profiles exhibit a periodic behavior of period $\pi/2$. This makes sense in the limit of a bacterial suspension in which (i) chains are far apart enough that chain-chain interactions can be neglected, which has been determined plausible in our case after microscopic observations allowing assessing bacterial suspensions densities before shearing (data not shown), and (ii) chains are far enough away from the nozzle walls, so that chain-wall interactions can be neglected, which appears also plausible in our case due to the high range of shear rates used, bacterial suspensions therefore likely to be more concentrated near the center of the liquid channel. For more densely packed suspensions, additional parameters taking into account both chain-chain and chain-wall interactions may need to be considered.

Whichever chain length considered, the minimal value of $\mathrm{Max_{STF}}$ reached over a half-rotation period remains below 25 % of the highest value of $\mathrm{Max_{STF}}$. The maximal value of $\mathrm{Max_{STF}}$, as well as the range of $\mathrm{Max_{STF}}$ reached over a half-rotation period, are respectively the highest and the largest for bacterial cells the closest to chain ends. Therefore, the more bacterial cells are close to the center of a chain, the more likely they are to be protected from damaging forces.

IV.2.2.3 Impact of the bacterial chain rotation angle

On a rotation period for quasi-rigid body motion, $\mathrm{Max_{STF}}$ is periodic for each cell of period $[\pi]$. Figure IV.2.8 represents the evolution of $\mathrm{Max_{STF}}$ over one period for the outer cells (left and right of the chain) and the center cell of a 3-cell chain. Location of the $\mathrm{Max_{STF}}$ is represented on pictures by cell by an open circle. We will call "outer cells" the two cells at each end of a chain, and "inner cells" all other cells. In the case of odd-numbered chains, the specific case of the bacterial cell located at the center of the chain will be called "center cell" (still belongs to "inner cells"). The chain rotation angle θ is defined as the angle taken at the center of the chain between the horizontal and the global orientation of the chain, defined by the tangent to the center of the chain. In the case of exact rigid body motion, θ is the angle between the horizontal and the chain

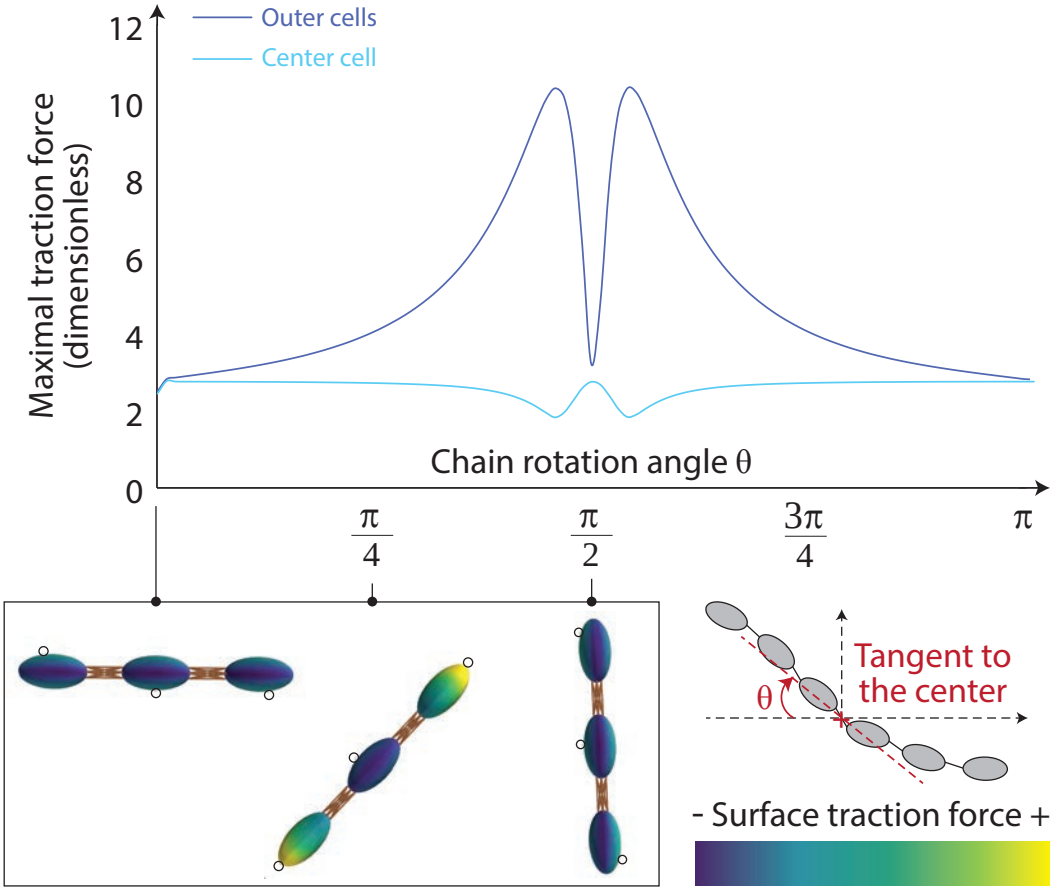

Figure IV.2.8: Maximal surface traction force (Max_{STF}) experienced by each bacterial cell within a 3-cell chain in a shear flow as a function of the chain rotation angle θ during a quarter rotation period; θ is the angle between the horizontal and the tangent to the center of the chain. Open circles on pictures represent the location of the Max_{STF} on each cell for a given θ.

itself, and can be measured from any point of the chain. Behaviors observed in Figure IV.2.8 for bacterial cells in 3-cell chains are similar to those of bacterial cells within 4-cell chains, outer cells and inner cells presenting similar behaviors, and therefore have not been represented here. Complete data set are available in Appendices C.1 for chains of 2, 3, and 4 cells and C.2 for 5-cell chains for more details.

Inner cells experienced a maximum Max_{STF} when the chain got exactly perpendicular to the flow *i.e.*, θ reached $\pi/2$ such as represented in Figure IV.2.8 for 3-cell chains. This

θ is indeed the closest the inner cells will ever get to full exposure to the shear flow. However, the intensity of this maximum remained small. One hypothesis that could explain this fact would be the existence of a local environment created by the outer cells, which would reduce the intensity of traction forces exerted on the inner cells. Also, although the inner cells may feel little traction forces, they should experience higher internal tension in order to maintain quasi-rigid body motion [Tornberg and Shelley, 2004]. This translates into higher stretching of the connections nearest to the center of the chain, such as presented in Figure IV.2.9. Indeed, springs connecting the inner cells

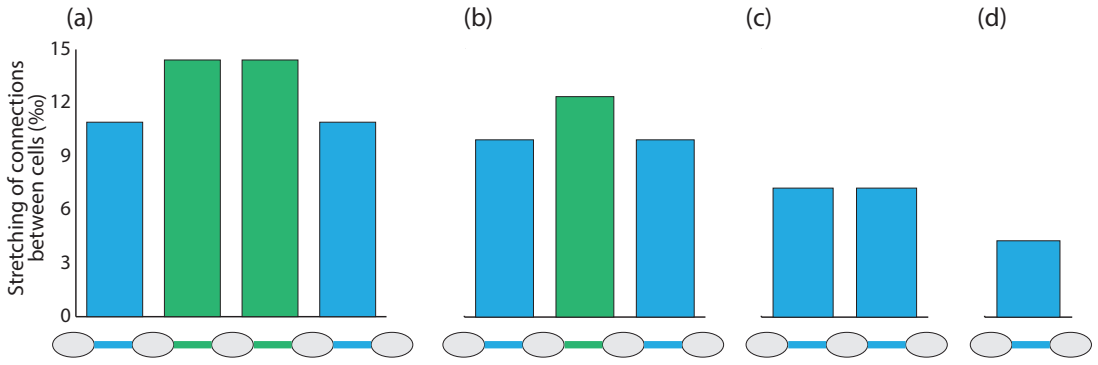

Figure IV.2.9: Stretching of connections (cluster of springs) between bacterial cells in 5-cell (a), 4-cell (b), 3-cell (c), and 2-cell (d) chains. Values are expressed in ‰ of the resting length d of each connection, which in the model is a dimensionless constant fixed to 1. Each bar matches the connection represented below.

to one another stretched more than springs connecting inner cells to outer cells, due to a higher local deformation of the chain during rotation. Stretching differences presented in Fig. IV.2.9 remained low because of the quasi-rigid body motion imposed, however this phenomenon is likely to amplify with increased chain flexibility. However, increased stretching and internal tension do not impact directly bacterial surface, and therefore we will not further detail these facts in the present study.

Outer cells experienced two maxima $\mathrm{Max}_{\mathrm{STF}}$ right before and just after the chain got perpendicular to the flow, that is, when drags on both chain ends were the highest (Fig. IV.2.8). These maxima are located at the free ends (cell poles) of the outer

cells (Fig. IV.2.8) which, in our case, may be the parts of bacterial cells that feature the most pili [Kankainen et al., 2009,Tripathi et al., 2012]. At these times, $\mathrm{Max}_{\mathrm{STF}}$ reached a minimum for the inner cells. This supports the previous hypothesis of a local environment created by outer cells in flow which would protect inner cells from the exterior shear flow. When the chain got perpendicular to the shear flow it suddenly relaxed and snapped (See Movies 1 and 2) due to full exposure to the flow. This snapping behavior explains the sudden decrease in $\mathrm{Max}_{\mathrm{STF}}$ observed for outer cells at $\pi/2$, *i.e.*, which coincide with the maximum $\mathrm{Max}_{\mathrm{STF}}$ reached for the inner cells. Indeed, when θ reaches $\pi/2$, the outer cells offered minimal resistance to the flow and therefore the local environment they may have created which would have protected the inner cell vanishes briefly while the chain snaps. Right after snapping was when most of the stretching shown in Fig. IV.2.9 occurs, therefore internal tension on inner cells and surface traction forces on outer cells reached a new maximum, then slowly decrease as the chain got parallel to the flow, thus minimizing exerted forces.

Overall, bacterial cells inside a chains are all the more protected from surface traction forces than they are closer to the center of the chain, but are likely to feel high internal tension forces all the more important than the chain is flexible. Bacterial cells on the outside of a chain may experience higher surface traction forces range during rotation, and the highest surface traction forces were found to be located near their cell poles, which may be the sites where pili are the most abundant.

IV.2.2.4 Impact of bacterial chain length

The impact of chain length on maximal surface traction forces exerted on individual bacterial cells within a chain in a shear flow has been investigated. Traction force profiles are presented for chains of 2 up to 5 cells over a period $[\pi]$ (corresponding to a half-rotation period) in Figures IV.2.10a, IV.2.11a for outer cells, and in Figures IV.2.10b, IV.2.11b for inner cells; data are compared with those obtained single cell (single body) in a shear flow (reference case). The case of 5-cell chains, undergoing the most deformation, is represented separately in Figures IV.2.11 for better readability. We will call F_{O} the

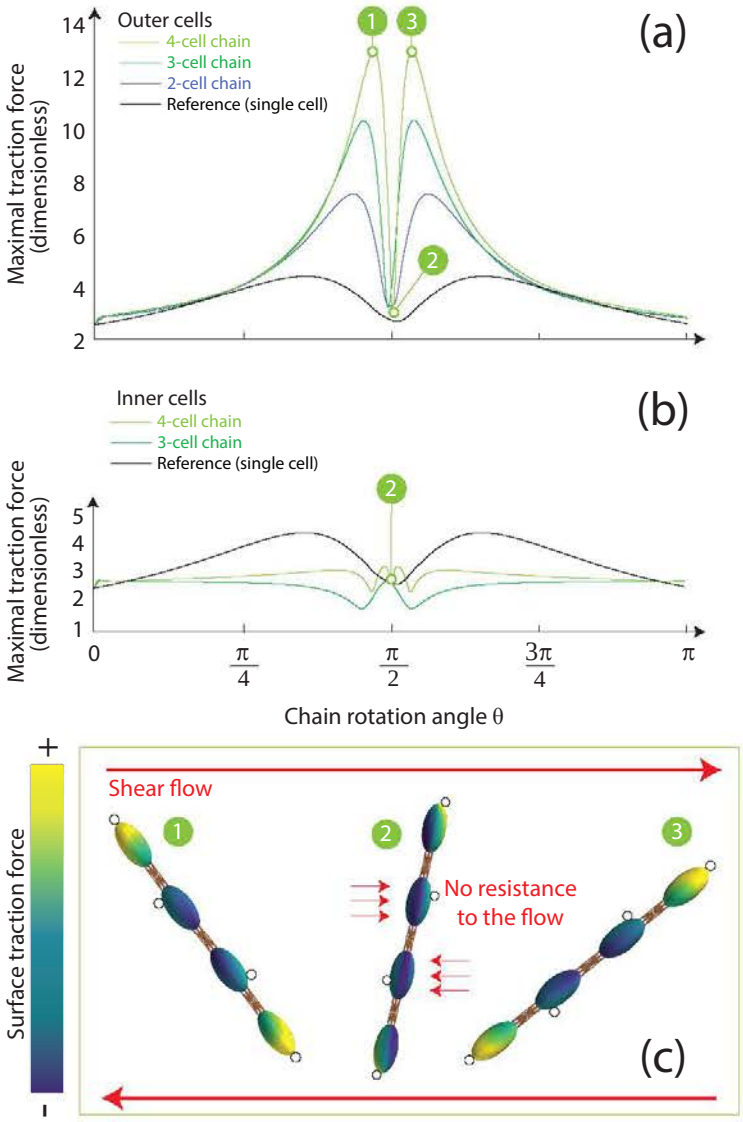

Figure IV.2.10: Maximal surface traction force ($\mathrm{Max_{STF}}$, dimensionless) experienced by outer bacterial cells (a) and inner bacterial cells (b) of 2, 3, and 4-cell chains over one period (corresponding to a half-rotation period) in quasi-rigid body motion. A visual output is provided for 4-cell chains; θ is the angle between the horizontal and the tangent to the center of the chain. Open circles on pictures represent the location of the $\mathrm{Max_{STF}}$ on each cell for a given θ. Results are compared with the $\mathrm{Max_{STF}}$ experienced by a single cell on the same period (reference case).

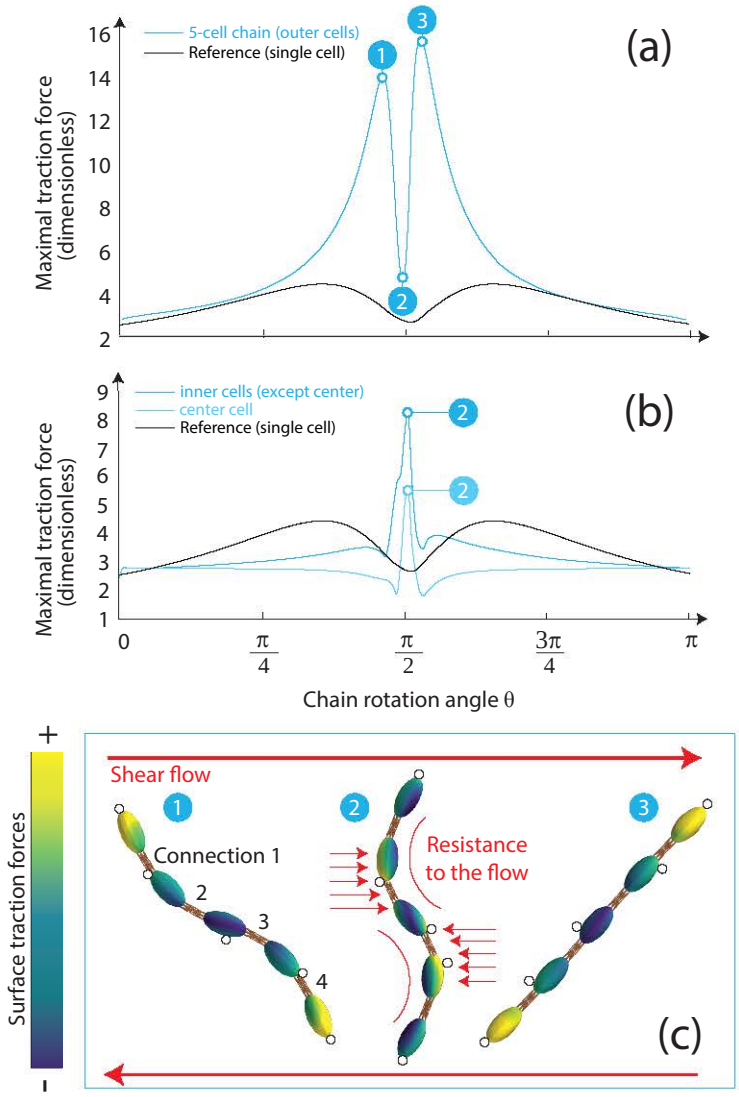

Figure IV.2.11: Maximal surface traction force (Max_{STF}, dimensionless) experienced by outer bacterial cells (a) and inner bacterial cells (b) of 5-cell chains over one period (corresponding to a half-rotation period) in quasi-rigid body motion. θ is the angle between the horizontal and the tangent to the center of the chain. Open circles and red dots on pictures represent the location of Max_{STF} for each body. Red dots stand for sensitive rupture points (SRP) identified near connection points. Results are compared with the Max_{STF} experienced by a single cell on the same period (reference case).

forces Max_{STF} applied on the outer cells of a chain (cells at both ends of a chain), and F_{I} the forces Max_{STF} applied on the inner cells of a chain (all other cells, including the

cell at the center of the chain).

IV.2.2.4.1 Impact on cells on the outside of a chain (outer cells)

It appeared that F_O(5-cell chains) > F_O(4-cell chains) > F_O(3-cell chains) > F_O(2-cell chains) > F_O(single cells) (Fig. IV.2.10a, IV.2.11a), therefore, that the longer the chain, the more likely outer cells are to get damaged by F_O. Highest F_O are reached for all chains from 2 to 5 cells right before and just after snapping when $\theta = \pi/2$ (the same phenomenon is observed on the reference case). The longer the chain, the briefer the snapping moment and the closer θ is to $\pi/2$ when highest F_O are reached (Fig. IV.2.10a, IV.2.10c, IV.2.11a, IV.2.11c). When the highest F_O are reached, once again cell poles of the outer cells are the most affected (Fig. IV.2.10c) which may cause important damage to surface adhesive proteins such as pili. Lowest values of F_O are reached for slightly different θ around $\pi/2$ depending on chain length from 2 to 5-cell (Fig. IV.2.10a, IV.2.10c), which can be attributed to the little flexibility allowed in quasi-rigid body motion, which may cause little change to the position of the outer cells relatively to the general orientation of the chain.

In the case of 5-cell chains presented in Fig. IV.2.11, an asymmetric behavior is observed when comparing F_O before and after snapping. This is due to the higher flexibility of this chain compared to the other ones (Fig. IV.2.11c). Indeed, because the stretching constant k_L was fixed arbitrarily for all chain lengths, the longer the chain, the more flexible it is. This limit of flexibility allows monitoring a S-shape deformation before and during snapping (Fig. IV.2.11c(1), (2)) as outer cells offer less and less resistance to the flow, whereas after $\pi/2$ the chain suddenly stiffens (Fig. IV.2.11c(3)), which leads to increased F_O and internal tension due to the stretching of the connections. When increasing k_L in order to get a more rigid behavior, F_O before and after snapping become symmetric again, of value similar to the highest value observed for the case presented in Fig. IV.2.11a, IV.2.11c (stiff chain).

IV.2.2.4.2 Impact on cells on the inside of a chain (inner cells) and potential link with chain breakage

Forces F_{I}(3-cell chains) and F_{I}(4-cell chains) were found both inferior to F_{I}(single cell) (Fig. IV.2.10b), suggesting that the chain environment may help protecting better the inner cells from F_{I}. However, this was not the case anymore for 5-cell, as all inner cells featured F_{I} higher than the single cell reference case (Fig. IV.2.11b). This is likely due to the more flexible behavior of chains longer than 4-cell which can be observed on Fig. IV.2.11c for 5-cell chains. Because of this higher flexibility, the local protective environment created by outer cells would vanish as θ gets close to $\pi/2$, due to increased bending of the outer parts of the chain, and the inner cells would not only feel the flow, but try to resist it, causing a local increase of F_{I} near the connection points of the inner cells (Fig. IV.2.11c(2)), therefore exposing the chain to potential breakage around these points. Right after snapping, a positive bump in F_{I} can be observed, likely to be due to the stretch induced by the sudden stiffening of the chain. As the chain keeps on stiffening and rotating after snapping, the local protective environment of the inner cells is recovered and F_{I} decreased again. A similar but smaller bump can also be observed before snapping, due to the same phenomenon however softened by the higher deformation of the chain. Similarly, bumps of F_{I} can be observed before and after snapping for 3-cell and 4-cell chains, due to small stiffening events (in the limit of quasi-rigid body motion allowing only very little stretching and bending).

Overall, in the limit of quasi-rigid body motion, small chains are better protected than long chains. As chains get long enough to present a more flexible behavior, outer cells become slightly less affected due to increased chain deformation, and inner cells are more likely to get damaged. Increased F_{I} due to higher flexibility may locate near the connection points between cells, which may favor chain breakage near these points.

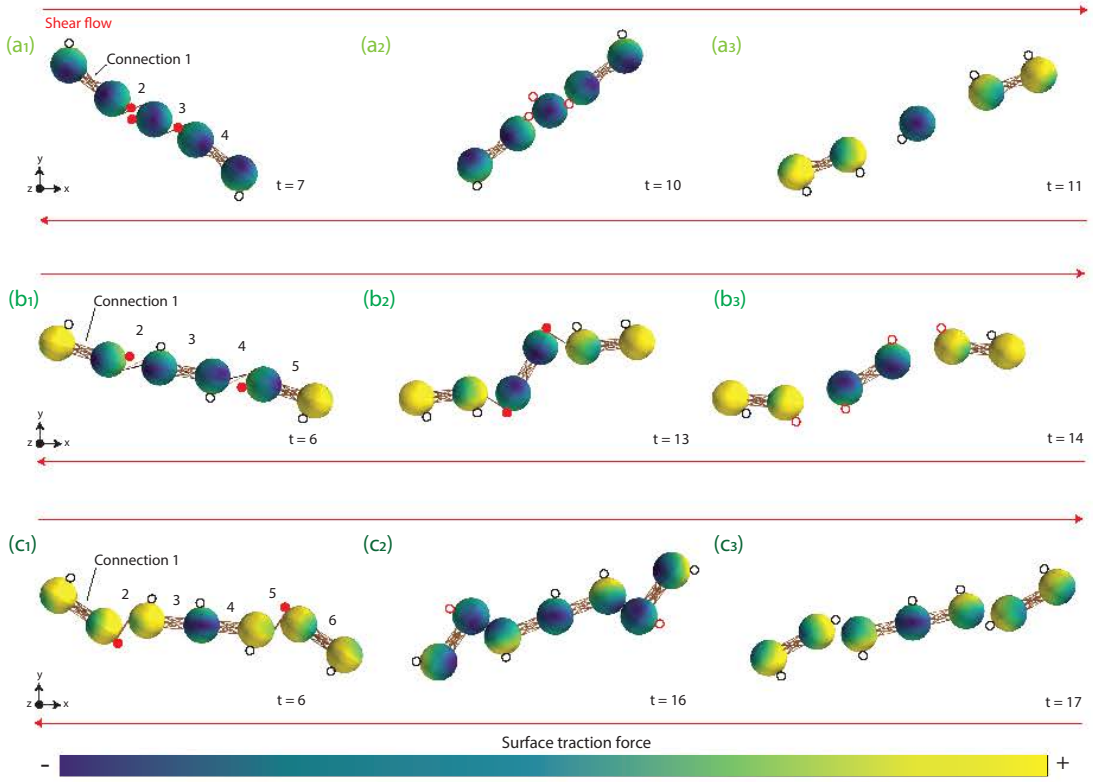

Figure IV.2.12: Location of sensitive rupture points (SRP) on 5-cell chains (a_1, a_2, a_3), 6-cell chains (b_1, b_2, b_3), and 7-cell chains (c_1, c_2, c_3) over time (dimensionless). Code was run without hydrodynamic interactions and bacterial cells were represented by spherical bodies. Open circles represent location of the maximal surface traction force (Max_{STF}) that do not impact connections between cells, red dots Max_{STF} creating SRP (near connection points) before breakage, and red circles Max_{STF} locations of previous SRP once connections were broken.

IV.2.2.5 Chain breakage as a function of chain length

IV.2.2.5.1 Breakage of 5-cell chains

Breakage may result from high Max_{STF} near connection points between cells in a chain. These forces may indeed weaken locally the strength of the connection, thus creating an environment conducive to rupture. This is more likely to occur for longer chains because of their increased flexibility leading to the creation of zones opposing a greater resistance to the flow (Fig. IV.2.10c, IV.2.11c). We will call these weaker zones "sensitive

rupture points (SRP)" for those near connection points. For the 5-cell chain presented in Fig. IV.2.11, two SRP could be identified on configurations (1) of Fig. IV.2.11c affecting connections 1 and 4, and three SRP could be identified on configuration (2) on connections 2 and 3. The three SRP identified in configuration (2) related to much higher forces than the SRP identified on the configuration (1) (Fig. IV.2.11b), as configuration (2) is the one opposing the most resistance to the flow. Therefore, breakage would be more likely to occur from the configuration (2), and would result in two 2-cell chains and one single cell (issued from the center of the chain). It can be observed that two of the SRP identified in this configuration are both located on connection 3, this connection thus totalizing forces equal to the sum of both peaks presented in Fig. IV.2.11b, whereas connection 2 only feels the highest peak (Fig. IV.2.11b). This suggests that connection 3 would break before connection 2, leading to a cascading fragmentation behavior. This type of fragmentation has previously been observed on thin brittle rods [Audoly and Neukirch, 2005] and was found to result from excessive bending, such as observed in configuration (2) of Fig. IV.2.11c, followed by sudden release, occurring right after snapping. The sudden relaxation of the curvature (which would correspond to chain stiffening in our case) was found to lead to a series of flexural waves, which locally increase the curvature in the rod and lead to cascading cracks [Audoly and Neukirch, 2005].

Breakage was directly observed on a chain of 5 spherical bodies (representing bacterial cells) by lowering down respectively the force and torque breakage thresholds, $\max_f$ and $\max_l$. The location of $\mathrm{Max}_{\mathrm{STF}}$ was monitored for each cell and SRP conducive to rupture were identified on Figure IV.2.12. On the 5-cell chain, similarly to what was observed for a chain of same length constituted of ellipsoids in Fig. IV.2.11c, 3 SRP could be identified in Fig. IV.2.12a_1 that led to increased stretching of connections 2 and 3. As suspected for the chain of ellipsoids, chain breakage of the chain of spheres effectively results into one single cell (previously center cell) and two 2-cell chains such as observed in Fig. IV.2.12a_2,a_3. However, although an asymmetry in the SRP distribution on connections 2 and 3 could be observed in both cases (ellipsoids and spheres), for a chain

of spheres two SRP were identified on connection 2 and one on connection 3, whereas the reverse was observed for a chain of ellipsoids (Fig. IV.2.10, IV.2.11). This rearrangement may be due to the fact that the configurations on which SRP have been identified, *i.e.* configurations (1) and (2) of Fig. IV.2.11c for chains of ellipsoids and configuration (a_1) of Fig. IV.2.12 for chains of spheres, are not exactly comparable to one another as the chain angle of Fig. IV.2.12a_1 differs from both other configurations. Indeed, as the simulations allowing observing breakage directly did not compute for full hydrodynamics interactions, the same exact same configurations as observed for the chain of ellipsoids in Fig. IV.2.11c could not be obtained for the chain of spheres. Nevertheless, fragmentation in three parts resulting from cascading cracks could still be observed.

IV.2.2.5.2 Breakage of 6-cell and 7-cell chains

Breakage was directly observed on chains of 6 and 7 spherical bodies (bacterial cells) in order to monitor whether the same fragmentation behavior could still be observed for chains longer than 5 cells (Fig. IV.2.12). Fragmentation in three parts could still be observed for both chain lengths. However, SRP were equally distributed on connections that effectively broke (no connection was observed to possess more than one SRP). The case of the 6-cell chains was found interestingly to feature 4 SRP, two of them reached in configuration (b_1) of Fig. IV.2.12, and the two other reached in configuration (b_2), all SRP affecting connections 2 and 4, first positioned near the outer bodies, then near the inner bodies. This would suggest a breaking mechanism occurring in two steps: the connections parts the more on the outside would weaken first, allowing increased stretching of connections 2 and 4 which would then weaken the connection points on the two cells the closest to the center, and eventually lead to breakage.

Only two SRP could be identified on 7-cell chains, on the outside of connections 2 and 4 (Fig. IV.2.12c_1). For 6-cell chains, the chain core of 2-cell chains was the one inducing chain deformation and breakage, and pairs of 2-cells on the outside only bent to initiate the weakening of connections 2 and 4 (Fig. IV.2.12b_1). On the contrary for 7-cell chains, the pairs of 2-cells on the outside are the one inducing chain deformation and breakage (Fig. IV.2.12c_1). This may be due to the fact that the center cell in 7-cell chains felt

the flow very little because it actually benefits from a double protection, from the core cells on both sides of it, as well as from the pairs of 2-cell chains on the outside that create a local environment around the chain when starting rotating. Thus well-isolated, this center cell would not feel the need of rotating and would therefore slow down any stretching motion that could be initiated by the three core cells. Therefore, connections breakage almost only depend on the motion of the pairs of 2 cells on the outside of the chain.

These observations suggest that fragmentation mechanisms of long chains of bodies (such as bacterial chains) may depend on chain length. Breakage may involve cascading cracks as observed for 5-cell chains (Fig. IV.2.11c, Fig. IV.2.12a$_1$, IV.2.12a$_2$, IV.2.12a$_3$) which however could not be generalized to all chains. Fragmentation behaviors observed on 6-cell and 7-cell chains appear specific of the chain length considered and an effect of the chain symmetry on chain breakage could be observed. All fragmentation behaviors observed (in quasi-rigid body motion) led to breakage in three parts, which is coherent with the behavior of thin brittle rods submitted to excessive bending [Audoly and Neukirch, 2005]. This may support the hypothesis formulated in Section IV.2.1.2.1 on 4-cell chains likely to break in three parts, leading to two single cells and one 2-cell chains. More simulations with longer chain length and involving full hydrodynamic interactions may be interesting to precise the breaking behaviors, which we aim to present in future work.

IV.2.2.5.3 Towards an integrated, mechanistic approach of chain breakage modeling

Numerous statistical models deal with chain fragmentation, especially related to polymer degradation or depolymerization [Aström, 2006, Banasiak, 2006, Banasiak and Noutchie, 2010, Carmona et al., 2014, El'darov et al., 1995, Forquin and Hild, 2010, Göpferich, 1996, Kostoglou, 2000, Mantzaris, 2005, Mao et al., 2017, Montroll and Simha, 1940, Paturej et al., 2011, Sjöstrand, 1988, Stickel et al., 2006, Ziff and McGrady, 1986]. Some reviews provide an experimental (chemical) basis to their models [El'darov et al., 1995, Göpferich, 1996] and often correlate breakage probability with polymer weight. Most models of

chain scission make assumptions on where chains are the most likely to break, and thus different models can be valid in different settings. Most common modeling assumptions include mid-chain or binary breakage [Mantzaris, 2005, Ziff and McGrady, 1986], end-chain scission [Kostoglou, 2000, Stickel et al., 2006], ternary breakage [Ziff and McGrady, 1986], and random breakage [Montroll and Simha, 1940, Ziff and McGrady, 1986]. Some models provide insight on the influence of chain length and position of bonds in the chain on the breakage phenomenon [Ziff and Stell, 1980]. A recent study also proposed a chain scission criterion based on the bond deformation energy attaining a critical value [Mao et al., 2017].

Fragmentation of brittle materials was studied independently from polymer fragmentation [Aström, 2006, Audoly and Neukirch, 2005, Forquin and Hild, 2010]. Models for brittle fragmentation include (i) instantaneous fragmentation (breakup generations are not distinguishable), and (ii) continuous fragmentation (generations of chronological fragment breakups can be identified) [Aström, 2006].

In the present study, as the behavior of chains is studied for quasi-rigid body motion, models for brittle rods may appear of better relevance than classical polymer degradation models, such as presented previously sections IV.2.2.5.1 and IV.2.2.5.2. For those type of models, the authors refer to two excellent papers, the review by Astrom et al. (2006) and the study of brittle rods by Audoly and Neukirch (2006) [Aström, 2006, Audoly and Neukirch, 2005].

When considering more flexible cases, which could occur for longer chains and/or for higher shear rates, the polymer models (bead-like chains) proposed by Ziff et al. (1986) were briefly investigated and tested in relation to our experimental data. These models take into account chain length and body position within the chain [Ziff and McGrady, 1986]. Ziff et al. present three different statistical models, respectively assuming binary, ternary, and random breakage of chains [Ziff and McGrady, 1986], which give expressions for the evolution of the proportion of chains of size x under various assumptions. The binary model used a breakage rate $F(x, y) = xy$ proportional to the product of the resulting fragments for the binary breakage case, which makes sense in a context of

parabolic distribution of the tension along the chain length such as what would occur in extensional flow [Ziff and McGrady, 1986]. The ternary model was only briefly presented and a constant breakage rate of $F(y, z, x - y - z) = 1$ for breakage of a chain of length x breaking into fragments of lengths y, z, and $x - y - z$ was used. The random model used a breakage rate independent of the position of the bond (connection) within the chain, $F(x, y) = (x + y)^{\alpha}$, increasing exponentially at power α with the initial length of the chain. All three expressions were briefly compared with our experimental data by scaling the chain proportion variables on the smallest shear rate used when performing spray-drying in our experiments, *i.e.* $\dot{\gamma} = 3 \times 10^5$ s^{-1}, but these models failed to provide good fits with our data, all three leading to a much higher single-cell proportion that observed experimentally (data not shown). The fact that two-cell chains were observed to be the most stable form of bacterial chains in flow was found difficult to explain through statistical modeling of polymer fragmentation.

IV.2.2.6 Possible advantages of the 2-cell chain configuration

The proportion of 2-cell chains represented more than 50 % of the resulting chain size distribution of LGG WT after shearing at $\dot{\gamma} = 3 \times 10^5$ s^{-1}, and 2-cell chains was found to be the most favorable chain configuration for bacterial cells in shear flow even at high shear rates, before flocs and about equally with single cells, for all tested strains. In an attempt to understand the advantages offered by this configuration compared to others, as the existing statistical and mechanistic models we tried to fit with our data failed to provide a satisfying explanation, we tackled the problem from a mechanical perspective by investigating the effect of $\mathrm{Max}_{\mathrm{STF}}$ at the surface of 2-cell chains, as well as conditions that may lead to 2-cell chains breakage using our model. Conditions leading to effective 2-cell chain breakage have been gathered for different cases in Table IV.2.8 and were determined for $d \in \{0.1, 0.5, 1\}$, $k_L \in \{1, 10, 100, 1000, 10000\}$, $r \in \{0.1, 0.2, 0.3\}$, $(\max_f, \max_l) \in \{(1, 1), (10, 10)\}$, $\dot{\gamma} \in \{1, 2, 3, 5, 10\}$. Different resting lengths of connections between cells were also investigated: d was scaled respectively with the half-length of the cell, the quarter-length of the cell, and the 20^{th}-length of the cell. In reality, the length of the

Body type	**Hydrodynamic interactions**	**Breakage conditions**				
		d	k_L	r	$\max_f$, $\max_l$	$\dot{\gamma}$
Sphere	Off	1	≥ 10	0.1	1,1	$\geq$1
Ellipsoid	Off	1	$\geq$ 10,000	0.1	1,1	$\geq$1
Ellipsoid	On	1	$\geq$ 10,000	0.1	1,1	$\geq$1
Sphere	Off	0.1	≥ 10	0.1	1,1	$\geq$2
Ellipsoid	Off	0.1	≥ 10	0.1	1,1	$\geq$2
Ellipsoid	Off	0.5	$\geq$ 10,000	0.1	1,1	$\geq$1
Ellipsoid	On	0.5	$\geq$ 10,000	0.1	1,1	$\geq$1

Table IV.2.8: Breakage conditions required for the rupture of 2-cell chains into single cells, depending on the system parameters d, k_L, r, $\max_f$, $\max_l$, respectively the resting length of the connection between the two cells, the stretching constant of the connection, the radius of the connection (determining bending abilities), and the force and torque threshold conducive to rupture, and of the applied shear rate $\dot{\gamma}$. Hydrodynamic interactions could be turned on or off depending on the version of the code that was used. Conditions were investigated for both dumbbells (2-cell chains with spherical bodies) and chains with ellipsoidal bodies were investigated.

connection linking two bacterial cells to one another in a chain depends on the growth stage of each cell [Cabeen and Jacobs-Wagner, 2005, Cabeen et al., 2009, Cava et al., 2013, Clark and Ruehl, 1919, Coley et al., 1978, Egan and Vollmer, 2013, Grover et al., 1977, Harry, 2001, Harry et al., 2006, Rosenberger et al., 1978, Turner et al., 2013, Way, 1996], as well as on various cell division characteristics such as the physico-chemical composition of the linkage [Altermann et al., 2004, Coley et al., 1978, Egan and Vollmer, 2013, Previc, 1970, Typas et al., 2012] and the cell growth differentiation phenomenon [Cava et al., 2013, Rosenberger et al., 1978, Grover et al., 1977, Turner et al., 2013, Cabeen et al., 2009]. It influences the perforation mechanism [Palumbo et al., 2006, Harry et al., 2006, Harry, 2001] and the symmetry or asymmetry of the division event [Egan and Vollmer, 2013, Harry et al., 2006, Harry, 2001, Monahan et al., 2014, Way, 1996, Previc, 1970].

When $d = 1$ *i.e.* the connection scales with the cell radius (or half-length in the case of ellipsoids), Max_{STF} exerted on 2-cell chains were still found higher than those exerted on single cells (Fig. IV.2.8), although lower than for all longer chains (Fig. IV.2.10,IV.2.11). Also compared to longer chains, breakage of 2-cells chains was much more difficult to observe. Only high bending capacities ($\varepsilon = 0.1$) combined with rela-

tively low stretching abilities $k_L \geq 10$ and the lowest possible rupture force and torque thresholds, *i.e.* $\max_f$=$\max_l$=1, allow visualizing dumbbell breakage for $\dot{\gamma} = 1$. When considering chains of ellipsoids, chains needed to be even stiffer to break as breakage was only observed from $k_L \geq 10,000$. This suggests that 2-cell bacterial chains constituted of ellipsoidal or rod-like cells, such as lactobacilli, would be more difficult to break than chains of beads, such as cocci. Indeed, the region between two spheres is narrower than the one between two ellipsoids of comparable half-length (bottleneck effect), and therefore, feels higher traction forces and would be more likely to break. Similar breakage conditions were observed for dumbbells of ellipsoidal cells separated by $d = 0.5$, whether or not hydrodynamic interactions were considered.

For $d = 0.1$ *i.e.* scaling with the 10^{th} of the sphere radius or ellipsoid half-length (so with the 20^{th} of the total cell length), dumbbell breakage could not be observed in the same conditions as for $d = 1$, whether considered bodies were spherical or ellipsoidal. A higher shear rate ($\dot{\gamma} = 2$) was necessary to lead to rupture (Table IV.2.8), which could then occur for more floppy chains as well (k_s as low as 10). This would suggest that when the bodies of a dumbbell are very close to one another, which could be the case of two bacterial cells shortly after occurrence of the cell division process, rupturing the connection between these cells could be very difficult. These 2-cell chains may actually behave like single cells of higher aspect ratios (4:1 *e.g.*). As cells elongate and the distance between them increase, breakage may be easier, as seen for $d \geq 0.5$.

This would explain why 2-cell chains are less likely to break than all other chain configurations when exposed to shearing, thus why the 2-cell chains proportion is the highest obtained after shearing even at low shear rates. Single cells may be a more favorable configuration than 2-cell chains looking at the surface traction forces, however as 2-cell chains are very difficult to break and bacteria in their native form mostly organized in long chains (Fig. III.4.1), single cells coherently did not represent an important proportion of the suspension after shearing at low shear rates. However, for increased shear rates applied repeatedly as shown in Tables IV.2.1, IV.2.2, and IV.2.3, all chain proportions reduce and the proportion of single cells increases. This is coherent with the

single cell configuration being a favorable configuration under shear (the most favorable configuration in terms of traction forces), however difficult to obtain from 2-cell chains as those are also favorable and hard to break.

IV.2.3 Proposed relationship between bacterial shape and functionality in a shear flow

Most bacterial functionality losses and chain breakage events were observed at very low shear rates ($\dot{\gamma} = 3.0 \times 10^5$), concomitantly with an important rise of the proportion of 2-cell chains. As seen from the simulations, long chains, such as the ones present initially in bacterial suspensions before shearing, experienced higher traction forces than smaller chains, especially at the chain ends. Also, as a chain gets perpendicular to the flow the maximum traction forces locate near contact points, previously described in this paper as "sensitive rupture points" (SRP), which may lead to breakage near those points. Combining experimental and numerical results, the shearing-induced rupture of bacterial chains can be envisioned as a protective process allowing preserving bacterial functionality, such as represented in Figure IV.2.13.

Initial (long) chains would first get broken near SRP, while cells at both ends of the chain would feel high surface traction forces ("shaving") leading to important surface damages *i.e.* functionality losses. On the contrary, cells closer to the center of the chain would experience little damage thanks to a local, protective environment created by the cells on the outside of the chains, which would act as buffers. Then, as chains shorten due to breakage, both shear stress exerted at contact points and surface traction forces exerted on cells would decrease, thus lowering the probability of surface damages and breakage. Ultimately, exerted stress and forces may become too low to induce either further chain breakage or cell surface damage, therefore the adhesive functionality of the resulting bacterial cells in small chains would remain preserved.

This proposed relationship between bacterial functionality and bacterial organization represents one more step towards a better understanding of the factors that could lead bacteria to shape differently when placed in favorable or detrimental environmental

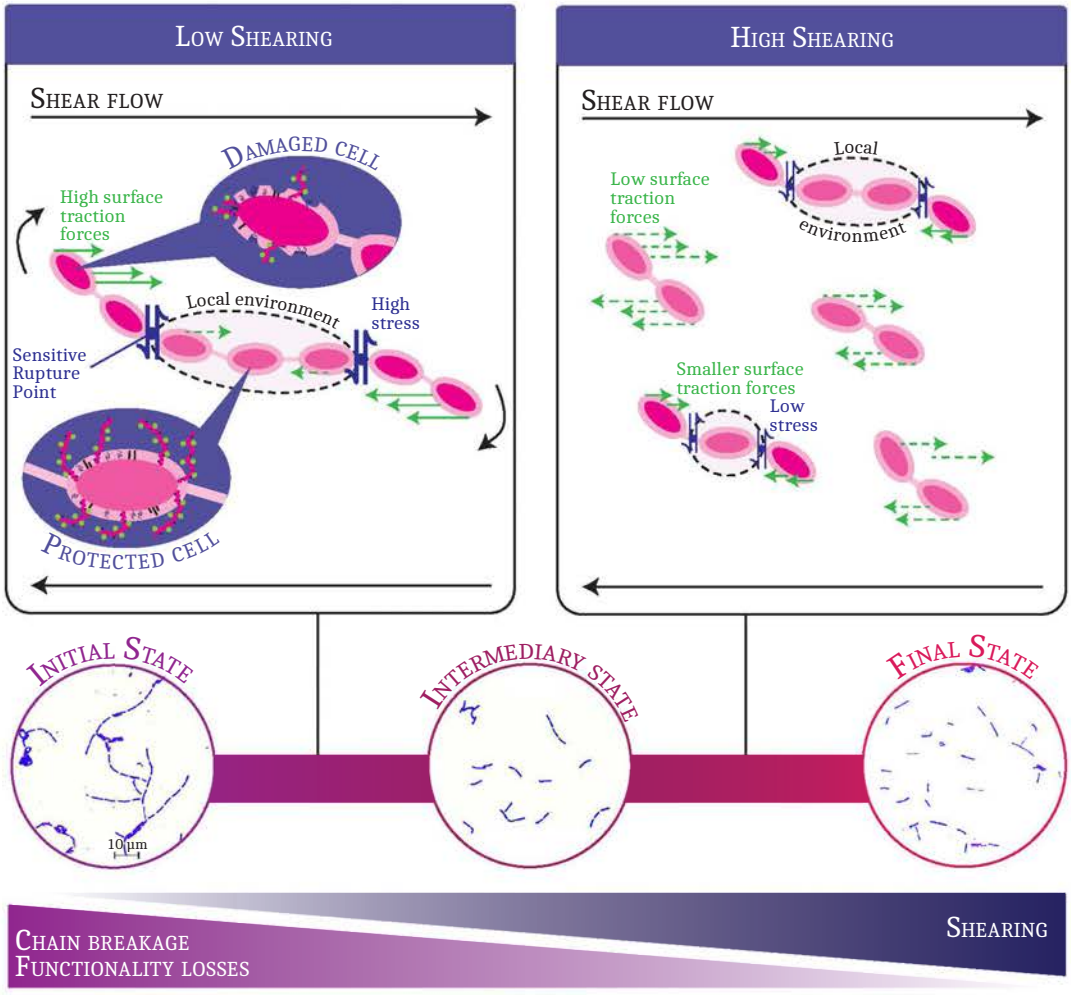

Figure IV.2.13: Proposed relationship between bacterial functionality and shearing-induced bacterial chain breakage. Microscopic pictures illustrating the initial, intermediary, and final state have been taken for *Lactobacillus rhamnosus* GG respectively for a control suspension (initial state), after one-time shearing at a rate of $3.0\times10^5 s^{-1}$ (intermediary state), and after repeated shearing at $11\times10^5 s^{-1}$.

conditions. As bacterial sensitivity to shear may depend on the composition of their growing medium, the impact of protective matrices embedding bacteria, such as dairy matrices (cheese- or yoghurt like) on bacterial organization and bacterial functionality when sheared (mimicking the food manufacturing process) may be explored in future work.

IV.3

Modeling bacterial adhesion in a shear flow: dynamics and damages

IV.3.1 Rigid body motion

We will begin our investigation by examining the particular dynamics of a rigid dumbbell in a shear flow, which we will call *Rigid Body Motion dynamics* (RBM dynamics). We will first consider the case of a dumbbell constituted of two spheres of identical size ($|\boldsymbol{r}_A| = A,\ |\boldsymbol{r}_a| = a,\ A = a$), connected by a rod of fixed length d ($d = a$). We will refer to this case throughout the text as the *reference symmetric case*. We will then consider the case of an asymmetric dumbbell ($|\mathbf{r}_A| = A,\ |\mathbf{r}_a| = a,\ A$), still connected by a rod of length d ($d = a$). This case will be referred throughout the text as the *reference asymmetric case* for a given radius A. A general representation of rigid body motion for an asymmetric dumbbell is presented in Figure IV.3.1. Quantities described on this figure will be used consistently throughout this section. This includes notations for the centroids $\mathbf{x}_A$, $\mathbf{x}_a$, the radii A, a, the distance d between the surface of the bodies, and the angle θ_A describing the rotation of the system over time. For the specific case of the system being initially horizontal (resting position), monitoring the behavior of the angle $\theta_A = f(t)$ allows keeping track of the system displacements over time in a shear flow. The norms of the vectors $\mathbf{R}$, $\mathbf{r}_A$, $\mathbf{r}_a$ will be written as R, r_A, r_a. The translational and

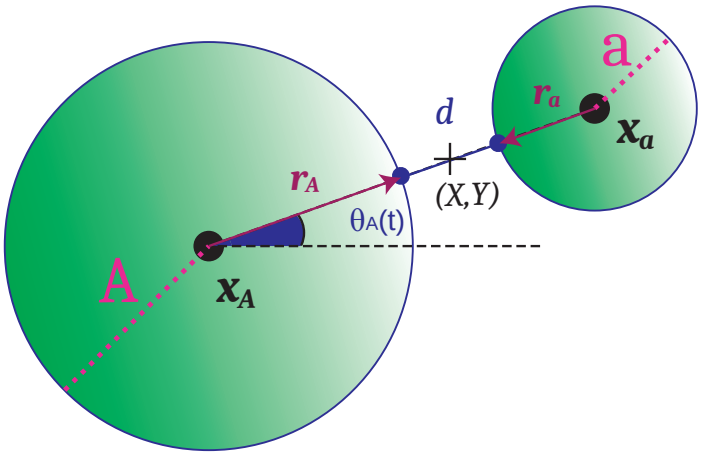

Figure IV.3.1: General representation of a rigid dumbbell (reference case). The angle θ_A keeps track of the position of the system comparatively to the horizontal. The coordinates of the system origin are (X, Y). Other quantities described on this figure are the centroids $\mathbf{x}_A$, $\mathbf{x}_a$, the radii A, a, the distance d between the surface of the bodies, and the vectors $\mathbf{r}_A$, $\mathbf{r}_a$.

angular velocities (not represented on Fig. IV.3.1) are called respectively $\mathbf{U}_A$, $\mathbf{U}_a$, $\mathbf{\Omega}_A$, and $\mathbf{\Omega}_a$. The forces exerted by the rod of length d on each body are called $\mathbf{F}_A$ and $\mathbf{F}_a$.

IV.3.1.1 Symmetric dumbbell

IV.3.1.1.1 Influence of hydrodynamic interactions

In this section we will solve analytically for the dynamics of a symmetric dumbbell such as described in Fig. IV.3.1 in the absence of hydrodynamic interactions (h.i.). We will then compare our solution to numerical results obtained while taking into account h.i. As a first pass we therefore have $\mathbf{r}_A = -\mathbf{r}_a$ at $t = 0$. Because we are solving locally *i.e.* for low Reynolds numbers, the sums of forces and torques applied on each body are all

equal to zero:

$$\mathbf{F}_A - 6\pi\mu A\left(\mathbf{U}_A - \left(A + \frac{A^2}{6}\nabla^2\right)\mathbf{u}^\infty(\mathbf{x}_A)\right) = \mathbf{0}, \tag{IV.3.1}$$

$$\mathbf{r}_A \times \mathbf{F}_A + \mathbf{M}_A - 8\pi\mu A^3\left(\mathbf{\Omega}_A - \frac{1}{2}\nabla\mathbf{u}^\infty(\mathbf{x}_A)\right) = \mathbf{0}, \tag{IV.3.2}$$

$$\mathbf{F}_a - 6\pi\mu a\left(\mathbf{U}_a - \left(a + \frac{a^2}{6}\nabla^2\right)\mathbf{u}^\infty(\mathbf{x}_a)\right) = \mathbf{0}, \tag{IV.3.3}$$

$$\mathbf{r}_a \times \mathbf{F}_a + \mathbf{M}_a - 8\pi\mu a^3\left(\mathbf{\Omega}_a - \frac{1}{2}\nabla\mathbf{u}^\infty(\mathbf{x}_a)\right) = \mathbf{0}. \tag{IV.3.4}$$

As the rod between the two bodies can be considered as an additional third body (we will write $\hat{\mathbf{e}}$ the unitary vector in the direction of $\mathbf{r}_A$):

$$-\mathbf{F}_A - \mathbf{F}_a = \mathbf{0} \implies \mathbf{F}_A = -\mathbf{F}_a = \mathbf{F}_r, \tag{IV.3.5}$$

$$-\mathbf{M}_a - \mathbf{M}_A + \frac{d}{2}\hat{\mathbf{e}} \times (-\mathbf{F}_a) - \frac{d}{2}\hat{\mathbf{e}} \times (-\mathbf{F}_A) = \mathbf{0}. \tag{IV.3.6}$$

And because the considered system is rigid, the following statements establishing a relationship between translational and angular velocities are also valid:

$$\mathbf{\Omega}_A = \mathbf{\Omega}_a = \mathbf{\Omega}, \tag{IV.3.7}$$

$$\mathbf{U}_a = \mathbf{U}_A + \mathbf{\Omega} \times (\mathbf{x}_a - \mathbf{x}_A). \tag{IV.3.8}$$

The back-flow terms $\nabla^2\mathbf{u}^\infty(\mathbf{x}_A), \nabla^2\mathbf{u}^\infty(\mathbf{x}_A)$ generated by one body over the other will be neglected in front of the velocities $\mathbf{U}_A, \mathbf{U}_a$ as they decay at a rate of $1/R^3$.
RBM dynamics depend on the dumbbell aspect ratio which we will call $\chi = (4a + d)/2a$. In the limit of bodies of identical size $A = a$ standing very far from one another in the initial state, *i.e.* $d \to \infty$ at $t = 0$, the rotation rate scales with $-(\dot{\gamma}/\chi^2)\ \hat{\mathbf{y}}$, giving the initial vertical impulse. Translational velocities later get into play as they scale with $(a\dot{\gamma}/\chi)\ \hat{\mathbf{y}}$. The horizontal component of the translational velocities remains constant and equal to $Y\dot{\gamma}$.
In order to be able to evaluate the behavior of the system as a function of time, we

define $\mathbf{\Omega}$, $\mathbf{U}_A$, and $\mathbf{U}_a$ in terms of $\theta_A(t)$ (Fig. IV.3.1). In two dimensions, the centroids coordinates can therefore be defined as functions of θ_A for general initial conditions (Fig. IV.3.1):

$$\begin{cases} x_{a_1} &= X + (d/2+a)\cos\theta_A, \\ x_{a_2} &= Y + (d/2+a)\sin\theta_A \end{cases} \quad and \quad \begin{cases} x_{A_1} &= X - (d/2+a)\cos\theta_A, \\ x_{A_2} &= Y - (d/2+a)\sin\theta_A \end{cases}$$

Solving for $\mathbf{U}_A$, $\mathbf{U}_a$, $\mathbf{\Omega} = \Omega_z \hat{\mathbf{z}}$ in relation to θ_A:

$$\mathbf{U}_A = \begin{pmatrix} \dot{\gamma} Y - \dfrac{a}{\alpha_2}\dot{\gamma}\left(\alpha_1 \sin\theta_A - \alpha_3 \sin(3\theta_A)\right) \\ \dfrac{\dot{\gamma} a}{16\alpha_2}\cos\theta_A\left(\alpha_4 + \alpha_3 \sin^2\theta_A\right) \end{pmatrix}, \tag{IV.3.9}$$

$$\mathbf{U}_a = \begin{pmatrix} \dot{\gamma} Y + \dfrac{\dot{\gamma} a}{\alpha_2}\left(\alpha_1 \sin\theta_A - \alpha_3 \sin(3\theta_A)\right) \\ -\dfrac{\dot{\gamma} a}{16\alpha_2}\cos\theta_A\left(\alpha_4 + \alpha_3 \sin^2\theta_A\right) \end{pmatrix}, \tag{IV.3.10}$$

$$\mathbf{\Omega} = \frac{-\dot{\gamma}}{\alpha_2}\left(1 + \frac{\alpha_3}{\alpha_4}\sin^2\theta_A\right)\hat{\mathbf{z}}, \tag{IV.3.11}$$

with (recalling the aspect ratio $\chi = (4a+d)/(2a)$),

$$\alpha_1 = (2a+d)(68a^2 + 36ad + 9d^2)/a^3 = 8(\chi-1)\left(9\chi^2 - 18\chi + 17\right), \tag{IV.3.12}$$

$$\alpha_2 = 8(28a^2 + 12ad + 3d^2)/(8a^2) = \frac{1}{2}\left(3\chi^2 - 6\chi + 7\right), \tag{IV.3.13}$$

$$\alpha_3 = 3(2a+d)^3/a^3 = 24(-1+\chi)^3, \tag{IV.3.14}$$

$$\alpha_4 = 8(2a+d)/a = 16(-1+\chi). \tag{IV.3.15}$$

Integrating $\dot{\theta}_A = \hat{\mathbf{z}} \cdot \mathbf{\Omega}$, we find the orientation as a function of time,

$$\theta_A(t) = -\tan^{-1}\left(\frac{\sqrt{\alpha_4}\tan\left(\frac{\dot{\gamma} t\sqrt{\alpha_3+\alpha_4}}{\alpha_2\sqrt{\alpha_4}} - \tan^{-1}\left(\frac{\sqrt{\alpha_3+\alpha_4}\tan(\theta_A(0))}{\sqrt{\alpha_4}}\right)\right)}{\sqrt{\alpha_3+\alpha_4}}\right) \tag{IV.3.16}$$

For the symmetric case, RBM dynamics can be entirely predicted by the equations (IV.3.9), (IV.3.10), (IV.3.11), (IV.3.16). These equations can be expressed in full or in function of the aspect ratio χ. Similarly, when expressed in terms of χ, the period T_{RBM} of a rigid dumbbell can be compared to the period of rotation of a single ellipsoid in a shear flow referred to as the Jeffery orbit [Jeffery, 1922]. The aspect ratio of the ellipsoid will be called χ_J:

$$T_{\text{RBM}} = \frac{2\pi\alpha_2\sqrt{\alpha_4}}{\dot{\gamma}\sqrt{\alpha_3+\alpha_4}} = \frac{\sqrt{2}\pi\sqrt{\chi-1}(3(\chi-2)\chi+7)}{\dot{\gamma}\sqrt{(\chi-1)(3(\chi-2)\chi+5)}}, \tag{IV.3.17}$$

$$T_J = \frac{2\pi}{\dot{\gamma}}\left(\chi_J + \frac{1}{\chi_J}\right). \tag{IV.3.18}$$

In the limit of $\chi_J \to \infty$, the Jeffery orbit scales with χ_J and therefore becomes infinitely long, whereas as $\chi \to \infty$, T_{RBM} converges towards $2\pi\dot{\gamma}\frac{7}{\sqrt{10}}$. Indeed, in the case of a single prolate body, as the aspect ratio increases the body looks more and more like an infinite rod, which requires very high forces in order to start rotating into the fluid. However, unlike the infinite rod, in the dumbbell case, as the distance between the two bodies becomes sufficiently large, T_{RBM} stabilizes when no hydrodynamic interactions are considered: both bodies experience traction forces as if they were alone in the fluid. When hydrodynamic forces are taken into account, the system reaches a higher rotation rate when getting perpendicular to the flow and T_{RBM} increases. Representative curves illustrating this phenomenon are presented in Figure IV.3.2.

Numerically, the RBM reference case is recovered for sufficiently large stretching and bending stiffnesses. The higher the distance between the bodies, the higher the stiffnesses need to be in order to ensure conservation of the dumbbell rigidity.

When comparing the model without h.i. and the numerical results obtained when taking into account all hydrodynamic interactions, $T_{\text{hydro}} \geq T_{\text{non hydro}}$ with $T_{\text{hydro}} = T_{\text{non hydro}}$ in the limit of $d \to \infty$ since hydrodynamic interactions can be neglected for spheres really far apart. Numerically, the range of d tested varied between 0.1 and 10 and this limit could never be reached. However, our results showed a trend confirming that the further apart bodies are, the closer $T_{\text{non hydro}}$ gets to T_{hydro} because the less hydrodynamic

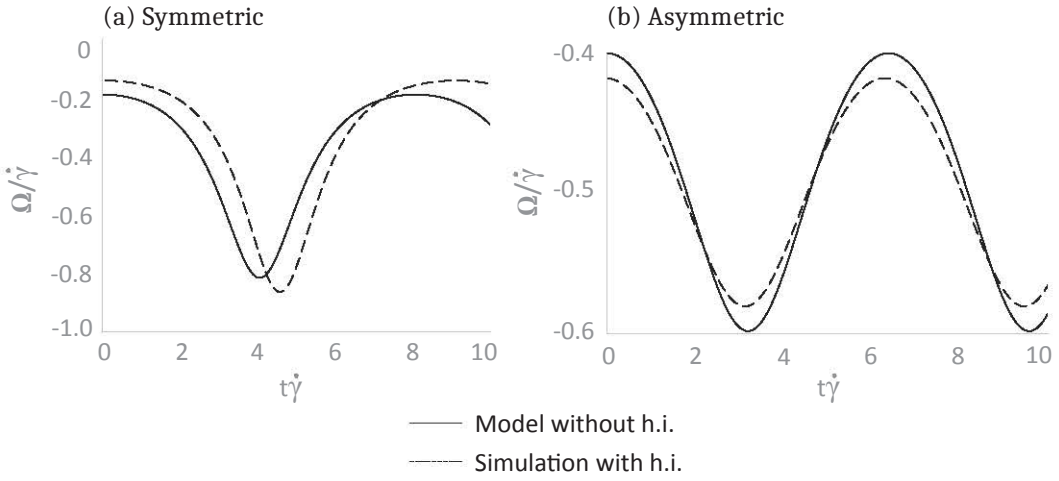

Figure IV.3.2: Rigid body motion (RBM) for a symmetric (a) and an asymmetric ($A = 5$, $a = 1$) (b) dumbbell in a shear flow: influence of the presence of hydrodynamic forces (h.i.) on the rotation rate. Bending and stretching stiffnesses were fixed high enough to ensure RBM, *i.e.* cluster radii controlling bending stiffness are $\varepsilon_{\text{sym}} = 0.1$, $\varepsilon_{\text{asym}} = 0.5$, and stretching stiffnesses are $k_s(\text{sym}) = 10,000$, $k_s(\text{asym}) = 20,000$. In both cases, distance between spheres was $d = 1$. Dimensionless velocity ($\boldsymbol{\Omega}/\dot{\gamma}$) and time ($t\dot{\gamma}$) are represented.

forces matter. In the limit of $d \to \infty$ (not reached numerically), $T_{\text{non hydro}} \approx T_{\text{hydro}}$ and $\log(\text{Error}) \approx -\log(d)$. Hence, the analytics developed for the RBM case in this section proved to provide a good estimate of the dynamics of a rigid dumbbell in the limit of two bodies being far apart. In fact, the model provided a surprisingly accurate estimate in the case presented on Figure IV.3.2, given the fact that bodies are actually very close to one another in this case ($d = 1 = a$).

IV.3.1.1.2 Traction forces

In this section we will present analytical expressions for traction forces $\boldsymbol{T} = f(t)$ exerted on the surface of a rigid dumbbell in a linear flow. These expressions have been established for the asymptotic case when bodies are far apart from one another, *i.e.* in the limit of large d. Numerical simulations using full h.i. will be used for comparison when plotting traction profiles. Color changes on the surface of the bodies attest visually for changes in exerted traction forces (Figure IV.3.3). Another asymptotic case is considered in Section

IV.3.1.2.2 when dealing with asymmetric dumbbells.

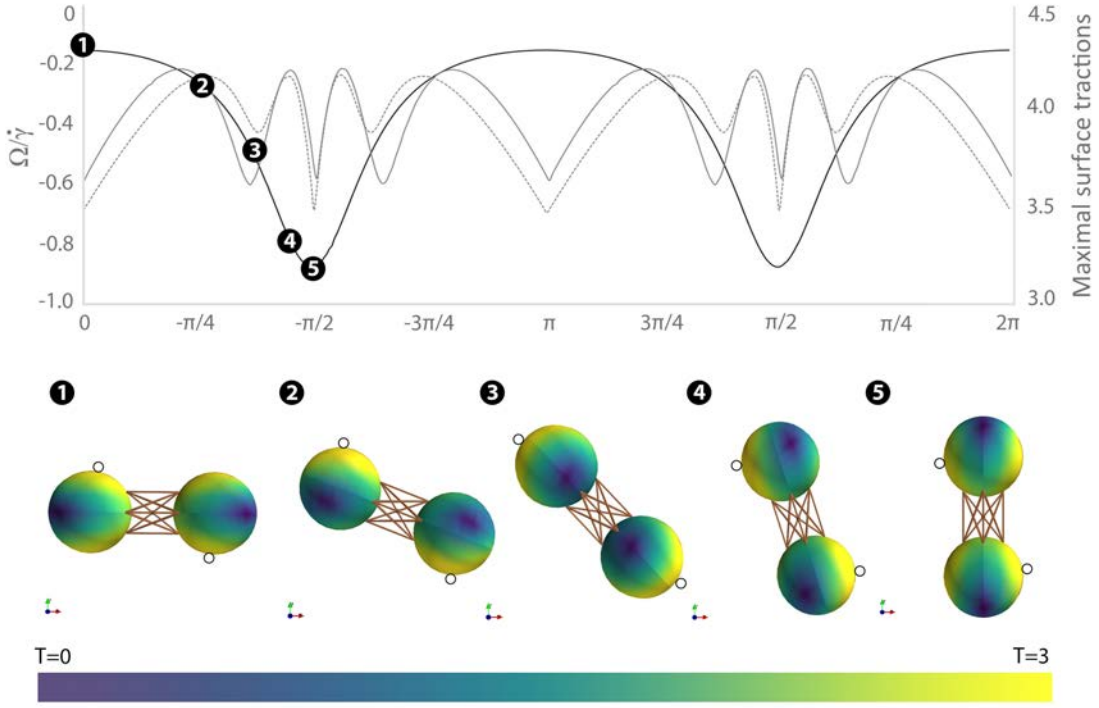

Figure IV.3.3: Traction forces exerted on the surface of a symmetric dumbbell during rigid body motion (RBM) in a shear flow. Correspondence with dynamics $\mathbf{\Omega}/\dot{\gamma} = f(t\dot{\gamma})$ with hydrodynamic interactions (h.i., solid black line), traction profile with h.i. (dotted grey line), and model traction profile (solid grey line) are represented over the course of one period (dimensionless numbers). Color scale changes on the pictures represent variations in surface traction forces over time; all traction forces superior to 3 show in yellow. An open circle on each body represents the location of the maximal traction force at a given time t. Cluster radius controlling bending stiffness is $\varepsilon = 0.5$, stretching stiffness is $k_s = 10,000$, distance between spheres is $d = 1.0$. See Movie 3 for similar case but with $\varepsilon = 0.1$.

For large d, the total surface traction applied on any of the bodies can be approximated by the sum of *(i)* the traction $\boldsymbol{T_F}$ due to the net force $\mathbf{F}$, *(ii)* the traction $\boldsymbol{T_L}$ due to the net torque $\mathbf{L}$, and *(iii)* the traction $\boldsymbol{T_{EE}}$ due to the linear background flow $\mathbf{EE}$. Analytical expressions for the maximum of each of these forces have been calculated for

general boundary conditions and are given below for a sphere of given radius length a.

$$\mathbf{T_F} = \frac{-\mathbf{F}}{4\pi a^2}, \tag{IV.3.19}$$

$$\mathbf{T_L} = -\frac{3(\mathbf{L} \times \mathbf{R})}{8\pi R^4}, \tag{IV.3.20}$$

$$\mathbf{T_{EE}} = 5\mu \mathbf{EE}.\frac{\mathbf{R}}{R}. \tag{IV.3.21}$$

Where μ is the dynamic viscosity of the fluid, and $\mathbf{R}$ is the direction of the rod connecting the two bodies and R its length. This asymptotic case was compared with numerical results obtained for d ranging from 0.1 to 10 for sufficiently large k_s and ε in order to recover RBM. It appears that even for d as small as 1, the model provides a good estimate of the traction forces exerted on the bodies (Fig. IV.3.3). These traction forces increase as the system gets in rotation in the shear flow and reach a maximum at $\pi/4$ $[\pi]$ (picture 2, Fig. IV.3.3). Once the system gets passed this angle, forces decrease until the system reaches a velocity of 0.5 (*i.e.* similar to the one experienced by a single sphere in a shear flow, picture 3) then, as the rotation rate keeps on increasing the tractions suddenly increase to reach new maxima around $\pi/2$ $[\pi]$ (picture 4). Traction forces maxima (reached at angles of $\pi/4$ $[\pi]$ and around $\pi/2$ $[\pi]$) are located on the sides of the bodies. The smallest traction forces are exerted once the system reaches an angle of $\pi/2$ $[\pi]$ *i.e.* gets perpendicular to the flow. In this position, the maximal traction forces are exerted on both sides of the bodies but actual forces values are very low (picture 5, Fig. IV.3.3). Surfaces the most exposed to the flow (top and bottom of the two bodies) experience even lower forces at this point. This is because the system is unstable in this position and rotates freely and quickly (the rotation rate is almost twice as high as the one of a single sphere in a shear flow at this point).

IV.3.1.2 Asymmetric dumbbell

IV.3.1.2.1 Dynamics

The dynamics of a rigid asymmetric dumbbell such as presented in Fig. IV.3.1 in the absence of hydrodynamic forces are described by Eqs. (IV.3.1)-(IV.3.6). These equations have been simplified using Eq. (IV.3.11), (IV.3.9), (IV.3.10) and can therefore be written as follows for resting initial conditions:

$$\mathbf{F}_r - 6\pi\mu A\mathbf{u_A} = \mathbf{0}, \tag{IV.3.22}$$

$$\mathbf{r}_A \times \mathbf{F}_r + \mathbf{M}_A - 8\pi\mu A^3\left(-\mathbf{\Omega}_A - \frac{\dot{\gamma}}{2}\hat{\mathbf{z}}\right) = \mathbf{0}, \tag{IV.3.23}$$

$$-\mathbf{F}_r - 6\pi\mu a\mathbf{u_a} = \mathbf{0}, \tag{IV.3.24}$$

$$\mathbf{r}_a \times (-\mathbf{F}_r) + \mathbf{M}_a - 8\pi\mu a^3\left(-\mathbf{\Omega}_a - \frac{\dot{\gamma}}{2}\hat{\mathbf{z}}\right) = \mathbf{0}, \tag{IV.3.25}$$

$$-\mathbf{M}_a - \mathbf{M}_A + \frac{d}{2}\hat{\mathbf{e}} \times 2\mathbf{F}_r = \mathbf{0}, \tag{IV.3.26}$$

$$\mathbf{U}_a - \mathbf{U}_A - \mathbf{\Omega} \times (\mathbf{x}_a - \mathbf{x}_A) = \mathbf{0}. \tag{IV.3.27}$$

When solving for general initial conditions *i.e.*= $\mathbf{x}_A = (X - \left(\frac{d}{2} + A\right), Y)$, $\mathbf{x}_a = (X + \left(\frac{d}{2}+\right), Y)$ we find:

$$\mathbf{U}_A = Y\hat{\mathbf{x}} + a\ VQ^{-1}\ \dot{\gamma}\ \hat{\mathbf{y}}, \tag{IV.3.28}$$

$$\mathbf{U}_a = Y\hat{\mathbf{x}} - A\ VQ^{-1}\ \dot{\gamma}\ \hat{\mathbf{y}}, \tag{IV.3.29}$$

$$\mathbf{\Omega} = -2Q^{-1}(a^4 + a^3A + aA^3 + A^4)\ \dot{\gamma}\ \hat{\mathbf{z}}, \tag{IV.3.30}$$

where

$$V = 2(a + A)(a^2 - aA + A^2)(a + A + d), \tag{IV.3.31}$$

$$Q = 4a^4 + 7a^3A + 4A^4 + 6a^2A(A + d) + aA(7A^2 + 6Ad + 3d^2). \tag{IV.3.32}$$

In the limit of $a \to A$, the expressions of $\mathbf{\Omega}$, $\mathbf{U}_A$, $\mathbf{U}_a$ for a symmetric dumbbell

described by Eq. (IV.3.11), (IV.3.9), (IV.3.10) are recovered. Whereas the rotation rate equally depends on both bodies, the vertical component of the translational velocity of one body is found to be linearly proportional to both the size of the other body and the shear rate. This means that in a case of two bodies presenting relative sizes differences, the small body is the one initiating the system rotation which is being stunted by the big body. In the limit of one body being really big compared to the other ($A \gg a$), the big body motion is independent from the small body motion, whereas the latter only depends on the big body motion. Indeed in this case, the position of the center of mass of the body A remains identical over time (this body rotates like what would do a sphere alone) whereas the small body attached to the surface spins at a very high rate around it, this rate being directly proportional to the size of the big body.

When expressing $\mathbf{\Omega}$ as a function of $\theta_A(t)$ as done previously for the symmetric case, we get the following expression:

$$\Omega_z(t) = \dot{\theta}_A(t) = \dot{\gamma}\frac{\alpha_5}{Q} + \dot{\gamma}\frac{\alpha_6}{Q}\sin^2\theta_A(t), \tag{IV.3.33}$$
$$\alpha_5 = -2(a^4 + a^3A + aA^3 + A^4), \quad \alpha_6 = -(3aA(a + A + d)^2).$$

Integrating, the orientation of the system is given by

$$\theta_A(t) = \tan^{-1}\left(\frac{\sqrt{\alpha_5}}{\sqrt{\alpha_5 + \alpha_6}}\tan\left[\frac{\sqrt{\alpha_5(\alpha_5 + \alpha_6)}}{Q}\ \dot{\gamma}t\right]\right). \tag{IV.3.34}$$

These dynamics are recovered numerically for sufficiently high values of k_s and ε in the limit of large d (neglecting hydrodynamic interactions). The bigger the size difference, the higher k_s and ε need to be in order to maintain RBM.

When comparing these expressions to outputs of simulations taking into account hydrodynamic interactions similarly to what we did before for the reference symmetric case (Section IV.3.1.1.1), we found that $T_{\text{hydro}} \leq T_{\text{non hydro}}$ with $T_{\text{hydro}} = T_{\text{non hydro}}$ in the limit of $d \to \infty$ (when h.i. become neglectable) or in the limit of $A \gg a$, in which latter case dynamics scale with the big body as the impact of the small body becomes

neglectable. Contrary to what happens for the symmetric case, when h.i. are taken into account the system reaches a lower rotation rate than for the model without h.i. when getting perpendicular to the flow (Fig. IV.3.2). This means that the bigger the big body is, the smaller the impact caused by the small body *i.e.* the closer the rotation rate is to 0.5 (rotation rate of a single sphere) and that this phenomenon is amplified by hydrodynamic interactions. Hydrodynamic interactions also lower the size difference threshold required to observe this phenomenon.

So far we have shown that h.i. impact the dynamics of a rigid dumbbell in a shear flow by amplifying the dominant trend. Hydrodynamic interactions delay the motion of symmetric dumbbells but the flipping itself occurs faster than in the absence of h.i.: both bodies work in synergy, either against the flow (longer lag period) or within the flow (quicker flipping). However, it appears that even for a small distance d between the bodies, the model gives surprisingly accurate results despite the fact that h.i. are not taken into account ($d = 1$ on Fig. IV.3.2 *e.g.*). In the asymmetric case, this is due to the fact that the velocity rate of the system is very close to the velocity rate of a sphere as soon as the difference in size between both bodies is large enough, *i.e.* that the influence of the small body on the rotation rate can be neglected. This is already the case for $A = 5$ and $a = 1$ (Fig. IV.3.2). Asymmetric dumbbells dynamics are slightly fastened when taking into account h.i.. The bigger the big body is, the faster the impact of the small body becomes neglectable, and this is all the more verified when h.i. are taken into account.

IV.3.1.2.2 Traction forces: aymptotic case of large A

We previously proposed analytical expressions for the traction forces exerted on the surface of bodies within a dumbbell. These expressions were established for rigid symmetric dumbbells in a shear flow, in the limit of bodies being far apart *i.e.* no h.i. (Section IV.3.1.1). For the specific case of an asymmetric dumbbell featuring two bodies of respective radii A and a, $A \gg a$, the total surface traction exerted on the small body a approximated for large d is likely to be mostly due to the drag caused by the big body A, thus causing to neglect other possible forces (lubrication theory). In this case, assuming a

velocity $\mathbf{\Omega_A} = \frac{\dot{\gamma}}{2}\hat{\mathbf{z}}$ for the body A in a shear flow of constant shear rate $\dot{\gamma}$, the total surface traction $\mathbf{T_a}$ exerted on the body a can be approximated by $\mathbf{T_a} \approx \dfrac{-3\dot{\gamma}(A+a+d)}{4a}\hat{\mathbf{x}}$. For big A, this expression scales linearly with the body size ratio $A:a$, as $\mathbf{T_a} \approx \dfrac{-3\dot{\gamma}A}{4}\dfrac{}{a}\hat{\mathbf{x}}$.

Another asymptotic case can be drawn for small d, as in this case the total surface traction perceived by the body a can be approximated using the stresslet generated by the body A in a shear flow in order to match the no-slip boundary condition. This stresslet is impacted by the presence of a small body near the surface of the main sphere thus creating an additional drag on the surface of this body. In 2D, the net traction force $\mathbf{f_a}$ exerted by surface area on the small body can therefore be expressed as follows:

$$\mathbf{f_a} = \begin{pmatrix} f_{a_1} \\ f_{a_2} \\ f_{a_3} \end{pmatrix} \quad \begin{cases} f_{a_1} &= \dfrac{y_a(5a^2A^3(4x_a^2 - y_a^2) + 3(A^5(4x_a^2 - y_a^2) - 5A^3x_a^2R^2 + R^7))\dot{\gamma}\mu}{4aR^7} \\ f_{a_2} &= \dfrac{x_a}{4a}(3 - \dfrac{A^3(5a^2(x_a^2 - 4y_a^2) + 3A^2(x_a^2 - 4y_a^2) + 15y_a^2R^2))}{R^7}\dot{\gamma}\mu \\ f_{a_3} &= 0 \end{cases} \tag{IV.3.35}$$

Where $\mathbf{R} = (x_a, y_a)$ with $\mathbf{R}$ the rod connecting the two bodies.
The value of traction forces applied on the small body depend on its position compared to the big body in rotation in the shear flow (Fig. IV.3.4) which, in RBM, corresponds to θ_A (Fig. IV.3.1). Therefore, it can be interesting to monitor $\mathrm{Max_{STF}}(\theta_A) = f(\theta_A)$, $\mathrm{Max_{STF}}(\theta_A)$ being the value of the maximal surface traction force applied on the surface of the small body for a given angle θ_A. In the limit of very large A ($A = \frac{1}{K},\ K \to 0$) for $d = 1$, $a = 1$, $\mathrm{Max_{STF}}$ can be approximated by the following expression for asymmetric rigid dumbbells (at first order in K):

$$\mathrm{Max_{STF}}(\theta_A, A) = \frac{5\dot{\gamma}\mu}{8A}\sqrt{\cos^2\theta_A(39 + (-89 + 12A)\cos^2 2\theta_A) + (39 + (89 - 12A)\cos^2 2\theta_A)\sin^2\theta_A} \tag{IV.3.36}$$

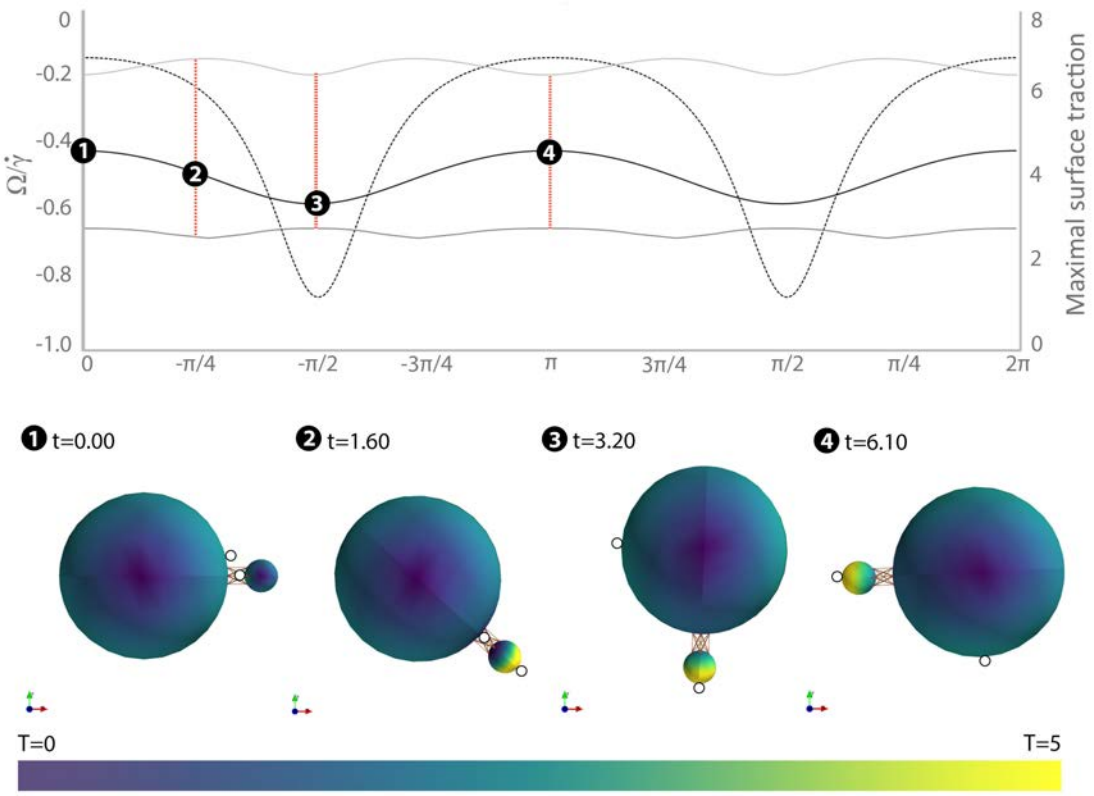

Figure IV.3.4: Traction forces exerted on the surface of a symmetric dumbbell during rigid body motion (RBM) in a shear flow with hydrodynamic interactions (h.i.) for the small (light grey) and big (dark grey) body (dotted grey line) of an asymmetric dumbbell in RBM ($A = 5$, $a = 1$, $d = 1$, $\varepsilon = 0.5$, $k_s = 100,000$). Correspondence with dynamics $\mathbf{\Omega}/\dot{\gamma}$ with h.i. (solid black line), as well as with reference case dynamics (symmetric dumbbell in RBM, dotted black line) are represented over the course of one rotation period (dimensionless numbers). Color scale changes on the pictures represent variations in surface traction forces over time; all traction forces superior to 3 show in yellow. An open circle on each body represents the location of the maximal traction force $\mathrm{Max}_{\mathrm{STF}}$ at a given time t.

This function is periodic of period $\frac{\pi}{2}$ and reaches three extrema on $[0, \frac{\pi}{2}]$, respectively for $\theta_A = 0$, $\theta_A = \frac{\pi}{4}$, and $\theta_A = \frac{\pi}{2}$. Depending on the value of A, these extrema are either maxima or minima. The behavior of $\mathrm{Max}_{\mathrm{STF}} = f(A)$ was studied further using the three

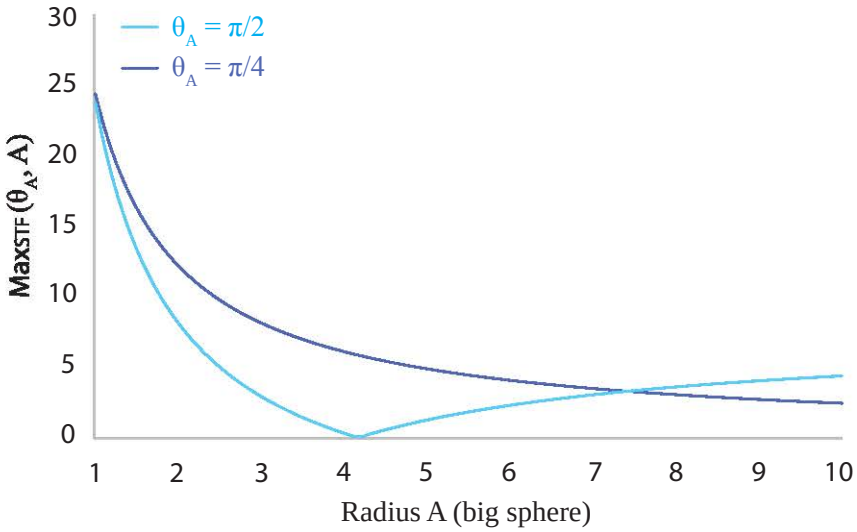

Figure IV.3.5: Influence of the size of the big body of radius A on the maximal surface traction force $\mathrm{Max}_{\mathrm{STF}}$ exerted on the small body $a = 1$ at $\theta_A = \pi/4$ and $\theta_A = \pi/2$, θ_A being the angle between the actual and the initial position of the small body relatively to the big body. Traction forces represented are issued from Eq. (IV.3.37), (IV.3.38), and (IV.3.39) and do not take hydrodynamic interactions into account.

following extrema functions:

$$\mathrm{Max}_{\mathrm{STF}}(0, A) = \frac{5\dot{\gamma}\mu}{8A} \mid -50 + 12A \mid \tag{IV.3.37}$$

$$\mathrm{Max}_{\mathrm{STF}}(\pi/4, A) = \frac{195}{8A}\dot{\gamma}\mu \tag{IV.3.38}$$

$$\mathrm{Max}_{\mathrm{STF}}(\pi/2, A) = \mathrm{Max}_{\mathrm{STF}}(0, A) \tag{IV.3.39}$$

Expressions of $\mathrm{Max}_{\mathrm{STF}}(\pi/4, A)$, $\mathrm{Max}_{\mathrm{STF}}(\pi/2, A)$ have been represented for $A \in [1, 10]$ in Figure IV.3.5. These expressions are equal for the size threshold $A_{thres} = 89/12 \approx 7.42$, and $\mathrm{Max}_{\mathrm{STF}}(\pi/2,\ A)$ reaches a minimum for $A = 25/6 \approx 4.16$. The periodicity of traction forces exerted on the small body for asymmetric rigid dumbbells, as well as the angles matching the minimal and maximal values of these traction forces over time, were in agreement with the traction profiles computed numerically with full h.i. The value of the numerical size threshold was lower than our theoretical value ($5 < A_{thres_{\mathrm{num}}} < 6$).

However, this issue can be addressed using a finer approximation for $\mathrm{Max}_{\mathrm{STF}}$. At third order in K instead of first order we found indeed a size threshold of $A_{thres} \approx 5.5071$ matching the interval observed for full h.i. (Fig. IV.3.6). The modified expression of $\mathrm{Max}_{\mathrm{STF}}$ at third order in K is given below:

$$\mathrm{Max}_{\mathrm{STF}}(\theta_A, A) = 5\dot{\gamma}\mu \ \frac{1}{16A^2} \ \sqrt{\kappa_1 \ (\cos\theta_A + \sin\theta_A) + \kappa_2 \ (\cos^2 3\theta_A - \sin^2 3\theta_A)} \tag{IV.3.40}$$

With

$$\begin{cases} \kappa_1 & = (136 + A(-8 - A(-11 + 12A))) \\ \kappa_2 & = (-1640 + A((424 + A(-89 + 12A))) \end{cases} \tag{IV.3.41}$$

Theoretical traction profiles using Eq. (IV.3.40) were plotted against numerical traction profiles screening for A around A_{thres} (Fig. IV.3.6). Theory and numerics both agree on values of θ_A leading to extrema during one full rotation in RBM. For $\theta_A \in [0, 2\pi]$ in the limit of large A:

- For $A < A_{thres}$, traction forces exerted on the small body are:
  - **maximal** for $\theta_A = -\pi/4$, $\theta_A = -3\pi/4$, $\theta_A = 3\pi/4$, and $\theta_A = \pi/4$
  - **minimal** for $\theta_A = 0$, $\theta_A = -\pi/2$, $\theta_A = -\pi$, and $\theta_A = \pi/2$

  This can be observed for example on Fig. IV.3.4. The picture (2) matches one of the maxima of the traction forces applied on the small body and corresponds to $\theta_A = -\pi/4$, whereas the pictures (3), (4) match two traction forces minima and correspond respectively to $\theta_A = -\pi/2$ and $\theta_A = -\pi$. Traction profiles for $A = 5$ represented in Fig. IV.3.6 also support this observation for both theoretical and numerical traction forces.

- For $A > A_{thres}$ such as presented in Fig. IV.3.6, traction forces exerted on the small body are:

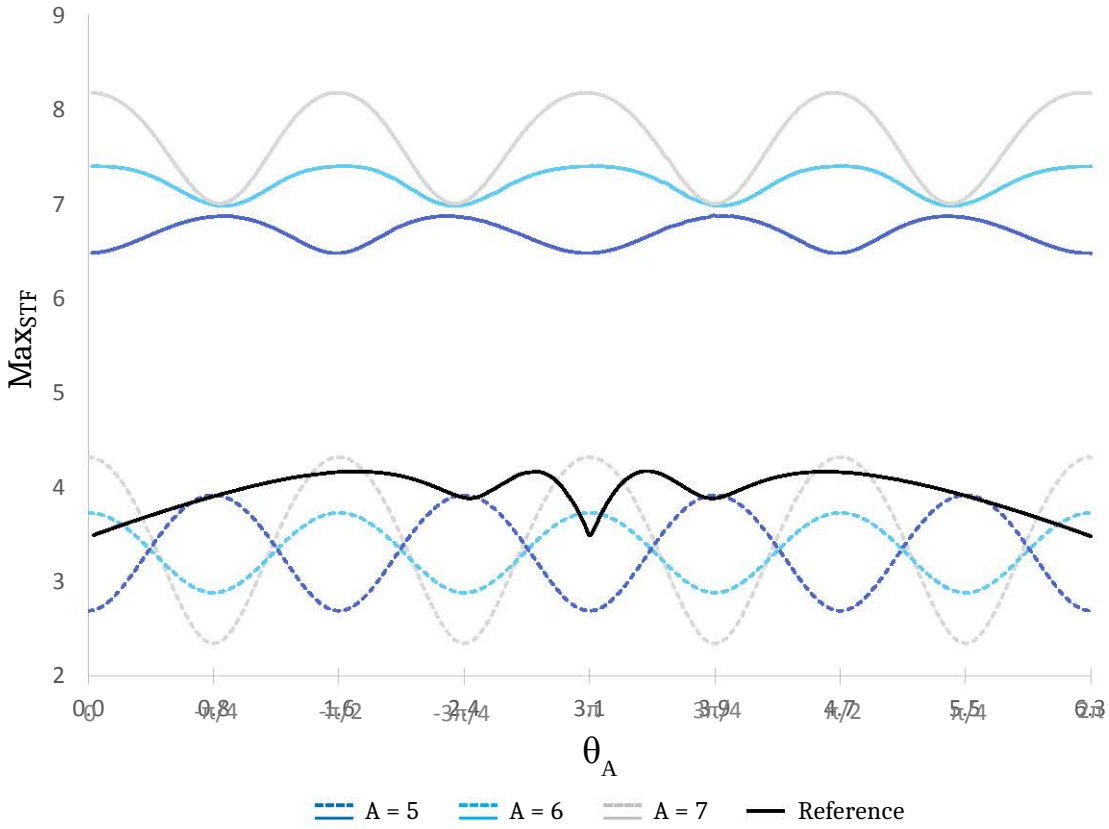

Figure IV.3.6: Theoretical (dotted lines) and numerical (solid lines) traction profiles for maximal surface traction forces $\mathrm{Max}_{\mathrm{STF}}$ exerted on the surface the small body of an asymmetric dumbbell ($A \in [\![5;7]\!]$, $a = 1$) during rigid body motion (RBM) in a shear flow. θ_A varies between $[0, 2\pi]$ (full system rotation) and represents the angle between the actual and the initial position of the small body relatively to the big body. Cluster radius controlling bending stiffness is $\varepsilon = 0.5$, distance between spheres is $d = 1.0$. Stretching stiffness was adjusted in order to maintain RBM. Traction profile of the reference symmetric case (RBM) is also presented for comparison.

- **maximal** for $\theta_A = 0$, $\theta_A = -\pi/2$, $\theta_A = -\pi$, and $\theta_A = \pi/2$
- **minimal** for $\theta_A = -\pi/4$, $\theta_A = -3\pi/4$, $\theta_A = 3\pi/4$, and $\theta_A = \pi/4$

The numerical values of the traction forces, however, were almost two times higher than the ones produced by our model (Fig. IV.3.6) and increase with A, therefore our theoretical evaluation of $\mathrm{Max}_{\mathrm{STF}}$ cannot provide reliable quantitative results. We can also

notice that for A insufficiently large, traction forces are not exactly periodic in $\pi/2$ but in π. This can be due to the fact that this model was established in the limit of small d and large A (as inspired from lubrication theory) whereas numerically, we still scaled d with a. Also, the nature of the connection between the two bodies is not specified in our model, whereas it can be argued that it also has an impact on the traction profiles exerted on both bodies. At this point, being aware of these limits, our theoretical $\mathrm{Max}_{\mathrm{STF}}$ only served as a basis to establish the periodicity of the traction forces as well as the size threshold determining the values of θ_A leading to maximal and minimal values of $\mathrm{Max}_{\mathrm{STF}}$. Numerical traction forces exerted on the big body were also monitored with full h.i., revealing an inverted periodicity compared to traction profiles obtained for the small body: when the forces are maximal on the small body, they are minimal on the big body, and vice versa. Also, the higher A, the lower the maximum traction value exerted on the big body as the closer the behavior of the system is to a single sphere, the impediment created by the small sphere becoming neglectable. This reaffirms the idea developed in Section IV.3.1.2.1 that the bodies in an asymmetric dumbbell act antagonistically, contrary to what happens for a symmetric dumbbell, which bodies work in synergy.

IV.3.2 Flexible dumbbells

In this section we consider that the two bodies of the dumbbell are connected by a cluster of springs which allows the system both to stretch and bend, leading to what we will call *"flexible dumbbells"*. This cluster is constituted of 4 springs in 2D (Figure IV.3.7) and of 16 springs in 3D. We will successively consider the case of symmetric, then asymmetric, flexible dumbbells. Some theoretical rationale will be provided to explain the dynamics of both cases, which are then further explored numerically. The impact of the shape of the small body (spherical versus ellipsoidal) on the dumbbell dynamics as well as on the surface traction forces experienced by both bodies will also be investigated. The stretching ability of the dumbbell is defined by its stretching stiffness k_s. The bending ability of the dumbbell is defined by the radius ε_i ($i \in \{A, a\}$) of the cluster of springs

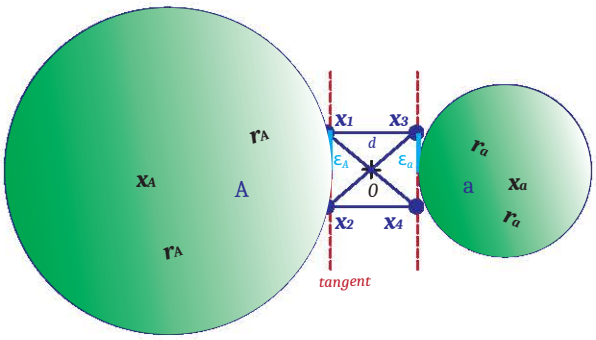

Figure IV.3.7: Flexible dumbbell system; in two dimensions bodies are connected by a cluster of four springs (dark blue) which ends are defined by contact points $\boldsymbol{x}_i$ located on surface tangents (red); the resting length of the two horizontal springs within the spring cluster is d; the spring cluster radius ε_i is defined by body and controls the bending ability on each side of the system. Other quantities described on this figure include the centroids $\mathbf{x_A}$, $\mathbf{x_a}$, the radii A, a, and the vectors $\hat{\mathbf{r}}_A$, $\hat{\mathbf{r}}_a$, $\hat{\mathbf{r}}_A^{\perp}$, $\hat{\mathbf{r}}_a^{\perp}$.

(Fig. IV.3.7). The start and end of each spring is defined by a contact point $\mathbf{x}_i$ ($i \in [\![1;4]\!]$ in 2D, $i \in [\![1;8]\!]$ in 3D) located on the surface tangent of each body, and the direction of each spring is indicated by a vector $\mathbf{R}_{ij}$ connecting the start of the spring x_i to the end of the spring x_j (for $(i,j) \in \mathbb{N}^2, \mathbf{R}_{ij} = \mathbf{x}_j - \mathbf{x}_i$). All these quantities will be used consistently throughout this section. Four angles have been defined in order to characterise the behavior of the system: θ_A, β, θ_a, and $\alpha\alpha$. (Fig. IV.3.8). θ_A and θ_a describe the position of the contact points on the surface of the bodies comparatively to the horizontal, and β is the angle formed between the cluster of springs defined by $\mathbf{R}$ and the reference RBM case. The angle $\alpha\alpha = \theta_A - \theta_a$ characterises potential offsetting of the small body relatively to the big one in case of asymmetry. In the specific case of the system initially being horizontal (resting position), θ_A describes the rotation of the system as if it were rigid (such as previously described in IV.3.1, Fig. IV.3.1), and θ_a describes slight displacements (wobbling) of the small body allowed by the stretching of the cluster of springs.

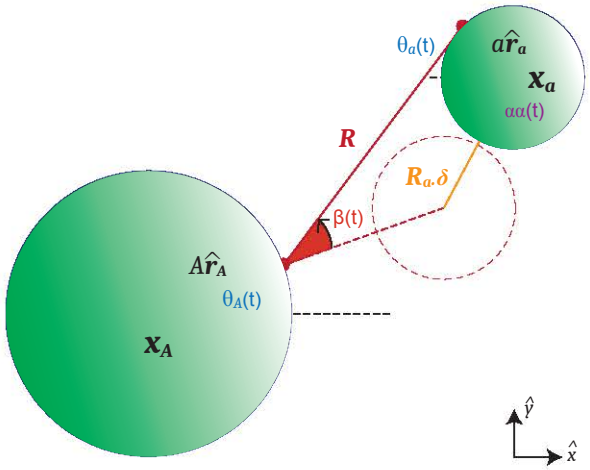

Figure IV.3.8: Monitoring the behavior of a flexible dumbbell in a shear flow through the evolution of four angles: $\beta(t)$ (difference between the direction of the cluster of springs represented by the vector $\mathbf{R}$ and the reference position of the rod in the RBM case; the vector $\mathbf{R_a}.\boldsymbol{\delta}$ represents the distance between the reference RBM position and the position allowed by a flexible system), θ_A and θ_a (positions of the contact points on each body's surface comparatively to the horizontal), and $\alpha\alpha$ (offset angle such as $\alpha\alpha = \theta_A - \theta_a$). The spring cluster is represented here by a single red line for clarity purposes. Other quantities described on this figure include the centroids $\mathbf{x_A}$, $\mathbf{x_a}$, the radii A, a, and the vectors $\hat{\mathbf{r}}_\mathbf{A}$, $\hat{\mathbf{r}}_\mathbf{A}$, $\hat{\mathbf{r}}_\mathbf{a}$.

IV.3.2.1 Symmetric case

IV.3.2.1.1 Influence of dumbbell flexibility on dumbbell dynamics: multiple timescales

In this section we solve for the dynamics of flexible dumbbells in 2D (3D dynamics can be extrapolated from this case). Considering a flexible dumbbell such as presented in Fig. IV.3.7, the coordinates of all four contact points for the 2D case are:

$$\mathbf{x}_1 = \mathbf{x}_A + A(\hat{\mathbf{r}}_A - \varepsilon\hat{\mathbf{r}}_A^{\perp}), \tag{IV.3.42}$$

$$\mathbf{x}_2 = \mathbf{x}_A + A(\hat{\mathbf{r}}_A + \varepsilon\hat{\mathbf{r}}_A^{\perp}), \tag{IV.3.43}$$

$$\mathbf{x}_3 = \mathbf{x}_a + a(\hat{\mathbf{r}}_a - \varepsilon\hat{\mathbf{r}}_a^{\perp}), \tag{IV.3.44}$$

$$\mathbf{x}_4 = \mathbf{x}_A + a(\hat{\mathbf{r}}_a + \varepsilon\hat{\mathbf{r}}_a^{\perp}). \tag{IV.3.45}$$

With $\hat{\mathbf{r}}_A = (\cos\theta_A, \sin\theta_A), \hat{\mathbf{r}}_A^{\perp} = (-\sin\theta_A, \cos\theta_A)$, $\hat{\mathbf{r}}_a = (-\cos\theta_a, -\sin\theta_a)$, and $\hat{\mathbf{r}}_a^{\perp} = (-\sin\theta_a, \cos\theta_a)$. For the symmetric case, we have equal bending ability on both sides of the cluster of springs ($\varepsilon_A = \varepsilon_a = \varepsilon$), and the offset angle $\alpha\alpha$ is equal to 0 ($\theta_A = \theta_a = \theta$). In 2D, the preferred length of the springs defined by $\mathbf{R}_{13}$ and $\mathbf{R}_{24}$ is equal to d, and those of the springs defined by $\mathbf{R}_{14}$ and $\mathbf{R}_{23}$ is $\sqrt{d^2 + 4\varepsilon}$. We will first determine the forces exerted each spring on the system:

$$\mathbf{f} = \mathbf{f}_{14} + \mathbf{f}_{23} + \mathbf{f}_{13} + \mathbf{f}_{24}, \tag{IV.3.46}$$

$$\mathbf{f}_{14} = k_s(|\mathbf{R}_{14}| - \sqrt{d^2 + 4\varepsilon})\frac{\mathbf{R}_{14}}{|\mathbf{R}_{14}|}, \tag{IV.3.47}$$

$$\mathbf{f}_{23} = k_s(|\mathbf{R}_{23}| - \sqrt{d^2 + 4\varepsilon})\frac{\mathbf{R}_{23}}{|\mathbf{R}_{23}|}, \tag{IV.3.48}$$

$$\mathbf{f}_{13} = k_s(|\mathbf{R}_{13}| - d)\frac{\mathbf{R}_{13}}{|\mathbf{R}_{13}|}, \tag{IV.3.49}$$

$$\mathbf{f}_{24} = k_s(|\mathbf{R}_{24}| - d)\frac{\mathbf{R}_{24}}{|\mathbf{R}_{24}|}. \tag{IV.3.50}$$

Then defining the torque expressions by body:

$$\tau_A = (\mathbf{x}_1 - \mathbf{x}_A) \times (\mathbf{f}_{13} + \mathbf{f}_{14}) + (\mathbf{x}_2 - \mathbf{x}_A) \times (\mathbf{f}_{23} + \mathbf{f}_{24}), \tag{IV.3.51}$$

$$\tau_a = (\mathbf{x}_3 - \mathbf{x}_a) \times (-\mathbf{f}_{13} - \mathbf{f}_{23}) + (\mathbf{x}_4 - \mathbf{x}_a) \times (-\mathbf{f}_{14} - \mathbf{f}_{24}). \tag{IV.3.52}$$

We will be solving for the semi-flexible case, *i.e.* only small displacements (bending and stretching) are allowed. The displacement along the horizontal axis will be called δ_1 and the one along the vertical axis will be called δ_2, $\boldsymbol{\delta} = \begin{pmatrix} \delta_1 \\ \delta_2 \end{pmatrix}$ being the displacement vector. Wobbling will show in small variations of $\theta_a = \theta$ (for the symmetric case). When only stretching is allowed, both torques are equal to 0 and the spring force is given by the

following expression (at first order for $\delta_1 \to 0,\ \delta_2 \to 0$):

$$\mathbf{f}_{stretching} = \begin{pmatrix} \delta_1 \left(2k_s + \dfrac{2d^2 k_s}{d^2 + 4\varepsilon^2} \right) \\ \delta_2 \dfrac{8k_s\varepsilon^2}{d^2+4\varepsilon^2} + \delta_1\delta_2 \left(\dfrac{4d^3 k_s}{(d^2+4\varepsilon^2)^2} + \dfrac{32k_s\varepsilon^4}{(d(d^2+4\varepsilon^2)^2} \right) \end{pmatrix}. \tag{IV.3.53}$$

When both stretching and bending are allowed, we will first study our system in a theoretical basis $(\hat{\tilde{\mathbf{x}}}, \hat{\tilde{\mathbf{y}}})$, which origin is the center of the big body A. Expressions for the forces and torques in this basis are given below:

$$\mathbf{f}_{th} = B\ ((1+2\eta^2)\delta_1 \hat{\tilde{\mathbf{x}}} + \eta^2(2\delta_2 + (2a+d)\theta)\ \hat{\tilde{\mathbf{y}}}), \tag{IV.3.54}$$

$$\boldsymbol{\tau}_{A_th} = B\eta^2\ ((2A+d)\delta_2 - (Ad + (2A+d)a - 2\varepsilon^2)\theta)\ \hat{\tilde{\mathbf{z}}}, \tag{IV.3.55}$$

$$\boldsymbol{\tau}_{a_th} = B\eta^2\ ((2a+d)\delta_2 - (d^2 + 2ad + 2a^2 + 2\varepsilon^2)\theta)\ \hat{\tilde{\mathbf{z}}}. \tag{IV.3.56}$$

With $B = \dfrac{4d^2k_s}{d^2+4\varepsilon^2}$ bending constant and $\eta = \dfrac{\varepsilon}{d}$ bending ratio. In order to get the expressions of the forces and torques in the real basis $(\hat{\mathbf{x}}, \hat{\mathbf{y}})$ such as presented in Fig. IV.3.8, the whole system is rotated using a rotation matrix $\mathbf{R}_A = \begin{pmatrix} \cos\theta_A & \sin\theta_A \\ -\sin\theta_A & \cos\theta_A \end{pmatrix}$ ($\theta_A = \theta$ for the symmetric case) *i.e.* the relation between the two basis is $\begin{pmatrix} \hat{\tilde{\mathbf{x}}} \\ \hat{\tilde{\mathbf{y}}} \end{pmatrix} = \mathbf{R}_A^{-1} \cdot \begin{pmatrix} \hat{\mathbf{x}} \\ \hat{\mathbf{y}} \end{pmatrix}$ and the expressions of the displacements in the new basis are $\delta_1 = \hat{\mathbf{r}}_A \cdot (\mathbf{x}_a - (\mathbf{x}_A + (A+a+d)\hat{\mathbf{r}}_A))$, $\delta_2 = \hat{\mathbf{r}}_A^{\perp} \cdot (\mathbf{x}_a - (\mathbf{x}_A + (A+a+d)\hat{\mathbf{r}}_A))$. Using the quantities describe on Fig. IV.3.8, the expressions of the forces and torques in the new basis in 2D are:

$$\mathbf{f} = B\ ((1+2\eta^2)\delta_1 \hat{\mathbf{r}}_a + \eta^2(2\delta_2 - (2a+d)\theta_a)\hat{\mathbf{r}}_A^{\perp}, \tag{IV.3.57}$$

$$\boldsymbol{\tau}_A = B\eta^2\ ((2A+d)\delta_2 - (Ad + a(2A+d) - 2\varepsilon^2)\theta_a)\ \hat{\mathbf{z}}, \tag{IV.3.58}$$

$$\boldsymbol{\tau}_a = B\eta^2\ ((2a+d)\delta_2 - (d^2 + 2ad + 2a^2 + 2\varepsilon^2)\theta_a)\ \hat{\mathbf{z}}. \tag{IV.3.59}$$

Similarly in 3D, eight contact points x_i define sixteen springs $R_{i,j}$ with associated forces $f_{i,j}$, allowing to determine the torque expression by body. Because these expressions are very complex, approximate, simpler expressions can be obtained by Taylor expanding for small displacements. Numerical values for $\dot{\theta}$ and $\dot{\beta}$ obtained from both these simple expressions of forces and torques, and from forces and torques issued from Taylor expansions at higher order were shown not to differ significantly in regard to the precision aimed when comparing with numerical simulations run with full hydrodynamics. The simplest expressions for forces and torques in 3D for flexible, symmetric dumbbells are

$$\mathbf{f} = B\boldsymbol{\delta}\hat{\boldsymbol{R}}_{\boldsymbol{v}} - \left(\frac{Bd2\eta^2(1+3\eta^2)}{2+8\eta^2+4\eta^4}\right)(\theta-\beta)\hat{\boldsymbol{R}}_{\boldsymbol{v}}, \tag{IV.3.60}$$

$$\boldsymbol{\tau_A} = -\frac{Bd\eta^2(2A+d)(1+3\eta^2)}{2+8\eta^2+4\eta^4}\beta\hat{\boldsymbol{z}} + \frac{d(1+5\eta^2+4\eta^4)}{2+8\eta^2+4\eta^4}\theta\hat{\boldsymbol{z}}, \tag{IV.3.61}$$

$$\boldsymbol{\tau_a} = -\frac{Bd\eta^2(2a+d)(1+3\eta^2)}{2+8\eta^2+4\eta^4}\beta\hat{\boldsymbol{z}} - \frac{d(1+5\eta^2+4\eta^4)}{2+8\eta^2+4\eta^4}\theta\hat{\boldsymbol{z}}, \tag{IV.3.62}$$

With $\hat{\boldsymbol{R}}_{\boldsymbol{v}} = (\boldsymbol{x_a} + a\hat{\boldsymbol{r}}_{\boldsymbol{a}}) - (\boldsymbol{x_A} + A\hat{\boldsymbol{r}}_{\boldsymbol{A}})$. These expressions can be used to solve Equations (IV.3.63), (IV.3.64), (IV.3.65), and (IV.3.66) for general initial conditions, then investigated for specific asymptotic cases (as the general solutions are, once again, very complex).

The dynamics of the flexible system in 2D are therefore governed by the following set of equations:

$$\mathbf{f} + 6\pi\mu A(\dot{\gamma}\mathbf{x}_{A_2}\hat{\mathbf{x}} - \mathbf{U}_A) = \mathbf{0}, \tag{IV.3.63}$$

$$-\mathbf{f} + 6\pi\mu a(\dot{\gamma}\mathbf{x}_{a_2}\hat{\mathbf{x}} - \mathbf{U}_a) = \mathbf{0}, \tag{IV.3.64}$$

$$\det(A\hat{\mathbf{r}}_A, \mathbf{f}) + 8\pi\mu A^3\left(-\frac{\dot{\gamma}}{2} - \Omega_{A_z}\right) + \tau_{A_z} = 0, \tag{IV.3.65}$$

$$\det(a\hat{\mathbf{r}}_a, -\mathbf{f}) + 8\pi\mu a^3\left(-\frac{\dot{\gamma}}{2} - \Omega_{a_z}\right) + \tau_{a_z} = 0. \tag{IV.3.66}$$

When solving for general initial conditions *i.e.* $\mathbf{x}_A = \left(X - \left(\frac{d}{2} + A\right), Y\right)$, $\mathbf{x}_a = (X +$

$\left(\frac{d}{2}+a\right), Y)$ for the symmetric case ($A = a$) for small displacements, we find the velocities

$$\mathbf{U}_A = \begin{pmatrix} \dot{\gamma}Y - \dfrac{1}{3\pi a\mu}\, B(2a+d)\left(\cos(\theta_a) - 2\eta^2\right) \;\; \sin^2\left(\frac{\theta_a}{2}\right) \\ \\ \dfrac{1}{6\pi a\mu}\, B(2a+d)\left(-2\eta^2 + \cos(\theta_a) - 1\right) \;\; \sin(\theta_a) \end{pmatrix}, \tag{IV.3.67}$$

$$\mathbf{U}_a = \begin{pmatrix} \dot{\gamma}Y + \dfrac{1}{3\pi a\mu}\, B(2a+d)\left(\cos(\theta_a) - 2\eta^2\right) \;\; \sin^2\left(\frac{\theta_a}{2}\right) \\ \\ -\dfrac{1}{6\pi a\mu}\, B(2a+d)\left(-2\eta^2 + \cos(\theta_a) - 1\right) \;\; \sin(\theta_a) \end{pmatrix}. \tag{IV.3.68}$$

and the rotation rate $\mathbf{\Omega}$, with $\mathbf{\Omega} = \dot{\theta}\ \hat{\mathbf{z}} = \mathbf{\Omega_A} = \mathbf{\Omega_a} = \dot{\theta}_A\ \hat{\mathbf{z}} = \dot{\theta}_a\ \hat{\mathbf{z}}$ in the symmetric case ($\alpha\alpha(t) = 0 \forall t$) is

$$\mathbf{\Omega} = -\frac{\dot{\gamma}}{2}\ \hat{\mathbf{z}} - \frac{B(2a+d)(4a+d)\eta^2}{8a^3\pi\mu}\sin\theta\ \hat{\mathbf{z}} \tag{IV.3.69}$$

which allows monitoring the rotation of the system over time (in the case of a system being initially horizontal). For small displacements, Equation (IV.3.69) can be Taylor-expanded for small θ at first order, revealing a direct dependence of $\dot{\theta}$ on θ as $\lim_{\theta\to 0}(\sin\theta) = \theta$. A simplified solution of Equation (IV.3.69) using this approximation is

$$\theta_{\text{app}}(t) = -\frac{\dot{\gamma}}{2}K + (\theta(0) + \frac{\dot{\gamma}}{2}K)e^{-Kt}, \tag{IV.3.70}$$
$$\text{with } K = \frac{B(2a+d)(4a+d)\eta^2}{8a^3\pi\mu}.$$

which shows that in case of small displacements, $\dot{\theta}_{\text{app}}$ dies off quickly because of its scaling with $1/K \propto 1/k_s$, therefore the stiffer the dumbbell, the quicker this angle freezes, conducing both bodies of the dumbbell to "lock" at an intermediate angle. However, if we allow for a little more displacements, with the only constraint of symmetry *i.e.* $A = a$,

$\theta_A = \theta_a = \theta$, the rotation rate becomes

$$\mathbf{\Omega} = -\frac{\dot{\gamma}}{2}\,\hat{\mathbf{z}} + \left(\frac{B(2a+d)\eta^2}{8a^3\pi\mu}(x_{a_2} - x_{A_2})\right)\cos\theta\;\hat{\mathbf{z}} + \left(\frac{1}{8a^3\pi\mu}(x_{A_1} - x_{a_1})\right)\sin\theta\;\hat{\mathbf{z}}. \tag{IV.3.71}$$

which this time depends both on $\cos\theta$ and $\sin\theta$ and translates into dumbbell tumbling. Equations (IV.3.69), (IV.3.71), and (IV.3.70) therefore bring to light the existence of two timescales governing the dynamics of flexible dumbbells, the *locking* and the *tumbling* regimes. Comparing with the RBM expression of $\mathbf{\Omega}$ presented in Equation (IV.3.11) which scales with $\sin^2\theta$, the dynamics of flexible dumbbells are very much slowed down compared to the RBM case, as the fastest regime (locking) only scales with $\sin\theta$.

To keep track of both locking and tumbling regimes as the flexible system gets into the flow, monitoring the angle β (Fig. IV.3.8) allowing to keep track of the bending of the cluster of springs which governs tumbling motion can prove useful. In the stiff limit *i.e.* not allowing stretching but only a little wobbling on both sides of the system, this angle can be expressed such as:

$$\beta(t) = \tan^{-1}\left(\frac{\hat{\mathbf{y}}\cdot(\hat{\mathbf{x}}_a(t) - \hat{\mathbf{x}}_A(t))}{\hat{\mathbf{x}}\cdot(\hat{\mathbf{x}}_a(t) - \hat{\mathbf{x}}_A(t))}\right), \tag{IV.3.72}$$

The coordinates for the small body can therefore be expressed such as:

$$x_{a_1} = x_{A_1} + (d + A + a)\cos\beta, \tag{IV.3.73}$$

$$x_{a_2} = x_{A_2} + (d + A + a)\sin\beta. \tag{IV.3.74}$$

The dynamics of the flexible symmetric case are therefore governed by the evolution of both angles β and θ as follows (recalling $B = \dfrac{4d^2k_s}{d^2+4\varepsilon}$ and $\eta = \varepsilon/d$):

$$\begin{cases} \dot{\theta}(t) = -\dfrac{\dot{\gamma}}{2} + K(\beta - \theta), \quad K = \dfrac{B(2a+d)(4a+d)\eta^2}{8a^3\pi\mu}, & \text{(IV.3.75)} \\ \dot{\beta}(t) = \dfrac{\dot{\gamma}}{2}(1 - \cos(2\beta)) + Q(\theta - \beta), \quad Q = \dfrac{4B\eta^2}{6\pi\mu a} & \text{(IV.3.76)} \end{cases}$$

As previously seen for small displacements, variations in θ scale with $1/B$, translating into a snapping behavior when $B \to \infty$, *i.e.* the angle between both bodies locks almost instantly.

What we know now about flexible symmetric dumbbells dynamics from Equations (IV.3.75) and (IV.3.76) is that

- at $t = 0$, $(1 - \cos 2(\beta)) = 0$, $(\theta - \beta) = 0 \to \dot{\beta}(0) = 0$, therefore no tumbling occurs, but
- at $t = 0$ (simultaneously), $\dot{\theta} = -\dfrac{\dot{\gamma}}{2}$, thus creating a motion of one body relatively to the other, leading to an almost instantaneous locking of the angle between both bodies,
- As soon as locking occurs, θ gets non-zero and therefore $(\theta - \beta)$ also becomes non-zero, leading to tumbling behavior,
- As β increases, $\cos(2\beta)$ accelerates the dumbbell motion as it starts getting into the flow.

However, these equations do not allow us to understand what may happen once tumbling is engaged, as other phenomena such as relaxation or other locking regime could may occur. Although solving for Equations (IV.3.63), (IV.3.64), (IV.3.65), and (IV.3.66) for general initial conditions can provide us with solutions describing the full dynamics of flexible dumbbells, these solutions are also much more complex and would still need to be analyzed in relation to some asymptotic cases for better understanding, which we aim to look at in future work.

IV.3.2.1.2 Numerical investigations of the dynamics

For now, aiming to achieve a more global picture of flexible symmetric dumbbell dynamics but not necessarily reaching out for detailed, analytic explanations, we studied the influenced of the flexibility level on dumbbell dynamics as well as on surface traction forces exerted on the surface of each body using numerical simulations, run with and without h.i.

Influence of k_s on regime dominance (locking or tumbling). In our numerical model the dumbbell flexibility depends on two parameters, namely the stretching stiffness k_s and the cluster radii ε_A, ε_a determining the bending stiffness. Because bending and stretching are interdependent behaviors (we previously established an expressions for the bending constant B as a function of ε_A, ε_a, and k_s for the symmetric case, see Equation (IV.3.54), (IV.3.55), and (IV.3.56)), we chose to present only the impact of stretching stiffness in this section. This impact was analyzed for a flexible symmetric dumbbell ($A = a = 1$) which two bodies are connected by a spring cluster of preferred length $d = 1$ and of cluster radius $\varepsilon = 0.1$, placed in a shear flow of $\dot{\gamma} = 1$. Stretching stiffnesses k_s studied ranged from 100 to 10,000.

Both locking and tumbling regimes were observed for each tested value of k_s. In locking regime, the two bodies move relatively to one another in compression and can be considered as two separate entities. Once the locked position is reached, the system starts tumbling and the dumbbell can be considered as one unique entity. When the rotation angle gets close to $\pi/2$, the system snaps, and relaxation occurs when the dumbbell aligns slowly with the flow after snapping, leading to a stretching of the connection: the system "unlocks", then locks again as tumbling continues. Movies 4 and 5 illustrate each regime for a flexible dumbbell ($A = a = 1,\ d = 1,\ \varepsilon = 0.1$).

When no h.i. are considered, dumbbell flexibility was found to influence the relative importance of one regime over the other (Figure IV.3.9) when monitoring the period of rotation T and the percentage of stretching of the cluster of springs. Stretching stiffnesses tested are $k_s \in \{90; 95; 100; 150; 200; 500; 900; 1,000; 10,000\}$. Parameters monitored were identical for $ks = 1,000$ and $k_s = 10,000$, suggesting that the system experiences RBM for $k_s \geq 1,000$, therefore values obtained for $k_s = 10,000$ were not represented on Fig. IV.3.9. The locking regime was considered dominant (DL) when the bodies kept on moving relatively to one another for more than 50 % of their period of rotation. A similar definition can be applied for dominant tumbling regime (DT). In very flexible systems ($k_s \in [90; 200[$) both regimes overlap, as tumbling occur while bodies are still moving relatively to one another. For stiffer systems ($k_s \in [200; 1000]$),

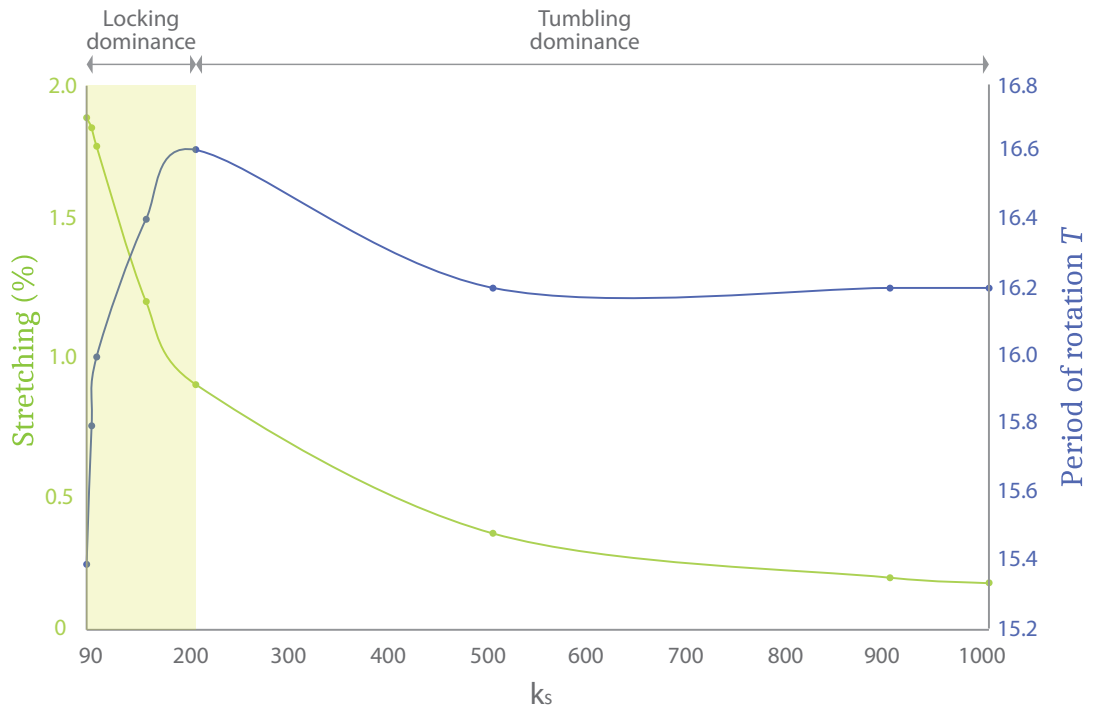

Figure IV.3.9: Regime dominance as a function of dumbbell flexibility (k_s is the dimensionless stretching modulus) for a symmetric dumbbell ($A = a = 1$, $d = 1$, $\varepsilon = 0.1$). Simulations presented have been run without hydrodynamic interactions. Period of rotation T have been averaged using up to 3 periods (dimensionless time). Stretching is expressed in percentages of the initial resting length d.

the locking regimes scaling proportionally with $1/k_s$, tumbling motion is dominant. A flexibility transition can be observed around $k_s = 200$ delimiting the dominant regime (Fig. IV.3.9).

Globally, as k_s increases, stretching decreases, and time delay with RBM decreases (data not shown). However, the evolution of the duration of the period of rotation was surprisingly found to be non-monotonous. Indeed, in the region of locking dominance, T increases with k_s (with an increasing rate going down as k_s goes up, as T increases ten times faster for $k_s \in [90, 100]$ compared to $k_s \in [100, 200]$), whereas in the region of tumbling dominance as k_s increases T decreases. A hypothesis to explain this non-monotony is that the apparent dumbbell aspect ratio changes depending on its flexibility (Figure IV.3.10). Indeed, the apparent aspect ratio χ of flexible dumbbells changes over

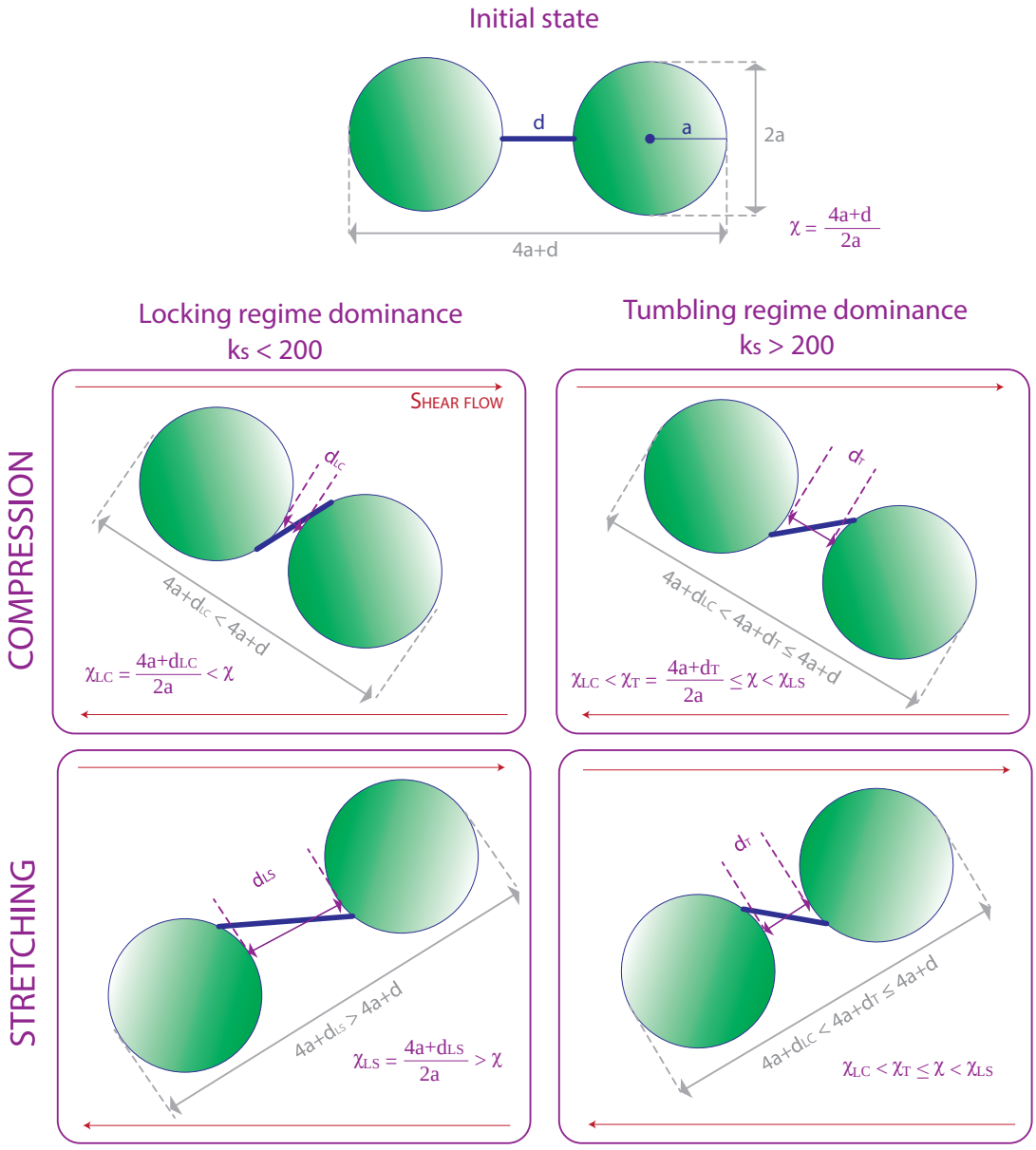

Figure IV.3.10: Evolution of the apparent aspect ratio χ of a flexible dumbbell in a shear flow depending on the dominant regime (locking or tumbling) and on the rotation phase (compression or stretching). Other quantities described on this figure include the distance between two sphere surfaces d, the sphere radius a, and the dimensionless stretching modulus k_s. LC = locking compression, LS = locking stretching, T = tumbling.

time in a shear flow due to periodic compression/relaxation phases. The more flexible the dumbbell is, the more bodies can compress and relax. Therefore, the minimum apparent aspect ratio χ_{LC} achieved by highly flexible dumbbells experiencing DL ($k_s < 200$) is close to 4:1, as if bodies were touching each other ($d_L \to 0$ for small k_s), and smaller than the aspect ratio χ_T of stiffer dumbbells experiencing DT ($d_L \to d$ for large k_s). As it is a well-known fact that the higher the aspect ratio of a body, the longer the period [Jeffery, 1922], it would be coherent to observe $\chi_L < \chi_T \leq \chi$ if we were only considering the compression phase. However, the dumbbells with the highest flexibility are also the ones that can stretch the most, leading to a maximum apparent aspect ratio χ_{LS} higher than the initial aspect ratio χ. Therefore, depending on the balance between stretching and compression, some dumbbells with intermediary flexibility ($k_s \approx 200$) may feature longer periods than both stiffer and more flexible dumbbells (Fig. IV.3.9). Similar results were observed with h.i. (data not shown).

Influence of regime dominance on rotation rate profiles. In this section, we will briefly compare the influence of the dominant regime (locking or tumbling) on rotation rate profiles as a function of the dumbbell rotation angle ζ (defined between the tangent to the dumbbell center and the horizontal) for a flexible, symmetric dumbbell, as presented in Figure IV.3.11. When experiencing DT, the dynamics of the dumbbells are very similar to those of dumbbells experiencing RBM (Section IV.3.1.1, Fig. IV.3.2 and IV.3.3), except from the fact that they feature a slight transient regime which is due to the dying off locking timescale (Fig. IV.3.11). However, when experiencing DL, this transient regime leads to the apparition of a second dynamic mode, due to compression phenomena: bodies get closer to one another, minimizing the dumbbell aspect ratio (see Fig. IV.3.10, and configurations (1) and (2) of Fig. IV.3.11) but slowing down dumbbell motion through the process. Once the dumbbell is compressed at its maximum, snapping occurs very quickly at $\zeta = \pi/2$ as the connection between bodies stretches intensely (configurations (3) and (4), Fig. IV.3.11), then slowly regain close to its resting length. This compression/stretching behavior is likely to play an important role on maximum surface traction exerted on the dumbbells, which are studied in the next section.

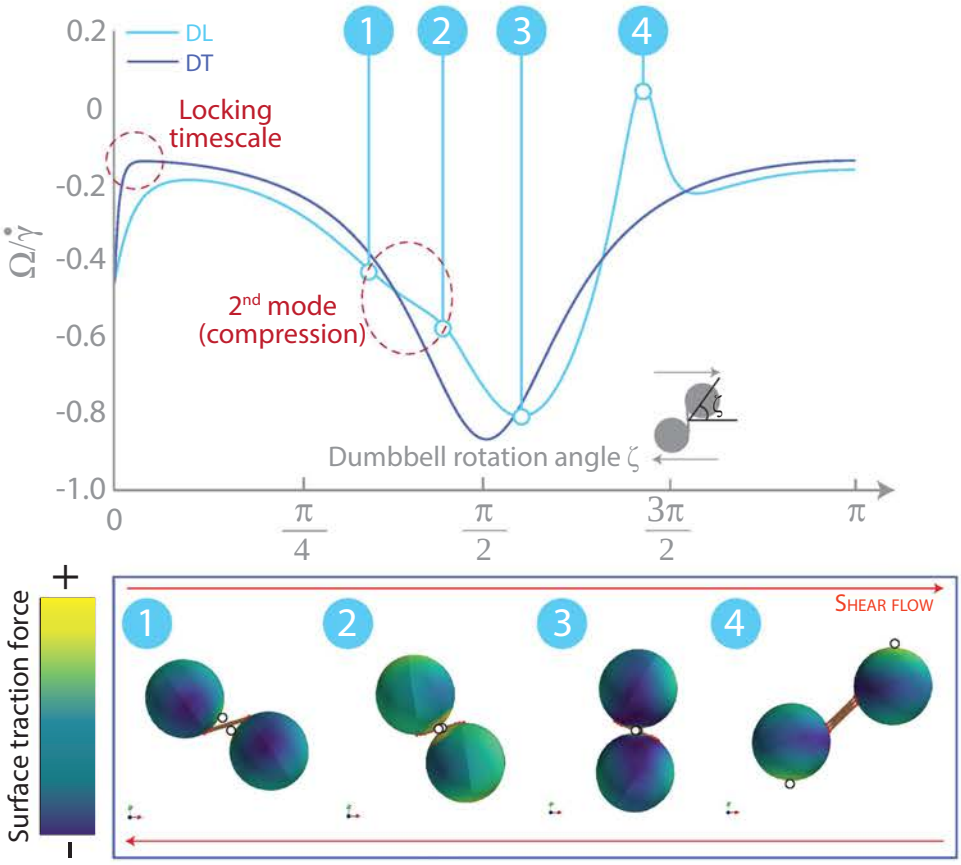

Figure IV.3.11: Representative rotation rates $\mathbf{\Omega}/\dot{\gamma} = f(t\dot{\gamma})$ over the course of a half-period (function of the dumbbell rotation angle ζ defined between the dumbbell orientation and the horizontal) for a flexible, symmetric dumbbell experiencing dominant locking (DL, light blue) and dominant tumbling (DT, dark blue) regimes in a shear flow $\dot{\gamma} = 1$. Corresponding visual outputs are presented for dumbbells in DL.

IV.3.2.1.3 Relationship between surface traction forces and dumbbell flexibility

The influence of dumbbell stretching stiffness k_s on surface traction forces exerted on the bodies of a flexible symmetric dumbbell was investigated for $k_s \in \{90; 100; 300; 500; 10,0000\}$. Highest and lowest values of maximal surface traction forces (Max_{STF}) achieved on the course of a period are presented in Table IV.3.1 and representative surface traction force profiles with and without h.i. are displayed in Figures IV.3.12 and IV.3.13 respectively for locking dominance and for tumbling dominance, with corresponding visual model outputs. Movies 4 and 5 illustrate the cases presented in Fig. IV.3.12 and IV.3.13.

k_s	Dominant regime	Highest Max_{STF}	Lowest Max_{STF}
90	Locking	400.00	3.37
100	Locking	379.82	3.39
300	Tumbling	4.24	3.47
500	Tumbling	4.21	3.48
10,000	RBM	4.17	3.48

Table IV.3.1: Influence of dumbbell flexibility on the maximal surface traction force Max_{STF} (dimensionless) exerted on the bodies with hydrodynamic interactions. RBM = Rigid Body Motion (reference).

Traction profiles are highly influenced by the dominant regime and by h.i. (Fig. IV.3.12 and IV.3.13, Table IV.3.1). Maxima and minima of Max_{STF} are reached for identical dumbbell rotation angle ζ (angle between the dumbbell direction and the horizontal) in both DL and DT (Fig. IV.3.12 and IV.3.13), and without h.i. all Max_{STF} values range between 2 and 6 (Fig. IV.3.12a, IV.3.13a). However, when h.i. are considered, the highest values of Max_{STF} achieved for DL are 10^2 higher than those achieved in DT (Fig. IV.3.12a, Table IV.3.1). The highest value of Max_{STF} in DL is reached when the dumbbell is the most compressed and opposes the most resistance to the flow (Fig. IV.3.12b, configuration (1), which matches configuration (2) of Fig. IV.3.11), whereas passed $\zeta = \pi/2$ the second maximum reached (four times lower than the first) is due to little resistance opposed after snapping when the transition between the compression and stretching phase occurs (Fig. IV.3.12b, configurations (3) and (4), matching config-

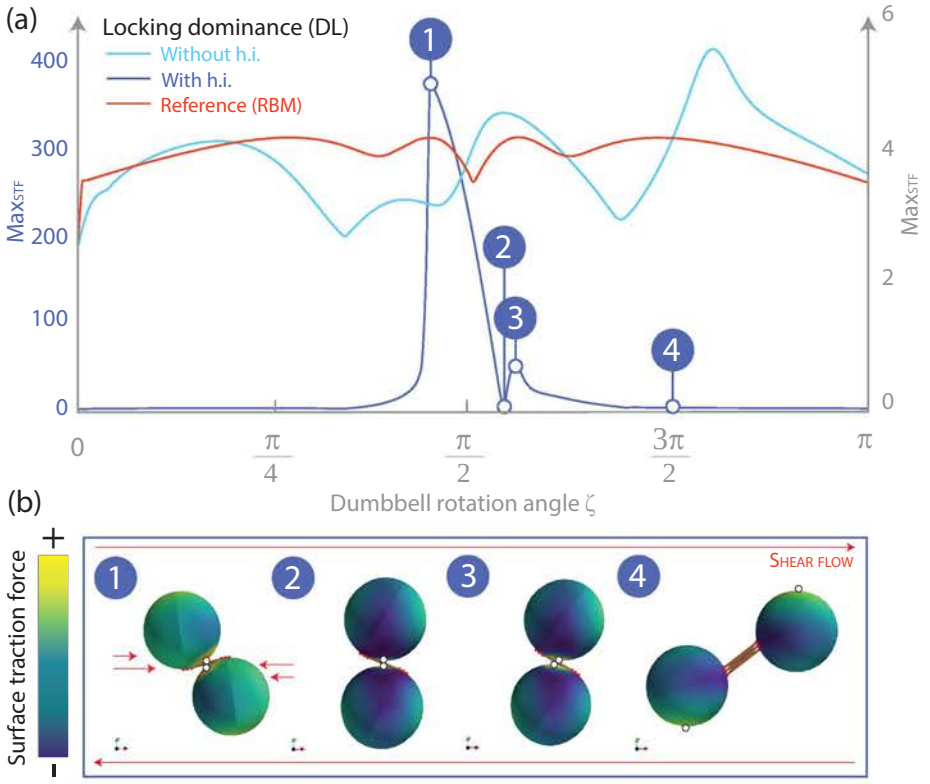

Figure IV.3.12: Representative maximal surface traction force ($\mathrm{Max}_{\mathrm{STF}}$) profiles (a) and corresponding visual outputs (b) for dominant locking regime ($k_s = 90$) in a shear flow ($\dot{\gamma} = 1$) over the course of a period. The left axis of (a) matches only data with hydrodynamic interactions. $\mathrm{Max}_{\mathrm{STF}}$ are tracked on each body by color changes. Open circles represent the location of $\mathrm{Max}_{\mathrm{STF}}$ on a given body for a given position. Rigid body motion (RBM) is also presented as a reference. The dumbbell rotation angle ζ is defined between the dumbbell orientation and the horizontal.

urations (2) and (4) of Fig. IV.3.11). The lowest values of $\mathrm{Max}_{\mathrm{STF}}$ do not change much with the regime nor with h.i., leading to a greater range of $\mathrm{Max}_{\mathrm{STF}}$ in the case of DL (in comparison, $\mathrm{Max}_{\mathrm{STF}}$ in DT ranges between 3-4, similarly to what occurs in RBM).

In case of DT, the maximum values of $\mathrm{Max}_{\mathrm{STF}}$ are reached just before and right after snapping, which occurs for a dumbbell rotation angle $\zeta = \pi/2$, and the minimum $\mathrm{Max}_{\mathrm{STF}}$ is reached at $\zeta = \pi/2$. These results are similar to what was observed for chains of ellipsoids at the limit of RBM, presented in Section IV.2.2.4. At all times (and in particular, when reaching maxima) for DT, $\mathrm{Max}_{\mathrm{STF}}$ are located on the body sides the

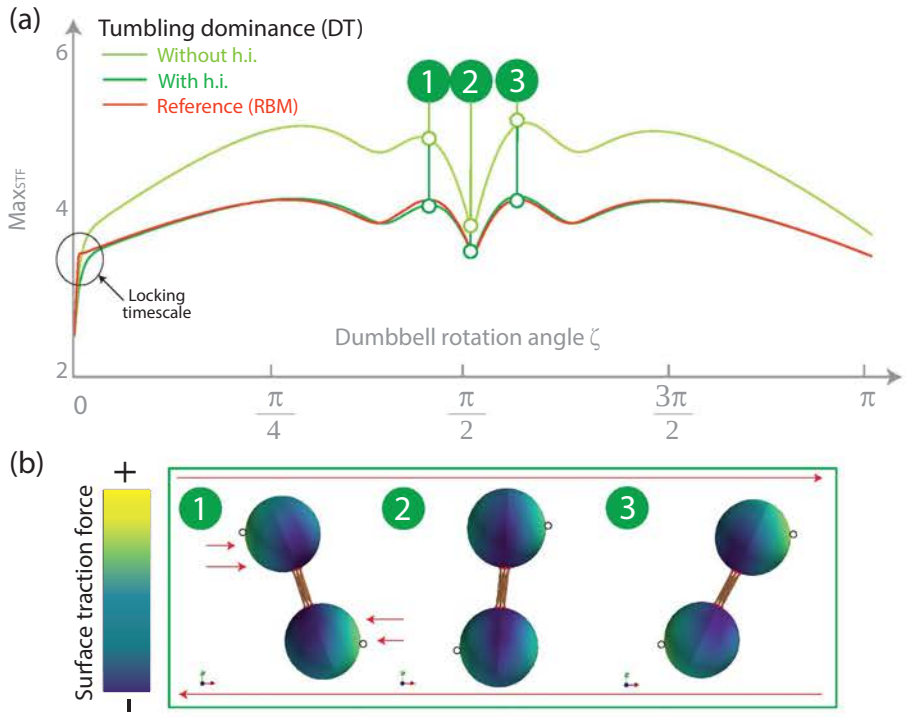

Figure IV.3.13: Representative maximal surface traction force (Max_{STF}) profiles (a) and corresponding visual outputs (b) for dominant tumbling regime ($k_s = 500$) in a shear flow ($\dot{\gamma} = 1$). Max_{STF} are tracked on each body by color changes. Open circles represent the location of Max_{STF} on a given body for a given position. Rigid body motion (RBM) is also presented as a reference. The dumbbell rotation angle ζ is defined between the dumbbell orientation and the horizontal.

more exposed to the flow (Fig. IV.3.13b, Movie 5) and never locate near connection points. On the contrary, for dumbbells in DL, Max_{STF} are located around connection points when the highest values are reached (Fig. IV.3.12b (1) and (3)) and locate on the sides of the bodies during the stretching phase (Fig. IV.3.12b (4)). This would suggest a higher probability of breakage of highly flexible dumbbells.

IV.3.2.2 Asymmetric case

IV.3.2.2.1 Analytical investigations around t=0

Similarly to the symmetric case (Section IV.3.2.1.1), we can solve for Equations (IV.3.63), (IV.3.64), (IV.3.65), and (IV.3.66) for the asymmetric case ($A \neq a$, in our case $A > a$)

introducing the offset angle $\alpha\alpha(t) = \theta_A - \theta_a$ such as represented in Fig. IV.3.8. In the symmetric case, $\alpha\alpha(t) = 0 \forall t$. However, in the asymmetric case, as $\theta_A \neq \theta_a$, $\alpha\alpha$ is not always equal to 0. Therefore, dynamics are governed by the evolution of three angles, θ_A, $\alpha\alpha$, and β. Solving for general initial conditions in the stiff limit *i.e.* $x_{a_1} = x_{A_1} + (A + d + a)\cos\beta$, $x_{a_2} = x_{A_2} + (A + d + a)\sin\beta$, $\theta_a = \theta_A - \alpha\alpha$ for $\dot{\theta}_A$, $\dot{\alpha\alpha}$, and $\dot{\beta}$ we find:

$$\begin{cases} \dot{\theta}_A = Q_1\alpha\alpha + Q_2(\beta - \theta_A) - \dfrac{\dot{\gamma}}{2}, & \text{(IV.3.77)} \\ \dot{\alpha\alpha} = Q_3\alpha\alpha + Q_4(\beta - \theta_A), & \text{(IV.3.78)} \\ \dot{\beta} = -\dfrac{\dot{\gamma}}{2}(1 - \cos(2\beta)) + Q_5(\beta - \theta_A) + Q_6\alpha\alpha. & \text{(IV.3.79)} \end{cases}$$

With $Q_i,\ i \in [\![1, 6]\!]$ constants are functions of A, d, B, η such as defined below:

$$\begin{cases} Q_1 = \dfrac{B\eta^2(2Ad + a(4A + d) - 2\varepsilon^2)}{8A^3\pi\mu}, \\ Q_2 = \dfrac{B\eta^2(A + d + a)(4A + d)}{8A^3\pi\mu}, \\ Q_3 = -\dfrac{B\eta^2(4a^2A^3 + 3aA^3d - a^4(4A + d) + 2a^3(-Ad + \varepsilon^2) + A^3(d^2 + 2\varepsilon^2))}{8a^3A^3\pi\mu}, \\ Q_4 = \dfrac{B\eta^2(a - A)(A + d + a)(4aA(a + A) + (a^2 + aA + A^2)d)}{8a^3A^3\pi\mu}, \\ Q_5 = -\dfrac{2B\eta^2(a + A)(A + d + a)}{aA(A + d + a)\pi\mu}, \\ Q_6 = -\dfrac{B\eta^2(a + A)(2a + d)}{aA(A + d + a)\pi\mu}. \end{cases}$$

As for the symmetric case, different timescales emerge, as:

- at $t = 0$, $1 - \cos(2\beta) = 0$, $\beta - \theta_A = 0$, and $\alpha\alpha(0) = 0$, therefore no tumbling or offsetting occurs, but

- at $t = 0$ (simultaneously), $\theta = -\frac{\dot{\gamma}}{2}$, thus creating a motion of one body relatively to the other (locking timescale), and

- as soon as locking occurs, θ_A and $\alpha\alpha$ get non-zero and therefore tumbling and offsetting occur,
- as β increases, the same dependence of $\dot{\beta}$ from $\cos(2\beta)$ as in the symmetric case accelerates the dumbbell motion as it starts getting into the flow.

Locking and offsetting are interdependent behaviors that occur on similar timescales. Dependence of $\dot{theta}_A$ in offsetting scales with $1/Q_1 \propto A^2/B$, therefore for very large big bodies the locking phenomenon gets amplified (offsetting and locking phenomena act in synergy), leading to what we will call a *swinging* behavior (see Movie 6 for $A = 10$, $a = 1$, $d = 1$, $\varepsilon = 0.1$, and $k_s = 3,000$). In absence of offset angle, variations in θ_A also scale with $1/Q_2 \propto Aa/B$, suggesting an balance between body size difference and dumbbell stiffness. The offsetting dynamics scale with $1/Q_3 \propto 1/(Ba)$, meaning that the smaller the small body, the more the offsetting phenomenon will get amplified. The impact of body size is tempered by the dumbbell stiffness B. Dependence of $\dot{\alpha\alpha}$ in θ_A scales with $1/Q_4 \propto 1/(B(a-A))$, suggesting this time a balance between body size difference and the dumbbell stiffness: the swinging behavior is amplified for highly asymmetric dumbbells (this is coherent with absence of offsetting phenomena for symmetric dumbbells) and tempered by low dumbbell flexibility. Offsetting and locking dynamics die off respectively proportionally to aA/B and $1/B(a-A)$, all the more quickly than body size difference is small and the dumbbell is stiff. For large big bodies and/or high dumbbell flexibility, tumbling can also be amplified by swinging as $\dot{beta}$ also features a dependence in $\alpha\alpha$ scaling with $1/Q_6 \propto A/B$.

Once again, Equations (IV.3.77), (IV.3.78), and (IV.3.79) do not provide us with full understanding of the dynamics occurring beyond tumbling, which we aim to achieve in the future. Dynamics will be studied numerically in the next section.

IV.3.2.2.2 Influence of body size ratio on dumbbells dynamics

Asymmetric, flexible dumbbells will be compared when experiencing either dominant locking regime (DL) or dominant tumbling (DT) for $A \in 2, 5, 10$ (the case of $A = a = 1$ having been previously treated in Section IV.3.2.1.2). Dynamics will be analyzed for each

dumbbell body using (i) the periodicity of period T (dimensionless number) of the body behavior, (ii) the first time $t_{\pi/2}$ at which the system rotation angle $\zeta = \pi/2$ (expressed in % of period completion), and (iii) the highest (absolute) rotation rate value $\mathbf{\Omega}_{\text{high}}$ reached over the course of one period.

		Behavior periodicity T (dimensionless)			
		Big sphere		**Small sphere**	
		DL	DT	DL	DT
Sphere radius A	2	14.80	14.40	14.80	15.20
	5	11.00	13.20	9.00	10.00
	10	12.60	13.00	10.20	11.80

Table IV.3.2: Impact of the dominant regime (locking or tumbling) and of the size of the big body (radius A) on the periodicity (period T, dimensionless) of the behaviors of the big and small bodies in flexible, asymmetric dumbbells. DL=dominant locking regime, DT=dominant tumbling regime.

Behavior periodicity. Table IV.3.2 describes the impact of the dominant regime (DL or DT) and of the size of the big body of radius A on the periodicity (period T, dimensionless) of the behaviors of the big and small bodies in flexible, asymmetric dumbbells.

As A increases from 2 to 5, all T decreased for all bodies, whether DL or DT was considered (Table IV.3.2), and T also decreases faster for the small body versus the big body, leading to an increased swinging periodicity (See Movies 6 and 7 respectively for $A = 10$, $a = 1$, and $A = 5$, $a = 1$, dominant locking behavior). This means that as A increases up to $A = 5$, the rotation of the system globally accelerates. However, between $A = 5$ and $A = 10$, T increases for the small body whether in DL or DT, as well as for big body experiencing DL (Table IV.3.2). This non-monotony may be correlated to a scaling transition, as for A large enough ($A > 5$) the small body only perceives a portion of the big body, as if it were attached to a wall, therefore experiencing a local field that would slow down the periodicity of its motion. Similarly, for A large enough, the big body would not feel the presence of the small body any more, which may have contributed to accelerating its rotation (due to the swinging phenomenon described in previous Section IV.3.2.2.1), and its behavior gets closer to a single sphere's. This

transition between decreasing/increasing period, occurring around $A = 5$, reminds of the transition in maximal Max_{STF} location described for asymmetric dumbbells in RBM (Section IV.3.1.2.2), where a threshold in A was identified between $A = 5$ and $A = 6$. It can therefore be suggested that a specific A_{thres} may originates both non-monotony in body behavior periodicity and maximal traction forces location. We hope to elucidate and clarify the role of this A_{thres} in future work.

When comparing DL and DT, it appears that DL mostly favor shorter T (Table IV.3.2)), which we can link to the synergistic behavior occurring in DL between the swinging of the small body and the rotation of the big body previously described (Section IV.3.2.2.1).

		Time $t_{\pi/2}$ (in % of T)			
		Big sphere		**Small sphere**	
		DL	DT	DL	DT
Sphere radius A	2	25.97	27.50	25.97	25.00
	5	29.63	25.56	29.55	24.75
	10	25.77	25.00	24.50	19.59

Table IV.3.3: Impact of the dominant regime (locking or tumbling) and of the size of the big body (radius A) on the first times $t_{\pi/2}$ (in % of T) at which the big and small body ($a = 1$) of flexible, asymmetric dumbbells reach a perpendicular to the flow ($\zeta = 2$ dumbbell rotation angle defined between the dumbbell orientation and the horizontal). DL=dominant locking regime, DT=dominant tumbling regime.

Reaching a perpendicular to the flow. Table IV.3.3 describes the impact of the dominant regime (DL or DT) and of the size of the big body of radius A on the first times $t_{\pi/2}$ (in % of T) at which the big and small body of flexible, asymmetric dumbbells reach a perpendicular to the flow. Overall, $t_{\pi/2}$, *i.e.* when a body gets perpendicular to the flow, is achieved around 25-30% of the period (considering each body behavior periodicity). If the system was perfectly rotating, $t_{\pi/2}$ would be achieved at exactly a quarter of period, as the shear rate considered is $\dot{\gamma} = 1$. Slight delays occurring here (0-5%) are due to interferences with the locking timescale.

For dumbbells experiencing DL, $t_{\pi/2}$ increases with A from $A = 2$ to $A = 5$ (dumbbells are delayed from getting into the flow), then decreases from $A = 5$ to $A = 10$. We

notice the same non-monotonous behavior than previously observed for body behavior periodicity (Section IV.3.2.2.2). For dumbbells experiencing DT, however, $t_{\pi/2}$ increases with A from $A = 2$ to $A = 10$, translating into accelerated motion as A gets bigger, following a logarithmic trend (as A gets large enough, the motion becomes once again closer to a single sphere's). In this same regime, it can also be noticed that as A increases, the small body motion is more and more delayed compared to the big body motion, as it gets dragged along into the flow due to almost permanent locking position (See Movies 8 and 9 respectively for $A = 10$, $a = 1$, and $A = 5$, $a = 1$, dominant tumbling regimes).

		Highest rotation rate $\mathbf{\Omega}_{\text{high}}$ (dimensionless)			
		Big sphere		**Small sphere**	
		DL	DT	DL	DT
Sphere radius A	2	-0.64	-0.67	-1.50	-1.27
	5	-0.53	-0.57	-1.96	-1.23
	10	-0.51	-0.52	-1.76	-0.90

Table IV.3.4: Impact of the dominant regime (locking or tumbling) and of the size of the big body (radius A) on highest absolute rotation rate $\mathbf{\Omega}_{\text{high}}$ (dimensionless) reached over the course of one period for both the big and small body ($a = 1$) of flexible, asymmetric dumbbells. DL=dominant locking regime, DT=dominant tumbling regime.

Highest absolute rotation rate. As A increases, the highest rotation rate $\mathbf{\Omega}_{\text{high}}$ of the big body decreases, whether in DL or in DT, as the behavior gets closer to a single sphere's, of constant rotation rate $\mathbf{\Omega}_{\text{high}} = -1/2$ for $\dot{\gamma} = 1$ (Table IV.3.4). Similarly, $\mathbf{\Omega}_{\text{high}}$ of the small body in DT decreases as A increases, translating into a stiffer behavior limiting swinging and making the small body experience a rotation closer the one of the big body. Highest rotation rates of the small body always remain two or three times higher than for the big body due to increased dragging, in addition to the background flow. For dumbbells experiencing DL, the small body is allowed to a lot of swinging, which eventually reduced as A gets large enough, in the limit of stiffer behavior (DL tends to translate into DT eventually for large A). The same threshold in A around $A = 5$ as previously described in sections IV.3.1.2.2 and IV.3.2.2.2 can be noticed.

Overall, it appears that DT and DL, as well as the body size ratio $A : a$ ($a =$

1 numerically) exert important influences on flexible asymmetric dumbbells dynamics. In DT, $t_{\pi/2}$ and highest rotation rates $\mathbf{\Omega}_{\text{high}}$ respectively increase and decrease with increasing A, whereas the periodicity of body behavior was found to be non-monotonous on $A \in [1, 10]$. In DL, T and $t_{\pi/2}$ feature non-monotonous behaviors, as well as $\mathbf{\Omega}_{\text{high}}$ for the small body. The existence of a threshold in A_{thres} was suggested, that would govern both flexible asymmetric dumbbells dynamics and maximal surface traction forces. DL, DT, and body size ratio were also always found to have amplified effect on the small body compared to the big body.

IV.3.2.2.3 Influence of body size ratio on surface traction forces

In this section we describe an interesting relationship that can be drawn between the body size ratio $A : a$ and Max_{STF} in case of flexible, asymmetric dumbbells experiencing DT, with and without h.i.. We then briefly compare Max_{STF} exerted on in DL versus DT as a function of body size ratio $A : a$.

Relationship between traction forces and body size ratio with and without hydrodynamic interactions. Max_{STF} was monitored for asymmetric dumbbells ($a = 1$, $A \in \{1; 2; 3; 4; 5; 10\}$; k_s and r were fixed to ensure DT) for both small and big bodies, with and without h.i. as respectively presented in Figures IV.3.14 and IV.3.15. Results without h.i. were obtained using the simple analytical expression of the traction force exerted by surface area on a small body attached to a big body in a shear flow that can be recalled from Section IV.3.1.2.2, implying a linear relationship between Max_{STF} and the body size ratio $A : a$. Hydrodynamic interactions play an important role on Max_{STF} exerted on the small body (Fig. IV.3.14), but have little effect on the big body (Fig. IV.3.15). When h.i. are not taken into account, Max_{STF} range from 5 to 45 for the small body whereas they only reach a maximum of 10 when h.i. are considered IV.3.14).

As the body size ratio increases, Max_{STF} respectively increase and decrease on the small and big body, which could be correlated with increased swinging behavior previously demonstrated (Section IV.3.2.2.1). However, when h.i. are considered, these trends

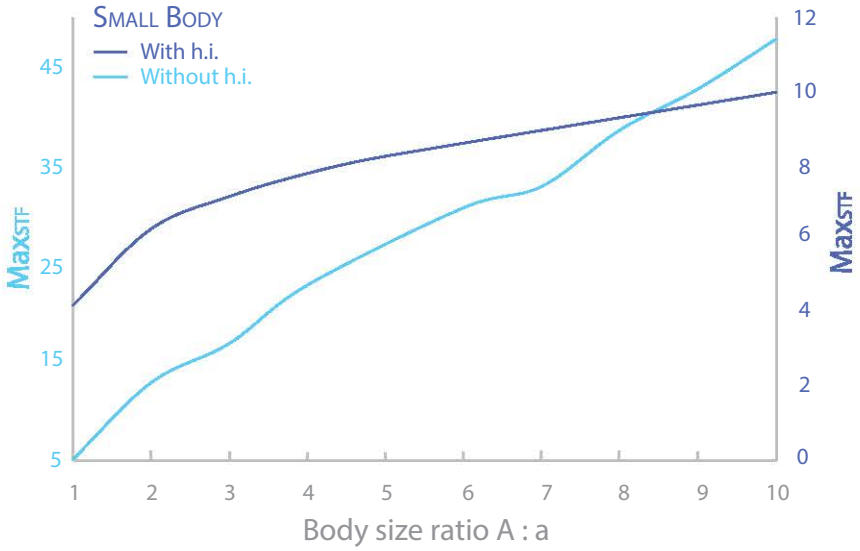

Figure IV.3.14: Influence of body size ratio A:a ($a = 1$, $A \in \{1; 2; 3; 4; 5; 10\}$) and hydrodynamic interactions (h.i.) on the maximal value reached by the maximal surface traction force ($\mathrm{Max}_{\mathrm{STF}}$) exerted on the small body of radius a of an asymmetric dumbbell experiencing dominant tumbling regime (DT) in a shear flow ($\dot{\gamma} = 1$).

are logarithmic, such as

$$\begin{cases} \text{Small body: } \mathrm{Max}_{\mathrm{STF}} \approx 2.46 \ln(A:a) + 4.35, \quad R^2 = 0.996, & \text{(IV.3.80)} \\ \text{Big body: } \mathrm{Max}_{\mathrm{STF}} \approx -0.91 \ln(A:a) + 4.10, \quad R^2 = 0.953, & \text{(IV.3.81)} \end{cases}$$

i.e. for sufficiently high body size ratios ($A \geq 5a$) $\mathrm{Max}_{\mathrm{STF}}$ reaches a plateau for both small and big bodies. This can be attributed to the fact that for $A : a$ high enough, the small body would only perceive the surface of the big body as a wall (experiencing periodic swinging), and the influence of the small body on $\mathrm{Max}_{\mathrm{STF}}$ perceived by the big body would become neglectable.

Combined influences of body size ratio and dominant regime. The maximal surface traction force exerted on both bodies of a flexible, asymmetric dumbbells in DL versus in DT has been represented for $A \in \{2, 4, 5, 10\}$ in Table IV.3.5. If $\mathrm{Max}_{\mathrm{STF}}$ globally evolve monotonously for dumbbells in DT, their evolution is much more complex in case of DL, featuring a double non-monotonous behavior. Indeed, $\mathrm{Max}_{\mathrm{STF}}$ decrease on

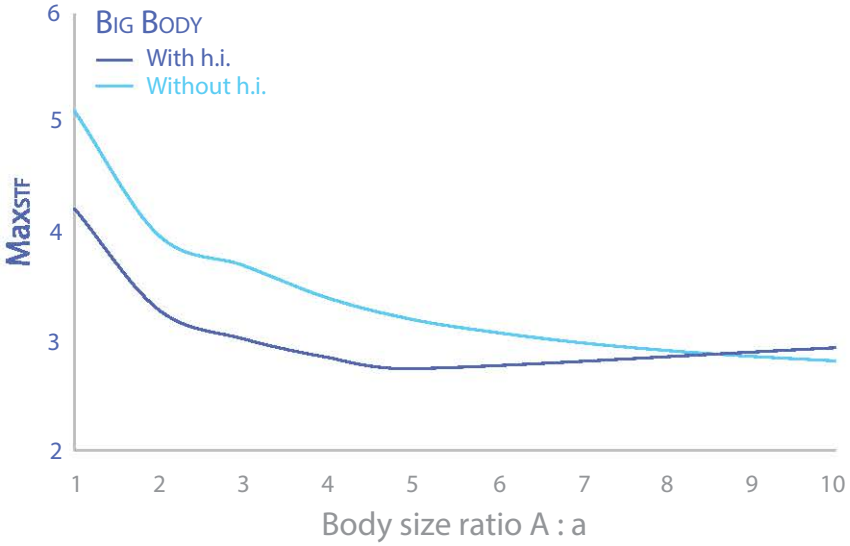

Figure IV.3.15: Influence of body size ratio A:a ($a = 1$, $A \in \{1; 2; 3; 4; 5; 10\}$) and hydrodynamic interactions (h.i.) on the maximal value reached by the maximal surface traction force (Max_{STF}) exerted on the big body of radius A of an asymmetric dumbbell experiencing dominant tumbling regime (DT) in a shear flow ($\dot{\gamma} = 1$).

		Max_{STF} **(dimensionless)**			
		Big sphere		**Small sphere**	
		DL	DT	DL	DT
Sphere radius A	2	10.07	3.28	10.88	6.28
	4	2.79	2.85	8.27	7.79
	5	11.84	2.74	18.18	8.25
	10	4.12	2.93	8.88	9.99

Table IV.3.5: Impact of the dominant regime (locking or tumbling) and of the size of the big body (radius A) on the maximal value of maximal surface traction forces Max_{STF} (dimensionless) exerted on both the big and small body ($a = 1$) of flexible, asymmetric dumbbells. DL=dominant locking regime, DT=dominant tumbling regime.

both bodies from $A = 2$ to $A = 4$, increase between $A = 4$ and $A = 5$, and decrease again sharply between $A = 5$ and $A = 10$. Range of Max_{STF} in DL is also far greater than in DT, and Max_{STF} in DL always remain superior to those in DT, suggesting bottleneck effects due to changing aspect ratios such as what occur in the symmetric case (Fig. IV.3.10). It appears very difficult to find a simple rationale guiding the evolution of

Max_{STF} in DL.

Two hypotheses can however be made: (i) the decrease in Max_{STF} from $A = 2$ to $A = 4$ (following the same trend as from $A = 1$ to $A = 2$ may result from the scaling out of the big body relatively to the small body, leading to increased stiffness of the connection and therefore less proximity can be achieved between both bodies, reducing the bottleneck effect due to compression, and (ii) the decrease in Max_{STF} from $A = 5$ to $A = 10$ may be due to a "second mode" of scaling out, this time the big body being large enough to be perceived as a wall by the small body, thus modifying locally the field perceived by the small body, whereas the big body gets closer to a single sphere's behavior. No satisfying explanation of the increase in Max_{STF} between $A = 4$ and $A = 5$ could be found for now. It may be the case that being close to a threshold in A such as previously observed when monitoring the dynamics on flexible asymmetric dumbbells (Section IV.3.2.2.2) induces very complex behaviors. More simulations would be needed in order to understand better those dynamics.

IV.3.3 Shape variations: spherical-ellipsoidal dumbbells

In this last section, we explore some possibilities of our model allowing us to change body shape in order to compare the dynamics and Max_{STF} applied to flexible, spherical dumbbells (SD) to those of mixed dumbbells (MD), constituted of one sphere of radius A and one ellipsoid of half-length a and half-width b (dimensionless numbers), such as represented in Figure IV.3.16a, with various body size ratios $A : a$. This part of our study has been motivated by adhesive interactions that may occur between lactic acid bacteria (modeled by ellipsoids) and spherical components, such as fat globules [Auty et al., 2001, Hickey et al., 2015b, Hickey et al., 2015a, Guerin et al., 2017b, Laloy et al., 1996, Lopez et al., 2006, Guerin et al., 2018b]. These interactions may play an important role in bacterial location and protection during food manufacturing of dairy products, such as cheese [Guerin et al., 2017b, Laloy et al., 1996, Jeanson et al., 2011], and may also impact probiotic delivery as interfering with adhesion to intestinal cells [Guerin et al., 2018b]. Most often, fat globule radius range between 0.5 and 5 μm, but in some case the

smallest globules (0.05 μm) can be approximately 100-fold smaller in diameter compared to the largest ones (10 μm) [Hickey et al., 2015a, Lopez, 2005, Truong et al., 2016]. Here, we will focus our investigations on spherical components of radius $A \in [\![1, 10]\!]$, which we will compare with the case of flexible asymmetric dumbbells previously described (Section IV.3.2.2). We will leave investigations of the impact of attachment orientation (Fig. IV.3.16b) and multiple attachments in case of bacterial chains (Fig. IV.3.16c, IV.3.16d) to future work.

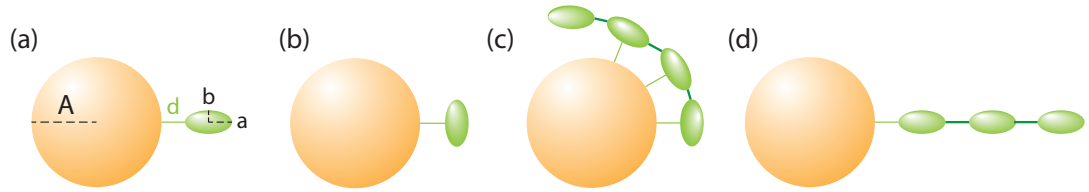

Figure IV.3.16: Exploring more complex configurations to model bacterial adhesion to a sphere of radius A: single cell (ellipsoid of aspect ratio b:a) attachment by cell tip (a) and cell side (b), multiple attachment of bacterial chains by cell side (c) and cell tip (d). Cases (b), (c), and (d) are left for future investigations.

IV.3.3.1 Particular case of A=a

When the spherical body of radius A scales with the ellipsoidal body (half-length a, $A \to a$), dynamics have a distinct behavior than for all other A, especially if the MD experience DL. Cases of DL and DT will be treated separately in this section. For each case, the dynamics and $\mathrm{Max}_{\mathrm{STF}}$ behavior will be briefly described.

IV.3.3.1.1 Dominant locking regime

Representative profiles of rotation rates $\Omega/\dot{\gamma}$ and $\mathrm{Max}_{\mathrm{STF}}$ over time (dimensionless, $t\dot{\gamma}$) are represented in Figure IV.3.17. Body shape appeared to exert a great influence on both MD dynamics and $\mathrm{Max}_{\mathrm{STF}}$ in DL when the sphere scales with the ellipsoid. In terms of dynamics, the sphere begins rotating when the ellipsoid does not feel the flow yet, due to differences in aspect ratios (the higher the aspect ratio, the more delayed the body gets into the flow). Consequently, as the ellipsoid motion is delayed by about a quarter of the sphere rotation period, very high forces start exerting on the narrow

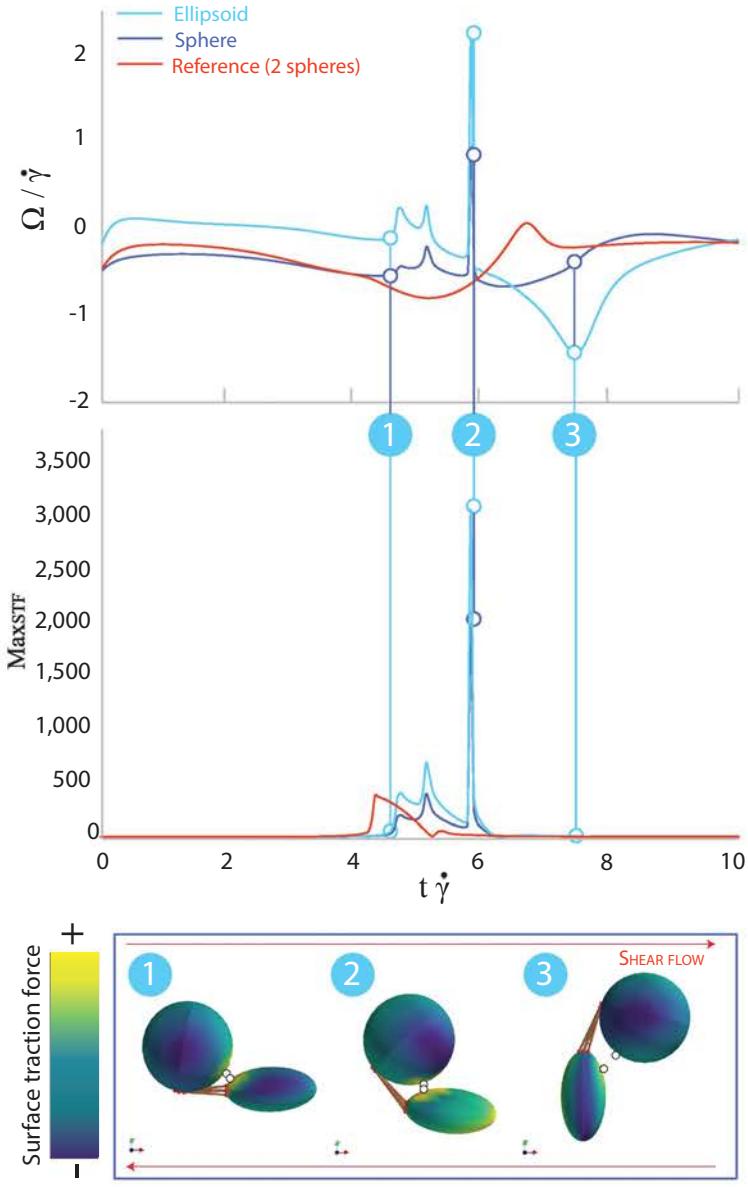

Figure IV.3.17: Dynamics (dimensionless rotation rate $\mathbf{\Omega}/\dot{\gamma}$) and maximum surface traction force $\mathrm{Max}_{\mathrm{STF}}$ exerted on mixed dumbbells (MD) constituted of one spherical ($A = 1$, dark blue) and one ellipsoidal body ($a = 1$, $b = 0.5$, light blue) experiencing dominant locking regime (DL) in a shear flow $\dot{\gamma} = 1$ over time $t\dot{\gamma}$ (dimensionless). Dynamics and $\mathrm{Max}_{\mathrm{STF}}$ exerted on spherical dumbbells ($A = a = 1$) are represented as a reference. Corresponding visual outputs allow $\mathrm{Max}_{\mathrm{STF}}$ tracking through color changes. Open circles represent the location of the maximal $\mathrm{Max}_{\mathrm{STF}}$ on a body in a given configuration.

region between both bodies (Fig. IV.3.17, configuration (1)), which become as close as able to bump repeatedly into each other while the ellipsoid is being forced into the flow (Fig. IV.3.17, configuration (2), which is similar for the two other traction peaks; see also Movie 10), leading to the series of three peaks observed both on dynamics as well as on $\mathrm{Max_{STF}}$ profiles. Peaks observed in the dynamics, corresponding to each bumping event, are slightly delayed compared to $\mathrm{Max_{STF}}$ peaks, which are the highest when the bodies are very close to one another without touching, as the narrow region between them experiences then a bottleneck effect increasing drastically $\mathrm{Max_{STF}}$. Once the ellipsoid gets forced into the flow but remains parallel to it (Fig. IV.3.17 (2)), the motion suddenly accelerates and the ellipsoid gets perpendicular to the flow, pushing away both bodies from one another (Fig. IV.3.17 (3)), leading to a relaxation phase in terms of traction forces, before both bodies regain close to horizontal. Compared to what occurs for the reference case of SD, only one main peak can be noticed in terms of $\mathrm{Max_{STF}}$ (actually, two peaks occur such as presented in Fig. IV.3.12, but the second one can be neglected in front of the first)), due to increased proximity between the bodies, but the symmetry does not lead to abnormal disturbances of the dynamics nor of $\mathrm{Max_{STF}}$ such as what occurs for MD. Changes in shapes therefore lead to more complex, and possible more detrimental behaviors in terms of forces and bumping events.

IV.3.3.1.2 Dominant tumbling regime

Dynamics. MD experiencing DT feature dynamics closer to SD, although asymmetric when comparing sphere versus ellipsoid dynamics in MD, such as represented in Figure IV.3.18. The sphere motion in MD is sensibly the same as in SD, with only increased locking timescale and delay in reaching a perpendicular to the flow (Fig. IV.3.18). The ellipsoid motion feature similar, but amplified dynamics.

Maximal surface traction forces. In DT, dynamics of MD were shown not to differ too much from SD dynamics. Investigating if similarly, $\mathrm{Max_{STF}}$ would not be influenced too much by body shape, we compared the maximum values and ranges reached by $\mathrm{Max_{STF}}$ with h.i. on (i) single cells of ellipsoidal and spherical shape, (ii) SD, (iii) MD,

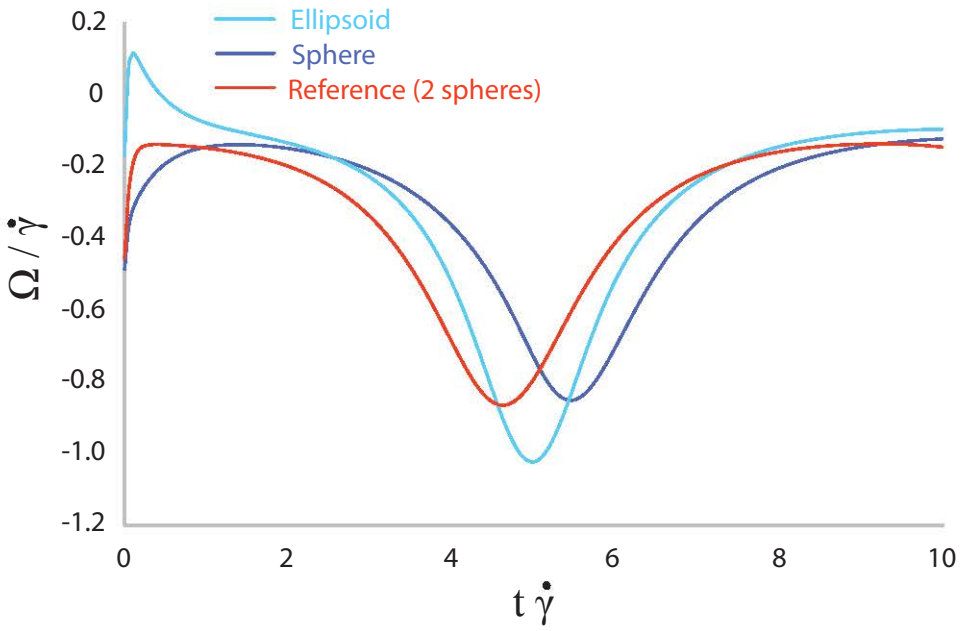

Figure IV.3.18: Dynamics (dimensionless rotation rate $\mathbf{\Omega}/\dot{\gamma}$ as a function of dimensionless time $t\dot{\gamma}$) of mixed dumbbells (MD) constituted of a sphere ($A = 1$, dark blue) and of an ellipsoid ($a = 1$, $b = 0.5$, light blue) experiencing dominant tumbling regime (DT) in a shear flow $\dot{\gamma} = 1$. Dynamics of spherical dumbbells (SD, reference case) are also represented (red line).

and (iv) two ellipsoids. Results are presented in Figure IV.3.19 for spheres of radius $A = 1$, ellipsoids of half-length $a = 1$ and half-width $b = 0.5$, and resting length of connection $d = 1$. Stretching and bending stiffnesses were fixed to ensure DT. Maximal values of $\mathrm{Max}_{\mathrm{STF}}$ on a single prolate body rotating freely in a shear flow are twice as high than for a single sphere, which experiences constant $\mathrm{Max}_{\mathrm{STF}}$ (Fig. IV.3.19). Similarly, symmetric dumbbells constituted of prolate ellipsoids experience maximum $\mathrm{Max}_{\mathrm{STF}}$ about twice as high as symmetric dumbbells constituted of spheres. The range of $\mathrm{Max}_{\mathrm{STF}}$ achieved over a period of rotation is also more important for ellipsoidal dumbbells than for spherical dumbbells, as the maximal value of $\mathrm{Max}_{\mathrm{STF}}$ is about 60 % higher than the minimal value for ellipsoidal dumbbells. Establishing a parallel with bacterial chain of rod-like and bead-like bacterial cells, rod-like chains would experience higher forces on their surface. However, $\mathrm{Max}_{\mathrm{STF}}$ exerted on a single bacterium attached to

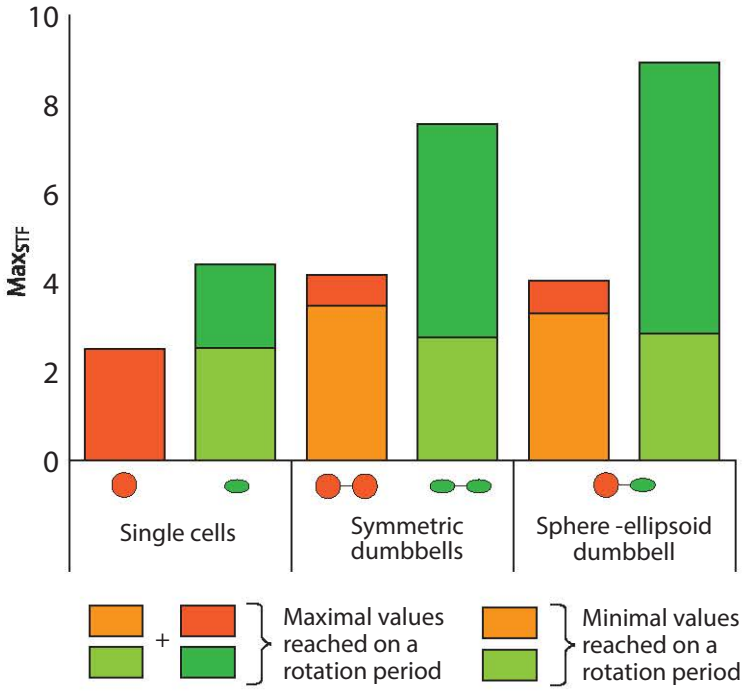

Figure IV.3.19: Maximal surface traction forces (Max_{STF}, dimensionless) with hydrodynamic interactions exerted on single body and dumbbells of various shapes (ellipsoidal and spherical experiencing dominant tumbling regime (DT) in a shear flow ($\dot{\gamma} = 1$). Minimal values (light colors) and maximal values (sum of light and dark colors) reached over one period of rotation are represented. Dark colors represent the range of values between which Max_{STF} vary over one period for a body in a given configuration. Systems parameters are $A = 1$, $a = 1$, $b = 0.5$, $d = 1$. Stretching and bending stiffnesses were fixed to ensure dominant tumbling regime.

a sphere of same dimensions in mixed dumbbells are even higher than those exerted on bacteria in an ellipsoidal dumbbell, whereas Max_{STF} exerted on the spherical part of mixed dumbbells are roughly the same than for a sphere in a spherical dumbbell. Moreover, in DT maximum Max_{STF} concentrate at the free tip of the ellipsoid (see Movie 11). This suggests that bacterial adhesion to a sphere may have unfavorable consequences on bacterial cells, which would experience greater forces on their surface which could potentially induce some damages. Body shape proved therefore to impact significantly Max_{STF}, even in DT.

IV.3.3.2 Case of flexible, asymmetric mixed dumbbells ($A > a$)

IV.3.3.2.1 Dynamics

The numerical dynamics of flexible, asymmetric MD are compared with those of flexible, asymmetric SD (reference, as described in Section IV.3.2.2.2), in DL and DT regimes for $A \in 2, 5, 10$ based on the same three indicators defined in Section IV.3.2.2.2, *i.e.* the behavior periodicity T, the time $t_{\pi/2}$, and the highest absolute rotation rate $\mathbf{\Omega}_{\text{high}}$.

		Behavior periodicity T (dimensionless)			
		Locking dominance		**Tumbling dominance**	
		Big sphere (MD)	Reference	Big sphere (MD)	Reference
Sphere radius A	2	14.20	14.80	15.00	14.40
	5	12.00	11.00	13.60	13.20
	10	13.20	12.60	13.00	13.00

Table IV.3.6: Impact of the dominant regime (locking or tumbling) and of the size of the big body (radius A) on behavior periodicity T (dimensionless) of the big body in asymmetric, mixed dumbbells (MD) and spherical dumbbells (SD, reference).

		Behavior periodicity T (dimensionless)			
		Locking dominance		**Tumbling dominance**	
		Ellipsoid	Reference	Ellipsoid	Reference
Sphere radius A	2	12.60	14.80	13.80	15.20
	5	8.80	9.00	11.20	10.00
	10	10.80	10.20	12.20	11.80

Table IV.3.7: Impact of the dominant regime (locking or tumbling) and of the size of the big body (radius A) on the behavior periodicity T (dimensionless) of the ellipsoid in asymmetric, mixed dumbbells (MD) and the small sphere of asymmetric, spherical dumbbells (SD, reference).

Behavior periodicity T. As A increases from 2 to 5, T decreased for all bodies and faster for the small body (whether ellipsoidal or spherical) (Table IV.3.7) than for the big body (Table IV.3.6), and between $A = 5$ and $A = 10$, all T increase for all small bodies, whether experiencing DL or DT (Table IV.3.7), as well as for big bodies experiencing DL (Table IV.3.6).

When comparing DL and DT, it appears that DL mostly favor shorter T for MD as well as for SD (Tables IV.3.6), IV.3.7), which we can link to the synergistic behavior occurring in DL between the swinging of the small body and the rotation of the big body previously described (Section IV.3.2.2.1.

T was lower for ellipsoids compared to small spheres for $A = 2$ and $A = 5$, but higher for $A = 10$ (Table IV.3.7), whether DL or DT were considered. On the contrary, when comparing big bodies in mixed dumbbells (MD) and spherical dumbbells (SD, reference), in DL T was higher for big bodies in MD compared to big bodies in SD for $A = 2$ and $A = 5$, and lower for $A = 10$ (Table IV.3.6). This suggests that the ellipsoidal shape has an amplified impact on T of both MD bodies compared to SD bodies. In DT, big spheres in MD always feature longer T compared to big spheres in SD, suggesting that the body shape impact may be greater on big bodies in DT compared to DL.

Overall, trends between MD and SD appear similar (Tables IV.3.6 and IV.3.7) but amplified for MD.

		Time $t_{\pi/2}$ (in % of T)			
		Locking dominance		**Tumbling dominance**	
		Big sphere (MD)	Reference	Big sphere (MD)	Reference
Sphere radius A	2	27.24	25.97	26.42	27.50
	5	27.61	29.63	24.63	25.56
	10	25.00	25.77	24.81	25.00

Table IV.3.8: Impact of the dominant regime (locking or tumbling) and of the size of the big body (radius A) on the first times $t_{\pi/2}$ (in % of T) at which the big body of asymmetric, mixed dumbbells (MD) and spherical dumbbells (SD, reference) reaches a perpendicular to the flow ($\zeta = \pi/2$).

Reaching a perpendicular to the flow. Once again, globally $t_{\pi/2}$ is reached about a quarter of period considering each body behavior periodicity T, with slight delays and advances due to timescales interferences (Tables IV.3.8 and IV.3.9). Delays and advances in reaching a perpendicular to the flow are amplified for MD compared to SD. The same non-monotonous behavior is observed both for MD and SD.

		Time $t_{\pi/2}$ (in % of T)			
		Locking dominance		**Tumbling dominance**	
		Ellipsoid	Reference	Ellipsoid	Reference
Sphere radius A	2	31.02	25.97	25.00	25.00
	5	28.00	29.55	21.72	24.75
	10	22.16	24.50	18.56	19.59

Table IV.3.9: Impact of the dominant regime (locking or tumbling) and of the size of the big body (radius A) on the first times $t_{\pi/2}$ (in % of T) at which the small body (ellipsoid) of asymmetric, mixed dumbbells (MD) and spherical dumbbells (SD, reference) reaches a perpendicular to the flow ($\zeta = \pi/2$).

		Highest rotation rate $\mathbf{\Omega}_{\text{high}}$ (dimensionless)			
		Locking dominance		**Tumbling dominance**	
		Big sphere	Reference	Big sphere	Reference
Sphere radius A	2	-0.57	-0.64	-0.69	-0.67
	5	-0.53	-0.53	-0.55	-0.57
	10	-0.51	-0.51	-0.51	-0.52

Table IV.3.10: Impact of the dominant regime (locking or tumbling) and of the size of the big body (radius A) on highest absolute rotation rate $\mathbf{\Omega}_{\text{high}}$ (dimensionless) reached over the course of one period for the big body of mixed dumbbells (MD) versus spherical dumbbells (SD, reference).

		Highest rotation rate $\mathbf{\Omega}_{\text{high}}$ (dimensionless)			
		Locking dominance		**Tumbling dominance**	
		Ellipsoid	Reference	Ellipsoid	Reference
Sphere radius A	2	-1.66	-1.50	-1.31	-1.27
	5	-1.91	-1.96	-1.01	-1.23
	10	-1.43	-1.76	-0.75	-0.90

Table IV.3.11: Impact of the dominant regime (locking or tumbling) and of the size of the big body (radius A) on highest absolute rotation rate $\mathbf{\Omega}_{\text{high}}$ (dimensionless) reached over the course of one period for the ellipsoid of mixed dumbbells (MD) versus the small sphere of spherical dumbbells (SD, reference).

Highest absolute rotation rate. As A increases, the behavior of the big sphere becomes closer to a single sphere's in both MD and SD, but much faster in MD (Table IV.3.10), both in DL and in DT. This suggests that the cost to free rotation of the big body created by attaching a small ellipsoid to it is inferior to the one created by a small

sphere. Similarly, Ω_{high} of the ellipsoid decreases faster when A increases compared to the small sphere's, although initial values were higher for ellipsoids compared small spheres at same A (Table IV.3.11). Shaping the small body as an ellipsoid would therefore less impact the spherical component's dynamics, whereas variations in the ellipsoid dynamics would be amplified compared to small sphere dynamics.

IV.3.3.2.2 Maximal surface traction forces

Knowing that it can be unfavorable for a bacterium cell to attach to a sphere in a shear flow in terms of Max_{STF} such as presented for $A = a = 1$ (Section IV.3.3.1.2), we want to know how unfavorable this adhesion could be depending on the sphere size, motivated by the biological rationale that fat globules usually range from 1 to 10 μm whereas the average length of a bacterium cell is about 1-2 μm [Tripathi et al., 2012, Lopez, 2005].

We investigated the evolution of Max_{STF} with h.i. on both the ellipsoidal body and the spherical body as a function of the sphere size for A radius of the sphere ranging in $\{2; 5; 10\}$. Both DL and DT were investigated using a shear flow of rate $\dot{\gamma} = 1$. Cases of SD experiencing DL and DT are also presented as references. Results are presented respectively in Table IV.3.12 and in Table IV.3.13 for the big and the small body for $A \in \{2, 5, 10\}$.

		Max_{STF} (dimensionless)			
		Locking dominance		**Tumbling dominance**	
		Big sphere	Reference	Big sphere	Reference
Sphere radius A	2	5.97	10.07	3.14	3.28
	5	2.63	11.84	2.68	2.74
	10	3.01	4.12	2.71	2.93

Table IV.3.12: Impact of the dominant regime (locking or tumbling) and of the size of the big body (radius A) on Max_{STF} (dimensionless) reached over the course of one period for the big body of mixed dumbbells (MD) versus spherical dumbbells (SD, reference).

When A increases in both DL and DT, Max_{STF} increase on the ellipsoidal body, and decrease on the big spherical body (except for the case of $A = 10$ in DL, which may be actually be at the limit between DL and DT, due to difficulties to reproduce DL for high body size ratios). Trends in Max_{STF} on mixed dumbbells with either DT or

		$\mathbf{Max_{STF}}$ **(dimensionless)**			
		Locking dominance		**Tumbling dominance**	
		Ellipsoid	Reference	Ellipsoid	Reference
Sphere radius A	2	10.91	10.88	12.96	6.28
	5	18.77	18.18	17.49	8.25
	10	21.69	8.88	24.53	9.99

Table IV.3.13: Impact of the dominant regime (locking or tumbling) and of the size of the big body (radius A) on $\mathrm{Max_{STF}}$ (dimensionless) reached over the course of one period for the ellipsoid of mixed dumbbells (MD) versus the small sphere of spherical dumbbells (SD, reference).

DL as function of spherical size are logarithmic, as were $\mathrm{Max_{STF}}$ trends on asymmetric dumbbells with DT, following

$$\mathrm{DL}\begin{cases}\text{Ellipsoid: } \mathrm{Max_{STF}} \approx 6.80\ln(A:a)+6.70, & R^2=0.968, \quad \text{(IV.3.82)}\\ \text{Sphere: } \mathrm{Max_{STF}} \approx -1.96\ln(A:a)+6.83, & R^2=0.728, \quad \text{(IV.3.83)}\end{cases}$$

$$\mathrm{DT}\begin{cases}\text{Ellipsoid: } \mathrm{Max_{STF}} \approx 6.52\ln(A:a)+6.47, & R^2=0.974, \quad \text{(IV.3.84)}\\ \text{Sphere: } \mathrm{Max_{STF}} \approx -0.56\ln(A:a)+3.78, & R^2=0.820. \quad \text{(IV.3.85)}\end{cases}$$

For big spheres in MD, the same non-monotonous behavior of $\mathrm{Max_{STF}}$ is observed for both DL and DT, which can be hypothesized for the same reasons presented in Section IV.3.2.2.3. However, if in DT $\mathrm{Max_{STF}}$ experienced by the big body in MD versus SD are very similar, in DL $\mathrm{Max_{STF}}$ are always lower on the big body of MD versus SD (Table IV.3.12). Small, ellipsoidal bodies would therefore decrease disturbances applied on the big body compared to small spheres.

When considering ellipsoids, $\mathrm{Max_{STF}}$ increase as A increases for both MD in DL and DT (Table IV.3.13). At the two extremes in size, $A = 2$ and $A = 10$, we can also noticed that $\mathrm{Max_{STF}}$ is higher for MD in DT compared to DL, for both the ellipsoid and the reference (small sphere). This is surprising, given the fact that is has been seen previously for flexible, symmetric SD that DL favored high $\mathrm{Max_{STF}}$ compared to DT (Fig. IV.3.12 and IV.3.13) due to a bottleneck effect occurring between the two bodies (Fig. IV.3.12b, configuration (1)). This suggests that shape may have a prevalent impact on $\mathrm{Max_{STF}}$

that interferes with the impact of the dominant regime. The case of $A = 5$ may be more complex as near the threshold in A previously described.

It also appears that Max_{STF} exerted on the ellipsoid are always higher than those exerted on the reference, whether in DL or in DT. Whereas it has been seen that Max_{STF} are lower for the big body of MD compared to SD, it could be argued that the ellipsoid took upon it Max_{STF} that are more equally distributed between the small and the big body of SD (Tables IV.3.12 and IV.3.13). This phenomenon amplifies as A increases. It therefore appears that shaping the small body as an ellipsoid increases forces on it compared to a sphere, and reduces forces applied to the big body compared to SD. This situation would thus be favorable to the big body, and unfavorable to the ellipsoid, by extension to the bacterial cell.

Overall, shaping the small body of a dumbbell as an ellipsoid was found to impact both dynamics and Max_{STF}. The ellipsoidal shape contributed to delay the rotation motion, especially for dumbbells experiencing DL and more importantly for small A. It also slow down behavior periodicity, especially for dumbbells in DT. Lastly, it contributes to decrease traction forces exerted on the big body (amplified phenomenon as A becomes large) but feels increased traction forces on it compared to a small sphere. Considering the situation from a bacterial cell perspective, adhering to a spherical component in a shear flow proved to be an unfavorable situation compared to being free in the flow or in a 2-cell chain. This situation would be all the more unfavorable than the sphere to which the cell has adhered is large.

In future work, we intend to compare Max_{STF} exerted on bacterial chains free in suspension, such as presented in Section IV.2.2, with Max_{STF} exerted on chains adhering to a sphere, as presented in Fig. IV.3.16c,d. We will also study the influence of the way bacteria adhere to spheres (Fig. IV.3.16b,c,d). Results are expected on whether adhering to a sphere may be beneficial depending on chain length, position in the chain, adhesion type (orientation), and adhesion strength.

IV.3.4 Dynamics and damages: spherical versus mixed dumbbells

Comparison of dynamics and surface traction forces exerted on spherical dumbbells experiencing RBM (a) or locking-tumbling regime (b) versus mixed flexible dumbbells (c) is presented in Figure IV.3.20. Spherical dumbbells experiencing RBM rotate at a rate $\dot{\theta}_A$

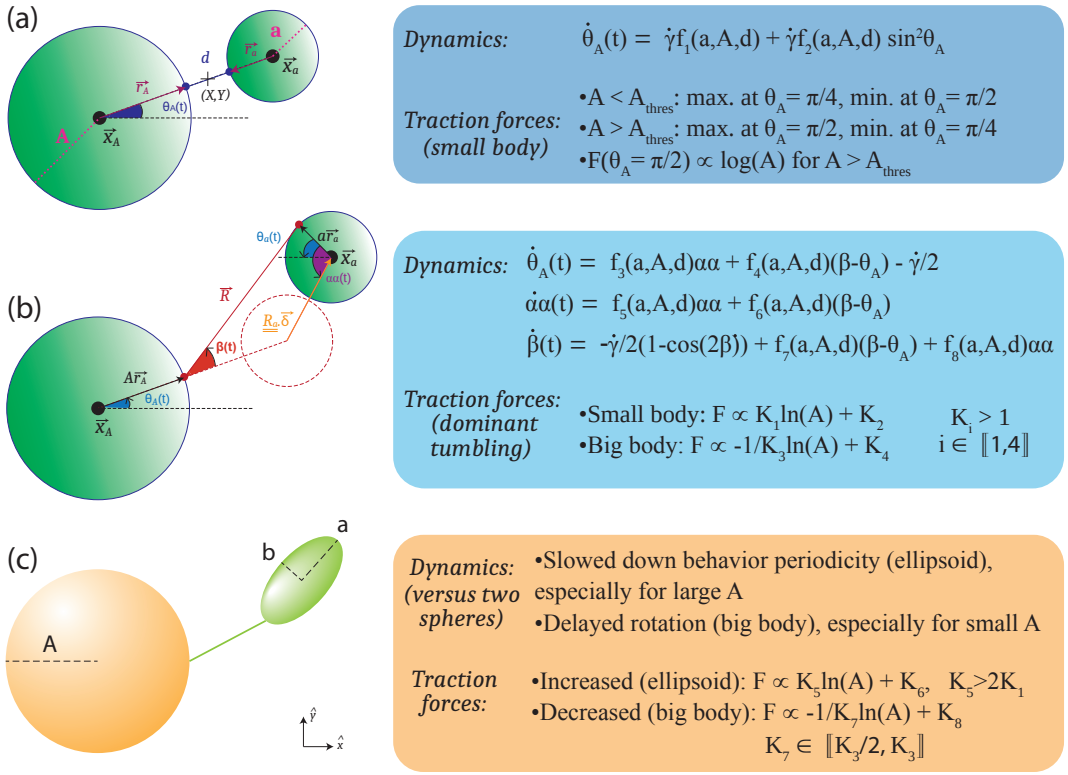

Figure IV.3.20: Main equations governing the dynamics and traction forces exerted on the surface of dumbbells experiencing rigid body motion (a) and flexible regimes (locking-tumbling, (b)), and main differences with mixed dumbbells constituted of a spherical body of varying size and an ellipsoid (c).

scaling with $\sin^2\theta_A$ (Fig. IV.3.20a), whereas dynamics of flexible dumbbells are governed by a two-frequency ("locking-tumbling" behavior, Fig. IV.3.20b). The locking behavior initiates dumbbell motion at $t = 0$ ($\dot{\theta}_A(0) = -\dot{\gamma}/2$, and the system starts tumbling ($\dot{\beta}$) as soon as $\dot{\theta}_A \neq 0$. In case of asymmetric flexible dumbbells, offsetting ($\dot{\alpha}\alpha$ may occur

that emphasize locking behavior. Traction forces exerted on a dumbbell experiencing RBM are non-monotonous functions depending on A (Fig. IV.3.20a) reaching extrema at $\theta_A \in \{\pi/2; \pi/4\}$, and for large A they become proportional to $\log A$. Traction forces experienced on dumbbells experiencing flexible regimes are higher for the small body and lower for the big body, proportionnally to $\ln A$ (Fig. IV.3.20b). Flexible dumbbells composed of a spherical body of varying size A and an ellipsoid ((Fig. IV.3.20c) present a slower periodicity of ellipsoid dynamics for large A, and a delayed rotation motion for small A. Traction forces respectively increases and decreases on the ellipsoid and the big body proportionally to $\ln A$, at higher rates than for spherical, flexible dumbbells ((Fig. IV.3.20b, c). In case of bacterial adhesion to spheres of various sizes, it appears that adhesion is unfavorable in terms of traction forces exerted on the bacterial cell, all the more than the sphere is big. Bacteria integrated in an adhesive matrix would therefore be more likely to suffer from surface damages *i.e.* functionality losses.

Part V

Conclusions and Perspectives

V.1

Thesis highlights

Precedent Ph.D. research projects completed in the Biomolecules Engineering Laboratory (LIBio) focused on optimizing probiotic bacteria encapsulation [Burgain, 2013, Guerin, 2017] and showed that adhesive interactions between the model strain *Lactobacillus rhamnosus* GG and dairy proteins play a key role in the encapsulation process [Guerin, 2017]. Recently, bacterial adhesion to food components has also been apprehended to help with protecting probiotics in functional foods [Hickey et al., 2015b, Mortazavian et al., 2012, Ranadheera et al., 2010, Sanders and Marco, 2010], but also to compete with bacterial adhesion to the host during intestinal delivery [Guerin et al., 2018b, Sun and Wu, 2017]. However the extent of probiotic adhesion to food components and possible outcomes of these adhesive interactions remained to be explored.

This project represents a first step in that direction, aiming to go beyond species characteristics to study the extent and main characteristics of bacterial adhesion to food components at the lactic acid bacteria group level. In particular, the specificity of adhesive interactions involved, as well as the sensitivity of bacterial adhesive abilities to stress have been investigated.

This thesis answered the three questions set out at the beginning of this dissertation (Chapter II):

1. What are the characteristics and strength of bacterial adhesion to dairy components

amongst the lactic acid bacteria group and, in particular, to β-lactoglobulin?

2. How does shear stress impact bacterial integrity (shape and functionality) for the model strain *Lactobacillus rhamnosus* GG?

3. What is the influence of bacterium-particle adhesive interactions on the dynamics and forces exerted on the bacterial cell?

Figures V.1.1 and V.1.2 on the next two pages present the highlights of this thesis project.

V.1.1 Identification and characterisation of LAB-food adhesive interactions

A high-throughput screening method has been developed that allowed identifying and evaluating quickly bacterial affinity to a range of components of interest for a wide number of strains. This method features three main steps (Fig. V.1.1) which are (i) immobilizing the component of interest on the surface of 96-well adherent microplates, (ii) incubating the bacterial strains into the same wells to allow bacterial adhesion to occur, followed by removal or non-adherent bacteria, and (iii) measuring bacterial growth, which has been found to be directly correlated to the number of bacteria able to adhere to the tested molecule. This method presents the advantage to simultaneously assess bacterial functionality and bacterial viability, as only functional, viable bacteria are able to grow in the microplates. It was validated on the model strain *Lactobacillus rhamnosus* GG (LGG) and three mutant strains, impaired in synthesis of some surface components involved in adhesion.

This method was then applied to a collection of 73 LAB strains screened for their adhesive affinities towards the major dairy protein β-lactoglobulin, in order to reveal shared adhesion characteristics. Less than 6 % of the strain collection were found to feature affinity towards β-lactoglobulin and, despite research efforts concentrated on genomics analysis, no underlying rationale relative to the presence of LPxTG-surface proteins, and in particular to pili gene clusters, or strain origins could be evidenced.

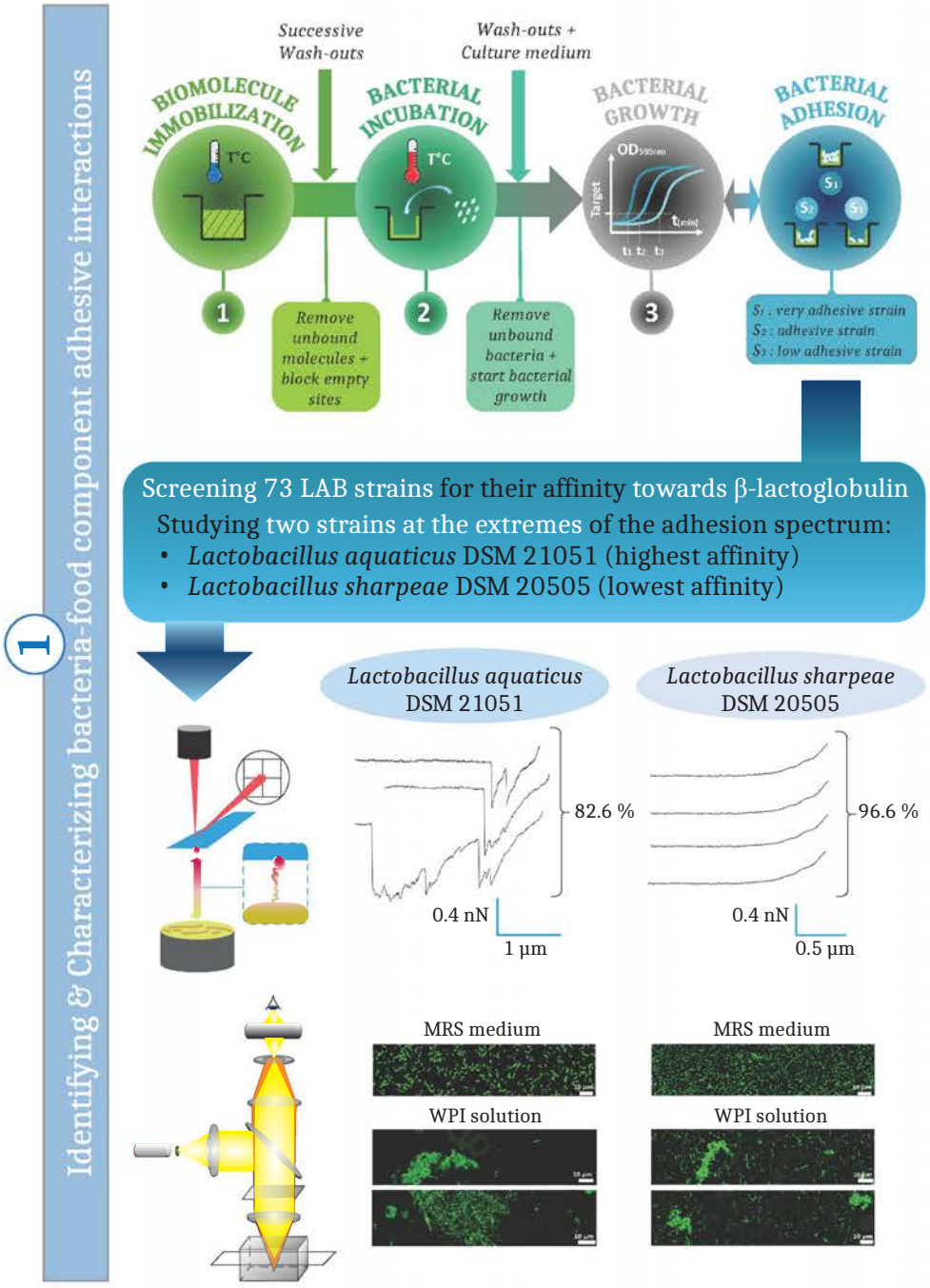

Figure V.1.1: Thesis project highlights: *Bacterial Adhesion to Food Components*: (objective 1).

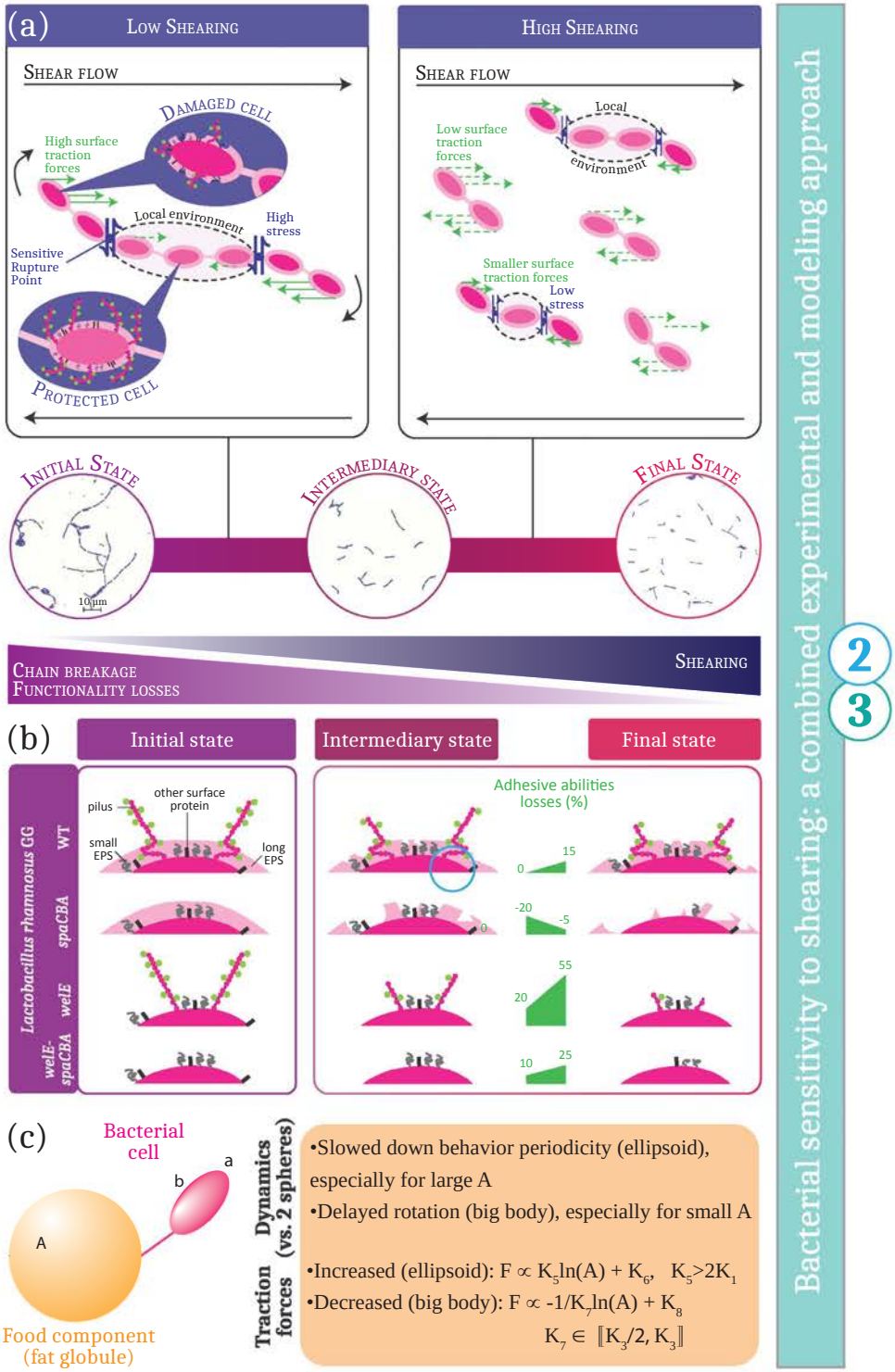

Figure V.1.2: Thesis project highlights: *Impact of Shearing on Bacteria* (objectives 2 & 3).

LAB adhesion behavior to dairy proteins could therefore not be accurately predicted from the bacterial surface information we disposed of.

Two strains at the extremes of the adhesive spectrum, *Lactobacillus aquaticus* DMS 21051 (highest affinity) and *Lactobacillus sharpeae* DMS 20505 (lowest affinity) were studied in further depth using atomic force microscopy (AFM) and confocal laser scanning microscopy (CLSM), as presented in Fig. V.1.1. *Lactobacillus aquaticus* DSM 21051 featured high adhesion specificity as deciphered by AFM, and presented similar, gathered spatial distribution (in flocs) in whey matrices composed of dissolved Whey Protein Isolated (WPI) powder as the control adhesive strain LGG WT. On the contrary, *Lactobacillus sharpeae* DSM 20505 was found to homogeneously disperse within the same matrices, similarly to the non-adhesive control strain, LGG *spaCBA*. These findings showed that LAB adhesion to β-lactoglobulin is highly specific and plays an important role on bacterial distribution in food matrices.

V.1.2 Impact of shearing on bacterial adhesive abilities and shape (bacterial suspension)

Because adhesive interactions involve bacterial surface components which may be sensitive to stresses applied during food and ferment manufacturing processes, the impact of shearing on bacterial functionality, viability, and shape, was studied using a combined experimental and modeling approach for bacteria alone in suspensions (Figure V.1.2a,b). Modeling was then pushed further to get a sense of how bacterial adhesion to food spherical components could impact shear-induced damages to bacterial cell surfaces (Figure V.1.2c).

A positive relationship between bacterial chain breakage and bacterial adhesive abilities preservation was revealed (Fig. V.1.2a). Indeed, the highest functionality losses were observed concomitantly with bacterial chain breakage, and modeling demonstrated that the smaller the chain, the less damaged it is likely to get, using a demonstrated correlation between surface adhesive protein (SAP) removal and traction forces exerted on a surface of a bacterial cell. As chains break, the forces applied on the remaining cells thus

get lower, preventing more damage to occur. Our model also evidenced regioselective damages, *i.e.*, that cells on the outside of a chain are more likely to be damaged than cells close to the center of the chain, due to local effects.

Shearing experiments demonstrated that 2-cell chains were likely the most favorable configuration for LGG cells in a shear flow, and that shearing may cause functionality losses up to 20 % for LGG wild type (WT) (Fig. V.1.2b). Functionality losses were found to be higher ($\sim$ 55 %) for the strain depleted of exopolysaccharides (EPS), suggesting a protective role of EPS towards surface molecules mediating adhesion. *A contrario*, LGG *spaCBA* (pili-depleted) featured increased adhesive abilities after shearing (+20 % of functionality gain), which may be due to partial removal of the EPS layer that would reveal underlying adhesive proteins.

V.1.3 Impact of shearing on bacterial adhesive abilities (bacteria-particle)

Further exploration with our model allow developing analytical predictions of the dynamics and traction forces exerted on the body surfaces of dumbbells, which stand for models of bacterial adhesion to spherical components in food matrices (Fig. V.1.2c). Dynamics of rigid body motion were first fully solved for, and results are compared with full, boundary integral simulations (including hydrodynamic interactions). Flexible dumbbells are then investigated, modeling the connection between bodies by a cluster of springs able to stretch and bend. Flexible dynamics are evidenced analytically to involve multiple timescales, leading to different behaviors depending on the dominant regime. Subsequent traction forces are analyzed numerically as functions of dumbbell flexibility and body size ratio and are found to feature non-monotonous, complex behaviors. Finally, the impact on body shape (ellipsoidal versus spherical) on dynamics and traction forces is studied, with an emphasis on the ellipsoidal, small body (in asymmetric, flexible "mixed" dumbbells), which may in our case stand for a bacterial cell. Adhesion to a sphere was found to be an unfavorable situation for bacterial cells in terms of potential damages inflicted to bacterial surfaces, all the more than the a sphere is large. Lactic acid

bacteria integrated in a food matrix containing large fat globules may therefore suffer more from shear stress during food structuration than in a food matrix containing small fat globules, thus decreasing the probiotic potential of the first matrix compared to the second.

V.2

Perspectives

The outcomes of this project pave the road to future research on more efficiently designed functional food matrices, and optimization of industrial processes to help preserving both probiotic bacterial viability and functionality.

Some interesting short-term ($\sim$ 6 months to 1-2 years) and long-term (at least 2 to 3 years) perspectives to this work are detailed in the next sections.

V.2.1 Short-term perspectives

V.2.1.1 Bacterial adhesion to food components

- **Pushing further bacterial surface analysis:**
  Our analysis of the pili-gene clusters and LPxTG-predicted proteins from the adhesive strains of our collection did not allow us to propose criteria to predict bacterial adhesion to β-lactoglobulin although good adhesive candidates were proposed as presented in Table IV.1.2. One way to refine our analysis would be to inactivate the genes corresponding to the most promising predicted-protein candidates and perform adhesion assays. This could be done first on the strain the most adhesive to β-lactoglobulin, *Lactobacillus aquaticus* DSM 21051, on which only five predicted LPxTG-proteins were identified [Sun et al., 2015]. Other bacterial surface components, such as components of the S-layer like proteins with low-energy bind-

ing featuring GW module (containing dipeptide Gly-Trp), as well as other protein secretion systems such as the TAT (twinarginine translocation) system, have also been identified to mediate adhesive behaviors, notably towards host tissues [Åvall Jääskeläinen and Palva, 2005, Chagnot et al., 2013, Desvaux et al., 2018, Desvaux et al., 2006, Hynönen and Palva, 2013]. The surface of the adhesive strains of our collection could thus be investigated further to see if other components than those examined could be predicted to be involved in adhesion to β-lactoglobulin. Complementary approaches to genomics, such as proteomics and transcriptomics, could also help identifying potential candidates that would mediate adhesion to β-lactoglobulin.

- **Researching a correlation between bacterial origin and bacterial adhesion:**
  The strains from our collection were isolated from very diverse environments, such as foods, faeces, blood, sewage water, plants, various animals and organs, etc. therefore it was difficult for us to study a relationship between the strain origin and its adhesive properties towards dairy components. However, a previous study has shown that strains isolated from a dairy environment presented stronger binding to milk proteins versus strains isolated from plants [Tarazanova et al., 2017]. This study focused on strains from the same species, *Lactococcus lactis*. In our case, it would be interesting to include more strains isolated from dairy sources to our collection, to test whether they would present higher adhesive affinities towards β-lactoglobulin than strains isolated from other environments, which could suggest a selective advantage.

- **Testing other dairy components:**
  Our results suggested that adhesion to β-lactoglobulin would not be a common characteristic of the LAB group. The affinity of our strain collection to other food components could also be evaluated in future work, in order to dispose of more comparison points to our study and to get a better understanding of the extent of adhesion to β-lactoglobulin in contrast to adhesion to other food com-

ponents. Other dairy components, such as milk fat globule membrane (MFGM) and α-lactalbumin, to which LGG has previously been shown to adhere [Gomand et al., 2018, Guerin et al., 2018a, Guerin et al., 2016], could be a good starting point. Similarly, it would be interesting to see if adhesive interactions to other dairy components would induce similar bacterial distribution in foods containing these components. The impact on bacterial distribution of more complex matrices including several components to which bacteria are likely to adhere could then also be investigated.

V.2.1.2 Impact of shearing on bacteria

- **Experimental investigation at the bacterial chain level:**

  Shearing was found to impact significantly bacterial adhesive abilities to β-lactoglobulin for bacteria alone in suspensions. This may have consequences on the design of some industrial processes in the food and ferment industry that feature steps generating shear stress, such as spray-drying. Modeling provided insight on the impact of shearing at the bacterial cell level, however no experiments were performed at this scale.

  Microfluidics with modeled bacterial chains could be a promising approach to do so, as an intermediary between pure biology and pure modeling. Models of bacterial chains could be printed in 3D in various semi-flexible materials, and breakage phenomena could be observed. Force sensors could be included that would allow monitoring the forces exerted on the different parts of the chain in a shear flow generated in microchannels. These experiments would be compared with our simulation results and help defining the application boundaries of our model. Microfluidics tools have previously been used to investigate chain breakage phenomena under high shear [Nghe et al., 2010] and dynamics of fiber-like suspensions [Berthet et al., 2016, du Roure et al., 2019].

  Other approaches could also be considered, such as exposing isolated bacterial chains of different lengths to a shear flow and calculating the forces applied on

their surfaces as a function of their bending angle *e.g.*. Experiments monitoring the bending angle of single bacterial cells submitted to flow have already been performed in previous studies [Amir et al., 2014].

- **Impact of shearing on bacteria within food matrices:**
  Modeling suggested that bacterial adhesion to food components may increase shear-induced damages on bacteria, depending on the size of the food component considered. More modeling could be performed aiming to describe more complex configurations, such as the adhesion of bacterial chains to food spherical components and the way bacterial cells adhere (see Fig. IV.3.16b,c,d), and even collective behavior of complex suspensions featuring bacterial chains and spherical components. A perspective coming out naturally of this work would be to investigate this direction experimentally, considering various monodisperse suspensions of fat globules, to which lactic acid bacteria are known to feature adhesive affinities [Gomand et al., 2018, Guerin et al., 2017b, Guerin et al., 2018b, Hickey et al., 2015b, Hickey et al., 2015a, Jeanson et al., 2011, Jeanson et al., 2015, Laloy et al., 1996, Lopez et al., 2006]. These suspensions would be obtained by homogenization of the same initial medium, to free from existing differences in MFGM composition that could exist between native globules of different sizes [Lopez, 2005, Luo et al., 2017, Michalski et al., 2002, Romeih et al., 2012]. The effect of shearing on bacterial surface within these different media could then be observed directly through AFM deflection images, which have previously been used to show the shaving effect of high-speed centrifugation on LGG [Tripathi et al., 2012].

- **Impact of shearing on bacterial adhesion to the intestines:**
  Considering that shearing also occur in some biological processes, such as digestion, it may be of use to consider the impact of shearing on bacterial adhesion to the intestines. This impact could be evaluated using the same methodology as described in Chapter III.2, replacing β-lactoglobulin solution by an equivalent solution of intestinal mucin (1 % v/v). These experiments could also be compared with more

precise investigations involving cultures of CaCo-2 cells.

- **Shearing impact combined with other stresses:**
  In industrial and biological processes, shear stress is usually combined with other stresses, such as heating stress and acid stress. A different, and likely higher, effect of these processes on bacterial functionality could therefore be expected, although in some cases, lactobacilli pili expression has been shown to be upregulated after acid exposure therefore increasing adhesive abilities [Bang et al., 2018]. The results obtained in our study could be compared with later experimental studies of the effect of digestion on lacic acid bacteria functionality, using *in vitro* digestion methods [Minekus et al., 2014,Thevenot, 2014], or experimental studies of the effect of spray-drying at pilot and industrial scales.

V.2.2 Long-term perspectives

V.2.2.1 Impact of bacterial adhesion on food matrices properties

Bacterial adhesion has been studied in this thesis in terms of specificity and impact on bacterial location in food matrices, however the impact on food matrices properties has not been investigated, although some recent studies have evidenced that physical properties of dairy products, such as viscosity and gel hardness, could be affected by bacterial surface properties [Tarazanova et al., 2018a].

In particular, bacterial adhesion could play a role on dairy matrix properties during the structuration of dairy products such as yogurts and cheeses, and especially in relation to fat. The importance of fat globules in the coagulation process has been especially highlighted in the past ten years [Michalski et al., 2002, Ion Titapiccolo et al., 2010, Corredig et al., 2011, Luo et al., 2017]. Fat globules have been found to modulate casein network formation depending on their size as well as on the composition of the milk fat globule membrane [Michalski et al., 2002, Ion Titapiccolo et al., 2010, Luo et al., 2017]. The impact of fat globules on rennet-induced gelation is also susceptible to be affected by the presence of bacteria. Lactic Acid Bacteria have indeed been found to gather around

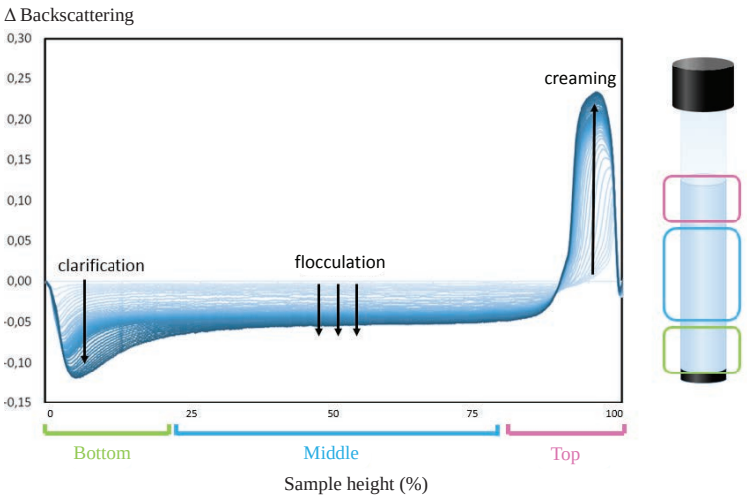

Figure V.2.1: Destabilization profile of a milk emulsion monitored using a Turbiscan analyzer. Phases sampled for bacterial concentration *i.e.* bottom, middle, and top, are represented on the tube as well as on the corresponding profile. Figure adapted from Cvetkovska, 2018 [Cvetkovska, 2018].

.

fat globules [Oberg et al., 1993, Laloy et al., 1996, Fitzsimons et al., 2001, Lopez et al., 2006] which may hinder the participation of fat globules to cheese network build-up.

Some work is currently being performed in our lab on the effect of bacterial surface adhesive molecules on the stability of various milk media (raw milk, homogenized milk, and skimmed milk) by monitoring creaming speed in tubes using a Turbiscan Lab Expert Stability Analyzer (Formulaction, Toulouse, France). To this end, the model strains LGG WT and *spaCBA*, respectively adhesive and non-adhesive to MFGM, are employed. Bacterial concentration and spatial distribution are also monitored at the top, middle, and bottom of the tubes using confocal microscopy, such as presented in Figure V.2.1, and apparent diffusive coefficient of bacteria and fat globules are evaluated by image analysis in order to interpret the dynamics of emulsion destabilization.

First results showed a decreased creaming speed in raw milk when LGG cells are present, and a correlation between the presence of adhesive molecules on bacterial surface and apparent bacterial diffusive coefficients. One hypothesis to explain the first fact could be that adhesive interactions between bacteria and fat globules would contribute to lower

creaming speed, thus impacting emulsion stability. This hypothesis will be investigated in future work, a new thesis project starting in September 2019.

V.2.2.2 Impact of stress on bacterial evolution

The proposed relationship between bacterial functionality and shape in a shear flow in Chapter IV.2 opens up perspectives on the role of bacterial shape in providing selective advantages in stressful environments.

Chaining was previously suggested to provide advantages against predation in grazing environments [Güde, 1979, Hahn and Höfle, 1999, Jürgens and Matz, 2002, Posch et al., 1999, Shikano et al., 1990, Young, 2006, Young, 2007] and allows better resistance in high-shear force environments for biofilm-forming bacteria, by increasing the number of contacts with surface elements, therefore limiting detachment events [Edwards et al., 1989, Young, 2006, Young, 2007]. In those latter environments, bacteria have also been observed to increase in size, featuring increased cell wall stretching [Berzins et al., 2001, Joshi et al., 1996, Wong et al., 2017]. Other forms of bacterial organization, such as bacterial filamentation, may also provide competitive advantages for colonization of biopassive surfaces [Möller et al., 2013].

The selective value of bacterial shape for lactic acid bacteria could be investigated relatively to shear stress, by recreating local shearing constraints in culture environments and studying the dynamics of shape evolution over several bacterial generations. Constraint environments could be inspired from previous studies that focused on the importance of mechanical constraints on bacterial cell shape and elongation of cell wall [Amir et al., 2014, Wong et al., 2017]. Important discoveries were made on molecular evolution and fitness gain for *Escherichia coli* by monitoring the evolution dynamics over thousands of generations by the Lenski group [Good et al., 2017]. Similar methodology could be applied, correlated with microscopic observations to characterise shape evolution.

The heterogeneity of bacterial functionality in bacterial chains, created by the regioselectivity of traction forces applied to chains in a shear flow (depending on the position of the cell within the chain) may also play a role in bacterial evolution. A recent review

describes the importance of microbial heterogeneity at single-cell level on population level strategies [Martins and Locke, 2015], pointing out that heterogeneity may play a key role in bacterial survival to unpredictable environmental changes. The cells closer to the center of a chain, more protected in a shear flow from damaging traction forces than the cells on the outside, would in that sense be the ones selected to survive and potentially allow the population to thrive again in the future. This shear-induced heterogeneity could be studied further experimentally using single-cell techniques, such as suggested by recent studies [Editorial, 2016,Bridier et al., 2015]. Modification of bacterial stress sensors using reporter genes (such as fluorescent protein promoters) could allow *in situ* visualization of exerted stress on bacterial cells in a chain in a shear flow [Bridier et al., 2015], for example in microfluidic devices. Other bacterial configurations, such as bacterial aggregates, could also be investigated in terms of created heterogeneity and collective behaviors that may lead to selective advantages.

Part VI

Bibliography

[Aarts et al., 1988] Aarts, P. A., van den Broek, S. A., Prins, G. W., Kuiken, G. D., Sixma, J. J., and Heethaar, R. M. (1988). Blood platelets are concentrated near the wall and red blood cells, in the center in flowing blood. *Arteriosclerosis: An Official Journal of the American Heart Association, Inc.*, 8(6):819–824.

[Abu-Lail and Camesano, 2003] Abu-Lail, N. I. and Camesano, T. A. (2003). Role of ionic strength on the relationship of biopolymer conformation, DLVO contributions, and steric interactions to bioadhesion of Pseudomonas putida KT2442. *Biomacromolecules*, 4(4):1000–1012.

[Adams and Corbett, 2018] Adams, J. and Corbett, D. (2018). Transient shear banding in the nematic dumbbell model of liquid crystalline polymers. *Physical review. E*, 97(5-1):052601.

[Agrawal, 2005] Agrawal, R. (2005). Probiotics: An emerging food supplement with health benefits. *Food Biotechnology*, 19(3):227–246.

[Aguirre and Collins, 1993] Aguirre, M. and Collins, M. D. (1993). Lactic acid bacteria and human clinical infection. *Journal of Applied Bacteriology*, 75(2):95–107.

[Alam et al., 2019] Alam, F., Kumar, S., and Varadarajan, K. M. (2019). Quantification of Adhesion Force of Bacteria on the Surface of Biomaterials: Techniques and Assays. *ACS Biomaterials Science & Engineering*, 5(5):2093–2110.

[Alamprese et al., 2005] Alamprese, C., Foschino, R., Rossi, M., Pompei, C., and Corti, S. (2005). Effects of lactobacillus rhamnosus GG addition in ice cream. *International Journal of Dairy Technology*, 58(4):200–206.

[Alamprese et al., 2002] Alamprese, C., Foschino, R., Rossi, M., Pompei, C., and Savani, L. (2002). Survival of lactobacillus johnsonii la1 and influence of its addition in retail-manufactured ice cream produced with different sugar and fat concentrations. *International Dairy Journal*, 12(2):201–208.

[Alegre et al., 2011] Alegre, I., Viñas, I., Usall, J., Anguera, M., and Abadias, M. (2011). Microbiological and physicochemical quality of fresh-cut apple enriched with the probiotic strain lactobacillus rhamnosus GG. *Food Microbiology*, 28(1):59–66.

[Altermann et al., 2004] Altermann, E., Buck, L. B., Cano, R., and Klaenhammer, T. R. (2004). Identification and phenotypic characterization of the cell-division protein CdpA. *Gene*, 342(1):189–197.

[Altieri, 2016] Altieri, C. (2016). Dairy propionibacteria as probiotics: recent evidences. *World Journal of Microbiology and Biotechnology*, 32(10):172.

[Altschul et al., 1990] Altschul, S. F., Gish, W., Miller, W., Myers, E. W., and Lipman, D. J. (1990). Basic local alignment search tool. *Journal of Molecular Biology*, 215(3):403–410.

[Amir et al., 2014] Amir, A., Babaeipour, F., McIntosh, D. B., Nelson, D. R., and Jun, S. (2014). Bending forces plastically deform growing bacterial cell walls. *Proceedings of the National Academy of Sciences*, 111(16):5778–5783.

[An and Friedman, 1998] An, Y. H. and Friedman, R. J. (1998). Concise review of mechanisms of bacterial adhesion to biomaterial surfaces. *Journal of Biomedical Materials Research*, 43(3):338–348.

[Ananta et al., 2005] Ananta, E., Volkert, M., and Knorr, D. (2005). Cellular injuries and storage stability of spray-dried lactobacillus rhamnosus GG. *International Dairy Journal*, 15(4):399–409.

[Andersson et al., 2006a] Andersson, M., Fällman, E., Uhlin, B. E., and Axner, O. (2006a). A sticky chain model of the elongation and unfolding of escherichia coli p pili under stress. *Biophysical Journal*, 90(5):1521–1534.

[Andersson et al., 2006b] Andersson, M., Fällman, E., Uhlin, B. E., and Axner, O. (2006b). Dynamic force spectroscopy of e. coli p pili. *Biophysical Journal*, 91(7):2717–2725.

[Apostolou et al., 2001] Apostolou, E., Kirjavainen, P. V., Saxelin, M., Rautelin, H., Valtonen, V., Salminen, S. J., and Ouwehand, A. C. (2001). Good adhesion properties of probiotics: a potential risk for bacteremia? *FEMS Immunology & Medical Microbiology*, 31(1):35–39.

[Armstrong et al., 2016] Armstrong, M. J., Beris, A. N., Rogers, S. A., and Wagner, N. J. (2016). Dynamic shear rheology of a thixotropic suspension: Comparison of an improved structure-based model with large amplitude oscillatory shear experiments. *Journal of Rheology*, 60(3):433–450.

[Arnaud et al., 1993] Arnaud, J. P., Lacroix, C., Foussereau, C., and Choplin, L. (1993). Shear stress effects on growth and activity of Lactobacillus delbrueckii subsp. bulgaricus. *Journal of Biotechnology*, 29(1):157–175.

[Aström, 2006] Aström, J. A. (2006). Statistical models of brittle fragmentation. *Advances in Physics*, 55(3-4):247–278.

[Audoly and Neukirch, 2005] Audoly, B. and Neukirch, S. (2005). Fragmentation of rods by cascading cracks: why spaghetti do not break in half. *Physical Review Letters*, 95(9):095505.

[Auletta et al., 2016] Auletta, S., Galli, F., Lauri, C., Martinelli, D., Santino, I., and Signore, A. (2016). Imaging bacteria with radiolabelled quinolones, cephalosporins and siderophores for imaging infection: a systematic review. *Clinical and Translational Imaging*, 4(4):229–252.

[Auty et al., 2001] Auty, M. a. E., Gardiner, G. E., McBrearty, S. J., O'Sullivan, E. O., Mulvihill, D. M., Collins, J. K., Fitzgerald, G. F., Stanton, C., and Ross, R. P. (2001). Direct in situ viability assessment of bacteria in probiotic dairy products using viability staining in conjunction with confocal scanning laser microscopy. *Applied and Environmental Microbiology*, 67(1):420–425.

[Avadhanula et al., 2006] Avadhanula, V., Rodriguez, C. A., DeVincenzo, J. P., Wang, Y., Webby, R. J., Ulett, G. C., and Adderson, E. E. (2006). Respiratory viruses augment the adhesion of bacterial pathogens to respiratory epithelium in a viral species- and cell type-dependent manner. *Journal of Virology*, 80(4):1629–1636.

[Axelsson, 2004] Axelsson, L. (2004). Lactic acid bacteria: classification and physiology. In *Lactic Acid Bacteria: Microbiological and Functional Aspects.*, pages 1–66. Seppo Salminen, Atte von Wright, Arthur Ouwehand, Boca Raton, London, New York, Singapore, marcel decker, inc., third edition edition.

[Azikri de Deus and Dupim, 2013] Azikri de Deus, H. P. and Dupim, G. S. P. (2013). On behavior of the thixotropic fluids. *Physics Letters A*, 377(6):478–485.

[Aziz et al., 2019] Aziz, K., Tariq, M., and Zaidi, A. (2019). Biofilm development in L. fermentum under shear flow and sequential GIT digestion. *FEMS Microbiology Letters*, 366(6).

[Badel et al., 2011] Badel, S., Bernardi, T., and Michaud, P. (2011). New perspectives for lactobacilli exopolysaccharides. *Biotechnology Advances*, 29(1):54–66.

[Bagchi et al., 1997] Bagchi, D., Garg, A., Krohn, R. L., Bagchi, M., Tran, M. X., and Stohs, S. J. (1997). Oxygen free radical scavenging abilities of vitamins c and e, and a grape seed proanthocyanidin extract in vitro. *Research Communications in Molecular Pathology and Pharmacology*, 95(2):179–189.

[Bajpai et al., 2015] Bajpai, V. K., Rather, I. A., Majumder, R., Shukla, S., Aeron, A., Kim, K., Kang, S. C., Dubey, R. C., Maheshwari, D. K., Lim, J., and Park, Y.-H. (2015). Exopolysaccharide and lactic acid bacteria: Perception, functionality and prospects. *Bangladesh Journal of Pharmacology*, 11(1):1–23.

[Balmforth et al., 2014] Balmforth, N. J., Frigaard, I. A., and Ovarlez, G. (2014). Yielding to stress: Recent developments in viscoplastic fluid mechanics. *Annual Review of Fluid Mechanics*, 46(1):121–146.

[Banasiak, 2006] Banasiak, J. (2006). Shattering and non-uniqueness in fragmentation models—an analytic approach. *Physica D: Nonlinear Phenomena*, 222(1):63–72.

[Banasiak and Noutchie, 2010] Banasiak, J. and Noutchie, S. O. (2010). Controlling number of particles in fragmentation equations. *Physica D: Nonlinear Phenomena*, 239(15):1422–1435.

[Bang et al., 2018] Bang, M., Yong, C.-C., Ko, H.-J., Choi, I.-G., and Oh, S. (2018). Transcriptional Response and Enhanced Intestinal Adhesion Ability of Lactobacillus rhamnosus GG after Acid Stress. *Journal of Microbiology and Biotechnology*, 28(10):1604–1613.

[Baravian et al., 1996] Baravian, C., Quemada, D., and Parker, A. (1996). Modelling thixotropy using a novel structural kinetics approach: Basis and application to a solution of iota carrageenan. *Journal of Texture Studies*, 27(4):371–390.

[Barbosa et al., 2015] Barbosa, J., Borges, S., and Teixeira, P. (2015). Pediococcus acidilactici as a potential probiotic to be used in food industry. *International Journal of Food Science & Technology*, 50(5):1151–1157.

[Barbosa and Teixeira, 2017] Barbosa, J. and Teixeira, P. (2017). Development of probiotic fruit juice powders by spray-drying: A review. *Food Reviews International*, 33(4):335–358.

[Barbé et al., 2013] Barbé, F., Ménard, O., Le Gouar, Y., Buffière, C., Famelart, M.-H., Laroche, B., Le Feunteun, S., Dupont, D., and Rémond, D. (2013). The heat treatment and the gelation are strong determinants of the kinetics of milk proteins digestion and of the peripheral availability of amino acids. *Food Chemistry*, 136(3):1203–1212.

[Barnes, 1997] Barnes, H. A. (1997). Thixotropy—a review. *Journal of Non-Newtonian Fluid Mechanics*, 70(1):1–33.

[Barnes et al., 2001] Barnes, L., Adams, M. R., Watts, J. F., Zhdan, P. A., and Chamberlain, A. H. L. (2001). Correlated XPS, AFM and bacterial adhesion studies on milk and milk proteins adherent to stainless steel. *Biofouling*, 17(1):1–22.

[Barnes et al., 1999] Barnes, L.-M., Lo, M. F., Adams, M. R., and Chamberlain, A. H. L. (1999). Effect of milk proteins on adhesion of bacteria to stainless steel surfaces. *Applied and Environmental Microbiology*, 65(10):4543–4548.

[Barrett and Süli, 2009] Barrett, J. W. and Süli, E. (2009). Numerical approximation of corotational dumbbell models for dilute polymers. *IMA Journal of Numerical Analysis*, 29(4):937–959.

[Barrett and Süli, 2018] Barrett, J. W. and Süli, E. (2018). Existence of global weak solutions to the kinetic Hookean dumbbell model for incompressible dilute polymeric fluids. *Nonlinear Analysis: Real World Applications*, 39:362–395.

[Bast et al., 2015] Bast, R., Sharma, P., Easton, H. K., Dessev, T. T., Lad, M., and Munro, P. A. (2015). Tensile testing to quantitate the anisotropy and strain hardening of mozzarella cheese. *International Dairy Journal*, 44:6–14.

[Beaussart et al., 2013] Beaussart, A., El-Kirat-Chatel, S., Herman, P., Alsteens, D., Mahillon, J., Hols, P., and Dufrêne, Y. F. (2013). Single-cell force spectroscopy of probiotic bacteria. *Biophysical Journal*, 104(9):1886–1892.

[Bellon-Fontaine et al., 1996] Bellon-Fontaine, M. N., Rault, J., and van Oss, C. J. (1996). Microbial adhesion to solvents: a novel method to determine the electron-donor/electron-acceptor or Lewis acid-base properties of microbial cells. *Colloids and Surfaces B: Biointerfaces*, 7(1):47–53.

[Bergonzelli et al., 2006] Bergonzelli, G. E., Granato, D., Pridmore, R. D., Marvin-Guy, L. F., Donnicola, D., and Corthésy-Theulaz, I. E. (2006). GroEL of Lactobacillus johnsonii La1 (NCC 533) is cell surface associated: potential role in interactions with the host and the gastric pathogen Helicobacter pylori. *Infection and Immunity*, 74(1):425–434.

[Berne et al., 2018] Berne, C., Ellison, C. K., Ducret, A., and Brun, Y. V. (2018). Bacterial adhesion at the single-cell level. *Nature Reviews Microbiology*, 16(10):616–627.

[Berry and Plazek, 1997] Berry, G. C. and Plazek, D. J. (1997). On the use of stretched-exponential functions for both linear viscoelastic creep and stress relaxation. *Rheologica Acta*, 36(3):320–329.

[Berthet et al., 2016] Berthet, H., du Roure, O., and Lindner, A. (2016). Microfluidic Fabrication Solutions for Tailor-Designed Fiber Suspensions. *Applied Sciences*, 6(12):385.

[Berzins et al., 2001] Berzins, A., Toma, M., Rikmanis, M., and Viesturs, U. (2001). Influence of Micromixing on Microorganisms and Products. *Acta Biotechnologica*, 21(2):155–170.

[Betoret et al., 2012] Betoret, E., Betoret, N., Arilla, A., Bennar, M., Barrera, C., Codoner, P., and Fito, P. (2012). No invasive methodology to produce a probiotic low humid apple snack with potential effect against helicobacter pylori. *Journal of Food Engineering*, 110(2):289–293.

[Betoret et al., 2003] Betoret, N., Puente, L., Diaz, M. J., Pagan, M. J., Garcia, M. J., Gras, M. L., Martinez-Monzo, J., and Fito, P. (2003). Development of probiotic-enriched dried fruits by vacuum impregnation. *Journal of Food Engineering*, 56(2):273–277.

[Bierne et al., 2007] Bierne, H., Sabet, C., Personnic, N., and Cossart, P. (2007). Internalins: a complex family of leucine-rich repeat-containing proteins in Listeria monocytogenes. *Microbes and Infection*, 9(10):1156–1166.

[Bird et al., 1987] Bird, R. B., Armstrong, R. C., and Hassager, O. (1987). *Dynamics of polymeric liquids. Vol. 1, 2nd Ed. : Fluid mechanics*, volume 1. U.S. Department of Energy Office of Scientific and Technical Information, United States, 2d. ed. fluid mechanics edition.

[Björnham and Axner, 2009] Björnham, O. and Axner, O. (2009). Multipili attachment of bacteria with helixlike pili exposed to stress. *The Journal of Chemical Physics*, 130(23):235102.

[Blair and W, 1953] Blair, S. and W, G. (1953). *Foodstuffs: their plasticity, fluidity and consistency.* Interscience.

[Bodelon et al., 2013] Bodelon, G., Palomino, C., and Fernandez, L. A. (2013). Immunoglobulin domains in escherichia coli and other enterobacteria: from pathogenesis to applications in antibody technologies. *FEMS microbiology reviews*, 37(2):204–250.

[Boekhorst et al., 2006] Boekhorst, J., Helmer, Q., Kleerebezem, M., and Siezen, R. J. (2006). Comparative analysis of proteins with a mucus-binding domain found exclusively in lactic acid bacteria. *Microbiology*, 152(1):273–280.

[Bonanno et al., 2017] Bonanno, L., Delubac, B., Michel, V., and Auvray, F. (2017). Influence of stress factors related to cheese-making process and to STEC detection procedure on the induction of stx phages from STEC o26:h11. *Frontiers in Microbiology*, 8.

[Bonito et al., 2006] Bonito, A., Clément, P., and Picasso, M. (2006). Mathematical analysis of a simplified Hookean dumbbells model arising from viscoelastic flows. *Journal of Evolution Equations*, 6(3):381–398.

[Bonn et al., 2017] Bonn, D., Denn, M. M., Berthier, L., Divoux, T., and Manneville, S. (2017). Yield stress materials in soft condensed matter. *Reviews of Modern Physics*, 89(3):035005.

[Borges et al., 2016a] Borges, S., Barbosa, J., Silva, J., Gomes, A. M., Pintado, M., Silva, C. L. M., Morais, A. M. M. B., and Teixeira, P. (2016a). A feasibility study of lactobacillus plantarum in fruit powders after processing and storage. *International Journal of Food Science & Technology*, 51(2):381–388.

[Borges et al., 2016b] Borges, S., Barbosa, J., and Teixeira, P. (2016b). Chapter 56 - gynecological health and probiotics a2 - watson, ronald ross. In Preedy, V. R., editor, *Probiotics, Prebiotics, and Synbiotics*, pages 741–752. Academic Press.

[Bos et al., 1999] Bos, R., van der Mei, H. C., and Busscher, H. J. (1999). Physico-chemistry of initial microbial adhesive interactions–its mechanisms and methods for study. *FEMS microbiology reviews*, 23(2):179–230.

[Bouchoux et al., 2010] Bouchoux, A., Gésan-Guiziou, G., Pérez, J., and Cabane, B. (2010). How to Squeeze a Sponge: Casein Micelles under Osmotic Stress, a SAXS Study. *Biophysical Journal*, 99(11):3754–3762.

[Boulos et al., 1999] Boulos, L., Prévost, M., Barbeau, B., Coallier, J., and Desjardins, R. (1999). LIVE/DEAD BacLight: application of a new rapid staining method for direct enumeration of viable and total bacteria in drinking water. *Journal of Microbiological Methods*, 37(1):77–86.

[Bove et al., 2013] Bove, P., Russo, P., Capozzi, V., Gallone, A., Spano, G., and Fiocco, D. (2013). Lactobacillus plantarum passage through an oro-gastro-intestinal tract simulator: Carrier matrix effect and transcriptional analysis of genes associated to stress and probiosis. *Microbiological Research*, 168(6):351–359.

[Boylston et al., 2004] Boylston, T. D., Vinderola, C. G., Ghoddusi, H. B., and Reinheimer, J. A. (2004). Incorporation of bifidobacteria into cheeses: challenges and rewards. *International Dairy Journal*, 14(5):375–387.

[Bridier et al., 2015] Bridier, A., Hammes, F., Canette, A., Bouchez, T., and Briandet, R. (2015). Fluorescence-based tools for single-cell approaches in food microbiology. *International Journal of Food Microbiology*, 213:2–16.

[Brookman, 1975] Brookman, J. S. G. (1975). Further studies on the mechanism of cell disruption by extreme pressure extrusion. *Biotechnology and Bioengineering*, 17(4):465–479.

[Brown et al., 2013] Brown, S., Santa Maria, J. P., and Walker, S. (2013). Wall Teichoic Acids of Gram-Positive Bacteria. *Annual review of microbiology*, 67.

[Brownlow et al., 1997] Brownlow, S., Morais Cabral, J. H., Cooper, R., Flower, D. R., Yewdall, S. J., Polikarpov, I., North, A. C., and Sawyer, L. (1997). Bovine beta-lactoglobulin at 1.8 angstrom resolution -still an enigmatic lipocalin. *Structure*, 5(4):481–495.

[Buck et al., 2005] Buck, B. L., Altermann, E., Svingerud, T., and Klaenhammer, T. R. (2005). Functional Analysis of Putative Adhesion Factors in Lactobacillus acidophilus NCFM. *Applied and Environmental Microbiology*, 71(12):8344–8351.

[Bunt et al., 1995] Bunt, C. R., Jones, D. S., and Tucker, I. G. (1995). The effects of pH, ionic strength and polyvalent ions on the cell surface hydrophobicity of Escherichia coli evaluated by the BATH and HIC methods. *International Journal of Pharmaceutics*, 113(2):257–261.

[Burgain, 2013] Burgain, J. (2013). *Microencapsulation de bactéries probiotiques dans des matrices laitières: Etude des mécanismes de formation par une approche multi-échelle*. Procédés Biotechnologiques et Alimentaires, Université de Lorraine, Vandoeuvre-lès-Nancy.

[Burgain et al., 2013a] Burgain, J., Gaiani, C., Cailliez-Grimal, C., Jeandel, C., and Scher, J. (2013a). Encapsulation of lactobacillus rhamnosus GG in microparticles: Influence of casein to whey protein ratio on bacterial survival during digestion. *Innovative Food Science & Emerging Technologies*, 19:233–242.

[Burgain et al., 2013b] Burgain, J., Gaiani, C., Francius, G., Revol-Junelles, A.-M., Cailliez-Grimal, C., Lebeer, S., Tytgat, H. L. P., Vanderleyden, J., and Scher, J. (2013b). In vitro interactions between probiotic bacteria and milk proteins probed by atomic force microscopy. *Colloids and Surfaces B: Biointerfaces*, 104:153–162.

[Burgain et al., 2011] Burgain, J., Gaiani, C., Linder, M., and Scher, J. (2011). Encapsulation of probiotic living cells: From laboratory scale to industrial applications. *Journal of Food Engineering*, 104(4):467–483.

[Burgain et al., 2014a] Burgain, J., Scher, J., Francius, G., Borges, F., Corgneau, M., Revol-Junelles, A. M., Cailliez-Grimal, C., and Gaiani, C. (2014a). Lactic acid bacteria in dairy food: Surface characterization and interactions with food matrix components. *Advances in Colloid and Interface Science*, 213:21–35.

[Burgain et al., 2014b] Burgain, J., Scher, J., Lebeer, S., Vanderleyden, J., Cailliez-Grimal, C., Corgneau, M., Francius, G., and Gaiani, C. (2014b). Significance of bacterial surface molecules interactions with milk proteins to enhance microencapsulation of lactobacillus rhamnosus GG. *Food Hydrocolloids*, 41:60–70.

[Burgain et al., 2015] Burgain, J., Scher, J., Lebeer, S., Vanderleyden, J., Corgneau, M., Guerin, J., Caillet, C., Duval, J. F. L., Francius, G., and Gaiani, C. (2015). Impacts of pH-mediated EPS structure on probiotic bacterial pili–whey proteins interactions. *Colloids and Surfaces B: Biointerfaces*, 134:332–338.

[Busscher and Weerkamp, 1987] Busscher, H. J. and Weerkamp, A. H. (1987). Specific and non-specific interactions in bacterial adhesion to solid substrata. *FEMS Microbiology Letters*, 46(2):165–173.

[Cabeen et al., 2009] Cabeen, M. T., Charbon, G., Vollmer, W., Born, P., Ausmees, N., Weibel, D. B., and Jacobs-Wagner, C. (2009). Bacterial cell curvature through mechanical control of cell growth. *The EMBO Journal*, 28(9):1208–1219.

[Cabeen and Jacobs-Wagner, 2005] Cabeen, M. T. and Jacobs-Wagner, C. (2005). Bacterial cell shape. *Nature Reviews Microbiology*, 3(8):601–610.

[Call and Klaenhammer, 2013] Call, E. K. and Klaenhammer, T. R. (2013). Relevance and application of sortase and sortase-dependent proteins in lactic acid bacteria. *Frontiers in Microbiology*, 4.

[Carlson et al., 1987a] Carlson, A., Hill, C. G., and Olson, N. F. (1987a). Kinetics of milk coagulation: II. kinetics of the secondary phase: Micelle flocculation. *Biotechnology and Bioengineering*, 29(5):590–600.

[Carlson et al., 1987b] Carlson, A., Hill, C. G., and Olson, N. F. (1987b). The kinetics of milk coagulation: IV. the kinetics of the gel-firming process. *Biotechnology and Bioengineering*, 29(5):612–624.

[Carmona et al., 2014] Carmona, H. A., Wittel, F. K., and Kun, F. (2014). From fracture to fragmentation: Discrete element modeling. *The European Physical Journal Special Topics*, 223(11):2369–2382.

[Carr et al., 2002] Carr, F. J., Chill, D., and Maida, N. (2002). The lactic acid bacteria: a literature survey. *Critical Reviews in Microbiology*, 28(4):281–370.

[Carvalho et al., 2004] Carvalho, A. S., Silva, J., Ho, P., Teixeira, P., Malcata, F. X., and Gibbs, P. (2004). Effects of various sugars added to growth and drying media upon thermotolerance and survival throughout storage of freeze-dried lactobacillus delbrueckii ssp. bulgaricus. *Biotechnology Progress*, 20(1):248–254.

[Castro et al., 2015] Castro, J. M., Tornadijo, M. E., Fresno, J. M., and Sandoval, H. (2015). Biocheese: A food probiotic carrier. *BioMed Research International*, 2015:e723056.

[Cava et al., 2013] Cava, F., Kuru, E., Brun, Y. V., and de Pedro, M. A. (2013). Modes of cell wall growth differentiation in rod-shaped bacteria. *Current Opinion in Microbiology*, 16(6):731–737.

[Chagnot et al., 2013] Chagnot, C., Zorgani, M. A., Astruc, T., and Desvaux, M. (2013). Proteinaceous determinants of surface colonization in bacteria: bacterial adhesion and biofilm formation from a protein secretion perspective. *Frontiers in Microbiology*, 4.

[Champagne et al., 2005] Champagne, C., Gardner, N. J., and Roy, D. (2005). Challenges in the addition of probiotic cultures to foods. *Critical Reviews in Food Science and Nutrition*, 45(1):61–84.

[Champagne and Gardner, 2008] Champagne, C. P. and Gardner, N. J. (2008). Effect of storage in a fruit drink on subsequent survival of probiotic lactobacilli to gastro-intestinal stresses. *Food Research International*, 41(5):539–543.

[Chapot-Chartier and Kulakauskas, 2014] Chapot-Chartier, M.-P. and Kulakauskas, S. (2014). Cell wall structure and function in lactic acid bacteria. *Microbial Cell Factories*, 13(1):S9.

[Charalampopoulos et al., 2002] Charalampopoulos, D., Pandiella, S., and Webb, C. (2002). Growth studies of potentially probiotic lactic acid bacteria in cereal-based substrates. *Journal of Applied Microbiology*, 92(5):851–859.

[Charalampopoulos and Pandiella, 2010] Charalampopoulos, D. and Pandiella, S. S. (2010). Survival of human derived lactobacillus plantarum in fermented cereal extracts during refrigerated storage. *LWT - Food Science and Technology*, 43(3):431–435.

[Charnchai et al., 2016] Charnchai, P., Jantama, S. S., Prasitpuriprecha, C., Kanchanatawee, S., and Jantama, K. (2016). Effects of the food manufacturing chain on the viability and functionality of bifidobacterium animalis through simulated gastrointestinal conditions. *PLOS ONE*, 11(6):e0157958.

[Charteris et al., 1998] Charteris, Kelly, Morelli, and Collins (1998). Development and application of an in vitro methodology to determine the transit tolerance of potentially probiotic lactobacillus and bifidobacterium species in the upper human gastrointestinal tract. *Journal of Applied Microbiology*, 84(5):759–768.

[Chiba et al., 1999a] Chiba, K., Teraoka, K., Iokito, Y., and Nakamura, K. (1999a). Brownian Dynamics Simulation of FENE Dumbbell Model for Dilute Polymer Solutions in Extensional Flow: Effect of Distribution of FENE Parameter and Relaxation Time. *Nihon Reoroji Gakkaishi*, 27(2):79–86.

[Chiba et al., 1999b] Chiba, K., Teraoka, K., Iokito, Y., and Nakamura, K. (1999b). Brownian Dynamics Simulation of FENE Dumbbell Model for Dilute Polymer Solutions in Shear Flow: Effects of Distributions of FENE Parameter and Relaxation Time. *Nihon Reoroji Gakkaishi*, 27(1):31–42.

[Chumphon et al., 2016] Chumphon, T., Sriprasertsak, P., and Promsai, S. (2016). Development of rice as potential carriers for probiotic lactobacillus amylovorus. *International Journal of Food Science & Technology*, 51(5):1260–1267.

[Clark and Ruehl, 1919] Clark, P. F. and Ruehl, W. H. (1919). Morphological Changes During the Growth of Bacteria. *Journal of Bacteriology*, 4(6):615–629.

[Coda et al., 2012] Coda, R., Lanera, A., Trani, A., Gobbetti, M., and Di Cagno, R. (2012). Yogurt-like beverages made of a mixture of cereals, soy and grape must: Microbiology, texture, nutritional and sensory properties. *International Journal of Food Microbiology*, 155(3):120–127.

[Coley et al., 1978] Coley, J., Tarelli, E., Archibald, A. R., and Baddiley, J. (1978). The linkage between teichoic acid and peptidoglycan in bacterial cell walls. *FEBS Letters*, 88(1):1–9.

[Coman et al., 2012] Coman, M. M., Cecchini, C., Verdenelli, M. C., Silvi, S., Orpianesi, C., and Cresci, A. (2012). Functional foods as carriers for SYNBIO, a probiotic bacteria combination. *International Journal of Food Microbiology*, 157(3):346–352.

[Comfort and Clubb, 2004] Comfort, D. and Clubb, R. T. (2004). A comparative genome analysis identifies distinct sorting pathways in gram-positive bacteria. *Infection and Immunity*, 72(5):2710–2722.

[Conway et al., 1987] Conway, P. L., Gorbach, S. L., and Goldin, B. R. (1987). Survival of lactic acid bacteria in the human stomach and adhesion to intestinal cells. *Journal of Dairy Science*, 70(1):1–12.

[Corbo et al., 2001] Corbo, M. R., Albenzio, M., De Angelis, M., Sevi, A., and Gobbetti, M. (2001). Microbiological and biochemical properties of canestrato pugliese hard cheese supplemented with bifidobacteria. *Journal of Dairy Science*, 84(3):551–561.

[Corcoran et al., 2008] Corcoran, B. M., Stanton, C., Fitzgerald, G., and Ross, R. P. (2008). Life under stress: the probiotic stress response and how it may be manipulated. *Current Pharmaceutical Design*, 14(14):1382–1399.

[Corcoran et al., 2005] Corcoran, B. M., Stanton, C., Fitzgerald, G. F., and Ross, R. P. (2005). Survival of probiotic lactobacilli in acidic environments is enhanced in the presence of metabolizable sugars. *Applied and Environmental Microbiology*, 71(6):3060–3067.

[Corredig et al., 2011] Corredig, M., Ion Titapiccolo, G., Gaygadzhiev, Z., and Alexander, M. (2011). Rennet-induced aggregation of milk containing homogenized fat globules. effect of interacting and non-interacting fat globules observed using diffusing wave spectroscopy. *International Dairy Journal*, 21(9):679–684.

[Cotter et al., 2005] Cotter, P. D., Hill, C., and Ross, R. P. (2005). Bacteriocins: developing innate immunity for food. *Nature Reviews. Microbiology*, 3(10):777–788.

[Cousin et al., 2012] Cousin, F. J., Foligné, B., Deutsch, S.-M., Massart, S., Parayre, S., Le Loir, Y., Boudry, G., and Jan, G. (2012). Assessment of the probiotic potential of a dairy product fermented by propionibacterium freudenreichii in piglets. *Journal of Agricultural and Food Chemistry*, 60(32):7917–7927.

[Cousin et al., 2015] Cousin, F. J., Lynch, S. M., Harris, H. M. B., McCann, A., Lynch, D. B., Neville, B. A., Irisawa, T., Okada, S., Endo, A., and O'Toole, P. W. (2015). Detection and Genomic Characterization of Motility in Lactobacillus curvatus: Confirmation of Motility in a Species outside the Lactobacillus salivarius Clade. *Applied and Environmental Microbiology*, 81(4):1297–1308.

[Cronin et al., 2011] Cronin, M., Ventura, M., Fitzgerald, G. F., and van Sinderen, D. (2011). Progress in genomics, metabolism and biotechnology of bifidobacteria. *International Journal of Food Microbiology*, 149(1):4–18.

[Cross, 1965] Cross, M. M. (1965). Rheology of non-newtonian fluids: a new flow equation for pseudoplastic systems. *Journal of colloid science*, 20(5):417–437.

[Cruz et al., 2009] Cruz, A. G., Antunes, A. E., Sousa, A. L. O., Faria, J. A., and Saad, S. M. (2009). Ice-cream as a probiotic food carrier. *Food Research International*, 42(9):1233–1239.

[Cvetkovska, 2018] Cvetkovska, L. (2018). Etude de la déstabilisation du lait en présence de bactéries lactiques. Rapport d'activité de stage, Université de Lorraine, Laboratoire d'Ingénierie des Biomolécules, Vandoeuvre-lès-Nancy.

[Céspedes et al., 2013] Céspedes, M., Cárdenas, P., Staffolani, M., Ciappini, M. C., and Vinderola, G. (2013). Performance in nondairy drinks of probiotic l. casei strains usually employed in dairy products. *Journal of Food Science*, 78(5):M756–M762.

[Córdoba et al., 2014] Córdoba, A., Schieber, J. D., and Indei, T. (2014). A single-chain model for active gels I: active dumbbell model. *RSC Advances*, 4(34):17935–17949.

[Dalgleish, 1979] Dalgleish, D. G. (1979). Proteolysis and aggregation of casein micelles treated with immobilized or soluble chymosin. *Journal of Dairy Research*, 46(4):653–661.

[Dalgleish, 2011] Dalgleish, D. G. (2011). On the structural models of bovine casein micelles—review and possible improvements. *Soft Matter*, 7(6):2265–2272.

[Daniel et al., 2006] Daniel, C., Poiret, S., Goudercourt, D., Dennin, V., Leyer, G., and Pot, B. (2006). Selecting lactic acid bacteria for their safety and functionality by use of a mouse colitis model. *Applied and Environmental Microbiology*, 72(9):5799–5805.

[Danne and Dramsi, 2012] Danne, C. and Dramsi, S. (2012). Pili of Gram-positive bacteria: roles in host colonization. *Research in Microbiology*, 163(9):645–658.

[Dave and Shah, 1998] Dave, R. I. and Shah, N. P. (1998). Ingredient supplementation effects on viability of probiotic bacteria in yogurt. *Journal of Dairy Science*, 81(11):2804–2816.

[Davies and Stokes, 2008] Davies, G. A. and Stokes, J. R. (2008). Thin film and high shear rheology of multiphase complex fluids. *Journal of Non-Newtonian Fluid Mechanics*, 148(1):73–87.

[De Bellis et al., 2010] De Bellis, P., Valerio, F., Sisto, A., Lonigro, S. L., and Lavermicocca, P. (2010). Probiotic table olives: Microbial populations adhering on olive surface in fermentation sets inoculated with the probiotic strain lactobacillus paracasei IMPC2.1 in an industrial plant. *International Journal of Food Microbiology*, 140(1):6–13.

[de Gennes, 2002] de Gennes, P.-G. (2002). Relaxation Anomalies in Linear Polymer Melts. *Macromolecules*, 35(9):3785–3786.

[De Kruif et al., 2012] De Kruif, C. G., Huppertz, T., Urban, V. S., and Petukhov, A. V. (2012). Casein micelles and their internal structure. *Advances in Colloid and Interface Science*, 171-172:36–52.

[De Man et al., 1960] De Man, J. C., Rogosa, M., and Sharpe, M. E. (1960). A medium for the cultivation of lactobacilli. *Journal of Applied Bacteriology*, 23(1):130–135.

[De Souza Lima et al., 2018] De Souza Lima, R., Gutierez, G., Arlabosse, P., and Re, M.-I. (2018). Changing spray-dried lactose-whey protein isolate particle structure with drying conditions. In *Proceedings of 21th International Drying Symposium*. Universitat Politècnica Valèncía.

[de Souza Mendes and Thompson, 2012] de Souza Mendes, P. R. and Thompson, R. L. (2012). A critical overview of elasto-viscoplastic thixotropic modeling. *Journal of Non-Newtonian Fluid Mechanics*, 187-188:8–15.

[de Vos, 2011] de Vos, W. M. (2011). Systems solutions by lactic acid bacteria: from paradigms to practice. *Microbial Cell Factories*, 10(Suppl 1):S2.

[De Vuyst, 2000] De Vuyst, L. (2000). Technology aspects related to the application of functional starter cultures. *Food Technology and Biotechnology*, 38(2):105–112.

[Deepika et al., 2011] Deepika, G., Rastall, R. A., and Charalampopoulos, D. (2011). Effect of food models and low-temperature storage on the adhesion of lactobacillus rhamnosus GG to caco-2 cells. *Journal of Agricultural and Food Chemistry*, 59(16):8661–8666.

[Degond et al., 2010] Degond, P., Lozinski, A., and Owens, R. G. (2010). Kinetic models for dilute solutions of dumbbells in non-homogeneous flows revisited. *Journal of Non-Newtonian Fluid Mechanics*, 165(9):509–518.

[Delcour et al., 1999] Delcour, J., Ferain, T., Deghorain, M., Palumbo, E., and Hols, P. (1999). The biosynthesis and functionality of the cell-wall of lactic acid bacteria. *Antonie van Leeuwenhoek*, pages p.159–184.

[Desvaux et al., 2018] Desvaux, M., Candela, T., and Serror, P. (2018). Surfaceome and Proteosurfaceome in Parietal Monoderm Bacteria: Focus on Protein Cell-Surface Display. *Frontiers in Microbiology*, 9.

[Desvaux et al., 2006] Desvaux, M., Dumas, E., Chafsey, I., and HÃ©braud, M. (2006). Protein cell surface display in Gram-positive bacteria: from single protein to macromolecular protein structure. *FEMS Microbiology Letters*, 256(1):1–15.

[Deutsch et al., 2012] Deutsch, S.-M., Parayre, S., Bouchoux, A., Guyomarc'h, F., Dewulf, J., Dols-Lafargue, M., Baglinière, F., Cousin, F. J., Falentin, H., Jan, G., and Foligné, B. (2012). Contribution of surface beta-glucan polysaccharide to physicochemical and immunomodulatory properties of propionibacterium freudenreichii. *Applied and Environmental Microbiology*, 78(6):1765–1775.

[Dewettinck et al., 2008] Dewettinck, K., Rombaut, R., Thienpont, N., Le, T. T., Messens, K., and Van Camp, J. (2008). Nutritional and technological aspects of milk fat globule membrane material. *International Dairy Journal*, 18(5):436–457.

[Dhanani and Bagchi, 2013] Dhanani, A. S. and Bagchi, T. (2013). The expression of adhesin EF-Tu in response to mucin and its role in Lactobacillus adhesion and competitive inhibition of enteropathogens to mucin. *Journal of Applied Microbiology*, 115(2):546–554.

[Diao et al., 2013] Diao, J., Burré, J., Vivona, S., Cipriano, D. J., Sharma, M., Kyoung, M., Südhof, T. C., and Brunger, A. T. (2013). Native alpha-synuclein induces clustering of synaptic-vesicle mimics via binding to phospholipids and synaptobrevin-2/VAMP2. *eLife*, 2:e00592.

[Diaz et al., 2016] Diaz, M., Ladero, V., del Rio, B., Redruello, B., Fernández, M., Martin, M. C., and Alvarez, M. A. (2016). Biofilm-forming capacity in biogenic amine-producing bacteria isolated from dairy products. *Frontiers in Microbiology*, 7.

[Dilly and Rajala, 2008] Dilly, A. K. and Rajala, R. V. S. (2008). Insulin growth factor 1 receptor/PI3k/AKT survival pathway in outer segment membranes of rod photoreceptors. *Investigative Ophthalmology & Visual Science*, 49(11):4765–4773.

[Dimitriou and McKinley, 2014] Dimitriou, C. J. and McKinley, G. H. (2014). A comprehensive constitutive law for waxy crude oil: a thixotropic yield stress fluid. *Soft Matter*, 10(35):6619–6644.

[Dimitrov et al., 2014] Dimitrov, Z., Gotova, I., and Chorbadjiyska, E. (2014). In vitro characterization of the adhesive factors of selected probiotics to caco-2 epithelium cell line. *Biotechnology & Biotechnological Equipment*, 28(6):1079–1083.

[Ditu et al., 2014] Ditu, L. M., Chifiriuc, M. C., Bezirtzoglou, E., Marutescu, L., Bleotu, C., Pelinescu, D., Mihaescu, G., and Lazar, V. (2014). Immunomodulatory effect of non-viable components of probiotic culture stimulated with heat-inactivated escherichia coli and bacillus cereus on holoxenic mice. *Microbial Ecology in Health and Disease*, 25.

[Doherty et al., 2010] Doherty, S. B., Wang, L., Ross, R. P., Stanton, C., Fitzgerald, G. F., and Brodkorb, A. (2010). Use of viability staining in combination with flow cytometry for rapid viability assessment of lactobacillus rhamnosus GG in complex protein matrices. *Journal of Microbiological Methods*, 82(3):301–310.

[Domínguez-Ramírez et al., 2013] Domínguez-Ramírez, L., Del Moral-Ramírez, E., Cortes-Hernández, P., García-Garibay, M., and Jiménez-Guzmán, J. (2013). beta-lactoglobulin's conformational requirements for ligand binding at the calyx and the dimer interphase: a flexible docking study. *PloS One*, 8(11):e79530.

[Douillard and de Vos, 2014] Douillard, F. P. and de Vos, W. M. (2014). Functional genomics of lactic acid bacteria: from food to health. *Microbial Cell Factories*, 13(1):S8.

[Douillard et al., 2013] Douillard, F. P., Ribbera, A., Kant, R., Pietilä, T. E., Järvinen, H. M., Messing, M., Randazzo, C. L., Paulin, L., Laine, P., Ritari, J., Caggia, C., Lähteinen, T., Brouns, S. J. J., Satokari, R., Ossowski, I. v., Reunanen, J., Palva, A., and Vos, W. M. d.

(2013). Comparative genomic and functional analysis of 100 lactobacillus rhamnosus strains and their comparison with strain GG. *PLOS Genetics*, 9(8):e1003683.

[Douëllou et al., 2018] Douëllou, T., Galia, W., Kerangart, S., Marchal, T., Milhau, N., Bastien, R., Bouvier, M., Buff, S., Montel, M.-C., and Sergentet-Thevenot, D. (2018). Milk fat globules hamper adhesion of enterohemorrhagic escherichia coli to enterocytes: In vitro and in vivo evidence. *Frontiers in Microbiology*, 9.

[Douëllou et al., 2017] Douëllou, T., Montel, M. C., and Sergentet, D. T. (2017). Invited review: Anti-adhesive properties of bovine oligosaccharides and bovine milk fat globule membrane-associated glycoconjugates against bacterial food enteropathogens. *Journal of Dairy Science*, 100(5):3348–3359.

[du Roure et al., 2019] du Roure, O., Lindner, A., Nazockdast, E. N., and Shelley, M. J. (2019). Dynamics of flexible fibers in viscous flows and fluids. *Annual Review of Fluid Mechanics*, 51(1):539–572.

[Dullaert and Mewis, 2006] Dullaert, K. and Mewis, J. (2006). A structural kinetics model for thixotropy. *Journal of Non-Newtonian Fluid Mechanics*, 139(1):21–30.

[Dutta et al., 2017] Dutta, J., Baijnath, S., Somboro, A. M., Nagiah, S., Albericio, F., de la Torre, B. G., Marjanovic-Painter, B., Zeevaart, J. R., Sathekge, M., Kruger, H. G., Chuturgoon, A., Naicker, T., Ebenhan, T., and Govender, T. (2017). Synthesis, in vitro evaluation, and 68ga-radiolabeling of CDP1 toward PET/CT imaging of bacterial infection. *Chemical Biology & Drug Design*, 90(4):572–579.

[D'Orazio et al., 2015] D'Orazio, G., Gennaro, P. D., Boccarusso, M., Presti, I., Bizzaro, G., Giardina, S., Michelotti, A., Labra, M., and Ferla, B. L. (2015). Microencapsulation of new probiotic formulations for gastrointestinal delivery: in vitro study to assess viability and biological properties. *Applied Microbiology and Biotechnology*, 99(22):9779–9789.

[E et al., 2004] E, W., Li, T., and Zhang, P. (2004). Well-Posedness for the Dumbbell Model of Polymeric Fluids. *Communications in Mathematical Physics*, 248(2):409–427.

[Ebner et al., 2014] Ebner, S., Smug, L. N., Kneifel, W., Salminen, S. J., and Sanders, M. E. (2014). Probiotics in dietary guidelines and clinical recommendations outside the european union. *World Journal of Gastroenterology*, 20(43):16095.

[Editorial, 2016] Editorial (2016). Single-cell microbiology. *Nature Biotechnology*, 34(11):1077.

[Edwards et al., 1989] Edwards, N., Beeton, S., Bull, A. T., and Merchuk, J. C. (1989). A novel device for the assessment of shear effects on suspended microbial cultures. *Applied Microbiology and Biotechnology*, 30(2):190–195.

[Edwards et al., 2008] Edwards, P., Creamer, L., and Jameson, G. (2008). Structure and Stability of Whey Proteins. In *Milk Proteins*, pages 163–203.

[Egan and Vollmer, 2013] Egan, A. J. F. and Vollmer, W. (2013). The physiology of bacterial cell division. *Annals of the New York Academy of Sciences*, 1277(1):8–28.

[El'darov et al., 1995] El'darov, E. G., Mamedov, F. V., Gol'dberg, V. M., and Zaikov, G. E. (1995). Kinetic Model of Polymer Degradation Occurring during Extrusion Process. *International Journal of Polymeric Materials and Polymeric Biomaterials*, 29(1-2):1–14.

[Elias-Argote et al., 2013] Elias-Argote, X., Laubscher, A., and Jimenez-Flores, R. (2013). Dairy Ingredients Containing Milk Fat Globule Membrane: Description, Composition, and Industrial Potential. In *Advances in Dairy Ingredients*, pages 71–98. Wiley-Blackwell, g.w. smithers & ry a. augustin edition.

[Endo et al., 2014] Endo, A., Teräsjärvi, J., and Salminen, S. (2014). Food matrices and cell conditions influence survival of lactobacillus rhamnosus GG under heat stresses and during storage. *International Journal of Food Microbiology*, 174:110–112.

[Engesser and Hammes, 1994] Engesser, D. M. and Hammes, W. P. (1994). Non-heme catalase activity of lactic acid bacteria. *Systematic and applied microbiology*, 17(1):11–19.

[Engler and Robinson, 1981a] Engler, C. R. and Robinson, C. W. (1981a). Disruption of Candida utilis cells in high pressure flow devices*. *Biotechnology and Bioengineering*, 23(4):765–780.

[Engler and Robinson, 1981b] Engler, C. R. and Robinson, C. W. (1981b). Effects of organism type and growth conditions on cell disruption by impingement. *Biotechnology Letters*, 3(2):83–88.

[Etzold et al., 2014] Etzold, S., Kober, O. I., Mackenzie, D. A., Tailford, L. E., Gunning, A. P., Walshaw, J., Hemmings, A. M., and Juge, N. (2014). Structural basis for adaptation of lactobacilli to gastrointestinal mucus. *Environmental Microbiology*, 16(3):888–903.

[Evers, 2004] Evers, J. M. (2004). The milk fat globule membrane: compositional and structural changes post secretion by the mammary secretory cell. *International Dairy Journal*, 14(8):661–674.

[Ewoldt and McKinley, 2017] Ewoldt, R. H. and McKinley, G. H. (2017). Mapping thixo-elasto-visco-plastic behavior. *Rheologica Acta*, 56(3):195–210.

[Faber et al., 2017] Faber, T. J., Jaishankar, A., and McKinley, G. H. (2017). Describing the firmness, springiness and rubberiness of food gels using fractional calculus. part i: Theoretical framework. *Food Hydrocolloids*, 62:311–324.

[Faraudo et al., 2013] Faraudo, J., Andreu, J. S., and Camacho, J. (2013). Understanding diluted dispersions of superparamagnetic particles under strong magnetic fields: a review of concepts, theory and simulations. *Soft Matter*, 9(29):6654.

[Fernandez et al., 2011] Fernandez, E. M., Valenti, V., Rockel, C., Hermann, C., Pot, B., Boneca, I. G., and Grangette, C. (2011). Anti-inflammatory capacity of selected lactobacilli in experimental colitis is driven by NOD2-mediated recognition of a specific peptidoglycan-derived muropeptide. *Gut*, 60(8):1050–1059.

[Finn et al., 2017] Finn, R. D., Attwood, T. K., Babbitt, P. C., Bateman, A., Bork, P., Bridge, A. J., Chang, H.-Y., Dosztányi, Z., El-Gebali, S., Fraser, M., Gough, J., Haft, D., Holliday, G. L., Huang, H., Huang, X., Letunic, I., Lopez, R., Lu, S., Marchler-Bauer, A., Mi, H., Mistry, J., Natale, D. A., Necci, M., Nuka, G., Orengo, C. A., Park, Y., Pesseat, S., Piovesan, D., Potter, S. C., Rawlings, N. D., Redaschi, N., Richardson, L., Rivoire, C., Sangrador-Vegas, A., Sigrist, C., Sillitoe, I., Smithers, B., Squizzato, S., Sutton, G., Thanki, N., Thomas, P. D., Tosatto, S. C. E., Wu, C. H., Xenarios, I., Yeh, L.-S., Young, S.-Y., and Mitchell, A. L. (2017). InterPro in 2017—beyond protein family and domain annotations. *Nucleic Acids Research*, 45:D190–D199.

[Firstenberg-Eden, 1981] Firstenberg-Eden, R. (1981). Attachment of bacteria to meat surfaces: A review. *Journal of Food Protection*, 44(8):602–607.

[Fischer, 1994] Fischer, W. (1994). Chapter 10 Lipoteichoic acids and lipoglycans. In Ghuysen, J. M. and Hakenbeck, R., editors, *New Comprehensive Biochemistry*, volume 27 of *Bacterial Cell Wall*, pages 199–215. Elsevier.

[Fischetti, 2019] Fischetti, V. A. (2019). Surface Proteins on Gram-Positive Bacteria. *Microbiology spectrum*, 7(4).

[Fitzsimons et al., 2001] Fitzsimons, N., Cogan, T., Condon, S., and Beresford, T. (2001). Spatial and temporal distribution of non-starter lactic acid bacteria in cheddar cheese. *Journal of Applied Microbiology*, 90(4):600–608.

[Foegeding et al., 2011] Foegeding, E. A., Daubert, C. R., Drake, M. A., Essick, G., Trulsson, M., Vinyard, C. J., and Velde, F. V. D. (2011). A comprehensive approach to understanding textural properties of semi- and soft-solid foods. *Journal of Texture Studies*, 42(2):103–129.

[Foegeding and Drake, 2007] Foegeding, E. A. and Drake, M. A. (2007). Invited review: Sensory and mechanical properties of cheese texture1. *Journal of Dairy Science*, 90(4):1611–1624.

[Fong et al., 2007] Fong, B. Y., Norris, C. S., and MacGibbon, A. K. H. (2007). Protein and lipid composition of bovine milk-fat-globule membrane. *International Dairy Journal*, 17(4):275–288.

[Ford et al., 2014] Ford, A. C., Quigley, E. M. M., Lacy, B. E., Lembo, A. J., Saito, Y. A., Schiller, L. R., Soffer, E. E., Spiegel, B. M. R., and Moayyedi, P. (2014). Efficacy of prebiotics, probiotics, and synbiotics in irritable bowel syndrome and chronic idiopathic constipation: Systematic review and meta-analysis. *The American Journal of Gastroenterology*, 109(10):1547–1561.

[Forquin and Hild, 2010] Forquin, P. and Hild, F. (2010). A Probabilistic Damage Model of the Dynamic Fragmentation Process in Brittle Materials. In *Advances in Applied Mechanics*, volume 44, pages 1–72. Elsevier.

[Foster et al., 1962] Foster, J. W., Cowan, R. M., and Maag, T. A. (1962). Rupture of Bacteria by Explosive Decompression. *Journal of Bacteriology*, 83(2):330–334.

[Fox, 1993] Fox, P. F. (1993). *Cheese: chemistry, physics and microbiology.*, volume 1. Springer Science+Business Media Dordrecht, 2nd edition. OCLC: 939445860.

[Fraggedakis et al., 2016] Fraggedakis, D., Dimakopoulos, Y., and Tsamopoulos, J. (2016). Yielding the yield-stress analysis: a study focused on the effects of elasticity on the settling of a single spherical particle in simple yield-stress fluids. *Soft Matter*, 12(24):5378–5401.

[Francius et al., 2009] Francius, G., Alsteens, D., Dupres, V., Lebeer, S., De Keersmaecker, S., Vanderleyden, J., Gruber, H. J., and Dufrêne, Y. F. (2009). Stretching polysaccharides on live cells using single molecule force spectroscopy. *Nature Protocols*, 4(6):939–946.

[Frederick and Armstrong, 2007] Frederick, C. O. and Armstrong, P. J. (2007). A mathematical representation of the multiaxial bauschinger effect. *Materials at High Temperatures*, 24(1):1–26.

[Fronzes et al., 2008] Fronzes, R., Remaut, H., and Waksman, G. (2008). Architectures and biogenesis of non-flagellar protein appendages in gram-negative bacteria. *The EMBO Journal*, 27(17):2271–2280.

[Furukawa et al., 2014] Furukawa, A., Marenduzzo, D., and Cates, M. E. (2014). Activity-induced clustering in model dumbbell swimmers: The role of hydrodynamic interactions. *Physical Review E*, 90(2):022303.

[Gadhiya et al., 2016] Gadhiya, D., Patel, A., and Prajapati, J. (2016). Current trend and future prospective of functional probiotic milk chocolates and related products: a review. *Czech Journal of Food Sciences*, 33:295–301.

[Gao et al., 2019] Gao, H., Ma, L., Li, T., Sun, D., Hou, J., Li, A., and Jiang, Z. (2019). Impact of ultrasonic power on the structure and emulsifying properties of whey protein isolate under various pH conditions. *Process Biochemistry*, 81:113–122.

[Gardiner et al., 1998] Gardiner, G., Ross, R. P., Collins, J. K., Fitzgerald, G., and Stanton, C. (1998). Development of a probiotic cheddar cheese containing human-derived lactobacillus paracaseiStrains. *Applied and Environmental Microbiology*, 64(6):2192–2199.

[Garrett et al., 2008] Garrett, T. R., Bhakoo, M., and Zhang, Z. (2008). Bacterial adhesion and biofilms on surfaces. *Progress in Natural Science*, 18(9):1049–1056.

[Gay et al., 1991] Gay, N. J., Packman, L. C., Weldon, M. A., and Barna, J. C. J. (1991). A leucine-rich repeat peptide derived from the drosophila toll receptor forms extended filaments with a beta-sheet structure. *FEBS Letters*, 291(1):87–91.

[Gentès et al., 2011] Gentès, M.-C., St-Gelais, D., and Turgeon, S. L. (2011). Gel formation and rheological properties of fermented milk with in situ exopolysaccharide production by lactic acid bacteria. *Dairy Science & Technology*, 91(5):645.

[Ghandi et al., 2012] Ghandi, A., Powell, I. B., Howes, T., Chen, X. D., and Adhikari, B. (2012). Effect of shear rate and oxygen stresses on the survival of lactococcus lactis during the atomization and drying stages of spray drying: A laboratory and pilot scale study. *Journal of Food Engineering*, 113(2):194–200.

[Giaouris et al., 2014] Giaouris, E., Heir, E., Hébraud, M., Chorianopoulos, N., Langsrud, S., Møretrø, T., Habimana, O., Desvaux, M., Renier, S., and Nychas, G.-J. (2014). Attachment and biofilm formation by foodborne bacteria in meat processing environments: Causes, implications, role of bacterial interactions and control by alternative novel methods. *Meat Science*, 97(3):298–309.

[Gidaspow and Chandra, 2014] Gidaspow, D. and Chandra, V. (2014). Unequal granular temperature model for motion of platelets to the wall and red blood cells to the center. *Chemical Engineering Science*, 117:107–113.

[Girard and Schaffer-Lequart, 2007] Girard, M. and Schaffer-Lequart, C. (2007). Gelation and resistance to shearing of fermented milk: Role of exopolysaccharides. *International Dairy Journal*, 17(6):666–673.

[Gobbetti et al., 1998] Gobbetti, M., Corsetti, A., Smacchi, E., Zocchetti, A., and De Angelis, M. (1998). Production of crescenza cheese by incorporation of bifidobacteria. *Journal of Dairy Science*, 81(1):37–47.

[Goh et al., 2005] Goh, S., Charalambides, M., and Williams, J. (2005). On the mechanics of wire cutting of cheese. *Engineering Fracture Mechanics*, 72(6):931–946.

[Goldin et al., 1992] Goldin, B. R., Gorbach, S. L., Saxelin, M., Barakat, S., Gualtieri, L., and Salminen, S. (1992). Survival of lactobacillus species (strain GG) in human gastrointestinal tract. *Digestive diseases and sciences*, 37(1):121–128.

[Goldsmith and Marlow, 1979] Goldsmith, H. L. and Marlow, J. C. (1979). Flow behavior of erythrocytes. II. particle motions in concentrated suspensions of ghost cells. *Journal of Colloid and Interface Science*, 71(2):383–407.

[Golowczyc et al., 2011] Golowczyc, M. A., Silva, J., Teixeira, P., De Antoni, G. L., and Abraham, A. G. (2011). Cellular injuries of spray-dried Lactobacillus spp. isolated from kefir and their impact on probiotic properties. *International Journal of Food Microbiology*, 144(3):556–560.

[Gomand et al., 2019a] Gomand, F., Borges, F., Burgain, J., Guerin, J., Revol-Junelles, A.-M., and Gaiani, C. (2019a). Food matrix design for effective lactic acid bacteria delivery. *Annual Review of Food Science and Technology*, 10(1):285–310.

[Gomand et al., 2019b] Gomand, F., Borges, F., Guerin, J., El-Kirat-Chatel, S., Francius, G., Dumas, D., Burgain, J., and Gaiani, C. (2019b). Adhesive Interactions Between Lactic Acid Bacteria and β-Lactoglobulin: Specificity and Impact on Bacterial Location in Whey Protein Isolate. *Frontiers in Microbiology*, 10(1512).

[Gomand et al., 2018] Gomand, F., Borges, F., Salim, D., Burgain, J., Guerin, J., and Gaiani, C. (2018). High-throughput screening approach to evaluate the adhesive properties of bacteria to milk biomolecules. *Food Hydrocolloids*, 84:537–544.

[Gomes et al., 1995] Gomes, A. M. P., Malcata, F. X., Klaver, F. a. M., and Grande, H. J. (1995). Incorporation and survival of Bifidobacterium sp. strain Bo and Lactobacillus acidophilus strain Ki in a cheese product. *Netherlands Milk and Dairy Journal*, 49(2-3):71–95.

[Gomes et al., 1998] Gomes, A. M. P., Vieira, M. M., and Malcata, F. X. (1998). Survival of probiotic microbial strains in a cheese matrix during ripening: Simulation of rates of salt diffusion and microorganism survival. *Journal of Food Engineering*, 36(3):281–301.

[Gonçalves and Cardarelli, 2019] Gonçalves, M. C. and Cardarelli, H. R. (2019). Changes in water mobility and protein stabilization of Mozzarella cheese made under different stretching temperatures. *LWT*, 104:16–23.

[Good et al., 2017] Good, B. H., McDonald, M. J., Barrick, J. E., Lenski, R. E., and Desai, M. M. (2017). The Dynamics of Molecular Evolution Over 60,000 Generations. *Nature*, 551(7678):45–50.

[Goodeve and Whitfield, 1938] Goodeve, C. F. and Whitfield, G. W. (1938). The measurement of thixotropy in absolute units. *Transactions of the Faraday Society*, 34(0):511–520.

[Granato et al., 2004] Granato, D., Bergonzelli, G. E., Pridmore, R. D., Marvin, L., Rouvet, M., and Corthésy-Theulaz, I. E. (2004). Cell Surface-Associated Elongation Factor Tu Mediates the Attachment of Lactobacillus johnsonii NCC533 (La1) to Human Intestinal Cells and Mucins. *Infection and Immunity*, 72(4):2160–2169.

[Granato et al., 2010] Granato, D., Branco, G. F., Cruz, A. G., Faria, J. d. A. F., and Shah, N. P. (2010). Probiotic dairy products as functional foods. *Comprehensive Reviews in Food Science and Food Safety*, 9(5):455–470.

[Granato et al., 1999] Granato, D., Perotti, F., Masserey, I., Rouvet, M., Golliard, M., Servin, A., and Brassart, D. (1999). Cell Surface-Associated Lipoteichoic Acid Acts as an Adhesion Factor for Attachment of Lactobacillus johnsonii La1 to Human Enterocyte-Like Caco-2 Cells. *Applied and Environmental Microbiology*, 65(3):1071–1077.

[Grangette et al., 2005] Grangette, C., Nutten, S., Palumbo, E., Morath, S., Hermann, C., Dewulf, J., Pot, B., Hartung, T., Hols, P., and Mercenier, A. (2005). Enhanced antiinflammatory capacity of a Lactobacillus plantarum mutant synthesizing modified teichoic acids. *Proceedings of the National Academy of Sciences of the United States of America*, 102(29):10321–10326.

[Grover et al., 1977] Grover, N. B., Woldringh, C. L., Zaritsky, A., and Rosenberger, R. F. (1977). Elongation of rod-shaped bacteria. *Journal of Theoretical Biology*, 67(2):181–193.

[Guergoletto et al., 2012] Guergoletto, K. B., Tsuruda, A. Y., Hirooka, E. Y., Martins, E. P., de Souza, J. C. B., Sivieri, K., Roig, S. M., and Garcia, S. (2012). *Dried probiotics for use in functional food applications*. INTECH Open Access Publisher.

[Guerin, 2017] Guerin, J. (2017). *Influence de l'ajout d'ingrédients fonctionnels laitiers sur l'encapsulation de L. rhamnosus GG*. Procédés Biotechnologiques et Alimentaires, Université de Lorraine, Vandoeuvre-lès-Nancy.

[Guerin et al., 2016] Guerin, J., Bacharouche, J., Burgain, J., Lebeer, S., Francius, G., Borges, F., Scher, J., and Gaiani, C. (2016). Pili of lactobacillus rhamnosus GG mediate interaction with beta-lactoglobulin. *Food Hydrocolloids*, 58:35–41.

[Guerin et al., 2017a] Guerin, J., Burgain, J., Borges, F., Bhandari, B., Desobry, S., Scher, J., and Gaiani, C. (2017a). Use of imaging techniques to identify efficient controlled release systems of lactobacillus rhamnosus GG during in vitro digestion. *Food Funct.*

[Guerin et al., 2018a] Guerin, J., Burgain, J., Francius, G., El-Kirat-Chatel, S., Beaussart, A., Scher, J., and Gaiani, C. (2018a). Adhesion of lactobacillus rhamnosus GG surface biomolecules to milk proteins. *Food Hydrocolloids*, 82:296–303.

[Guerin et al., 2017b] Guerin, J., Burgain, J., Gomand, F., Scher, J., and Gaiani, C. (2017b). Milk fat globule membrane glycoproteins: Valuable ingredients for lactic acid bacteria encapsulation? *Critical Reviews in Food Science and Nutrition*, 0(0):1–13.

[Guerin et al., 2017c] Guerin, J., Petit, J., Burgain, J., Borges, F., Bhandari, B., Perroud, C., Desobry, S., Scher, J., and Gaiani, C. (2017c). Lactobacillus rhamnosus GG encapsulation by spray-drying: Milk proteins clotting control to produce innovative matrices. *Journal of Food Engineering*, 193:10–19.

[Guerin et al., 2018b] Guerin, J., Soligot, C., Burgain, J., Huguet, M., Francius, G., El-Kirat-Chatel, S., Gomand, F., Lebeer, S., Le Roux, Y., Borges, F., Scher, J., and Gaiani, C. (2018b). Adhesive interactions between milk fat globule membrane and lactobacillus rhamnosus GG inhibit bacterial attachment to caco-2 TC7 intestinal cell. *Colloids and Surfaces B: Biointerfaces*, 167:44–53.

[Gulati et al., 2008] Gulati, P., Gaspers, L. D., Dann, S. G., Joaquin, M., Nobukuni, T., Natt, F., Kozma, S. C., Thomas, A. P., and Thomas, G. (2008). Amino acids activate mTOR complex 1 via ca2+/CaM signaling to hVps34. *Cell Metabolism*, 7(5):456–465.

[Guo et al., 2016] Guo, Q., Ye, A., Lad, M., Dalgleish, D., and Singh, H. (2016). Impact of colloidal structure of gastric digesta on in-vitro intestinal digestion of whey protein emulsion gels. *Food Hydrocolloids*, 54:255–265.

[Göpferich, 1996] Göpferich, A. (1996). Mechanisms of polymer degradation and erosion. *Biomaterials*, 17(2):103–114.

[Güde, 1979] Güde, H. (1979). Grazing by protozoa as selection factor for activated sludge bacteria. *Microbial Ecology*, 5(3):225–237.

[Habashi et al., 2011] Habashi, J. P., Doyle, J. J., Holm, T. M., Aziz, H., Schoenhoff, F., Bedja, D., Chen, Y., Modiri, A. N., Judge, D. P., and Dietz, H. C. (2011). Angiotensin II type 2 receptor signaling attenuates aortic aneurysm in mice through ERK antagonism. *Science*, 332(6027):361–365.

[Haffner et al., 2016] Haffner, F. B., Diab, R., and Pasc, A. (2016). Encapsulation of probiotics: insights into academic and industrial approaches. *Materials 2016, Vol. 3, Pages 114-136*.

[Hahn and Höfle, 1999] Hahn, M. W. and Höfle, M. G. (1999). Flagellate Predation on a Bacterial Model Community: Interplay of Size-Selective Grazing, Specific Bacterial Cell Size, and Bacterial Community Composition. *Applied and Environmental Microbiology*, 65(11):4863–4872.

[Halpin et al., 2008] Halpin, R. M., O'Connor, M. M., McMahon, A., Boughton, C., O'Riordan, E. D., O'Sullivan, M., and Brady, D. B. (2008). Inhibition of adhesion of streptococcus mutans to hydroxylapatite by commercial dairy powders and individual milk proteins. *European Food Research and Technology*, 227(5):1499.

[Harry et al., 2006] Harry, E., Monahan, L., and Thompson, L. (2006). Bacterial Cell Division: The Mechanism and Its Precision. In *International Review of Cytology*, volume 253, pages 27–94. Academic Press.

[Harry, 2001] Harry, E. J. (2001). Bacterial cell division: regulating Z-ring formation. *Molecular Microbiology*, 40(4):795–803.

[Hayek and Ibrahim, 2013] Hayek, S. A. and Ibrahim, S. A. (2013). Current limitations and challenges with lactic acid bacteria: A review. *Food and Nutrition Sciences*, 04(11):73–87.

[Hede et al., 2008] Hede, P. D., Bach, P., and Jensen, A. D. (2008). Two-fluid spray atomisation and pneumatic nozzles for fluid bed coating/agglomeration purposes: A review. *Chemical Engineering Science*, 63(14):3821–3842.

[Heilmann et al., 1996] Heilmann, C., Schweitzer, O., Gerke, C., Vanittanakom, N., Mack, D., and Götz, F. (1996). Molecular basis of intercellular adhesion in the biofilm-forming staphylococcus epidermidis. *Molecular Microbiology*, 20(5):1083–1091.

[Helland et al., 2004] Helland, M. H., Wicklund, T., and Narvhus, J. A. (2004). Growth and metabolism of selected strains of probiotic bacteria in milk- and water-based cereal puddings. *International Dairy Journal*, 14(11):957–965.

[Heller, 2001] Heller, K. J. (2001). Probiotic bacteria in fermented foods: product characteristics and starter organisms. *The American Journal of Clinical Nutrition*, 73(2):374s–379s.

[Hermansson, 1999] Hermansson, M. (1999). The DLVO theory in microbial adhesion. *Colloids and Surfaces B: Biointerfaces*, 14(1):105–119.

[Hernández Cifre et al., 2003] Hernández Cifre, J. G., Barenbrug, T. M. A. O. M., Schieber, J. D., and van den Brule, B. H. A. A. (2003). Brownian dynamics simulation of reversible polymer networks under shear using a non-interacting dumbbell model. *Journal of Non-Newtonian Fluid Mechanics*, 113(2):73–96.

[Hickey et al., 2015a] Hickey, C., Auty, M., Wilkinson, M., and Sheehan, J. (2015a). The influence of cheese manufacture parameters on cheese microstructure, microbial localisation and their interactions during ripening: A review. *Trends in Food Science & Technology*, 41(2):135–148.

[Hickey et al., 2015b] Hickey, C. D., Sheehan, J. J., Wilkinson, M. G., and Auty, M. A. E. (2015b). Growth and location of bacterial colonies within dairy foods using microscopy techniques: a review. *Frontiers in Microbiology*, 6(99):1–8.

[Hinrichs and Keim, 2007] Hinrichs, J. and Keim, S. (2007). Process-induced stabilizing bonds in fermented milk products. *Milchwissenschaft*, 62(4):422–425.

[Holt, 1992] Holt, C. (1992). Structure and Stability of Bovine Casein Micelles. In Anfinsen, C. B., Richards, F. M., Edsall, J. T., and Eisenberg, D. S., editors, *Advances in Protein Chemistry*, volume 43, pages 63–151. Academic Press.

[Holzmüller et al., 2016] Holzmüller, W., Gmach, O., Griebel, A., and Kulozik, U. (2016). Casein precipitation by acid and rennet coagulation of buttermilk: Impact of pH and temperature on the isolation of milk fat globule membrane proteins. *International Dairy Journal*, 63:115–123.

[Holzmüller and Kulozik, 2016] Holzmüller, W. and Kulozik, U. (2016). Isolation of milk fat globule membrane (MFGM) material by coagulation and diafiltration of buttermilk. *International Dairy Journal*, 63:88–91.

[Homayouni, 2008] Homayouni, A. (2008). Growth and survival of some probiotic strains in simulated ice cream conditions. *Journal of Applied Sciences*, pages 379–382.

[Horne, 1998] Horne, D. S. (1998). Casein Interactions: Casting Light on the Black Boxes, the Structure in Dairy Products. *International Dairy Journal*, 8(3):171–177.

[Horvath et al., 2009] Horvath, P., Coûté-Monvoisin, A.-C., Romero, D. A., Boyaval, P., Fremaux, C., and Barrangou, R. (2009). Comparative analysis of CRISPR loci in lactic acid bacteria genomes. *International Journal of Food Microbiology*, 131(1):62–70.

[Houzé et al., 2005] Houzé, G., Cases, E., Colas, B., and Cayot, P. (2005). Viscoelastic properties of acid milk gel as affected by fat nature at low level. *International Dairy Journal*, 15(10):1006–1016.

[Huang et al., 2016] Huang, S., Rabah, H., Jardin, J., Briard-Bion, V., Parayre, S., Maillard, M.-B., Loir, Y. L., Chen, X. D., Schuck, P., Jeantet, R., and Jan, G. (2016). Hyperconcentrated sweet whey, a new culture medium that enhances propionibacterium freudenreichii stress tolerance. *Applied and Environmental Microbiology*, 82(15):4641–4651.

[Huc et al., 2014] Huc, D., Mariette, F., and Michon, C. (2014). Rheological characterisation of semi-hard cheese using lubricated squeezing flow test. *International Dairy Journal*, 36(2):101–109.

[Hynönen and Palva, 2013] Hynönen, U. and Palva, A. (2013). Lactobacillus surface layer proteins: structure, function and applications. *Applied Microbiology and Biotechnology*, 97(12):5225–5243.

[Iaconelli et al., 2015] Iaconelli, C., Lemetais, G., Kechaou, N., Chain, F., Bermúdez-Humarán, L. G., Langella, P., Gervais, P., and Beney, L. (2015). Drying process strongly affects probiotics viability and functionalities. *Journal of Biotechnology*, 214:17–26.

[Ion Titapiccolo et al., 2010] Ion Titapiccolo, G., Alexander, M., and Corredig, M. (2010). Rennet-induced aggregation of homogenized milk: Impact of the presence of fat globules on the structure of casein gels. *Dairy Science & Technology*, 90(6):623–639.

[Ishikawa, 2019] Ishikawa, T. (2019). Stability of a Dumbbell Micro-Swimmer. *Micromachines*, 10(1):33.

[Isihara, 1951] Isihara, A. (1951). Theory of High Polymer Solutions (The Dumbbell Model). *The Journal of Chemical Physics*, 19(4):397–403.

[Islam et al., 2014] Islam, M. T., Oishi, A., Machida, C., Ogura, A., Kin, S., Honjoh, K.-i., and Miyamoto, T. (2014). Combined effects of selected food additives on adhesion of various foodborne pathogens onto microtiter plate and cabbage leaves. *Food Control*, 46:233–241.

[Ismail et al., 2007] Ismail, M., Ayyad, K., and Hamad, M. (2007). Manufacture of Mozzarella cheese using Glucono-Delta-Lactone. In *Proceedings of the 10th Egyptian Conference for Dairy Science and Technology*, pages 415–432, Cairo, Egypt.

[Isolauri et al., 1991] Isolauri, E., Rautanen, T., Juntunen, M., Sillanaukee, P., and Koivula, T. (1991). A human lactobacillus strain (lactobacillus casei sp strain GG) promotes recovery from acute diarrhea in children. *Pediatrics*, 88(1):90–97.

[Jaglic et al., 2014] Jaglic, Z., Desvaux, M., Weiss, A., Nesse, L. L., Meyer, R. L., Demnerova, K., Schmidt, H., Giaouris, E., Sipailiene, A., Teixeira, P., Ka aniova, M., Riedel, C. U., and Knochel, S. (2014). Surface adhesins and exopolymers of selected foodborne pathogens. *Microbiology*, 160:2561–2582.

[Javanmard et al., 2018] Javanmard, M., Wong, E., Howes, T., and Stokes, J. R. (2018). Application of the thixotropic elasto-viscoplastic model as a structure probing technique for acid milk gel suspensions. *Journal of Food Engineering*, 222:250–257.

[Jeanson et al., 2011] Jeanson, S., Chadœuf, J., Madec, M. N., Aly, S., Floury, J., Brocklehurst, T. F., and Lortal, S. (2011). Spatial distribution of bacterial colonies in a model cheese. *Applied and Environmental Microbiology*, 77(4):1493–1500.

[Jeanson et al., 2015] Jeanson, S., Floury, J., Gagnaire, V., Lortal, S., and Thierry, A. (2015). Bacterial colonies in solid media and foods: A review on their growth and interactions with the micro-environment. *Frontiers in Microbiology*, 6.

[Jeffery, 1922] Jeffery, G. B. (1922). The motion of ellipsoidal particles immersed in a viscous fluid. *Proc. R. Soc. Lond. A*, 102(715):161–179.

[Jensen et al., 2014] Jensen, H., Roos, S., Jonsson, H., Rud, I., Grimmer, S., van Pijkeren, J.-P., Britton, R. A., and Axelsson, L. (2014). Role of Lactobacillus reuteri cell and mucus-binding protein A (CmbA) in adhesion to intestinal epithelial cells and mucus in vitro. *Microbiology (Reading, England)*, 160(Pt 4):671–681.

[Jiang and Kurath, 1996] Jiang, Y. and Kurath, P. (1996). Characteristics of the Armstrong-Frederick type plasticity models. *International Journal of Plasticity*, 12(3):387–415.

[Johnson-Henry et al., 2016] Johnson-Henry, K. C., Abrahamsson, T. R., Wu, R. Y., and Sherman, P. M. (2016). Probiotics, prebiotics, and synbiotics for the prevention of necrotizing enterocolitis. *Advances in Nutrition: An International Review Journal*, 7(5):928–937.

[Jolly and Stingele, 2001] Jolly, L. and Stingele, F. (2001). Molecular organization and functionality of exopolysaccharide gene clusters in lactic acid bacteria. *International Dairy Journal*, 11(9):733–745.

[Jones et al., 2014] Jones, P., Binns, D., Chang, H.-Y., Fraser, M., Li, W., McAnulla, C., McWilliam, H., Maslen, J., Mitchell, A., Nuka, G., Pesseat, S., Quinn, A. F., Sangrador-Vegas, A., Scheremetjew, M., Yong, S.-Y., Lopez, R., and Hunter, S. (2014). InterProScan 5: genome-scale protein function classification. *Bioinformatics*, 30(9):1236–1240.

[Joshi et al., 1996] Joshi, J. B., Elias, C. B., and Patole, M. S. (1996). Role of hydrodynamic shear in the cultivation of animal, plant and microbial cells. *The Chemical Engineering Journal and the Biochemical Engineering Journal*, 62(2):121–141.

[Joshi et al., 2003] Joshi, N. S., Muthukumarappan, K., and Dave, R. I. (2003). Understanding the role of calcium in functionality of part skim Mozzarella cheese. *Journal of Dairy Science*, 86(6):1918–1926.

[Juge, 2012] Juge, N. (2012). Microbial adhesins to gastrointestinal mucus. *Trends in Microbiology*, 20(1):30–39.

[Jürgens and Matz, 2002] Jürgens, K. and Matz, C. (2002). Predation as a shaping force for the phenotypic and genotypic composition of planktonic bacteria. *Antonie van Leeuwenhoek*, 81:413–434.

[Kailasapathy et al., 2008] Kailasapathy, K., Harmstorf, I., and Phillips, M. (2008). Survival of lactobacillus acidophilus and bifidobacterium animalis ssp. lactis in stirred fruit yogurts. *LWT - Food Science and Technology*, 41(7):1317–1322.

[Kailasham et al., 2018] Kailasham, R., Chakrabarti, R., and Prakash, J. R. (2018). Rheological consequences of wet and dry friction in a dumbbell model with hydrodynamic interactions and internal viscosity. *The Journal of Chemical Physics*, 149(9):094903.

[Kankainen et al., 2009] Kankainen, M., Paulin, L., Tynkkynen, S., Ossowski, I. v., Reunanen, J., Partanen, P., Satokari, R., Vesterlund, S., Hendrickx, A. P. A., Lebeer, S., Keersmaecker, S. C. J. D., Vanderleyden, J., Hämäläinen, T., Laukkanen, S., Salovuori, N., Ritari, J., Alatalo, E., Korpela, R., Mattila-Sandholm, T., Lassig, A., Hatakka, K., Kinnunen, K. T., Karjalainen, H., Saxelin, M., Laakso, K., Surakka, A., Palva, A., Salusjärvi, T., Auvinen, P., and Vos, W. M. d. (2009). Comparative genomic analysis of lactobacillus rhamnosus GG reveals pili containing a human- mucus binding protein. *Proceedings of the National Academy of Sciences*, 106(40).

[Karimi et al., 2011] Karimi, R., Mortazavian, A. M., and Cruz, A. G. D. (2011). Viability of probiotic microorganisms in cheese during production and storage: a review. *Dairy Science & Technology*, 91(3):283–308.

[Katsikogianni and Missirlis, 2004] Katsikogianni, M. and Missirlis, Y. F. (2004). Concise review of mechanisms of bacterial adhesion to biomaterials and of techniques used in estimating bacteria-material interactions. *Eur Cell Mater*, 8(3).

[Keaveny and Shelley, 2011] Keaveny, E. E. and Shelley, M. J. (2011). Applying a second-kind boundary integral equation for surface tractions in stokes flow. *Journal of Computational Physics*, 230(5):2141–2159.

[Kelly and O'Kennedy, 2001] Kelly, P. and O'Kennedy, B. (2001). The effect of casein/whey protein ratio and minerals on the rheology of fresh cheese gels using a model system. *International Dairy Journal*, 11(4-7):525–532.

[Khalid and others, 2011] Khalid, K. and others (2011). An overview of lactic acid bacteria. *International Journal of Biosciences*, 1(3):1–13.

[Khan et al., 2011] Khan, M. I., Arshad, M. S., Anjum, F. M., Sameen, A., Aneeq-ur-Rehman, and Gill, W. T. (2011). Meat as a functional food with special reference to probiotic sausages. *Food Research International*, 44(10):3125–3133.

[Kiekens et al., 2019] Kiekens, S., Vandenheuvel, D., Broeckx, G., Claes, I., Allonsius, C., De Boeck, I., Thys, S., Timmermans, J.-P., Kiekens, F., and Lebeer, S. (2019). Impact of spray-drying on the pili of Lactobacillus rhamnosus GG: Spray-drying affects functionality probiotics. *Microbial Biotechnology*, pages 1–7.

[Kim and Bhowmik, 1990] Kim, S. S. and Bhowmik, S. (1990). Survival of lactic acid bacteria during spray drying of plain yogurt. *Journal of Food Science*.

[Kimoto-Nira et al., 2015] Kimoto-Nira, H., Yamasaki, S., Sasaki, K., Moriya, N., Takenaka, A., and Suzuki, C. (2015). New lactic acid bacterial strains from traditional mongolian fermented milk products have altered adhesion to porcine gastric mucin depending on the carbon source: Altered adhesion activity by c-source. *Animal Science Journal*, 86(3):325–332.

[Kindstedt et al., 2004] Kindstedt, P., Carić, M., and Milanović, S. (2004). Pasta-filata cheeses. In Fox, P. F., McSweeney, P. L. H., Cogan, T. M., and Guinee, T. P., editors, *Cheese: Chemistry, Physics and Microbiology*, volume 2 of *Major Cheese Groups*, pages 251–277. Academic Press.

[Kinoshita et al., 2008] Kinoshita, H., Uchida, H., Kawai, Y., Kawasaki, T., Wakahara, N., Matsuo, H., Watanabe, M., Kitazawa, H., Ohnuma, S., Miura, K., Horii, A., and Saito, T. (2008). Cell surface Lactobacillus plantarum LA 318 glyceraldehyde-3-phosphate dehydrogenase (GAPDH) adheres to human colonic mucin. *Journal of Applied Microbiology*, 104(6):1667–1674.

[Klaenhammer et al., 2005] Klaenhammer, T. R., Barrangou, R., Buck, B. L., Azcarate-Peril, M. A., and Altermann, E. (2005). Genomic features of lactic acid bacteria effecting bioprocessing and health. *FEMS Microbiology Reviews*, 29(3):393–409.

[Kleerebezem and Hugenholtz, 2003] Kleerebezem, M. and Hugenholtz, J. (2003). Metabolic pathway engineering in lactic acid bacteria. *Current Opinion in Biotechnology*, 14(2):232–237.

[Klemm and Schembri, 2000] Klemm, P. and Schembri, M. A. (2000). Bacterial adhesins: function and structure. *International Journal of Medical Microbiology*, 290(1):27–35.

[Klindt-Toldam et al., 2016] Klindt-Toldam, S., Larsen, S. K., Saaby, L., Olsen, L. R., Svenstrup, G., Müllertz, A., Knøchel, S., Heimdal, H., Nielsen, D. S., and Zielińska, D. (2016). Survival of lactobacillus acidophilus NCFM and bifidobacterium lactis HN019 encapsulated in chocolate during in vitro simulated passage of the upper gastrointestinal tract. *LWT - Food Science and Technology*, 74:404–410.

[Kline et al., 2010] Kline, K. A., Dodson, K. W., Caparon, M. G., and Hultgren, S. J. (2010). A tale of two pili: assembly and function of pili in bacteria. *Trends in microbiology*, 18(5):224–232.

[Kline et al., 2009] Kline, K. A., Fälker, S., Dahlberg, S., Normark, S., and Henriques-Normark, B. (2009). Bacterial adhesins in host-microbe interactions. *Cell Host & Microbe*, 5(6):580–592.

[Klu et al., 2014] Klu, Y. A. K., Phillips, R. D., and Chen, J. (2014). Survival of four commercial probiotic mixtures in full fat and reduced fat peanut butter. *Food Microbiology*, 44:34–40.

[Klu et al., 2012] Klu, Y. A. K., Williams, J. H., Phillips, R. D., and Chen, J. (2012). Survival of lactobacillus rhamnosus GG as influenced by storage conditions and product matrixes. *Journal of Food Science*, 77(12):M659–M663.

[Kobayashi and Yamamoto, 2010] Kobayashi, H. and Yamamoto, R. (2010). Tumbling motion of a single chain in shear flow: A crossover from brownian to non-brownian behavior. *Physical Review E*, 81(4).

[Kobe and Kajava, 2001] Kobe, B. and Kajava, A. V. (2001). The leucine-rich repeat as a protein recognition motif. *Current Opinion in Structural Biology*, 11(6):725–732.

[Kontopidis et al., 2002] Kontopidis, G., Holt, C., and Sawyer, L. (2002). The ligand-binding site of bovine beta-lactoglobulin: evidence for a function? *Journal of Molecular Biology*, 318(4):1043–1055.

[Kontopidis et al., 2004] Kontopidis, G., Holt, C., and Sawyer, L. (2004). Invited review: beta-lactoglobulin: binding properties, structure, and function. *Journal of Dairy Science*, 87(4):785–796.

[Korolczuk, 1993] Korolczuk, J. (1993). Flow behaviour of low solids fresh cheeses. *Journal of Dairy Research*, 60(4):593–601.

[Kostoglou, 2000] Kostoglou, M. (2000). Mathematical analysis of polymer degradation with chain-end scission. *Chemical Engineering Science*, 55(13):2507–2513.

[Kothari et al., 2016] Kothari, D. C., Luckham, D. P., and Lawrence, D. C. J. (2016). Determination of mechanical and rheological properties of cheese by indentation. *Mathematical Sciences*, 5(4):35–44.

[Kowalik et al., 2018] Kowalik, J., Lobacz, A., Zulewska, J., and Dec, B. (2018). Analysis and mathematical modelling of the behaviour of escherichia coli in the mascarpone cheese during cold storage. *International Journal of Food Science & Technology*, 53(6):1541–1548.

[Kravchuk and Stokes, 2013] Kravchuk, O. and Stokes, J. R. (2013). Review of algorithms for estimating the gap error correction in narrow gap parallel plate rheology. *Journal of Rheology*, 57(2):365–375.

[Kubota et al., 2008] Kubota, H., Senda, S., Nomura, N., Tokuda, H., and Uchiyama, H. (2008). Biofilm formation by lactic acid bacteria and resistance to environmental stress. *Journal of Bioscience and Bioengineering*, 106(4):381–386.

[Lablée, 1988] Lablée, J. (1988). Evolution de la théorie fromagère et utilisation de la glucono-delta-lactone. *Bulletin de l'Académie Vétérinaire de France*, 61(2):191–198.

[Lacroix and Yildirim, 2007] Lacroix, C. and Yildirim, S. (2007). Fermentation technologies for the production of probiotics with high viability and functionality. *Current Opinion in Biotechnology*, 18(2):176–183.

[Lakemond and Van Vliet, 2007] Lakemond, C. M. M. and Van Vliet, T. (2007). Rheology of acid skim milk gels. In Dickinson, E., editor, *Special Publications*, pages 26–36. Royal Society of Chemistry, Cambridge.

[Laličić-Petronijević et al., 2015] Laličić-Petronijević, J., Popov-Raljić, J., Obradović, D., Radulović, Z., Paunović, D., Petrušić, M., and Pezo, L. (2015). Viability of probiotic strains lactobacillus acidophilus NCFMand bifidobacterium lactis HN019 and their impact on sensory and rheological properties of milk and dark chocolates during storage for 180 days. *Journal of Functional Foods*, 15:541–550.

[Laloy et al., 1996] Laloy, E., Vuillemard, J.-C., El Soda, M., and Simard, R. E. (1996). Influence of the fat content of cheddar cheese on retention and localization of starters. *International Dairy Journal*, 6(7):729–740.

[Lamichhane et al., 2018] Lamichhane, P., Kelly, A. L., and Sheehan, J. J. (2018). Symposium review: Structure-function relationships in cheese. *Journal of Dairy Science*, 101(3):2692–2709.

[Lamothe et al., 2012] Lamothe, S., Corbeil, M.-M., Turgeon, S. L., and Britten, M. (2012). Influence of cheese matrix on lipid digestion in a simulated gastro-intestinal environment. *Food and Function*, 3(7):724–731.

[Lane et al., 2012] Lane, J. A., Mariño, K., Rudd, P. M., Carrington, S. D., Slattery, H., and Hickey, R. M. (2012). Methodologies for screening of bacteria–carbohydrate interactions: Anti-adhesive milk oligosaccharides as a case study. *Journal of Microbiological Methods*, 90(1):53–59.

[Lange et al., 2001] Lange, H., Taillandier, P., and Riba, J.-P. (2001). Effect of high shear stress on microbial viability. *Journal of Chemical Technology & Biotechnology*, 76(5):501–505.

[Larsen et al., 2007] Larsen, N., Nissen, P., and Willats, W. G. T. (2007). The effect of calcium ions on adhesion and competitive exclusion of lactobacillus ssp. and e. coli o138. *International Journal of Food Microbiology*, 114(1):113–119.

[Larson, 2015] Larson, R. G. (2015). Constitutive equations for thixotropic fluids. *Journal of Rheology*, 59(3):595–611.

[Lavermicocca, 2006] Lavermicocca, P. (2006). Highlights on new food research. *Digestive and Liver Disease*, 38:S295–S299.

[Lavermicocca et al., 2005] Lavermicocca, P., Valerio, F., Lonigro, S. L., Angelis, M. D., Morelli, L., Callegari, M. L., Rizzello, C. G., and Visconti, A. (2005). Study of adhesion and survival of lactobacilli and bifidobacteria on table olives with the aim of formulating a new probiotic food. *Applied and Environmental Microbiology*, 71(8):4233–4240.

[Le et al., 2013] Le, D. T. L., Tran, T.-L., Duviau, M.-P., Meyrand, M., Guérardel, Y., Castelain, M., Loubière, P., Chapot-Chartier, M.-P., Dague, E., and Mercier-Bonin, M. (2013). Unraveling the role of surface mucus-binding protein and pili in muco-adhesion of Lactococcus lactis. *PloS One*, 8(11):e79850.

[Le et al., 2009] Le, T. T., Van Camp, J., Rombaut, R., van Leeckwyck, F., and Dewettinck, K. (2009). Effect of washing conditions on the recovery of milk fat globule membrane proteins during the isolation of milk fat globule membrane from milk. *Journal of Dairy Science*, 92(8):3592–3603.

[Lebeer et al., 2012] Lebeer, S., Claes, I., Tytgat, H. L. P., Verhoeven, T. L. A., Marien, E., Ossowski, I. v., Reunanen, J., Palva, A., Vos, W. M. d., Keersmaecker, S. C. J. D., and Vanderleyden, J. (2012). Functional analysis of lactobacillus rhamnosus GG pili in relation to adhesion and immunomodulatory interactions with intestinal epithelial cells. *Applied and Environmental Microbiology*, 78(1):185–193.

[Lebeer et al., 2010] Lebeer, S., Vanderleyden, J., and De Keersmaecker, S. C. J. (2010). Host interactions of probiotic bacterial surface molecules: comparison with commensals and pathogens. *Nature Reviews Microbiology*, 8(3):171–184.

[Lebeer et al., 2008] Lebeer, S., Vanderleyden, J., and Keersmaecker, S. C. J. D. (2008). Genes and molecules of lactobacilli supporting probiotic action. *Microbiology and Molecular Biology Reviews*, 72(4):728–764.

[Lebeer et al., 2009] Lebeer, S., Verhoeven, T. L. A., Francius, G., Schoofs, G., Lambrichts, I., Dufrêne, Y., Vanderleyden, J., and Keersmaecker, S. C. J. D. (2009). Identification of a gene cluster for the biosynthesis of a long, galactose-rich exopolysaccharide in lactobacillus rhamnosus GG and functional analysis of the priming glycosyltransferase. *Applied and Environmental Microbiology*, 75(11):3554–3563.

[Lechardeur et al., 2012] Lechardeur, D., Cesselin, B., Liebl, U., Vos, M. H., Fernandez, A., Brun, C., Gruss, A., and Gaudu, P. (2012). Discovery of intracellular heme-binding protein HrtR, which controls heme efflux by the conserved HrtB-HrtA transporter in lactococcus lactis. *Journal of Biological Chemistry*, 287(7):4752–4758.

[Lecuyer et al., 2011] Lecuyer, S., Rusconi, R., Shen, Y., Forsyth, A., Vlamakis, H., Kolter, R., and Stone, H. A. (2011). Shear stress increases the residence time of adhesion of pseudomonas aeruginosa. *Biophysical Journal*, 100(2):341–350.

[Lee and Lim, 1980] Lee and Lim, H. (1980). New device for continuously monitoring the optical density of concentrated microbial cultures. *Biotechnology and Bioengineering*, 22(3):639–642.

[Lee et al., 2000] Lee, Y. K., Lim, C. Y., Teng, W. L., Ouwehand, A. C., Tuomola, E. M., and Salminen, S. (2000). Quantitative approach in the study of adhesion of lactic acid bacteria to intestinal cells and their competition with enterobacteria. *Applied and Environmental Microbiology*, 66(9):3692–3697.

[Lee and Salminen, 2009] Lee, Y. K. and Salminen, S. (2009). *Handbook of Probiotics and Prebiotics*. John Wiley & Sons.

[Lewis et al., 2014] Lewis, C. L., Craig, C. C., and Senecal, A. G. (2014). Mass and density measurements of live and dead gram-negative and gram-positive bacterial populations. *Applied and Environmental Microbiology*, 80(12):3622–3631.

[Li et al., 2008] Li, B., Du, T., Li, H., Gu, L., Zhang, H., Huang, J., Hertz, L., and Peng, L. (2008). Signalling pathways for transactivation by dexmedetomidine of epidermal growth factor receptors in astrocytes and its paracrine effect on neurons. *British Journal of Pharmacology*, 154(1):191–203.

[Liu, 2003] Liu, S. Q. (2003). Practical implications of lactate and pyruvate metabolism by lactic acid bacteria in food and beverage fermentations. *International journal of food microbiology*, 83(2):115–131.

[Liu et al., 2019] Liu, Y., Yu, Y., Liu, C., Regenstein, J. M., Liu, X., and Zhou, P. (2019). Rheological and mechanical behavior of milk protein composite gel for extrusion-based 3d food printing. *LWT*, 102:338–346.

[Livney, 2010] Livney, Y. D. (2010). Milk proteins as vehicles for bioactives. *Current Opinion in Colloid & Interface Science*, 15(1):73–83.

[Lopez, 2005] Lopez, C. (2005). Focus on the supramolecular structure of milk fat in dairy products. *Reproduction Nutrition Development*, 45(4):497–511.

[Lopez et al., 2006] Lopez, C., Maillard, M.-B., Briard-Bion, V., Camier, B., and Hannon, J. A. (2006). Lipolysis during ripening of emmental cheese considering organization of fat and preferential localization of bacteria. *Journal of Agricultural and Food Chemistry*, 54(16):5855–5867.

[Lourens-Hattingh and Viljoen, 2001] Lourens-Hattingh, A. and Viljoen, B. C. (2001). Yogurt as probiotic carrier food. *International Dairy Journal*, 11(1):1–17.

[Lowe et al., 2003] Lowe, L. L., Allen Foegeding, E., and Daubert, C. R. (2003). Rheological properties of fine-stranded whey protein isolate gels. *Food Hydrocolloids*, 17(4):515–522.

[Lu et al., 2015] Lu, S., Giuliani, M., Harvey, H., Burrows, L. L., Wickham, R. A., and Dutcher, J. R. (2015). Nanoscale pulling of type IV pili reveals their flexibility and adhesion to surfaces over extended lengths of the pili. *Biophysical Journal*, 108(12):2865–2875.

[Lucas et al., 2004] Lucas, A., Sodini, I., Monnet, C., Jolivet, P., and Corrieu, G. (2004). Probiotic cell counts and acidification in fermented milks supplemented with milk protein hydrolysates. *International Dairy Journal*, 14(1):47–53.

[Lucey et al., 2003] Lucey, J. A., Johnson, M. E., and Horne, D. S. (2003). Invited review: Perspectives on the basis of the rheology and texture properties of cheese. *Journal of Dairy Science*, 86(9):2725–2743.

[Luo et al., 2017] Luo, J., Wang, Y., Guo, H., and Ren, F. (2017). Effects of size and stability of native fat globules on the formation of milk gel induced by rennet. *Journal of Food Science*, 82(3):670–678.

[Luo and Yin, 2017] Luo, W. and Yin, Z. (2017). Global existence and well-posedness for the FENE dumbbell model of polymeric flows. *Nonlinear Analysis: Real World Applications*, 37:457–488.

[Lupien-Meilleur et al., 2016] Lupien-Meilleur, J., Roy, D., and Lagacé, L. (2016). Viability of probiotic bacteria in a maple sap beverage during refrigerated storage. *LWT - Food Science and Technology*, 74:160–167.

[Ly et al., 2006] Ly, M. H., Vo, N. H., Le, T. M., Belin, J.-M., and Waché, Y. (2006). Diversity of the surface properties of Lactococci and consequences on adhesion to food components. *Colloids and Surfaces. B, Biointerfaces*, 52(2):149–153.

[Mackenzie et al., 2010] Mackenzie, D. A., Jeffers, F., Parker, M. L., Vibert-Vallet, A., Bongaerts, R. J., Roos, S., Walter, J., and Juge, N. (2010). Strain-specific diversity of mucus-binding proteins in the adhesion and aggregation properties of Lactobacillus reuteri. *Microbiology (Reading, England)*, 156(Pt 11):3368–3378.

[MacKenzie et al., 2009] MacKenzie, D. A., Tailford, L. E., Hemmings, A. M., and Juge, N. (2009). Crystal structure of a mucus-binding protein repeat reveals an unexpected functional immunoglobulin binding activity. *The Journal of Biological Chemistry*, 284(47):32444–32453.

[Macías-Rodríguez et al., 2009] Macías-Rodríguez, M. E., Zagorec, M., Ascencio, F., Vázquez-Juárez, R., and Rojas, M. (2009). Lactobacillus fermentum BCS87 expresses mucus- and mucin-binding proteins on the cell surface. *Journal of Applied Microbiology*, 107(6):1866–1874.

[Madureira et al., 2011] Madureira, A. R., Amorim, M., Gomes, A. M., Pintado, M. E., and Malcata, F. X. (2011). Protective effect of whey cheese matrix on probiotic strains exposed to simulated gastrointestinal conditions. *Food Research International*, 44(1):465–470.

[Madureira et al., 2005] Madureira, A. R., Pereira, C. I., Truszkowska, K., Gomes, A. M., Pintado, M. E., and Malcata, F. X. (2005). Survival of probiotic bacteria in a whey cheese vector submitted to environmental conditions prevailing in the gastrointestinal tract. *International Dairy Journal*, 15(6):921–927.

[Maffettone and Marrucci, 1992] Maffettone, P. L. and Marrucci, G. (1992). The nematic dumbbell model. *Journal of Rheology*, 36(8):1547–1561.

[Majorek et al., 2012] Majorek, K. A., Porebski, P. J., Dayal, A., Zimmerman, M. D., Jablonska, K., Stewart, A. J., Chruszcz, M., and Minor, W. (2012). Structural and immunologic characterization of bovine, horse, and rabbit serum albumins. *Molecular Immunology*, 52(3-4):174–182.

[Makarova et al., 2006] Makarova, K., Slesarev, A., Wolf, Y., Sorokin, A., Mirkin, B., Koonin, E., Pavlov, A., Pavlova, N., Karamychev, V., Polouchine, N., Shakhova, V., Grigoriev, I., Lou, Y., Rohksar, D., Lucas, S., Huang, K., Goodstein, D. M., Hawkins, T., Plengvidhya, V., Welker, D., Hughes, J., Goh, Y., Benson, A., Baldwin, K., Lee, J.-H., Díaz-Muñiz, I., Dosti, B., Smeianov, V., Wechter, W., Barabote, R., Lorca, G., Altermann, E., Barrangou, R., Ganesan, B., Xie, Y., Rawsthorne, H., Tamir, D., Parker, C., Breidt, F., Broadbent, J., Hutkins, R., O'Sullivan, D., Steele, J., Unlu, G., Saier, M., Klaenhammer, T., Richardson, P., Kozyavkin, S., Weimer, B., and Mills, D. (2006). Comparative genomics of the lactic acid bacteria. *Proceedings of the National Academy of Sciences of the United States of America*, 103(42):15611–15616.

[Makhal et al., 2013] Makhal, S., Kanawjia, S. K., and Giri, A. (2013). A dual-acidification process for the manufacture of direct-acidified Cottage cheese. *International Journal of Dairy Technology*, 66(4):552–561.

[Makinen et al., 2012] Makinen, K., Berger, B., Bel-Rhlid, R., and Ananta, E. (2012). Science and technology for the mastership of probiotic applications in food products. *Journal of Biotechnology*, 162(4):356–365.

[Mandlik et al., 2008] Mandlik, A., Swierczynski, A., Das, A., and Ton-That, H. (2008). Pili in Gram-positive bacteria: assembly, involvement in colonization and biofilm development. *Trends in microbiology*, 16(1):33–40.

[Mantzaris, 2005] Mantzaris, N. V. (2005). Transient and asymptotic behaviour of the binary breakage problem. *Journal of Physics A Mathematical General*, 38:5111–5132.

[Mao et al., 2017] Mao, Y., Talamini, B., and Anand, L. (2017). Rupture of polymers by chain scission. *Extreme Mechanics Letters*, 13:17–24.

[Maresso and Schneewind, 2008] Maresso, A. W. and Schneewind, O. (2008). Sortase as a target of anti-infective therapy. *Pharmacological Reviews*, 60(1):128–141.

[Marshall et al., 1971] Marshall, K. C., Stout, R., and Mitchell, R. (1971). Mechanism of the Initial Events in the Sorption of Marine Bacteria to Surfaces. *Microbiology,*, 68(3):337–348.

[Martinez-Monzo et al., 1998] Martinez-Monzo, J., Martínez-Navarrete, N., Chiralt, A., and Fito, P. (1998). Mechanical and structural changes in apple (var. granny smith) due to vacuum impregnation with cryoprotectants. *Journal of Food Science*, 63(3):499–503.

[Martins and Locke, 2015] Martins, B. M. and Locke, J. C. (2015). Microbial individuality: how single-cell heterogeneity enables population level strategies. *Current Opinion in Microbiology*, 24:104–112.

[Martins et al., 2013] Martins, E. M. F., Ramos, A. M., Vanzela, E. S. L., Stringheta, P. C., de Oliveira Pinto, C. L., and Martins, J. M. (2013). Products of vegetable origin: A new alternative for the consumption of probiotic bacteria. *Food Research International*, 51(2):764–770.

[Masmoudi, 2008] Masmoudi, N. (2008). Well-posedness for the FENE dumbbell model of polymeric flows. *Communications on Pure and Applied Mathematics*, 61(12):1685–1714.

[Massaguer-Roig et al., 1984] Massaguer-Roig, S., Rizvi, S. S. H., and Kosikowski, F. V. (1984). Characterization of thixotropic behavior of soft cheeses. *Journal of Food Science*, 49(3):668–670.

[Mather, 2000] Mather, I. H. (2000). A Review and Proposed Nomenclature for Major Proteins of the Milk-Fat Globule Membrane1,2. *Journal of Dairy Science*, 83(2):203–247.

[McClements, 2015] McClements, D. J. (2015). Enhancing nutraceutical bioavailability through food matrix design. *Current Opinion in Food Science*, 4:1–6.

[McCrea et al., 2000] McCrea, K. W., Hartford, O., Davis, S., Eidhin, D. N., Lina, G., Speziale, P., Foster, T. J., and Höök, M. (2000). The serine-aspartate repeat (sdr) protein family in staphylococcus epidermidis. *Microbiology*, 146(7):1535–1546.

[McCulloch, 2008] McCulloch, E. (2008). *Experimental and Finite Element Modeling of Ultrasonic Cutting of Food*. University of Glasgow.

[McMahon and Oberg, 2011] McMahon, D. and Oberg, C. (2011). Cheese: Pasta-filata Cheeses: Low-Moisture Part-Skim Mozzarella (Pizza Cheese). In J.W. Fuquay, P. F. and McSweeney, P., editors, *Encyclopedia of Dairy Sciences*, volume 1, pages 737–744. Academic Press, San Diego, USA, 2nd edition.

[McMahon and Oommen, 2008] McMahon, D. J. and Oommen, B. S. (2008). Supramolecular structure of the casein micelle. *Journal of Dairy Science*, 91(5):1709–1721.

[McSweeney and O'Mahony, 2016] McSweeney, P. L. H. and O'Mahony, J. A., editors (2016). *Advanced dairy chemistry*, volume 1B: Proteins: Applied Aspects. Springer, fourth edition edition.

[Mende et al., 2013] Mende, S., Peter, M., Bartels, K., Rohm, H., and Jaros, D. (2013). Addition of purified exopolysaccharide isolates from S. thermophilus to milk and their impact on the rheology of acid gels. *Food Hydrocolloids*, 32(1):178–185.

[Meng et al., 2008] Meng, X. C., Stanton, C., Fitzgerald, G. F., Daly, C., and Ross, R. P. (2008). Anhydrobiotics: The challenges of drying probiotic cultures. *Food Chemistry*, 106(4):1406–1416.

[Mercier et al., 2000] Mercier, C., Domakova, E., Tremblay, J., and Kulakauskas, S. (2000). Effects of a muramidase on a mixed bacterial community. *FEMS Microbiology Letters*, 187(1):47–52.

[Mewis and Wagner, 2009] Mewis, J. and Wagner, N. J. (2009). Thixotropy. *Advances in Colloid and Interface Science*, 147-148:214–227.

[Meyrand et al., 2013] Meyrand, M., Guillot, A., Goin, M., Furlan, S., Armalyte, J., Kulakauskas, S., Cortes-Perez, N. G., Thomas, G., Chat, S., Péchoux, C., Dupres, V., Hols, P., Dufrêne, Y. F., Trugnan, G., and Chapot-Chartier, M.-P. (2013). Surface proteome analysis of a natural isolate of Lactococcus lactis reveals the presence of pili able to bind human intestinal epithelial cells. *Molecular & cellular proteomics: MCP*, 12(12):3935–3947.

[Michalski et al., 2002] Michalski, M. C., Cariou, R., Michel, F., and Garnier, C. (2002). Native vs. damaged milk fat globules: membrane properties affect the viscoelasticity of milk gels. *Journal of Dairy Science*, 85(10):2451–2461.

[Miller et al., 2006] Miller, E., Garcia, T., Hultgren, S., and Oberhauser, A. F. (2006). The mechanical properties of e. coli type 1 pili measured by atomic force microscopy techniques. *Biophysical Journal*, 91(10):3848–3856.

[Minekus et al., 2014] Minekus, M., Alminger, M., Alvito, P., Ballance, S., Bohn, T., Bourlieu, C., Carrière, F., Boutrou, R., Corredig, M., Dupont, D., Dufour, C., Egger, L., Golding, M., Karakaya, S., Kirkhus, B., Feunteun, S. L., Lesmes, U., Macierzanka, A., Mackie, A., Marze, S., McClements, D. J., Ménard, O., Recio, I., Santos, C. N., Singh, R. P., Vegarud, G. E., Wickham, M. S. J., Weitschies, W., and Brodkorb, A. (2014). A standardised static in vitro digestion method suitable for food – an international consensus. *Food and Function*, 5(6):1113–1124.

[Mitchell and Spagnolie, 2017] Mitchell, W. H. and Spagnolie, S. E. (2017). A generalized traction integral equation for stokes flow, with applications to near-wall particle mobility and viscous erosion. *Journal of Computational Physics*, 333:462–482.

[Miyoshi et al., 2006] Miyoshi, Y., Okada, S., Uchimura, T., and Satoh, E. (2006). A mucus adhesion promoting protein, MapA, mediates the adhesion of Lactobacillus reuteri to Caco-2 human intestinal epithelial cells. *Bioscience, Biotechnology, and Biochemistry*, 70(7):1622–1628.

[Mizuno and Lucey, 2005] Mizuno, R. and Lucey, J. A. (2005). Effects of two types of emulsifying salts on the functionality of nonfat pasta filata cheese. *Journal of Dairy Science*, 88(10):3411–3425.

[Mohammadi and Mortazavian, 2011] Mohammadi, R. and Mortazavian, A. M. (2011). Review article: Technological aspects of prebiotics in probiotic fermented milks. *Food Reviews International*, 27(2):192–212.

[Monaco et al., 1987] Monaco, H. L., Zanotti, G., Spadon, P., Bolognesi, M., Sawyer, L., and Eliopoulos, E. E. (1987). Crystal structure of the trigonal form of bovine beta-lactoglobulin and of its complex with retinol at 2.5 a resolution. *Journal of Molecular Biology*, 197(4):695–706.

[Monahan et al., 2014] Monahan, L. G., Liew, A. T. F., Bottomley, A. L., and Harry, E. J. (2014). Division site positioning in bacteria: one size does not fit all. *Frontiers in Microbiology*, 5:19.

[Montroll and Simha, 1940] Montroll, E. W. and Simha, R. (1940). Theory of Depolymerization of Long Chain Molecules. *The Journal of Chemical Physics*, 8(9):721–726.

[Morelli, 2007] Morelli, L. (2007). In vitro assessment of probiotic bacteria: From survival to functionality. *International Dairy Journal*, 17(11):1278–1283.

[Morra and Cassinelli, 1996] Morra, M. and Cassinelli, C. (1996). Staphylococcus epidermidis adhesion to films deposited from hydroxyethylmethacrylate plasma. *Journal of Biomedical Materials Research*, 31(2):149–155.

[Morra and Cassinelli, 1998] Morra, M. and Cassinelli, C. (1998). Bacterial adhesion to polymer surfaces: A critical review of surface thermodynamic approaches. *Journal of Biomaterials Science, Polymer Edition*, 9(1):55–74.

[Mortazavian et al., 2010] Mortazavian, A. M., Khosrokhavar, R., Rastegar, H., and Mortazaei, G. R. (2010). Effects of dry matter standardization order on biochemical and microbiological characteristics of freshly made probiotic doogh (iranian fermented milk drink). *Italian Journal of Food Science*, 22(1):98–104.

[Mortazavian et al., 2012] Mortazavian, A. M., Mohammadi, R., and Sohrabvandi, S. (2012). *Delivery of probiotic microorganisms into gastrointestinal tract by food products.* INTECH Open Access Publisher.

[Mukai et al., 2002] Mukai, T., Asasaka, T., Sato, E., Mori, K., Matsumoto, M., and Ohori, H. (2002). Inhibition of binding of Helicobacter pylori to the glycolipid receptors by probiotic Lactobacillus reuteri. *FEMS immunology and medical microbiology*, 32(2):105–110.

[Muliawan and Hatzikiriakos, 2007] Muliawan, E. B. and Hatzikiriakos, S. G. (2007). Rheology of mozzarella cheese. *International Dairy Journal*, 17(9):1063–1072.

[Muller et al., 2010] Muller, J., Stanton, C., Sybesma, W., Fitzgerald, G., and Ross, R. (2010). Reconstitution conditions for dried probiotic powders represent a critical step in determining cell viability. *Journal of Applied Microbiology*, 108(4):1369–1379.

[Munoz et al., 2011] Munoz, R., Yarza, P., Ludwig, W., Euzéby, J., Amann, R., Schleifer, K.-H., Oliver Glöckner, F., and Rosselló-Móra, R. (2011). Release LTPs104 of the all-species living tree. *Systematic and Applied Microbiology*, 34(3):169–170.

[Muthukumarappan and Swamy, 2017] Muthukumarappan, K. and Swamy, G. J. (2017). Chapter 10 - rheology, microstructure, and functionality of cheese. In Ahmed, J., Ptaszek, P., and Basu, S., editors, *Advances in Food Rheology and Its Applications*, Woodhead Publishing Series in Food Science, Technology and Nutrition, pages 245–276. Woodhead Publishing.

[Muzzio et al., 2017] Muzzio, N. E., Pasquale, M. A., Diamanti, E., Gregurec, D., Moro, M. M., Azzaroni, O., and Moya, S. E. (2017). Enhanced antiadhesive properties of chitosan/hyaluronic acid polyelectrolyte multilayers driven by thermal annealing: Low adherence for mammalian cells and selective decrease in adhesion for gram-positive bacteria. *Materials Science and Engineering: C*, 80:677–687.

[Muñoz-Provencio et al., 2009] Muñoz-Provencio, D., Llopis, M., Antolín, M., Torres, I. d., Guarner, F., Pérez-Martínez, G., and Monedero, V. (2009). Adhesion properties of lactobacillus casei strains to resected intestinal fragments and components of the extracellular matrix. *Archives of Microbiology*, 191(2):153–161.

[Möller et al., 2013] Möller, J., Emge, P., Vizcarra, I. A., Kollmannsberger, P., and Vogel, V. (2013). Bacterial filamentation accelerates colonization of adhesive spots embedded in biopassive surfaces. *New Journal of Physics*, 15(12):125016.

[Møller et al., 2013] Møller, S. M., Bertram, H. C., Andersen, U., Lillevang, S. K., Rasmussen, A., and Hansen, T. B. (2013). Physical sample structure as predictive factor in growth modeling of Listeria innocua in a white cheese model system. *Food Microbiology*, 36(1):90–102.

[Nagara et al., 2017] Nagara, Y., Takada, T., Nagata, Y., Kado, S., and Kushiro, A. (2017). Microscale spatial analysis provides evidence for adhesive monopolization of dietary nutrients by specific intestinal bacteria. *PLOS ONE*, 12(4):e0175497.

[Navarre and Schneewind, 1999] Navarre, W. W. and Schneewind, O. (1999). Surface proteins of gram-positive bacteria and mechanisms of their targeting to the cell wall envelope. *Microbiology and molecular biology reviews: MMBR*, 63(1):174–229.

[Nghe et al., 2010] Nghe, P., Tabeling, P., and Ajdari, A. (2010). Flow-induced polymer degradation probed by a high throughput microfluidic set-up. *Journal of Non-Newtonian Fluid Mechanics*, 165(7-8):313–322.

[Niki et al., 2000] Niki, R., Motoshima, H., and Tsukasaki, F. (2000). Viscoelastic properties of acid-induced milk gel at different gelation temperatures. In Nishinari, K., editor, *Hydrocolloids*, pages 447–451. Elsevier Science, Amsterdam.

[Ningtyas et al., 2018] Ningtyas, D. W., Bhandari, B., Bansal, N., and Prakash, S. (2018). Effect of homogenisation of cheese milk and high-shear mixing of the curd during cream cheese manufacture. *International Journal of Dairy Technology*, 71(2):417–431.

[Nishiyama et al., 2013] Nishiyama, K., Ochiai, A., Tsubokawa, D., Ishihara, K., Yamamoto, Y., and Mukai, T. (2013). Identification and characterization of sulfated carbohydrate-binding protein from Lactobacillus reuteri. *PloS One*, 8(12):e83703.

[Nishiyama et al., 2016] Nishiyama, K., Sugiyama, M., and Mukai, T. (2016). Adhesion Properties of Lactic Acid Bacteria on Intestinal Mucin. *Microorganisms*, 4(3).

[Notermans et al., 1991] Notermans, S., Dormans, J. A. M. A., and Mead, G. C. (1991). Contribution of surface attachment to the establishment of micro-organisms in food processing plants: A review. *Biofouling*, 5(1):21–36.

[Nualkaekul et al., 2012] Nualkaekul, S., Deepika, G., and Charalampopoulos, D. (2012). Survival of freeze dried lactobacillus plantarum in instant fruit powders and reconstituted fruit juices. *Food Research International*, 48(2):627–633.

[Oberg et al., 1993] Oberg, C. J., McManus, W. R., and McMahon, D. J. (1993). Microstructure of mozzarella cheese during manufacture. *Food structure*, 12(2):12.

[O'Connell, 2003] O'Connell, D. (2003). Dock, lock and latch. *Nature Reviews Microbiology*, 1(3):171.

[Okochi et al., 2017] Okochi, M., Sugita, T., Asai, Y., Tanaka, M., and Honda, H. (2017). Screening of peptides associated with adhesion and aggregation of lactobacillus rhamnosus GG in vitro. *Biochemical Engineering Journal*, 128:178–185.

[Omar et al., 1995] Omar, Z. B., Raphaelides, S., and Kesteloot, R. (1995). Texture evaluation of french acid-type fresh cheeses. *Journal of Texture Studies*, 26(3):325–338.

[Ong and Shah, 2009] Ong, L. and Shah, N. P. (2009). Probiotic cheddar cheese: Influence of ripening temperatures on survival of probiotic microorganisms, cheese composition and organic acid profiles. *LWT - Food Science and Technology*, 42(7):1260–1268.

[Ong et al., 1999] Ong, Y.-L., Razatos, A., Georgiou, G., and Sharma, M. M. (1999). Adhesion forces between e. coli bacteria and biomaterial surfaces. *Langmuir*, 15(8):2719–2725.

[Onogi, 1970] Onogi, S. (1970). *Proceedings Of The Fifth International Congress On Rheology*, volume 4. University of Tokyo Press and University of Park Press, Tokyo, Japan and Baltimore, Maryland, and Manchester, England, university of tokyo press edition.

[Ouwehand et al., 2001] Ouwehand, A. C., Tuomola, E. M., Tölkkö, S., and Salminen, S. (2001). Assessment of adhesion properties of novel probiotic strains to human intestinal mucus. *International Journal of Food Microbiology*, 64(1):119–126.

[Pabst and Gregorová, 2007] Pabst, W. and Gregorová, E. (2007). Characterization of particles and particle systems. Technical report, Institute of Chemical Technology, Prague, Czech Republic.

[Palumbo et al., 2006] Palumbo, E., Deghorain, M., Cocconcelli, P. S., Kleerebezem, M., Geyer, A., Hartung, T., Morath, S., and Hols, P. (2006). d-Alanyl Ester Depletion of Teichoic Acids in Lactobacillus plantarum Results in a Major Modification of Lipoteichoic Acid Composition and Cell Wall Perforations at the Septum Mediated by the Acm2 Autolysin. *Journal of Bacteriology*, 188(10):3709–3715.

[Pandey et al., 2015] Pandey, K. R., Naik, S. R., and Vakil, B. V. (2015). Probiotics, prebiotics and synbiotics- a review. *Journal of Food Science and Technology*, 52(12):7577–7587.

[Pappelbaum Karin I. et al., 2013] Pappelbaum Karin I., Gorzelanny Christian, Grässle Sandra, Suckau Jan, Laschke Matthias W., Bischoff Markus, Bauer Corinne, Schorpp-Kistner Marina, Weidenmaier Christopher, Schneppenheim Reinhard, Obser Tobias, Sinha Bhanu, and Schneider Stefan W. (2013). Ultralarge von willebrand factor fibers mediate luminal staphylococcus aureus adhesion to an intact endothelial cell layer under shear stress. *Circulation*, 128(1):50–59.

[Pasqualin Cavalheiro et al., 2015] Pasqualin Cavalheiro, C., Ruiz-Capillas, C., Herrero, A. M., Jiménez-Colmenero, F., Ragagnin de Menezes, C., and Martins Fries, L. L. (2015). Application of probiotic delivery systems in meat products. *Trends in Food Science & Technology*, 46(1):120–131.

[Patel et al., 2016] Patel, D. K., Shah, K. R., Pappachan, A., Gupta, S., and Singh, D. D. (2016). Cloning, expression and characterization of a mucin-binding GAPDH from Lactobacillus acidophilus. *International Journal of Biological Macromolecules*, 91:338–346.

[Patrício et al., 2014] Patrício, P., Almeida, P. L., Portela, R., Sobral, R. G., Grilo, I. R., Cidade, T., and Leal, C. R. (2014). Living bacteria rheology: Population growth, aggregation patterns, and collective behavior under different shear flows. *Physical Review E*, 90(2):022720.

[Patton et al., 2006] Patton, T., Barrett, J., Brennan, J., and Moran, N. (2006). Use of a spectrophotometric bioassay for determination of microbial sensitivity to manuka honey. *Journal of Microbiological Methods*, 64(1):84–95.

[Paturej et al., 2011] Paturej, J., Milchev, A., Rostiashvili, V. G., and Vilgis, T. A. (2011). Polymer chain scission at constant tension —An example of force-induced collective behaviour. *EPL (Europhysics Letters)*, 94(4):48003.

[Paéz et al., 2012] Paéz, R., Lavari, L., Vinderola, G., Audero, G., Cuatrin, A., Zaritzky, N., and Reinheimer, J. (2012). Effect of heat treatment and spray drying on lactobacilli viability and resistance to simulated gastrointestinal digestion. *Food Research International*, 48(2):748–754.

[Pedersen et al., 2012] Pedersen, M. B., Gaudu, P., Lechardeur, D., Petit, M.-A., and Gruss, A. (2012). Aerobic respiration metabolism in lactic acid bacteria and uses in biotechnology. *Annual Review of Food Science and Technology*, 3:37–58.

[Persat et al., 2015] Persat, A., Nadell, C. D., Kim, M. K., Ingremeau, F., Siryaporn, A., Drescher, K., Wingreen, N. S., Bassler, B. L., Gitai, Z., and Stone, H. A. (2015). The mechanical world of bacteria. *Cell*, 161(5):988–997.

[Piacentini, 2014] Piacentini, E. (2014). Droplet Size. In Drioli, E. and Giorno, L., editors, *Encyclopedia of Membranes*, pages 1–2. Springer Berlin Heidelberg, Berlin, Heidelberg.

[Piette and Idziak, 1989] Piette, J. P. and Idziak, E. S. (1989). New method to study bacterial adhesion to meat. *Applied and Environmental Microbiology*, 55(6):1531–1536.

[Pike et al., 1996] Pike, A. C., Brew, K., and Acharya, K. R. (1996). Crystal structures of guinea-pig, goat and bovine alpha-lactalbumin highlight the enhanced conformational flexibility of regions that are significant for its action in lactose synthase. *Structure*, 4(6):691–703.

[Pizarro-Cerdá and Cossart, 2006] Pizarro-Cerdá, J. and Cossart, P. (2006). Bacterial adhesion and entry into host cells. *Cell*, 124(4):715–727.

[Pokusaeva et al., 2011] Pokusaeva, K., Fitzgerald, G. F., and van Sinderen, D. (2011). Carbohydrate metabolism in bifidobacteria. *Genes & Nutrition*, 6(3):285–306.

[Ponnuraj et al., 2003] Ponnuraj, K., Bowden, M. G., Davis, S., Gurusiddappa, S., Moore, D., Choe, D., Xu, Y., Hook, M., and Narayana, S. V. (2003). A "dock, lock, and latch" structural model for a staphylococcal adhesin binding to fibrinogen. *Cell*, 115(2):217–228.

[Pontefract, 1991] Pontefract, R. D. (1991). Bacterial adherence: Its consequences in food processing. *Canadian Institute of Food Science and Technology Journal*, 24(3):113–117.

[Poortinga et al., 2002] Poortinga, A. T., Bos, R., Norde, W., and Busscher, H. J. (2002). Electric double layer interactions in bacterial adhesion to surfaces. *Surface Science Reports*, 47(1):1–32.

[Posch et al., 1999] Posch, T., Šimek, K., Vrba, J., J, P., Nedoma, J., Sattler, B., B, S., and Psenner, R. (1999). Predator-induced changes of bacterial size-structure and productivity studied on an experimental microbial community. *Aquatic Microbial Ecology*, 18:235–246.

[Possemiers et al., 2010] Possemiers, S., Marzorati, M., Verstraete, W., and Van de Wiele, T. (2010). Bacteria and chocolate: A successful combination for probiotic delivery. *International Journal of Food Microbiology*, 141(1):97–103.

[Pot, 2007] Pot, B. (2007). The taxonomy of lactic acid bacteria. In *Bactéries lactiques: de la génétique aux ferments*, Collections Sciences et Techniques Agroalimentaires, pages 1–152. Corrieu, Georges, Luquet, François-Marie, lavoisier, france / tec et doc edition.

[Pouzot et al., 2006] Pouzot, M., Nicolai, T., Benyahia, L., and Durand, D. (2006). Strain hardening and fracture of heat-set fractal globular protein gels. *Journal of Colloid and Interface Science*, 293(2):376–383.

[Pretzer et al., 2005] Pretzer, G., Snel, J., Molenaar, D., Wiersma, A., Bron, P. A., Lambert, J., Vos, W. M. d., Meer, R. v. d., Smits, M. A., and Kleerebezem, M. (2005). Biodiversity-Based Identification and Functional Characterization of the Mannose-Specific Adhesin of Lactobacillus plantarum. *Journal of Bacteriology*, 187(17):6128–6136.

[Previc, 1970] Previc, E. P. (1970). Biochemical determination of bacterial morphology and the geometry of cell division. *Journal of Theoretical Biology*, 27(3):471–497.

[Proft and Baker, 2009] Proft, T. and Baker, E. N. (2009). Pili in gram-negative and gram-positive bacteria — structure, assembly and their role in disease. *Cellular and Molecular Life Sciences*, 66(4):613.

[Pönisch et al., 2017] Pönisch, W., Weber, C. A., Juckeland, G., Biais, N., and Zaburdaev, V. (2017). Multiscale modeling of bacterial colonies: how pili mediate the dynamics of single cells and cellular aggregates. *New Journal of Physics*, 19(1):015003.

[Qi and Onwulata, 2011a] Qi, P. X. and Onwulata, C. I. (2011a). Physical properties, molecular structures, and protein quality of texturized whey protein isolate: Effect of extrusion moisture content. *Journal of Dairy Science*, 94(5):2231–2244.

[Qi and Onwulata, 2011b] Qi, P. X. and Onwulata, C. I. (2011b). Physical Properties, Molecular Structures, and Protein Quality of Texturized Whey Protein Isolate: Effect of Extrusion Temperature. *Journal of Agricultural and Food Chemistry*, 59(9):4668–4675.

[Quemada, 1998] Quemada, D. (1998). Rheological modelling of complex fluids: II. Shear thickening behavior due to shear induced flocculation. *The European Physical Journal Applied Physics*, 2(2):175–181.

[Quinto et al., 2014] Quinto, E. J., Jiménez, P., Caro, I., Tejero, J., Mateo, J., and Girbés, T. (2014). Probiotic lactic acid bacteria: A review. *Food and Nutrition Sciences*, 05(18):1765–1775.

[Quirynen and Bollen, 1995] Quirynen, M. and Bollen, C. M. (1995). The influence of surface roughness and surface-free energy on supra- and subgingival plaque formation in man. A review of the literature. *Journal of Clinical Periodontology*, 22(1):1–14.

[Radziwill-Bienkowska et al., 2016] Radziwill-Bienkowska, J. M., Le, D. T. L., Szczesny, P., Duviau, M.-P., Aleksandrzak-Piekarczyk, T., Loubière, P., Mercier-Bonin, M., Bardowski, J. K., and Kowalczyk, M. (2016). Adhesion of the genome-sequenced lactococcus lactis subsp. cremoris IBB477 strain is mediated by specific molecular determinants. *Applied Microbiology and Biotechnology*, 100(22):9605–9617.

[Ranadheera et al., 2012] Ranadheera, C. S., Evans, C. A., Adams, M. C., and Baines, S. K. (2012). In vitro analysis of gastrointestinal tolerance and intestinal cell adhesion of probiotics in goat's milk ice cream and yogurt. *Food Research International*, 49(2):619–625.

[Ranadheera et al., 2010] Ranadheera, R., Baines, S., and Adams, M. (2010). Importance of food in probiotic efficacy. *Food Research International*, 43(1):1–7.

[Rangel et al., 2013] Rangel, D. E., Marín-Medina, N., Castro, J. E., González-Mancera, A., and Forero-Shelton, M. (2013). Observation of bacterial type i pili extension and contraction under fluid flow. *PLOS ONE*, 8(6):e65563.

[Rathore et al., 2012] Rathore, S., Salmerón, I., and Pandiella, S. S. (2012). Production of potentially probiotic beverages using single and mixed cereal substrates fermented with lactic acid bacteria cultures. *Food Microbiology*, 30(1):239–244.

[Rawle, 2003] Rawle, A. (2003). Basic Principles of Particle Size Analysis. *Surface Coatings International Part A: Coatings Journal*, 86(2):58–65.

[Reichmann and Gründling, 2011] Reichmann, N. T. and Gründling, A. (2011). Location, synthesis and function of glycolipids and polyglycerolphosphate lipoteichoic acid in Gram-positive bacteria of the phylum Firmicutes. *FEMS microbiology letters*, 319(2):97–105.

[Reunanen et al., 2012] Reunanen, J., Ossowski, I. v., Hendrickx, A. P. A., Palva, A., and Vos, W. M. d. (2012). Characterization of the SpaCBA pilus fibers in the probiotic lactobacillus rhamnosus GG. *Appl. Environ. Microbiol.*, 78(7):2337–2344.

[Riccio, 2004] Riccio, P. (2004). The proteins of the milk fat globule membrane in the balance. *Trends in Food Science & Technology*, 15:458–461.

[Rintahaka et al., 2014] Rintahaka, J., Yu, X., Kant, R., Palva, A., and von Ossowski, I. (2014). Phenotypical analysis of the Lactobacillus rhamnosus GG fimbrial spaFED operon: surface expression and functional characterization of recombinant SpaFED pili in Lactococcus lactis. *PloS One*, 9(11):e113922.

[Riveros et al., 2009] Riveros, B., Ferrer, J., and Bórquez, R. (2009). Spray drying of a vaginal probiotic strain of lactobacillus acidophilus. *Drying Technology*, 27(1):123–132.

[Robert and Sherman, 1988] Robert, F. and Sherman, P. (1988). The influence of surface friction on the calculation of stress relaxation parameters for processed cheese. *Rheologica Acta*, 27(2):212–215.

[Rodgers, 2007] Rodgers, S. (2007). Incorporation of probiotic cultures in foodservice products: an exploratory study. *Journal of Foodservice*, 18(3):108–118.

[Rohm et al., 2014] Rohm, H., Ullrich, F., Schmidt, C., Löbner, J., and Jaros, D. (2014). Gelation of cross-linked casein under small and large shear strain. *Journal of Texture Studies*, 45(2):130–137.

[Romeih et al., 2012] Romeih, E. A., Moe, K. M., and Skeie, S. (2012). The influence of fat globule membrane material on the microstructure of low-fat cheddar cheese. *International Dairy Journal*, 26(1):66–72.

[Roos and Jonsson, 2002] Roos, S. and Jonsson, H. (2002). A high-molecular-mass cell-surface protein from lactobacillus reuteri 1063 adheres to mucus components. *Microbiology (Reading, England)*, 148:433–442.

[Rosenberg and Doyle, 1990] Rosenberg, M. and Doyle, R. J. (1990). *Microbial Cell-Surface Hydrophobicity*. American Society for Microbiology.

[Rosenberger et al., 1978] Rosenberger, R. F., Grover, N. B., Zaritsky, A., and Woldringh, C. L. (1978). Surface growth in rod-shaped bacteria. *Journal of Theoretical Biology*, 73(4):711–721.

[Rosendale et al., 2008] Rosendale, D. I., Maddox, I. S., Miles, M. C., Rodier, M., Skinner, M., and Sutherland, J. (2008). High-throughput microbial bioassays to screen potential new zealand functional food ingredients intended to manage the growth of probiotic and pathogenic gut bacteria. *International Journal of Food Science & Technology*, 43(12):2257–2267.

[Roszak and Colwell, 1987] Roszak, D. B. and Colwell, R. R. (1987). Survival strategies of bacteria in the natural environment. *Microbiological Reviews*, 51(3):365–379.

[Ruas-Madiedo et al., 2002] Ruas-Madiedo, P., Hugenholtz, J., and Zoon, P. (2002). An overview of the functionality of exopolysaccharides produced by lactic acid bacteria. *International Dairy Journal*, 12(2):163–171.

[Russell and Diez-Gonzalez, 1997] Russell, J. B. and Diez-Gonzalez, F. (1997). The effects of fermentation acids on bacterial growth. *Advances in Microbial Physiology*, 39:205–234.

[Russo et al., 2014] Russo, P., de Chiara, M. L. V., Vernile, A., Amodio, M. L., Arena, M. P., Capozzi, V., Massa, S., and Spano, G. (2014). Fresh-cut pineapple as a new carrier of probiotic lactic acid bacteria. *BioMed Research International*, 2014:e309183.

[Russo et al., 2015] Russo, P., Peña, N., de Chiara, M. L. V., Amodio, M. L., Colelli, G., and Spano, G. (2015). Probiotic lactic acid bacteria for the production of multifunctional fresh-cut cantaloupe. *Food Research International*, 77, Part 4:762–772.

[Rutter and Vincent, 1984] Rutter, P. R. and Vincent, B. (1984). Physicochemical Interactions of the Substratum, Microorganisms, and the Fluid Phase. In Marshall, K. C., editor, *Microbial Adhesion and Aggregation*, Life Sciences Research Reports, pages 21–38, Berlin, Heidelberg. Springer.

[Rößle et al., 2010] Rößle, C., Auty, M. A., Brunton, N., Gormley, R. T., and Butler, F. (2010). Evaluation of fresh-cut apple slices enriched with probiotic bacteria. *Innovative Food Science & Emerging Technologies*, 11(1):203–209.

[Saarela et al., 2006a] Saarela, M., Virkajärvi, I., Alakomi, H.-L., Sigvart-Mattila, P., and Mättö, J. (2006a). Stability and functionality of freeze-dried probiotic bifidobacterium cells during storage in juice and milk. *International Dairy Journal*, 16(12):1477–1482.

[Saarela et al., 2006b] Saarela, M., Virkajärvi, I., Nohynek, L., Vaari, A., and Mättö, J. (2006b). Fibres as carriers for lactobacillus rhamnosus during freeze-drying and storage in apple juice and chocolate-coated breakfast cereals. *International Journal of Food Microbiology*, 112(2):171–178.

[Sachdeva and Buchheim, 1997] Sachdeva, S. and Buchheim, W. (1997). Recovery of phospholipids from buttermilk using membrane processing. *Recovery of phospholipids from buttermilk using membrane processing*, 49(1):47–68.

[Salaün et al., 2005] Salaün, F., Mietton, B., and Gaucheron, F. (2005). Buffering capacity of dairy products. *International Dairy Journal*, 15(2):95–109.

[Samaey et al., 2011] Samaey, G., Lelièvre, T., and Legat, V. (2011). A numerical closure approach for kinetic models of polymeric fluids: Exploring closure relations for FENE dumbbells. *Computers & Fluids*, 43(1):119–133.

[Sanders et al., 2014] Sanders, M. E., Klaenhammer, T. R., Ouwehand, A. C., Pot, B., Johansen, E., Heimbach, J. T., Marco, M. L., Tennilä, J., Ross, R. P., Franz, C., Pagé, N., Pridmore, R. D., Leyer, G., Salminen, S., Charbonneau, D., Call, E., and Lenoir-Wijnkoop, I. (2014). Effects of genetic, processing, or product formulation changes on efficacy and safety of probiotics. *Annals of the New York Academy of Sciences*, 1309(1):1–18.

[Sanders and Marco, 2010] Sanders, M. E. and Marco, M. L. (2010). Food formats for effective delivery of probiotics. *Annual Review of Food Science and Technology*, 1(1):65–85.

[Santhanalakshmi and Balaji, 2001] Santhanalakshmi, J. and Balaji, S. (2001). Binding studies of crystal violet on proteins. *Colloids and Surfaces A: Physicochemical and Engineering Aspects*, 186(3):173–177.

[Santivarangkna et al., 2007] Santivarangkna, C., Kulozik, U., and Foerst, P. (2007). Alternative drying processes for the industrial preservation of lactic acid starter cultures. *Biotechnology Progress*, 23(2):302–315.

[Santivarangkna et al., 2008] Santivarangkna, C., Kulozik, U., and Foerst, P. (2008). Inactivation mechanisms of lactic acid starter cultures preserved by drying processes. *Journal of Applied Microbiology*, 105(1):1–13.

[Sato et al., 2017] Sato, T., Takase, K., and Taniguchi, T. (2017). Multiscale Simulation of Polymer Melt Spinning by Using the Dumbbell Model. *Nihon Reoroji Gakkaishi*, 44(5):265–280.

[Saxelin et al., 2003] Saxelin, M., Korpela, R., and Mäyrä-Mäkinen, A. (2003). 1 - introduction: classifying functional dairy products. In *Functional Dairy Products*, Woodhead Publishing Series in Food Science, Technology and Nutrition, pages 1–16. Woodhead Publishing.

[Saxelin et al., 2010] Saxelin, M., Lassig, A., Karjalainen, H., Tynkkynen, S., Surakka, A., Vapaatalo, H., Järvenpää, S., Korpela, R., Mutanen, M., and Hatakka, K. (2010). Persistence of probiotic strains in the gastrointestinal tract when administered as capsules, yoghurt, or cheese. *International Journal of Food Microbiology*, 144(2):293–300.

[Schieber, 1991] Schieber, J. D. (1991). A Hookean dumbbell model with Basset forces for dilute polymer solutions. *The Journal of Chemical Physics*, 94(11):7526–7533.

[Schieber, 1993] Schieber, J. D. (1993). Internal viscosity dumbbell model with a Gaussian approximation. *Journal of Rheology*, 37(6):1003–1027.

[Schmidt, 1982] Schmidt, D. G. (1982). Association of caseins and casein micelle structure. *Developments in dairy chemistry*.

[Schneewind and Missiakas, 2014a] Schneewind, O. and Missiakas, D. (2014a). Lipoteichoic Acids, Phosphate-Containing Polymers in the Envelope of Gram-Positive Bacteria. *Journal of Bacteriology*, 196(6):1133–1142.

[Schneewind and Missiakas, 2014b] Schneewind, O. and Missiakas, D. (2014b). Sec-secretion and sortase-mediated anchoring of proteins in gram-positive bacteria. *Biochimica Et Biophysica Acta*, 1843(8):1687–1697.

[Scholler et al., 2008] Scholler, N., Gross, J. A., Garvik, B., Wells, L., Liu, Y., Loch, C. M., Ramirez, A. B., McIntosh, M. W., Lampe, P. D., and Urban, N. (2008). Use of cancer-specific yeast-secreted in vivo biotinylated recombinant antibodies for serum biomarker discovery. *Journal of Translational Medicine*, 6:41.

[Scott and Zähner, 2006] Scott, J. R. and Zähner, D. (2006). Pili with strong attachments: Gram-positive bacteria do it differently. *Molecular Microbiology*, 62(2):320–330.

[Segers and Lebeer, 2014] Segers, M. E. and Lebeer, S. (2014). Towards a better understanding of lactobacillus rhamnosus GG - host interactions. *Microbial Cell Factories*, 13(1):S7.

[Servin and Coconnier, 2003] Servin, A. L. and Coconnier, M.-H. (2003). Adhesion of probiotic strains to the intestinal mucosa and interaction with pathogens. *Best Practice & Research Clinical Gastroenterology*, 17(5):741–754.

[Sharma et al., 1980] Sharma, H. S., Bassette, R., Mehta, R. S., and Dayton, A. D. (1980). Yield and Curd Characteristics of Cottage Cheese Made by the Culture and Direct-Acid-Set Methods. *Journal of Food Protection*, 43(6):441–446.

[Sharma et al., 2016a] Sharma, P., Munro, P. A., Dessev, T. T., and Wiles, P. G. (2016a). Shear work induced changes in the viscoelastic properties of model mozzarella cheese. *International Dairy Journal*, 56:108–118.

[Sharma et al., 2016b] Sharma, P., Munro, P. A., Dessev, T. T., Wiles, P. G., and Buwalda, R. J. (2016b). Effect of shear work input on steady shear rheology and melt functionality of model mozzarella cheeses. *Food Hydrocolloids*, 54:266–277.

[Sharma et al., 2018] Sharma, P., Munro, P. A., Dessev, T. T., Wiles, P. G., and Foegeding, E. A. (2018). Strain hardening and anisotropy in tensile fracture properties of sheared model mozzarella cheeses. *Journal of Dairy Science*, 101(1):123–134.

[Sharma et al., 2017] Sharma, P., Munro, P. A., Gillies, G., Wiles, P. G., and Dessev, T. T. (2017). Changes in creep behavior and microstructure of model mozzarella cheese during working. *LWT - Food Science and Technology*, 83:184–192.

[Sharma and Cherayil, 2011] Sharma, R. and Cherayil, B. J. (2011). Work fluctuations in an elastic dumbbell model of polymers in planar elongational flow. *Physical Review E*, 83(4):041805.

[Sharp et al., 2008] Sharp, M., McMahon, D., and Broadbent, J. (2008). Comparative evaluation of yogurt and low-fat cheddar cheese as delivery media for probiotic lactobacillus casei. *Journal of Food Science*, 73(7):M375–M377.

[Sheehan et al., 2007] Sheehan, V. M., Ross, P., and Fitzgerald, G. F. (2007). Assessing the acid tolerance and the technological robustness of probiotic cultures for fortification in fruit juices. *Innovative Food Science & Emerging Technologies*, 8(2):279–284.

[Shikano et al., 1990] Shikano, S., Luckinbill, L. S., and Kurihara, Y. (1990). Changes of traits in a bacterial population associated with protozoal predation. *Microbial Ecology*, 20(1):75–84.

[Shimaoka et al., 2001] Shimaoka, T., Kume, N., Minami, M., Hayashida, K., Sawamura, T., Kita, T., and Yonehara, S. (2001). LOX-1 supports adhesion of gram-positive and gram-negative bacteria. *The Journal of Immunology*, 166(8):5108–5114.

[Shori, 2015] Shori, A. B. (2015). The potential applications of probiotics on dairy and non-dairy foods focusing on viability during storage. *Biocatalysis and Agricultural Biotechnology*, 4(4):423–431.

[Shori, 2016] Shori, A. B. (2016). Influence of food matrix on the viability of probiotic bacteria: A review based on dairy and non-dairy beverages. *Food Bioscience*, 13:1–8.

[Sieuwerts et al., 2008] Sieuwerts, S., Bok, F. A. M. d., Hugenholtz, J., and Vlieg, J. E. T. v. H. (2008). Unraveling microbial interactions in food fermentations: from classical to genomics approaches. *Applied and Environmental Microbiology*, 74(16):4997.

[Signoretto et al., 2012] Signoretto, C., Canepari, P., Stauder, M., Vezzulli, L., and Pruzzo, C. (2012). Functional foods and strategies contrasting bacterial adhesion. *Current Opinion in Biotechnology*, 23(2):160–167.

[Singh et al., 2015] Singh, H., Ye, A., and Ferrua, M. J. (2015). Aspects of food structures in the digestive tract. *Current Opinion in Food Science*, 3:85–93.

[Sjöstrand, 1988] Sjöstrand, T. (1988). Status of fragmentation models. *International Journal of Modern Physics A*, 03(04):751–823.

[Sleytr and Beveridge, 1999] Sleytr, U. B. and Beveridge, T. J. (1999). Bacterial S-layers. *Trends in Microbiology*, 7(6):253–260.

[Smith, 1998] Smith, D. A. (1998). Direct Tests of Muscle Cross-Bridge Theories: Predictions of a Brownian Dumbbell Model for Position-Dependent Cross-Bridge Lifetimes and Step Sizes with an Optically Trapped Actin Filament. *Biophysical Journal*, 75(6):2996–3007.

[Smithers et al., 1996] Smithers, G. W., John Ballard, F., Copeland, A. D., de Silva, K. J., Dionysius, D. A., Francis, G. L., Goddard, C., Grieve, P. A., McIntosh, G. H., Mitchell, I. R., Pearce, R. J., and Regester, G. O. (1996). New Opportunities from the Isolation and Utilization of Whey Proteins. *Journal of Dairy Science*, 79(8):1454–1459.

[Sonomoto and Yokota, 2011] Sonomoto, K. and Yokota, A. (2011). *Lactic Acid Bacteria and Bifidobacteria: Current Progress in Advanced Research*. Horizon Scientific Press.

[Stack et al., 2010] Stack, H. M., Kearney, N., Stanton, C., Fitzgerald, G. F., and Ross, R. P. (2010). Association of beta-glucan endogenous production with increased stress tolerance of intestinal lactobacilli. *Applied and Environmental Microbiology*, 76(2):500–507.

[Stackebrandt and Teuber, 1988] Stackebrandt, E. and Teuber, M. (1988). Molecular taxonomy and phylogenetic position of lactic acid bacteria. *Biochimie*, 70(3):317–324.

[Stadler et al., 2011] Stadler, F. J., Rajan, M., Agarwal, U. S., Liu, C.-Y., George, K. E., Lemstra, P. J., and Bailly, C. (2011). Rheological characterization in shear of a model dumbbell polymer concentrated solution. *Rheologica Acta*, 50(5):491.

[Steinitz, 2000] Steinitz, M. (2000). Quantitation of the blocking effect of tween 20 and bovine serum albumin in ELISA microwells. *Analytical Biochemistry*, 282(2):232–238.

[Stickel et al., 2006] Stickel, J. J., Phillips, R. J., and Powell, R. L. (2006). A constitutive model for microstructure and total stress in particulate suspensions. *Journal of Rheology*, 50(4):379–413.

[Stiles and Holzapfel, 1997] Stiles, M. E. and Holzapfel, W. H. (1997). Lactic acid bacteria of foods and their current taxonomy. *International Journal of Food Microbiology*, 36(1):1–29.

[Sullan et al., 2013] Sullan, R. M. A., Beaussart, A., Tripathi, P., Derclaye, S., El-Kirat-Chatel, S., Li, J. K., Schneider, Y.-J., Vanderleyden, J., Lebeer, S., and Dufrêne, Y. F. (2013). Single-cell force spectroscopy of pili-mediated adhesion. *Nanoscale*, 6(2):1134–1143.

[Sun and Wu, 2017] Sun, X. and Wu, J. (2017). Food derived anti-adhesive components against bacterial adhesion: Current progresses and future perspectives. *Trends in Food Science & Technology*, 69:148–156.

[Sun et al., 2015] Sun, Z., Harris, H. M. B., McCann, A., Guo, C., Argimón, S., Zhang, W., Yang, X., Jeffery, I. B., Cooney, J. C., Kagawa, T. F., Liu, W., Song, Y., Salvetti, E., Wrobel, A., Rasinkangas, P., Parkhill, J., Rea, M. C., O'Sullivan, O., Ritari, J., Douillard, F. P., Paul Ross, R., Yang, R., Briner, A. E., Felis, G. E., de Vos, W. M., Barrangou, R., Klaenhammer, T. R., Caufield, P. W., Cui, Y., Zhang, H., and O'Toole, P. W. (2015). Expanding the biotechnology potential of lactobacilli through comparative genomics of 213 strains and associated genera. *Nature Communications*, 6:8322.

[Surber et al., 2019] Surber, G., Jaros, D., and Rohm, H. (2019). Shear and extensional rheology of acid milk gel suspensions with varying ropiness. *Journal of Texture Studies*, 1:1–9.

[Takamura et al., 1981] Takamura, K., Adler, P., Goldsmith, H., and Mason, S. G. (1981). Particle motions in sheared suspensions. *Journal of Colloid and Interface Science*, 81(2):516–530.

[Talà et al., 2019] Talà, L., Fineberg, A., Kukura, P., and Persat, A. (2019). Pseudomonas aeruginosa orchestrates twitching motility by sequential control of type IV pili movements. *Nature Microbiology*, page 1.

[Tarazanova et al., 2017] Tarazanova, M., Huppertz, T., Beerthuyzen, M., van Schalkwijk, S., Janssen, P., Wels, M., Kok, J., and Bachmann, H. (2017). Cell surface properties of lactococcus lactis reveal milk protein binding specifically evolved in dairy isolates. *Frontiers in Microbiology*, 8:1691.

[Tarazanova et al., 2018a] Tarazanova, M., Huppertz, T., Kok, J., and Bachmann, H. (2018a). Altering textural properties of fermented milk by using surface-engineered lactococcus lactis. *Microbial Biotechnology*, 11(4):770–780.

[Tarazanova et al., 2018b] Tarazanova, M., Huppertz, T., Kok, J., and Bachmann, H. (2018b). Influence of lactococcal surface properties on cell retention and distribution in cheese curd. *International Dairy Journal*, 85:73–78.

[Taskila, 2017] Taskila, S. (2017). Industrial production of starter cultures. In *Starter Cultures in Food Production*, pages 79–100. John Wiley & Sons, Ltd.

[Tassell and Miller, 2011] Tassell, M. L. V. and Miller, M. J. (2011). Lactobacillus adhesion to mucus. *Nutrients*, 3(5):613–636.

[Tavares et al., 2014] Tavares, G. M., Croguennec, T., Carvalho, A. F., and Bouhallab, S. (2014). Milk proteins as encapsulation devices and delivery vehicles: Applications and trends. *Trends in Food Science & Technology*, 37(1):5–20.

[Teixeira et al., 1995] Teixeira, P. C., Castro, M. H., Malcata, F. X., and Kirby, R. M. (1995). Survival of lactobacillus delbrueckii ssp. bulgaricus following spray-drying. *Journal of Dairy Science*, 78(5):1025–1031.

[Thevenot, 2014] Thevenot, J. (2014). *Etude en systèmes digestifs artificiels de la survie et de la pathogénicité des Escherichia Coli entérohémorragiques (EHEC). Influence de la matrice alimentaire et de l'administration de souches probiotiques.* Biotechnologie, Microbiologie et Santé, Université Blaise Pascal et Université d'Auvergne, Clermont-Ferrand.

[Toh et al., 2013] Toh, H., Oshima, K., Nakano, A., Takahata, M., Murakami, M., Takaki, T., Nishiyama, H., Igimi, S., Hattori, M., and Morita, H. (2013). Genomic adaptation of the Lactobacillus casei group. *PloS One*, 8(10):e75073.

[Toma et al., 1991] Toma, M. K., Ruklisha, M. P., Vanags, J. J., Zeltina, M. O., Lelte, M. P., Galinine, N. I., Viesturs, U. E., and Tengerdy, R. P. (1991). Inhibition of microbial growth and metabolism by excess turbulence. *Biotechnology and Bioengineering*, 38(5):552–556.

[Tornberg and Shelley, 2004] Tornberg, A.-K. and Shelley, M. J. (2004). Simulating the dynamics and interactions of flexible fibers in stokes flows. *Journal of Computational Physics*, 196(1):8–40.

[Tripathi and Giri, 2014] Tripathi, M. K. and Giri, S. K. (2014). Probiotic functional foods: Survival of probiotics during processing and storage. *Journal of Functional Foods*, 9:225–241.

[Tripathi et al., 2013] Tripathi, P., Beaussart, A., Alsteens, D., Dupres, V., Claes, I., von Ossowski, I., de Vos, W. M., Palva, A., Lebeer, S., Vanderleyden, J., and Dufrêne, Y. F. (2013). Adhesion and nanomechanics of pili from the probiotic lactobacillus rhamnosus GG. *ACS Nano*, 7(4):3685–3697.

[Tripathi et al., 2012] Tripathi, P., Dupres, V., Beaussart, A., Lebeer, S., Claes, I. J. J., Vanderleyden, J., and Dufrêne, Y. F. (2012). Deciphering the nanometer-scale organization and assembly of lactobacillus rhamnosus GG pili using atomic force microscopy. *Langmuir*, 28(4):2211–2216.

[Truong et al., 2016] Truong, T., Palmer, M., Bansal, N., and Bhandari, B. (2016). Effect of milk fat globule size on physical properties of milk. In *Effect of Milk Fat Globule Size on the Physical Functionality of Dairy Products*, SpringerBriefs in Food, Health, and Nutrition, pages 35–45. Springer, Cham.

[Tufarelli and Laudadio, 2016] Tufarelli, V. and Laudadio, V. (2016). An overview on the functional food concept: prospectives and applied researches in probiotics, prebiotics and synbiotics. *Journal of Experimental Biology and Agricultural Sciences*, 4(3):273–278.

[Turner et al., 2013] Turner, R. D., Hurd, A. F., Cadby, A., Hobbs, J. K., and Foster, S. J. (2013). Cell wall elongation mode in Gram-negative bacteria is determined by peptidoglycan architecture. *Nature Communications*, 4:1496.

[Typas et al., 2012] Typas, A., Banzhaf, M., Gross, C. A., and Vollmer, W. (2012). From the regulation of peptidoglycan synthesis to bacterial growth and morphology. *Nature Reviews Microbiology*, 10(2):123–136.

[Tytgat et al., 2016] Tytgat, H. L. P., Teijlingen, N. H. v., Sullan, R. M. A., Douillard, F. P., Rasinkangas, P., Messing, M., Reunanen, J., Satokari, R., Vanderleyden, J., Dufrêne, Y. F., Geijtenbeek, T. B. H., Vos, W. M. d., and Lebeer, S. (2016). Probiotic Gut Microbiota Isolate Interacts with Dendritic Cells via Glycosylated Heterotrimeric Pili. *PLOS ONE*, 11(3):e0151824.

[Uneyama et al., 2014] Uneyama, T., Miyata, T., and Nitta, K.-h. (2014). Self-Consistent Field Model Simulations for Statistics of Amorphous Polymer Chains in Crystalline Lamellar Structures. *The Journal of Chemical Physics*, 141(16):164906. arXiv: 1410.3257.

[Utratna et al., 2017] Utratna, M., Annuk, H., Gerlach, J. Q., Lee, Y. C., Kane, M., Kilcoyne, M., and Joshi, L. (2017). Rapid screening for specific glycosylation and pathogen interactions on a 78 species avian egg white glycoprotein microarray. *Scientific Reports*, 7(1):6477.

[Valerio et al., 2006] Valerio, F., Bellis, P. D., Lonigro, S. L., Morelli, L., Visconti, A., and Lavermicocca, P. (2006). In vitro and in vivo survival and transit tolerance of potentially probiotic strains carried by artichokes in the gastrointestinal tract. *Applied and Environmental Microbiology*, 72(4):3042–3045.

[van den Brule, 1990] van den Brule, B. H. A. A. (1990). The non-isothermal elastic dumbbell: A model for the thermal conductivity of a polymer solution. *Rheologica Acta*, 29(5):416–422.

[van Loosdrecht et al., 1987] van Loosdrecht, M. C., Lyklema, J., Norde, W., Schraa, G., and Zehnder, A. J. (1987). Electrophoretic mobility and hydrophobicity as a measured to predict the initial steps of bacterial adhesion. *Applied and Environmental Microbiology*, 53(8):1898–1901.

[Van Loosdrecht et al., 1987] Van Loosdrecht, M. C., Lyklema, J., Norde, W., Schraa, G., and Zehnder, A. J. (1987). The role of bacterial cell wall hydrophobicity in adhesion. *Applied and Environmental Microbiology*, 53(8):1893–1897.

[van Loosdrecht et al., 1989] van Loosdrecht, M. C. M., Lyklema, J., Norde, W., and Zehnder, A. J. B. (1989). Bacterial adhesion: A physicochemical approach. *Microbial Ecology*, 17(1):1–15.

[van Loosdrecht et al., 1990] van Loosdrecht, M. C. M., Norde, W., Lyklema, J., and Zehnder, A. J. B. (1990). Hydrophobic and electrostatic parameters in bacterial adhesion. *Aquatic Sciences*, 52(1):103–114.

[van Oss, 1989] van Oss, C. J. (1989). Energetics of cell-cell and cell-biopolymer interactions. *Cell Biophysics*, 14(1):1–16.

[van Vliet, 2008] van Vliet, T. (2008). Strain hardening as an indicator of bread-making performance: A review with discussion. *Journal of Cereal Science*, 48(1):1–9.

[Vandenberghe et al., 2017] Vandenberghe, E., Charalambides, M., Mohammed, I., De Ketelaere, B., De Baerdemaeker, J., and Claes, J. (2017). Determination of a critical stress and distance criterion for crack propagation in cutting models of cheese. *Journal of Food Engineering*, 208:1–10.

[Vaudaux et al., 1990] Vaudaux, P., Yasuda, H., Velazco, M., Huggler, E., Ratti, I., Waldvogel, F., Lew, D., and Proctor, R. (1990). Role of host and bacterial factors in modulating staphylococcal adhesion to implanted polymer surfaces. *Journal of Biomaterials Applications*, 5(2):134–153.

[Vijaya Kumar et al., 2015] Vijaya Kumar, B., Vijayendra, S. V. N., and Reddy, O. V. S. (2015). Trends in dairy and non-dairy probiotic products - a review. *Journal of Food Science and Technology*, 52(10):6112–6124.

[Vinderola et al., 2000a] Vinderola, C. G., Bailo, N., and Reinheimer, J. A. (2000a). Survival of probiotic microflora in argentinian yoghurts during refrigerated storage. *Food Research International*, 33(2):97–102.

[Vinderola et al., 2002] Vinderola, C. G., Costa, G. A., Regenhardt, S., and Reinheimer, J. A. (2002). Influence of compounds associated with fermented dairy products on the growth of lactic acid starter and probiotic bacteria. *International Dairy Journal*, 12(7):579–589.

[Vinderola et al., 2000b] Vinderola, C. G., Prosello, W., Ghiberto, D., and Reinheimer, J. A. (2000b). Viability of probiotic (bifidobacterium, lactobacillus acidophilus and lactobacillus casei) and nonprobiotic microflora in argentinian fresco cheese. *Journal of Dairy Science*, 83(9):1905–1911.

[Vinderola et al., 2012] Vinderola, G., Zacarías, M., Bockelmann, W., Neve, H., Reinheimer, J., and Heller, K. (2012). Preservation of functionality of bifidobacterium animalis subsp. lactis INL1 after incorporation of freeze-dried cells into different food matrices. *Food Microbiology*, 30(1):274–280.

[Vogt et al., 1987] Vogt, R. V., Phillips, D. L., Omar Henderson, L., Whitfield, W., and Spierto, F. W. (1987). Quantitative differences among various proteins as blocking agents for ELISA microtiter plates. *Journal of Immunological Methods*, 101(1):43–50.

[von Ossowski et al., 2010] von Ossowski, I., Reunanen, J., Satokari, R., Vesterlund, S., Kankainen, M., Huhtinen, H., Tynkkynen, S., Salminen, S., de Vos, W. M., and Palva, A. (2010). Mucosal adhesion properties of the probiotic Lactobacillus rhamnosus GG SpaCBA and SpaFED pilin subunits. *Applied and Environmental Microbiology*, 76(7):2049–2057.

[Von Ossowski et al., 2011] Von Ossowski, I., Satokari, R., Reunanen, J., Lebeer, S., Keersmaecker, S. C. J. D., Vanderleyden, J., Vos, W. M. d., and Palva, A. (2011). Functional Characterization of a Mucus-Specific LPxTG Surface Adhesin from Probiotic Lactobacillus rhamnosus GG. *Applied and Environmental Microbiology*, 77(13):4465–4472.

[Wadhwani et al., 2011] Wadhwani, R., McManus, W. R., and McMahon, D. J. (2011). Improvement in melting and baking properties of low-fat Mozzarella cheese. *Journal of Dairy Science*, 94(4):1713–1723.

[Walstra, 1990] Walstra, P. (1990). On the Stability of Casein Micelles. *Journal of Dairy Science*, 73(8):1965–1979.

[Wang et al., 2013] Wang, X., Ge, J., Liu, B., Hu, Y., and Yang, M. (2013). Structures of SdrD from staphylococcus aureus reveal the molecular mechanism of how the cell surface receptors recognize their ligands. *Protein & Cell*, 4(4):277–285.

[Wang et al., 2009] Wang, Y., Yu, B., Wei, J. j., Li, F. c., and Kawaguchi, Y. (2009). Direct Numerical Simulation on drag-reducing flow by polymer additives using a spring-dumbbell model. *Progress in Computational Fluid Dynamics, An International Journal*, 9(3/4/5):217.

[Watanabe and Matsumiya, 2017] Watanabe, H. and Matsumiya, Y. (2017). Revisit the Elongational Viscosity of FENE Dumbbell Model. *Nihon Reoroji Gakkaishi*, 45(4):185–190.

[Watanabe et al., 2010] Watanabe, M., Kinoshita, H., Nitta, M., Yukishita, R., Kawai, Y., Kimura, K., Taketomo, N., Yamazaki, Y., Tateno, Y., Miura, K., Horii, A., Kitazawa, H., and Saito, T. (2010). Identification of a new adhesin-like protein from Lactobacillus mucosae ME-340 with specific affinity to the human blood group A and B antigens. *Journal of Applied Microbiology*, 109(3):927–935.

[Way, 1996] Way, J. C. (1996). The mechanism of bacterial asymmetric cell division. *BioEssays*, 18(2):99–101.

[Weaver et al., 2011] Weaver, W. M., Dharmaraja, S., Milisavljevic, V., and Carlo, D. D. (2011). The effects of shear stress on isolated receptor–ligand interactions of staphylococcus epidermidis and human plasma fibrinogen using molecularly patterned microfluidics. *Lab on a Chip*, 11(5):883–889.

[Wei et al., 2016] Wei, Y., Solomon, M. J., and Larson, R. G. (2016). Quantitative nonlinear thixotropic model with stretched exponential response in transient shear flows. *Journal of Rheology*, 60(6):1301–1315.

[Wei et al., 2018] Wei, Y., Solomon, M. J., and Larson, R. G. (2018). A multimode structural kinetics constitutive equation for the transient rheology of thixotropic elasto-viscoplastic fluids. *Journal of Rheology*, 62(1):321–342.

[Weidenmaier and Peschel, 2008] Weidenmaier, C. and Peschel, A. (2008). Teichoic acids and related cell-wall glycopolymers in Gram-positive physiology and host interactions. *Nature Reviews Microbiology*, 6(4):276–287.

[Welman and Maddox, 2003] Welman, A. D. and Maddox, I. S. (2003). Exopolysaccharides from lactic acid bacteria: perspectives and challenges. *Trends in Biotechnology*, 21(6):269–274.

[Weng, 1980] Weng, G. J. (1980). Dislocation theories of work hardening and yield surfaces of single crystals. *Acta Mechanica*, 37(3):217–230.

[Whittaker et al., 1996] Whittaker, C., Klier, C., and Kolenbrander, a. P. E. (1996). Mechanisms of adhesion by oral bacteria. *Annual Review of Microbiology*, 50(1):513–552.

[Wong et al., 2017] Wong, F., Renner, L. D., Özbaykal, G., Paulose, J., Weibel, D. B., van Teeffelen, S., and Amir, A. (2017). Mechanical strain sensing implicated in cell shape recovery in escherichia coli. *Nature Microbiology*, 2(9):17115.

[Yang et al., 2017] Yang, S., Phan, H. V., Bustamante, H., Guo, W., Ngo, H. H., and Nghiem, L. D. (2017). Effects of shearing on biogas production and microbial community structure during anaerobic digestion with recuperative thickening. *Bioresource Technology*, 234:439–447.

[Ye et al., 2016] Ye, A., Cui, J., Dalgleish, D., and Singh, H. (2016). Formation of a structured clot during the gastric digestion of milk: Impact on the rate of protein hydrolysis. *Food Hydrocolloids*, 52:478–486.

[Yeo et al., 2011] Yeo, S.-K., Ewe, J.-A., Tham, C. S.-C., and Liong, M.-T. (2011). Carriers of probiotic microorganisms. In Liong, M.-T., editor, *Probiotics*, number 21 in Microbiology Monographs, pages 191–220. Springer Berlin Heidelberg.

[Yoo and Lee, 1993] Yoo, B. and Lee, C. M. (1993). Thermoprotective effect of sorbitol on proteins during dehydration. *Journal of Agricultural and Food Chemistry*, 41(2):190–192.

[Young, 2006] Young, K. D. (2006). The Selective Value of Bacterial Shape. *Microbiology and Molecular Biology Reviews*, 70(3):660–703.

[Young, 2007] Young, K. D. (2007). Bacterial morphology: why have different shapes? *Current Opinion in Microbiology*, 10(6):596–600.

[Yu et al., 1987] Yu, C., Lee, A. M., and Roseman, S. (1987). The sugar-specific adhesion/deadhesion apparatus of the marine bacterium Vibriofurnissii is a sensorium that continuously monitors nutrient levels in the environment. *Biochemical and Biophysical Research Communications*, 149(1):86–92.

[Zhang and Zhou, 1998] Zhang, H. and Zhou, C. (1998). A dumbbell dispersion model of viscous drops of liquid/liquid mixing in steady-state plane hyperbolic flow fluids. *Acta Polymerica Sinica*, pages 707–708.

[Zhang et al., 2011] Zhang, Z.-G., Ye, Z.-Q., Yu, L., and Shi, P. (2011). Phylogenomic reconstruction of lactic acid bacteria: an update. *BMC Evolutionary Biology*, 11(1):1.

[Zhou et al., 2010] Zhou, M., Theunissen, D., Wels, M., and Siezen, R. J. (2010). LAB-Secretome: a genome-scale comparative analysis of the predicted extracellular and surface-associated proteins of Lactic Acid Bacteria. *BMC Genomics*, 11(1):651.

[Ziff and McGrady, 1986] Ziff, R. M. and McGrady, E. D. (1986). Kinetics of polymer degradation. *Macromolecules*, 19(10):2513–2519.

[Ziff and Stell, 1980] Ziff, R. M. and Stell, G. (1980). Kinetics of polymer gelation. *The Journal of Chemical Physics*, 73(7):3492–3499.

[Zita and Hermansson, 1994] Zita, A. and Hermansson, M. (1994). Effects of Ionic Strength on Bacterial Adhesion and Stability of Flocs in a Wastewater Activated Sludge System. *Applied and Environmental Microbiology*, 60(9):3041–3048.

[Åvall Jääskeläinen and Palva, 2005] Åvall Jääskeläinen, S. and Palva, A. (2005). Lactobacillus surface layers and their applications. *FEMS Microbiology Reviews*, 29(3):511–529.

[Önneby et al., 2013] Önneby, K., Pizzul, L., Bjerketorp, J., Mahlin, D., Håkansson, S., and Wessman, P. (2013). Effects of di- and polysaccharide formulations and storage conditions on survival of freeze-dried sphingobium sp. *World Journal of Microbiology and Biotechnology*, 29(8):1399–1408.

Part VII

Scientific valorization

VII.1

Publications

J. Guerin, J. Burgain, **F. Gomand**, J. Scher, C. Gaiani. Milk fat globule membrane glycoproteins: Valuable ingredients for lactic acid bacteria encapsulation? *Critical Reviews in Food Science and Nutrition*, 2017, 1-13. IF 2018 = 6.70.

J. Guerin, C. Soligot, J. Burgain, M. Huguet, G. Francius, S. El-Kirat-Chatel, **F. Gomand**, S. Lebeer, Y. Le Roux, F. Borges, J. Scher, C. Gaiani. Adhesive interactions between milk fat globule membrane and Lactobacillus rhamnosus GG inhibit bacterial attachment to Caco-2 TC7 intestinal cells. *Colloids and Surfaces B: Biointerfaces*, 2018, 167:44-53. IF 2018 = 3.97.

F. Gomand, F. Borges, J. Burgain, J. Guerin, C. Gaiani. High-throughput screening approach to evaluate the adhesive behavior of bacteria to milk biomolecules. *Food Hydrocolloids*, 2018, 84:537-544. IF 2018 = 5.83.

F. Gomand, F. Borges, J. Burgain, J. Guerin, A.M. Revol-Junelles, C. Gaiani. Food matrix design for effective Lactic Acid Bacteria delivery. *Annual Review of Food Science and Technology*, 2019, 10:285-310. IF 2018 = 8.51, ranked first journal in Food Science. *Available online.*

F. Gomand, F. Borges, J. Guerin, S. El-Kirat-Chatel, G. Francius, D. Dumas, J. Burgain, C. Gaiani. Adhesive interactions between lactic acid bacteria and β-lactoglobulin: specificity and impact on bacterial location in whey protein isolate. *Frontiers in Microbiology*, 2019, 10:1512. IF 2018 = 4.26. *Open access*.

F. Gomand, S. Spagnolie, J. Petit, J. Burgain, F. Borges, C. Gaiani. Shaving and breaking bacterial chains with a viscous flow: a theoretical and experimental spraying study. Draft. Predicted journal: *Soft Matter*.

F. Gomand, C. Gaiani, F. Borges, and S. Spagnolie. How to model cheese structuration? An overview of mathematical frameworks and perspectives for further development. Draft. Predicted journal: *Annual Review of Food Science and Technology*.

F. Gomand, W. Mitchell, and S. Spagnolie. Elastic dumbbells in a shear flow: dynamics and damages. Draft. Predicted journal: *Journal of Fluids and Structures*.

VII.2

Oral communications

F. Gomand, F. Borges, J. Burgain, J. Guerin, C. Gaiani. High-throughput screening approach to evaluate the adhesive behavior of bacteria to milk biomolecules. *3rd Food Structure and Functionality Forum Symposium & 3rd IDF Symposium on Microstructure of Dairy Products*, Montreal, QC, Canada, June 3-6, 2018.

F. Gomand, S. Spagnolie, J. Petit, J. Burgain, F. Borges, C. Gaiani. Shaving and breaking bacterial chains with a viscous flow: a theoretical and experimental spraying study. *International Scientific Conference on Probiotics, Prebiotics, Gut Mirobiota and Health*, Prague, Czech Republic, June 17-20, 2019.

F. Gomand, S. Spagnolie, J. Petit, J. Burgain, F. Borges, C. Gaiani. Shaving and breaking bacterial chains with a viscous flow: a theoretical and experimental spraying study. *Fluid and Elasticity*, Malaga, Spain, June 24-26, 2019.

VII.3

Poster presentations

F. Gomand, F. Borges, J. Burgain, J. Guerin, C. Gaiani. High-throughput screening approach to evaluate the adhesive behavior of bacteria to milk biomolecules. *25th International Conference on Bioencapsulation*, La Chapelle-sur-Erdre (Nantes), France, July 3-6, 2017.

F. Gomand, F. Borges, J. Burgain, J. Guerin, C. Gaiani. High-throughput screening approach to evaluate the adhesive behavior of bacteria to milk biomolecules. *Seminary of the doctoral school SIReNa (Natural Resources Science and Engineering, in French "Science et Ingénierie des Ressources Naturelles"*, Vandoeuvre-lès-Nancy, France, February 7, 2019.

VII.4

International collaborations

International bonds were formed during this project which involved the Biomolecule Engineering Laboratory (LIBio, Université de Lorraine, Vandoeuvre-lès-Nancy, France) and the Applied Math Lab (Department of Mathematics, University of Wisconsin-Madison, Madison, WI, USA). I initiated this multidisciplinary collaboration in November 2016 and pursued it during the three years of this project, including 8 months that I spent in the Applied Math Lab (Jan-Aug. 2018) thanks to a Fulbright scholarship. As new research questions have arisen, this collaboration will likely be pursued in future years.

Other international collaborations may also ultimately result from this work, such as later collaborations with researchers working at the Center for Computational Biology (CCB), Flatiron Institute, Simons Foundation, NY, USA, where I spent 2 months as a Visitor in the Biophysical Modeling team when holding my Fulbright scholar status, or with the Courant Institute, NY, USA, some members of this Institute being already involved in collaboration with the Biophysical Modeling team.

VII.5

Communication and science popularization

As both a LUE and Fulbright grantee, I have participated in numerous communication events and was also interviewed several times for internal press releases (FactUeL, ENSAIA journal Croq'Infos, Fulbright and LUE events), which main goals were to promote multidisciplinary and novative research fields, and international franco-american collaborations and understanding.

Involved in scientific tutoring since 2012 including two years during which I trained students who were preparing for national exams to enter French schools of higher education (Grandes Ecoles), I value passing along knowledge to others and seeing them put into practice. I love the contact with my students and always worked closely with them in order to design my courses specifically to fulfill their needs. In 2018, I got involved in a "science discovery" program for children in primary school (Accompagnement en Sciences et Technologies à l'Ecole Primaire, ASTEP). I organized various activities and workshops with a class of twenty-three 10-year old children around probiotic bacteria and food manufacturing.

VII.6

Teaching

I taught food science and engineering to MSc. students through lectures and lab work (64h/year). My teaching duties were divided into:

- Food science lectures (14h) on milk coagulation and cheese manufacturing (first-year master students). Key points discussed included the importance of dairy industry within the global food industry context and main stakeholders, mechanisms involved in enzymatic and acid milk coagulation, main manufacturing steps involved in cheese manufacturing, their implications and possible alternatives,

- Food engineering lectures (12h) on automation in food industry. I entirely designed this class for students in their last year of Master in Food Science. Key points discussed included importance and advantages of automation in food science, with a focus on integrated vision systems, logic systems and the GRAFCET method ("GRAphe Fonctionnel de Commande Etapes/Transitions" or in English *functional diagram of commands between steps and transitions*), control and regulated systems (closed and open loop feedback) using Laplace transforms and PID (proportional–integral–derivative) controllers,

- Lab work (number of hours varied depending on the year, not less than 38h) on the physico-chemistry of milk and dairy products (to students in their last year of

Bachelor to their last year of MSc.). Key manipulations included titration of dairy minerals and dairy powder characterisation,

- Participating to the selection process of the Master MILQ ("Master Industrie Laitière et Qualité", in English "Master for quality in the dairy industry"),
- Supervising two interns who performed quality, R&D, and supply chain duties in food industry all along their last year of MSc. (respectively in meat and dairy industries).

Part VIII

Appendices

A

Genomic information on the collection of 73 lactic acid bacteria strains

Bacteria name			Genomic information[6]					Optimal temperature of incubation	Minimal Adhesion Value (MAV)
Genus	**Species**	**Strain DSM n°**	**Pili-positive strain[7]**	**Number of pili clusters**	**Similarities with LGG WT pili[8]**	**Proteins with LPxTG motif**	**Number of sortase enzymes**		
Fructobacillus	*fructosus*	20349	no	0		0	0	30	-114.15
Lactobacillus	*acetotolerans*	20749	no	0		0	1	30	-294.34
Lactobacillus	*acidophilus*	20079	no	0		11	1	37	-342.31
Lactobacillus	algidus	15638	no	0		7	1	24 (room temperature)	-3.54
Lactobacillus	alimentarius	20249	no	0		5	1	30	-248.52
Lactobacillus	*amylovorus*	16698	no	0		6	1	37	-187.77
Lactobacillus	*animalis*	20602	yes	1	yes	7	2	37	-170.06
Lactobacillus	*apodemi*	16634	yes	1	yes	17	2	37	-128.17
Lactobacillus	*aquaticus*	21051	no	0		5	1	37	61.54
Lactobacillus	*bifermentans*	20003	no	0		19	1	30	-210.88

[6]Information about pili and surface proteins has been adapted from Sun et al. (2015)
[7]Strains featuring pili-encoding genes
[8]Strains harboring at least 1 pilus gene cluster with a similar gene order as L. rhamnosus GG WT

Lactobacillus	*brantae*	23927	yes	1	no	13	5	37	6.97
Lactobacillus	*brevis*	20054	no	0		7	1	30	-254.13
Lactobacillus	*camelliae*	22697	yes	1	yes	16	2	37	-29.13
Lactobacillus	*capillatus*	19910	no	0		2	1	30	-115.67
Lactobacillus	*casei*	20011	yes	2	yes	11	4	30	-22.52
Lactobacillus	*composti*	18527	yes	1	yes	6	2	30	-54.47
Lactobacillus	*concavus*	17758	yes	1	yes	4	2	37	-159.69
Lactobacillus	*diolivorans*	14421	no	0		4	2	30	-321.00
Lactobacillus	*farciminis*	20184	no	0		5	1	30	-69.13
Lactobacillus	*fermentum*	20055	no	0		5	1	30	-11.95
Lactobacillus	*florum*	22689	no	0		6	1	30	-213.06
Lactobacillus	*fuchuensis*	14340	no	0		11	2	22 (room temperature)	-325.35
Lactobacillus	*gallinarum*	10532	no	0		11	1	37	-10.06
Lactobacillus	*hammesii*	16381	yes	1	no	18	3	30	-185.59
Lactobacillus	*harbinensis*	16991	yes	1	no	5	7	37	-121.67
Lactobacillus	*hominis*	23910	no	0		16	1	37	-297.22
Lactobacillus	*hordei*	19519	no	0		2	1	30	-37.30
Lactobacillus	*johnsonii*	10533	no	0		8	1	37	-60.55
Lactobacillus	*kefiri*	20587	no	0		3	1	30	-786.90
Lactobacillus	*kimchiensis*	24716	no	0		6	1	23 (room temperature)	-162.29
Lactobacillus	*koreensis*	27983	yes	1	no	9	3	30	-138.28
Lactobacillus	*lindneri*	20690	no	0		6	1	30	-386.89
Lactobacillus	*manihotivorans*	13343	yes	4	yes	9	7	30	-20.84
Lactobacillus	*mucosae*	13345	no	0		15	1	37	-16.69
Lactobacillus	*murinus*	20452	yes	2	yes	14	4	37	12.79
Lactobacillus	*nagelii*	13675	no	0		3	1	30	-354.36
Lactobacillus	*namurensis*	19117	no	0		15	1	30	-516.20
Lactobacillus	*nantensis*	16982	no	0		8	1	30	-131.37
Lactobacillus	*nasuensis*	26653	yes	3	yes	20	5	30	-129.58
Lactobacillus	*nodensis*	19682	no	0		7	1	30	-206.13
Lactobacillus	*pantheris*	15945	yes	2	yes	13	5	37	-63.20
Lactobacillus	*parabuchneri*	15352	yes	1	no	11	3	30	-70.89
Lactobacillus	*paracasei* subsp. *paracasei*	5622	yes	3	yes	9	4	30	-293.21
Lactobacillus	*paracasei* subsp. *tolerans*	20258	yes	1	yes	6	3	30	-38.62
Lactobacillus	*paralimentarius*	13238	no	0		5	1	30	-124.26
Lactobacillus	*pasteurii*	23907	no	0		11	1	37	-317.66
Lactobacillus	*paucivorans*	22467	yes	1	no	23	3	30	-242.57
Lactobacillus	*pentosus*	20314	no	0		17	1	30	-99.69
Lactobacillus	*perolens*	12744	yes	1	no	11	3	30	-45.19
Lactobacillus	*plantarum*	13273	no	0		17	1	37	12.65
Lactobacillus	*pobuzihii*	28122	yes	1	no	1	1	37	-616.96

Lactobacillus	*psittaci sakei*	15354	no	0		14	1	37	-35.72
Lactobacillus	subsp. *sakei*	20017	no	0		3	2	30	-116.07
Lactobacillus	*salivarius*	20555	yes	1	no	10	3	37	-31.69
Lactobacillus	*satsu-mensis*	16230	no	0		3	1	30	-490.01
Lactobacillus	*selango-rensis*	13344	yes	1	no	6	4	30	-63.69
Lactobacillus	*senioris*	24302	yes	1	no	3	3	37	-171.35
Lactobacillus	*senma-zukei*	21775	yes	1	no	17	3	30	-403.90
Lactobacillus	*sharpeae*	20505	yes	5	yes	17	5	30	-858.76
Lactobacillus	*similis*	23365	no	0		21	1	37	-780.53
Lactobacillus	*thailen-densis*	22698	yes	2	yes	11	6	37	-161.03
Lactobacillus	*versmol-densis*	14857	no	0		4	1	30	-70.60
Lactobacillus	*vini*	20605	no	0		1	1	37	-40.14
Leuconostoc	*mesente-roides* subsp. *mesen-teroides*	20343	yes	1	no	1	2	30	-69.05
Pediococcus	*acidilac-tici*	19927	no	0		3	1	30	-83.40
Pediococcus	*claus-senii*	14800	yes	1	no	3	2	30	-106.35
Pediococcus	*ethanoli-durans*	22301	yes	1	no	9	4	37	-257.24
Pediococcus	*inopi-natus*	20285	yes	1	no	10	4	30	-46.32
Pediococcus	*parvulus*	20332	yes	2	yes	10	6	30	-476.83
Pediococcus	*stilesii*	18001	no	0		0	1	30	-11.10
Weissela	*confusa*	20196	yes	1	yes	2	3	30	-50.80
Weissela	*halotole-rans*	20190	no	0		1	1	30	-137.23
Weissela	*virides-cens*	20410	no	0		7	1	30	-39.56
Lactobacillus	*rhamno-sus*	GG WT	yes	1	/	14	/	37	104.05
Lactobacillus	*rhamno-sus*	GG *spaCBA*	no	0	/	13	/	37	-386.00

Table A.1: The collection of 73 lactic acid bacteria (LAB) strains screened for potential adhesive interactions with β-lactoglobulin; *Lactobacillus rhamnosus* GG (LGG) "wild type" (WT) and *spaCBA* (pili-depleted strain) are used as control strains.

B

Impact of shearing on bacterial chain size distribution

B.1 *Lactobacillus rhamnosus* GG "wild type" (WT)

Type of chains	Shear rate $\dot{\gamma}$ (s^{-1})							
	Control	**244**	**3.0×10^5**	**3.7×10^5**	**4.2×10^5**	**4.9×10^5**	**11×10^5 (OT)**	**11×10^5 (R)**
Single cell	0 ± 0	0 ± 0	3.88 ± 1.18	8.08 ± 2.10	10.18 ± 1.60	10.72 ± 2.38	22.40 ± 1.67	38.06 ± 2.01
2-cell	4.85 ± 1.55	4.99 ± 1.38	56.87 ± 3.63	48.79 ± 3.21	65.20 ± 2.43	57.89 ± 3.55	55.02 ± 2.00	47.45 ± 2.39
3-cell	1.96 ± 1.00	2.16 ± 1.27	5.96 ± 1.51	6.20 ± 1.68	4.96 ± 1.23	5.17 ± 1.40	3.37 ± 0.45	1.37 ± 0.43
4-cell	12.54 ± 2.43	10.30 ± 2.46	18.91 ± 3.84	6.05 ± 1.23	11.22 ± 1.65	6.34 ± 1.74	2.65 ± 0.51	1.63 ± 0.35
5-cell	4.31 ± 1.33	4.70 ± 1.48	2.53 ± 0.79	1.56 ± 0.75	0.55 ± 0.38	1.56 ± 0.90	0.50 ± 0.20	0 ± 0
6-cell	8.98 ± 1.91	10.57 ± 1.93	2.11 ± 1.00	1.77 ± 0.89	0.48 ± 0.32	2.03 ± 0.81	0.20 ± 0.14	0.08 ± 0.08
7-cell	6.19 ± 1.93	4.44 ± 1.33	0.49 ± 0.48	0.43 ± 0.42	0.18 ± 0.18	0.43 ± 0.42	0.14 ± 0.13	0 ± 0
8-cell	8.58 ± 2.05	6.61 ± 1.43	0.31 ± 0.30	0.25 ± 0.24	0 ± 0	0 ± 0	0.09 ± 0.09	0 ± 0
9-cell	1.92 ± 1.00	5.54 ± 1.77	0 ± 0	0 ± 0	0 ± 0	0 ± 0	0 ± 0	0 ± 0
10-cell	3.87 ± 1.50	2.09 ± 0.87	0.38 ± 0.37	0 ± 0	0 ± 0	0 ± 0	0 ± 0	0 ± 0
> 10-cell	23.89 ± 3.24	29.03 ± 4.72	0 ± 0	0 ± 0	0 ± 0	0 ± 0	0 ± 0	0 ± 0
Flocs	22.90 ± 2.25	19.58 ± 3.63	8.56 ± 1.83	26.87 ± 3.86	7.24 ± 1.67	15.86 ± 2.49	15.63 ± 1.97	11.41 ± 2.22

Table B.1: *Lactobacillus rhamnosus* GG "wild type" chain distribution (% by type of chains) before and after spray-drying for shear rates ranging from 244 s^{-1} to 11×10^5 s^{-1}; OT = one-time shearing, R = repeated shearing. Standard errors are presented.

B.2 *Lactobacillus rhamnosus* GG *spaCBA*

Type of chains	Shear rate $\dot{\gamma}$ (s^{-1})							
	Control	**244**	**3.0×10^5**	**3.7×10^5**	**4.2×10^5**	**4.9×10^5**	**11×10^5 (OT)**	**11×10^5 (R)**
Single cell	1.25 ± 0.53	1.12 ± 0.52	4.30 ± 0.86	5.30 ± 0.82	9.42 ± 1.21	14.56 ± 1.47	16.50 ± 1.29	35.69 ± 1.09
2-cell	6.73 ± 1.22	9.28 ± 1.13	34.37 ± 1.98	44.84 ± 2.78	45.22 ± 1.55	52.15 ± 1.62	47.59 ± 1.47	43.22 ± 1.05
3-cell	2.09 ± 0.58	3.22 ± 0.82	11.99 ± 1.60	10.17 ± 1.40	8.01 ± 1.00	7.14 ± 0.55	4.99 ± 0.43	3.42 ± 0.31
4-cell	6.25 ± 1.15	9.96 ± 1.42	19.54 ± 1.46	15.05 ± 1.77	10.57 ± 0.60	8.76 ± 0.77	5.80 ± 0.71	1.68 ± 0.29
5-cell	2.99 ± 0.90	3.54 ± 0.79	3.54 ± 0.65	1.72 ± 0.50	2.07 ± 0.38	1.20 ± 0.27	0.87 ± 0.25	0.14 ± 0.08
6-cell	3.68 ± 0.95	7.14 ± 0.99	2.53 ± 0.77	4.36 ± 0.83	1.12 ± 0.28	1.21 ± 0.29	0.40 ± 0.16	0.04 ± 0.04
7-cell	3.79 ± 0.86	3.09 ± 0.92	1.53 ± 0.41	1.08 ± 0.51	0.44 ± 0.19	0.27 ± 0.14	0 ± 0	0 ± 0
8-cell	7.74 ± 1.52	4.97 ± 0.99	0.78 ± 0.31	0.85 ± 0.38	0.18 ± 0.10	0.03 ± 0.03	0 ± 0	0 ± 0
9-cell	2.17 ± 0.64	4.07 ± 0.72	0 ± 0	0 ± 0	0 ± 0	0.10 ± 0.067	0 ± 0	0 ± 0
10-cell	5.13 ± 1.01	2.42 ± 0.64	0 ± 0	0 ± 0	0 ± 0	0 ± 0	0 ± 0	0 ± 0
> 10-cell	26.59 ± 3.00	17.40 ± 2.00	0 ± 0	0.17 ± 0.17	0 ± 0	0 ± 0	0 ± 0	0 ± 0
Flocs	31.58 ± 2.71	33.80 ± 1.60	21.41 ± 1.44	16.46 ± 1.27	22.98 ± 1.19	14.58 ± 1.33	23.85 ± 1.22	15.81 ± 0.65

Table B.2: *Lactobacillus rhamnosus* GG *spaCBA* chain distribution (% by type of chains) before and after spray-drying for shear rates ranging from 244 s^{-1} to 11×10^5 s^{-1}; OT = one-time shearing, R = repeated shearing. Standard errors are presented.

B.3 *Lactobacillus rhamnosus* GG *welE*

Type of chains	Shear rate $\dot{\gamma}$ (s^{-1})							
	Control	**244**	**3.0×10^5**	**3.7×10^5**	**4.2×10^5**	**4.9×10^5**	**11×10^5 (OT)**	**11×10^5 (R)**
single cell	0.18 ± 0.18	1.22 ± 0.58	5.46 ± 0.73	7.04 ± 1.36	15.33 ± 1.94	22.24 ± 2.05	17.91 ± 1.80	51.97 ± 2.43
2-cell	9.33 ± 1.38	22.91 ± 2.57	48.80 ± 1.32	60.50 ± 2.57	56.39 ± 2.12	53.68 ± 2.38	57.99 ± 1.77	33.47 ± 2.02
3-cell	3.99 ± 1.06	4.98 ± 1.11	6.96 ± 0.90	8.02 ± 1.18	9.11 ± 1.20	4.22 ± 0.64	3.72 ± 0.68	2.86 ± 0.89
4-cell	11.52 ± 1.34	13.95 ± 1.19	13.30 ± 0.84	13.53 ± 1.36	10.26 ± 1.49	4.40 ± 0.62	3.63 ± 0.55	0.33 ± 0.22
5-cell	3.87 ± 0.80	3.40 ± 0.84	2.60 ± 0.44	1.51 ± 0.45	2.30 ± 0.92	0.71 ± 0.28	0.45 ± 0.17	0 ± 0
6-cell	8.00 ± 1.34	6.68 ± 1.04	2.69 ± 0.56	2.13 ± 0.68	1.63 ± 0.51	0.53 ± 0.24	0.19 ± 0.09	0 ± 0
7-cell	3.60 ± 0.92	5.16 ± 0.91	0.98 ± 0.29	0.50 ± 0.34	0 ± 0	0.27 ± 0.22	0.03 ± 0.03	0.07 ± 0.07
8-cell	7.23 ± 1.51	5.22 ± 0.71	0.24 ± 0.11	0.12 ± 0.11	0 ± 0	0 ± 0	0.14 ± 0.13	0 ± 0
9-cell	4.29 ± 0.89	2.33 ± 0.62	0.33 ± 0.16	0 ± 0	0 ± 0	0 ± 0	0.14 ± 0.14	0 ± 0
10-cell	5.70 ± 1.37	4.71 ± 0.86	0.07 ± 0.06	0 ± 0	0 ± 0	0 ± 0	0 ± 0	0 ± 0
> 10-cell	25.33 ± 2.68	14.94 ± 1.40	0 ± 0	0 ± 0	0 ± 0	0 ± 0	0.55 ± 0.53	0 ± 0
Flocs	16.93 ± 1.48	14.51 ± 1.84	18.55 ± 1.03	6.65 ± 0.99	4.98 ± 0.92	13.95 ± 1.92	15.24 ± 1.52	11.30 ± 1.03

Table B.3: *Lactobacillus rhamnosus* GG *welE* chain distribution (% by type of chains) before and after spray-drying for shear rates ranging from 244 s^{-1} to 11×10^5 s^{-1}; OT = one-time shearing, R = repeated shearing. Standard errors are presented.

C

Maximal surface traction forces applied to cells in bacterial chains of various length

C.1 Maximal surface traction forces on 2-cell, 3-cell, and 4-cell chains

Time	**2 ellipsoids**		**3 ellipsoids**			**4 ellipsoids**			
	L	R	L	M	R	L	ML	MR	R
0	2.4900	2.4900	2.4859	2.4284	2.4859	2.4845	2.4225	2.4225	2.4845
0.25	2.8007	2.8007	2.8064	2.7556	2.8064	2.7908	2.7704	2.7704	2.7908
0.5	2.8408	2.8408	2.8479	2.7439	2.8479	2.8384	2.7629	2.7629	2.8384
0.75	2.8828	2.8828	2.8796	2.7424	2.8796	2.8732	2.7565	2.7565	2.8732
1	2.9280	2.9280	2.9109	2.7419	2.9109	2.9024	2.7504	2.7504	2.9024
1.25	2.9765	2.9765	2.9430	2.7415	2.9430	2.9294	2.7476	2.7476	2.9294
1.5	3.0290	3.0290	2.9759	2.7409	2.9759	2.9554	2.7526	2.7526	2.9554
1.75	3.0873	3.0873	3.0102	2.7403	3.0102	2.9818	2.7579	2.7579	2.9818
2	3.1514	3.1514	3.0458	2.7396	3.0458	3.0085	2.7634	2.7634	3.0085
2.25	3.2216	3.2216	3.0830	2.7388	3.0830	3.0358	2.7690	2.7690	3.0358
2.5	3.3008	3.3008	3.1221	2.7379	3.1221	3.0637	2.7746	2.7746	3.0637
2.75	3.3883	3.3883	3.1627	2.7369	3.1627	3.0924	2.7803	2.7803	3.0924
3	3.4870	3.4870	3.2064	2.7357	3.2064	3.1221	2.7861	2.7861	3.1221
3.25	3.5938	3.5938	3.2526	2.7344	3.2526	3.1528	2.7919	2.7919	3.1528
3.5	3.7147	3.7147	3.3016	2.7330	3.3016	3.1847	2.7977	2.7977	3.1847
3.75	3.8501	3.8501	3.3543	2.7314	3.3543	3.2172	2.8037	2.8037	3.2172

4	3.9992	3.9992	3.4096	2.7296	3.4096	3.2517	2.8097	2.8097	3.2517
4.25	4.1689	4.1689	3.4702	2.7276	3.4702	3.2876	2.8157	2.8157	3.2876
4.5	4.3586	4.3586	3.5350	2.7251	3.5350	3.3251	2.8219	2.8219	3.3251
4.75	4.5716	4.5716	3.6049	2.7226	3.6049	3.3644	2.8282	2.8282	3.3644
5	4.8094	4.8094	3.6808	2.7199	3.6808	3.4058	2.8345	2.8345	3.4058
5.25	5.0796	5.0796	3.7606	2.7168	3.7606	3.4496	2.8410	2.8410	3.4496
5.5	5.3820	5.3820	3.8497	2.7133	3.8497	3.4941	2.8476	2.8476	3.4941
5.75	5.7201	5.7201	3.9458	2.7094	3.9458	3.5426	2.8544	2.8544	3.5426
6	6.0924	6.0924	4.0501	2.7049	4.0501	3.5936	2.8613	2.8613	3.5936
6.25	6.4945	6.4945	4.1642	2.6998	4.1642	3.6475	2.8684	2.8684	3.6475
6.5	6.9069	6.9069	4.2899	2.6940	4.2899	3.7047	2.8756	2.8756	3.7047
6.75	7.2842	7.2842	4.4233	2.6873	4.4233	3.7656	2.8830	2.8830	3.7656
7	7.5345	7.5345	4.5736	2.6796	4.5736	3.8310	2.8906	2.8906	3.8310
7.25	7.4825	7.4825	4.7385	2.6707	4.7385	3.8974	2.8984	2.8984	3.8974
7.5	6.8548	6.8548	4.9205	2.6603	4.9205	3.9711	2.9061	2.9061	3.9711
7.75	5.3928	5.3928	5.1224	2.6481	5.1224	4.0493	2.9144	2.9144	4.0493
8	3.4153	3.4153	5.3483	2.6336	5.3483	4.1329	2.9230	2.9230	4.1329
8.25	3.3761	3.3761	5.5946	2.6164	5.5946	4.2224	2.9318	2.9318	4.2224
8.5	5.3514	5.3514	5.8743	2.5956	5.8743	4.3187	2.9410	2.9410	4.3187
8.75	6.8358	6.8358	6.1868	2.5704	6.1868	4.4228	2.9504	2.9504	4.4228
9	7.4804	7.4804	6.5381	2.5382	6.5381	4.5360	2.9601	2.9601	4.5360
9.25	7.5403	7.5403	6.9339	2.4995	6.9339	4.6520	2.9702	2.9702	4.6520
9.5	7.2903	7.2903	7.3746	2.4508	7.3746	4.7823	2.9806	2.9806	4.7823
9.75	6.9107	6.9107	7.8691	2.3888	7.8691	4.9232	2.9914	2.9914	4.9232
10	6.4951	6.4951	8.4131	2.3093	8.4131	5.0762	3.0025	3.0025	5.0762
10.25	6.0899	6.0899	8.9969	2.2076	8.9969	5.2429	3.0140	3.0140	5.2429
10.5	5.7161	5.7161	9.5857	2.0800	9.5857	5.4254	3.0258	3.0258	5.4254
10.75	5.3744	5.3744	10.1066	1.9309	10.1066	5.6263	3.0379	3.0379	5.6263
11	5.0703	5.0703	10.3983	1.8105	10.3983	5.8423	3.0503	3.0503	5.8423
11.25	4.7987	4.7987	10.1613	1.9378	10.1613	6.0847	3.0628	3.0628	6.0847
11.5	4.5600	4.5600	8.9344	2.2436	8.9344	6.3522	3.0753	3.0753	6.3522
11.75	4.3463	4.3463	6.3317	2.5700	6.3317	6.6486	3.0876	3.0876	6.6486
12	4.1565	4.1565	3.2049	2.7359	3.2049	6.9782	3.0992	3.0992	6.9782
12.25	3.9866	3.9866	4.7870	2.6640	4.7870	7.3463	3.1097	3.1097	7.3463
12.5	3.8376	3.8376	7.9265	2.3750	7.9265	7.7593	3.1183	3.1183	7.7593
12.75	3.7028	3.7028	9.7750	2.0323	9.7750	8.2188	3.1223	3.1223	8.2188
13	3.5822	3.5822	10.3954	1.8201	10.3954	8.7373	3.1220	3.1220	8.7373
13.25	3.4759	3.4759	10.2841	1.8835	10.2841	9.3169	3.1132	3.1132	9.3169
13.5	3.3785	3.3785	9.8256	2.0335	9.8256	9.9613	3.0910	3.0910	9.9613
13.75	3.2920	3.2920	9.2401	2.1702	9.2401	10.6688	3.0474	3.0474	10.6688
14	3.2153	3.2153	8.6368	2.2813	8.6368	11.4203	2.9698	2.9698	11.4203
14.25	3.1451	3.1451	8.0639	2.3685	8.0639	12.1679	2.8391	2.8391	12.1679
14.5	3.0824	3.0824	7.5401	2.4365	7.5401	12.8006	2.6233	2.6233	12.8006
14.75	3.0261	3.0261	7.0715	2.4899	7.0715	13.0905	2.3888	2.3888	13.0905
15	2.9745	2.9745	6.6507	2.5320	6.6507	12.6202	2.8403	2.8403	12.6202
15.25	2.9272	2.9272	6.2779	2.5656	6.2779	10.7709	3.1989	3.1990	10.7708
15.5	2.8836	2.8836	5.9468	2.5938	5.9468	7.0799	3.2259	3.2259	7.0798
15.75	2.8425	2.8425	5.6516	2.6158	5.6516	2.9488	2.7996	2.7996	2.9487

16	2.8036	2.8036	5.3920	2.6341	5.3920	6.3182	3.1505	3.1505	6.3183
16.25	2.7662	2.7662	5.1553	2.6492	5.1553	10.3475	3.1231	3.1231	10.3476
16.5	2.8001	2.8001	4.9438	2.6620	4.9438	12.4951	2.7877	2.7877	12.4951
16.75	2.8401	2.8401	4.7545	2.6728	4.7545	13.1090	2.3636	2.3636	13.1090
17	2.8821	2.8821	4.5833	2.6820	4.5833	12.8621	2.6680	2.6680	12.8621
17.25	2.9272	2.9272	4.4278	2.6898	4.4278	12.2245	2.8932	2.8932	12.2245
17.5	2.9757	2.9757	4.2899	2.6966	4.2899	11.4551	3.0335	3.0335	11.4551
17.75	3.0288	3.0288	4.1611	2.7025	4.1611	10.6785	3.1161	3.1161	10.6785
18	3.0863	3.0863	4.0446	2.7077	4.0446	9.9467	3.1630	3.1630	9.9467
18.25	3.1502	3.1502	3.9384	2.7121	3.9384	9.2810	3.1871	3.1871	9.2810
18.5	3.2203	3.2203	3.8408	2.7161	3.8408	8.6836	3.1968	3.1968	8.6836
18.75	3.2994	3.2994	3.7534	2.7195	3.7534	8.1508	3.1974	3.1974	8.1508
19	3.3868	3.3868	3.6706	2.7225	3.6706	7.6788	3.1921	3.1921	7.6788
19.25	3.4853	3.4853	3.5951	2.7252	3.5951	7.2566	3.1832	3.1832	7.2566
19.5	3.5919	3.5919	3.5258	2.7276	3.5258	6.8815	3.1720	3.1721	6.8815
19.75	3.7126	3.7126	3.4614	2.7297	3.4614	6.5459	3.1608	3.1608	6.5459
20	3.8477	3.8477	3.4030	2.7316	3.4030	6.2448	3.1478	3.1478	6.2448
20.25	3.9965	3.9965	3.3479	2.7332	3.3479	5.9737	3.1346	3.1346	5.9737
20.5	4.1660	4.1660	3.2970	2.7347	3.2970	5.7332	3.1214	3.1214	5.7332
20.75	4.3550	4.3550	3.2495	2.7363	3.2495	5.5105	3.1084	3.1084	5.5105
21	4.5679	4.5679	3.2055	2.7374	3.2055	5.3095	3.0957	3.0957	5.3095
21.25	4.8051	4.8051	3.1637	2.7384	3.1637	5.1271	3.0834	3.0834	5.1271
21.5	5.0748	5.0748	3.1244	2.7393	3.1244	4.9607	3.0714	3.0714	4.9607
21.75	5.3768	5.3768	3.0872	2.7401	3.0872	4.8082	3.0598	3.0598	4.8082
22	5.7145	5.7145	3.0517	2.7408	3.0517	4.6679	3.0486	3.0486	4.6679
22.25	6.0860	6.0860	3.0181	2.7413	3.0181	4.5429	3.0378	3.0378	4.5429
22.5	6.4877	6.4877	2.9855	2.7418	2.9855	4.4231	3.0273	3.0273	4.4231
22.75	6.8999	6.8999	2.9540	2.7422	2.9540	4.3135	3.0173	3.0173	4.3135
23	7.2787	7.2787	2.9235	2.7425	2.9235	4.2126	3.0075	3.0075	4.2126
23.25	7.5322	7.5322	2.8938	2.7427	2.8938	4.1192	2.9981	2.9981	4.1192
23.5	7.4872	7.4872	2.8648	2.7429	2.8648	4.0324	2.9890	2.9890	4.0324
23.75	6.8715	6.8715	2.8363	2.7429	2.8363	3.9513	2.9802	2.9802	3.9513
24	5.4237	5.4237	2.8081	2.7429	2.8081	3.8783	2.9716	2.9716	3.8783
24.25	3.4444	3.4444	2.8008	2.7429	2.8008	3.8080	2.9633	2.9633	3.8080
24.5	3.3484	3.3484	2.8303	2.7427	2.8303	3.7428	2.9552	2.9552	3.7428
24.75	5.3200	5.3200	2.8604	2.7425	2.8604	3.6822	2.9474	2.9474	3.6822
25	6.8184	6.8184	2.8911	2.7422	2.8911	3.6253	2.9397	2.9397	3.6253

Table C.1: Maximal surface traction forces ($\mathrm{Max}_{\mathrm{STF}}$) applied to each bacterial cell (ellipsoid body) of chains of 2, 3, and 4cells over time. L=Left cell, ML=middle left cell, MR=middle right cell, R=right cell.

C.2 Maximal surface traction forces on 5-cell chains

Time	**5 ellipsoids**				
	L	ML	C	MR	R
0	2.4839	2.4207	2.4166	2.4207	2.4839
0.25	2.7909	2.7605	2.7660	2.7605	2.7909
0.5	2.8330	2.7629	2.7623	2.7629	2.8330
0.75	2.8666	2.7652	2.7569	2.7652	2.8666
1	2.8967	2.7649	2.7530	2.7649	2.8967
1.25	2.9243	2.7626	2.7503	2.7626	2.9243
1.5	2.9500	2.7589	2.7483	2.7589	2.9500
1.75	2.9751	2.7542	2.7469	2.7542	2.9751
2	2.9996	2.7488	2.7458	2.7488	2.9996
2.25	3.0237	2.7505	2.7450	2.7505	3.0237
2.5	3.0478	2.7566	2.7444	2.7566	3.0478
2.75	3.0720	2.7629	2.7439	2.7629	3.0720
3	3.0964	2.7694	2.7435	2.7694	3.0964
3.25	3.1213	2.7761	2.7431	2.7761	3.1213
3.5	3.1467	2.7829	2.7428	2.7829	3.1467
3.75	3.1727	2.7899	2.7424	2.7899	3.1727
4	3.1995	2.7969	2.7421	2.7969	3.1995
4.25	3.2261	2.8041	2.7418	2.8041	3.2261
4.5	3.2544	2.8114	2.7414	2.8114	3.2544
4.75	3.2836	2.8188	2.7410	2.8188	3.2836
5	3.3136	2.8263	2.7407	2.8263	3.3136
5.25	3.3447	2.8340	2.7403	2.8340	3.3447
5.5	3.3769	2.8417	2.7398	2.8417	3.3769
5.75	3.4105	2.8496	2.7394	2.8496	3.4105
6	3.4455	2.8576	2.7389	2.8576	3.4455
6.25	3.4822	2.8658	2.7383	2.8658	3.4822
6.5	3.5185	2.8741	2.7378	2.8741	3.5185
6.75	3.5582	2.8826	2.7372	2.8826	3.5582
7	3.5994	2.8913	2.7365	2.8913	3.5994
7.25	3.6425	2.9002	2.7358	2.9002	3.6425
7.5	3.6875	2.9093	2.7351	2.9093	3.6875
7.75	3.7347	2.9185	2.7343	2.9185	3.7347
8	3.7844	2.9281	2.7335	2.9281	3.7844
8.25	3.8369	2.9378	2.7325	2.9378	3.8369
8.5	3.8926	2.9478	2.7316	2.9478	3.8926
8.75	3.9476	2.9581	2.7305	2.9581	3.9476
9	4.0087	2.9687	2.7294	2.9687	4.0087
9.25	4.0730	2.9797	2.7281	2.9797	4.0730
9.5	4.1407	2.9906	2.7268	2.9906	4.1407
9.75	4.2123	3.0022	2.7254	3.0022	4.2123
10	4.2881	3.0142	2.7238	3.0142	4.2881
10.25	4.3688	3.0266	2.7221	3.0266	4.3688
10.5	4.4547	3.0395	2.7203	3.0395	4.4547

10.75	4.5468	3.0528	2.7183	3.0528	4.5468
11	4.6402	3.0667	2.7161	3.0667	4.6402
11.25	4.7442	3.0810	2.7137	3.0810	4.7442
11.5	4.8552	3.0960	2.7110	3.0960	4.8552
11.75	4.9738	3.1115	2.7082	3.1115	4.9738
12	5.1009	3.1277	2.7050	3.1277	5.1009
12.25	5.2375	3.1446	2.7015	3.1446	5.2375
12.5	5.3848	3.1622	2.6976	3.1622	5.3848
12.75	5.5443	3.1806	2.6933	3.1806	5.5443
13	5.7175	3.1997	2.6884	3.1997	5.7175
13.25	5.9063	3.2198	2.6830	3.2198	5.9063
13.5	6.1056	3.2406	2.6770	3.2406	6.1056
13.75	6.3284	3.2624	2.6701	3.2624	6.3284
14	6.5722	3.2850	2.6624	3.2850	6.5722
14.25	6.8397	3.3084	2.6536	3.3084	6.8397
14.5	7.1345	3.3326	2.6436	3.3326	7.1345
14.75	7.4608	3.3574	2.6322	3.3574	7.4608
15	7.8234	3.3824	2.6190	3.3824	7.8234
15.25	8.2283	3.4073	2.6033	3.4073	8.2283
15.5	8.6766	3.4313	2.5858	3.4313	8.6766
15.75	9.1824	3.4532	2.5655	3.4532	9.1824
16	9.7498	3.4713	2.5423	3.4713	9.7498
16.25	10.3850	3.4835	2.5158	3.4835	10.3850
16.5	11.0926	3.4857	2.4863	3.4857	11.0926
16.75	11.8638	3.4719	2.4544	3.4719	11.8638
17	12.6725	3.4368	2.4222	3.4368	12.6725
17.25	13.4286	3.3759	2.3930	3.3759	13.4286
17.5	13.9366	3.2844	2.3697	3.2844	13.9366
17.75	13.8100	3.1713	2.3438	3.1713	13.8100
18	12.5523	3.8144	2.2769	3.8144	12.5523
18.25	10.0302	4.8659	2.1036	4.8659	10.0302
18.5	7.0606	5.7757	1.8632	5.7757	7.0606
18.75	4.9436	6.0596	3.0405	6.0596	4.9436
19	4.6312	7.4551	4.9304	7.4551	4.6312
19.25	7.0944	8.1595	5.4952	8.1595	7.0944
19.5	11.7479	5.7902	3.5995	5.7902	11.7479
19.75	14.6624	4.1286	2.6137	4.1286	14.6624
20	15.6426	3.5413	1.9563	3.5413	15.6426
20.25	15.5172	3.4377	1.7817	3.4377	15.5172
20.5	14.8341	3.7196	1.9179	3.7196	14.8341
20.75	13.9292	3.8511	2.0660	3.8511	13.9292
21	12.9830	3.9032	2.1868	3.9032	12.9830
21.25	12.0789	3.9085	2.2824	3.9085	12.0789
21.5	11.2477	3.8898	2.3580	3.8898	11.2477
21.75	10.4993	3.8582	2.4182	3.8582	10.4993
22	9.8309	3.8199	2.4665	3.8199	9.8309
22.25	9.2354	3.7788	2.5056	3.7788	9.2354
22.5	8.7047	3.7372	2.5377	3.7372	8.7047

22.75	8.2339	3.6962	2.5641	3.6962	8.2339
23	7.8095	3.6565	2.5862	3.6565	7.8095
23.25	7.4296	3.6198	2.6047	3.6198	7.4296
23.5	7.0880	3.5837	2.6205	3.5837	7.0880
23.75	6.7796	3.5497	2.6339	3.5497	6.7796
24	6.5001	3.5176	2.6455	3.5176	6.5001
24.25	6.2456	3.4874	2.6555	3.4874	6.2456
24.5	6.0187	3.4589	2.6642	3.4589	6.0187
24.75	5.8054	3.4321	2.6718	3.4321	5.8054
25	5.6109	3.4067	2.6785	3.4067	5.6109

Table C.2: Maximal surface traction forces (Max_{STF}) applied to each bacterial cell (ellipsoid body) of 5-cell chains over time. L=Left cell, ML=middle left cell, C=Center cell, MR=middle right cell, R=right cell.

Part IX

Résumé de la thèse en français

IX.1

Introduction et objectifs

Les capacités adhésives des bactéries sont indissociables de leur survie au sein de nombreux environnements. Elles leur permettent de se nourrir [Nagara et al., 2017, Yu et al., 1987], de se déplacer [Persat et al., 2015, Talà et al., 2019], de résister au stress [Björnham and Axner, 2009, Persat et al., 2015] et de coloniser différents milieux [An and Friedman, 1998, Katsikogianni and Missirlis, 2004, Kline et al., 2010, O'Connell, 2003, Lebeer et al., 2008, Lebeer et al., 2012, Pizarro-Cerdá and Cossart, 2006, Segers and Lebeer, 2014, Tripathi et al., 2013, Tassell and Miller, 2011, Whittaker et al., 1996]. Les interactions adhésives bactéries-hôte sont responsables de la mise en place d'infections dans le cas des bactéries pathogènes [An and Friedman, 1998, Katsikogianni and Missirlis, 2004, Ong and Shah, 2009, Pizarro-Cerdá and Cossart, 2006, Proft and Baker, 2009, Roszak and Colwell, 1987, Whittaker et al., 1996], mais peuvent aussi générer des bénéfices santé chez l'hôte dans le cas de bactéries probiotiques, telles que les bactéries lactiques (LAB) [Agrawal, 2005, Borges et al., 2016b, Cousin et al., 2015, Daniel et al., 2006, Ford et al., 2014, Johnson-Henry et al., 2016, Lee and Salminen, 2009, Ouwehand et al., 2001, Pandey et al., 2015, Quinto et al., 2014, Servin and Coconnier, 2003, Tufarelli and Laudadio, 2016]. Les LAB forment un groupe de bactéries Gram positif, non sporulantes, anaérobies ou aérobies facultatives qui produisent de l'acide lactique comme composé principal de leur catabolisme [Stackebrandt and Teuber, 1988, Stiles and Holzapfel, 1997]. Elles sont très utilisées comme levains en agroalimentaire et, plus récemment, ont suscité un intérêt accru du fait de leur potentiel probiotique [Carr et al., 2002, Hayek and Ibrahim, 2013, Khalid and others, 2011, Pokusaeva et al., 2011, Quinto et al., 2014]. Afin de prodiguer leurs effets santé à l'hôte, ces bactéries doivent arriver dans l'intestin à la fois vivantes et fonctionnelles. Des stratégies ont donc été développées afin

d'assurer leur protection jusqu'à leur relargage dans l'intestin.

Récemment, des phénomènes d'adhésion ont également été observés entre LAB et composants de la matrice alimentaire, notamment au sein de certaines viandes [Firstenberg-Eden, 1981, Piette and Idziak, 1989], céréales [Chumphon et al., 2016] et produits laitiers [Burgain et al., 2014a, Gomand et al., 2019b, Gomand et al., 2018, Guerin et al., 2016]. Ces interactions sont susceptibles de jouer un rôle important en termes de protection et d'efficacité de relargage des probiotiques dans l'intestin, qui a été mis en avant par plusieurs revues de la littérature [Gomand et al., 2019a, Hickey et al., 2015b, Mortazavian et al., 2012, Ranadheera et al., 2010, Sanders and Marco, 2010]. Des études récentes ont montré que l'adhésion bactérienne aux composants alimentaires pouvait notamment moduler la distribution des bactéries dans l'aliment [Jeanson et al., 2011, Jeanson et al., 2015, Okochi et al., 2017, Laloy et al., 1996, Lopez et al., 2006], modifier les propriétés rhéologiques de la matrice [Laloy et al., 1996, Lopez et al., 2006, Tarazanova et al., 2018a], et entrer en compétition avec l'adhésion aux cellules intestinales [Guerin et al., 2018b, Sun and Wu, 2017].

Ces interactions adhésives sont possibles grâce à la présence de protéines à la surface des cellules bactériennes, dont font partie les pili, qui sont des protéines filamentaires sortase-dépendantes ancrées par liaisons chimiques de haute énergie à la paroi bactérienne [Kline et al., 2010, Schneewind and Missiakas, 2014b]. Ces protéines de surface sont sensibles au stress pouvant être généré lors de certaines étapes industrielles de fabrication alimentaire ou fermentaire, susceptibles d'endommager la paroi des cellules et donc d'engendrer une diminution des capacités adhésives bactériennes. L'atomisation de suspensions bactériennes, en particulier, ainsi que les étapes de brassage du lait et d'étirement de la matrice fromagère (dans le cas de fromages de type "pâte filée"), génèrent un stress de cisaillement conduisant à des modifications significatives de la surface bactérienne [Arnaud et al., 1993, Berzins et al., 2001, Kiekens et al., 2019, Lange et al., 2001, Taskila, 2017, Tripathi et al., 2012].

Cependant, la majorité des études menées jusqu'à présent sur l'adhésion bactérienne aux composants de l'aliment se sont concentrées seulement sur quelques souches [De Bellis et al., 2010, Chumphon et al., 2016, Tarazanova et al., 2017, Tarazanova et al., 2018a, Tarazanova et al., 2018b, Utratna et al., 2017]. Il est par conséquent difficile d'avoir une vision d'ensemble du phénomène d'adhésion bactérienne aux composants de la matrice alimentaire à l'échelle de groupes de souches, tels que le groupe LAB. Le développement d'outils permettant de caractériser l'adhésion et ses effets sur les bactéries au sein de matrices alimentaires répondrait donc au besoin de l'industrie de mieux comprendre les conditions permettant d'améliorer ou de réduire

la viabilité et la fonctionnalité des bactéries probiotiques à l'échelle du groupe LAB. En particulier, une meilleure compréhension de l'impact d'étapes industrielles génératrices de stress pour les bactéries permettrait d'optimiser les procédés de fabrication en vue d'un meilleur relargage des probiotiques dans le tractus intestinal.

Mon projet de thèse répond aux trois questions suivantes :

1. L'adhésion bactérie-β-lactoglobuline présente-elle des caractéristiques communes au sein du groupe des bactéries lactiques ?
2. Quel est l'effet du cisaillement sur l'intégrité cellulaire (organisation spatiale et capacités adhésives) de *Lactobacillus rhamnosus* GG ?
3. Quelle est l'influence des interactions adhésives bactérie-particule sur la dynamique du système et les forces exercées sur la bactérie ?

Le chapitre IX.2 répond à l'objectif 1, et le chapitre IX.3 aux objectifs 2 et 3.

IX.2

Adhésion bactérie-aliment: ampleur et conséquences spatiales

Une méthode de criblage haut-débit a été développée, permettant d'évaluer l'affinité adhésive d'une centaine de souches vis-à-vis d'une gamme de biomolécules d'intérêt. Cette méthode comporte trois étapes principales, représentées en Figure IX.2.1, qui sont (i) l'immobilisation de la biomolécule d'intérêt sur des microplaques de 96 puits à haute valeur adhésive, (ii) l'incubation des souches bactériennes sur ces mêmes microplaques, permettant la mise en place des interactions adhésives bactérie-biomolécule. Cette étape est suivie de lavages successifs permettant d'éliminer les bactéries non-adhérentes, puis (iii) un suivi de la croissance bactérienne est effectué. Il a été démontré que le temps apparent de croissance d'une souche est directement correlé au nombre de bactéries capables d'adhérer à la biomolécule testée. Cette méthode présente l'avantage d'évaluer à la fois les capacités adhésives des bactéries et leur viabilité, car seules les bactéries vivantes et fonctionnelles sont capables de pousser sur microplaques. Elle a été validée sur la souche modèle *Lactobacillus rhamnosus* GG (LGG) ainsi que sur trois souches présentant diverses mutations de surface modifiant leurs capacités adhésives.

Cette méthode a ensuite été appliquée à une collection de 73 souches LAB, dont l'affinité adhésive a été évaluée vis-à-vis d'une protéine laitière majeure du lactosérum, la β-lactoglobuline. Le but était de déterminer si les interactions adhésives de souches issue d'un même groupe présentaient des caractéristiques communes, et si celles-ci pouvaient être prédites à partir de la composition de surface de ces bactéries. Un phénomène d'adhésion à la β-lactoglobulin a été observé seulement sur quatre souches, soit moins de 6 % de notre collection. L'étude génomique

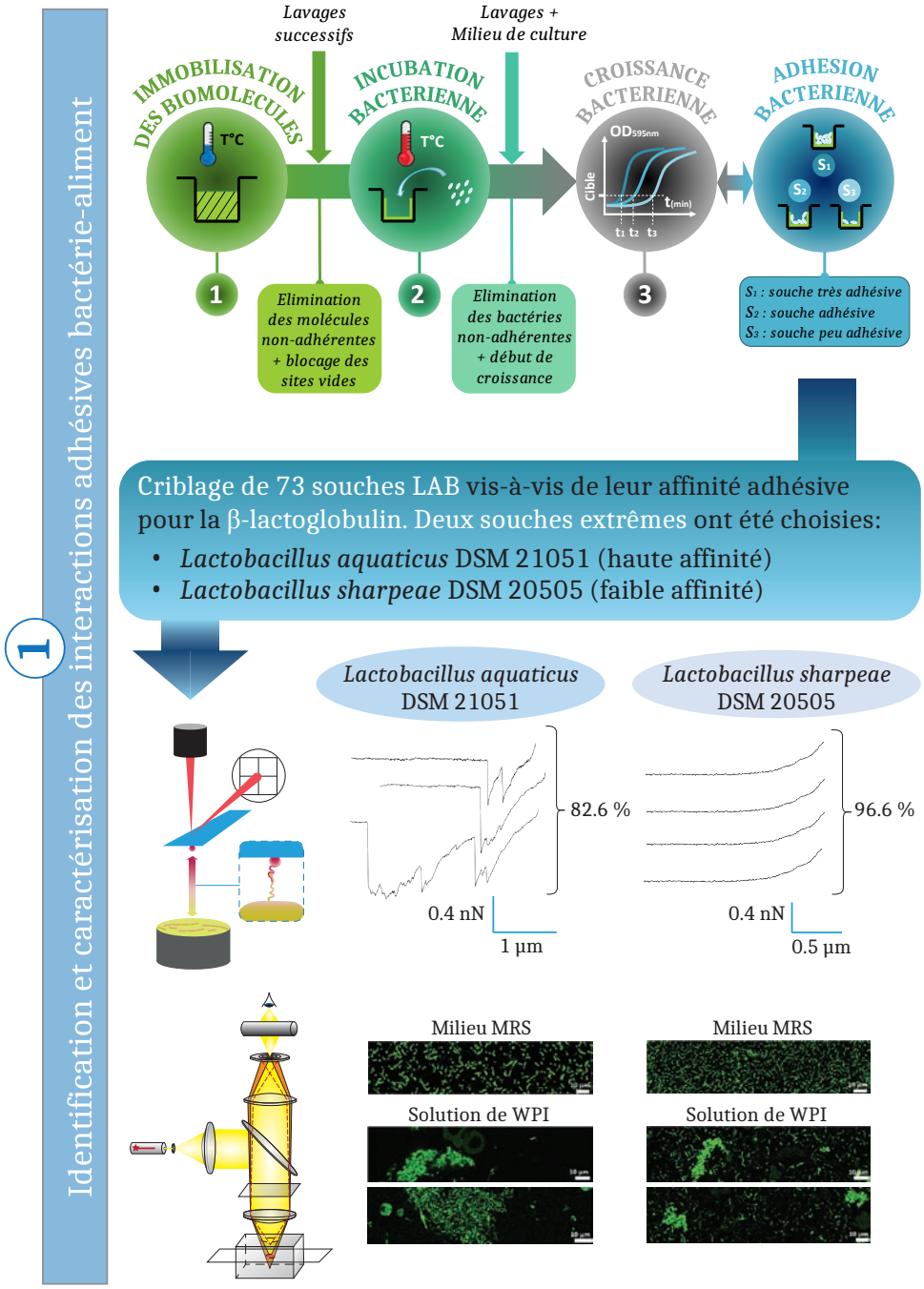

Figure IX.2.1: Ampleur du phénomène d'adhésion bactérie-aliment et ses conséquences sur la répartition spatiale bactérienne (objectif 1).

réalisée sur les souches adhérentes, focalisée sur les protéines prédites à motif LPxTG, ainsi que sur les clusters de gènes responsables de l'expression de pili, n'a pas permis de tirer de conclusions quant aux acteurs moléculaires qui seraient impliqués dans l'adhésion à la β-lactoglobuline. Deux souches extrêmes en termes d'adhésion, *i.e.* la souche la plus adhérente de la collection, *Lactobacillus aquaticus* DSM 21051, et la souche la moins adhérente, *Lactobacillus sharpeae* DSM 20505, ont été étudiées plus en détail par microscopie à force atomique (AFM), ainsi que par microscopie confocale (CLSM). Les résultats principaux de cette étude sont présenté en Fig. IX.2.1. Il a été mis en évidence que l'adhésion de *Lactobacillus aquaticus* DSM 21051 à la β-lactoglobuline est hautement spécifique, comme en témoigne la signature caractéristique observable sur les courbes de retraits d'AFM présentées en Fig. IX.2.1. Il a également été démontré que ces interactions adhésives influençaient de manière importante la répartition des bactéries au sein d'une matrice contenant de la β-lactoglobuline, constituée d'extrait de lactosérum (Whey Protein Isolate, WPI). Des agrégats de cellules bactériennes ont été observés au sein de cette matrice pour la souche adhésive *Lactobacillus aquaticus* DSM 21051, tandis qu'une répartition plus homogène a été observée dans le cas des cellules de *Lactobacillus sharpeae* DSM 20505. Des répartitions similaires ont été observées pour les souches témoins adhésive (LGG WT) et non-adhésive (LGG *spaCBA*).

Ces découvertes mettent en évidence la spécificité d'adhésion des bactéries LAB à la β-lactoglobulin, qui ne semble pas être une caractéristique partagée par la majorité des LAB, ainsi que le rôle-clé joué par ces interactions sur la répartition des bactéries au sein de la matrice alimentaire.

IX.3

Impact du cisaillement sur les capacités adhésives et la rupture de chaînes bactériennes

Les protéines de la surface bactérienne impliquées dans les phénomènes d'adhésion aux composants alimentaires sont sensibles au stress pouvant survenir lors d'étapes industrielles de fabrication de l'aliment et des ferments, comme l'atomisation ou le brassage du lait. L'impact du cisaillement sur l'intégrité des cellules bactériennes a été étudié en termes de viabilité, pertes de capacités adhésives, et modification de la forme bactérienne (en chaînes, cellules isolées, agrégats, etc.). Cette impact a été appréhendé à travers une double approche, à la fois expérimentale et théorique grâce à des simulations numériques et une modélisation analytique. Les principaux résultats obtenus sont présentés en Figure IX.3.1.

Les expériences ont été réalisées à l'échelle de la suspension bactérienne, tandis que la modélisation mathématique s'est attachée à la description des phénomènes à l'échelle de la cellule. L'intensité du phénomène d'arrachage des protéines à la surface des cellules bactériennes a été correlée à l'intensité des forces de traction appliquées en surface des cellules au sein d'un flux de cisaillement. Ces forces de traction sont celles qui ont été étudiées par la suite en modélisation.

Une relation positive entre fonctionnalité adhésive et forme bactérienne a été suggérée en combinant résultats expérimentaux et résultats de modélisation (Fig. IX.3.1a). En effet, les pertes les plus importantes en termes de capacités adhésives (suivant une exponentielle décrois-

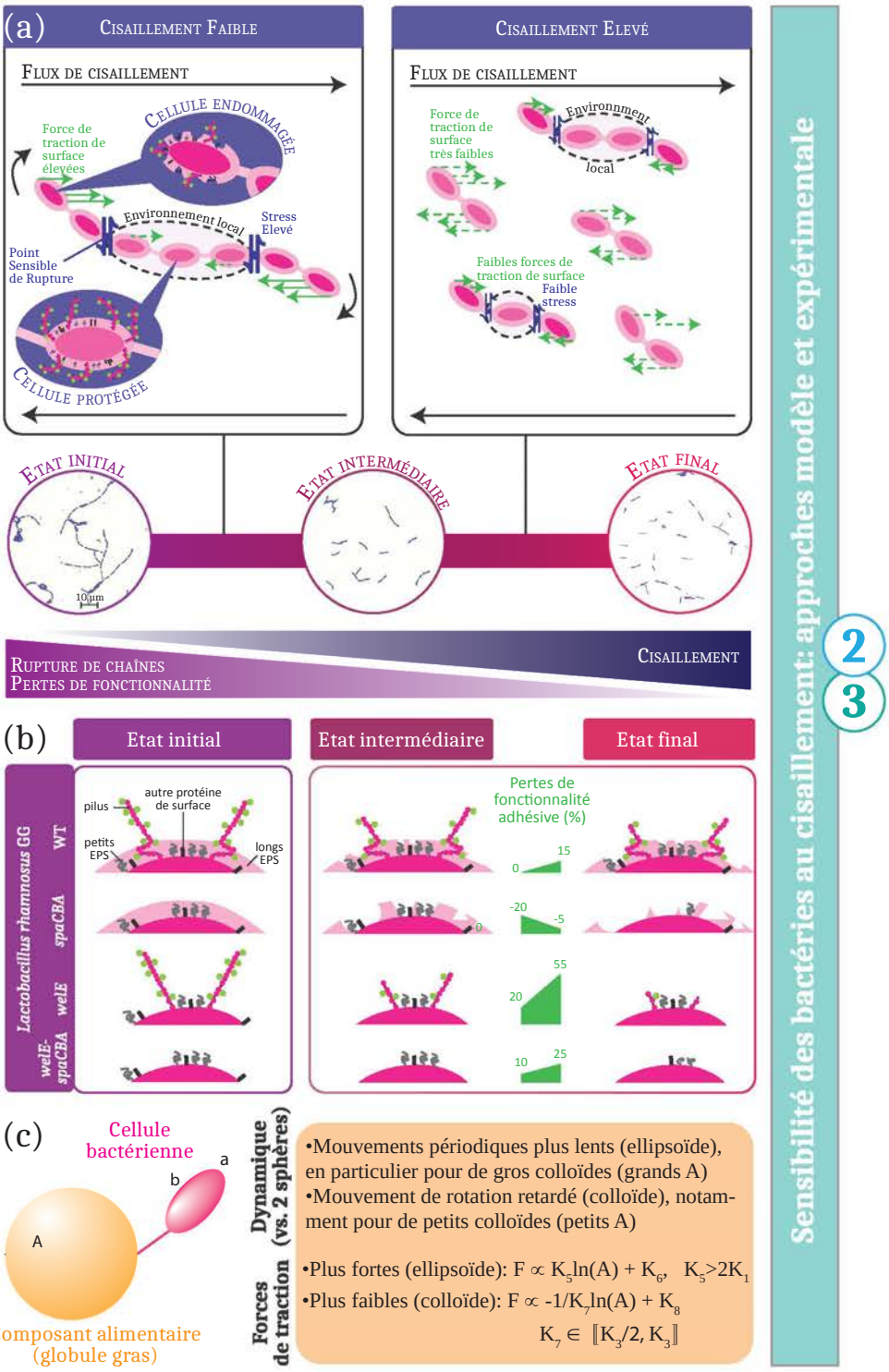

Figure IX.3.1: Impact du cisaillement sur les capacités adhésives et la rupture de chaînes bactériennes (objectifs 2 et 3).

sante en fonction du taux de cisaillement appliqué) ont été observées en parallèle d'un phénomène de rupture des chaînes bactériennes. Or, notre modèle a également permis de montrer que, plus une chaîne est longue, plus les forces de traction appliquées aux cellules sont importantes. Les chaînes plus petites issues de la rupture de chaînes plus longues subiront ainsi des forces de traction plus faibles, limitant les dommages subits en surface. La rupture de chaînes bactériennes permettrait ainsi de protéger la fonctionalité des cellules issues de cette rupture. Notre modèle a également mis en évidence une régiosélectivité des forces de traction et donc des dommages subits par les cellules bactériennes au sein d'une chaîne : ainsi, les cellules aux extrémités de la chaînes sont susceptibles d'être plus endommagées par le cisaillement que les cellules proches du centre de la chaîne, du fait d'effets locaux observés. Cette régiosélectivité est créatrice d'hétérogénéité au sein d'une même chaîne, et serait susceptible de participer à la sélectivité naturelle.

Les expériences ont mis en évidence le fait que la configuration en chaînes de deux cellules était la plus favorisée au sein d'un environnment soumis à des forces de cisaillement. Les pertes maximales de capacités adhésives observées ont été respectivement de 20 % et 55 % pour LGG WT et LGG *welE* (souche mutante sans exopolysaccharides (EPS)), suggérant un rôle protecteur des EPS vis-à-vis des molécules de surface impliquées dans les phénomènes d'adhésion. *A contrario*, un gain en capacités adhésives s'élevant jusqu'à 20 % a été observé pour la souche mutante sans pili LGG *spaCBA*, qui pourrait s'expliquer par un arrachage partiel de la couche d'EPS, permettant d'exposer d'autres protéines adhésives sous-jacentes.

L'influence de l'adhésion bactérienne à des composants alimentaires, tels que les globules gras, sur l'intégrité des protéines adhésives à la surface de cellules bactériennes soumises à un cisaillement, a été étudiée par modélisation. L'adhésion d'une bactérie à un colloïde de taille variable a été modélisée par un système constitué de deux corps. L'un est sphérique de rayon A (colloïde), l'autre ellipsoïdal de longueur $2a$ et de largeur $2b$ (cellule bactérienne), comme représenté en Fig. IX.3.1c). Ces corps sont connectés l'un à l'autre par un faisceau de ressorts, caractérisé par deux constantes, l'une de rigidité et l'autre d'élasticité. Ce système haltéroïde a été comparé à des haltères (*dumbbells*) rigides et flexibles. Les dynamiques de ces systèmes ont été étudiées à travers des paramètres de périodicité et de vitesse maximale de rotation. Les forces de traction exercées sur ces corps au sein d'un flux de cisaillement ont également été étudiées, à la fois en termes d'intensité et de localisation sur chaque corps. Dans le cas des systèmes flexibles, un comportement à double fréquence a été observé, se traduisant par un mouvement de balancier (*swinging*) pour le corps le plus petit et un mouvement de rotation pour le corps le plus grand, entraînant à sa suite l'ensemble du système. L'adhésion d'un corps ellipsoïdal à un colloïde

plus gros, mais de taille variable, augmente les forces de traction sur l'ellipsoïde, de manière logarithmique avec le rayon A du colloïde, et diminue les forces de tractions exercées sur le colloïde. Dans ce contexte et pour la configuration étudiée (Fig. IX.3.1c), l'adhésion bactérienne à un globule gras aurait donc un effet défavorable sur l'intégrité des protéines bactériennes de surface.

IX.4

Conclusion et perspectives

Cette thèse a permis de répondre aux trois objectifs énoncés en introduction, à savoir (i) la mise en place d'une méthode haut-débit permettant d'évaluer rapidement la présence d'interactions adhésives entre bactéries et composants de la matrice alimentaire pour un grand nombre de souches, (ii) la détermination de caractéristiques communes d'adhésion à l'échelle du groupe LAB, en termes de spécificité d'adhésion, mais aussi d'impact sur la répartition spatiale des bactéries au sein de matrices alimentaires, et (iii) l'impact du cisaillement (pris comme exemple de stress mécanique) sur la fonctionalité, viabilité et forme bactérienne.

Ce projet est un premier pas en direction d'une meilleure compréhension des phénomènes d'adhésion bactéries-aliment susceptibles d'influer sur la protection des probiotiques dans la matrice et l'efficacité de leur relargage.

Les perspectives de poursuite de ces travaux sont multiples. On distinguera notamment les perspectives à court terme ($\sim$ 6 mois à 1-2 ans) des perspectives à long terme (minimum 2 à 3 ans).

Parmi les perspectives à court terme, on peut envisager de replacer l'adhésion des LAB à la β-lactoglobuline dans un contexte plus général d'adhésion à la matrice laitière, en appliquant la méthode haut-débit développée à d'autres composants du lait, comme la membrane des globules gras (MFGM) et l'α-lactalbumine. L'impact de l'adhésion sur la répartition des bactéries au sein de matrices alimentaires pourrait aussi être étudié sur des matrices de composition plus complexes, plus proches du lait. Des analyses plus complètes de la surface bactérienne des souches adhérentes pourraient également être réalisées, prenant en compte d'autres types de protéines que celles à ancrage LPxTG, comme les protéines liées au système de sécrétion TAT (twinargi-

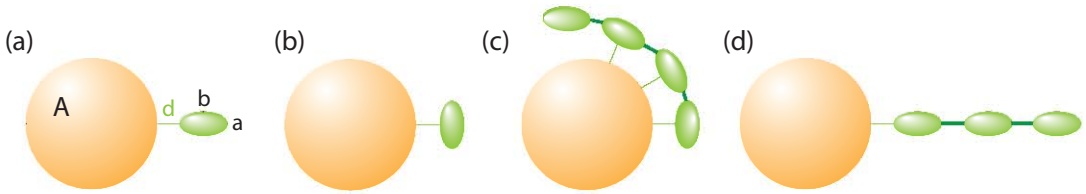

Figure IX.4.1: Etude de configurations plus complexes d'adhésion entre bactéries et globules gras par le biais de simulations numériques.

nine translocation), ou mobilisant d'autres techniques, comme la protéomique. Ces analyses permettraient potentiellement de proposer de meilleures protéines bactériennes candidates pour expliquer les mécanismes d'adhésion aux protéines laitières. Concernant l'impact du cisaillement sur l'intégrité bactérienne, des expériences pourraient être réalisées à l'échelle de la cellule pour confirmer les résultats obtenus par modélisation et mieux définir le domaine d'application de notre modèle. Ces expériences pourraient utiliser des outils développés en microfluidique, qui permettraient de suivre *in situ* la dynamique et les forces de traction exercées sur les cellules d'une chaîne. L'adhésion bactérie-globule gras et son impact sur l'intégrité de la surface bactérienne pourrait aussi être étudiée expérimentalement, en utilisant des suspensions monodisperses de globules gras puis en procédant à des observations microscopiques via AFM. Des configurations plus complexes que celle étudiée dans ce projet (Figure IX.4.1a) pourraient également être explorées par le biais de simulations numériques, comme présentées en Fig. IX.4.1b, c, et d. Enfin, l'impact du stress de cisaillement pourrait être combiné à celui d'autres stress, afin de se rapprocher des conditions réelles procédés (stress hydrique lié au séchage lors de l'atomisation des ferments par exemple) ou biologiques (stress acide lors de la digestion).

Parmi les perspectives à long terme, deux directions principales de recherche peuvent être proposées, qui sont (i) l'impact de l'adhésion et des propriétés de surface des cellules bactériennes sur les propriétés de la matrice alimentaire, notamment lors de sa structuration, et (ii) l'impact de stress environnementaux sur l'évolution bactérienne et la sélectivité naturelle. L'impact des propriétés de surface de la souche modèle LGG sur la structuration de matrices laitières sera étudié au sein d'une nouvelle thèse, débutant en septembre. Des premières expériences ont permis de montrer que les protéines adhésives bactériennes jouent un rôle sur le coefficient de diffusivité des bactéries, ainsi que sur la vitesse de crémage du lait cru, que l'on peut corréler à l'affinité de la souche étudiée pour la membrane des globules gras présents dans le lait.

La relation proposée entre fonctionalité et rupture de chaînes bactériennes au sein d'un flux

de cisaillement suggère l'existence d'avantages sélectifs conférés par la configuration en chaînes par rapport à la configuration en cellules isolées dans cet environnement. Ce phénomène pourrait être étudié à l'échelle expérimentale, en recréant des contraintes de cisaillement en conditions de cultures, afin de suivre l'évolution naturelle des phénotypes bactériens sur plusieurs générations.

Notre modèle ayant également mis en évidence un phénomène de régiosélectivité des forces de traction appliquées sur les cellules d'une chaîne bactérienne soumise à un cisaillement, ce phénomène serait alors créateur d'hétérogénéité à l'échelle d'un individu au sein d'une population. Une revue a récemment mis en avant l'intérêt de l'hétérogénéité pour la survie de populations bactériennes soumises à des changements environnementaux imprévisibles [Martins and Locke, 2015]. L'hétérogénéité née du cisaillement au sein d'une population bactérienne pourrait ainsi être étudiée plus en détails en relation avec les avantages évolutifs qu'elle pourrait conférer à certains individus, en utilisant des approches de single-cell [Editorial, 2016, Bridier et al., 2015].

Abstract

In the last decade, there has been an increasing interest in the potential health effects associated with consumption of Lactic Acid Bacteria (LAB) in foods. Adhesive interactions between bacteria and food components are likely to play a key role on bacterial probiotic action by modulating both bacterial protection and distribution within food matrices. Research presented in this thesis aims a better understanding of these interactions to help optimizing functional food design. Indeed, the adhesive behavior of most LAB, as well as the impact of adhesive interactions on food structuration, remain mostly unknown. Furthermore, some food manufacturing steps, such as spray-drying, may induce stress on bacteria, which can cause partial loss of bacterial adhesive capacities. In case of bacteria integrated within an adhesive matrix, the effect of adhesive interactions on bacterial protection from stress can also be questioned. A high-throughput screening method was first designed to screen quickly a hundred of strains for their adhesive affinities towards a given range of biomolecules of interest. This method was then applied to a 73-LAB strains collection which allowed identifying common characteristics amongst adhesive strains, especially in terms of adhesion specificity. Two studies (experimental and theoretical) were performed in parallel to determine the impact of shear stress on bacterial functionality and bacterial chains integrity. These studies suggest that the stress-induced breaking-down process of bacterial chains can be thought of as a functionality protective process. The proposed model predicts regioselectivity of damages inflicted to bacterial cells within a chain, which intensity would vary with chain length. When applied to bacteria-spherical component adhesive interactions within a food matrix submitted to shearing, the model suggests an unfavorable impact of adhesion on bacterial cell damages, which would be all the more important than spheres are big. This multidisciplinary research project points out several key findings that may help with designing more efficient food matrices for optimized LAB delivery.

Keywords: lactic acid bacteria, adhesion, food, shear flow, modeling, stress resistance.

Résumé

Les bactéries lactiques (LAB) ont suscité ces dernières années un intérêt accru en agroalimentaire du fait de leur potentiel probiotique, *i.e.* des potentiels bénéfices santé associés à leur consommation. Les interactions adhésives entre bactéries et composants alimentaires sont susceptibles de jouer un rôle-clé à la fois sur la protection et la répartition des bactéries au sein de l'aliment, impactant donc leur action probiotique. Les travaux réalisés au cours de cette thèse ont pour objectif une meilleure compréhension de ces interactions, afin d'optimiser la fonctionnalité d'aliments contenant des LAB. En effet, le comportement adhésif de la majorité des LAB, ainsi que l'effet des interactions adhésives sur la structuration de l'aliment, sont encore mal connus. En outre, certaines étapes de fabrication alimentaire, telles que l'atomisation, peuvent être génératrices de stress pour les bactéries et donc partiellement compromettre leur capacité à adhérer. Dans le cas où ces bactéries seraient intégrées au sein d'une matrice adhésive, il est également légitime de s'interroger sur les effets de cette adhésion sur la protection des bactéries vis-à-vis du stress infligé. Une méthode de criblage haut-débit a d'abord été développée dans l'objectif d'évaluer rapidement l'affinité adhésive d'une centaine de souches vis-à-vis d'une gamme de biomolécules d'intérêt. Cette méthode a ensuite été appliquée à une collection de 73 souches LAB et a permis de dégager des caractéristiques communes parmi les souches adhérentes, notamment en termes de spécificité d'adhésion. Deux études (expérimentale et théorique) ont été menées conjointement sur l'impact du stress de cisaillement sur la fonctionnalité et l'intégrité des chaînes bactériennes. Ces études suggèrent que la rupture de chaînes bactériennes induite par un stress mécanique serait un processus protecteur de la fonctionnalité bactérienne. Le modèle construit prédit une régiosélectivité des dommages infligés aux cellules bactériennes en chaînes, dont l'intensité dépendrait également de la longueur de chaîne. Appliqué aux interactions adhésives bactéries-particules dans une matrice alimentaire soumise au cisaillement, le modèle suggère un impact défavorable de cette adhésion sur les dommages infligés aux bactéries, d'autant plus important que les particules sont de grande taille. Ce travail pluridisciplinaire apporte ainsi plusieurs éléments-clé qui seront utiles lors la conception et production d'aliments fonctionnels optimisés par rapport à leur action probiotique.

Mots-clés: bactéries lactiques, adhésion, aliment, cisaillement, modélisation, résistance au stress